Towards Sustainable Buildings with Free-Form Geometries

Development and Application of Flexible NFRP in Load-Bearing Structures

Dahy, Hanaa

Published in:
Biocomposite Materials

DOI (link to publication from Publisher):
10.1007/978-981-33-4091-6_2

Publication date:
2021

Document Version
Publisher's PDF, also known as Version of record

Composites Science and Technology

Mohamed Thariq Hameed Sultan
Mohd Shukry Abdul Majid
Mohd Ridzuan Mohd Jamir
Azwan Iskandar Azmi
Naheed Saba *Editors*

Biocomposite Materials

Design and Mechanical Properties Characterization

Springer

Composites Science and Technology

Series Editor

Mohammad Jawaid, Lab of Biocomposite Technology, Universiti Putra Malaysia, INTROP, Serdang, Malaysia

Composites Science and Technology (CST) book series publishes the latest developments in the field of composite science and technology. It aims to publish cutting edge research monographs (both edited and authored volumes) comprehensively covering topics shown below:

- Composites from agricultural biomass/natural fibres include conventional composites-Plywood/MDF/Fiberboard
- Fabrication of Composites/conventional composites from biomass and natural fibers
- Utilization of biomass in polymer composites
- Wood, and Wood based materials
- Chemistry and biology of Composites and Biocomposites
- Modelling of damage of Composites and Biocomposites
- Failure Analysis of Composites and Biocomposites
- Structural Health Monitoring of Composites and Biocomposites
- Durability of Composites and Biocomposites
- Biodegradability of Composites and Biocomposites
- Thermal properties of Composites and Biocomposites
- Flammability of Composites and Biocomposites
- Tribology of Composites and Biocomposites
- Bionanocomposites and Nanocomposites
- Applications of Composites, and Biocomposites

To submit a proposal for a research monograph or have further inquries, please contact springer editor, Ramesh Premnath (ramesh.premnath@springer.com).

More information about this series at http://www.springer.com/series/16333

Mohamed Thariq Hameed Sultan ·
Mohd Shukry Abdul Majid ·
Mohd Ridzuan Mohd Jamir ·
Azwan Iskandar Azmi · Naheed Saba
Editors

Biocomposite Materials

Design and Mechanical Properties Characterization

Springer

Editors
Mohamed Thariq Hameed Sultan
Department of Aerospace Engineering,
Faculty of Engineering
Universiti Putra Malaysia
Serdang, Selangor, Malaysia

Mohd Shukry Abdul Majid
Faculty of Mechanical Engineering
Technology
Universiti Malaysia Perlis (UniMAP)
Arau, Perlis, Malaysia

Mohd Ridzuan Mohd Jamir
Faculty of Mechanical Engineering
Technology
Universiti Malaysia Perlis (UniMAP)
Arau, Perlis, Malaysia

Azwan Iskandar Azmi
Faculty of Mechanical Engineering
Technology
Universiti Malaysia Perlis (UniMAP)
Arau, Perlis, Malaysia

Naheed Saba
Laboratory of Biocomposite Technology,
Institute of Tropical Forestry and Forest
Products (INTROP)
Universiti Putra Malaysia
Serdang, Selangor, Malaysia

Composites Science and Technology
ISBN 978-981-33-4090-9 ISBN 978-981-33-4091-6 (eBook)
https://doi.org/10.1007/978-981-33-4091-6

This Springer imprint is published by the registered company Springer Nature Singapore Pte Ltd.
The registered company address is: 152 Beach Road, #21-01/04 Gateway East, Singapore 189721, Singapore

Preface

The use of biocomposite materials has received significant attention in recent years, in particular, due to the proliferated awareness of and drive towards more environmentally sustainable technologies. In many cases, bio-based materials offer lightweight applications, added functionality such as damping/impact absorption and occupational health benefits. Thus bio-based materials have become a pressing issue both for academia and industry. A significant market driver for high volume applications is the potential to disassociate material costs from the inconsistent price of oil and energy.

This book chapter offers ranges of biocomposites, and the natural fibres, bio-based polymers and bio-based core materials used to produce them and present the current best practice in design, mechanical characterisation and applications. The term "*biocomposite*" referred in the book represent fibre-reinforced polymer composite materials where the fibres and matrix are bio-based. Kenaf, Jute, Pineapple leaves (PALF), Hemp, and coir are frequent natural fibre reinforcements in biocomposites and have excellent mechanical properties. Loose fibre, non-woven mats and woven fabrics are the most common forms of natural fibre for composites, with aligned variants offering the best mechanical properties. Fibre treatments such as salinisation or acetylation can be used to reduce moisture uptake and advance compatibility with polymers. Artificial bio-based fibre reinforcements, such as regenerated cellulose, are also available and offer higher homogeneity. In addition to the studies aimed at refining basic mechanical properties and functionalities of the materials, other studies dedicated to developing eco-friendly composites and biomedical materials for use in tissue engineering, scaffolds and implants.

We are thankful to all authors who contributed their valuable research in our edited book. Editors are also thankful to Springer team for supporting and cooperation during the whole project. Though the progress of the book has been delayed by the COVID-19 pandemic that swept the world, we have made through, and it is a true testament to the perseverance of all authors involved in the project. Thanks all.

Serdang, Malaysia — Mohamed Thariq Hameed Sultan
Arau, Malaysia — Mohd Shukry Abdul Majid
Arau, Malaysia — Mohd Ridzuan Mohd Jamir
Arau, Malaysia — Azwan Iskandar Azmi
Kuala Lumpur, Malaysia — Naheed Saba

Contents

About the Editors

Prof. Ir. Ts. Dr. Mohamed Thariq Hameed Sultan is a Professional Engineer (PEng) registered under the Board of Engineers Malaysia (BEM), a Professional Technologist (PTech) registered under the Malaysian Board of Technologists, and also a Charted Engineer (CEng) registered with the Institution of Mechanical Engineers United Kingdom, currently attached to the Universiti Putra Malaysia as the Head of the Biocomposite Technology Laboratory, Institute of Tropical Forestry and Forest Products (INTROP), UPM Serdang, Selangor, Malaysia. Being the Head of the Biocomposite Technology Laboratory, he is also appointed as an Independent Scientific Advisor to Aerospace Malaysia Innovation Centre (AMIC) based in Cyberjaya, Selangor, Malaysia. He received his Ph.D. from the University of Sheffield, UK. He has about 10 years of experience in teaching as well as in research. His area of research interests includes hybrid composites, advance materials, structural health monitoring, and impact studies. So far he has published more than 100 international journal papers and received many awards locally and internationally. In December 2017, he was awarded a Leaders in Innovation Fellowship (LIF) by the Royal Academy of Engineering (Raeng), UK. He is also the Honourable Secretary of the Malaysian Society of Structural Health Monitoring (MSSHM) based in UPM Serdang, Selangor, Malaysia. Currently, he is also attached to the Institution of Engineers Malaysia (IEM) as the Deputy Chairman in the Engineering Education Technical Division (E2TD).

Dr. Mohd Shukry Abdul Majid received his Bachelor of Engineering in Mechanical Engineering from University Manchester Institute of Science and Technology (UMIST) in 2001. Upon his return to Malaysia, he worked as a research and development (R&D) engineer at a semiconductor industry before joining Universiti Malaysia Perlis (UniMAP) as a lecturer in 2004. He completed his M.Sc. in Mechanical Systems Engineering from the University of Liverpool in 2005 and his Ph.D. in Composite Engineering from Newcastle University, UK in 2011. Currently, he is serving Universiti Malaysia Perlis as an Associate Professor at Faculty of Mechanical Engineering Technology. An advocate of interdisciplinary research, his research interests lie in the strength of material's area with emphasis

on the composite piping, looking at the performance of composite structures, NDE's of composites and natural fibre/green composites, hybrid reinforced/filled polymer composites, lignocellulosic reinforced/filled polymer and biodegradable composites. His aptitude for high-quality research of international standing has been supported by his 188 Scopus indexed publications with *47 (32 Q1) publications in ISI-ranked Journals having a cumulative impact factor (CIF) of 148.948*. He received his professional engineer qualification (Ir.) from Board of Engineer Malaysia (BEM) in Mac 2016 and has been a Chartered Engineer (CEng) from the Engineering Council, UK since 2014. Dr. Mohd Shukry has been honoured with numerous local and international awards for his achievements. He is the first recipient from Technical University Network (MTUN) to have been awarded Malaysia's Research Star Award 2017, as one of Malaysia's most promising and influential researchers by the Ministry of Higher Education Malaysia (MOHE).

Dr. Mohd Ridzuan Mohd Jamir is a Professional Engineer (PEng) registered under the Board of Engineers Malaysia (BEM), a Professional Technologist (PTech) registered under the Malaysian Board of Technologists, and also a Chartered Engineer (CEng) registered with the Institution of Mechanical Engineers United Kingdom, currently attached to the Universiti Malaysia Perlis as an Associate Professor at Faculty of Mechanical Engineering Technology. He obtained Diploma in Mechanical Engineering from Universiti Teknologi Malaysia (UTM) in 2006. He graduated in Bachelor of Engineering (Mechanical) and Master of Engineering (Mechanical) from Universiti Teknologi Malaysia (UTM) in the year of 2009 and 2010, respectively. He also worked as Quality Assurance Engineer in Venture Pintarmas Sdn Bhd in Johor Baharu in 2010 before joined Universiti Malaysia Perlis (UniMAP) in the same year. He received his Ph.D. in Mechanical Engineering from Universiti Malaysia Perlis (UniMAP) in 2016. He has about 10 years of experience in teaching as well as in research. An advocate of interdisciplinary research, his research interests includes the strength of material's area with emphasis on the natural fibre composite, looking at the performance of composite structures and tribological properties, hybrid reinforced/filled polymer composites, lignocellulosic reinforced/filled polymer and biodegradable composites. He has published more than 100 international journal research paper with Scopus index and ISI ranked journal publications. In addition, he is also a regular reviewer for high-impacts ISI ranked journals.

Dr. Azwan Iskandar Azmi received his bachelor's degree in Mechanical Engineering from Purdue University, USA in 1999 and Master's in Advanced Manufacturing Technology from Universiti Teknologi Malaysia in 2003. In 2013, he completed his doctoral study at The University of Auckland, New Zealand in Mechanical Engineering with specialisation in the area of fibre reinforced composite machining. He is currently serving the Faculty of Mechanical Engineering Technology, Universiti Malaysia Perlis (UniMAP) as Associate Professor. Dr. Azwan is a Professional Engineer (PEng) registered under the Board of Engineers Malaysia (BEM), a Professional Technologist (PTech) registered under the

Malaysian Board of Technologists (MBOT), and also a Chartered Engineer (CEng) registered with the Institution of Mechanical Engineers (IMechE) in the UK. He has more than 10 years of experience in teaching, research, and industries. His area of research interests includes machining and machinability of carbon, glass, and their hybrid composites. Currently, the research also covers the drilling and milling of lignocellulosic reinforced polymer composites. His interest extends on the machinability study of difficult-to-cut metal alloys such as titanium, Inconel, and nickel-titanium (NiTi) alloys. So far, he has more than 50 research articles in renowned international journals, proceedings and review papers. He has been awarded with research funds from Ministry of Higher Education Malaysia (MOHE) and Ministry of Science Technology and Innovation (MOSTI). Due to the research outputs, Dr. Azwan has served as technical reviewer for a number of reputable high impact ISI ranked journals and international conferences.

Dr. Naheed Saba completed her Ph.D. (Nanocomposites) with Distinction from Laboratory of Biocomposites Technology, Institute of Tropical Forestry and Forest Products (INTROP), Universiti Putra Malaysia, Serdang, Selangor, Malaysia in 2017. She completed her masters in chemistry and also completed her postgraduate diploma in environment and sustainable development from India. She has published over 50 scientific Peer review Articles in International Journal and 4–5 Articles come under top cited articles in Construction and Building Materials, and Polymers Journal during 2016–2019. She edited six books from Elsevier and also published more than 25 book chapters in Springer, Elsevier, and Wiley publication. She attended few international conferences and presented research papers. Her research interest areas are nanocellulosic materials, fire-retardant materials, natural fiber-ereinforced polymer composites, biocomposites, hybrid composites, and nanocomposites. She is also recipient of International Graduate Research Fellowship and Graduate on time (GOT) award from Universiti Putra Malaysia, Malaysia. Presently she is Editor-in-Chief of The Journal of Composites and Advance Materials (ISSN 2716-8018) is a peer-reviewed bi-annual journal. She is also reviewer of several international journals such as Cellulose, Constructions and Building Materials, Composite Part A,Composite Part B, Journal of Polymers and The Environment, Journal of Energy Storage, Journal of Elastomers and Plastics, Journal of Materials Research and Technology, BioResources, and Carbohydrate Polymers. Her H-index = 17 (Scopus); H-Index = 20 (Google Scholar).

Green Biocomposites for Packaging Applications

Florencia Versino, Olivia Valeria López, and María Alejandra García

Abstract In recent years, research on environmentally sustainable packaging has been gaining momentum, primarily driven by consumer ecological consciousness. Green biocomposites play an important role in novel and innovative materials for the emerging sustainable packaging industry, being intrinsically biobased and biodegradable. Therefore, the following chapter is aimed to make an overview of the main trends on green biocomposites study and development, their environmental impact and their importance in future production systems. A revision of the polymeric matrices and fillers most widely used for green biocomposites and bionanocomposites manufacture is done, and the results of the latest investigations on the subject are discussed. Besides, their role in active and intelligent packaging is reviewed as well as their implementation for 3D printing technologies. Finally, the relevance of these materials study and development in terms of environmental impact is herein considered, remarking the importance of adequate life cycle assessment of the developed green biocomposites in comparison to conventional materials used for similar packaging applications.

Keywords Bioplastics · Packaging · Sustainable · Biodegradable · Biomass

F. Versino (✉) · M. A. García
Centro de Investigación y Desarrollo en Criotecnología de Alimentos (CIDCA), UNLP-CONICET-CICPBA, La Plata, Argentina
e-mail: florencia.versino@ing.unlp.edu.ar
URL: https://www.cidca.quimica.unlp.edu.ar

O. V. López
Planta Piloto de Ingeniería Química (PLAPIQUI), UNS-CONICET, Bahía Blanca, Argentina
URL: https://www.plapiqui.conicet.gov.ar

F. Versino
Departamento de Ingeniería Química, Universidad Nacional del La Plata, La Plata, Argentina

M. T. Hameed Sultan et al. (eds.), *Biocomposite Materials*, Composites Science and Technology, https://doi.org/10.1007/978-981-33-4091-6_1

1 Introduction

Composite materials comprise a wide range of materials, which consist of at least two compounds that differ on their physical or chemical characteristics interacting in a way that leads to a single material with hopefully better properties than its components separately. Generally, composites are comprised by a polymeric continues phase (known as matrix) and a dispersed phase (known as reinforcement), though some are prepared by mixture of two or more polymers (Shekar and Ramachandra 2018). The vast amount of possible compounds combinations in composite materials development has driven these materials market growth in various fields of application, mainly automotive, marine, aerospace, and construction industries (Rodriguez et al. 2012; Ramamoorthy et al. 2019). They were first developed as a low-cost alternatives to pure components and as high-performance and low-weight materials. Most early studies, as well as current work, focus on biobased and biodegradable compounds to develop the herein called green biocomposites which are expected not only to be cost-effective but also more environmentally friendly. This type of materials have become of interest for their use in the packaging industry where conventional composites face some limitations: their waste management and recycling are difficult and still underdeveloped generating large non-biodegradable plastic waste, while contributing to petrochemical resources depletion (La Mantia and Morreale 2011; Shekar and Ramachandra 2018). Packaging materials must be sufficiently resistant to protect and preserve the product from production through transportation and storage until consumption, but are discarded usually with little to no reuse (Song et al. 2009). Hence the development of green biocomposites, mainly those which are not only biobased but also biodegradable, has been extensively studied.

Petit et al. (2019) showed that despite of monetary savings there is a strong preference of consumers for smaller food packages, even individual portions, over larger packages because of anticipated food waste association. This proves, on the one hand, that consumers have a key role in market tendency building, thus waste management and environmental public education is of critical importance to move towards more sustainable production systems. On the other hand, smaller and portioned food packages prevent food waste, yet resulting in greater litter generation from packaging, therefore new packaging systems that could minimise both types of wastes need to be developed. In this that regard, biodegradable packaging plays a central role. Moreover, a cost-effective package should be the cheapest option that could preserve the products in good conditions until it is consumed in order to avoid products loses due to damage or expiration. In addition, packaging should be designed as to minimise raw materials and energy use in its production and reduce the energy consumption in transportation. Some alternatives oriented in this regard are, for instance, the thickness reduction on PET bottles design or the square profile design of bottles in order to optimise pallet space utilisation. The minimisation of raw materials use and products losses, as well as the reduction of transport volume and weight not only help reduce costs but also make a more efficient use of the valuable resources (Emblem 2012).

Nowadays, thanks to the worldwide greater environmental awareness, leading consumer goods companies are committed to a more holistic approach to good production, packaging, and distribution in turn of more sustainable processes to avoid pollution and further resources depletion. Efficient and cost-effective production and design of packaging materials, involving raw materials use reduction and development of new biobased and biodegradable packaging materials, are very much part of this holistic worldview (Farmer 2013). Consequently, in comparison to petroleum-based products, sustainable biobased products may have benefits for all agents comprised: the producers and customers as well as the whole environment (Georgios et al. 2016).

Briefly, in developing and designing sustainable alternatives for the packaging industry the whole process from cradle to grave should be considered. In the production stage, the type of raw material employed, its environmental impact with respect to resources consumption (water, earth, energy, etc.) during processing and transportation and the pollution that from its use is derived must be considered. During the shelf-life stage, its efficiency to preserve the specific packed-products properties as to prevent product loses, taking into account mechanical resistance, permeability and, eventually, active packaging properties should be contemplated. Lastly, in the end-of-life stage, the possibility of materials reuse, recycling or finally energy recovery or composting (in the case of biodegradable materials) must be evaluated. There is still much study and work to do in this respect, yet there is a common objective of adapting our products and processes to the future requirements, tending toward more conscious and sustainable production.

In general, the mechanical properties of composites are improved by fillers addition due to their higher strength and stiffness than those of polymers. An extensive revision and comparison of these properties has already been presented (Georgios et al. 2016; Castillo et al. 2017; Ramamoorthy et al. 2019). Therefore, this chapter aims to an extensive revision of the state-of-the-art on biobased and biodegradable composite materials investigations for packaging applications. On the one hand, the type of polymer matrices will be revised, especially its use in active packaging systems. On the other hand, different types and sizes of filler employed and processing techniques will be discussed. Various studies have gathered and compared different composites and green composites properties. Thus, even though a wide range of biocomposites properties will be discussed herein, it will certainly be incomplete owing to the versatility and numerous possibilities of formulations of composites materials comprising: polymer matrix type; filler type, size and form; additives type and content (such as plasticizer, cross-linking agents, among others); processing techniques employed; and processing conditions.

2 Green Composites Formulations, Processing, Structure, and Final Properties

2.1 Towards Greener Composites

As it was previously mentioned, polymer composites were first developed in order to reduce costs and weight. Besides, by these means there was also an implied reduction in conventional polymers use, which could contribute to decreasing petroleum reserves depletion and all environmental impact derived from its overuse. In addition, the use of basically recyclable polymers (mainly polyolefins), meaning that post-consumer plastics recovered from waste management systems could be partially used in place of virgin raw material, was a step forward greener or environmentally friendly composite material (La Mantia and Morreale 2011).

A step further led to the substitution of mineral inorganic fillers (such as glass fibre) by natural-organic fillers (for instance, wood flour or fibres extracted from plants). The latter present several advantages from an ecological point of view: they are essentially biodegradable and renewable materials; they are usually derived from relatively abundant plants (often from wastes) and therefore very cheap; they are also more safe to process both for employees and processing equipment; they can be easily incinerated; in comparison to inorganic fillers lead to lighter composites; and allow obtaining composite materials with thermal and acoustic insulation (Joshi et al. 2004; Dittenber and GangaRao 2012; Sapuan et al. 2016; Castillo et al. 2017).

Even though green composites containing novel sustainable natural fillers have drawn several researches for different industrial applications as a way of achieving a more efficient use of resources, some limitations regarding composites ductility, processability, and dimensional stability have arisen (La Mantia and Morreale 2011; Nayak and Khuntia 2019). These problems derive mostly from the hydrophilic nature of bioreinforcements and their low thermal stability. Numerous chemical and physical modifications of organic fillers can be performed in order to improve both fibre properties as well as fibre-polymer interaction, and consequently the composites final performance (Azwa et al. 2013; Shalwan and Yousif 2013; Castillo et al. 2017).

Nonetheless, an integrally sustainable approach with real environmental impact can only be obtained by substituting conventional oil-based polymers by biobased and biodegradable ones. These, however, present new limitations regarding especially lower mechanical performance and dimensional stability. Thus, these materials should be studied and developed for certain applications where very high mechanical resistance and durability are not relevant properties, which is the case of most packaging uses. Researches on green biocomposites are currently focused on the selection of the most suitable biodegradable matrix for each type of product and the optimization of formulations and processing conditions. Much of these investigations are exploring novel sustainable natural fillers as bioreinforcement-agents, being agricultural waste or by-products key players in the search of circular production systems.

As regards the biomaterials market situation, it can be stated that even though bioplastics have had a strong growth in the world market in the last decade, it is still in an opening phase. According to a report by the company Allied Analytics LLP, 4869 thousand tons of bioplastics were commercialized in 2014 and it is estimated that for the 2018–2024 period the annual growth rate is 20.45% (Allied Analytics LLP 2018). This growth is due not only to the various potential applications of these materials but also to favourable government policies aimed at increasing the production and consumption of environmentally friendly and sustainable products. Yet, significant research efforts are required to develop green biocomposites with similar performance to their petroleum-based counterparts being as well cost-competitive.

2.2 Polymer Matrices

Before analysing and comparing different polymer matrices used in green biocomposites, a proper classification of polymers should be stated. Usually, it would be considered as green biocomposites such composites that necessarily consist of a *bioplastic* as polymeric phase. This term comprises all plastics that are either biodegradable or bio-based or both (Fig. 1), hence there are bio-based polymers that are not biodegradable (i.e. green polyolefins) or biodegradable materials that are petroleum-based (i.e. polycaprolactone). However, to the extent of this chapter will be considered for green composite constituent those that are necessarily biodegradable.

As for non-biodegradable polymer matrices used in the field of green composites (which could be or not biobased), these are mainly polyolefins (as well as some polyurethanes or phenolic resins) in combination with natural fillers: mostly lignocellulosic fibres (Netravali and Chabba 2003; Iyer et al. 2015; Dey and Ray 2018; Dixit and Yadav 2019; Hidalgo-Salazar and Salinas 2019) or mineral fillers (Hatakeyema et al. 2005; Cazan et al. 2019; Hanken et al. 2019). The greener option in this case is the use of the biobased counterpart.

As for biodegradable bioplastics from fossil origin, most composite works reported employ polycaprolactone (PCL) or polyvinyl alcohol (PVA) as polymer matrix and in some cases combined with other biobased biodegradables polymer, such as starch and chitosan (Liu et al. 2010; Ludueña et al. 2012; Tănase et al. 2015; Xiong et al. 2018; Ahmed et al. 2019; Huang et al. 2019; Wang et al. 2019; Wu et al. 2019). Even though these polymer matrices usually have better mechanical properties and water resistance than natural polymers and, thanks to their biocompatibility, are more suitable for biomedical applications, they have a considerably higher cost (Chen et al. 2013; Trakoolwannachai et al. 2019; Zhang et al. 2019).

Natural polymers and biodegradable bioplastics synthesised from biomass (i.e. polylactic acid (PLA) or polyhydroxyalkanoates (PHAs)) are the most desirable polymeric matrices from an environmental point of view, owing that culture practices are sustainable with controlled water usage and minimum or no agrochemical application. In comparison to conventional plastic, these bioplastics have various advantages: low-cost (in the case of natural biopolymers), great availability, and

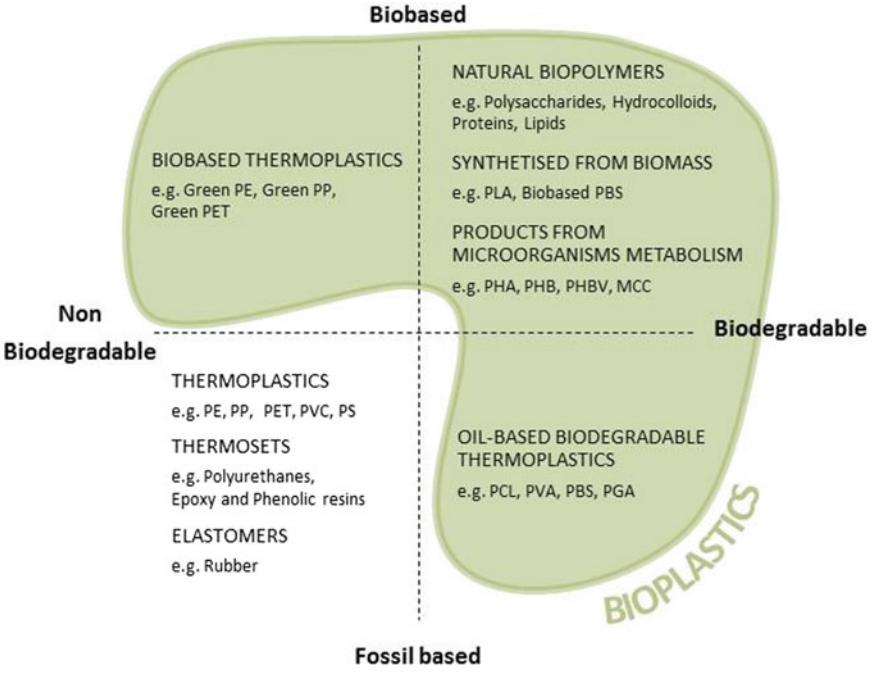

Fig. 1 Polymers classification according to biodegradability and source. *Note* PE: polyethylene; PP: polypropylene; PET: polyethylene terephthalate; PVC: polyvinyl chloride PS: polystyrene; PLA: polylactic acid; PBS: poly butylene succinate; PHA: polyhydroxyalkanoate; PHB: polyhydroxybutyrate; PHBV: Poly(3-hydroxybutyrate-co-3-hydroxyvalerate); MCC: microcrystalline cellulose; PCL: polycaprolactone; PVA: polyvinyl alcohol; PGA: polyglycolic acid

biodegradability (Ramamoorthy et al. 2019). The most widely applied renewable resources include plant oils, polysaccharides (primarily cellulose and starch), and proteins; most of them used as well as precursors for synthesised resin (Georgios et al. 2016). The major limitations for the application of these biopolymers are due to their lower thermal, water, and mechanical resistance. For instance, PLA is sensitive to hydrolytic degradation under melt processing condition in the presence of small amounts of moisture (Mukherjee and Kao 2011); and starch can only be thermo-processed in presence of plasticisers being unplasticised films extremely brittle (López et al. 2008; Versino et al. 2019). Besides, bioplastics production is not cost-competitive nowadays with commodity traditional polymers, not due to the raw materials cost but rather their low volume production (Georgios et al. 2016). The literature review show a vast amount of studies on biodegradable and biobased polymers, being these key to developing eco-friendly and sustainable packaging; PLA, (Mukherjee and Kao 2011; Arrieta et al. 2014; Fortunati et al. 2015; Yusoff et al. 2016; Piekarska et al. 2017; Komal et al. 2020), starch (Famá et al. 2009; Vercelheze et al. 2012; Bodirlau et al. 2013; Versino and García 2014; López et al. 2015; Merci

et al. 2019) and their combination with other bioplastics (Kaisangsri et al. 2012, 2014; De Oliveira et al. 2019) are the most used matrices for green biocomposites.

2.3 Natural Fillers

Natural fillers can be both organic and inorganic. In this regard, layered silicates (clays), carbon nanotubes, and mineral nanoparticles (talc), among others, are the most widely used inorganic fillers in composite materials (Castillo et al. 2017). These are usually nanosized fillers (meaning that at least one of their dimensions is smaller than 100 nm) that have proven to induce important changes in composites properties even at very low concentrations (Castillo et al. 2015). Even though these fillers are not biodegradable nor renewable, they are usually natural fillers and would be expected to be generally innocuous to the environment when the biocomposite is composted. Nonetheless, their toxicity is still under study (Yu et al. 2019).

Organic fibres, on the other hand, are typically lignocellulosic materials derived from plant tissue, thus fully biodegradable and annually renewable. They are made of three principal components: cellulose, lignin, and hemicellulose. Cellulose is the most abundant compound of the fibres which is accountable for their inherent strength and stability, while hemicellulose contributes to maintain the structure of the fibre, and lignin protects the matrix from pathogen attack (Taiz and Zeiger 2002). Natural plant fibres are a more economic and environmentally friendly alternative to synthetic ones: they are organic renewable material with low energy process requirements, and therefore carbon dioxide neutral if composted (John and Thomas 2008). Moreover, they can be obtained from agricultural or wood wastes, contributing to a more sustainable material production (Versino et al. 2019). Additionally, they are less abrasive to processing equipment, essentially cheaper, and present lower density (Sapuan et al. 2016). Mohanty et al. (2000), Väisänen et al. (Väisänen et al. 2016), and Djafari Petroudy (2017) have extensively reviewed the composition and mechanical properties of the most industrially used natural fibres. Natural organic fibres density there reported vary from 0.7 to 1.5 gm/cm^3, significantly lower than that of glass fibre (2.5 gm/cm^3). In general, the reinforcing efficiency of plant fibres depend on cellulose nature and crystallinity, and its alignment in the cell walls: high cellulose content and low microfibril angle (MFA, defined as the angle microfibrils make with respect to the fibre axis) are desirable (Georgios et al. 2016; Djafari Petroudy 2017). Comparatively, ramie, hemp and flax fibres showed the higher cellulose content and lower MFA and, correspondingly, the highest tensile strength and Young's moduli, indicating superior mechanical resistance.

Biofibres have a low thermal stability which limits both processing conditions and the recyclability of the composites containing them. If they are exposed to high processing temperatures (typically circa 200 °C) for a certain time, their mechanical properties can be significantly degraded. For instance, it has been reviewed a 10% drop on naked ramie fibres tensile strength with a 10 min exposure at 200 °C, while this effect was retarded in PP/sisal fibre composite signifying that the fibre

was protected by the polymer matrix (Ramamoorthy et al. 2019). Moreover, Chaitanya et al. (2019) proved that there is a marked deterioration of PLA/sisal fibre biocomposites thermal stability with recycling cycles.

Another major disadvantage of natural organic fillers is their hydrophilicity and moisture content. This affect their mechanical properties and dimensional stability and those of the composites that contain them, as well as the interfacial adhesion between the fillers and the polymer (generally hydrophobic) that has an important impact on their dispersion in the matrix (La Mantia and Morreale 2011). Therefore, research has been focused on the modification of natural fillers surface in order to improve polymer-filler interaction and fibres properties. Even when both components are essentially hydrophilic, the addition of the untreated filler could lead to poor mechanical properties in comparison to the neat polymer if filler particles agglomeration occurs. In this respect, both chemical and physical modifications of natural fibres have been widely studied and reported (Kalia et al. 2009; Kabir et al. 2012). The most used treatment is mercerization (alkali treatment) with dilute NaOH solution, a basic treatment in paper industry which partially removes lignin, waxes and oils from the fibres. This treatment distorts the packed crystalline cellulose structure, generating rougher fibre surface and more porous structure which improves wetting. Alkali modification is usually followed by fibre acetylation which helps stabilise cell walls and improve water resistance (increase hydrophobicity). La Mantia and Morreale (2011) have made a clear recount of the chemical modification used on natural fillers, remarking that treatments with TDI (reaction with toluene-2,4-diisocyanate), dicumylperoxide, and silanes appear to be the most effective in mechanical properties improvement, whereas mercerization and acetylation enhances thermal and dimensional stability. Ozone and plasma treatments have also been reported, indicating a greater wettability and roughness of the treated fibres, which enhanced polymer-filler interaction and therefore improved the mechanical properties of the composites obtained with different polymer matrices, both bio and conventional ones (De Oliveira et al. 2017; Ventura et al. 2017; Fazeli et al. 2019; Putra et al. 2020; Sánchez et al. 2020).

However, various factors should be assessed when choosing fillers treatments for green composites: cost (especially in the case of complicated techniques which can make some methods impractical for industrial applications), energy consumption, type and amount of effluents generated, reagents toxicity in long term exposures (for safe work conditions), and the global environmental impact of the process. In this regard, plasma treatments are arising great interest since they have low energy and chemical reagents use, require no water and can be incorporated to continuous processes (Ventura et al. 2017).

Another alternative to produce green composites with improved components interfacial adhesion and filler dispersion is the addition of small amounts of a third component which acts as compatibilizer between the filler and the polymer matrix by forming chemical bonds (either covalent or Van der Waals kind) with both parts (La Mantia and Morreale 2011). Lysine-diisocyanate and esterified lignin, for example, have been used as coupling agents in different green biocomposites reported in the literature (Lee and Wang 2006; Anugwom et al. 2019). The use of

non-toxic and preferably biobased compatibilizer should be preferentially studied for new sustainable green biocomposites development.

Yet one of the major problems in the use of natural-organic fillers is the variation of properties from botanical sources, harvesting seasons, and regions with different solar radiation, precipitations, soil composition, and minimum/maximum day temperatures. An attempt to address this problem is to mix batches of different harvest fibres of the same type or different type of fibres (Georgios et al. 2016).

3 Processing

Biocomposites are manufactured using various conventional techniques for plastic processing, typically extrusion and later compression and injection moulding. For each composite formulation, processing parameters such as temperature, pressure, and time need to be studied to optimise the materials end properties. Likewise, not only the filler and resin intrinsic properties but also the filler-polymer interface characteristics are critical for the composite's final properties (Shekar and Ramachandra 2018). The mayor limitations in green biocomposite processing is due to the hygroscopic nature of the fillers and their poor thermal resistance (La Mantia and Morreale 2011). The presence of moisture, as well as the use of water as plasticiser (especially in the case of starch-based materials), generally leads to the formation of water vapour during processing which can interfere with polymer filler adhesion, generating structural defects (i.e. voids) in the final product during moulding if a venting system is not provided. Consequently, natural fillers are usually dried to some extent (approx. 2–3%) to avoid fibre agglomeration during processing without compromising their mechanical performance (Singh et al. 2017).

Processing techniques as well as composite formulation have proven to have an impact on the biocomposites final properties. An interesting work by Morreale et al. (2008) on MaterBi® based composites with wood flour, showed that filler content was the process variable which had the greater impact on the materials rigidity, while impact strength was significantly modified by mixing speed and the filler aspect ratio. Ashori and Nourbakhsh (2010) also concluded that aspect ratio had a greater effect on the mechanical properties of PP composites with oak and pine fibres than particle size. Many other authors have shown how comparatively different processing parameters have statistically greater impact over biocomposites properties (Dauda et al. 2007; Castillo et al. 2013; Muthuraj et al. 2016).

Due to the relatively low thermal stability of natural-organic fillers, processing temperature conditions of green composites are limited, being 140–190 °C the reported typical processing temperature range for extrusion, blend-mixing and thermo-moulding of different polymer matrices (Morreale et al. 2008; López et al. 2015; Jumaidin et al. 2016; Mendes et al. 2016; Scaffaro et al. 2018; Versino et al. 2019). An electromagnetic induction system for PLA/jute fabric composite proposed by Tanaka et al. (2008) allows the instant heating of the mold surface, therefore reducing production cycle times, and consequently, process costs and possible

thermal degradation of the composites components. The casting method of composite materials is generally performed at low temperatures and is widely employed in laboratory or small production scale studies, yet due to its high solvent use it is difficult to scale-up to industrial proportions. However, the study of filler-matrix in casting systems is simple and of great use to understand the composites components interactions.

In addition, as the inclusion of fibres tends to increase the molten-polymer batter viscosity, higher shear forces are needed to make the filler-polymer mixtures flow. Therefore, the rheology study of the biocomposites formulations is of great importance in terms of processing conditions needed as well as its potential scale-up. Besides, the rheological responses are closely related to the fillers dispersion and orientation, as well as their interactions with the polymer matrix (Wang et al. 2018; Borchani et al. 2019). In general, rheological rotational studies show an increase in the viscosity of green biocomposites under melt flow conditions, indicating an overall hindrance of its processability (Scaffaro et al. 2018; Wang et al. 2018; Xiao et al. 2019). A similar trend was observed on corn TPS biocomposites during melt-mixing process, where an increase in the mixing maximum torque which is associated to the material viscosity during processing and hence to the melt resistance to flow (Vallejos et al. 2011; Versino et al. 2019). However, an opposite effect was observed when working on cassava TPS biocomposites with cassava roots by-products, which was attributed to a thermodynamic favourability of the diffusion process of plasticisers into cassava starch granules with filler addition (Versino et al. 2015), probably due to amylopectin content and chain length differences between starch botanical origins. Moreover, Scaffaro et al. (2018) and Xiao et al. (2019) observed a more marked shear-thinning effect (decrease in apparent viscosity at higher oscillatory frequencies) on biocomposites with higher fillers loads (>20%) that indicate a greater interaction among particles, which is disrupted at higher frequencies by disentanglement and reorientation of the fillers and the polymer chains in the flow direction. Another interesting study carried out by Borchani et al. (2019) showed the impact of different alkali fibres treatments on Mater-Bi® based biocomposites on the rheological behaviour of the molten mixture, exhibiting a greater gel network strength of treated fibres biocomposites due to the greater interaction between the matrix and the treated filler.

Rheological behaviour under melt flow conditions results of important design parameters also for biocomposites for 3D printing applications, an alternative which is also currently being widely studied. The development of green biocomposites 3D-printing filaments may result of great interest for the packaging industry, allowing to enhance the package mechanical resistance compared to neat polymer filaments, as well as the possibility of designing specially featured packages to minimize products damage and package volume. Le Duigou et al. (2019) developed PLA/flax fibre filaments with better mechanical properties than many other natural fibres biocomposites.

4 Packaging Applications

Green composite materials have been studied and used in many industrial applications such as construction (windows frames, doors, insulating panels), furniture, railroad sleepers, automotive parts, gardening items, packaging, and various other applications of low cost and not high mechanical performance requirements (La Mantia and Morreale 2011; Gurunathan et al. 2015; Dey and Ray 2018). A possible greener and convenient trend under study is the use of recycled polymers instead of virgin ones in order to reduce production costs and develop more sustainable materials. Many shoes and clothing international brands have moved towards this eco-friendlier, yet biocomposite materials are not extensively employed. In this regard, packaging applications are the most promising scenario for green biocomposites use and development, since it represents 30–35% of the urban solid waste annually generated (Tencati et al. 2016), have mild mechanical resistance requirements, and are usually discarded after single use, especially for food-packaging where recycling is more complex and water consuming. Biodegradable biobased composites are one of the most promising sustainable alternatives for packaging applications. A review by Tang et al. (2012) summarizes the barrier and mechanical properties of the most typically studied biopolymer and biobased composites films for food packaging applications, remarking that poor mechanical and water vapour barrier properties represent the greatest limitations of these materials. However, new and enhanced materials have been developed to date, with strong focus on active and intelligent packaging. The first has an specific function different from the usual protective characteristic of the package that results from the presence or controlled-release of an active compound (i.e. antimicrobial activity, gas scavenging, etc.), while the latter provides information to the consumer regarding the products conditions based in some measurable quality parameter sensed by the packaging material (i.e. pH, temperature limits, etc.).

Furthermore, the use of 3D printing of green biocomposites has also gained interest in the packaging industry. By this technology customised structures can be designed with structural optimised properties in order to minimise virgin materials use by reducing the thickness needed to achieve the same mechanical property and waste due to cuts. Besides, 3D printable green biocomposites are innovative and promising candidates for biodegradable and flexible materials as well as for sensors development for intelligent packaging applications. For instance, Dai et al. (2019) remarked that according to their rheological and mechanical properties, composite materials with cellulose nanofibres (CNF) are promising alternative for 3D printing.

On the other hand, green biocomposites have lately been studied as expanded or foam-like materials used as loose-fill packaging and disposable food trays usually employed in food delivery in our modern urban society. Polystyrene (PS) is generally used for these applications, yet it is a petroleum-based and non-biodegradable polymer which is rather difficult to recollect and recycle in waste management systems, therefore new biodegradable and biobased alternatives are under investigation (Soykeabkaew et al. 2015). Davis and Song (2006) after analysing the biobased biodegradable packaging impact on waste management systems in comparison to

oil-based polymer packaging materials, the first can have a positive environmental effect if composted in situ or provided an appropriate collection, transport, and special treatment of compostable waste.

Diverse biocomposites and bionanocomposites have been developed and studied as sustainable alternatives for packaging materials due to the pressing environmental concerns derived from the extensive use of non-sustainable oil-based polymers. These materials require different properties depending on the product that must be protected within the package (i.e. food, pharmaceutical or electronic products), though good mechanical and gas barrier properties are most desirable characteristics.

4.1 Thermoplastic Green Biocomposites

Thermoplastics green biocomposites present a wide range of properties and characteristics that are suitable for packaging applications, from blown-extrusion bags to thermoformed trays and containers.

Most biodegradable materials present either poor mechanical or barrier properties, thus composite materials combining more than one type of bioplastic have been studied due to their enhanced final properties. One of the most widely used bioplastic nowadays is PLA since it is nontoxic, biodegradable, biocompatible, and presents comparable mechanical and thermal properties to conventional plastics such as PS and PET. Nevertheless, PLA has some existing limitations: such as inherent brittleness, low impact resistance, poor crystallization behaviour, poor toughness, etc. (Ghosh et al. 2019). In order to tailor the materials properties and reduce the production cost, blends of PLA with other bioplastics and biocomposites have been widely studied (Madhavan Nampoothiri et al. 2010). Burzic et al. (2019) found that PLA/PHA (80/20) blends significantly improved PLA crystallization and impact strength without comprising the biobased origin and biodegradable character of the materials. PLA biocomposites films by blown extrusion with functionalised chitosan and Arabic gum were developed by Ghosh et al. (2019), showing better tear resistance and thermomechanical properties and may as well stimulate the enzymatic biodegradation of the composites. Blends with starch have also been widely studied as a means of materials cost reduction and lessening of environmental impact, since starch is an abundant, renewable, biodegradable, and cheap biopolymer. Even lower environmental impact could be achieved by using starch derived from starch extraction wastewater as reported by Broeren et al. (2017). Due to the hygroscopic character of starch and the hydrophobic nature of PLA, weak adhesion is obtained in simple PLA/starch blends, being needed appropriate coupling strategies (Müller et al. 2016). Several research studies evaluated the grafting process and the use of compatibilizers with promising results (Lee and Wang 2006; Shirai et al. 2013; Yang et al. 2013; Akrami et al. 2016; Ibrahim and Ab Wahab 2017). De Oliveira et al. (2019) compared the life cycle impact of neat thermoplastic PLA and PLA/starch/cotton fibre biocomposites, the latter proved to have a better overall performance in terms of eco-efficiency though the end-of-life step of the material was not contemplated.

Moreover, other PLA biocomposites with natural filler obtained from different waste materials, such as algae collected from beaches, trees sawdust or agro-industrial wastes, have shown a marked improve in films mechanical properties and good optical properties (Fortunati et al. 2015; Agustin-Salazar et al. 2018; Scaffaro et al. 2018; Orue et al. 2019; Silva et al. 2019). Generally, a surface treatment (i.e. alkali treatment) of the natural organic fillers is needed to improve adhesion between PLA matrix and filler particles. Likewise, a recent study on PLA composites with a natural inorganic filler showed that surface treatment drastically affect the biocomposites mechanical behaviour, observing a significant increase in materials toughness when calcium carbonate particles treated with stearic acid were used in presence of 20 %wt. of plasticiser (Aliotta et al. 2019). The authors concluded that the surface treatment is crucial for a better dispersion of filler particles in the matrix, thus when immersed in a plasticised polymer matrix (more ductile and with higher chain mobility) the dispersed filler dissipate energy by void formation, deboning and matrix ligament yielding. An interesting result was found by Singh et al. (2019) in PLA biocomposites reinforced with halloysite nanotubes and chitosan powder: the synergic effect of both fillers efficiently enhanced the materials ductility without compromising the tensile resistance even in the absence of plasticisers.

Starch itself represents a promising cheap, fully biodegradable and a raw material with low environmental impact for green biocomposites. Starch blends with chitosan, gelatine or soy protein have also been reported for food packaging applications (Versino et al. 2016). Some starch-based blends are nowadays commercially available with trademarks as Mater-Bi® (Novamont, Italy), Bioplast® (Biotech, Germany), Novon™ (Chisso, Japan and Warner-Lambert, USA), Biopar® (Biop Biopolymer Technologies AG, Germany), Gaialene® (Roquette, France) and Solanyl® (Rodenburg Biopolymers, Netherlands) (Gurunathan et al. 2015). Besides, starch-based composite materials both with natural organic and inorganic fillers have been extensively studied and reviewed by Castillo et al. (2017). In previous works, bagasse and peels from root tubers starch extraction where used as biocomposites fillers based on corn and cassava TPS. An increase in the mechanical resistance of the reinforced materials up to 1.5% filler content was observed in films obtained by thermomoulding, though water resistance and permeability was not improved (Versino et al. 2015, 2019; López et al. 2015). Similar results were obtained by Merci et al. (2019) for cassava starch-based composites with soybean hulls or microcrystalline cellulose, showing lower water vapour permeability in composites with 2.5% of filler. Water vapour permeability and solubility of PLA/starch composite films were also improved by adding a chitosan crosslinked layer over the blend composite (Soares et al. 2013). Li et al. (2018) developed starch/nanocellulose biocomposites with good fibre dispersion up to 15% fibre content and improved mechanical resistance and hydrophobicity (increase in contact angle). Many nanocellulose based biocomposite have been developed and presented remarkable results in terms of optical, barrier, and mechanical properties; yet its production is considerably high energy consuming which lessens its eco-friendly character being necessary technological developments in this respect (Shanmugam et al. 2019). Consequently, nanocellulose based materials are being studied and developed for high-value applications,

especially as biobased sustainable and innovative materials for flexible electronics, energy storage devices, and water treatment membranes (Fang et al. 2019).

Starch as well as other biopolymers such as chitosan, carboxymethyl cellulose, and gelatine have poor mechanical performance and low water resistance, thus biocomposites and bionanocomposites are nowadays being studied as innovative ways of producing innovative novel sustainable packaging materials (Youssef and El-Sayed 2018). The development of the latter is of special interest in active or intelligent packaging (this will be discussed further on in this chapter), but its study and use have risen concern with respect to the nanoparticles' diffusion and potential toxicity.

4.2 Green Foam Biocomposites

Another type of materials that can be produced from green biocomposites is foam like materials, that have risen especial interest as an eco-friendlier alternative to expended polystyrene (PS) packaging. This non-biodegradable synthetic polymer is widely used in disposable food containers and packaging for products susceptible to mechanical damage. However it is difficult to collect in adequate conditions for its recycling. Besides, a life cycle assessment for warehouse appliances carried out by Razza et al. (2015) showed that starch based prototype packaging materials obtained by microwave technology, implied a reduction in non-renewable energy resources consumption (50%) and greenhouse gas emissions (60%) compared to expanded PS counterparts. In this regard, according to Guan and Hanna (2004), starch foams are a promising alternative for PS, especially for loose-fill packaging application. These materials should be light, compressible, and resistant enough to protect and stabilise packaged articles. Furthermore, starch can be easily processed by extrusion-cooking (method commonly used in the food industry) into loose-fill foam (Mitrus and Moscicki 2014). Starch-based foams can also be moulded into trays, another disposal packaging application in which they can substitute expanded PS materials. Starches from different botanical sources have been studied in this regard (Georges et al. 2018; Cruz-Tirado et al. 2019). Yet starch itself is a brittle and water sensitive polymer, thus the use of modified starches and its mixture with other bioplastics or fillers with better mechanical and water resistance have been widely reported. Soykeabkaew et al. (2015) summarised a wide range of processing techniques, types of starches modifications, and many blending examples used to overcome poor properties of native starch.

In order to produce hydrophobic starch, acetylation and esterification have been studied by Bergel et al. (2018b). The authors found that contents up to 20%wt. of the modified starches reduced water absorption and increased impact resistance, though presenting higher density than the native starch foams. Similarly, Guan et al. had proposed acetylated starch composites foams both with corn cob fibre and cellulose (Guan and Hanna 2004) and with PLA (Guan et al. 2005). These authors evaluated processing conditions, additives type and quantity, and starch degree of acetylation on the final packaging properties. Pornsuksomboon et al. (2016) developed

50/50 composite foams with native and citric acid modified cassava starch with higher thermal stability and lower water sorption, and similar thickness and density than native starch foams. Another recent work used crosslinked starch with cellulose biocomposites foams, with enhanced flexion properties and water resistance for 5%wt. cellulose contents (Hassan et al. 2019). Other authors have suggested the use of more hydrophobic and resistant bioplastics coatings as a means of overcoming starch foams detrimental characteristics with positive results (Bergel et al. 2017, 2018a).

Starch composite foams blended with different concentrations of plant proteins, kraft fibre, and palm oil were studied by Kaisangsri et al. (2014) with the aim of improving the mechanical performance and water resistance of these biocomposites. All fillers reduced water absorption and water solubility index, especially zein and gluten protein, while kraft fibre gave the highest flexural and compressive strength, yet water resistance was significantly lower than the expanded polystyrene foam. The same authors developed starch/chitosan/kraft fibre biocomposites foams with lower density, higher water absorption, and higher mechanical resistance and flexibility than starch foams and starch/kraft fibre biocomposites (Kaisangsri et al. 2012). Likewise, Cruz-Tirado et al. (2017) used sugarcane bagasse and asparagus peel fibre as reinforcement, though no significant improvement was observed in mechanical properties up to 40% fibre loading. On the other hand, Mello and Mali (2014) have obtained trays from cassava starch and malt bagasse by thermo-moulding, and have thoroughly evaluated the effect of the presence of this agro-industrial by-product on final properties of the expanded trays, demonstrating that the addition of 10% of the residue significantly decreased their hygroscopicity. Similarly, the residue from pressing sesame cake has been incorporated into expanded cassava starch-based materials (Machado et al. 2017), showing that the incorporation of 20% or more of this residual product gave place to biocomposite foams with comparable mechanical properties to those of commercial expanded PS.

Recently, different inorganic fillers were used as reinforcement of starch-based composite foams (Matsuda et al. 2013; Chiarathanakrit et al. 2019) as well as food waste mainly calcium based, were also revised as starch foams fillers (Chiarathanakrit et al. 2018; Kaewtatip et al. 2018). All biocomposites resulted in higher density, more resistant, and more thermally stable expanded materials. Remarkably, Kaewtatip et al. (2018) found that egg shell powder is a more effective filler than shrimp shells or commercial calcium carbonate.

Natural fillers with other biodegradable bioplastics have been reported. In a recent work, Adu et al. (2019) developed an interesting highly strong and fully biodegradable PVA/nanocellulose biocomposite by an innovative freezing method, though the scaling and cost evaluation of this manufacturing system should be analysed. Moreover, Bocz et al. (2016) studied PLA biocomposites foams with cellulose and basalt fibres as fillers using supercritical CO_2 as foaming agent, obtaining highly expanded materials with increased crystallinity than neat PLA foams. However, the best mechanical performance (compression test) was obtained when only talc was added as nucleating agent, attributed to the more homogenous cell formation. Furthermore, a biocomposite foam based on PBTA and peach palm tree fibres (an agricultural

residue) was proposed by Pereira da Silva et al. (2017), showing enhanced mechanical properties with and without silane treatment of the fibres when compared to other natural fibres. However, better poymer/filler interaction and thus final material properties were obtained for treated filler.

In summary, a wide range of biocomposite foams have been developed and studied over the last decade, being starch the most widely reported biopolymer used for packaging applications due to its comparatively lower cost. Nonetheless, in order to enhance these biobased and biodegradable composites, further investigations on the use of different cost-effective, low-energy-consuming, and innocuous foaming agents are necessary.

4.3 Active Green Composite Films

The main objective of packaging is to retain the products goodness. Packaging design, quality, and efficiency are of great importance in food industry since it has to comply with several requirements, most often strictly regulated. Food packaging must try to extend the products shelf life as much as possible, preserving their organoleptic characteristics and nutrients, and guaranteeing food safety. It must protect the product form contamination at any point of the food supply chain (for example, cross contamination with other food products). Likewise, it must provide the consumer with the whole products composition and production information and be appealing from a marketing point of view. Consequently, the market demands a wide range of requirements and specifications for food packaging and labelling (Kalpana et al. 2019). Appropriate selection of packaging materials can help reduce food waste by helping consumers purchase the proper quantity they will consume and minimise food spoilage, while indirectly minimising energy and water consumption and plastic waste generation. According to the Food and Agriculture Organization (FAO, United Nations) estimation, almost half of the total worldwide food loses, that rise to approximately 1.3 billion tonnes per year, occur at processing, distribution, and consumption stages. Though intelligent and active packaging can help in terms of diminishing food waste, their use also increases packaging value and overall products cost, being needed in each case a cost-benefit analysis.

Intelligent packaging has emerged as a means of information communication for producers, retailers, and consumers based on their ability to sense, detect, and record both external or internal changes in the product (Majid et al. 2018). Most indicators are intended for freshness and leakage detection by temperature or pH indicators, or by headspace gases and biological sensors integrated with data carriers such as bar codes and radio frequency identification (RFID) tags. An extensive and up-to-date review of intelligent packaging materials have been recently carried out by Kalpana et al. (2019), providing valuable information on different types of sensor and data carriers and combination on both biobased and conventional packaging materials that could be used or studied for tailoring intelligent packaging systems for specific applications.

At large, intelligent packaging are a type of active packaging, meaning that a compound with a specific function is incorporated to the material, usually a polymer, which detects and also informs the consumer that some indicator of freshness or safety of the product has been altered during transport, distribution or storage. The use of active packaging in food is intended to extend the products preservation replacing conventional food processing techniques that are costly and can alter the food nutritional quality or produce undesirable organoleptic characteristics modifications (high thermal and pressure treatments, brining, acidification, dehydration and additive preservatives). Active materials are usually obtained by the development of composite materials including the active compound itself or other material particles that contain the active agent. These polymeric matrices have the potential of gradually releasing the active agents (antioxidants and antimicrobials) or absorbing undesirable food degradation products or promoters (ethylene, oxygen, and water) (Majid et al. 2018).

One of the most studied biopolymer in active food films is chitosan due to its intrinsic antimicrobial activity. Chitosan is a biodegradable polymer derived from chitin, that can be extracted from oceanic food waste (shellfish processing by-products) (Salaberria et al. 2015). The biocompatibility and antimicrobial activity of chitosan have promoted the development of innovative novel composites materials for wound dressings and drug controlled delivery systems (Jayakumar et al. 2011; Chen et al. 2013; Ghazaie et al. 2019; Zhang et al. 2019). Many biocomposite materials based on chitosan with antifungal and antimicrobial activity for packaging applications have been investigated (Lopez et al. 2014; Salaberria et al. 2015; Tan et al. 2015; Basu et al. 2017; Zhang et al. 2017; Niu et al. 2018; Moeini et al. 2019; Wang et al. 2019). Basu et al. (2017) developed chitosan based bionanocomposites reinforced with PLA nanoparticles loaded with quercetin (a flavonoid with bactericide and antioxidant capacity), with five times higher antioxidant capacity and microbial deterrent capacity, without compromising its water vapour barrier and mechanical performance. Likewise, a fully biobased and biodegradable composite from chitosan, ascorbate, and methylcellulose with antioxidant and UV-light absorption capacity were recently developed (Tan et al. 2020). An interesting composite material prepared with polyvinyl alcohol (PVA) and quaternary ammonium salt modified chitosan (HACC) was designed by Min et al. (2020) with both antifogging and antimicrobial activity. The antifogging characteristic is important in food packaging of fresh products for two clear reasons: fog hinders the products clear observation and water condensation on the package surface may lead as well to bacteria and fungi growth and further food deterioration. At present, the HACC/PVA coating was applied over PET trays to compare the shelf life extension of strawberries (as an example of fresh food preservation) but could equally be applied over bioplastic trays to produce a fully green biocomposite packaging.

Another trend in active packaging materials for food industry involves the addition of essential natural oils as active compounds to biobased composite polymer matrices. Roy and Rhim (2019) developed gelatine/curcumin composite films with remarkable antimicrobial activity against foodborne pathogenic bacteria as well as good antioxidant activity. Another co-antimicrobial composite system based on chitosan

and pine resin modified nanocellulose were proposed by Niu et al. (2018). Contrary to expectations, Kamdem et al. (2019) discovered that the inclusion of carvacrol to chitosan/xylan composites was not effective to increase the antimicrobial capacity of the films. A wide range of other natural essential oils based biocomposites were reviewed by Chiralt and Atar (2016).

Furthermore, bionanocomposites have been investigated for intelligent and active packaging materials. Silver nanoparticles have proven to present antimicrobial activity being included in different bioplastic matrices (Ortega et al. 2017; Chi et al. 2019; Liang et al. 2019; Yu et al. 2019; Ceran et al. 2020). Passaretti et al. (2019) developed starch/bentonite (a natural clay) bionanocomposties with UV-barrier capacity as secondary package to protect coloured beverage or food products susceptible to UV radiation. A recent study presented unbleached softwood kraft sheets functionalised with gold nanoparticles as antioxidant packaging material, resulting in an integral green manufacturing process (Bumbudsanpharoke and Ko 2018). Antimicrobial biocomposites with zinc oxide nanoparticles were developed with different polymeric matrices: chitosan (Al-Naamani et al. 2016); gelatine (Ejaz et al. 2018); PVA/starch with pH sensing capacity (Jayakumar et al. 2019); PLA/PCL (Ahmed et al. 2019); biobased polyurethane and chitosan (Saral Sarojini et al. 2019). Many other innovative and interesting works have been recently reviewed by Youssef and El-Sayed (2018). However, since nanoparticles present a high diffusivity, their release during the use and end-of-life of the material and their impact on human health and the environment is currently being thoroughly studied (Han et al. 2018; Yu et al. 2019), yet further research on different nanoparticles and polymeric systems is needed.

4.4 3D Printing Composite Filaments

Recently, 3D printing has arisen as an attractive technology for a vast range of new applications. Diverse materials from conventional thermoplastics and bioplastics to ceramics and metals are some of the materials that can be 3D printed. An interesting and complete review by Lee et al. (2017) summarises the different 3D printing technologies and materials developed to date, their operation fundaments, resolution and fabrication speed, energy consumption, properties, and thus its application feasibility. 3D printing offers the possibility of obtaining customised products in a relatively fast and low-cost manner, especially for applications were high precision reproducibility and design is needed, such as biomedical and electronics though nowadays is increasingly being used for massive products design for agriculture, healthcare, automotive, and aerospace industries (Sahrubudinh et al. 2019).

Although, a large amount of research work on various 3D materials have been complied and reviewed in the literature lately (Lee et al. 2017; Bekas et al. 2019; Dai et al. 2019; Liu et al. 2019; Sahrubudinh et al. 2019), few studies have been reported on biocomposite materials for 3D printing. PLA biocomposite filaments with natural organic fibres have been developed with potential packaging applications

(Murphy and Collins 2018; Le Duigou et al. 2019; Xiao et al. 2019). Cellulose based biocomposites have also been evaluated for potential 3D printing being a versatile polymeric matrix for bionanocomposites development for intelligent packaging (Dai et al. 2019). Likewise, an antioxidant PLA/lignin biocomposite was developed by Domínguez-Robles et al. (2019) for pharmaceutical and biomedical applications, though similar materials could be studied for active green packaging materials. 3D printing green bionanocomposites have a great potentiality to be employed in active and intelligent packaging, yet further investigations on biocomposites design and 3D printing technology and operation conditions optimisation are needed.

5 Environmental Impact Considerations

Unfortunately, there is discrepancy with respect to whether "green biocomposites" are fully sustainable materials for two main reasons:

1. Their recyclability is limited due to thermal degradations in successive reprocessing cycles.
2. Their biodegradability is sometimes limited only to the filler (when polymer matrix is biobased but not biodegradable) and because composting processes are not always integrated to waste management systems.

Therefore, the use of fully biobased and biodegradable materials and the improvement of waste management systems and regulations, together with the ecological consciousness education of producers, retailers, and consumers is crucial to move forward more sustainable packaging materials. Most recently, there is a growing tendency of consumers towards selecting eco-friendly and sustainable goods and, above all, those buyers more ecologically aware expressed that they were keen to pay more for these products (Han et al. 2009). This is key considering that bioplastics, and thus green biocomposites produced from them, still present high prices with respect to conventional polymers. Due to the growing bioplastics markets, prices are slowly dropping, yet further cost reductions are needed in order to have competitive prices (La Mantia and Morreale 2011). A more ecological and economical option is the use of residual biomass from current industrial processes as raw material for green biocomposites, with the aim of reducing costs as well as developing processes with minimum effluents generation towards circular production systems, especially in the case of biodegradable materials.

Correspondingly, as previously stated, the use of biobased polymers and fillers presents various environmental advantages, mainly because of their biodegradable character, which helps reduce plastic waste generation and fossil-based resources use, minimising the carbon footprint. These aspects have been further investigated by life cycle assessment (LCA) of various biobased and biocomposite materials designed especially for packaging applications (Zabaniotou and Kassidi 2003; Bohlmann

2004; Tencati et al. 2016; De Oliveira et al. 2019). The impact of agricultural production of most biobased compounds must be contemplated in LCA of green biocomposite materials, being eutrophication, fertiliser and pesticides use, and water and soil use and degradation the main environmental impact factors for this activity. Besides, the replacement of commodity polymers for biodegradable matrices or the inclusion of natural fillers usually require physical or chemical modification of the compounds in order to obtain similar or enhanced properties in comparison to conventional materials. These treatments imply additional production costs and can sometimes not be eco-friendly.

Therefore, ideally future research should be conducted focusing not only on the mechanical, thermal, and barrier properties of the developed materials but also on their biodegradability under composting conditions. Besides, it is relevant the analysis of its overall effects on soil conditions; the toxicity and eco-compatibility of any used additive; the assessment of energy and resources (water, soil, etc.) consumption in both raw materials obtention and biocomposites processing; and the global life cycle analysis of the product considering the impact of raw material manufacture and real end-of-life of each produced material with the current waste management systems employed.

6 Conclusion and Future Perspective

It is of common knowledge that every human activity has an impact on the environment. Global awareness has been lately raised on the consequence that the current socioeconomic system has brought. Consequently, sustainability is currently considered the guideline for present and future world development. The concept of sustainability implies a commitment of solidarity with future generation, achieving the desired socio-economic and cultural growth while making a rational use of the existing natural resources, preserving the species and the environment. In this regard, there is a worldwide trend towards the generation of regulations aimed at circularity of production systems. The objective of circular systems is to keep products, materials, and resources (water, energy) in circulation for as long as possible, minimising the generation of waste and reducing costs, hence achieving more sustainable processes.

Packaging design and production play a key role in this respect, since packaging (a single use material) constitute an important source of solid waste. The development of biobased and biodegradable composite materials is needed for more environmentally sustainable packaging. Research towards developing materials with optimised properties in terms of product preservation, minimum resources use, and waste generation along the whole *cradle-to-grave* path will lead to more ecologically responsible packaging materials. This implies a reduction of energy, water, and soil use in raw materials manufacture, transport and distribution, storage and retail, consumption and disposal of both the product and the package.

Biobased materials help transform primary products into value-added ones, particularly when residual biomass is used as raw material for biocomposites. This is an

important growing opportunity for developing countries where agriculture is one of the main economic activities, playing a central role in the elaboration of strategies towards more equitable markets within the perspective of sustainable development. In addition, biomass derived compounds have a net lower environmental impact, though more ecological practices are being promoted as well in agricultural production to reduce solid waste generation, water eutrophication, and soil depletion problems.

On the other hand, the biodegradability character of green biocomposites could help reduce plastic waste generation derived from the packaging industry if adequate composting systems are integrated to waste management programs. Additives and processes implied in their manufacture should also be as innocuous as possible in order to achieve totally green materials.

Finally, the great versatility of biocomposites materials enables the development of customised packaging materials for different products as well as intelligent alternatives with enhanced properties, thus ensuring the quality, wholesomeness, integrity, and safety of the product for longer time. In summary, the development of green biocomposites for the packaging industry can meet the sustainability requirement of modern society.

References

Adu C, Rahatekar S, Filby J et al (2019) Structural packaging foams prepared by uni-directional freezing of paper sludge cellulose nanofibres and poly (vinyl alcohol). Mater Lett 253:242–245. https://doi.org/10.1016/j.matlet.2019.06.050

Agustin-Salazar S, Cerruti P, Medina-Juárez LÁ et al (2018) Lignin and holocellulose from pecan nutshell as reinforcing fillers in poly (lactic acid) biocomposites. Int J Biol Macromol 115:727–736. https://doi.org/10.1016/j.ijbiomac.2018.04.120

Ahmed J, Mulla M, Jacob H et al (2019) Polylactide/poly(ε-caprolactone)/zinc oxide/clove essential oil composite antimicrobial films for scrambled egg packaging. Food Packag Shelf Life 21:100355. https://doi.org/10.1016/j.fpsl.2019.100355

Akrami M, Ghasemi I, Azizi H et al (2016) A new approach in compatibilization of the poly(lactic acid)/thermoplastic starch (PLA_TPS) blends. Carbohydr Polym 144:254–262. https://doi.org/10.1016/j.carbpol.2016.02.035

Al-Naamani L, Dobretsov S, Dutta J (2016) Chitosan-zinc oxide nanoparticle composite coating for active food packaging applications. Innov Food Sci Emerg Technol 38:231–237. https://doi.org/10.1016/j.ifset.2016.10.010

Aliotta L, Cinelli P, Coltelli MB, Lazzeri A (2019) Rigid filler toughening in PLA-calcium carbonate composites: effect of particle surface treatment and matrix plasticization. Eur Polym J 113:78–88. https://doi.org/10.1016/j.eurpolymj.2018.12.042

Anugwom I, Lahtela V, Kallioinen M, Kärki T (2019) Lignin as a functional additive in a biocomposite: influence on mechanical properties of polylactic acid composites. Ind Crops Prod 140. https://doi.org/10.1016/j.indcrop.2019.111704

Arrieta MP, Fortunati E, Dominici F et al (2014) PLA-PHB/cellulose based films: mechanical, barrier and disintegration properties. Polym Degrad Stab 107:139–149. https://doi.org/10.1016/j.polymdegradstab.2014.05.010

Ashori A, Nourbakhsh A (2010) Reinforced polypropylene composites: effects of chemical compositions and particle size. Bioresour Technol 101:2515–2519. https://doi.org/10.1016/j.biortech.2009.11.022

Azwa ZN, Yousif BF, Manalo ACAC, Karunasena W (2013) A review on the degradability of polymeric composites based on natural fibres. Mater Des 47:424–442. https://doi.org/10.1016/j.matdes.2012.11.025

Basu A, Kundu S, Sana S et al (2017) Edible nano-bio-composite film cargo device for food packaging applications. Food Packag Shelf Life 11:98–105. https://doi.org/10.1016/j.fpsl.2017.01.011

Bekas DG, Hou Y, Liu Y, Panesar A (2019) 3D printing to enable multifunctionality in polymer-based composites: a review. Compos Part B Eng 179:107540. https://doi.org/10.1016/j.compositesb.2019.107540

Bergel BF, da Luz LM, Santana RMC (2017) Comparative study of the influence of chitosan as coating of thermoplastic starch foam from potato, cassava and corn starch. Prog Org Coatings 106:27–32. https://doi.org/10.1016/j.porgcoat.2017.02.010

Bergel BF, da Luz LM, Santana RMC (2018a) Effect of poly(lactic acid) coating on mechanical and physical properties of thermoplastic starch foams from potato starch. Prog Org Coatings 118:91–96. https://doi.org/10.1016/j.porgcoat.2018.01.029

Bergel BF, Dias Osorio S, da Luz LM, Santana RMC (2018b) Effects of hydrophobized starches on thermoplastic starch foams made from potato starch. Carbohydr Polym 200:106–114. https://doi.org/10.1016/j.carbpol.2018.07.047

Bocz K, Tábi T, Vadas D et al (2016) Characterisation of natural fibre reinforced PLA foams prepared by supercritical CO_2 assisted extrusion. Express Polym Lett 10:771–779. https://doi.org/10.3144/expresspolymlett.2016.71

Bodirlau R, Teaca CA, Spiridon I (2013) Influence of natural fillers on the properties of starch-based biocomposite films. Compos Part B Eng 44:575–583. https://doi.org/10.1016/j.compositesb.2012.02.039

Bohlmann GM (2004) Biodegradable packaging life-cycle assessment. Environ Prog 23:342–346. https://doi.org/10.1002/ep.10053

Borchani KE, Carrot C, Jaziri M (2019) Rheological behavior of short Alfa fibers reinforced Mater-Bi® biocomposites. Polym Test 77:105895. https://doi.org/10.1016/j.polymertesting.2019.05.011

Broeren MLM, Kuling L, Worrell E, Shen L (2017) Environmental impact assessment of six starch plastics focusing on wastewater-derived starch and additives. Resour Conserv Recycl 127:246–255. https://doi.org/10.1016/j.resconrec.2017.09.001

Bumbudsanpharoke N, Ko S (2018) The green fabrication, characterization and evaluation of catalytic antioxidation of gold nanoparticle-lignocellulose composite papers for active packaging. Int J Biol Macromol 107:1782–1791. https://doi.org/10.1016/j.ijbiomac.2017.10.046

Burzic I, Pretschuh C, Kaineder D et al (2019) Impact modification of PLA using biobased biodegradable PHA biopolymers. Eur Polym J 114:32–38. https://doi.org/10.1016/j.eurpolymj.2019.01.060

Castillo LA, Barbosa SE, Capiati NJ (2013) Influence of talc morphology on the mechanical properties of talc filled polypropylene. J Polym Res. https://doi.org/10.1007/s10965-013-0152-2

Castillo LA, López OV, Ghilardi J et al (2015) Thermoplastic starch/talc bionanocomposites. Influence of particle morphology on final properties. Food Hydrocoll 51:432–440. https://doi.org/10.1016/j.foodhyd.2015.05.030

Castillo LA, López O V, Ninago MD, et al (2017) Composites and nanocomposites based on starches. effect of mineral and organic fillers on processing, structure, and final properties of starch. In: Starch-based materials in food packaging: processing, characterization and applications. pp 125–151

Cazan C, Cosnita M, Isac L (2019) The influence of temperature on the performance of rubber—PET-HDPE waste -based composites with different inorganic fillers. J Clean Prod 208:1030–1040. https://doi.org/10.1016/j.jclepro.2018.10.045

Ceran ÖB, Şimşek B, Şara ON (2020) Preparation and characterization novel dioctyl terephthalate blended polyvinyl alcohol-composite films incorporated with the graphene oxide and silver nanoparticles. Polym Test 106315. https://doi.org/10.1016/j.polymertesting.2019.106315

Chaitanya S, Singh I, Il Song J (2019) Recyclability analysis of PLA/Sisal fiber biocomposites. Compos Part B Eng 173:106895. https://doi.org/10.1016/j.compositesb.2019.05.106

Chen C, Liu L, Huang T et al (2013) Bubble template fabrication of chitosan/poly(vinyl alcohol) sponges for wound dressing applications. Int J Biol Macromol 62:188–193. https://doi.org/10.1016/j.ijbiomac.2013.08.042

Chi H, Song S, Luo M et al (2019) Effect of PLA nanocomposite films containing bergamot essential oil, TiO_2 nanoparticles, and Ag nanoparticles on shelf life of mangoes. Sci Hortic (Amsterdam) 249:192–198. https://doi.org/10.1016/j.scienta.2019.01.059

Chiarathanakrit C, Riyajan SA, Kaewtatip K (2018) Transforming fish scale waste into an efficient filler for starch foam. Carbohydr Polym 188:48–53. https://doi.org/10.1016/j.carbpol.2018.01.101

Chiarathanakrit C, Mayakun J, Prathep A, Kaewtatip K (2019) Comparison of the effects of calcified green macroalga (Halimeda macroloba Decaisne) and commercial $CaCO_3$ on the properties of composite starch foam trays. Int J Biol Macromol 121:71–76

Chiralt A, Atar L (2016) Essential oils as additives in biodegradable films and coatings for active food packaging. Trends Food Sci Technol 48:51–62. https://doi.org/10.1016/j.tifs.2015.12.001

Cruz-Tirado JP, Siche R, Cabanillas A, et al (2017) Properties of baked foams from oca (Oxalis tuberosa) starch reinforced with sugarcane bagasse ans aparagus peel fiber. In: Procedia engineering. pp 175–185

Cruz-Tirado JP, Vejarano R, Tapia-Blácido DR et al (2019) Biodegradable foam tray based on starches isolated from different Peruvian species. Int J Biol Macromol 125:800–807. https://doi.org/10.1016/j.ijbiomac.2018.12.111

Dai L, Cheng T, Duan C et al (2019) 3D printing using plant-derived cellulose and its derivatives: a review. Carbohydr Polym 203:71–86. https://doi.org/10.1016/j.carbpol.2018.09.027

Dauda M, Yoshiba M, Miura K, Takahashi S (2007) Processing and mechanical property evaluation of maize fiber reinforced green composites. Adv Compos Mater Off J Japan Soc Compos Mater 16:335–347. https://doi.org/10.1163/156855107782325168

Davis G, Song JH (2006) Biodegradable packaging based on raw materials from crops and their impact on waste management. Ind Crops Prod 23:147–161. https://doi.org/10.1016/j.indcrop.2005.05.004

Allied Analytics LLP (2018) Bioplastics market by type and application: global opportunity analysis and industry forecast, 2018–2024. Pune, India

De Oliveira DM, Hilário Cioffi MO, De Carvalho Benini KCC, Cornelis Voorwald HJ (2017) Effects of plasma treatment on the sorption properties of coconut fibers. Procedia Eng 200:357–364. https://doi.org/10.1016/j.proeng.2017.07.050

De Oliveira SA, Nunes de Macedo JR, dos Rosa D S (2019) Eco-efficiency of poly (lactic acid)-Starch-Cotton composite with high natural cotton fiber content: environmental and functional value. J Clean Prod 217:32–41. https://doi.org/10.1016/j.jclepro.2019.01.198

Dey P, Ray S (2018) An overview of the recent trends in manufacturing of green composites—considerations and challenges. Mater Today Proc 5:19783–19789. https://doi.org/10.1016/j.matpr.2018.06.341

Dittenber DB, GangaRao HVS (2012) Critical review of recent publications on use of natural composites in infrastructure. Compos Part A Appl Sci Manuf 43:1419–1429. https://doi.org/10.1016/j.compositesa.2011.11.019

Dixit S, Yadav VL (2019) Optimization of polyethylene/polypropylene/alkali modified wheat straw composites for packaging application using RSM. J Clean Prod 240:118228. https://doi.org/10.1016/j.jclepro.2019.118228

Djafari Petroudy SR (2017) Physical and mechanical properties of natural fibers. In: Advanced high strength natural fibre composites in construction. Elsevier Ltd, pp 59–83

Domínguez-Robles J, Martin NK, Fong ML et al (2019) Antioxidant pla composites containing lignin for 3D printing applications: a potential material for healthcare applications. Pharmaceutics 11:5–7. https://doi.org/10.3390/pharmaceutics11040165

Ejaz M, Arfat YA, Mulla M, Ahmed J (2018) Zinc oxide nanorods/clove essential oil incorporated type B gelatin composite films and its applicability for shrimp packaging. Food Packag Shelf Life 15:113–121. https://doi.org/10.1016/j.fpsl.2017.12.004

Emblem HJ (2012) Packaging and environmental sustainability. Packag Technol 65–86. https://doi.org/10.1533/9780857095701.1.65

Famá L, Gerschenson L, Goyanes S (2009) Starch-vegetable fibre composites to protect food products. Carbohydr Polym 75:230–235. https://doi.org/10.1016/J.CARBPOL.2008.06.018

Fang Z, Hou G, Chen C, Hu L (2019) Nanocellulose-based films and their emerging applications. Curr Opin Solid State Mater Sci 23:100764. https://doi.org/10.1016/j.cossms.2019.07.003

Farmer N (2013) Present status and trends in innovations in packaging for food, beverages and other fast-moving consumer goods. In: Trends in packaging of food, beverages and other fast-moving consumer goods (FMCG). Woodhead Publishing Limited, pp 1–21

Fazeli M, Florez JP, Simão RA (2019) Improvement in adhesion of cellulose fibers to the thermoplastic starch matrix by plasma treatment modification. Compos Part B Eng 163:207–216. https://doi.org/10.1016/j.compositesb.2018.11.048

Fortunati E, Luzi F, Puglia D et al (2015) Processing of PLA nanocomposites with cellulose nanocrystals extracted from Posidonia oceanica waste: innovative reuse of coastal plant. Ind Crops Prod 67:439–447. https://doi.org/10.1016/j.indcrop.2015.01.075

Georges A, Lacoste C, Damien E (2018) Effect of formulation and process on the extrudability of starch-based foam cushions. Ind Crops Prod 115:306–314. https://doi.org/10.1016/j.indcrop.2018.02.001

Georgios K, Silva A, Furtado S (2016) Applications of green composite materials. Biodegrad Green Compos 312–337. https://doi.org/10.1002/9781118911068.ch10

Ghazaie M, Ghiaci M, Soleimanian-Zad S, Behzadi-teshnizi S (2019) Preparing natural biocomposites of N-quaternary chitosan with antibacterial activity to reduce consumption of antibacterial drugs. J Hazard Mater 371:224–232. https://doi.org/10.1016/j.jhazmat.2019.03.003

Ghosh T, Bhasney SM, Katiyar V (2019) Blown films fabrication of poly lactic acid based biocomposites: thermomechanical and migration studies. Mater Today Commun 100737. https://doi.org/10.1016/j.mtcomm.2019.100737

Guan J, Hanna MA (2004) Functional properties of extruded foam composites of starch acetate and corn cob fiber. Ind Crops Prod 19:255–269. https://doi.org/10.1016/j.indcrop.2003.10.007

Guan J, Eskridge KM, Hanna MA (2005) Acetylated starch-polylactic acid loose-fill packaging materials. Ind Crop Prod 22:109–123. https://doi.org/10.1016/j.indcrop.2004.06.004

Gurunathan T, Mohanty S, Nayak SK (2015) A review of the recent developments in biocomposites based on natural fibres and their application perspectives. Compos Part A 77:1–25. https://doi.org/10.1016/j.compositesa.2015.06.007

Han C, Zhao A, Varughese E, Sahle-Demessie E (2018) Evaluating weathering of food packaging polyethylene-nano-clay composites: release of nanoparticles and their impacts. NanoImpact 9:61–71. https://doi.org/10.1016/j.impact.2017.10.005

Han H, Hsu (Jane) LT, Lee JS (2009) Empirical investigation of the roles of attitudes toward green behaviors, overall image, gender, and age in hotel customers' eco-friendly decision-making process. Int J Hosp Manag 28:519–528. https://doi.org/10.1016/j.ijhm.2009.02.004

Hanken RBL, Arimatéia RR, Farias GMG, et al (2019) Effect of natural and expanded vermiculite clays on the properties of eco-friendly biopolyethylene-vermiculite clay biocomposites. Compos Part B Eng 175. https://doi.org/10.1016/j.compositesb.2019.107184

Hassan MM, Tucker N, Le Guen MJ (2019) Thermal, mechanical and viscoelastic properties of citric acid-crosslinked starch/cellulose composite foams. Carbohydr Polym 115675. https://doi.org/10.1016/j.carbpol.2019.115675

Hatakeyema H, Tanamachi N, Matsumura H et al (2005) Bio-based polyurethane composite foams with inorganic fillers studied by thermogravimetry. Thermochim Acta 431:155–160. https://doi.org/10.1016/j.tca.2005.01.065

Hidalgo-Salazar MA, Salinas E (2019) Mechanical, thermal, viscoelastic performance and product application of PP-rice husk Colombian biocomposites. Compos Part B Eng 176:107135. https://doi.org/10.1016/j.compositesb.2019.107135

Huang D, De HuZ, Ding Y et al (2019) Seawater degradable PVA/PCL blends with water-soluble polyvinyl alcohol as degradation accelerator. Polym Degrad Stab 163:195–205. https://doi.org/10.1016/j.polymdegradstab.2019.03.011

Ibrahim N, Ab Wahab MK (2017) Acidolysis effect on starch in polylactic acid (PLA)/thermoplastic starch (TPS) blend. Solid State Phenom 264, SSP:156–159. https://doi.org/10.4028/www.scientific.net/SSP.264.156

Iyer KA, Flores AM, Torkelson JM (2015) Comparison of polyolefin biocomposites prepared with waste cardboard, microcrystalline cellulose, and cellulose nanocrystals via solid-state shear pulverization. Polymer (Guildf) 75:78–87. https://doi.org/10.1016/j.polymer.2015.08.029

Jayakumar A, K.V. H, T.S. S et al (2019) Starch-PVA composite films with zinc-oxide nanoparticles and phytochemicals as intelligent pH sensing wraps for food packaging application. Int J Biol Macromol 136:395–403. https://doi.org/10.1016/j.ijbiomac.2019.06.018

Jayakumar R, Prabaharan M, Sudheesh Kumar PT et al (2011) Biomaterials based on chitin and chitosan in wound dressing applications. Biotechnol Adv 29:322–337. https://doi.org/10.1016/j.biotechadv.2011.01.005

John MJ, Thomas S (2008) Biofibres and biocomposites. Carbohydr Polym 71:343–364. https://doi.org/10.1016/j.carbpol.2007.05.040

Joshi SV, Drzal LT, Mohanty AK, Arora S (2004) Are natural fiber composites environmentally superior to glass fiber reinforced composites? Compos Part A Appl Sci Manuf 35:371–376. https://doi.org/10.1016/j.compositesa.2003.09.016

Jumaidin R, Sapuan SM, Jawaid M et al (2016) Characteristics of thermoplastic sugar palm Starch/Agar blend: Thermal, tensile, and physical properties. Int J Biol Macromol 89:575–581. https://doi.org/10.1016/j.ijbiomac.2016.05.028

Kabir MM, Wang H, Lau KT, Cardona F (2012) Chemical treatments on plant-based natural fibre reinforced polymer composites: an overview. Compos Part B 43:2883–2892. https://doi.org/10.1016/j.compositesb.2012.04.053

Kaewtatip K, Chiarathanakrit C, Riyajan SA (2018) The effects of egg shell and shrimp shell on the properties of baked starch foam. Powder Technol 335:354–359. https://doi.org/10.1016/j.powtec.2018.05.030

Kaisangsri N, Kerdchoechuen O, Laohakunjit N (2012) Biodegradable foam tray from cassava starch blended with natural fiber and chitosan. Ind Crops Prod 37:542–546. https://doi.org/10.1016/j.indcrop.2011.07.034

Kaisangsri N, Kerdchoechuen O, Laohakunjit N (2014) Characterization of cassava starch based foam blended with plant proteins, kraft fiber and palm oil. Carbohydr Polym 110:70–77. https://doi.org/10.1016/j.carbpol.2014.03.067

Kalia S, Kaith BS, Kaur I (2009) Pretreatments of natural fibers and their application as reinforcing material in polymer composites-a review. Polym Eng Sci 49:1253–1272. https://doi.org/10.1002/pen.21328

Kalpana S, Priyadarshini SR, Maria Leena M et al (2019) Intelligent packaging: trends and applications in food systems. Trends Food Sci Technol 93:145–157. https://doi.org/10.1016/j.tifs.2019.09.008

Kamdem DP, Shen Z, Nabinejad O (2019) Development of biodegradable composite chitosan-based films incorporated with xylan and carvacrol for food packaging application. Food Packag Shelf Life 21:100344. https://doi.org/10.1016/j.fpsl.2019.100344

Komal UK, Lila MK, Singh I (2020) PLA/banana fiber based sustainable biocomposites: a manufacturing perspective. Compos Part B Eng 180:107535. https://doi.org/10.1016/j.compositesb.2019.107535

La Mantia FP, Morreale M (2011) Green composites: a brief review. Compos Part A Appl Sci Manuf 42:579–588. https://doi.org/10.1016/j.compositesa.2011.01.017

Le Duigou A, Barbé A, Guillou E, Castro M (2019) 3D printing of continuous flax fibre reinforced biocomposites for structural applications. Mater Des 180:107884. https://doi.org/10.1016/j.matdes.2019.107884

Lee JY, An J, Chua CK (2017) Fundamentals and applications of 3D printing for novel materials. Appl Mater Today 7:120–133. https://doi.org/10.1016/j.apmt.2017.02.004

Lee SH, Wang S (2006) Biodegradable polymers/bamboo fiber biocomposite with bio-based coupling agent. Compos Part A Appl Sci Manuf 37:80–91. https://doi.org/10.1016/j.compositesa.2005.04.015

Li M, Tian X, Jin R, Li D (2018) Preparation and characterization of nanocomposite films containing starch and cellulose nano fibers. Ind Crop Prod 123:654–660. https://doi.org/10.1016/j.indcrop.2018.07.043

Liang J, Wang J, Li S et al (2019) The size-controllable preparation of chitosan/silver nanoparticle composite microsphere and its antimicrobial performance. Carbohydr Polym 220:22–29. https://doi.org/10.1016/j.carbpol.2019.05.048

Liu H, Huang Y, Yuan L et al (2010) Isothermal crystallization kinetics of modified bamboo cellulose/PCL composites. Carbohydr Polym 79:513–519. https://doi.org/10.1016/j.carbpol.2009.08.037

Liu J, Sun L, Xu W et al (2019) Current advances and future perspectives of 3D printing natural-derived biopolymers. Carbohydr Polym 207:297–316. https://doi.org/10.1016/j.carbpol.2018.11.077

Lopez O, Garcia MA, Villar MA et al (2014) Thermo-compression of biodegradable thermoplastic corn starch films containing chitin and chitosan. LWT—Food Sci Technol 57:106–115. https://doi.org/10.1016/j.lwt.2014.01.024

López OV, García MA, Zaritzky NE (2008) Film forming capacity of chemically modified corn starches. Carbohydr Polym 73:573–581. https://doi.org/10.1016/j.carbpol.2007.12.023

López OV, Versino F, Villar MA, García MA (2015) Agro-industrial residue from starch extraction of Pachyrhizus ahipa as filler of thermoplastic corn starch films. Carbohydr Polym 134:324–332. https://doi.org/10.1016/j.carbpol.2015.07.081

Ludueña L, Vázquez A, Alvarez V (2012) Effect of lignocellulosic filler type and content on the behavior of polycaprolactone based eco-composites for packaging applications. Carbohydr Polym 87:411–421. https://doi.org/10.1016/j.carbpol.2011.07.064

Machado CM, Benelli P, Tessaro IC (2017) Sesame cake incorporation on cassava starch foams for packaging use. Ind Crops Prod 102:115–121. https://doi.org/10.1016/J.INDCROP.2017.03.007

Madhavan Nampoothiri K, Nair NR, John RP (2010) An overview of the recent developments in polylactide (PLA) research. Bioresour Technol 101:8493–8501. https://doi.org/10.1016/j.biortech.2010.05.092

Majid I, Nayik A, Dar M, Nanda V (2018) Novel food packaging technologies: Innovations and future prospective. J Saudi Soc Agric Sci 17:454–462. https://doi.org/10.1016/j.jssas.2016.11.003

Matsuda DKM, Verceheze AES, Carvalho GM et al (2013) Baked foams of cassava starch and organically modified nanoclays. Ind Crops Prod 44:705–711. https://doi.org/10.1016/j.indcrop.2012.08.032

Mello LRPF, Mali S (2014) Use of malt bagasse to produce biodegradable baked foams made from cassava starch. Ind Crops Prod 55:187–193. https://doi.org/10.1016/J.INDCROP.2014.02.015

Mendes JF, Paschoalin RT, Carmona VB et al (2016) Biodegradable polymer blends based on corn starch and thermoplastic chitosan processed by extrusion. Carbohydr Polym 137:452–458. https://doi.org/10.1016/j.carbpol.2015.10.093

Merci A, Marim RG, Urbano A, Mali S (2019) Films based on cassava starch reinforced with soybean hulls or microcrystalline cellulose from soybean hulls. Food Packag Shelf Life 20:100321. https://doi.org/10.1016/J.FPSL.2019.100321

Min T, Zhu Z, Sun X et al (2020) Highly efficient antifogging and antibacterial food packaging film fabricated by novel quaternary ammonium chitosan composite. Food Chem 308:125682. https://doi.org/10.1016/j.foodchem.2019.125682

Mitrus M, Moscicki L (2014) Extrusion-cooking of starch protective loose-fill foams. Chem Eng Res Des 92:778–783. https://doi.org/10.1016/J.CHERD.2013.10.027

Moeini A, Mallardo S, Cimmino A, et al (2019) Thermoplastic starch and bioactive chitosan submicroparticle biocomposites: antifungal and chemico-physical properties of the films. Carbohydr Polym 115627. https://doi.org/10.1016/J.CARBPOL.2019.115627

Mohanty AK, Misra M, Hinrichsen G (2000) Biofibres, biodegradable polymers and biocomposites: An overview. Macromol Mater Eng 276(277):1–24. https://doi.org/10.1002/(SICI)1439-2054(20000301)276:1%3c1:AID-MAME1%3e3.0.CO;2-W

Morreale M, Scaffaro R, Maio A, La Mantia FP (2008) Mechanical behaviour of mater-bi®/wood flour composites: a statistical approach. Compos Part A Appl Sci Manuf 39:1537–1546. https://doi.org/10.1016/j.compositesa.2008.05.015

Mukherjee T, Kao N (2011) PLA based biopolymer reinforced with natural fibre: a review. J Polym Environ 19:714–725. https://doi.org/10.1007/s10924-011-0320-6

Müller P, Bere J, Fekete E et al (2016) Interactions, structure and properties in PLA/plasticized starch blends. Polymer (Guildf). https://doi.org/10.1016/j.polymer.2016.09.031

Murphy CA, Collins MN (2018) Microcrystalline cellulose reinforced polylactic acid biocomposite filaments for 3D printing. Polym Compos 39:1311–1320. https://doi.org/10.1002/pc.24069

Muthuraj R, Misra M, Defersha F, Mohanty AK (2016) Influence of processing parameters on the impact strength of biocomposites: a statistical approach. Compos Part A Appl Sci Manuf 83:120–129. https://doi.org/10.1016/j.compositesa.2015.09.003

Nayak S, Khuntia SK (2019) Development and study of properties of Moringa oleifera fruit fibers/polyethylene terephthalate composites for packaging applications. Compos Commun 15:113–119. https://doi.org/10.1016/j.coco.2019.07.008

Netravali AN, Chabba S (2003) Composites get greener. Mater Today 6:22–29. https://doi.org/10.1016/S1369-7021(03)00427-9

Niu X, Liu Y, Song Y et al (2018) Rosin modified cellulose nanofiber as a reinforcing and co-antimicrobial agents in polylactic acid/chitosan composite film for food packaging. Carbohydr Polym 183:102–109. https://doi.org/10.1016/j.carbpol.2017.11.079

Ortega F, Giannuzzi L, Arce VB, García MA (2017) Active composite starch films containing green synthetized silver nanoparticles. Food Hydrocoll 70:152–162. https://doi.org/10.1016/j.foodhyd.2017.03.036

Orue A, Eceiza A, Arbelaiz A (2019) The use of alkali treated walnut shells as filler in plasticized poly(lactic acid) matrix composites. Ind Crops Prod 111993. https://doi.org/10.1016/j.indcrop.2019.111993

Passaretti MG, Ninago MD, Di Anibal C et al (2019) Composite films with UV barrier capacity to minimize flavored waters degradation. Food Packag Shelf Life 21:100334. https://doi.org/10.1016/j.fpsl.2019.100334

Pereira da Silva JS, Farias da Silva JM, Soares BG, Livi S (2017) Fully biodegradable composites based on poly(butylene adipate-co-terephthalate)/peach palm trees fiber. Compos Part B Eng 129:117–123. https://doi.org/10.1016/j.compositesb.2017.07.088

Petit O, Lunardo R, Rickard B (2019) Small is beautiful: the role of anticipated food waste in consumers' avoidance of large packages. J Bus Res 0–1. https://doi.org/10.1016/j.jbusres.2019.10.003

Piekarska K, Piorkowska E, Bojda J (2017) The influence of matrix crystallinity, filler grain size and modification on properties of PLA/calcium carbonate composites. Polym Test 62:203–210. https://doi.org/10.1016/j.polymertesting.2017.06.025

Pornsuksomboon K, Holló BB, Szécsényi KM, Kaewtatip K (2016) Properties of baked foams from citric acid modified cassava starch and native cassava starch blends. Carbohydr Polym 136:107–112. https://doi.org/10.1016/j.carbpol.2015.09.019

Putra AEE, Renreng I, Arsyad H, Bakri B (2020) Investigating the effects of liquid-plasma treatment on tensile strength of coir fibers and interfacial fiber-matrix adhesion of composites. Compos Part B Eng 183:107722. https://doi.org/10.1016/j.compositesb.2019.107722

Ramamoorthy SK, Åkesson D, Rajan R, et al (2019) Mechanical performance of biofibers and their corresponding composites. In: Mechanical and physical testing of biocomposites, fibre-reinforced composites and hybrid composites. Elsevier Ltd, pp 259–292

Razza F, Degli Innocenti F, Dobon A et al (2015) Environmental profile of a bio-based and biodegradable foamed packaging prototype in comparison with the current benchmark. J Clean Prod 102:493–500. https://doi.org/10.1016/J.JCLEPRO.2015.04.033

Rodriguez S, Margem FM, Monteiro SN, Calado V (2012) Thermogravimetric behavior of natural fibers reinforced polymer composites—an overview. Mater Sci Eng, A 557:17–28. https://doi.org/10.1016/j.msea.2012.05.109

Roy S, Rhim J (2019) Preparation of antimicrobial and antioxidant gelatin/curcumin composite films for active food packaging application. Colloids Surfaces B Biointerfaces 188:110761. https://doi.org/10.1016/j.colsurfb.2019.110761

Sahrubudinh N, Lee TC, Ramlan R (2019) An overview on 3D printing technology: technological, materials, and applications. Procedia Manuf 35:1286–1296. https://doi.org/10.1016/j.promfg.2019.06.089

Salaberria AM, Diaz RH, Labidi J, Fernandes SCM (2015) Preparing valuable renewable nanocomposite films based exclusively on oceanic biomass: Chitin nanofillers and chitosan. React Funct Polym 89:31–39. https://doi.org/10.1016/j.reactfunctpolym.2015.03.003

Sánchez ML, Patiño W, Cárdenas J (2020) Physical-mechanical properties of bamboo fibers-reinforced biocomposites: Influence of surface treatment of fibers. J Build Eng 28. https://doi.org/10.1016/j.jobe.2019.101058

Sapuan SM, Tamrin KF, Nukman Y et al (2016) Natural fiber-reinforced composites: types, development, manufacturing process, and measurement. Compr Mater Finish 1–3:203–230. https://doi.org/10.1016/B978-0-12-803581-8.09183-9

Saral Sarojini K, Indumathi MP, Rajarajeswari GR (2019) Mahua oil-based polyurethane/chitosan/nano ZnO composite films for biodegradable food packaging applications. Int J Biol Macromol 124:163–174. https://doi.org/10.1016/j.ijbiomac.2018.11.195

Scaffaro R, Lopresti F, Botta L (2018) PLA based biocomposites reinforced with Posidonia oceanica leaves. Compos Part B Eng 139:1–11. https://doi.org/10.1016/j.compositesb.2017.11.048

Shalwan A, Yousif BF (2013) In state of art: mechanical and tribological behaviour of polymeric composites based on natural fibres. Mater Des 48:14–24. https://doi.org/10.1016/j.matdes.2012.07.014

Shanmugam K, Doosthosseini H, Varanasi S, et al (2019) Nanocellulose films as air and water vapour barriers: A recyclable and biodegradable alternative to polyolefin packaging. Sustain Mater Technol 22. https://doi.org/10.1016/j.susmat.2019.e00115

Shekar HSS, Ramachandra M (2018) Green composites: a review. Mater Today Proc 5:2518–2526. https://doi.org/10.1016/j.matpr.2017.11.034

Shirai MA, Grossmann MVE, Mali S et al (2013) Development of biodegradable flexible films of starch and poly(lactic acid) plasticized with adipate or citrate esters. Carbohydr Polym 92:19–22. https://doi.org/10.1016/j.carbpol.2012.09.038

Silva CG, Campini PAL, Rocha DB, Rosa DS (2019) The influence of treated eucalyptus microfibers on the properties of PLA biocomposites. Compos Sci Technol 179:54–62. https://doi.org/10.1016/j.compscitech.2019.04.010

Singh AA, Afrin S, Karim Z (2017) Green composites: versatile material for future. In: Jawaid M, Sapuan SM, Alothman OY (eds), Green biocomposites: design and applications, 1st edn. Springer International Publishing, pp 29–44

Singh AA, Sharma S, Srivastava M, Majumdar A (2019) Modulating the properties of polylactic acid for packaging applications using biobased plasticizers and naturally obtained fillers. Int J Biol Macromol In Press: https://doi.org/10.1016/j.ijbiomac.2019.10.246

Soares FC, Yamashita F, Müller CMO, Pires ATN (2013) Thermoplastic starch/poly(lactic acid) sheets coated with cross-linked chitosan. Polym Test 32:94–98. https://doi.org/10.1016/j.polymertesting.2012.09.005

Song JH, Murphy RJ, Narayan R, Davies GBH (2009) Biodegradable and compostable alternatives to conventional plastics. Philos Trans R Soc B Biol Sci 364:2127–2139. https://doi.org/10.1098/rstb.2008.0289

Soykeabkaew N, Thanomsilp C, Suwantong O (2015) A review: Starch-based composite foams. Compos Part A Appl Sci Manuf 78:246–263. https://doi.org/10.1016/j.compositesa.2015.08.014

Taiz L, Zeiger E (2002) Photosynthesis: the light reactions. Plant Physiology, 3rd edn. Oxford University Press Inc, Oxford, UK, pp 111–145

Tan W, Zhang J, Zhao X et al (2020) Preparation and physicochemical properties of antioxidant chitosan ascorbate/methylcellulose composite films. Int J Biol Macromol 146:53–61. https://doi.org/10.1016/j.ijbiomac.2019.12.044

Tan YM, Lim SH, Tay BY et al (2015) Functional chitosan-based grapefruit seed extract composite films for applications in food packaging technology. Mater Res Bull 69:142–146. https://doi.org/10.1016/j.materresbull.2014.11.041

Tanaka K, Katsura T, Kinoshita Y et al (2008) Mechanical properties of jute fabric reinforced thermoplastic moulded by high-speed processing using electromagnetic induction. WIT Trans Built Environ 97:211–219. https://doi.org/10.2495/HPSM080231

Tănase EE, Popa ME, Râpă M, Popa O (2015) Biological evaluation of some PVA/starch composites as sustainable food packaging candidates. J Biotechnol 208:S58–S59. https://doi.org/10.1016/j.jbiotec.2015.06.174

Tang XZ, Kumar P, Alavi S, Sandeep KP (2012) Recent advances in biopolymers and biopolymer-based nanocomposites for food packaging materials. Crit Rev Food Sci Nutr 52:426–442. https://doi.org/10.1080/10408398.2010.500508

Tencati A, Pogutz S, Moda B et al (2016) Prevention policies addressing packaging and packaging waste: some emerging trends. Waste Manag 56:35–45. https://doi.org/10.1016/j.wasman.2016.06.025

Trakoolwannachai V, Kheolamai P, Ummartyotin S (2019) Characterization of hydroxyapatite from eggshell waste and polycaprolactone (PCL) composite for scaffold material. Compos Part B Eng 173. https://doi.org/10.1016/j.compositesb.2019.106974

Väisänen T, Haapala A, Lappalainen R, Tomppo L (2016) Utilization of agricultural and forest industry waste and residues in natural fiber-polymer composites: a review. Waste Manag 54:62–73. https://doi.org/10.1016/j.wasman.2016.04.037

Vallejos ME, Curvelo AAS, Teixeira EM et al (2011) Composite materials of thermoplastic starch and fibers from the ethanol–water fractionation of bagasse. Ind Crops Prod 33:739–746. https://doi.org/10.1016/j.indcrop.2011.01.014

Ventura H, Claramunt J, Rodríguez-Pérez MA, Ardanuy M (2017) Effects of hydrothermal aging on the water uptake and tensile properties of PHB/flax fabric biocomposites. Polym Degrad Stab 142:129–138. https://doi.org/10.1016/j.polymdegradstab.2017.06.003

Vercelheze AES, Fakhouri FM, Dall'Antônia LH et al (2012) Properties of baked foams based on cassava starch, sugarcane bagasse fibers and montmorillonite. Carbohydr Polym 87:1302–1310. https://doi.org/10.1016/j.carbpol.2011.09.016

Versino F, García MA (2014) Cassava (Manihot esculenta) starch films reinforced with natural fibrous filler. Ind Crops Prod 58. https://doi.org/10.1016/j.indcrop.2014.04.040

Versino F, López OV, García MA (2015) Sustainable use of cassava (Manihot esculenta) roots as raw material for biocomposites development. Ind Crops Prod 65:79–89. https://doi.org/10.1016/j.indcrop.2014.11.054

Versino F, Lopez OV, Garcia MA, Zaritzky NE (2016) Starch-based films and food coatings: an overview. Starch/Staerke 68:1026–1037. https://doi.org/10.1002/star.201600095

Versino F, López OV, García MA (2019) Exploitation of by-products from cassava and ahipa starch extraction as filler of thermoplastic corn starch. Compos Part B Eng. https://doi.org/10.1016/j.compositesb.2019.107653

Wang K, Lim PN, Tong SY, Thian ES (2019) Development of grapefruit seed extract-loaded poly(ε-caprolactone)/chitosan films for antimicrobial food packaging. Food Packag Shelf Life 22:100396. https://doi.org/10.1016/j.fpsl.2019.100396

Wang Y, Xu C, Wu D et al (2018) Rheology of the cellulose nanocrystals filled poly(ε-caprolactone) biocomposites. Polymer (Guildf) 140:167–178. https://doi.org/10.1016/j.polymer.2018.02.050

Wu L, Huang S, Zheng J et al (2019) Synthesis and characterization of biomass lignin-based PVA super-absorbent hydrogel. Int J Biol Macromol 140:538–545. https://doi.org/10.1016/j.ijbiomac.2019.08.142

Xiao X, Chevali VS, Song P et al (2019) Polylactide/hemp hurd biocomposites as sustainable 3D printing feedstock. Compos Sci Technol 184:107887. https://doi.org/10.1016/j.compscitech.2019.107887

Xiong F, Wu Y, Li G et al (2018) Transparent nanocomposite films of lignin nanospheres and poly(vinyl alcohol) for UV-absorbing. Ind Eng Chem Res 57:1207–1212. https://doi.org/10.1021/acs.iecr.7b04108

Yang X, Finne-Wistrand A, Hakkarainen M (2013) Improved dispersion of grafted starch granules leads to lower water resistance for starch-g-PLA/PLA composites. Compos Sci Technol 86:149–156. https://doi.org/10.1016/j.compscitech.2013.07.013

Youssef AM, El-Sayed SM (2018) Bionanocomposites materials for food packaging applications: concepts and future outlook. Carbohydr Polym 193:19–27. https://doi.org/10.1016/j.carbpol.2018.03.088

Yu Z, Wang W, Kong F et al (2019) Cellulose nanofibril/silver nanoparticle composite as an active food packaging system and its toxicity to human colon cells. Int J Biol Macromol 129:887–894. https://doi.org/10.1016/j.ijbiomac.2019.02.084

Yusoff RB, Takagi H, Nakagaito AN (2016) Tensile and flexural properties of polylactic acid-based hybrid green composites reinforced by kenaf, bamboo and coir fibers. Ind Crops Prod 94:562–573. https://doi.org/10.1016/j.indcrop.2016.09.017

Zabaniotou A, Kassidi E (2003) Life cycle assessment applied to egg packaging made from polystyrene and recycled paper. J Clean Prod 11:549–559. https://doi.org/10.1016/S0959-6526(02)00076-8

Zhang X, Xiao G, Wang Y et al (2017) Preparation of chitosan-TiO_2 composite film with efficient antimicrobial activities under visible light for food packaging applications. Carbohydr Polym 169:101–107. https://doi.org/10.1016/j.carbpol.2017.03.073

Zhang Y, Jiang M, Zhang Y et al (2019) Novel lignin–chitosan–PVA composite hydrogel for wound dressing. Mater Sci Eng, C 104:110002. https://doi.org/10.1016/j.msec.2019.110002

Towards Sustainable Buildings with Free-Form Geometries: Development and Application of Flexible NFRP in Load-Bearing Structures

Hanaa Dahy

Abstract The application of non-renewable building materials including concrete and metals in construction industries have caused a major impact on the environment including the destruction of more than 45% of the global resources, the consumption of 35% of energy and nearly 40% of energy-related emissions (UN Secretary-General's High-Level Panel on Global 2012). In order to help in reducing these extending impacts, the building sector started considering three reduction of these dreadful impacts through increasing the environmentally-friendly building materials with Natural Fiber Reinforced Polymer Composites (NFRP), specially through WPCs (Wood Polymer Composites) since the 90s. The use of natural fibers in composites form in the building sector is historically applied since the phrase time when straw and mud were mixed to form the first known bricks in history. After the discovery of cement, it became the largest dominant material in the industry till our current time, in spite of its huge environmental damage. Natural fibres (NF) have been mostly applied in non-structural applications. Accordingly, this paper discusses applying reinforcement scenarios in the form of novel core and veneer reinforcement to enhance a load-bearing capacity to reach to improved mechanical properties that could enable building a demo- shell construction system. In this research natural fiber reinforced polymer composite (NFRP) produced from agricultural residues in the form of straw fibres (SF) mixed with three different types of polymers including (polylactide (PLA), a TPE (Thermoplastic elastic polymer) and high-density polyethylene (HDPE)) were developed through extrusion processes, then laminated or veneered to elevate the material properties needed to be reached to apply in load-bearing structures. The thermoplastic elastic polymers (TPE) were applied to enhance elasticity and flexibility in reaching sophisticated geometries. The

H. Dahy (✉)
BioMat Department, University of Stuttgart, Institute of Building Structures and Structural Design, 70174 Stuttgart, Germany
e-mail: h.dahy@itke.uni-stuttgart.de

Department of Planning, Section of Sustainable Design and Transition, Aalborg University, 2450 Copenhagen SV, Denmark

FEDA (Faculty of Engineering, Department of Architecture), Ain Shams University, 11517 Cairo, Egypt

M. T. Hameed Sultan et al. (eds.), *Biocomposite Materials*, Composites Science and Technology, https://doi.org/10.1007/978-981-33-4091-6_2

mechanical strength was controlled by veneering. The targeted and reached material properties were applied in structural simulations that were later used in predicting the structural performance of a physical experimental shell construction that were built to validate the settled hypothesis of reinforcement of elastic/semi-elastic lignocellulosic cores to be applied in load-bearing systems. The paper will highlight the material samples development and testing, followed by an analysis and interpretation to the possibility of usage and appliance in load-bearing structures. Finally, the physical built demonstrator in the form of the experimental shell construction is shortly illustrated to showcase the validity of the settled hypothesis.

Keywords Natural fiber reinforced polymer composite (NFRP) · Biocomposites · Sustainable construction system · Veneered biocomposites · Sustainable load-bearing systems

1 Introduction

Biocomposite materials, i.e. natural fibre reinforced polymeric composites (NFRP) (Dahy 2017a, b) are materials fabricated from at least two main components, a fibre and a matrix (also known as binder), where at least one of the two main components is biomass-based. Wood consumption worldwide became questionable since the late twentieth century. This is due to the international trend of preserving the forests and retaining the needed eco-life equilibrium through changing the forestry behaviour and the amounts of consumed wood annually. Accordingly, searching for another available source of annually renewable natural fibres' source became an international demand.

On the other hand and since resource-intensive materials like steel, concrete etc. were and are still the predominant used materials in the building industry, different emerging technologies based on biocomposites' application started growing since the 1990s, namely Wood Polymer Composites (WPC) (Vogt, C. Wood Plastic Composites (WPC) 2020) from wood and annually generated agricultural residues like straw bond by thermoplastics.

Biocomposites using long lignocellulosic fibres started in the automotive industry by Ford in the 1940s, then faded for decades till it started back in the 1990s. Only few examples have been realized in the building industry. One of them is the pedestrian bridge made by Eindhoven University of Technology (Blok and Teuffel 2017). The main bridge girder was composed of hemp and flax fibres attached to a Polylactic Acid (PLA)-based foam core. Another example is the BioMat Research Pavilion completed in 2018 at University of Stuttgart Campus (Dahy 2019a, b) as well as the BioMat Tailored Fibre Placed (TFP) Biocomposite Camopy realized in 2019 (Dahy et al. 2020).

Green biocomposites is a term that is used to describe that the main components of the biocomposite (fibre and binder) are both biomass-based. In that case, the positive value of applying those composites is doubled. One of the developed materials discussed here in the chapter is a green biocomposite that has been also veneered and mechanically tested.

2 Material Preparation

Three NFRP materials were prepared using 70–80% straw fiber by wt. with a fiber size of 1–5 mm. The mixture was prepared by dry mixing the original components then directly extruding the composition using a double-screw lab-extruder without pre-pelletizing the biocomposite. Three types of polymers were used for production including polylactide (PLA), a thermoplastic elastic polymer (TPE) of PVA (Polyvinyl Acetate)-basis as well as high-density polyethylene (HDPE) polymer matrix, (Table 1). Before extrusion, the pre-blending of straw fibers and polymer matrix with coupling and lubricant agents were carried out. All biocomposite samples were extruded at an extrusion speed of average 18 cm/min, temperatures ranged between 120–160 °C and diverse pressing forces ranging from 30–140 Bar were applied to reach a final homogenous mixture with an acceptable extruded profile with no visinary trapped air gases in the surface. Mechanical tests were carried out on the three biocomposite charges that were visually and qualitatively pre-selected and inspected, showing the best quality out of the series of charges pre-compounded at different further fibre-ratios than those final selected ones given here. The mechanical properties of thee biocomposite samples were tested after oak veneer lamination was applied to the extruded samples for the aim of increasing bending strength and stiffness.

Table 1 Biocomposites samples preparation

Charges	Material composition	Percentage (%)
1	Straw fibres (SF) Thermoplastic elastic polymer (TPE)	80 20
2	Straw fibres (SF) Polylactide (PLA) Thermoplastic elastic polymer (TPE) (Coupling agent)	70 15 13 2
3	Straw fibres (SF) High density polyethylene (HDPE) (Coupling agent)	70 28 2

2.1 Material Lamination Process Through Veneering

Lamination is a basic process known and applied in construction building materials, including the known laminated timber beam products. In this research, vacuum lamination processes were applied to enhance increased mechanical properties and strength through veneering the extruded NFRP samples. Before veneering through a selected PVA-based glue, the extruded biocomposite materials were rubbed to activate the capillary surface reaction to improve the gluing process. The veneering lamination process was assisted by means of vacuum appliance. The presence of a vacuum pump helped in eliminating air-pockets between the sandwich layers, composed of the extruded NFRP of the core and two oak veneer layers on both sides. The veneer itself was reinforced with plastic threads from the back-side, which helped in further reinforcement of the whole sandwich panel as needed. Applying vacuum has also assisted on reaching high-quality surfaces and the process took place for half an hour then left under pressure for a complete 24 h till the glue hardening process has been completed.

3 Standards for Test Specimens Preparation

The test samples were prepared and calibrated according to the norm DIN EN 325:1993, the wood-based panels standard (DIN EN 1993). Samples were measured using digital caliper measurement with 0,01 accuracy. Due to extrusion irregularities, the samples' thicknesses were measured from four points throughout the length and the thickness mean value was calculated accordingly, then typed as inputs in the used measuring machine. This is one of the necessary steps needed for testing prior to the bending test to be able to determine the elastic modulus. Further calibration conditions included preparing the samples at a relative humidity of (65 ± 5) % and a temperature of (23 ± 1) °C.

3.1 Bending Test

Five samples were prepared from the pre-defined material cores that were presented in Table 1 and veneered with oak veneer from both sides to create the sandwich panels shown in (Fig. 1a) as described in 2.1 through vacuuming. The veneer fibres were fibre-oriented, which is different from the free-fibre orientation of the extruded core. A Universal bending machine (Zwick Z1455) setup for three-point bending test according to the pre-mentioned standard was applied hereby. The bending test setup included setting a 100 mm distance between both bottom supports. The upper supporting cylinder of the machine was 15 ± 0.5 mm and the loading cylinder diameter was also 30 ± 0.5 mm. The flexural loading speed was set to 25 mm/min

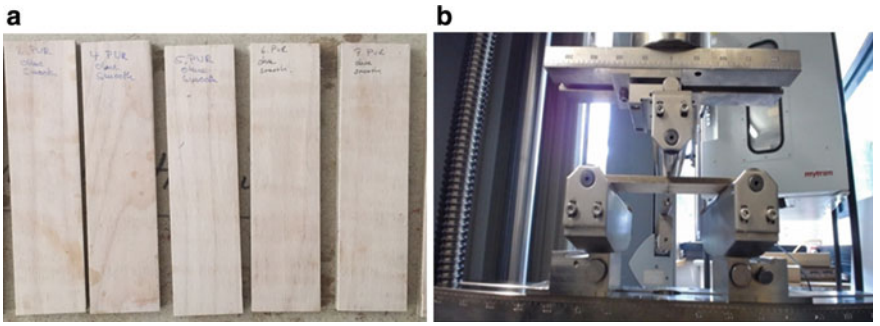

Fig. 1 **a** Bending test specimens after lamination, **b** specimens under three-point bending test

with pre-load of 0.1 N/mm^2, according to the testing standard DIN EN 310:1993, Wood-based panels; for the determination of modulus of elasticity in bending and of bending strength (DIN EN 1993).

3.2 Tensile Test

The tensile test was carried out on a universal testing machine set according to DIN EN 789 standard of tensile test for wood-based panels (DIN EN 2004). The testing machine setup under a uniform test speed of 10 mm/min with a pre-load of 0.01 N/mm^2 at room temperature(23 ± 1 °C). The five tested samples had bone-like cross-sections according to the Fig. 2. The tensile test specimens dimensions: $b_2 = 42$ mm, $b_1 = 28$ mm, $l_3 = 210$ mm, $l_2 = 171$ mm, $l_1 = 90$ mm and $t = 6$ mm.

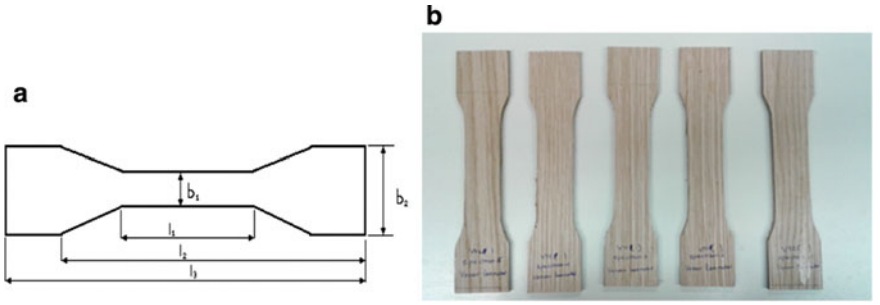

Fig. 2 **a** Dimension of specimens for tensile test and **b** tensile test specimens after veneering

Table 2 Average elasticity modulus of biocomposite samples after bending and tensile test

Samples	No. of specimens	Elasticity modulus (GPa)	Tensile modulus (GPa)
1	5	1.8–2.5	–
2	5	4.5–5.2	1.1–1.5
3	5	5.5–6.3	1.4–2.8

4 Test Results and Discussion

4.1 Bending Test

Table 2 shows the modulus of elasticity after the three-point bending test for five specimens of each material charge as defined in 3.1. Most of the samples were brittle prior to veneering, then the breaking performance was improved through the veneering reinforcement. For the first sample, the specimens has shown a good strength performance in compression stress from the applied bending force (Fig. 3a), exhibiting a clear elastic deformation due to the elastic properties already highly present in the TPE applied. In the second sample, a brittle like fracture were observed and weak flexural stress resistance existed. In the third sample, the straw fibers (SF) and HDPE composition were compatible, and the NFRP composite resulted here has shown the highest flexural stress resistance even before veneering took place. SF and HDPE were found the best biocomposite developed in this case with the best mechanical performance. Within the test and during breaking, delamination occurred, which was mostly at the bottom veneer layer due to the tensile stress created during loading condition.

4.2 Tensile Test

During veneering, adhesives were applied and the methods used to activate the layers to which adhesion was applied, especially the core, have all played an important role in upgrading the NFRP biocomposites' strengths. The value of tensile strength of the second veneered sample was around 1.1–1.5 GPa. In Fig. 4a, sample 2 from SF and PLA has shown high deformation. The average tensile strength of the third biocomposite sample from SF and HDPE ranged from 1.4–2.8 GPa after veneering was applied (Table 2) and its elasticity modulus increased 10 times after veneering was applied in comparison to previous measurements without veneering or reinforcement. It is worth mentioning that failures were mostly seen in the form of delamination and in the veneer layers themselves, which reflects that the biocomposites cores could not hold alone bearing tensile loads. This indicates the scope in this paper, that only through veneering to appropriate biocomposite core mixtures and with appropriate gluing conditions and glue types, advanced mechanical performances were reached

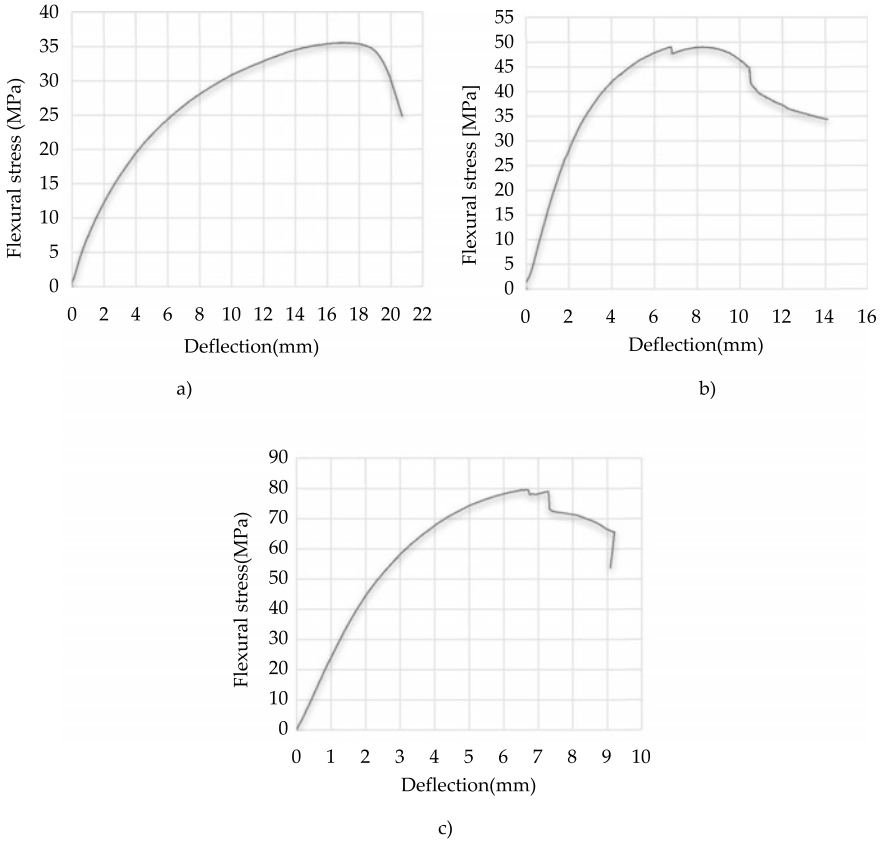

Fig. 3 Flexural stress versus deflection graph **a** sample 1, **b** sample 2 and **c** sample 3

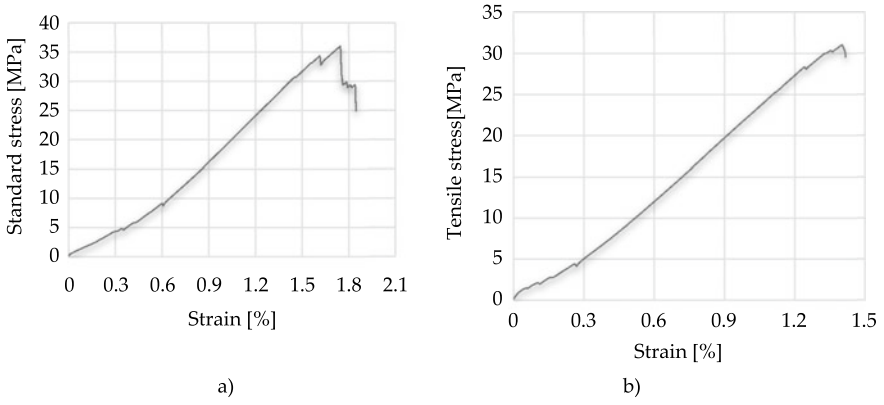

Fig. 4 Tensile stress versus strain graph **a** sample 2 and **b** sample 3

and accordingly load-bearing elements were developed when correctly applied in certain appropriate loading conditions like that tested in the BioMat Pavilion 2018 in the form of a shell construction system as shown in part 5.

5 Potential Applications in Sustainable Building Structures

In sustainable constructions, biocomposites can be used for small load-bearing structures such as pedestrian bridge structures (Blok and Teuffel 2017), cladding systems, flooring finishes and free-form furniture as from (Bioflexi) another development by the author (Dahy and Knippers 2016; Horn et al. 2018).

The presented experiments were a part of the Research Project 'BioProfile' funded by Fachagentur Nachwachsende Rohstoffe e. V. (FNR) and conducted at the University of Stuttgart, by Department of Biobased Materials and Materials Cycles in Architecture (BioMat) at Institute of Building Structures and Structural Design (ITKE), lead by the BioMat director, the author. The BioProfile project pursues research on extruded and coextruded profiles for windows frames and exterior architectural applications, especially façade panels, made of plant residues as a source for natural fibres reinforced by biopolymers. The extruded profiles analyzed in this paper took place in the Fraunhofer- WKI center in Braunschweig in Germany with both the company ETS and BioMat assistances.

During this research study, BioMat realized a Biocomposite Experimental Pavilion, which is an experimental load-bearing structure made using biocomposites. This pavilion that was realized in 2018 was a 3.6 m-high shell structure with a 9.5 m span, covering an area of 55 m^2. It was located on the campus of the University of Stuttgart in the city centre between August–December 2018, as shown in (Fig. 10). Its special feature is the modular construction of lightweight, single-curved elements that form a double-curved shell with individual segments consisting of veneer-reinforced elastic/semi-elastic biocomposite cores. The structure is supported by three crossed beams.

The original target values for the settling of the shell global geometry was dependant on the results of the material developments given in this paper. The reinforcement strategy through veneering that enabled the original elastic/semi-elastic cores to reach higher mechanical performance were set as a main parameter in the whole development of the shell-construction.

The initial structural simulations integrated those material properties, which have shown that the developed biocomposites would not allow a single shell layer, therefore a second structural layer was developed and attached to the first one. This interconnection and double layering enabled homogenous loads' distribution in all directions. The presence of the three crossed laminated beams was essential and the loads were transferred to three superficial foundation footages that were located at different heights, according to the existing site conditions (Fig. 5). The parametric model of the shell was developed using Rhinoceros and Grasshopper softwares,

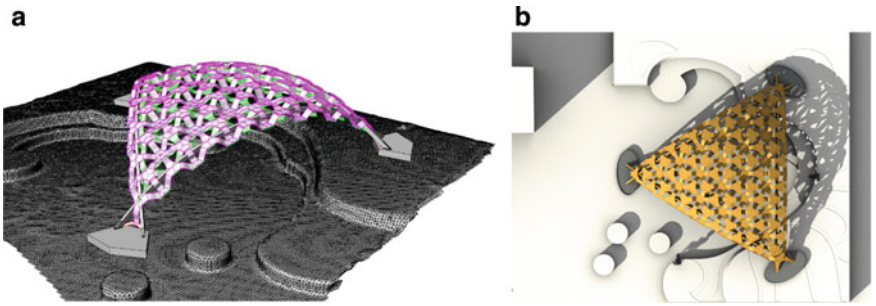

Fig. 5 Parametric model of the global geometry of the designed shell **a** perspective view on the 3D-laser scanned data and **b** layout of the model

enabling the control over the number of variations of the three-legged elements (Dahy et al. 2019a, b).

In (Fig. 6), the fabrication of one element is illustrated and in (Fig. 7), the combination of the elements in one unit is illustrated. Consequently, 360 panels for the three-legged elements: upper elements, lower elements, upper edged elements and lower edged elements were fabricated (Fig. 8a) and the panels were assembled in 4 stages (Fig. 8b). In (Fig. 9) a detail of the relationship between the biocomposite panels and the wooden structural beam is illustrated and in (Fig. 10) the final experimental pavilion is shown.

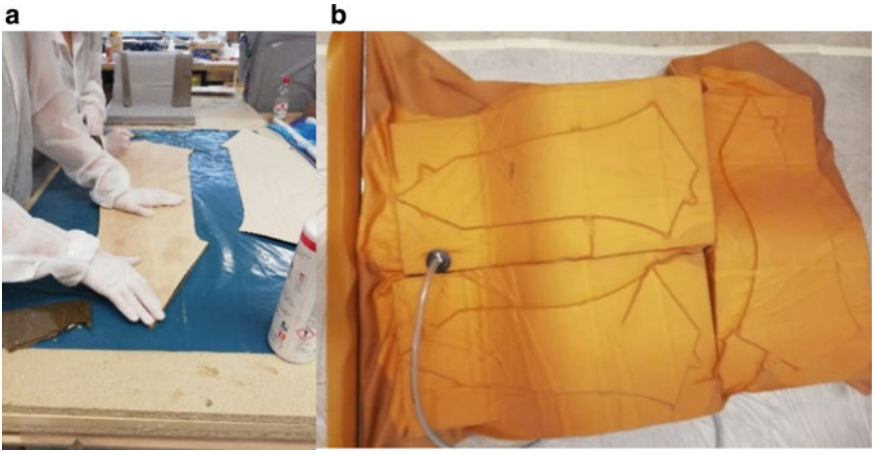

Fig. 6 Lamination process **a** reinforcement of the bio-composites by 3D veneer layers and **b** vacuum-assisted veneer-reinforcement lamination process

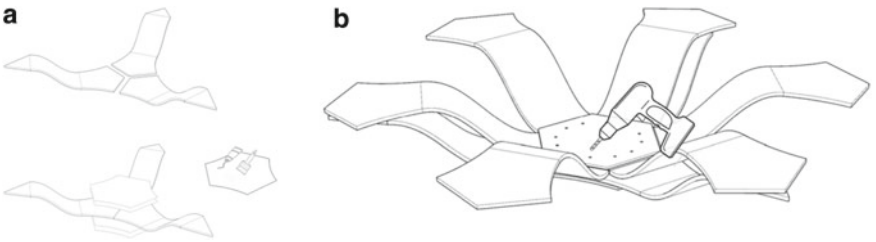

Fig. 7 Combining the legs to form the building units. **a** Combing each three leg-units and **b** combining six legs units to another three-legs unit to form the double shell structure

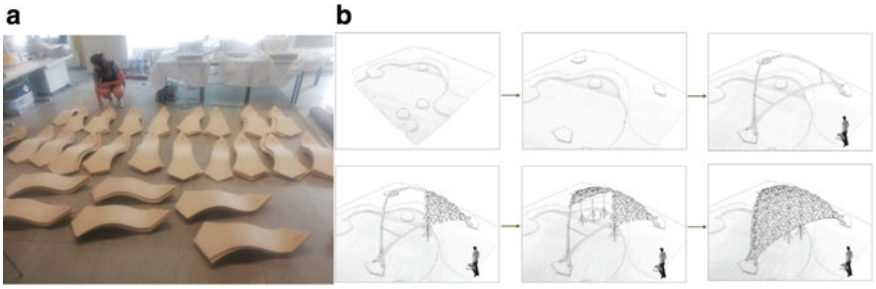

Fig. 8 Off-site and on-site construction phases **a** off-site segments ordering **b** sequence of fixing larger segments on site

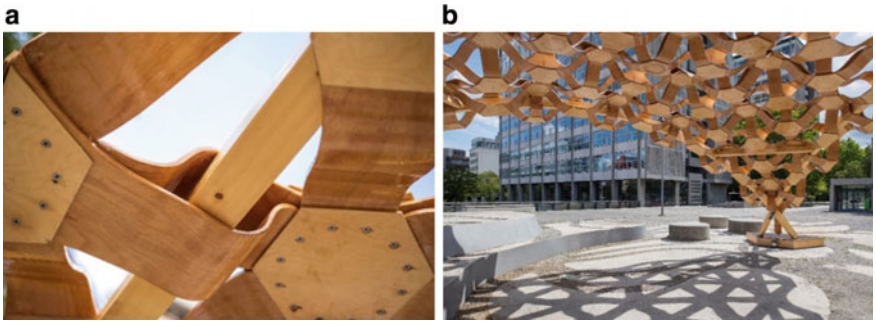

Fig. 9 Detailing in the structure **a** relation between biocomposites and the timber beam **b** relation between diverse biocomposites units in the structure

6 Conclusion

In this paper, an emphasis on veneering in elevanting the properties of biocomposite cores to reach up to load-bearing capacity for future sustainable constructions have been illustrated. The development of multi biocomposites extruded cores with free-fibre oriented straw fibres was highlighted. It was intended to enduce the presence

Fig. 10 Night-view for the biomat Pavilion 2018

of thermoplastic elastic polymers to enduce elasticity, hence flexibility in reaching sophisticated geometries and free-forms that are nowadays urgently needed in the building industry. On the other hand, it was intended to fix veneer though cloused vacuum-assisted lamination process that would fix the final geometries needed and enduce the targeted elevanted mechanical properties to build through the developed innovative building elements new structural applications. This was showcased through the built experimental pavilion in which the same target values for the developed materials was applied in the structural analysis. In the physical world, another biocomposite sandwich panel was developed using a different ligno-cellulosic elastic core, but the same mechanical values were applied.

The modulus of elasticity was comparable to medium density fiberboard (MDF) and the target was reached to elevate the mechanical properties and to optimize the geometry of the shell to make proper advantage of the still relatively low mechanical properties in comparison to conventional glass fibre reinforced composites (GFRP).

In this research, biocomposites were given a further chance to investigate elevating their properties to compete with conventional building materials towards more future sustainable constructions. Biocomposites have many advantages, but also disadvantages including water-absorption sensitivity. On the mechanical side, properties can be elevated by different means through oriented fibre-reinforcement as illustrated in this paper. But on the other hand, further research work is recommended to further go in that direction and especially to find environmentally-friendly means of improving the weathering resistance of these groups of materials. This will help enabling them to further compete globally in the building materials market and accordingly reach the needed target of reaching to a high percentage of appliance in reality, hence achieving a large percentage of targeting the urgently needed sustainability in this industrial field, the building industry world.

Acknowledgements The author thanks all students, employees, technicians and agencies involved in this project. This work was the direct result of cooperation between around 40 architecture students over two semesters participating in the (Flexible Forms) Design Studio in the semesters: WS17/18 and SS18 supervised by the author: Hanaa Dahy, the director of BioMat group at ITKE with her team: Jan Petrs, Piotr Baszynski and Michaela Mey, with the support from the University of Stuttgart and the Baden-Württemberg Foundation. Financial support was from the German Agency for Renewable Resources (FNR) under the Ministry of Food and Agriculture (BMEL), and scientific cooperation took place with Fraunhofer-Institut für Holzforschung (Fraunhofer WKI) and industrial partners Mathias Stange ETS and Profine GmbH in the framework of the Research Project (BioProfile) FKZ 22021516. International collaboration has taken place with the Technical University Eindhoven in the Netherlands (TU/e) - Department of Built Environment Prof. Patrick Teuffel, Dr. Arjan Habraken and M.Sc. Dirk Bos, in addition to local collaboration with various institutes of the University of Stuttgart, including the Institute of Construction and Structural Design (KE) - Prof. Urlike Kuhlmann and Mr. Janusch Töpler as well as the Institute of Engineering Geodesy (IIGS) Prof. Volker Schwieger and Gabriel Kerekes. Wooden beams were fabricated and supported by Burgbacher Holztechnologie GmbH with assistance of Mr. Steffen Haller, weathering resistant coatings were provided by Hexion Stuttgart GmbH.

References

Blok R, Teuffel PM (25–28 September, 2017) Bio-based composite bridge—lessons learned published. In: Proceedings of the IASS annual symposium 2017 interfaces: architecture, engineering science. Hamburg, Germany

Dahy H, Knippers J (2016) (PATENT) Flexible high-density fiberboard and method for manufacturing the same. EP3166765A1; Filed 8. July 2014 Published 13 January 2016. Based on Same Patent, Also Applied as WO2016005026A1; CN106604806A; US20170144327, EP2965882 A1

Dahy H (2017a) Biocomposite materials based on annual natural fibres and biopolymers—design, fabrication and customized applications in architecture. Constr Build Mater 147:212–220

Dahy H (2017b) Efficient fabrication of sustainable building products from annually generated non-wood cellulosic fibres and bioplastics with improved flammability resistance. Waste Biomass Valorizat No 1–9. https://doi.org/10.1007/s12649-017-0135-3. Springer Netherlands. Print ISSN 1877–2641, Online ISSN 1877-265X

Dahy H (2019a) Materials as a design tool' design philosophy applied in three innovative research pavilions out of sustainable building materials with controlled end-of-life scenarios. Buildings 9:64

Dahy H (2019b) Natural fibre-reinforced polymer composites (NFRP) fabricated from lignocellulosic fibres for future sustainable architectural applications, case studies: segmented-shell construction, acoustic panels, and furniture. Sensors 19(3):738

Dahy H, Petrs J, Bos DH, Baszynski P, Habraken APHW, Teuffel PM (2019a) BioMat Pavilion 2018: development, fabrication and erection of a double curved segmented shell from biocomposite elements. In: Lázaro C, Bletzinger KU, Oñate E (eds), Proceedings of the IASS annual symposium 2019—structural membranes 2019 form and force

Dahy H, Petrs J, Baszynski P (2019b) Experimental biocomposite pavilion: segmented shell construction—design, material development and erection. ACADIA Conference 2019, Texas, USA

Dahy H, Petrs J, Baszynski P (2020) Design and fabrication of two 1:1 architectural demonstrators based on biocomposites from annually renewable resources displaying a future vision for sustainable architecture. FABRICATE 2020, UCL, UK

DIN EN 325:1993 (1993) Wood-based panels; determination of dimensions of test pieces. European Committee for Standardization

DIN EN 310:1993 (1993) Wood-based panels; determination of modulus of elasticity in bending and of bending strength. European Committee for Standardization

DIN EN 789:2004 (2004) Determination of mechanical properties of wood based panels. European Committee for Standardization

Horn R, Dahy H, Gantner J, Speck O, Leistner P (2018) Bio-inspired sustainability assessment for building product development—concept and case study. Sustain Special Issue Sustain Construct 10(1):130. https://doi.org/10.3390/su10010130

UN Secretary-General's High-Level Panel on Global Sustainability (2012) Resilient people, resilient planet: a future worth choosing, overview. United Nations: New York, NY, USA

Vogt, C. Wood Plastic Composites (WPC) (27 January, 2020) Markets in North America, Japan and Europe with emphasis on Germany, 2005. Available online: http://biocompositescc.com/wpcdata/File/06%20pr_wpcstudy_engl.pdf. Accessed on 27 Jan 2020

PLA Hybrid Composites Reinforced with Nanomaterials

Narendra Reddy

Abstract Poly(lactic acid) (PLA) is the most common synthetic biopolymer that is derived from renewable resources and is biodegradable. PLA is used for commodity and specialized applications such as medical implants. Low processing temperatures, good mechanical and thermal stability and ability to obtain PLA in different configurations and structures make it an ideal biopolymer. However, PLA has several limitations, primarily, relatively poor resistance to chemicals. Several modifications have been done to improve the performance and properties of PLA and its products. Developing biocomposites by blending PLA with other biopolymers, nanomaterials including nanoclay have been done. Biocomposites have been developed by blending polysaccharides such as cellulose, starch, chitin and also proteins with PLA. Transparent and high performance biocomposites useful for food, medical and other applications have been developed from the blends. Despite numerous approaches, there are several limitations of PLA based biocomposites which presents scope for further research and development.

Keywords Biocomposites · Blends · Polysaccharides · Proteins · Nanoclay · Nanowhiskers

1 Introduction

Poly (lactic acid) is one of the most common synthetic biopolymers used extensively for food packaging, pharmaceutical, medical, textile and other applications. Biodegradability, production from a renewable resource, low melting temperature and solubility in common solvents are some of the advantages of using PLA. However, PLA is prone to hydrolysis under alkaline conditions, is relatively more susceptible to chemicals and products made from PLA do not have desired performance properties. Hence, considerable efforts have been made to modify PLA and improve its applications. Extensive studies have also been done to incorporate other

N. Reddy (✉)
Center for Incubation Innovation Research and Consultancy, Jyothy Institute of Technology, Bengaluru, Thataguni Post 560109, India
e-mail: narendra.r@ciirc.jyothyit.ac.in

M. T. Hameed Sultan et al. (eds.), *Biocomposite Materials*, Composites Science and Technology, https://doi.org/10.1007/978-981-33-4091-6_3

biopolymers and additives to enhance the performance of PLA based materials. Nanomaterials (fibers, particles, whiskers, capsules etc.) have been extensively used to improve the performance of polymers. Similarly, nanoclays have also been known to increase the mechanical properties, thermal stability, compatibility etc. Extensive studies have been done to study the feasibility of improving the performance and applications of PLA materials through the addition of nanomaterials. In this chapter, we provide a review of the various cellulose, starch, protein and clay-based nanomaterials used to improve the properties, processing and applications of PLA.

2 PLA Reinforced with Cellulosic Nanomaterials

Cellulosic materials have been the preferred reinforcement or additives for PLA to improve tensile, thermal, mechanical and performance properties. A variety of cellulosic materials including plants, trees, bacteria etc. are converted into nanofibrils, nanoparticles and nanowhiskers for potential reinforcement of PLA. Since cellulose is considerably stable and does not dissolve in common solvents, various approaches have been used to process cellulose and obtain the nanomaterials. Some of the common cellulosic materials used, techniques adopted for conversion and methods used to incorporate the nanomaterials into PLA are given in Table 1 (Kian et al. 2019).

Films for food packaging applications were prepared using a blend of PLA, lignin nanoparticles, microcrystalline cellulose and umbelliferone (7-hydroxycoumarin), a natural plant extract with antioxidant and antimicrobial properties (Iglesias Montes et al. 2019). The three components were added in desired ratios into a twin screw extruder and processed into films at 180–200 °C. Thickness of the films formed was between 80 and 85 μm. Further, bilayer films were formed by assembling the monolayer films and compression molding at 155 °C for 1 min at a pressure of 25 bar. Interestingly, the thickness of the bilayer films was lower than the sum of the thicknesses of the individual layers. No major change in structure of PLA was observed due to the addition of the cellulose or lignin and morphological analysis showed good interaction between the components. Although films containing more than 15% antioxidant tended to be brittle due to increased inhomogeneity, highest elongation and strength were obtained in the films containing nanoparticles and the antioxidant (Table 2).

Both lignin and umbelliferone contributed to the substantially high antioxidant properties of the films. Since hydrophobic PLA and hydrophilic microcrystalline cellulose (MCC) have poor interactions, chemical modification of MCC was done to improve the dispersion and compatibility with PLA. For the modification, MCC was acetylated using acetic acid to obtain an acetyl content of up to 17%. To obtain the nanocomposites, PLA was dissolved in chloroform to which the modified and unmodified MCC were added. Later, the mixture was poured onto Teflon molds to form nanocomposites with 0–to 17% of MCC. Acetylation helped in increasing the viscoelastic properties and compatibility. Addition of modified cellulose made

Table 1 Methods used to convert cellulosic sources into nanomaterials and different approaches to reinforce them into PLA (Kian et al. 2019). Reproduced with permission from Elsevier

Source	Chemical pretreatment	Principal treatment	Post-treatment	Fabrication techniques of PLA nanocomposites
Flax fiber	Elemental chlorine-free (ECF) bleaching sequence treatment	Hydrochloric acid hydrolysis	Dialysis, sonication, vacuum filtration	–
Flax fabric	Sodium hydroxide, sodium carbonate; hydrogen peroxide	Sulfuric acid hydrolysis	Washing, centrifugation, dialysis, ultrasonication	–
Refined industrial flax stem fibers	Toluene, ethanol; sodium chlorite, acetic acid; sodium bisulfite	Sulfuric acid hydrolysis	Centrifugation, ultrasonication, dialysis	–
Bleached flax yarns	Sodium hydroxide	Sulfuric acid hydrolysis	Centrifugation, neutralization (by adding aqueous NaOH)	Evaporation casting of PLA in chloroform solvent
Hemp fiber	Sodium hydroxide, sodium chlorite, acetic acid	Defibrillation (microfluidizer)	–	–
Pristine hemp fiber	Toluene, ethanol; sodium chlorite, acetic acid; sodium bisulphate; sodium hydroxide	Sulfuric acid hydrolysis; physical modification with acid phosphate ester of ethoxylatednonylphenol surfactant	Centrifugation, dialysis, sonication	Evaporation casting of PLA/PBS blend with functionalized nanocellulose in chloroform solvent

(continued)

Table 1 (continued)

Source	Chemical pretreatment	Principal treatment	Post-treatment	Fabrication techniques of PLA nanocomposites
Hemp pristine fiber	Toluene, ethanol; sodium chlorite, acetic acid; sodium bisulphate; sodium hydroxide	Sulfuric acid hydrolysis	Centrifugation, dialysis, sonication	–
Hemp yarns	–	Sodium hydroxide, sodium hypochlorite (oxidation hydrolysis under continuous agitation and sonication)	–	–
Jute fiber	Sodium hydroxide; sodium chlorite, sodium sulphite; hydrogen peroxide	Sulfuric acid hydrolysis	Centrifugation	–
Waste jute bags	Toluene, ethanol; soda cooking (in basic reactor); hydrogen peroxide; hydrochloric acid hydrolysis (in ultrasonicator)	Homogenization	–	–
Jute fiber	Sodium hydroxide; sodium hypochlorite, sodium sulphate	Sulfuric acid hydrolysis	Neutralization (by adding aqueous NaOH), discoloring (by adding aqueous NaOCl), vacuum filtration	–

(continued)

Table 1 (continued)

Source	Chemical pretreatment	Principal treatment	Post-treatment	Fabrication techniques of PLA nanocomposites
Jute fiber	Caustic soda; sodium chlorite	Oxalic acid hydrolysis; steam explosion	Centrifugation, mechanical agitation, sonication, neutralization (by adding aqueous NaOH)	–
Pristine jute fiber	Sodium hydroxide, dimethyl sulfoxide	TEMPO-mediated oxidation	Centrifugation, high-speed homogenization, ultrasonication	–
Jute fiber	Toluene; sodium hydroxide; hydrogen peroxide	Sulfuric acid hydrolysis; formic acid hydrolysis	Filtration (using nylon membrane), neutralization (by rinsing with distilled water)	–
Jute fiber	Sodium hydroxide, dimethyl sulfoxide	TEMPO-mediated oxidation	Centrifugation	–
Jute felts	Sodium hydroxide, dimethyl sulfoxide	Sulfuric acid hydrolysis	Sonication, neutralization (by adding aqueous NaOH), centrifugation	–
Water retted kenaf fiber	Sodium hydroxide, anthraquinone (in rotatory digester); three-stage bleaching	Mechanical shearing (supermasscolloider); grinding	–	–
Kenaf fiber	Sodium hydroxide; sodium chlorite, acetic acid	Sulfuric acid hydrolysis; hydrochloric acid hydrolysis	Centrifugation, dialysis, homogenization, addition with chloroform	–

(continued)

Table 1 (continued)

Source	Chemical pretreatment	Principal treatment	Post-treatment	Fabrication techniques of PLA nanocomposites
Kenaf core wood	Sodium hydroxide; sodium chlorite, acetic acid	Sulfuric acid hydrolysis	Centrifugation, dialysis	–
Kenaf stem fiber	Sodium hydroxide	Homogenization	–	–
Roselle microcrystalline cellulose	–	Sulfuric acid hydrolysis	Centrifugation, dialysis, ultrasonication	–
Mulberry pulp	–	Sulfuric acid hydrolysis	Centrifugation, ultrasonication, dialysis	–
Ramie fiber	Sodium hydroxide	Sulfuric acid hydrolysis; physical modification with organosilanization	Centrifugation, dialysis, homogenization, filtration, neutralization (by adding aqueous NaOH)	Melt-extrusion of PLA with functionalized nanocellulose in absence of solvent
Ramie fiber	Sodium hydroxide	Sulfuric acid hydrolysis	Centrifugation, dialysis, homogenization, filtration, addition with chloroform	–

Table 2 Tensile properties of monolayer and bilayer films of neat PLA and those reinforced with lignin, cellulose and umbelliferone (Iglesias Montes et al. 2019). Reproduced with permission through open access publishing

Sample	Modulus (GPa)	Strength (MPa)	Elongation (%)
Neat PLA	1.4 ± 0.2	41.5 ± 3.9	16.2 ± 4.2
PLA, 3% CNC	1.2 ± 0.1	28.1 ± 4.0	4.9 ± 0.8
PLA, 3% LNP	1.3 ± 0.1	34.2 ± 1.5	8.4 ± 0.9
PLA, 15% UMB	1.2 ± 0.3	28.8 ± 9.3	37.0 ± 4.2
PLA/PLA	1.6 ± 0.2	35.0 ± 6.2	16.4 ± 5.3
PLA/PLA, 3% CNC	1.4 ± 0.1	38.3 ± 2.9	5.6 ± 1.2
PLA/PLA, 3% LNP	1.5 ± 0.3	36.7 ± 4.1	6.3 ± 0.8
PLA/PLA, 15% UMB	1.6 ± 0.1	38.4 ± 2.2	4.5 ± 0.9
PLA 3CNC/PLA 15% UMB	2.1 ± 0.1	52.9 ± 2.2	2.9 ± 0.3
PLA 3LNP/PLA 15% UMB	2.0 ± 0.3	48.4 ± 4.4	3.0 ± 0.2

the films translucent (Fig. 1), reduced hydrophilicity and improved thermal stability. Acetylated cellulose had considerably higher dispersibility and also increased the Tg of PLA. Increase in modulus and decrease in strength was also observed with 17% cellulose in the composites (Tingaut et al. 2009). In another study, it has been shown that acetylated nanocellulose fibers (length 50 μm and diameter 50 nm) provided better phase affinity, higher dispersibility and orientation compared to nanocellulose coupled with silane or unmodified PLA (Ying et al. 2018). Coupling reaction did not affect the modulus of the nanofibers whereas acetylation decreased modulus by about 10% which was attributed to strong hydrogen bonding between PLA and acetylated nanocellulose. Morphological observations showed that pristine nanofibers had poor dispersion with aggregates formed of 1–2 μm in size. Both coupled and acetylated fibers had better dispersion based on visual observation (Fig. 2) and a parameter called interaction energy parameter. Acetylated nanofibers also provided increased tensile properties typically by about 38% but higher tensile strength up to 51% was possible depending on the amount of nanofibers in the blend (Fig. 3).

Cellulose nanocrystals extracted from sugarcane bagasse were combined with PLA to develop composites with improved thermal stability (Gan and Wen 2019). Bagasse was delignified and later acid hydrolyzed with 6 M sulfuric acid and 11 M phosphoric acid at 55 °C for 30 min. Cellulose nanocrystals formed were obtained after dialysis and freeze drying. To form the composites, the nanocellulose and PLA were dissolved in chloroform to obtain a CNC concentration of 10%and the solution was cast to form films. Cellulose nanocrystals had diameters between 5.5 and 6.2 nm

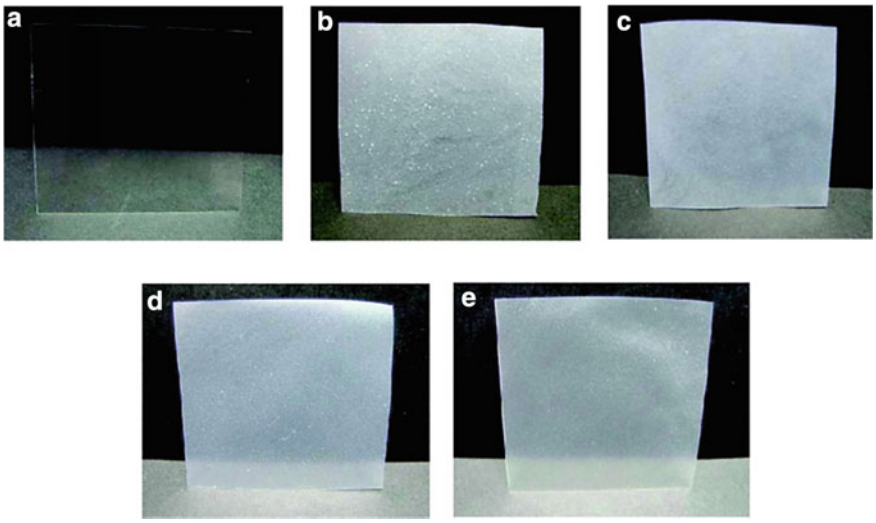

Fig. 1 Changes in the appearance (transparency) of neat PLA (**a**) films reinforced with acetylated microcrystalline cellulose. **b** (0%), **c** (3.5%), **d** (8.5%) and **e** (17%) nanocellulose reinforced films (Tingaut et al. 2009). Reproduced with permission from American Chemical Society

and length of 235–300 nm with aspect ratio between 37–55. However, agglomeration of the CNCs was also noticed due to intermolecular hydrogen bonding. XPS and FTIR studies confirmed the addition of sulphate and phosphate groups on the surface of cellulose due to the acid treatment. Composites containing phosphoric acid treated nanocellulose provided considerably higher thermal stability compared to neat or sulfuric acid treated cellulose (Gan and Wen 2019). In a related approach, highly crystalline cellulose nanofibers were modified to add a high density of carboxylate groups and later grafted onto PLA and made into composites. Cellulose pulp obtained from northern softwood and sugarcane bagasse pulp (non-wood) were treated with 2,2,6,6-Tetramethylpiperidine-1-oxyl (TEMPO) and surface oxidation was done to obtain treated cellulose (Fig. 4). Ion-exchange with lithium chloride was done resulting in TEMPO oxidized cellulose nanofibers. The modified cellulose nanofibers were grafted onto PLA through ring open polymerization. Extent of grafting and molar ratios of carboxylate groups on the PLA were controlled by varying the reaction conditions. Carboxylate content of the materials increased significantly after treating with TEMPO and further after oxidation. A carboxylate content of 1.03 mmol/g was obtained for the oxidized cellulose compared to 0.03 mmol/g for the untreated sugarcane bagasse pulp. However, the crystallinity and crystal size of the modified cellulose was lower compared to unmodified cellulose pulp but higher than the crystallinity of neat PLA. It was suggested that inclusion of modified cellulose nanofibers would be a feasible approach to improve the thermal and performance properties of PLA for various applications (Chuensangjun et al. 2019a; b). An improved process and higher conversion of carboxylate groups along with higher crystallinity of cellulose

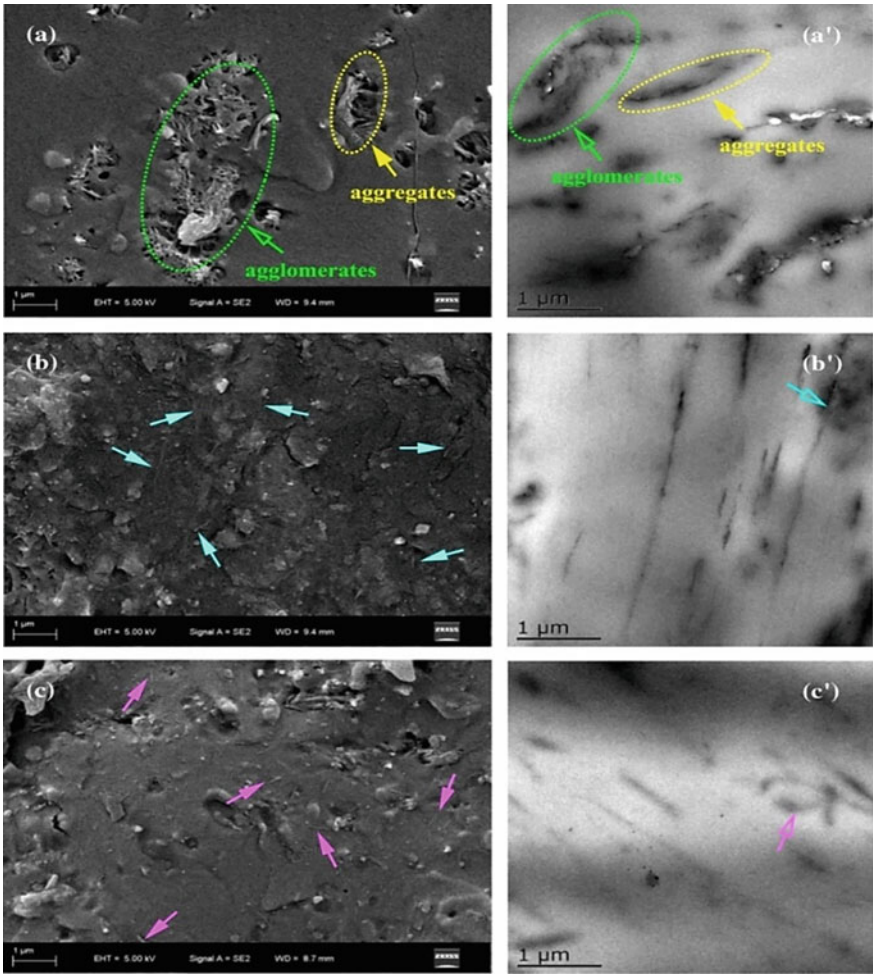

Fig. 2 SEM (left) and TEM (right) images of neat (untreated fibers) PLA and PLA films containing coupled **b** and acetylated **c** nanocellulose fibers showing differences in dispersion and compatibility (Ying et al. 2018). Reproduced with permission from Springer Nature

was obtained when the ring open polymerization was done using lipase as catalyst. A carboxylate group content of 1.63–1.68 mmol/g was obtained and the PLA in the composites developed had crystallinity of 76% and crystal size of 3.8 nm. Better dispersibility of modified cellulose and higher thermal stability of composites was also possible by using the catalyst and ring open polymerization (Chuensangjun et al. 2019a; b).

Grafting of cellulose nanocrystals onto PLA was also done using an in-situ ring opening polymerization approach of L-lactide. The cellulose nanocrystals were made from softwood pulp and had width of 13 nm and length of 140 nm. Nanocrystals and

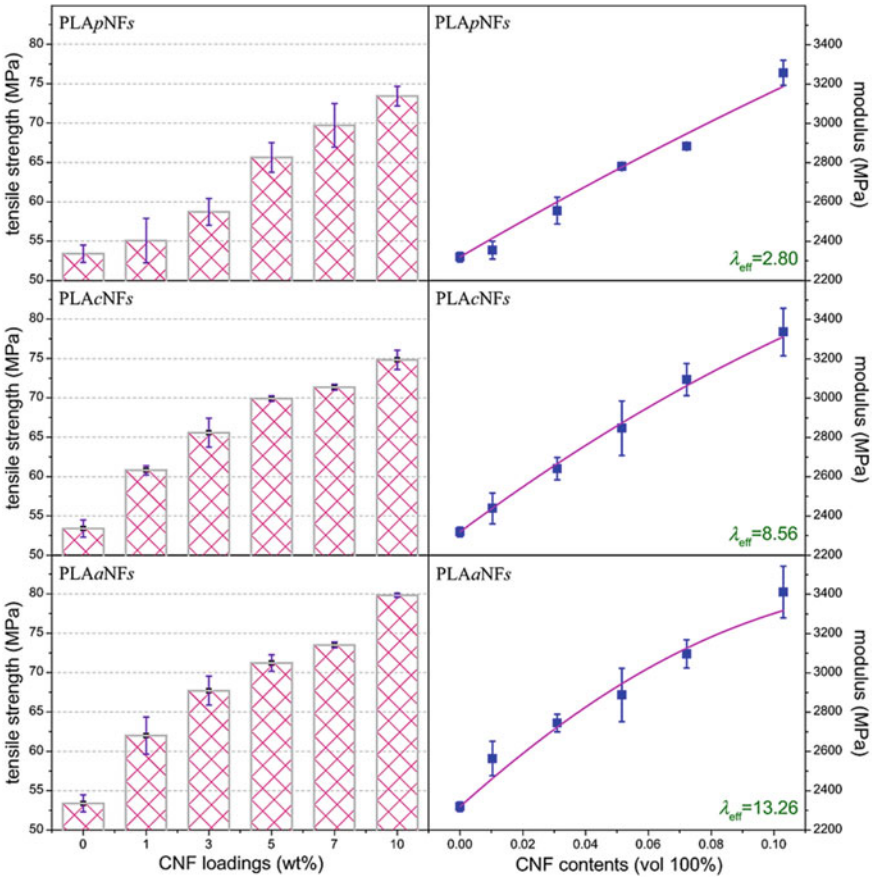

Fig. 3 Tensile strength and modulus of PLA films with untreated nanocellulose fibers (PLApNFs) and those containing nanocellulose fibers after coupling (PLAcNFs) and acetylation (PLAaNFs) (Ying et al. 2018). Reproduced with permission from Springer Nature

the L-lactide were dissolved in DMSO in the presence of a initiator and an catalyst. The polymerization reaction was performed over a period of 17 h under nitrogen atmosphere. Depending on the reaction conditions, a grafting ratio of 84–152% was obtained (Miao and Hamad 2016). The polymerized PLA containing nanocrystals was made into films using solution casting and also co-extrusion. Grafted nanomaterials had better dispersibility in chloroform compared to unmodified PLA. Considerable decrease in water contact angle but no major change in thermal behavior was observed due to the grafting of the nanocrystals. However, oxygen and water vapor permeability had decreased thereby increasing the barrier properties. Water vapor permeability rates between 2244 and 3137 (ml.mm)/(Cm^2.s.c.Hg) and oxygen transmission rates similar or better than that of commercially used PET, PE and cellulose acetate members were achieved making the PLA-celluose nanocrystal films suitable

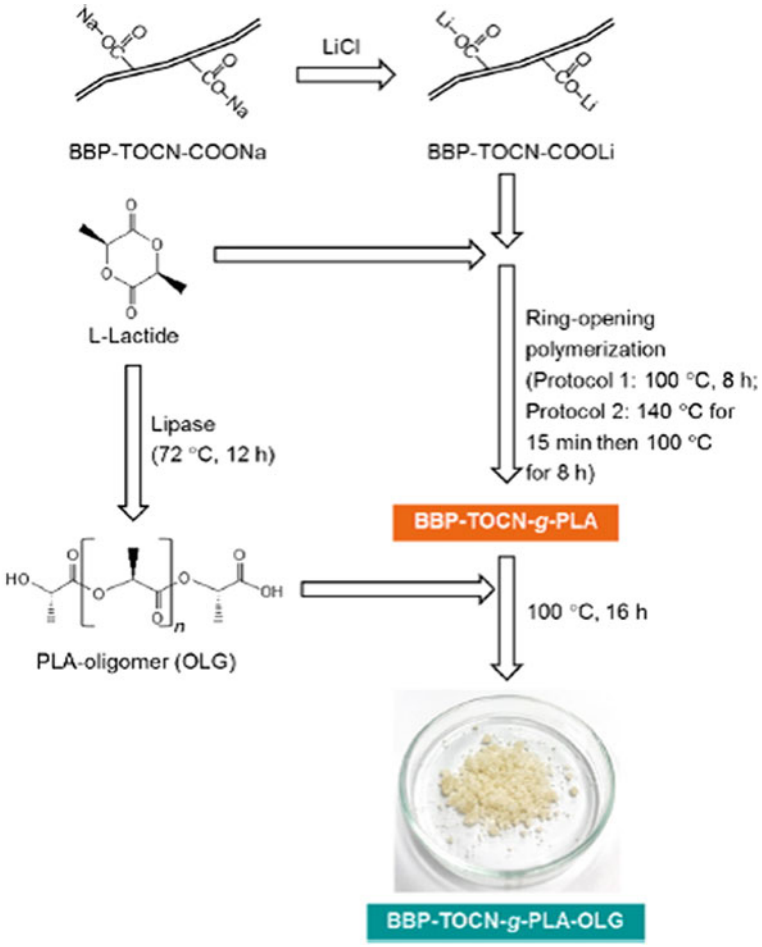

Fig. 4 Schematic of the process of preparing the PLA composites grafted with cellulose nanofibers obtained from bagasse pulp modified using TEMPO (Chuensangjun et al. 2019a; b). The oxidation was done using lipase as catalyst to obtain higher carboxylate groups and crystallinity

for food packaging applications. Similarly, up to 1100% increase in modulus was possible since the nanocrystals functioned as excellent nucleating agent (Miao and Hamad 2016).

An algae *Posidonia oceanica* has been used as a source of cellulose fibers and cellulose nanoparticles for reinforcing PLA. The algae was extensively bleached to obtain fibers and these fibers were converted into cellulose nanoparticles by acid hydrolysis with a yield of 14%. The nanoparticles were also modified with a surfactant to improve dispersion and compatibility when used as reinforcement in PLA nanocomposite films. PLA was dissolved in chloroform into which treated and untreated nanocellulose was added and the solution was made into 50 μm thick

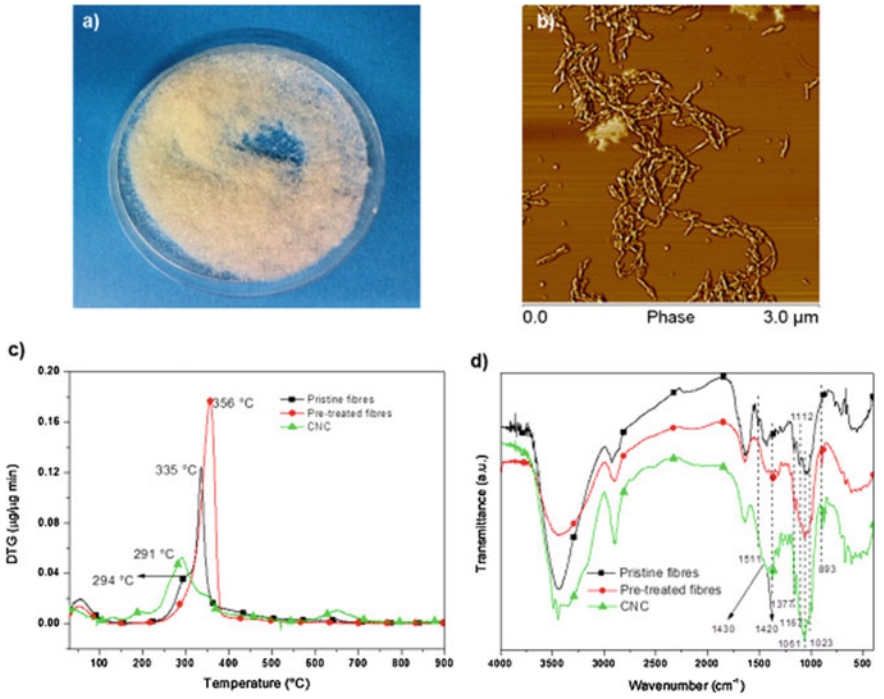

Fig. 5 Digital image **a**; AFM structure **b**, thermal behavior **c** and chemical structure **d** of the cellulose materials prepared from *Posidonia oceanica* (Fortunati et al. 2015). Reproduced with permission from Elsevier

films by solution casting (Fortunati et al. 2015). Nanocrystals obtained had a length of 180 nm and diameter of 4.9 nm and had typical cellulose I structure (Fig. 5). Acid hydrolysis reduced the thermal stability of the nanocellulose but did not affect the transparency of PLA films. Addition of the nanocrystals into PLA increased the porosity but reduced brittleness at concentration of 3% and after modification with the detergent. Also, better crystallization was observed in the PLA films containing the nanocellulose. Considerable increase in the mechanical properties of PLA particularly when reinforced with surfactant modified nanocellulose was observed (Table 3).

Zinc oxide nanoparticles were used in addition to cellulose nanocrystals from *Posidonia oceanica* to further improve the properties of PLA for food packaging applications. Cellulose nanocrystals (length of 180 nm and diameter of 4.9 nm) extracted from *Posidonia oceanica* and zinc oxide nanoparticles were added into PLA (Luzi et al. 2017). The nanocrystals were modified by treating with phosphate ester of ethoxylatednonyl phenol and a surfactant. PLA and modified nanocellulose were dissolved in chloroform separately and later combined together (Fig. 6). ZnO nanoparticles were also dispersed in chloroform and combined with PLA to form binary blends and later combined with the cellulose and PLA solution to form tertiary

Table 3 Effect of unmodified (CNC) and surfactant modified cellulose nanocrystals (SCNC) on mechanical properties of PLA films (Fortunati et al. 2015). Reproduced with permission from Elsevier

Composition	Yield strength (MPa)	Elongation at yield (%)	Breaking strength (MPa)	Breaking elongation (%)	Young's modulus (MPa)
Neat PLA	14.7 ± 5.1	2.3 ± 0.5	16.5 ± 3.1	278 ± 34	1205 ± 100
PLA, 1% CNC	31.3 ± 1.6	3.0 ± 0.5	27.1 ± 6.3	200 ± 53	1330 ± 90
PLA, 1% SCNC	22.9 ± 4.2	2.6 ± 0.6	22.9 ± 1.2	286 ± 25	993 ± 190
PLA, 3% CNC	42.1 ± 2.0	2.7 ± 0.6	21.9 ± 3.5	101 ± 28	1930 ± 170
PLA 3% SCNC	25.7 ± 4.8	3.1 ± 0.1	20.2 ± 1.9	210 ± 48	800 ± 100

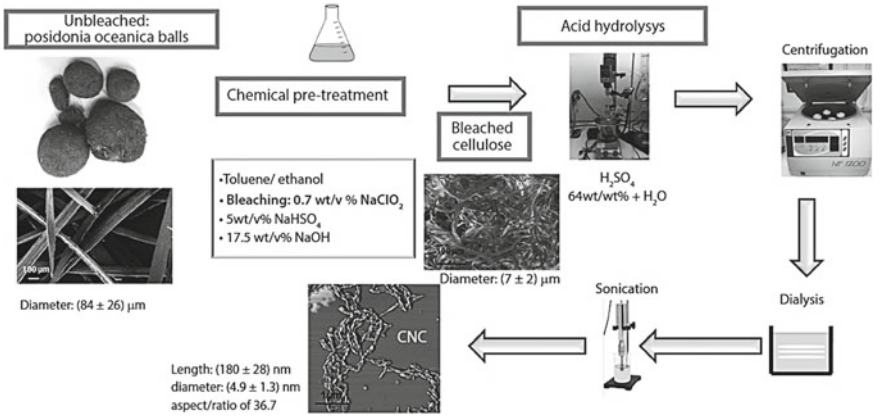

Fig. 6 Schematic of the preparation of cellulose nanocrystals for reinforcing with PLA (Luzi et al. 2017). Reproduced with permission through Creative Commons CC licence

blends (Luzi et al. 2017). Fibers were obtained after casting the solution and drying it under appropriate conditions. Addition of the nanomaterials into PLA separately did not affect the morphology of the nanocomposites whereas a more compact structure was formed in the case of the tertiary blends. Both tensile strength and elongation of PLA films increased due to the addition of the nanoparticles whereas water vapor permeability decreased which is preferable for food packaging applications (Table 4). There was no major effect of ZnO on the antimicrobial activity of the films.

A combination of inorganic nanofillers and cellulose fibers were used to reinforce PLA and obtain composites with improved properties (Piekarska et al. 2016). PLA used had density of 1.24 g/cm^3 with d and l-lactide content of 2.5 and 97.5%, respectively. Calcium carbonate (80 nm) (NCC), Closite 30B (MMT), and cellulose nanofibers (CF) were used individually and also in combination to reinforce

Table 4 Mechanical properties and water vapor permeability of PLA reinforced with ZnO and/or cellulose nanocrystals (Luzi et al. 2017). Reproduced with permission through Creative Commons CC license

Sample	Strength (MPa)	Elongation (%)	Modulus (MPa)	Water vapor permeability g mm/kPa h m^2	
				11–53% RH	100–53% RH
PLA	16.5 ± 3.1	277 ± 33	1205 ± 100	0.051 ± 0.004	0.067 ± 0.006
PLA 1s-CNC	22.9 ± 1.2	286 ± 25	993 ± 190	0.047 ± 0.002	0.063 ± 0.002
PLA 0.1 ZnO	20.5 ± 2.0	105 ± 10	1163 ± 33	0.048 ± 0.005	0.063 ± 0.007
PLA 0.5 ZnO	38.3 ± 3.6	87 ± 8	1210 ± 50	0.046 ± 0.003	0.058 ± 0.002
PLA 1s-CNC 0.1 ZnO	21.7 ± 1.6	250 ± 45	975 ± 60	0.044 ± 0.001	0.056 ± 0.001
PLA 1s-CNC 0.5 ZnO	23.7 ± 0.8	205 ± 15	990 ± 40	0.041 ± 0.002	0.052 ± 0.005

the PLA. PLA blends with NCC and MMT were made by melt mixing the materials and later combining with CF, when hybrid films were developed. Films of thickness 1 and 0.5 mm were extruded which were later compression molded into designated samples at 180 °C for 3 min. The clay particles had good dispersibility and did not show any agglomeration and addition of CF favored further dispersion. However, thermal stability of the hybrid PLA/MMT/CF films was lower than that of PLA/MMT but better than that of PLA/CF. Tensile properties of PLA improved with addition of both MMT or NCC but the improvement was further enhanced when CF was included into the MMT and NCC (Table 5).

PLLA based surfactants were developed and used as matrix with cellulose nanocrystals extracted from ramie fibers (Mariano et al. 2017). Nanocellulose obtained had average length of 200 nm, width of 7 nm and % crystallinity was 85%. The PLA based surfactants (PEG-b-PLLA) and Im-PLLA were prepared from L-lactide and other chemicals through ring opening polymerization. The prepared surfactants were combined with CNCs and solution cast to form films on a glass plate. Films formed were combined with PLA and extruded in a twin screw extruder at 170 °C and 200 bar pressure to form the composite samples. Addition of the surfactant PEG-b-PLLA increased the transmittance whereas Im-PLLA decreased the transmittance as indicated in Fig. 7. Thermal stability of the films had also increased due to the addition of Im-PLLA which was suggested to be due to the improved ionic interactions between the polymer and cellulose nanocrystals. However, it was also postulated that the surfactant could cause a decrease in molecular weight and shortening of PLA chains which leads to plasticization effect and reduces the crystallinity of the matrix (Mariano et al. 2017).

Table 5 The properties of PLA films reinforced with MMT, NCC, CF and their hybrids (Piekarska et al. 2016). Reproduced with permission from Elsevier

Sample	Temperature (°C)	Yield stress (MPa)	Stress at break (MPa)	Elongation (%)	Storage modulus (MPa)
PLA	25	49.3 ± 0.1	47.3 ± 0.1	29.0 ± 3.8	3011 ± 43
PLA/CF	25	–	44.8 ± 1.2	7.1 ± 0.3	3500 ± 8
PLA/NCC	25	44.1 ± 2.4	42.2 ± 2.2	31.7 ± 0.7	3296 ± 4
PLA/NCC/CF	25	–	41.5 ± 0.1	5.8 ± 0.5	4340 ± 45
PLA/MMT	25	49.9 ± 1.6	45.1 ± 0.7	7.8 ± 0.6	3600 ± 63
PLA/MMT/CF	25	–	42.1 ± 2.1	5.1 ± 0.3	4578 ± 34
PLA	35	47.5 ± 0.5	42.8 ± 0.7	37.4 ± 6.4	2938 ± 43
PLA/CF	35	33.4 ± 3.0	32.5 ± 1.4	6.2 ± 0.1	3410 ± 8
PLA/NCC	35	43.0 ± 0.7	32.7 ± 1.8	47.4 ± 4.0	3216 ± 2
PLA/NCC/CF	35	35.8 ± 2.9	29.8 ± 1.0	6.2 ± 0.1	4224 ± 46
PLA/MMT	35	43.8 ± 0.6	37.2 ± 0.2	9.4 ± 1.3	3515 ± 47
PLA/MMT/CF	35	28.7 ± 4.0	27.6 ± 4.1	4.4 ± 0.3	4444 ± 58

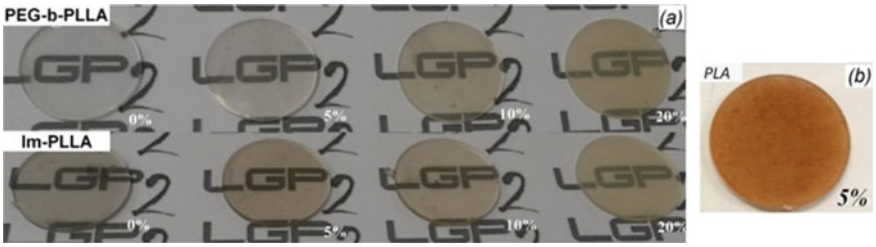

Fig. 7 Effect of adding various levels of modified surfactants onto PLA and injection molded into discs **a** and image of unmodified PLA composites (Mariano et al. 2017). Reproduced with permission from American Chemical Society through open access publishing

A ternary blend of microcrystalline cellulose, nanocrystal cellulose and nanolignin was combined with unmodified and modified PLA to develop films with antimicrobial properties for food packaging applications (Yang et al. 2016). Different combinations of the three polymers were used to develop films with varying properties. Films containing 3% nanocellulose had good transparency to UV light but the presence of lignin in the films led to blocking of UV light. Changes were also observed in the thermal and crystal behavior which led to grafted PLA providing better compatibility and hence improved crystallization and thermal resistance. A lowest crystallization temperature of 96 °C was possible due to the presence of cellulose and lignin nanoparticles. Addition of cellulose led to larger increase in tensile properties compared to lignin nanoparticles. Pure PLA films were susceptible to microbes whereas addition of 3% lignin provided high resistance and even 1% cellulose in the ternary blend

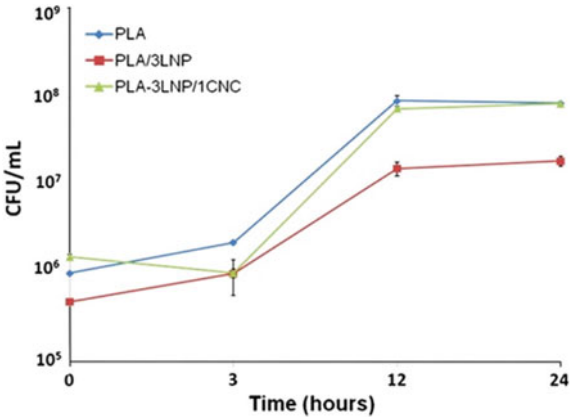

Fig. 8 Ability of PLA and cellulose nanoparticles and lignin nanoparticle containing blend films to resist growth of Pseudomonas *syringae pv.* tomato (Pst) after incubation for up to 24 h (Yang et al. 2016). Reproduced with permission from Elsevier

leads to marginal decrease (Fig. 8). It was suggested that the ternary films could be used to detect pathogens in food when used as packaging (Yang et al. 2016).

Nanowhiskers extracted from oil palm empty fruit bunch fibers were used to improve the properties of PLA films (Haafiz et al. 2016). Cellulose nanowhiskers (with lengths of about 100 nm and widths of about 10 nm) were extracted using the acid hydrolysis approach. Chemical modifications were done to the whiskers to improve swelling. Modified nanocellulose whiskers were added into PLA dissolved in chloroform in 1, 3 or 5 weight % and cast into films. Atomic force microscopy (AFM) images confirmed the nanoscale dimensions but revealed that the cellulose was in spherical shape before hydrolysis but converted into rod like whiskers after hydrolysis. Uniform distribution and good interaction but poor interfacial adhesion was observed between nanowhiskers and PLA up to a fiber content of 3%. Higher levels of reinforcement led to agglomeration and also reduction in properties. Due to these changes, strength and modulus of the films increases but elongation decreases with increasing levels of nanocellulose in the films. However, thermal behavior of PLA films was found to improve after the addition of the nanocellulose (Haafiz et al. 2016).

3 PLA Reinforced with Nanofibers from Bacteria

Similar to plant sources, nanofibrils obtained from bacterial cellulose have also been studied for potential improvement in the performance of PLA films (Martinez-Sanz et al. 2012). Bacterial cellulose was prepared from the strain *Gluconacetobacter* xylinus 7351 and used to improve the properties of PLA having molecular weight of 150,000 g/mol. The cellulose developed was treated with sulfuric acid at 50 °C for three days to form the nanowhiskers with a yield of about 79%. The PLA and bacterial cellulose nanowhiskers were dissolved using HFIP and electrospun into fibers using a voltage of 10–12 kV and extrusion speed of 0.66 mL/h. Nanocomposites were

developed from the cellulose using three different approaches: electrospinning, solution casting and injection molding. Films developed using electrospun nanowhiskers showed lesser reduction in transparency and more homogenous distribution. Considerable differences in fracture morphology were observed due to the differences in compatibility (Fig. 9). Melting and glass transition were not affected due to the addition of the nanocellulose. However, melting enthalpy and cold crystallization

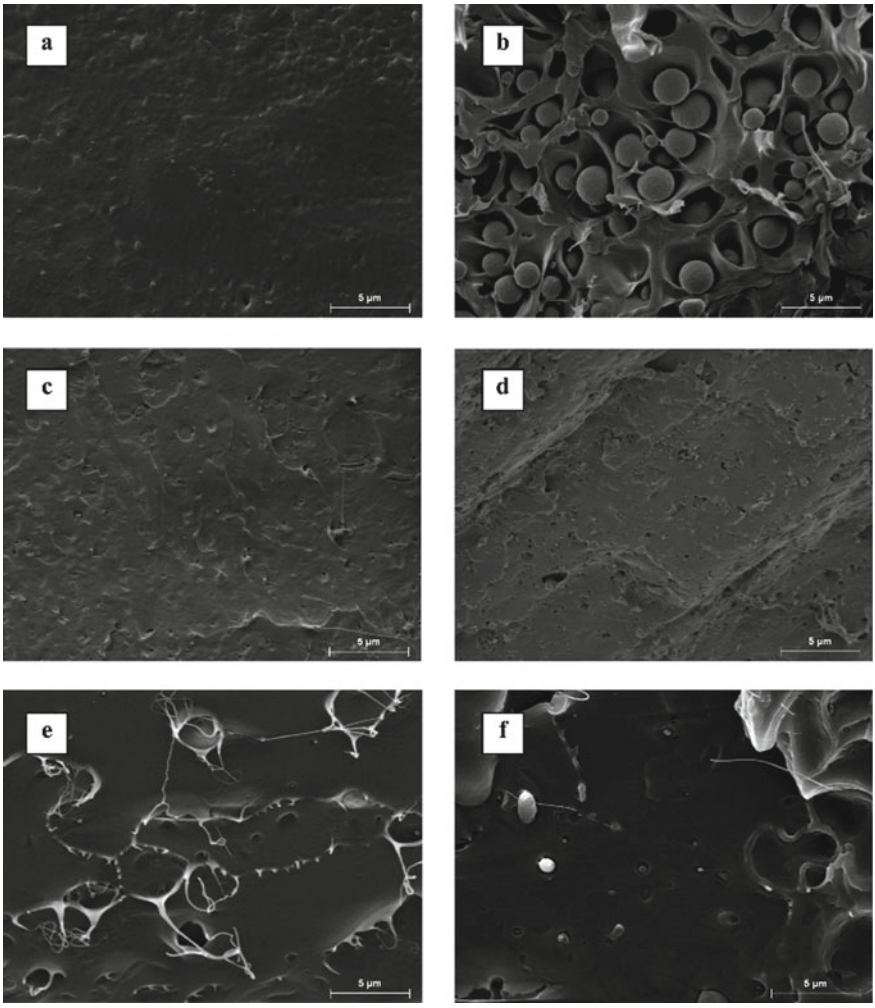

Fig. 9 SEM images of pure PLA **a** PLA films made using 16% EVOH **b**, 1% bacterial cellulose containing film made using electrospinning **c**, 2% bacterial cellulose containing film made using electrospinning **d**, 2% cellulose freeze dried **e**, 2% bacterial cellulose made using extrusion, **f** (Martínez-Sanz et al. 2012). Reproduced with permission from American Chemical Society

Table 6 Thermal behavior of PLA and PLA nanocomposites containing bacterial cellulose incorporated into PLA using various techniques. Melting enthalpy (ΔHm), cold crystallization temperature (Tcc), cold crystallization enthalpy (ΔHCC), PLA crystallinity (Xc), and glass transition temperature (Tg) (Martínez-Sanz et al. 2012). Reproduced with permission from American Chemical Society

Samples	T_m (°C)	ΔH_m (J/g) PLA	T_{CC} (°C)	ΔH_{CC} (J/g) PLA	X_c (%)	T_{g1} (°C)	T_{g2} (°C)
PLA	150.8 ± 2.5	26 ± 0.7	119 ± 1.8	12 ± 0.5	16 ± 0.3	60 ± 1.8	60 ± 1.1
1% ES	151.6 ± 1.5	22 ± 0.5	105 ± 0.9	4.3 ± 3.7	19 ± 4.6	59 ± 0.0	59 ± 0.3
2% ES	148.5 ± 2.0	25 ± 1.1	110 ± 1.4	13 ± 0.9	13 ± 0.2	58 ± 0.5	59 ± 0.8
3% ES	150.3 ± 3.2	18 ± 0.6	109 ± 1.9	2.6 ± 1.6	17 ± 1.1	59 ± 0.6	59 ± 0.3
1% FD	150.9 ± 2.1	24 ± 0.8	119 ± 1.6	9.4 ± 0.6	16 ± 1.1	58 ± 1.3	59 ± 1.0
2% FD	150.2 ± 0.7	24 ± 2.9	120 ± 3.3	9.3 ± 0.4	16 ± 2.6	57 ± 2.3	59 ± 0.1
PLA, 16% EVOH	151.3 ± 1.5	22 ± 1.0	123 ± 1.7	8.1 ± 1.9	15 ± 1.0	56 ± 0.5	59 ± 0.5
1% P	151.0 ± 2.4	27 ± 0.4	121 ± 2.1	11 ± 0.4	18 ± 0.8	59 ± 1.3	59 ± 1.3
2% P	149.8 ± 0.1	26 ± 0.1	120 ± 1.2	7.6 ± 3.7	19 ± 3.9	59 ± 1.2	59 ± 0.3

temperature were affected by the method adopted to add the cellulose nanowhiskers into PLA (Table 6).

About 17% increase in elastic modulus and 14% in tensile strength were obtained when 2–3% nanowhiskers were incorporated. Water vapor permeability decreased by 43% at 3% fiber loading whereas significant improvements in oxygen barrier properties were noticed even when the nanofiber loading was 1%. Bacterial nanocellulose, particularly after electrospinning were found ideal to improve the barrier and mechanical properties required for food packaging and other applications (Martínez-Sanz et al. 2012). Bacterial cellulose pellicles prepared by mechanical disintegration having width of about 150 nm and tape-like structure were added into molten PLA (molecular weight between 195,000 and 205,00 Da and density of 1.24 g/cm^3) and extruded in the form of sheets of about 0.5 mm thickness. No changes were observed in the degradation temperature of PLA but the glass transition and cold crystallization was found to increase due to the addition of bacterial cellulose. Ability of the bacterial cellulose to act as a nucleating agent and even dispersion in the matrix were suggested to be the reasons for the changes in thermal behavior. Good interfacial interaction leading to decreased segmental mobility lead to increase in modulus. About 15% increase in strength and 10% increase in tensile modulus was possible even with an addition of 5% of nanofibers (Panaitescu et.al. 2017).

It was observed that compression molding sheets of electrospun PLA nanofibers at specific temperature and time leads to formation of transparent films with substantial improvement in toughness (Somord et al. 2018). Utilizing this phenomenon of self-reinforcement, PLA nanocomposites with improved performance properties were prepared by adding modified and unmodified bacterial cellulose (Somord et al. 2018). Bacterial cellulose was cultivated from *Gluconacetobacter xylinus* strain TISTR 975

and obtained in the form of pellicles with thickness of 1 cm. These pellicles were homogenized and maintained as a suspension in water. The bacterial cellulose was also treated with 3-(trimethyoxysilyl) propyl methacrylate to improve adhesion and compatibility with PLA. Electrospun PLA mats were placed in a filter and BC or modified BC (MBC) suspension (1 or 10%) was poured onto the mats. Additional PLA mats were stacked and BC was added onto the PLA as shown in Fig. 10. After the desired layers of PLA and BC were added, the multilayer structure was treated with ethanol, rinsed in water and dried at 50 °C for 150 min. Rectangular pieces of 3 cm × 3 cm × 150 μm were cut from the PLA-BC treated membranes and placed in a mold and compression molded to form films. Films without and those containing 1% cellulose were transparent but the transparency decreased with increasing bacterial cellulose content. Addition of BC lead to improvement in tensile properties due to the reinforcing effect which was more pronounced when MBC was used (Table 7). Thermal resistance increased and water vapor permeability had decreased after the addition of bacterial cellulose (Somord et al. 2018).

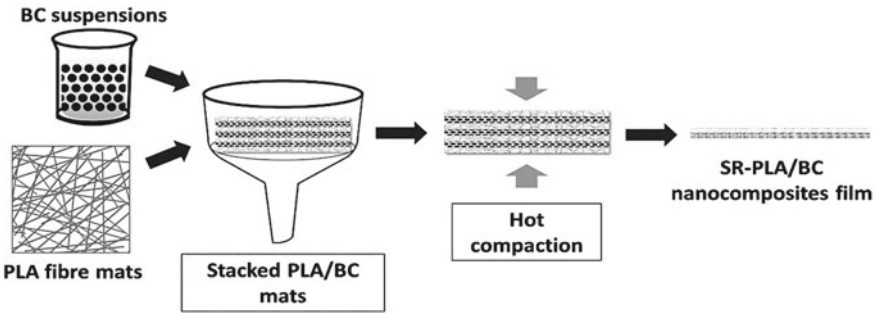

Fig. 10 Schematic of the process of converting bacterial cellulose reinforced PLA nanocomposites through self-reinforcement technique (Somord et al. 2018). Reproduced with permission through Creative Commons Attribution License

Table 7 Tensile properties of neat PLA electrospun membranes, self-reinforced PLA and those reinforced with 1 or 10% of BC or MBC (Somord et al. 2018). Reproduced with permission through Creative Commons Attribution License

Sample	Strength (MPa)	Modulus (GPa)	Elongation (%)	Toughness (MJ/m^3)
PLA	49.9 ± 3.0	2.8 ± 0.1	5.2 ± 2.4	2.2 ± 1.0
Neat SR-PLA	61.2 ± 2.0	2.2 ± 0.3	15.6 ± 8.9	8.5 ± 5.0
SR-PLA-1% BC	70.1 ± 2.0	3.0 ± 0.2	0.2 ± 1.2	3.6 ± 0.9
SR-PLA-1% MBC	79.5 ± 4.9	3.1 ± 0.3	46.8 ± 6.2	35.0 ± 4.4
SR-PLA-10% BC	79.6 ± 1.8	3.5 ± 0.1	3.1 ± 0.3	1.7 ± 0.3
SR-PLA-10% MBC	87.5 ± 3.5	3.8 ± 0.1	2.8 ± 0.2	1.9 ± 0.5

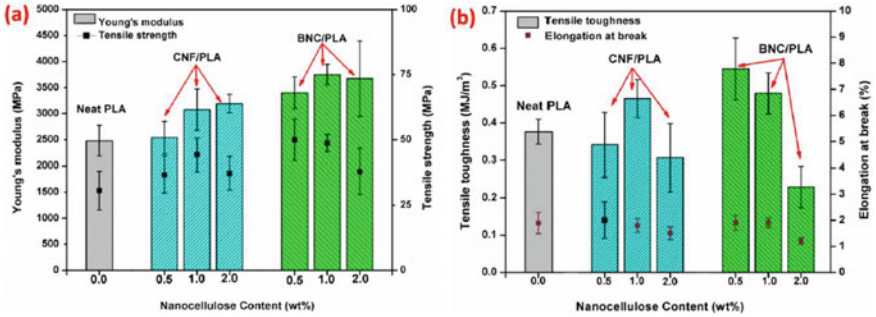

Fig. 11 Tensile properites of PLA films reinforced with cellulose nanofibrils (CNC) and bacterial nanocellulose (BNC) with increasing content of nanofibers (Gitari et al. 2019)

In a comparative study, it was found that bacterial nanocellulose was able to provide better mechanical properties than cellulose nanofibrils obtained from softwood (Gitari et al. 2019). It was reported that during the extraction of nanofibers from bacteria, formation of carbonate occurs which reduces bonding between the nanocellulose and improves dispersion in the PLA matrix. Both the nanofibers and nanocellulose decreased glass transition whereas nanofibrils increased and nanocellulose decreased the cold crystallization temperature. In terms of mechanical properties, there was an increase of Young's modulus from about 2500 to 3672 MPa. Similarly, strength of the composites containing bacterial nanocellulose increased to 50 MPa, higher than that for the cellulose fibers (Fig. 11). Elongation and toughness of the films decreased due to the addition of the nanomaterials (Gitari et al. 2019).

4 PLA Composites Reinforced with Chitin-Based Nanomaterials

In addition to cellulose, other polysaccharides particularly starch and chitin/chitosan have also been used as reinforcement for developing PLA nanocomposites. A summary of the various attempts made to use chitin and starch in PLA nanocomposites is given in Table 8.

As seen from the table, both nanocrystals and nanofibrils from chitin have been formed and incorporated into PLA through solution casting or thermoplastic processing. Substantial improvements in mechanical and performance properties could be achieved due to the reinforcing effect (Scaffaro et al. 2017). In a recent study by Coltelli et al., chitin nanofibrils (20 μm in length and 90 nm in width) were combined with poly(ethylene glycol) (PEG) and used to develop PLA nanocomposites. Since chitin nanofibrils tend to agglomerate in water suspensions and it is difficult to incorporate them into PLA, the fibrils were first combined with PEG in 1:1 ratio and made into pre-composites. This pre-composite was combined with PLA

Table 8 Types of chitin/starch used as reinforcement for developing PLA nanocomposites and resulting properties (Scaffaro et al. 2017). Reproduced with permission from Springer Nature

Content (wt%)	Filler modification	Other components	Preparation method	Main results
ChNCs up to 10%	Acetylation	–	Solvent casting	E = +37%, TS = +45%
ChNCs 1%	–	TEC	Extrusion	E = +67%, TS = +28%
ChNCs 1%	–	Glycerol triacetate, polybutylene adipate-co-terephthalate, talc	Film blowing	E = +75%, TS = +65%
ChNCs up to 5%	–	PHBV, DMAC	CO_2 Foaming	TS = +133%
ChNCs up to 10%	l-Lactide	–	Solvent casting	E = +133%, TS = +63%
ChNCs up to 10%	l-Lactide	–	Electrospinning	E = +143%, TS = +49%
ChNCs up to 5%	l-Lactide	MgO	Injection molding	E = + 18%, TS = +33%
SNCs 3.2%	PLA	–	Grafting reaction	Successful grafting of PLA onto SNCs
SNCs up to 8%	Cross-linking	–	Solvent casting	E = +35%, TS = +12%
SNCs up to 30%	PCL	–	Solvent casting	TS = +132%, ε_b = +400%
SNCs up to 2%	Ozone-mediated styrene grafting	–	Solvent casting	WVP up to − 52%, DTG_{peak} up to +130 °C

in a twin screw extruder and made into specimens by injection molding at 180 °C, 650 bars pressure, holding time of 15 s and mold temperature of 135 °C. Addition of PEG increased the compatibility between chitin and PLA leading to improved thermal resistance. Although no major improvements in tensile strength or modulus were observed, elongation of the nanocomposites was high at about 150%. It was suggested that PEG formed a coating on the nanofibrils and improved extensibility but formed a layer between chitin and PLA preventing reinforcing effect (Coltelli et al. 2019). In another approach, chitin obtained from crabs were made into nanowhiskers by acid hydrolysis and later by treating chitin powder in 5% KOH solution and boiling for 6 h. The powder obtained was bleached and retreated with 3 mol/L HCl at 102 °C for 5 h. The obtained chitin nanowhiskers were further modified by grafting l-lactide via ring-opening polymerization. The modified and unmodified chitin whiskers were added into PLA dissolved in chloroform and later solution cast to form films. FTIR and NMR studies confirmed successful grafting of oligo(L-lactide) side chains onto

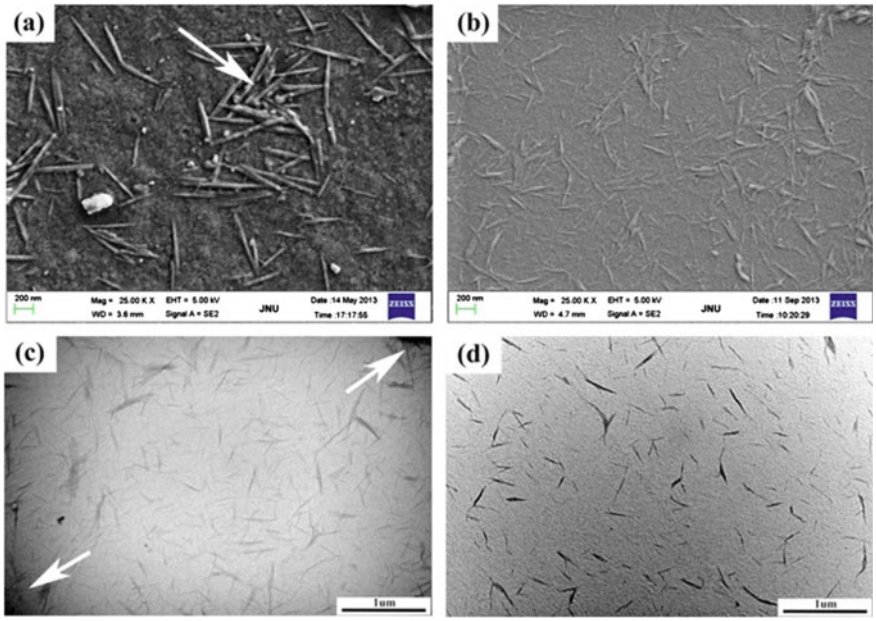

Fig. 12 SEM (**a** and **b**) and TEM (**c** and **d**) images of unmodified and grafted chitin nanowhiskers (Li et al. 2016). Reproduced with permission from Elsevier

chitin. No major changes in the crystallinity or crystal size of chitin were noticed due to the grafting. Length of unmodified nanowhiskers was between 200 and 800 nm and diameter was between 20 and 70 nm (Li et al. 2016). Comparatively, the grafted whiskers had length between 150 and 400 nm and diameter was between 5 and 55 nm. The decrease in the diameter of the fibrils and better dispersibility in PLA matrix was noticed in the SEM and TEM images (Fig. 12) (Li et al. 2016). When incorporated into PLA, the whiskers caused changes in the crystallization rates and spherulite formation. Marginal decrease in crystallinity and melting temperature was also noticed. Substantial increase in tensile properties with highest strength of 30.5 MPa and modulus of 1.5 GPa and fracture energy of 333 J/mm were obtained when 5% grafted whiskers were used as reinforcement (Fig. 13). Nanocomposites containing grafted PLA also exhibited better cytocompatibility to MC3T3-E1 cells. Considerable effect of chitin nanocrystals (diameter between 7 and 25 nm, length between 314 and 1571 nm and crystallinity of 91%) on the crystallinity, thermal behavior and mechanical properties was observed when used as reinforcement for triethyl citrate plasticized poly (lactic acid).

Chitin nanoparticles and plasticizer were dissolved and made into a solution and added into an extruder along with PLA. Amount of components added was controlled to obtain a nanocrystal concentration of 1%. PLA pellets extruded were compression molded into films by processing at 190 °C for 3.5 min at a pressure of 4 MPa. After compression, the films were cooled to room temperatures at two different rates (fast

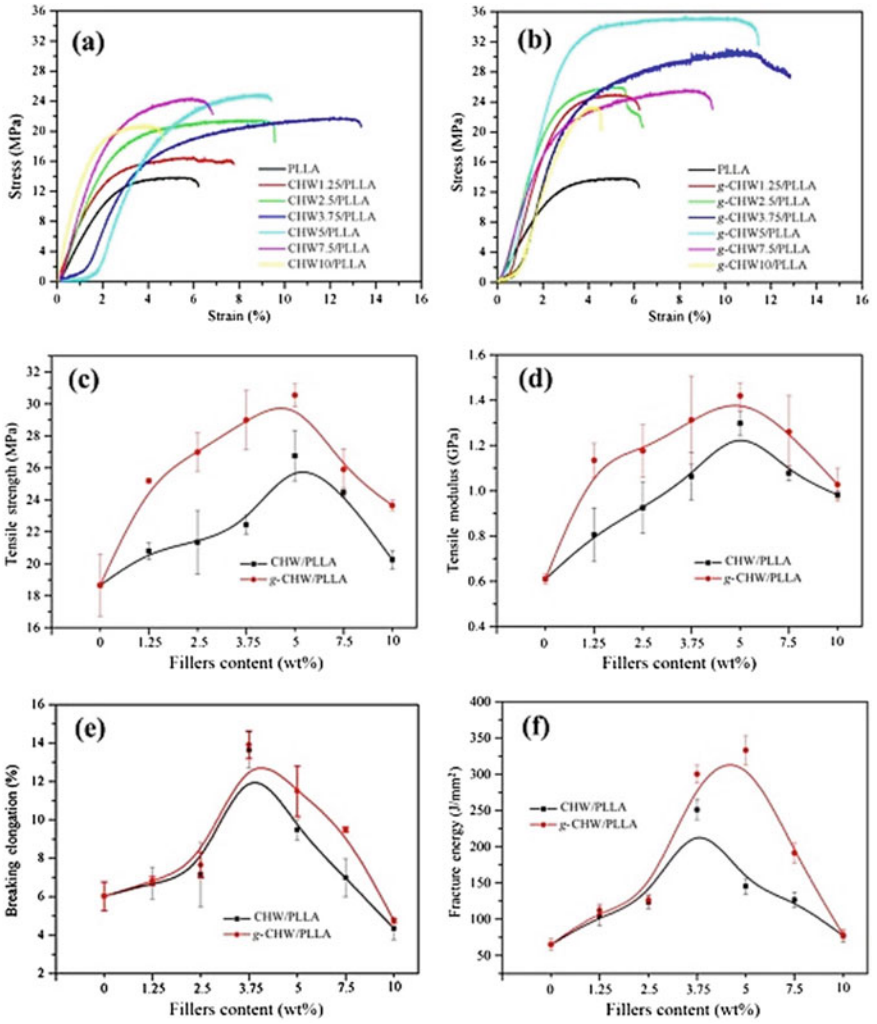

Fig. 13 Effect of addition of unmodified and grafted chitin nanowhiskers on the tensile properties of PLA nanocomposites (Li et al. 2016). Reproduced with permission from Elsevier

cooling for 5 min or slow cooling for 20 min) to vary the crystallization rate and extent of PLA. Differences in the cooling rates affected the crystallinity, transparency and tensile properties, particularly elongation. Faster cooling provided films with higher transparency (Fig. 15) and crystallinity and improvement in tensile properties was observed until 1% reinforcement (Hererra et al. 2016). Changes in the tensile properties of the PLA nanocomposites obtained using fast or slow cooling are shown in Table 9 and Fig. 14.

Table 9 Effect of fast cooling (FC) and slow cooling (SC) on the tensile properties of PLA films with and without chitin nanoparticles (Hererra et al. 2016). Reproduced with permission from Elsevier

Type of PLA	Yield strength (MPa)	Ultimate strength (MPa)	Young's modulus (GPa)	Elongation at break (%)	Work of fracture (MJ/m^2)
FC PLA-TEC	3.7 ± 1.2	22.4 ± 4.1	0.3 ± 0.2	305 ± 53	32.2 ± 12.8
FC-PLA-TEC-ChNc	21.4 ± 3.9	21.0 ± 2.0	1.2 ± 0.4	262 ± 24	36.9 ± 4.4
SC PLA-TEC	19.6 ± 1.2	15.8 ± 1.1	0.6 ± 0.1	91 ± 38	16.1 ± 6.4
SC-PLA-TEC-ChNc	20.9 ± 0.5	20.3 ± 0.5	1.0 ± 0.3	16 ± 4	2.9 ± 0.8

Fig. 14 Influence of cooling rates on the transparency of neat and chitin nanowhisker reinforced PLA as seen visually and using an optical microscope (Hererra et al. 2016). Reproduced with permission from Elsevier

5 PLA Containing Starch-Based Nanomaterials

Starch nanocrystals prepared from two sources, high amylopectin maize starch and acetylated starch were prepared and used as fillers for PLA. Starch nanocrystals were prepared by acid hydrolysis and later acetylated by treating with glacial acetic acid to obtain a degree of substitution of 0.99. The PLA and starch nanoparticles were dispersed in dichloromethane and cast onto glass plates to form films. PLA reinforced with unmodified starch had a rougher morphology due to agglomeration of the particles and poor bonding between PLA and starch. The roughness was found to increase with increasing amount of nanofillers. Acetylation of starch improved adhesion and interfacial interaction that provided a relatively smoother surface to the nanocomposites (Fig. 15). A significant decrease (25%) in oxygen permeability was

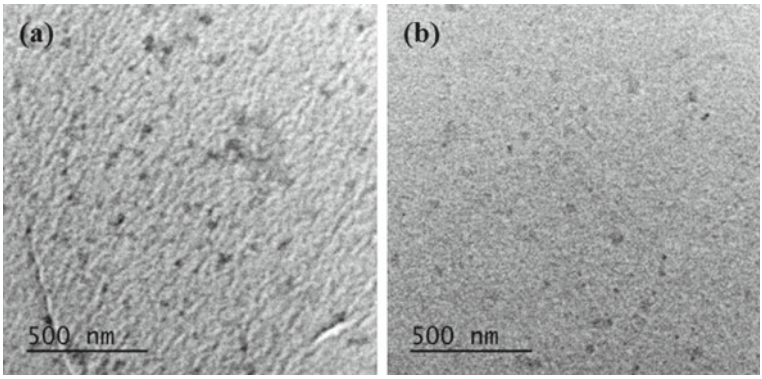

Fig. 15 TEM images of PLA films containing unmodified (left) and acetylated starch nanocrystals (right) show differences in agglomeration and interaction (Takkalkar et al. 2019). Reproduced with permission from Springer Nature

observed for the films reinforced with acetylated nanostarch. Similarly, the mechanical properties of the starch nanofiller containing PLA were higher but elongation was lower compared to neat PLA (Takkalkar et al. 2019).

Starch nanocrystals were prepared by acid hydrolysis of starch by treating with sulfuric acid at 40 °C for 5 days. Lactic acid was grafted onto the nanocrystals using tetrahydrofuran at 60 °C for 30 min. PLA nanocomposites were prepared by adding the modified starch (5–30%) into PLA solution and later casting the solution into films (Zamir et al. 2019). Grafted samples showed a decrease in atomic concentration of C-H from 13 to 4% and an increase in COO concentration confirming grafting. There was no change in the crystal structure or % crystallinity of starch before and after grafting. Considerable increase in thermal stability with initial weight loss of 4% for grafted samples compared to 37% for the ungrafted samples was suggested to be due to the hydrophobicity imparted after grafting which was also confirmed by the contact angle measurements. In terms of the nanocomposites, the Tg of PLA did not show any major change but the cold crystallization temperature decreased from 124 to 113 °C when 30% modified starch nanocrystals were included. Addition of up to 5% modified starch nanocrystals did increase crystallization of PLA but the crystallization decreased at higher concentrations. Modulus of the composites showed marginal increase up to a nanoparticle concentration of 10% (Zamir et al. 2019).

Instead of directly adding nanomaterials into PLA, a novel approach of combining cellulose nanocrystals with starch and poly(vinyl alcohol), electrospinning the blend and later adding the electrospun fibers into PLA to form films was followed. Addition of cellulose nanocrystals into starch nanofibers had improved the dispersibility of the polymers in PLA. Although starch and cellulose had poor crystallinity, there was no major influence on the crystallinity of the blend PLA films (Dicastillo et al. 2017). Marginal increase in strength and elongation were observed in the PLA films but agglomeration occurred at higher concentrations. Decrease in transparency and

water vapor permeability were also attributed to the presence of electrospun fibers containing the cellulose nanoparticles (Dicastillo et al. 2017).

6 Nanoclay Reinforced PLA Composites

Nanoclay of different dimensions and properties has been used to reinforce or improve performance of PLA. A nanoclay C30B was dispersed in dichloromethane and ultrasonicated for 3 h at 200 W and homogenized for 90 min. PLA solution was also predispersed in dichloromethane and combined with the nanoclay solution. The suspension was cast onto molds, cured at 23 °C for 16 h and later dried at 50 °C for 24 h to form the films. Compared to nanocellulose crystals or cellulose nanofibers made from sisal fibers, the clay reinforced PLA had inferior oxygen barrier, mechanical and also thermal properties (Fig. 16) (Trifol et al. 2016).

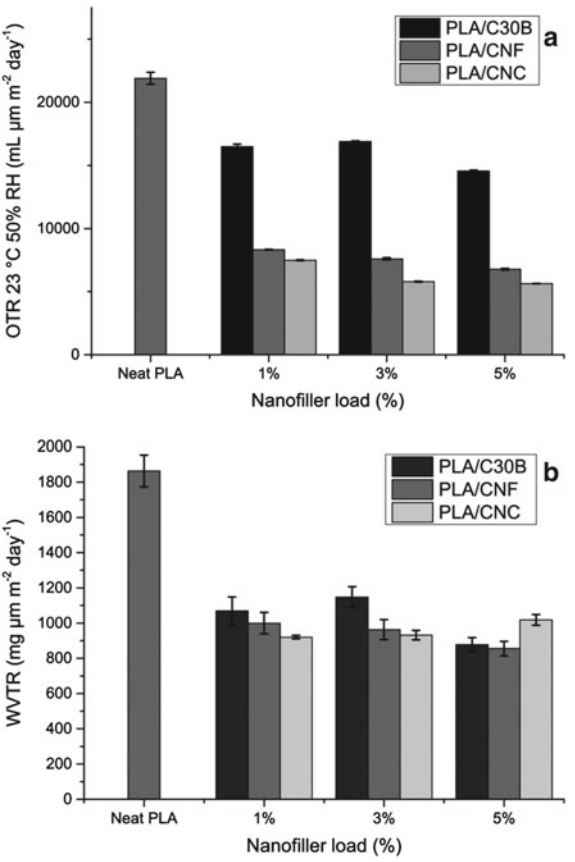

Fig. 16 Comparison of the oxygen and water vapor permeability of PLA containing cellulose nanofibers, nanocrystals and nanoclay C30B (Trifol et al. 2016). Reproduced with permission from John Wiley and Sons

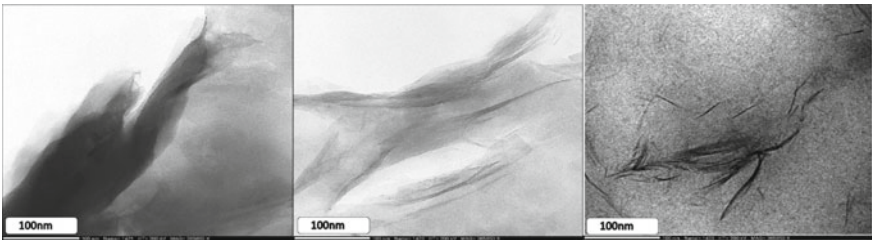

Fig. 17 TEM images depicting the intercalating behavior of PLLA films modified with MMT (left), organically modified 350 (center) and C30B clay (right) (Fordiani et al. 2013). Reproduced with permission from John Wiley and Sons

Hence, hybrid nanocomposites were made using a combination of PLA, nanoclay and cellulose nanofibers. Clay used was an organo-modified montmorillonite (MMT) having particle size of 16–22 μm and modified using octadecylamine. Cellulose nanowhiskers were separated from microcrystalline cellulose using a sequential chemical extraction and ultrasonification approach. Extracted cellulose whiskers were combined with PLA and modified MMT and cast into films. PLA was found to have polar interactions with both clay and cellulose. Tensile properties of the hybrid films increased up to a cellulose content of 3% and ductility of the films also improved (10–90%). Although the nanoclay was well dispersed and intercalated with PLA, it was suggested that modifications to cellulose to improve interactions would probably lead to better film properties (Arjmandi et al. 2015a; b). A green modification approach was used to improve intercalation of nanoclay with PLA (Fordiani et al. 2013). To achieve the enhanced intercalation, a complex containing ulvan and glycoproteins was extracted from seaweeds and used an as additive to PLA and the improvement in properties was studied using C30B clay and MMT. TEM images (Fig. 17) showed considerably improved intercalation and less aggregation for the modified clay containing films compared to C30B or MMT containing films. It was found that the nanoclay improved crystallization kinetics and also caused decrease in interfacial energy leading to the better intercalation.

In an attempt to increase the properties of hybrid PLA films, cellulose nanowhiskers obtained from MCC were modified through acid hydrolysis to obtain an average particle size of 50 μm and later combined with PLA and nanoclay. The hybrid constituents were combined together using chloroform and cast into films with different levels of nanoclay and cellulose (Arjmandi et al. 2016). Presence of cellulose nanowhiskers substantially increased the biodegradation of the samples and hence the weight loss. Increasing cellulose content caused higher degradation with a maximum weight loss of 2.5% after 8 weeks of burying the samples containing 9% cellulose. Similarly, thermal stability improved whereas activation energy decreased due to the addition of cellulose, particularly above 5%. It was suggested that the cellulose and PLA had polar interactions which led to increase in tensile strength from 18 to 36 MPa at 1% reinforcement. However, agglomeration of the nanowhiskers at higher concentrations leads to substantial decrease in strength. Elongation of the films also showed

a similar trend with strength, but the modulus of the films continually increases with cellulose content. Nanoclay in the hybrid films showed good intercalation and assisted in the dispersion of the cellulose nanowhiskers. Presence of nanowhiskers reduced water vapor transmission but did not affect the transparency (Arjmandi et al. 2016). Although the presence of nanoclay was found to improve performance properties of hybrid PLA films, the role of nanoclay with respect to its ability to replace cellulose nanowhiskers was not clearly understood. When nanoclay content was progressively increased and cellulose content was decreased, it was found that highest tensile strength could be obtained at a cellulose content of 1% and nanoclay content of 4% with 79% improvement in ductility (Fig. 18). Higher nanoclay content increased thermal stability whereas cellulose increased biodegradability Arjmandi et al. 2015a, b).

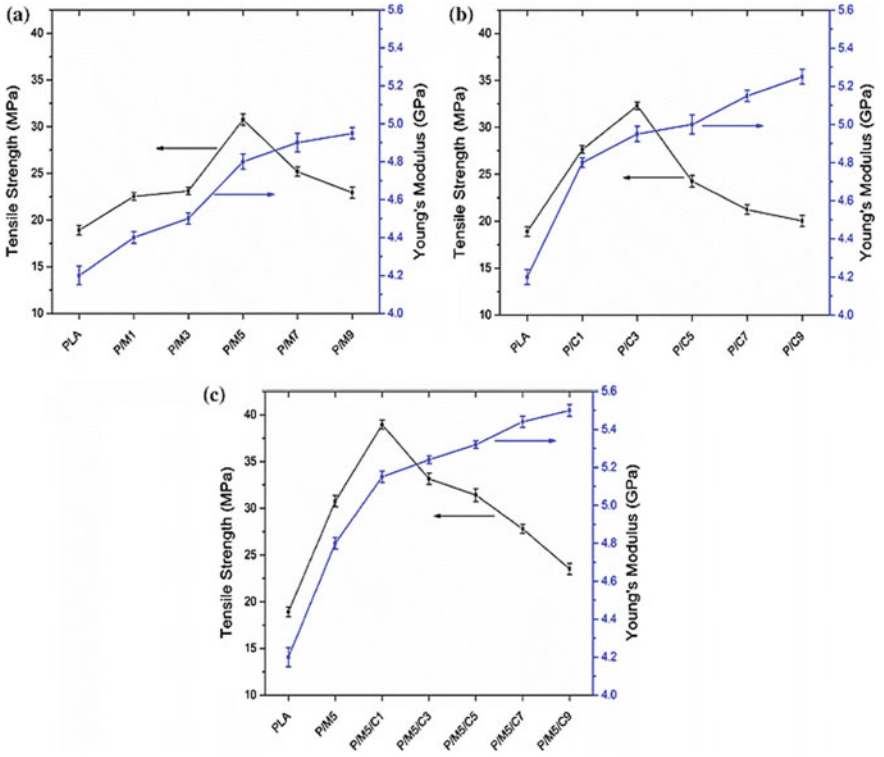

Fig. 18 Influence of amount of nanoclay and cellulose nanowhiskers on the tensile properties of PLA films (Arjmandi et al. 2015a; b). Reproduced with permission from Springer Nature

Table 10 Properties of films developed from CNF, PLA and their blends containing 1% casein as compatibilizer (Khakola et al. 2018). Reproduced with permission from Elsevier

Parameter	CNF	PLA	CNF/PLA	CNF/PLA, 1% casein
Density (g/cm^3)	1.23 ± 0.01	1.21 ± 0.01	1.02 ± 0.02	1.08 ± 0.01
Tensile strength (MPa)	86 ± 6	1.6 ± 0.1	70 ± 5	78 ± 5
Tensile index (Nm/g)	99 ± 12	1.4 ± 0.0	69 ± 3	72 ± 5
Breaking strain (%)	1.8 ± 0.2	318 ± 13	2.3 ± 0.3	5.3 ± 0.3
Elastic modulus (GPa)	10.1 ± 0.6	0.01	5.6 ± 0.4	6.3 ± 0.3
Tensile energy absorbed (J/g)	1.1 ± 0.1	3.3 ± 0.2	1.7 ± 01	2.7 ± 01

7 Protein Compatibilized PLA Nanocomposites

Another approach to improve the compatibility between cellulose nanoparticles and PLA was attempted by using the milk protein casein (Khakola et al. 2018). Nanofibrillar cellulose was prepared by treating bleached softwood kraft pulp with sodium for defibrillation and later with mechanical refining. Casein proteins were dispersed in water and later treated with bicarbonate and heated for 30 min at 45 °C to cause thermal denaturation. Casein and cellulose nanofibril suspensions were combined with PLA latex and filtered to form a powder which was later compression molded at 80 °C, 1800 Pa for 2 h. Work of adhesion (52–60 mJ/m^2) and pull-out force (372–420 mJ/m^2) showed considerable increase with the incorporation of casein into the PLA and cellulose nanofibrils containing films. Presence of casein increased the density of the composite films, decreased the number of voids which could promote better stress distribution between the matrix and reinforcement confirming that casein functioned as a compatibilizer. Consequently, considerable increase in tensile properties had occurred (Table 10). It was reported that casein compatibilized PLA could be used to develop 3D shaped cellulose-based packaging materials.

8 Conclusions and Future Perspectives

Nanomaterials have proven to effectively improve the performance properties of poly (lactic acid) based materials. Cellulose based nanofibers, nanoparticles derived from wood and non-wood sources including bacteria have been predominantly used as reinforcement/fillers. Several authors have also developed hybrid PLA nanocomposites combining nanoclay, proteins or other additives to improve the compatibility between PLA and the additives. Similarly, chemical modifications such as grafting have also been adopted. Inclusion of nanomaterials has primarily led to increase in mechanical properties, decrease in water and oxygen transmission and even resistance to heat and UV radiation. However, use of nanofillers above the optimum concentration has led to decrease in properties including transparency, strength and

modulus. Although most studies confirm some interaction between the nanomaterials and PLA and improvement in properties, suitability of the composites developed for specific applications has not been reported. Using available literature, additional studies have to be conducted to tailor the composites for targeted applications, particularly for food and medical applications due to the inherent advantages of PLA. Similarly, new processing techniques other than the conventional solution casting and injection molding should be studied.

References

Arjmandi R, Hassan A, Haafiz MKM, Zakaria Z (2015) Partial replacement effect of montmorillonite with cellulose nanowhiskers on polylactic acid nanocomposites. Int J Biol Macromol 81:91–99

Arjmandi R, Hassan A, Eichhorn SJ, Haafiz MKM, Zakaria Z, Tanjung FA (2015) Enhanced ductility and tensile properties of hybrid montmorillonite/cellulose nanowhiskers reinforced polylactic acid nanocomposites. J Mater Sci 50(8):3118–3130

Arjmandi R, Azman Hassan A, Haafiz MKM, Zakaria Z, Islam MS (2016). Effect of hydrolysed cellulose nanowhiskers on properties of montmorillonite/polylactic acid nanocomposites. Int J Biol Macromol 82:998–1010

Chuensangjun C, Kanomata K, Kitaoka T, Chisti Y, Sirisansaneeyakul S (2019a) Surface-modified cellulose nanofibers-graft-poly (lactic acid) s made by ring-opening polymerization of l-lactide. J Polym Environ 27(4):847–861

Chuensangjun C, Kitaoka T, Chisti Y, Sirisansaneeyakul S (2019b) Chemo-enzymatic preparation and characterization of cellulose nanofibers-graft-poly (lactic acid)s. Eur Polymer J 114:308–318

Coltelli M-B, Cinelli P, Gigante V, Aliotta L, Morganti P, Panariello L, Lazzeri A (2019) Chitin nanofibrils in poly (lactic acid)(PLA) nanocomposites: dispersion and thermo-mechanical properties. Int J Mol Sci 20(3):504

Fordiani F, Aubry T, Pillin I, Grohens Y (2013) Enhancement of polylactide nucleation by montmorillonites intercalated with a green seaweed byproduct. J Appl Polym Sci 127(1):724–732

Fortunati E, Luzi F, Puglia D, Petrucci R, Kenny JM, Torre L (2015) Processing of PLA nanocomposites with cellulose nanocrystals extracted from Posidonia oceanica waste: innovative reuse of coastal plant. Indus Crops Products 67:439–447

Gan I, Chow WS (2019) Synthesis of phosphoric acid-treated sugarcane bagasse cellulose nanocrystal and its thermal properties enhancement for poly (lactic acid) nanocomposites. J Thermoplas Compos Mater 32(5):619–634

Gitari B, Chang BP, Misra M, Navabi A, Mohanty AK (2019) A comparative study on the mechanical, thermal, and water barrier properties of PLA nanocomposite films prepared with bacterial nanocellulose and cellulose nanofibrils. BioResources 14(1):1867–1889

Haafiz MKM, Hassan A, Khalil HPSA, Fazita MRN, Islam MS, Inuwa IM, Marliana MM, Hussin MH (2016) Exploring the effect of cellulose nanowhiskers isolated from oil palm biomass on polylactic acid properties. Int J Biol Macromol 85:370–378

Herrera N, Salaberria AM, Mathew AP, Oksman K (2016) Plasticized polylactic acid nanocomposite films with cellulose and chitin nanocrystals prepared using extrusion and compression molding with two cooling rates: effects on mechanical, thermal and optical properties. Compos A Appl Sci Manuf 83:89–97

Iglesias Montes ML, Luzi F, Dominici F, Torre L, Cyras VP, Manfredi LB, Puglia D (2019) Design and characterization of PLA bilayer films containing lignin and cellulose nanostructures in combination with umbelliferone as active ingredient. Front Chem 7:157

Khakalo A, Filpponen I, Rojas OJ (2018) Protein-mediated interfacial adhesion in composites of cellulose nanofibrils and polylactide: enhanced toughness towards material development. Compos Sci Technol 160:145–151

Kian LK, Saba N, Jawaid M, Sultan MTH (2019) A review on processing techniques of bast fibers nanocellulose and its polylactic acid (PLA) nanocomposites. Int J Biol Macromol 121:1314–1328

Li C, Liu H, Luo B, Wen W, He L, Liu M, Zhou C (2016) Nanocomposites of poly (l-lactide) and surface-modified chitin whiskers with improved mechanical properties and cytocompatibility. Eur Polymer J 81:266–283

López de Dicastillo C, Roa K, Garrido L, Pereira A, Galotto M (2017) Novel polyvinyl alcohol/starch electrospun fibers as a strategy to disperse cellulose nanocrystals into poly (lactic acid). Polymers 9(4):117

Luzi F, Fortunati E, Jiménez A, Puglia D, Chiralt A, Torre L (2017) PLA nanocomposites reinforced with cellulose nanocrystals from posidonia oceanica and ZnO nanoparticles for packaging application. J Renew Mater 5(2):103–115

Mariano M, Pilate F, de Oliveira FB, Khelifa F, Dubois P, Raquez JM, Dufresne A (2017) Preparation of cellulose nanocrystal-reinforced poly (lactic acid) nanocomposites through noncovalent modification with PLLA-based surfactants. ACS Omega 2(6):2678–2688

Martínez-Sanz M, Lopez-Rubio A, Lagaron JM (2012) Optimization of the dispersion of unmodified bacterial cellulose nanowhiskers into polylactide via melt compounding to significantly enhance barrier and mechanical properties. Biomacromol 13(11):3887–3899

Miao C, Hamad WY (2016) In-situ polymerized cellulose nanocrystals (CNC)—poly (l-lactide) (PLLA) nanomaterials and applications in nanocomposite processing. Carbohyd Polym 153:549–558

Panaitescu DM, Frone AN, Chiulan I, Gabor RA, Spataru IC, Căşărică A (2017)Biocomposites from polylactic acid and bacterial cellulose nanofibers obtained by mechanical treatment.BioResources 12(1):662–672

Piekarska K, Sowinski P, Piorkowska E, Haque MMU, Pracella M (2016) Structure and properties of hybrid PLA nanocomposites with inorganic nanofillers and cellulose fibers. Compos Part A Appl Sci Manuf 82:34–41

Scaffaro R, Botta L, Lopresti F, Maio A, Sutera F (2017) Polysaccharide nanocrystals as fillers for PLA based nanocomposites. Cellulose 24(2):447–478

Somord K, Somord K, Suwantong O, Thanomsilp C, Peijs T, Soykeabkaew N (2018) Self-reinforced poly (lactic acid) nanocomposites with integrated bacterial cellulose and its surface modification. Nanocomposites 4(3):102–111

Soykeabkaew (2016) Self-reinforced poly (lactic acid) nanocomposites of high toughness. Polymer 103:347–352

Takkalkar P, Griffin G, Kao N (2019) Enhanced mechanical and barrier performance of poly (lactic acid) based nanocomposites using surface acetylated starch nanocrystals. J Polymers Environ 1–11

Tingaut P, Zimmermann Y, Lopez-Suevos F (2009) Synthesis and characterization of bionanocomposites with tunable properties from poly (lactic acid) and acetylated microfibrillated cellulose Biomacromol 11(2):454–464

Trifol J, Plackett D, Sillard C, Hassager O, Daugaard AE, Julien B, Szabo P (2016) A comparison of partially acetylated nanocellulose, nanocrystalline cellulose, and nanoclay as fillers for high-performance polylactide nanocomposites. J Appl Polymer Sci 133(14)

Yang W, Fortunati E, Dominici F, Giovanale G, Mazzaglia A, Balestra GM, Kenny JM, Puglia D (2016) Synergic effect of cellulose and lignin nanostructures in PLA based systems for food antibacterial packaging. Eur Polymer J 79:1–12

Ying Z, Defeng Wu, Wang Z, Xie W, Qiu Y, Wei X (2018) Rheological and mechanical properties of polylactide nanocomposites reinforced with the cellulose nanofibers with various surface treatments. Cellulose 25(7):3955–3971

Zamir SS, Frouzanmehr MR, Nagalakshmaiah M, Ajji A, Robert M, Elkoun S (2019) Chemical compatibility of lactic acid-grafted starch nanocrystals (SNCs) with polylactic acid (PLA). Polym Bull 76(7):3481–3499

Effect of Cellulose Nanocrystals on the Mechanical Properties of Polymeric Composites

Matthew J. Dunlop, Bishnu Acharya, and Rabin Bissessur

Abstract The demands of modern society are increasingly driving a shift from nonrenewable petroleum-based materials to more sustainable renewable resources. As the most prevalent natural polymer on Earth, cellulose has attracted broad interest for use as a green additive or replacement for unsustainable petroleum-based materials. The cellulose polymer arranges naturally into microscale semi-crystalline cellulose fibrils which can be degraded, typically by chemical treatments, to yield the nanoscale crystalline region of the cellulose polymer. These nanoscale crystals display a high aspect ratio with length from 100 to 3000 nm and width from 3 to 50 nm. They also possess excellent mechanical properties, comparable to high cost synthetic reinforcing nanomaterials such as carbon nanotubes. The morphology of these cellulose nanocrystals (CNCs) is highly dependent on natural cellulose source material and the utilized CNC preparation conditions. When utilizing CNC as a reinforcing filler material within a polymer matrix, the resulting nanocomposite often displays properties dependent on the morphology of the filler. This chapter discusses the benefits, drawbacks and differences between CNC sources with focus on the resulting CNC morphology and its effect on the mechanical properties of CNC containing polymeric nanocomposites. In addition, recent findings in the area of hybrid multifiller CNC reinforced polymeric nanocomposites will be highlighted and contrasted with monofiller CNC polymeric nanocomposites.

Keywords Cellulose nanocrystals · Polymeric nanocomposites · Mechanical properties · Hybrid

B. Acharya (✉)
Department of Chemical and Biological Engineering, University of Saskatchewan, Saskatoon S7N 5A9, Canada
e-mail: bsp874@usask.ca

M. J. Dunlop · R. Bissessur
Department of Chemistry, University of Prince Edward Island, Charlottetown C1A 4P3, Canada

M. T. Hameed Sultan et al. (eds.), *Biocomposite Materials*, Composites Science and Technology, https://doi.org/10.1007/978-981-33-4091-6_4

1 Cellulose Background

The natural polymer cellulose has been utilized by humanity for thousands of years and can still be commonly found today, as before, in numerous applications including wooden homes, paper books, and cotton-based clothing. Being the most abundant natural polymer on Earth, cellulose has been utilized for wide ranging applications across diverse demographics (Ummartyotin and Manuspiya 2015). Cellulose is commonly known as a linear polysaccharide with repeat units of cellobiose, which is comprised of β-1,4-glycosidic linkages between neighboring glucose residues. The extended nature of these linkages allows for the precise interaction of neighboring chains over long ranges to form a rigid and ordered structure. Therefore, cellulose does not generally occur naturally as a single polymer chain but is synthesized as a natural fiber from many cellulose polymer chains, described as cellulose fibrils (Fig. 1). The cellulose chains associate strongly in this way via both inter-chain and intra-chain hydrogen bonding between glucose residues. The precise manner of this interaction leads to cellulose fibers which are often largely crystalline.

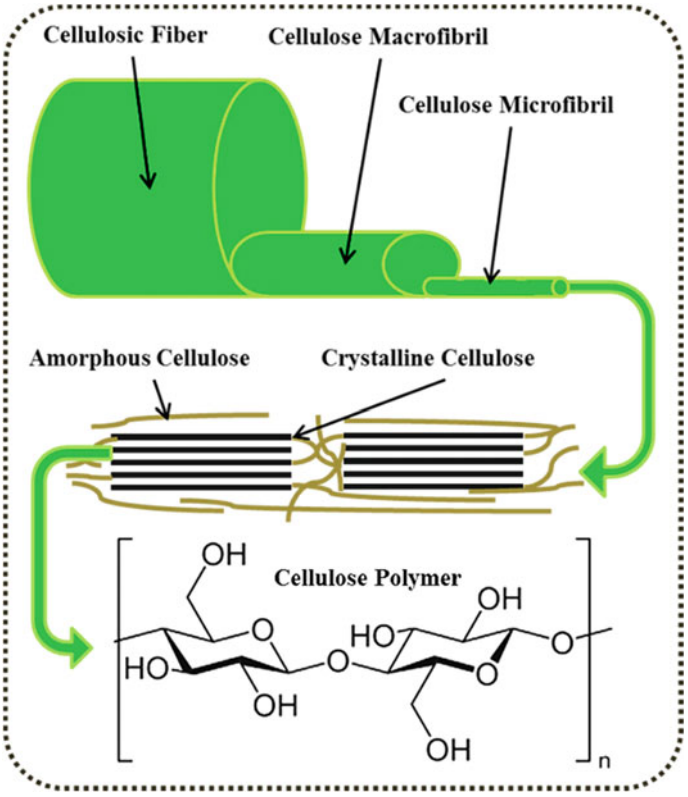

Fig. 1 Schematic illustration of a natural cellulosic fiber and its structural components

Cellulose is primarily found in forests where trees are thought to be the most important and abundant source, however cellulose can be found in all plants to various degrees (Beck-Candanedo et al. 2005). Additionally, cellulose can be found in bacteria (Roman and Winter 2004), algae (Revol 1982) and many other natural materials (de Rodriguez et al. 2006), (de Menezes et al. 2009). Interestingly there exists only a single animal source of cellulose, which is found in the marine invertebrate animal tunicate (Zhao and Li 2014). Regardless of the source, cellulose is almost always arranged in nature as either macro or microfibrils which contain crystalline regions of ordered cellulose polymer chains and amorphous regions with disordered cellulose polymer chains. All naturally synthesized cellulose is formed as Cellulose I which has two structures, the triclinic metastable cellulose Iα and the stable monoclinic cellulose Iβ crystal structure (Fig. 2). Natural cellulose can also be converted to Cellulose II, Cellulose III and Cellulose IV using various thermal or chemical treatments (Ciolacu and Popa 2011). The amount of cellulose present in a given cellulose containing material, the percentage of the cellulose which is crystalline, and the structural polymorph of the crystalline cellulose present is highly dependent on the specific cellulose source. Plant sources such as wood contain roughly 50% cellulose, of which only around 50% is crystalline, and the crystalline cellulose is arranged in both the cellulose Iα and the Iβ crystal structure (Park et al. 2010). Alternatively, the tunicate derived cellulose containing tunic is roughly 60% cellulose,

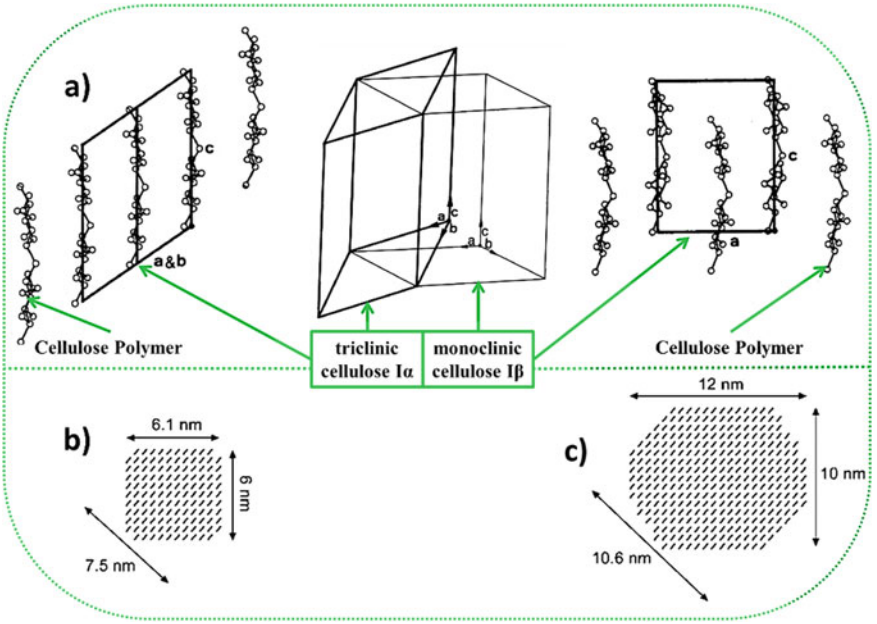

Fig. 2 **a** Schematic illustration of the difference between the triclinic cellulose Iα and monoclinic cellulose Iβ crystal structure. Typical cross-section of **b)** plant sourced and **c)** tunicate sourced CNCs. Adapted from Sugiyama et al. (1991) and Elazzouzi-Hafraoui et al. (2007)

which is between 70 and 95% crystalline and arranged almost exclusively in the Iβ crystal structure (Berrill 1950).

Of increasing interest today is the isolation of nanoscale cellulose crystals from natural resources and its utilization as a mechanical reinforcement in polymeric composites. To isolate these cellulose nanocrystals (CNC) researchers have used a variety of individual and combined methods, which generally fall under the categories of chemical treatment, mechanical treatment or enzymatic treatment (Klemm et al. 2011). Isolation methodologies are not the focus of this chapter and are described in more detail by others (Le Normand et al. 2014) (Jonoobi et al. 2015). However, given the wide range of natural cellulose sources and CNC isolation methods, it is apparent that CNC isolated from different sources with similar or different CNC isolation methodologies will yield CNC products with a wide range of morphologies. The focus of this chapter is to examine the effect of CNC morphology on the properties of CNC embedded polymeric nanocomposites. Particular attention will be paid to the mechanical properties of the polymeric nanocomposites, and how those properties change when the morphology of the CNC reinforcement is varied. To define a realistic scope for the chapter, discussion will be limited to CNC based polymeric composites where the CNC is in the form of discreet individual crystalline rods, also described throughout literature as cellulose whiskers or nanocrystalline cellulose (NCC).

2 Nanocellulose

2.1 Advantages at the Nanoscale

First isolated by the French chemist Anselme Payen in 1839, cellulose is ubiquitous in modern society (Purves 1954). However, it was not until the early 1980s that nanocellulose materials began to draw broad interest from the scientific community (Turbak et al. 1983). Nanomaterials are broadly defined as materials with at least one dimension in the nanoscale. Nanocellulose therefore, simply represents some arrangement of cellulose with one or more nanoscale dimensions. One of the primary advantages of nanocellulose compared to bulk cellulose is its high specific surface area (Kim et al. 2002). This high surface area allows for a greater degree of interaction between nanocellulose and the polymeric matrices which the nanocellulose is embedded within. In this section, the different classes of nanocellulose will be briefly described with an emphasis on CNCs.

2.2 Classes of Nanocellulose

There does not exist at this point a standardized nomenclature for describing nanocellulose materials. Generally, cellulose is known to contain amorphous and crystalline

regions and nanocellulose is simply segments of the cellulose polymer with at least one dimension (typically the diameter) in the nanoscale. Nanocellulose which contains both amorphous and crystalline regions typically arrange into a fibrous structure which is commonly denoted as either nanofibrillated cellulose (NFC) or cellulose nanofibers (CNFs). When the amorphous cellulose regions are removed (typically by acid hydrolysis), what remains are discreet rod like cellulose crystals. These are referred to as nanocrystalline cellulose (NCC) or cellulose nanocrystals (CNCs). Likewise, cellulose of microscale dimensions and crystalline structure is referred to as microcrystalline cellulose (MCC). When microscale cellulose contains crystalline and amorphous regions, a fibrous structure results described as microfibrillated cellulose (MFC). Other terms and abbreviations have been used to describe cellulose sourced nanoscale and microscale materials throughout literature. In the context of this chapter however, we limit ourselves to discussing the effect of crystalline cellulose nanomaterials (CNC and NCC) on the mechanical properties of polymeric nanocomposites.

2.3 Cellulose Nanocrystals

Reminiscent of the crystalline regions within elementary fibers of the natural cellulose source, CNCs are pure cellulose crystals generally shaped like whiskers or thin rods. They exhibit a large length compared to a relatively narrow width (Table 1), which contributes to the high aspect ratio (the length/width) of CNCs. The CNC morphology (aspect ratio, crystal structure, polydispersity and crystallinity) is highly variable and is dependent on the cellulose source, the CNC extraction process

Table 1 CNC morphology and its variance with CNC source material and preparation conditions. L = CNC length and W = CNC width (diameter)

Source	Preparation method	Length (nm)	Width (nm)	Aspect ratio (L/W)	References
Wood	H_2SO_4 hydrolysis	100–300	3–5	20–100	Beck-Candanedo et al. (2005)
Cotton	HCl hydrolysis	100–150	5–10	10–30	Araki et al. (2001)
Ramie	H_2SO_4 hydrolysis	70–200	5–15	~12	De Menezeset al. (2009)
Sisal	H_2SO_4 hydrolysis	100–300	3–5	~60	De Rodriguez et al. (2006)
Tunicates	H_2SO_4 hydrolysis	>1000	10–20	~100	Kimura et al. (2005)
Bacteria	H_2SO_4 hydrolysis	100–1000	10–50	2–100	George and Bawa (2010)
Bacteria	HCl hydrolysis	160–420	15–25	7–23	George (2012)

and the methods used to measure the morphological properties. Typical widths for CNCs are in the range 2–50 nm, and lengths between 100 and 3000 nm depending on the source material, processing conditions and measurement techniques (Habibi et al. 2010). These materials are highly crystalline, with percent crystallinity varying from 50 to 95% depending on the cellulose source, measurement technique and the data analysis method. Given their nanoscale dimensions, CNCs also exhibit high surface area in the range of 150–250 $m^2\ g^{-1}$ (Shaheen and Emam 2018). The abundant hydroxyl groups present on the surface of CNCs allow for a diverse array of possible chemical modifications on the CNCs including etherification, oxidation, silylation, esterification, polymer grafting and others (Salas et al. 2014). This allows for hydrophilic CNCs to be incorporated into both hydrophilic and hydrophobic matrices, provided that the appropriate surface chemistry is imbued to the CNCs prior to incorporation within the polymer matrix of interest. The numerous CNC surface modifications available provide researchers with a diverse panoply of experimental approaches to incorporate CNCs into polymer matrices. By incorporating CNCs within a polymer matrix, properties of the resulting nanocomposite can be varied. CNCs are well known to alter the thermal, structural, and morphological properties of polymeric nanocomposites; however mechanical properties are often the most sensitive to CNC addition (Klemm et al. 2011).

2.4 CNC Commercial Production

The production of cellulose worldwide is estimated to be in the range of 1010–1011 tons yearly (Azizi Samir et al. 2005). In order to meet the growing demand from academia, government and industry, the worldwide production of CNCs from this abundant cellulose stock is increasing in volume, and diverse cellulose sources are being utilized. It was recently proposed by 'The Technical Association of the Pulp and Paper Industry' (TAPPI) that in the year 2020 the gross world productions of nanocellulose materials may exceed $600 billion (Endes et al. 2016). There are numerous large scale production facilities capable of isolating kilograms of CNC from plant based sources. The largest is Canada based CelluForce©, a result of the partnership between FPInovations and the Domtar Corporation, which boasts a CNC production capacity of ~1000 kg CNC/day (Sharma et al. 2019). At the Forest Products Laboratory in Madison Wisconsin USA, CNCs are extracted from wood at a rate of ~10 kg/day (Chauve and Bras 2014). According to the 2016 report (Frost & Sullivan 2016), "Emerging Applications of Nanocellulose Technology", several other private and public organizations are also producing CNCs at a ~10 kg/day rate including the Israeli company Melodea Ltd, the India Council for Agricultural Research, and Canada's Blue Goose Biorefineries. In an effort to reduce the environmental impact of CNC isolation, (Mathew et al. 2014) used mild mechanical and chemical means to isolate ~600 g/day of CNCs from cellulose containing waste streams in a bioethanol producing pilot plant. All of these examples however rely on plant-based sources,

primarily wood pulp, from which to extract the CNCs. Some production of bacterial CNCs (~17 g/day) (Chen et al. 2018) and algal CNCs (~36 g/day) (El Achaby et al. 2018; Masaoka et al. 2014; Masaoka et al. 1993) exist, however these are of much smaller scale than the plant based CNC sources. Tunicates likewise are converted to CNCs in very small, typically laboratory scale quantities of several grams or less (Jonoobi et al. 2015; Zhao and Li 2014). There is increasing interest in scaling this process up to a pilot plant scale (Dunlop et al. 2018), and recently the first known kilogram scale processing of tunicates to of CNCs was reported (Dunlop et al. 2020).

3 Sources of CNCs

3.1 Plants

The primary sources of CNCs produced today are derived from plants, due in part to their natural abundance and accessibility. There is also a preexisting infrastructure in place to harvest and pretreat many plant sources of CNC. The best example of this is wood based CNCs, which are sourced primarily from the bleached Kraft wood pulp used conventionally to produce paper. Other examples include the packaging, pharmaceutical and textile industries which each have existing methods for the harvesting, pretreatment and processing of plant based CNC precursors (Moon et al. 2011). Generally the processing of plants to isolate plant based CNC is similar and consists of two main steps. Firstly, the removal of non-cellulose materials such as hemicellulose, lignin and other materials; followed by the removal of amorphous cellulose regions to yield individualized CNCs. An acid hydrolysis is typically used to remove amorphous cellulose regions, the most common being a sulfuric acid hydrolysis process. When sulfuric acid is utilized to extract CNCs, the surface of the nanocrystals is modified with sulphate groups. This imparts a negative surface charge to the CNC, increasing repulsion between the crystals, leading to a greatly increased CNC stability in an aqueous solution. In this way, numerous plants have been utilized for the extraction of CNCs, which include potato tubers (Dufresne et al. 2000), sugar beets (Leitner et al. 2007), ramie (Habibi and Dufresne 2008), cotton (Elazzouzi-Hafraoui et al. 2007), and many others (de Rodriguez et al. 2006, Helbert et al. 1996, Wang and Mohini 2007, Zuluaga et al. 2007). Plant sourced CNCs contain a mixture of cellulose Iα and Iβ crystal structures; with higher order plants such as trees and shrubs containing more cellulose Iβ, and lower order plants such as fungi and algae containing more cellulose Iα (de Souza Lima et al. 2004).

3.2 Tunicates

Named for their 'tunic like' cellulose containing epidermis, tunicates are unique among animals in their ability to biosynthesize cellulose (Zhao and Li 2014). The cellulose produced in tunicates is arranged in microfibrils and acts as a reinforcing skeletal-type network structure; this provides rigidity and support to the remaining protein and lipid materials which comprise the tunic (Kimura and Itoh 2007). In 2002 the genome of the common ascidian tunicate 'Ciona intestinalis' was sequenced for the first time, in part to enhance understanding of cellulose biosynthesis and function in tunicates (Dehal et al. 2002). Over recent years, tunicates have been increasingly viewed as an attractive source for the production of CNCs (Zhao and Li 2014; Dunlop et al. 2018). Primarily, this is due to the unique properties which tunicate CNCs exhibit compared to plant sourced CNCs. Tunicate CNCs exhibit the highest aspect ratio (~70–100) of all CNC sources. Additionally, tunicate derived CNCs are predominantly the cellulose Iβ allomorph, rather than the mixture of the cellulose Iα and the Iβ crystal structure displayed in plant sourced CNCs. Similar to plant sourced CNC, the isolation of tunicate sourced CNC occurs in two general steps. Firstly, the cellulose containing tunic is cleaned, deproteinated and bleached to remove the non cellulose tunic components. Next the purified tunic cellulose, referred to as tunicin, is hydrolyzed in acid to yield tunicate CNCs. As with plant CNCs, sulfuric acid is the most common acid used for the hydrolysis process. This leads to CNCs with surface sulfate groups that reduce agglomeration and increase the colloidal stability of the dispersed CNCs.

3.3 Other Sources

Numerous other cellulose sources exist, which can be utilized as a source of CNCs. Some species of bacteria have the ability to biosynthesize and secrete cellulose microfibrils. Bacterially synthesized microfibrils display a high aspect ratio, typically higher than 50 (Brown and Laborie 2007). The exact bacteria and the growing conditions utilized will determine the morphology of the isolated CNCs. One common bacteria known as Acetobacter produces highly crystalline cellulose microfibrils with a cellulose Iα crystal structure (Tokoh et al. 1998). However, by altering the culturing conditions, the width of the microfibrils and the ratio of cellulose Iα to cellulose Iβ can be tailored (Yamamoto and Horn 1994). Interestingly, when some species of algae are treated in acid, the cellulose microfibrils present in the algal cell wall can be hydrolyzed to form CNCs. Like with other cellulose sources, the properties of isolated CNCs are dependent on the natural source material and preparation conditions. The algae Micrasterias and Valonia provide good examples of the contrast in CNC properties across algae species. Micrasterias CNCs are primarily cellulose Iβ and exhibit a rectangular cross-section (Hanley et al. 1997), whereas Valonia CNCs are primarily cellulose Iα and exhibit a square cross-section (Revol 1982). Cellulose

isolated from Valonia has been shown to display exceptional crystallinity, in some cases exceeding 95% crystallinity (Sugiyama et al. 1991).

4 Composites

Cellulose based composite materials date back thousands of years and have served many functions. Due to improvements in technology and scientific advancement, we are able today to prepare cellulose based nanocomposite materials. Given that a wide variety of cellulose based nanomaterials currently exist with diverse morphologies, we will narrow the focus of this chapter to cellulose based nanocomposite materials whose composition is limited to CNCs incorporated within a polymeric matrix. Since all cellulose sources yield CNCs which are highly polydisperse, and the range of naturally sourced CNC morphologies is highly variable; we will further simplify our composites into three main classes.

i. Low aspect ratio plant CNC based polymeric nanocomposites
ii. High aspect ratio tunicate CNC based polymeric nanocomposites
iii. Hybrid CNC mixtures in polymeric nanocomposites

Throughout the literature, researchers have used low aspect ratio CNCs from plant-based sources to prepare polymeric nanocomposites. However due to the nature of the plant based cellulose source, CNC isolation process, and characterization technique; these CNCs cover a wide range of aspect ratio distributions, different shapes in cross-section, changing ratios of cellulose Iα to Iβ and so on. Likewise, for high aspect ratio tunicates, a range of morphologies are reported throughout literature and these vary for similar reasons as plant-based CNC sources. We feel, given the variability in CNC morphology across natural sources and the inconsistencies in CNCs used between literature reports, that it is reasonable to separate CNC based composites into these three previously mentioned classes, visualized in Fig. 3. This will allow for simple comparison between the effect of high aspect ratio, low aspect ratio and hybrid mixtures of high and low aspect ratio CNCs, on the mechanical properties of polymeric nanocomposites.

4.1 Mechanical Reinforcement of CNCs in Polymeric Nanocomposites

The mechanical reinforcement observed in CNC reinforced polymeric nanocomposites is thought to arise from two main factors. The first and most obvious factor being the impressive mechanical properties which CNC crystals display. Comparable to high cost, synthetic reinforcing nanomaterials such as carbon nanotubes (Moon et al. 2011), CNCs display a Young's modulus from 110 to 220 GPa and tensile strength

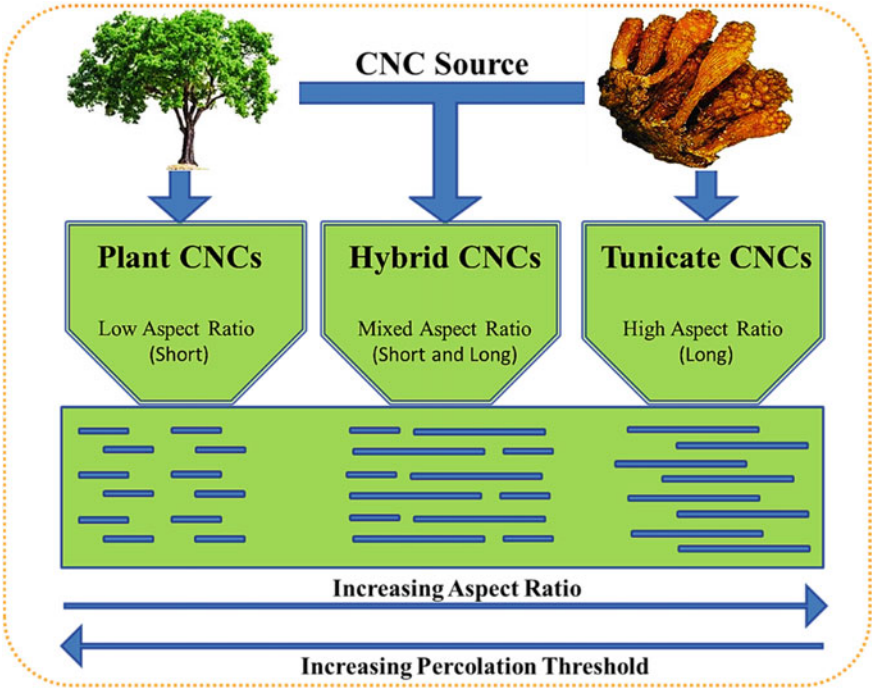

Fig. 3 Visualizing the incorporation of long high aspect ratio tunicate derived CNCs, short low aspect ratio plant derived CNCs and hybrid mixtures of high and low aspect ratio (long and short) CNCs within polymeric nanocomposites

in the range of 7.5–7.7 GPa (Lin et al. 2012). The second factor relates to the stress transfer between the polymer matrix and CNC filler. Strong interactions between matrix and filler such as covalent linkages or noncovalent interactions like hydrogen bonding allow for stress to be transferred from the viscoelastic polymer matrix to the elastic CNC reinforcement. The weaker the interaction between matrix and filler, the weaker the stress transfer from matrix to filler, leading to reduced reinforcement and lower nanocomposite mechanical properties (Kargarzadeh et al. 2017) (Dunlop et al. 2019). The first factor regarding superb individual CNC mechanical properties is largely consistent regardless of the CNC source or processing conditions. However, increased variability is observed when stress transfer is considered. Stress transfer can vary with numerous factors such as the surface chemistry of the filler and matrix, the nanocomposite preparation methodology, the presence of plasticizers or solvents, aggregation of the CNCs and the CNC morphology among others (Klemm et al. 2011). In short, any factor that modifies the formation or final structure of the percolating CNC network within the polymeric matrix will affect the mechanical properties of the resulting nanocomposite (Dufresne et al. 2000, Dufresne 2008). When fitting experimentally determined mechanical properties to expected mechanical properties, two general models are most often used: the percolation model (Takayanagi

et al. 1964) and the Halpin-Kardos model (Halpin and Kardos 1972). The percolation model predicts the modulus of a nanocomposite material by assuming that the polymer matrix is too soft to contribute to the nanocomposite modulus, which is instead dominated by an interconnected or 'percolating' network of stiff filler material that has a continuous order and structure throughout the nanocomposite deriving from strong filler-filler interactions. Conversely the Halpin-Kardos model assumes a perfect distribution of the filler within the matrix polymer with no filler-filler interactions present. Both models are dependent on the average aspect ratio (length/width) of the CNCs. The percolation model predictions in particular are heavily dependent on the aspect ratio of the CNC filler material, with high aspect ratio fillers percolating the polymeric matrix and providing mechanical enhancements at lower loading levels (Peng et al. 2011). An illustration of the effect of CNC aspect ratio on nanocomposite properties is illustrated by the work of (Azizi Samir et al. 2005). In this study three CNC types were dispersed within a poly(S-co-BuA) polymer matrix to yield nanocomposite materials. The nanocomposite reinforced with high aspect ratio (~67) tunicate CNCs showed the greatest modulus increase and thermal stability compared to the neat polymer matrix. The bacterial sourced CNCs with aspect ratio (~60) showed the second greatest modulus and thermal improvements, followed by the low aspect ratio (~10) plant sourced CNCs. Notably, the aspect ratio dependence of the percolation threshold for a rigid rod like reinforcement within a polymeric matrix has been demonstrated to extend to various rigid filler materials such as carbon nanotubes (Wong et al. 2009) and others (Jiang et al. 2007). In this section the effect of CNC morphology is investigated as it relates to the mechanical properties of CNC containing polymeric nanocomposites.

4.2 Nanocomposites Based on Plant Sourced CNCs

Plant sourced CNCs are short, generally low aspect ratio, crystals which contain a mixture of the cellulose Iα and the Iβ crystal structure. Higher order plants tend to exhibit higher degrees of the cellulose Iβ allomorph whereas lower order plants contain more of the cellulose Iα allomorph. There exist a plethora of reports and reviews on numerous aspects of plant CNC based polymeric nanocomposites (Moon et al. 2011; Kim et al. 2015; Oksman and Sain 2005). Primarily this is due to the prevalence, low cost and commercial availability of plant sourced CNCs compared to other sources. As with all CNC reinforced polymeric nanocomposites, the mechanical behavior of these materials are dependent on the aspect ratio of the CNCs, however plant sources of CNC generally exhibit a narrow and low aspect ratio distribution (de Rodriguez et al. 2006). Recently Hendren et al. combined wood derived CNCs with poly (5-triethoxysilyl-2-norbornene) (PTESN) to form nanocomposite solvent cast films (Hendren et al. 2019). When the mechanical properties of the films were probed it was found that the Young's modulus and storage modulus increases as CNC loading is increased. At 20% CNC addition the Young's modulus almost doubled from 540 to 970 MPa and the storage modulus tripled from 400 to 1200 MPa. In another recent

study, (Chen et al. 2019) compared starch-based bionanocomposite films which incorporated nanocellulose isolated from several different non wood fibers. Of the various nanocellulose materials tested, the bamboo sourced nanocellulose displayed the best reinforcement at the lowest filler content. This was primarily ascribed to the aspect ratio of the bamboo sourced nanocellulose being the highest of all the nanocellulose studied. In an effort to further improve the mechanical properties of polymeric nanocomposites containing plant sourced CNCs, some authors have begun to incorporate polymeric dispersants into these composite materials in an effort to limit CNC aggregation and increase the stress transfer between polymeric matrix and CNC reinforcement (Meesorn et al. 2017). It has been demonstrated for poly (ethylene oxide-co-epichlorohydrin), polyurethane and poly(methyl acrylate) matrices, that by using polyvinyl alcohol as a polymeric dispersant for CNCs, significant improvements in mechanical properties are achievable (Meesorn et al. 2017) (Miri et al. 2016). This is thought to arise from improved dispersion and reduced aggregation of the CNC filler material. By taking advantage of the hydrophilic nature of the polyvinyl alcohol and CNCs, (Meesorn et al. 2019) was able to prepare a polymeric nanocomposite from poly (ethylene oxide-co-epichlorohydrin), polyvinyl alcohol and CNCs which displayed tunable mechanical properties with humidity level. When dry the polymer matrix displayed a storage modulus of 2.7 MPa, rising to 50 MPa when reinforced with 10% wt. plant CNCs. Interestingly when 5% wt. of polyvinyl alcohol is added to the same nanocomposite system the resulting storage modulus is 200 MPa, four times higher than without CNCs and almost 75 times higher than the unmodified polymer matrix. Notably, the Young's modulus and tensile strength also increased when polyvinyl was added as a polymeric dispersant. When wet a similar trend is observed however the storage modulus is significantly lower, primarily due to hydrogen bonding competition between the composite components and the aqueous solution (Rusli et al. 2010).

4.3 Nanocomposites Based on Tunicate Sourced CNCs

Tunicate sourced CNCs are long high aspect ratio crystals comprised almost exclusively of cellulose Iβ. The first study of polymeric nanocomposites comprising tunicate CNCs was reported by (Favier et al. 1995) who combined these nanoscale crystals with the polymer latex. This resulted in a nanocomposite material with improved mechanical properties at low CNC content, particularly when the nanocomposite was heated beyond the glass transition temperature of the polymer matrix. Improved mechanical properties were also documented for a composite system comprised of amorphous poly(β-hydroxyoctanoate) and tunicate derived CNCs, the reinforcement documented by (Dubief et al. 1999) resulted from the formation of a rigid network of high aspect ratio CNC filler material. By combining either of the hydrophobic matrices poly(styrene-co-butadiene) or polybutadiene with hydrophilic tunicate derived CNCs, Dagnon et al. were able to prepare a biomimetic and stimuli-responsive polymeric nanocomposite (Dagnon et al. 2012). At 17% by volume,

the tunicate CNCs enhanced the storage modulus of the nanocomposites three-fold compared to the neat polymer matrix. Above the glass transition the mechanical enhancements in storage modulus were similar to the results of Favier et al., where CNCs act as rigid stabilizers for the glassy state polymer matrix. The authors noted that even when swollen in aqueous media, the mechanical reinforcement which CNCs imbue to the polymeric nanocomposites is preserved, however the overall mechanical properties of all samples is reduced. This was determined to result from the tunicate CNCs acting as hydrophilic channels which aid in the uptake of water molecules which solvate the CNCs and limit their stress transfer to the polymer matrix while lessening the strength of CNC filler-filler interactions. These findings were built on by (Jorfi et al. 2013) who prepared physiologically responsive and mechanically adaptive polymeric nanocomposites for eventual use in biomedical applications.

4.4 Hybrid Nanocomposites comprised of Multiple CNC Sources

In recent years, the production of hybrid polymeric nanocomposite materials, which combine multiple nanoscale filler materials within the same polymeric matrix, has gained significant interest. The properties of hybrid polymeric nanocomposites depend primarily on the polymer and nanoscale fillers used. Interestingly, it has been demonstrated that hybrid polymeric nanocomposite materials which utilize nanoscale fillers of different morphologies, often show mechanical properties which exceed monofiller nanocomposites at the same filler loading level (Sapkota et al. 2017, Yeng et al. 2011, El Miri et al. 2016). This indicates that there exists a cooperative interaction between nanoscale fillers of different morphology, which leads to these enhanced properties. Herein we will discuss hybrid polymeric nanocomposites in the context of highly elastic rod like nanomaterials with different aspect ratios (long and short CNCs), being used to provide reinforcement in a soft polymer matrix. There exists a small but growing body of work in this area which highlights the growing potential of, and unique advantages to, using long and short rod like nanomaterials within a common polymer matrix.

As discussed previously, numerous researchers have reported polymeric nanocomposite materials which contain either plant sourced or tunicate sourced CNCs (Meesorn et al. 2017, Samir et al. 2005). Across these reports, the difference in morphology (aspect ratio) of the CNC reinforcement is primarily credited with the differences in mechanical properties observed between nanocomposite materials reinforced with CNCs of a different morphology but the same volume fraction (Jorfi et al. 2013). The large aspect ratio of tunicate CNCs allow them to percolate and form an interconnected network within the polymer matrix at a lower concentration than CNCs with a lower aspect ratio. The structure and orientation of this percolation network determines in large part the stress transfer between the soft polymer matrix and the ridged reinforcing filler material (Šturcová et al. 2005).This percolating

network is known to change its structure and orientation based on the morphology of the filler materials. Using Raman spectroscopy techniques, (Rusli et al. 2011) demonstrated that enhanced stress transfer from CNC filler to epoxy polymer matrix was observed for tunicate CNCs compared to wood CNCs. The authors attributed this difference in stress transfer to the changing morphology of the CNC reinforcement. A pioneering 2011 study by (Yeng et al. 2011) combined nanoscale graphene sheets and carbon nanotubes within an epoxy resin. Surprisingly, the authors found that hybrid combinations of the two filler materials which display very different morphologies displayed a synergistic reinforcing effect within the epoxy. The tensile strength of the hybrid nanocomposites increased by over 35% compared to the neat epoxy, whereas the monofiller graphene containing nanocomposite displayed roughly 1% improvement in tensile strength.

Building off this study, (El Miri et al. 2016) prepared polyvinyl alcohol based nanocomposite materials which incorporated a hybrid combination of plant sourced CNCs and graphene oxide nanosheets. The authors found synergistic behavior between the two nanoscale filler materials within the polyvinyl alcohol polymer matrix. This resulted in improved mechanical performance for hybrid multifiller materials compared to the neat polymer matrix or monofiller nanocomposites with the same volume fraction of reinforcement. The Young's modulus and ultimate tensile strength of the hybrid nanocomposite increased 320% and 124% respectively compared to the neat polymer matrix; the CNC reinforced monofiller nanocomposite only increased by 77% and 12%, respectively.

The initial study which incorporated both low aspect ratio plant and high aspect ratio tunicate sourced CNCs together within the same polymer matrix was accomplished by (Sapkota et al. 2017). They reported an aspect ratio dependence on the percolation threshold and proposed a modified percolation model, based on the aspect ratio distribution of the CNC source material, to predict experimental mechanical performance for this class of hybrid polymeric nanocomposites. Additionally the authors noted that the experimental modulus of the polymeric nanocomposite material is strongly weighted towards the contribution of high aspect ratio filler material with little effect from the low aspect ratio filler material. Recently, our group built on the research by (Sapkota et al. 2017) and (El Miri et al. 2016) and prepared polymeric nanocomposite materials with plant and tunicate derived CNCs incorporated within a polyvinyl alcohol matrix. We found that not only does the tunicate derived CNCs display higher reinforcement than plant CNCs, but when the high and low aspect ratio CNC fillers are combined in a 1:1 ratio they display cooperative behavior with respect to the elastic modulus of the nanocomposites. We determined that hybrid CNC mixtures display higher elastic modulus than either the plant or the tunicate containing monofiller nanocomposites, at the same filler content (Dunlop et al. 2019). This was attributed to a modification of the percolating network resulting in increased stress transfer to the polymer matrix, which was supported by an increase in the structural order of the nanocomposite materials as revealed by X-ray diffraction.

5 Effect of Morphology on Mechanical Performance

Generally, when discussing CNC morphology researchers report average lengths, widths and aspect ratio based on some form of statistical analysis, usually derived from experimental micrographs. It is important to consider when discussing the aspect ratio dependence of CNC imparted reinforcement in polymeric nanocomposites, that CNCs aspect ratios reported in literature are averages with corresponding polydispersity. Interestingly, when comparing CNC sources the polydispersity of the CNCs seems to scale with the average aspect ratio of the CNCs (Azizi Samir et al. 2005) (Natarajan et al. 2018).

Currently, the consensus is that it is the higher aspect ratio of the CNCs which leads to the enhanced stress transfer in polymeric nanocomposites (Azizi Samir et al. 2005; Sapkota et al. 2017). For this reason, tunicate CNCs were shown to carry stress to a greater degree than low aspect plant CNCs by (Šturcová et al. 2005; Rusli et al. 2011). It should be noted however that the tunicate CNCs are also significantly more polydisperse than plant sourced CNCs (de Souza Lima et al. 2004).

To the best of our knowledge, in the current literature CNC aspect ratio is generally considered the main factor in the expected reinforcement of polymeric matrices (Azizi Samir et al. 2005; de Souza Lima et al. 2004; Sapkota et al. 2017). Recently however, hybrid CNC nanocomposites have shown surprisingly high mechanical properties, even surpassing tunicate derived CNC reinforcement at the same CNC content (Fig. 4).

The average aspect ratio of the hybrid CNC mixture is lower than the tunicate CNCs, and yet as filler the hybrid CNCs show superior mechanical properties than

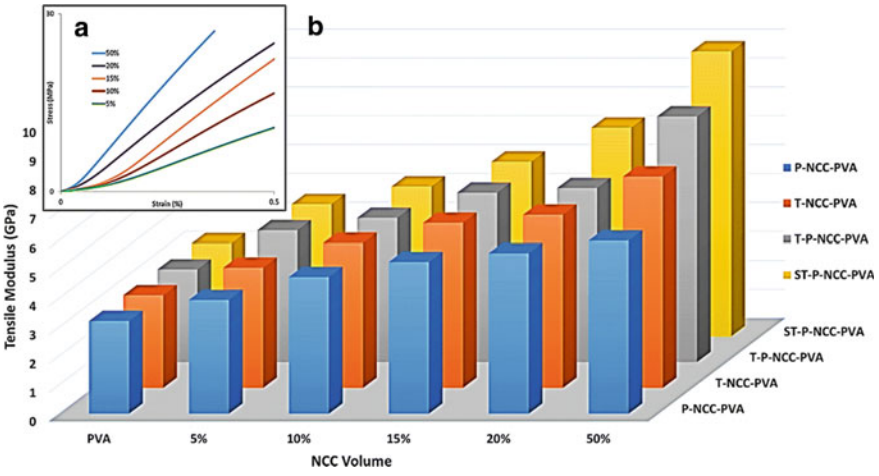

Fig. 4 DMA stress versus strain overlay of hybrid nanocomposites at increasing CNC content **a)**, and **b)** measured Young's modulus for all composites including monofiller P-NCC-PVA and T-NCC-PVA as well as the hybrid T-P-NCC-PVA and ST-P-NCC-PVA

the monofiller tunicate CNCs. This unusual result for hybrid nanocomposite materials could potentially be explained by the increased polydispersity of CNCs in the hybrid nanocomposite case, rather than solely considering the average aspect ratio of the multifiller CNC reinforcement. More detailed studies which investigate the use of highly polydisperse hybrid multifiller CNC reinforcements in polymeric composites are needed to better understand the unique mechanical properties which these materials exhibit. Future work in this area will further elucidate whether CNC reinforcement in polymeric composites is in part polydispersity dependent or is primarily dependent on the aspect ratio of the CNC filler.

6 Conclusion and Future Perspective

Clearly there exists a strong and growing interest in the use of CNCs to modify the properties of polymeric matrices. Among the most important of these is the effect of CNCs on the mechanical properties of the corresponding polymeric nanocomposite material. CNCs from any source with any morphology have the potential to reinforce polymeric matrices, provided that the CNC and polymer share compatible surface chemistry and that the polymers elastic modulus is lower than the CNC. It has been shown that high aspect ratio CNCs, such as those sourced from tunicates; reinforce polymers at a lower CNC concentration than low aspect ratio CNCs such as those sourced from plants. When plant and tunicate CNCs are combined within the same polymer matrix, the resulting hybrid polymeric nanocomposites can display mechanical properties superior to either plant or tunicate CNCs individually dispersed within the polymer matrix. These findings have brought into question the notion that the aspect ratio of CNCs is the primary morphological factor when determining CNC reinforcement in polymeric matrices. We posit that the polydispersity of the CNC reinforcement may also play an important factor, and expect that future work towards understanding the effect of CNC morphology on the mechanical properties of monofiller and hybrid multifiller polymeric composites will be explored.

References

Araki J, Wada M, Kuga S (2001) Steric stabilization of a cellulose microcrystal suspension by poly (ethylene glycol) grafting. Langmuir 17(1):21–27

Azizi Samir MAS, Alloin F, Dufresne A (2005) Review of recent research into cellulosic whiskers, their properties and their application in nanocomposite field.Biomacromolecules 6(2):612–626

Beck-Candanedo S, Roman M, Gray DG (2005) Effect of reaction conditions on the properties and behavior of wood cellulose nanocrystal suspensions.Biomacromolecules 6(2):1048–1054

Berrill NJ (1950) The Tunicata. The Ray Society, London

Brown EE, Laborie M-P (2007) Bioengineering bacterial cellulose/poly (ethylene oxide) nanocomposites. Biomacromol 8(10):3074–3081

Chauve G, Bras J (2014)Industrial point of view of nanocellulose materials and their possible applications. In: Handbook of green materials: 1 Bionanomaterials: separation processes, characterization and properties, pp 233–252

Chen G et al. (2018) Scale-up of production of bacterial nanocellulose using submerged cultivation.J Chem Technol Biotechnol 93(12):3418–3427

Chen Q, Liu Y, Chen G (2019) A comparative study on the starch-based biocomposite films reinforced by nanocellulose prepared from different non-wood fibers. Cellulose 26(4):2425–2435

Ciolacu D, Popa VI (2011) Cellulose allomorphs: structure, accessibility and reactivity. Environ Eng Manage J 10(3):467–468

Dagnon KL et al. (2012) Water-triggered modulus changes of cellulose nanofiber nanocomposites with hydrophobic polymer matrices.Macromolecules 45(11):4707–4715

de Menezes AJ et al. (2009) Extrusion and characterization of functionalized cellulose whiskers reinforced polyethylene nanocomposites.Polymer 50(19):4552–4563

de Rodriguez NLG, Thielemans W, Dufresne A (2006) Sisal cellulose whiskers reinforced polyvinyl acetate nanocomposites.Cellulose 13(3):261–270

de Souza Lima MM, Redouane B (2004) Rodlike cellulose microcrystals: structure, properties, and applications.Macromol Rapid Commun 25(7):771–787

Dehal P et al. (2002) The draft genome of Ciona intestinalis: insights into chordate and vertebrate origins.Science 298(5601):2157–2167

Dubief D, Samain E, Dufresne A (1999) Polysaccharide microcrystals reinforced amorphous poly (β-hydroxyoctanoate) nanocomposite materials. Macromolecules 32(18):5765–5771

Dufresne A, Dupeyre D, Vignon MR (2000) Cellulose microfibrils from potato tuber cells: processing and characterization of starch–cellulose microfibril composites. J Appl Polym Sci 76(14):2080–2092

Dufresne A (2008) Polysaccharide nanocrystal reinforced nanocomposites. Can J Chem 86(6):484–494

Dunlop MJ, Acharya B, Bissessur R (2018) Isolation of nanocrystalline cellulose from tunicates. J Environ Chem Eng 6(4):4408–4412

Dunlop MJ, Acharya B, Bissessur R (2019) Study of plant and tunicate based nanocrystalline cellulose in hybrid polymeric nanocomposites.Cellulose 1–13

El Achaby M et al. (2018) Reuse of red algae waste for the production of cellulose nanocrystals and its application in polymer nanocomposites.Int J Biol Macromol 106:681–691

El Miri N, El Achaby M, Fihri A, Larzek M, Zahouily M, Abdelouahdi K, Barakat A, Solhy A (2016) Synergistic effect of cellulose nanocrystals/graphene oxide nanosheets as functional hybrid nanofiller for enhancing properties of PVA nanocomposites. Carbohydr Polym 137:239–248

Elazzouzi-Hafraoui S et al. (2007) The shape and size distribution of crystalline nanoparticles prepared by acid hydrolysis of native cellulose.Biomacromolecules 9.1:57–65

Endes C et al (2016) A critical review of the current knowledge regarding the biological impact of nanocellulose. J Nanobiotechnol 14(1):78

Favier V, Chanzy H, Cavaillé JY (1995) Polymer nanocomposites reinforced by cellulose whiskers.Macromolecules 28(18):6365–6367

Frost & Sullivan—Market Research (2016) Emerging applications of nanocellulose technology. In: Sustainable, bio-based nanomaterials, nanofibrillated cellulose (NFC), nanocrystalline cellulose (NCC) and bacterial nanocellulose (BNC) to expand application base. Release date 09-may-2016. Region global. Research code: D6DF-01–00–00–00SKU: CM01226-GL-TR_18536

George J, Bawa AS (2010) Synthesis and characterization of bacterial cellulose nanocrystals and their PVA nanocomposites.Adv Mater Res 123. Trans Tech Publications

George J (2012) High performance edible nanocomposite films containing bacterial cellulose nanocrystals. Carbohyd Polym 87(3):2031–2037

Habibi Y, Dufresne A (2008) Highly filled bionanocomposites from functionalized polysaccharide nanocrystals. Biomacromol 9(7):1974–1980

Habibi Y, Lucia LA, Rojas OJ (2010) Cellulose nanocrystals: chemistry, self-assembly, and applications. Chem Rev 110(6):3479–3500

Halpin JC, Kardos JL (1972) Moduli of crystalline polymers employing composite theory. J Appl Phys 43(5):2235–2241
Hanley SJ et al. (1997) Atomic force microscopy and transmission electron microscopy of cellulose from Micrasterias denticulata; evidence for a chiral helical microfibril twist.Cellulose 4(37):209
Helbert W, Cavaille JY, Dufresne A (1996) Thermoplastic nanocomposites filled with wheat straw cellulose whiskers. Part I: processing and mechanical behavior. Polym Compos 17(4):604–611
Hendren KD et al. (2019) Cellulose nanocrystal-reinforced poly (5-triethoxysilyl-2-norbornene) composites.Polym Chem
Jiang B et al. (2007) The effect of non-symmetric distribution of fiber orientation and aspect ratio on elastic properties of composites.Compos Part B: Eng 38(1):24–34
Jonoobi M et al. (2015) Different preparation methods and properties of nanostructured cellulose from various natural resources and residues: a review.Cellulose 22(2):935–969
Jorfi M et al. (2013) Physiologically responsive, mechanically adaptive bio-nanocomposites for biomedical applications.ACS Appl Mater Interfaces 5(4):1517–1526
Kargarzadeh H et al. (2017) Recent developments on nanocellulose reinforced polymer nanocomposites: a review.Polymer 132:368–393
Khalil HPSA et al. (2014) Production and modification of nanofibrillated cellulose using various mechanical processes: a review.Carbohydr Polym 99:649–665
Kim D-Y, Nishiyama Y, Kuga S (2002) Surface acetylation of bacterial cellulose. Cellulose 9(3–4):361–367
Kim J-H, et al. (2015) Review of nanocellulose for sustainable future materials.Int J Precision Eng Manuf Green Technol 2(2):197–213
Kimura S, Itoh T (2007) Biogenesis and function of cellulose in the tunicates. In: Brown RM, Saxena I (eds) Cellulose: molecular and structural biology. Springer, Netherlands, pp 217 236
Kimura F et al. (2005) Magnetic alignment of the chiral nematic phase of a cellulose microfibril suspension.Langmuir 21(5):2034–2037
Klemm D et al. (2011) Nanocelluloses: a new family of nature-based materials.Angew Chem Int Ed 50(24):5438–5466
Le Normand M, Moriana R, Ek M (2014)Isolation and characterization of cellulose nanocrystals from spruce bark in a biorefinery perspective.Carbohydr Polym 111:979–987
Leitner J et al. (2007) Sugar beet cellulose nanofibril-reinforced composites.Cellulose 14(5):419–425
Lin N, Huang J, Dufresne A (2012) Preparation, properties and applications of polysaccharide nanocrystals in advanced functional nanomaterials: a review. Nanoscale 4(11):3274–3294
Malcolm Jr R, Saxena IM (eds) (2007) Cellulose: molecular and structural biology: selected articles on the synthesis, structure, and applications of cellulose. Springer Science & Business Media
Masaoka S, Ohe T, Sakota N (1993) Production of cellulose from glucose by Acetobacter xylinum.J Ferment Bioeng 75(1):18–22
Mathew AP et al. (2014)Process scale up and characterization of wood cellulose nanocrystals hydrolysed using bioethanol pilot plant.Indus Crops Products 58:212–219
Meesorn W et al. (2017) A simple and versatile strategy to improve the mechanical properties of polymer nanocomposites with cellulose nanocrystals.Macromolecules 50(6):2364–2374
Meesorn W, Zoppe JO, Weder C (2019) Stiffness-changing of polymer nanocomposites with cellulose nanocrystals and polymeric dispersant. Macromol Rapid Commun 40(9):1800910
Moon RJ et al. (2011) Cellulose nanomaterials review: structure, properties and nanocomposites.Chem Soc Rev 40(7):3941–3994
Natarajan B et al. (2018) Binary cellulose nanocrystal blends for bioinspired damage tolerant photonic films.Adv Funct Mater 28(26):1800032. Beck-Candanedo S, Roman M, Gray DG (2005) Effect of reaction conditions on the properties and behavior of wood cellulose nanocrystal suspensions.Biomacromolecules 6(2):1048–1054
Oksman K, Sain M (2005) Cellulose nanocomposites: processing, characterization and properties
Park S et al. (2010) Cellulose crystallinity index: measurement techniques and their impact on interpreting cellulase performance.Biotechnol Biofuels 3(1):10

Peng BL et al (2011) Chemistry and applications of nanocrystalline cellulose and its derivatives: a nanotechnology perspective. Can J Chem Eng 89(5):1191–1206
Purves CB (1954) Chemical nature of cellulose and its derivatives. In: Cellulose and cellulose derivatives, part 1, pp 29–98
Revol J-F (1982) On the cross-sectional shape of cellulose crystallites in Valonia ventricosa. Carbohyd Polym 2(2):123–134
Roman M, Winter WT (2004) Effect of sulfate groups from sulfuric acid hydrolysis on the thermal degradation behaviour of bacterial cellulose. Biomacromol 5:1671–1677
Rusli R et al. (2011) Stress transfer in cellulose nanowhisker composites influence of whisker aspect ratio and surface charge.Biomacromolecules 12(4):1363–1369
Rusli R et al. (2010) Stress-transfer in anisotropic and environmentally adaptive cellulose whisker nanocomposites.Biomacromolecules 11(3):762–768
Salas C et al. (2014) Nanocellulose properties and applications in colloids and interfaces.Curr Opin Colloid Interface Sci 19(5):383–396
Sapkota J et al. (2017) Polymer nanocomposites with nanorods having different length distributions.Polymer 110:284–291
Sapkota J, Garcia JCM, Lattuada M (2017) Reinterpretation of the mechanical reinforcement of polymer nanocomposites reinforced with cellulose nanorods. J Appl Polym Sci 134(35):45254
Shaheen ThI, Emam HE (2018) Sono-chemical synthesis of cellulose nanocrystals from wood sawdust using acid hydrolysis. Int J Biol Macromol 107:1599–1606
Sharma A et al. (2019) Commercial application of cellulose nano-composites-a review.Biotechnol Rep, e00316
Šturcová A, Davies GR, Eichhorn SJ (2005) Elastic modulus and stress-transfer properties of tunicate cellulose whiskers. Biomacromol 6(2):1055–1061
Sugiyama J, Vuong R, Chanzy H (1991) Electron diffraction study on the two crystalline phases occurring in native cellulose from an algal cell wall. Macromolecules 24(14):4168–4175
Takayanagi M, Uemura S, Minami S (1964) Application of equivalent model method to dynamic rheo-optical properties of crystalline polymer.J Polym Sci Part C: Polym Symposia 5(1). Wiley Subscription Services, Inc., A Wiley Company, New York
Tokoh C et al. (1998) Cellulose synthesized by Acetobacter xylinum in the presence of acetyl glucomannan.Cellulose 5(4):249–261
Turbak AF, Snyder FW, Sandberg KR (1983) Microfibrillated cellulose, a new cellulose product: properties, uses, and commercial potential.J. Appl. Polym. Sci. Appl. Polym. Symp. (United States) 37. No. CONF-8205234-Vol. 2. ITT Rayonier Inc., Shelton, WA
Ummartyotin S, Manuspiya H (2015) A critical review on cellulose: from fundamental to an approach on sensor technology. Renew Sustain Energy Rev 41:402–412
Wang B, Sain M (2007) Isolation of nanofibers from soybean source and their reinforcing capability on synthetic polymers. Compos Sci Technol 67(11–12):2521–2527
Wong KKH et al. (2009) The effect of carbon nanotube aspect ratio and loading on the elastic modulus of electrospun poly (vinyl alcohol)-carbon nanotube hybrid fibers.Carbon 47(11):2571–2578
Yamamoto H, Horn F (1994) In Situ crystallization of bacterial cellulose I. Influences of polymeric additives, stirring and temperature on the formation celluloses I α and I β as revealed by cross polarization/magic angle spinning (CP/MAS) 13 C NMR spectroscopy. Cellulose 1(1):57–66
Yang S-Y et al. (2011) Synergetic effects of graphene platelets and carbon nanotubes on the mechanical and thermal properties of epoxy composites.Carbon 49(3):793–803
Zhao Y, Li J (2014) Excellent chemical and material cellulose from tunicates: diversity in cellulose production yield and chemical and morphological structures from different tunicate species. Cellulose 21(5):3427–3441
Zuluaga R et al. (2007) Cellulose microfibrils from banana farming residues: isolation and characterization.Cellulose 14(6):585–592

Lignocellulosic Fiber-Reinforced PLA Green Composites: Effects of Chemical Fiber Treatment

Farkhondeh Hemmati, Tara Farizeh, and Jamshid Mohammadi-Roshandeh

Abstract Bio-based polymer composites have been introduced as the most promising alternatives for the petroleum-based polymer composites, owing to the depletion of fossil fuel resources, global energy crisis and growing concerns about environmental pollutants. Among them, the green biocomposites totally based on plants, which consist of lignocellulosic fibers as reinforcement agents and biopolymers as matrices, have many beneficial advantages in a wide range of applications such as availability, renewability, eco-friendly, biodegradability and low density. The most frequently used green composites are the plant fiber-reinforced poly(lactic acid) (PLA) biocomposites. Regardless to the sustainability and ecologically friendly properties, PLA/plant fiber biocomposites must be modified to gain a comparable performance with the petroleum-based composites. Different chemical, physical, physiochemical and biological modification methods have been developed to treat the lignocellulosic fibers for improving the matrix/filler interfacial adhesion and biocomposite final properties. Through the literature, the most widely applied methods are the fiber chemical modifications. In this chapter, the effects of different chemical treatments of plant fibers, as the most feasible modification processes, in the PLA-based biocomposites have been discussed and the importance of choosing proper reaction conditions on controlling the biocomposite performance is clarified.

Keywords Poly (lactic acid) · Plant fibers · Biocomposites · Chemical treatment

1 Introduction

In recent decades, biodegradable polymers have been considered as promising substitutes for the petroleum-based polymers owing to the growing environmental awareness and worldwide concerns about the global warming and plastic pollutants (Sharif et al. 2019; Siakeng et al. 2019a). Using biodegradable plastics may alleviates the environmental problems caused by the large amounts of non-biodegradable plastic

F. Hemmati (✉) · T. Farizeh · J. Mohammadi-Roshandeh
Caspian Faculty of Engineering, College of Engineering, University of Tehran, Guilan, Iran
e-mail: f.hemmati@ut.ac.ir

M. T. Hameed Sultan et al. (eds.), *Biocomposite Materials*, Composites Science and Technology, https://doi.org/10.1007/978-981-33-4091-6_5

wastes from huge daily consumptions of humans (Singhvi et al. 2019). Recently, poly(lactic acid) (PLA) or polylactide, among different biodegradable polymers, has been attracted a great attention as the most promising substitute for the fossil fuel-based polymers (Avérous 2008; Singhvi et al. 2019). In fact, this biopolymer is a renewable and compostable thermoplastic aliphatic polyester, which has contributed to the global plastic market, due to the reasonable price and favorable properties (Saeidlou et al. 2012). With repeating unit of $C_3H_6O_3$, PLA is a nontoxic, biocompatible and bio-based polymer that can be completely produced from the annual renewable resources such as corn starch and sugar beets (Avinc and Khoddami 2009; Ding et al. 2018; Nofar et al. 2019).

The production process of PLA requires about 50% less non-renewable energy in comparison with the synthetic process of common synthetic plastics like polypropylene (PP), polyethylene (PE), polystyrene (PS), etc. (Ding et al. 2018). This eco-friendly polyester has high modulus and good transparency, comparable with PE, PS and poly(ethylene terephthalate) (PET), and can be shaped as fibers, films and household goods using common melt-processing machineries (Saeidlou et al. 2012; Sharif et al. 2019). Although PLA has been recognized as a proper substitute for synthetic polymers in packaging, electronics, non-woven fibers and household products, most of its primary applications have been limited to the biomedical field (Sharif et al. 2019). Appropriate mechanical properties, good biocompatibility and biodegradability, non-toxicity and thermal plasticity of PLA make it suitable for sutures, blood vessels, drug-delivery systems, resorbable implants and tissue scaffold in this field (Savioli Lopes et al. 2012). It is worth noting that the limitation of the primary uses of PLA in the biomedical applications was resulted from the low availability, high cost of production and low molecular weight (M_w) of the synthesized biopolymer. However, the recent developments in the dextrose fermentation process of corn starch has eventuated in the cost reduction of lactic acid (LA), which is the building block of PLA chains (Avinc and Khoddami 2009). Hydrolytic degradation of PLA macromolecules converts the chains into the LA monomers (Ding et al. 2018). There are different synthesis methods for the PLA production. Some of them have been applied in industrial scales.

2 PLA Synthesis Methods and Properties

2.1 PLA Synthesis

Synthesis of PLA, usually begins with producing LA monomer and finishes with polymerization of an intermediate material known as lactide (Singhvi et al. 2019). Overall, there are two feedstocks for the LA production. One of them is the petroleum resources by which LA is obtained through the chemical synthesis route. The other one is the natural feedstock by which LA is synthesized through the carbohydrate fermentation process. The biotechnology method of LA production provides more

that 90% market share (Hamad et al. 2015). The reasons behind paying special attention to the natural feedstock can be traced to the less dependence on the fossil fuels, less greenhouse gas emissions, use of biocatalysts and the possibility of producing LA with higher purity (Singhvi et al. 2019). LA can be synthesized by the bacterial fermentation of the food crops such as corn, wheat, rice, potato, sugar beet, sugar cane or agricultural wastes such as whey and cellulosic biomass (Ahmed and Varshney 2011).This method of synthesis mostly leads to an optically active enantiomer of LA, called Levo-lactic acid (L-LA) (Hamad et al. 2015). Nonetheless, the chemical route results in a racemic mixture of two optically active isomers of LA, Levo- (L-LA) and Dextro-lactic acid (D-LA), which can be considered as the main drawback of this method (Singhvi et al. 2019).

As a matter of fact, Lactic acid or 2-hydroxypropionic acid ($CH_3CHOHCOOH$) has a chiral carbon atom and can be synthesized to form L or D optical active enantiomers (Sharif et al. 2019). A mixture of approximately 99.5% L-form and 0.5% D-Form yields from the bacterial fermentation. The properties of L and D enantiomers are similar, except for the rotation direction of the plane polarized light. The rotation of the polarized light for L-LA isomer is clockwise, whereas the rotation for D-LA is counterclockwise (Avinc and Khoddami 2009). The chemical structures of the possible stereoisomerisms of LA and natural fermentation route of LA is schematically shown in Fig. 1. Undoubtedly, the ratio and distribution of these stereoisomers along the PLA backbone substantially change the properties and processability of the biopolymer (Hassan et al. 2013).

As it is also illustrated in Fig. 1, there are three common procedures for the PLA synthesis: (I) polycondensation of the LA monomer and increasing the PLA molecular weight using coupling agents, (II) ring-opening polymerization (ROP) of LA cyclic dimer, and (III) direct methods including azeotropic dehydration polycondensation and enzymatic polymerization (Savioli Lopes et al. 2012).

In the first route (polycondensation), the condensation reaction of the bifunctional LA monomer is performed under vacuum and at high temperatures. However, the method just yields to the PLA prepolymers with low to moderate molecular weights ($M_w = 10{,}000$–$20{,}000$ g/mol) owing to the problems in the water removal and impurities. This method is feasible through solution and melt polymerization processes. It is a single-stage process, fairly economical and easy to control. However, the low molecular weight of the synthesized PLA makes it inadequate for the plastic industrial applications. Using chain extenders or esterification-promoting agents is a common solution to modify the low molecular weight of PLA chains (Singhvi et al. 2019). One may keep in mind that this modification leads to higher costs and complexity of the synthesis process. Moreover, the presence of active chain-extending agents, oligomers and metallic impurities, which are applied as catalysts, are the main disadvantages of this synthesis method (Avérous 2008).

The mentioned second procedure for the PLA synthesis is the most widely used method for producing the PLA chains with high molecular weight. Because of the importance and prevalence of this method, PLA is also called polylactide. ROP reaction includes three stages: (I) condensation polymerization of LA, (II) depolymerization of PLA to the LA cyclic dimer or lactide and (III) ring-opening polymerization

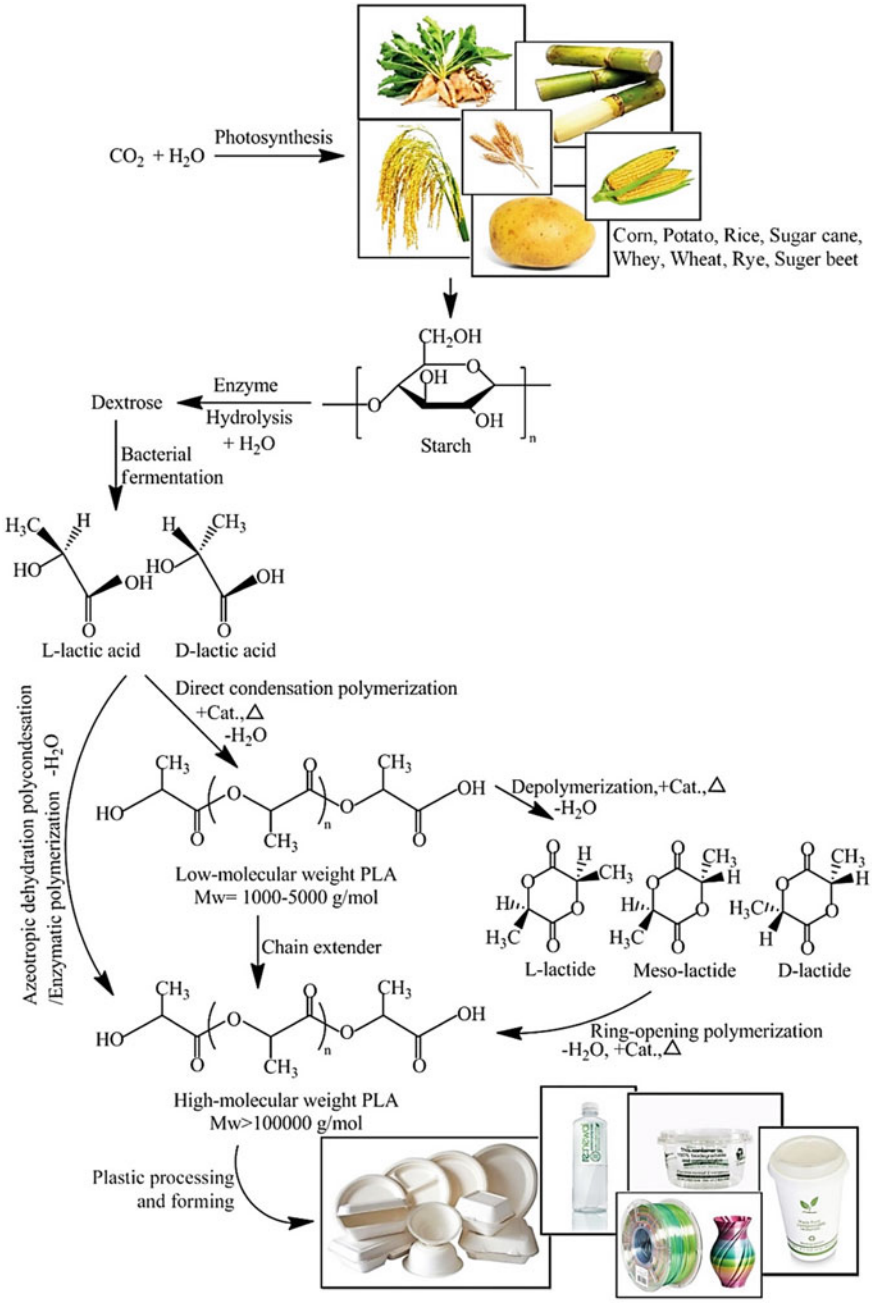

Fig. 1 Schematic drawing for the synthesis of lactic acid, lactide and PLA (Avérous 2008; Avinc and Khoddami 2009; Sharif et al. 2019)

of lactide (Ding et al. 2018; Singhvi et al. 2019). The PLA synthesis through ROP procedure is relatively mild and has higher rates. Nevertheless, the need for the additional separation and purification process of lactide makes ROP method more complex and expensive. It must be noted that catalysts based on metals such as tin, aluminum, lead, zinc and etc. must be employed in ROP reaction, which their residual traces are not approving in some application fields such as biomedical or food industries (Avinc and Khoddami 2009; Singhvi et al. 2019). Since an asymmetric carbon center is present in LA, the synthesis of Lactide can lead to different stereoisomeric forms including D-lactide, L-lactide and meso-lactide (Avinc and Khoddami 2009). Possible stereochemistry configurations of lactide are also shown in Fig. 1.

The PLA polymers synthesized purely from L-lactide or D-lactide are called poly(L-lactic acid) (PLLA) and poly(D-lactic acid) (PDLA), respectively. The ROP polymerization of L-lactide and D-lactide mixture with minimum content of 10% of one the stereoisomers bring about an amorphous PLA (Ding et al. 2018). A wide range of PLA polymers with completely different properties can be synthesized through the ROP procedure. This can be achieved by controlling the ratio and sequences of the stereoisomeric units of L- and D-lactide in the synthesized PLA linear macromolecules through changing the reaction temperature and time and the catalyst type and composition (Avinc and Khoddami 2009; Siakeng et al. 2019a). The ROP synthesis of PLA is possible through different polymerization methods including solution, bulk, melt and suspension polymerization processes. However, in industrial scale, it is preferred to apply the bulk and melt polymerization processes by using lower amounts of non-toxic catalysts (Avérous 2008).

The third method mentioned in the feasible PLA synthesis procedures is a direct route for the PLA synthesis having high molecular weight. This method is more eco-friendly and necessitates mild reaction conditions. The enzymatic synthesis method of PLA yields polyester chains with proper structures by using low cost raw materials (Singhvi et al. 2019). Although direct methods based on azeotropic dehydration polycondensation and enzymatic polymerization have some advantages, but more researches are required for this synthesis route to be commercialized (Siakeng et al. 2019a). As mentioned before, the optical isomers of the PLA building blocks provide great opportunities to synthesize a wide range of PLA grades with different microstructures and properties by controlling the stereochemistry of the chain repeating units.

2.2 PLA Properties

One may know that the stereochemistry of the macromolecular repeating units determines the crystallinity degree, crystal morphology, mechanical performance, degradation rate and thermal properties of PLA (Ding et al. 2018). In fact, completely amorphous or semi-crystalline biodegradable PLA can be synthesized by controlling the composition and sequence of the optically active isomers in the chain backbones. Moreover, the PLA crystallinity behavior depends on the molecular weight,

branching, thermal history and additives (Ahmed and Varshney 2011). It can be seen in Fig. 2, the ratio of L and D stereoisomers and distribution of them across the chain backbone along with the polymerization degree determine the melting temperature (T_m) and glass transition temperature (T_g). For instance, a highly crystalline PLA polymer can be synthesized from a combination of L- and D-lactide monomers with less than 2% of D isomer content. Amorphous PLA is obtained at D-lactide content more than 15%. Moreover, the synthesized PLA from meso-lactide is also amorphous (Avinc and Khoddami 2009). On the other hand, pure PLLA is relatively stiff semi-crystalline material with ordered molecular structure and maximum T_m of 175–180 °C. Increasing the D-lactide level as an optical impurity in the PLA chain, at a constant molecular weight, leads to a decrease in the crystalline order, crystallization kinetics, T_m and T_g (See Fig. 2a). Furthermore, the desired hardness, toughness, biodegradation rate, melting temperature and crystallinity degree can be attained by adding D-lactide units to the PLLA chain. Normally, the D optical isomer as an impurity is present in the lactic acid obtained from the bacterial fermentation process (Avinc and Khoddami 2009). As it is evident in Fig. 2a, an augmentation in the molecular weight (M_n) up to $10\frac{Kg}{mol}$ increases the T_m and T_g of PLA, while these temperatures remain constant by increasing the molecular weight more than $100\frac{Kg}{mol}$. Melting temperature of the PLA oligomer is 90 °C and for PLA with M_n of $100\frac{Kg}{mol}$ reaches 185 °C (Saeidlou et al. 2012).

Desirable properties of PLA such as transparency, high modulus, strength and rigidity, glossy appearance, good barrier properties and processability make it as an appropriate substitute for the petroleum-based plastics such as PET, PS, PP and high density polyethylene (HDPE) in various applications (Nofar et al. 2019; Siakeng et al. 2019a). Some of these uses are packaging applications, films, fibers and textiles, construction products and automobile parts (Nofar et al. 2019). PLA (Biomer L9000 grade) has properties such as Young modulus of about 3.6 GPa, tensile strength of about 70 MPa, strain at break of about 2.4%, flexural strength of about 98 $\frac{N}{m^2}$, impact strength of about 16.5 kJ, notched impact strength of about 3.3 $\frac{KJ}{m^2}$, melt flow index of

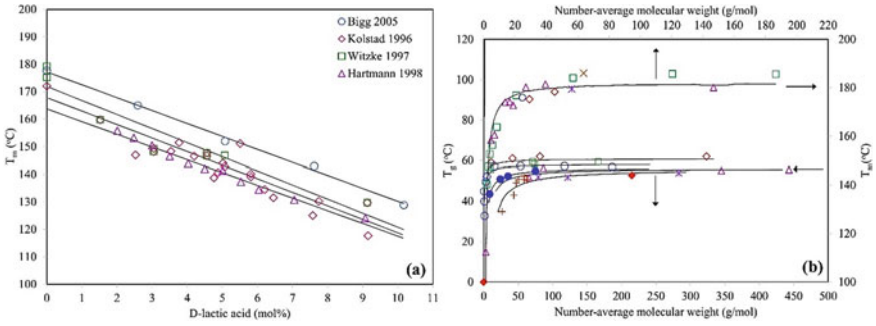

Fig. 2 **a** Melting point versus D-lactic acid content in PLA chain, **b** Melting point and glass transition temperature versus number-average molecular weight. Adapted to (Bigg 2005; Hartmann 1998; Kolstad 1996; Saeidlou et al. 2012; Witzke 1997)

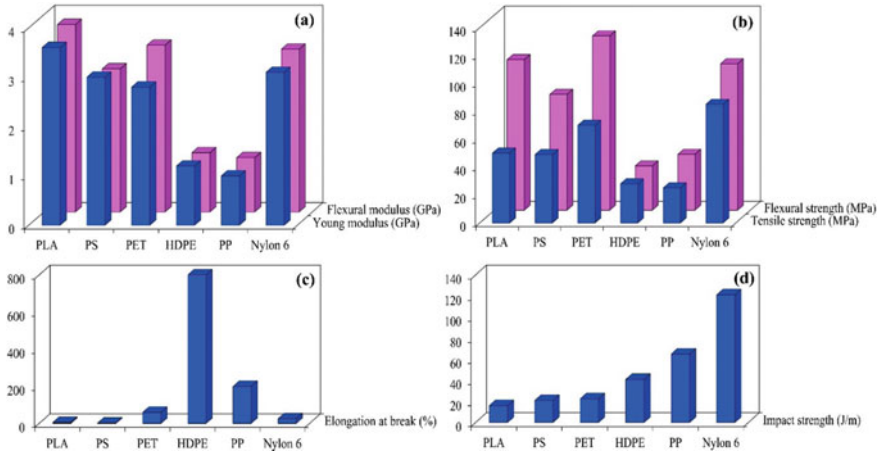

Fig. 3 **a** Young and flexural modulus, **b** tensile and flexural strength, **c** elongation at break and **d** impact strength of PLA and some of common plastics

3–6 $\frac{g}{10\,min}$, density of about 1.25 $\frac{g}{cm^3}$ and moisture absorption of about 0.3% (Hassan et al. 2013). Some properties of PLA are compared with the analogues properties of the highly consumed plastics in Fig. 3. It can be found in Fig. 3 that despite its biodegradability, PLA has comparable properties with common synthetic polymers, especially for Young modulus, flexural modulus and tensile strength. Furthermore, PLA can be processed and shaped to final products similar to other thermoplastic materials by using common melt processing techniques such as extrusion, injection-molding, blow molding, thermoforming extrusion-coating and spinning (Hassan et al. 2013). PLA under shear flow field in the molten state follows the power-law like most of the petroleum-based polymers. For sheer rates up to 10 s^{-1}, it shows a Newtonian behavior, and for higher sheer rates, it demonstrates a shear-thinning melt behavior (Hamad et al. 2015). Pseudoplastic index of PLA melt is in the range of 0.2–0.3, depending on the chain structure.

Moreover, entanglement threshold of PLA chains happens at molecular weights of about $10^4 \frac{g}{mol}$. Molecular weight distribution and branching significantly affect the melt viscosity of PLA (Avérous 2008). The zero-shear viscosity of PLA melt is roughly scaled the molecular weight with power of 3.4–4 (Ahmed and Varshney 2011). PLA dissolves in solvents such as chloroform, acetonitrile, dioxane, furan and fluorinated and chlorinated organic compounds. PLA's non-solvents includes water, alcohols (such as methanol and ethanol) and alkanes (such as hexane and heptane) (Avérous 2008; Sharif et al. 2019). This aliphatic polyester is rather hydrophobic with surface energy of 49 $\frac{mJ}{m^2}$. PLA chains with L-lactide content of 92% and meso-lactide level of 8% have dispersive surface energy (γ^d) of 37 $\frac{mJ}{m^2}$ and polar surface energy (γ^p) of 11 $\frac{mJ}{m^2}$. The water absorption of PLA films is low similar to PET films. In packaging applications, the permeability of PLA films against CO_2 and O_2 gases is lower than PS and is in the range of PET permeability (Ahmed and Varshney 2011).

In the biodegradation process, PLA chains are primitively degraded by hydrolysis reaction after being in moisture exposure for several months. The degradation process of PLA mainly consists of two steps: first, random and non-enzymatic chain scission of ester groups in abiotic conditions that results in a decrease in the molecular weight. Second step includes further molecular weight loss to reach the monomers and oligomers with low molecular weight. This process continues until the final mineralization under biotic degradation conditions. At this stage, the microorganisms can begin to metabolize the residues and produce CO_2 and water (Savioli Lopes et al. 2012). Hence, the natural life cycle of biomasses is also possible for this biopolymer. Additionally, after serving the original purpose, it can be recycled and hydrolyzed to its building blocks, LA molecules (Hassan et al. 2013).

Despite considerable advantages of PLA as a thermoplastic, which make it a competitive plastic with the common synthetic polymers such as PS, PE and PET, there are some disadvantages that limit the potential application range of PLA. Some of the major drawbacks of PLA are listed below:

1. Intrinsic brittleness: PLA fractures in very small strains, less than 10% (See Fig. 3). PLA is brittle even more than PS. The combination of brittle mechanical behavior with low impact strength confines the PLA applications (Hassan et al. 2013; Siakeng et al. 2019a). Different plasticizers such as lactide monomer, poly(ethylene glycol) (PEG) and poly(propylene glycol) (PPG) with low molecular weights and fatty acids are used to improve the brittle fracture behavior (Avérous 2008).
2. Slow biodegradation: The biodegradation rate of PLA depends on the crystallinity degree, molecular weight, molecular orientation, permeability, surface characteristics, chain stereochemistry and environmental conditions. In some cases, biodegradation of PLA took several years reportedly. The required long period of time for PLA biodegradation besides the high crystallinity degree of the residual fragments may cause problems. For instance, a second surgery was reported to be performed for removal a PLA-based implant after three years from the first surgery for implant embedment (Sharif et al. 2019).
3. Low dimensional stability: The T_g of PLA is low (50–60 °C), comparing with the other polyesters. This temperature for PET is about 80 °C. This low temperature normally leads to low heat distortion temperature (HDT) and Vicat softening point. Hence, the service temperature for the PLA-based products are limited. For example, PLA is not suitable for packaging of foodstuffs containing hot liquids (Saeidlou et al. 2012; Sharif et al. 2019).
4. Slow crystallization rate: Due to the low crystallization rate of the biopolymer chains, the processability and service conditions of PLA have some limitations (Nofar et al. 2019). If the PLA chains can be crystallized to high extents, the corresponding HDT and Vicat softening point would shift to larger temperatures more than 30 °C and 100 °C, respectively (Saeidlou et al. 2012).
5. Low thermal stability: The rheological behavior of PLA melt is different from the behavior of common petroleum-based polymers and it has lower melt strength owing to the low chemical stability of PLA chains in the melt

processing conditions. Consequently, PLA has narrower processing window (Siakeng et al. 2019a). Poor melt strength and low crystallization rate of PLA (as mentioned earlier) impose some restrictions on the processability, formability and foamability of the biopolymer (Nofar et al. 2019).

6. Hydrophobicity: The water contact angle of PLA is about 80°. Hence, the biological cells may have less tendency to adhere on the PLA surface (Sharif et al. 2019).
7. Throughout the literature, lots of researches have been devoted to find effective solutions for the mentioned disadvantages (Nofar et al. 2019). One relatively economical approach to improve the final properties of the PLA-based products is using the lignocellulosic fibers as reinforcement agents in the PLA matrix. This approach is expected to make a considerable improvement in the PLA performance, while maintains the renewable and biodegradable nature of the PLA-based products.

3 Lignocellulosic Fibers as Reinforcement Agents

Fillers are used in polymers to improve the properties and decrease the cost of final products. The common and conventional fillers of polymers are glass and carbon fibers, kevlar, silica, calcium carbonate, clay, graphite, carbon black and carbon nanotubes (Zhang et al. 2017). Using synthetic fibers as reinforcement agents in plastic matrices gives the composites the desired durability and structural properties required in many applications. However, the energy crisis, depletion of petroleum resources and growing environmental concerns have led to a growing demand for the renewable resources (Sisti et al. 2018). Unlike man-made fibers, natural fibers as renewable resources do not cause environmental issues in their manufacturing process and disposal. Moreover, natural fibers have some advantages such as light weight, low cost, renewability, biodegradability, recyclability, flexibility, ecologically friendly, versatility and high specific strength (Zhang et al. 2017; Zimniewska and Wladyka-Przybylak 2016).

Based on the used resources, natural fibers are categorized to three distinct groups, including animal, mineral and plant fibers. The animal fibers such as wool, silk and hair are used for reinforcing purposes have proteins as their major component. The mineral fibers like asbestos have been also applied to reinforce polymers. However, their applications have carcinogenic effects by inhalation and ingestion. Plant fibers, which are lignocellulosic materials, contain cellulose as a main constituent. It has been repeatedly reported that the plant fibers have higher strength and stiffness comparing to the animal fibers. Therefore, plant fibers are the most appropriate reinforcement agents for polymer matrices among all natural fibers (Mochane et al. 2019; Zhang et al. 2017).

Plant fibers have gotten a special place as reinforcement agents in the composite market in recent decades and today, the plant fiber-based biocomposites are extensively used in different industries from automotive to construction sectors (Sisti et al.

2018). There is a wide range of fibrous plants, more than 2000 species, which can be applied as reinforcement agents in polymers. However, only plants having high fiber contents have been applied on industrial scale, owing to the possibility for easy and effective fiber extraction (Zimniewska and Wladyka-Przybylak 2016). The most important fibers used in polymer-based composites are flax, hemp, jute, ramie, kenaf, sisal, coir, abaca and pineapple leaf fibers (Siakeng et al. 2019a; Sisti et al. 2018; Zimniewska and Wladyka-Przybylak 2016).

Based on the utilization routes, the plants used in the natural fiber fabrication process are classified into primary and secondary plants. Primary plants are those that are cultivated just for fiber production such as cotton, jute, java-kapok, hemp and kenaf. In contrast, secondary plants are the ones from which fibers are produced as by-products like banana, coconut coir, pineapple, oil palm and rice straw (Siakeng et al. 2019a).

The lignocellulosic fibers have enough potential to replace the synthetic fibers such as glass fibers in reinforcing polymers. In addition to their renewability and biodegradability, natural fibers have been considered as beneficial reinforcement agents because of their favorable properties such as low density and appropriate mechanical performance. The natural fibers with a density of 1.15–1.5 $\frac{g}{cm^3}$ are much lighter than E-glass fibers with a density of 2.4 $\frac{g}{cm^3}$. The usage of plant fibers, as renewable resources, leads to the fabrication of "green" products, which are recyclable on industrial scale. As a result, this eventuates in less emission of greenhouse gases and reduced generation of pollutant wastes. For example, the cultivation of hemp in an agricultural land with area of 1 ha leads to the absorption of approximately 3.5 tons of atmospheric carbon dioxide gas in one harvest season. On the other hand, the production of 1 ton of polypropylene (PP) synthetic plastic release 3 tons of CO_2 gas into the atmosphere (Zimniewska and Wladyka-Przybylak 2016).

Moreover, plant fibers like flax, hemp and ramie fibers have relatively good mechanical properties and their specific modulus and strength are comparable to the synthetic glass fibers (Kozlowski and Wladyka-Przybylak 2004). In Fig. 4, the physical appearance and some of the physical and mechanical properties of lignocellulosic fibers and synthetic fibers are compared with each other.

It is clear from this figure that the elongation at break for natural fibers are often higher than the ones for glass and carbon fibers, hence resulting in a better performance of natural fiber-reinforced composites. Furthermore, plant fibers are suitable for the production of thermal insulators, because of the low thermal conductivity of natural fibers in the range of 0.29–0.32 $\frac{W}{m.K}$ (Kozlowski and Wladyka-Przybylak 2004). In general, the advantages of lignocellulosic fibers in polymer-based composites over the synthetic fibers can be briefly mentioned as follows: Sustainability and renewability, easy accessibility and lower cost, biodegradability, thermal recyclability, acceptable specific strength and other specific properties, easy extraction of fibers, low density, good thermal properties, more friendly processing and less tool wear, no skin irritation and improved energy recovery.

Their main disadvantages can be outlined as follows: Lower strength specially impact strength, higher moisture absorption and fiber swelling, limited maximum processing temperatures, poor flame resistance, variable quality (The properties of

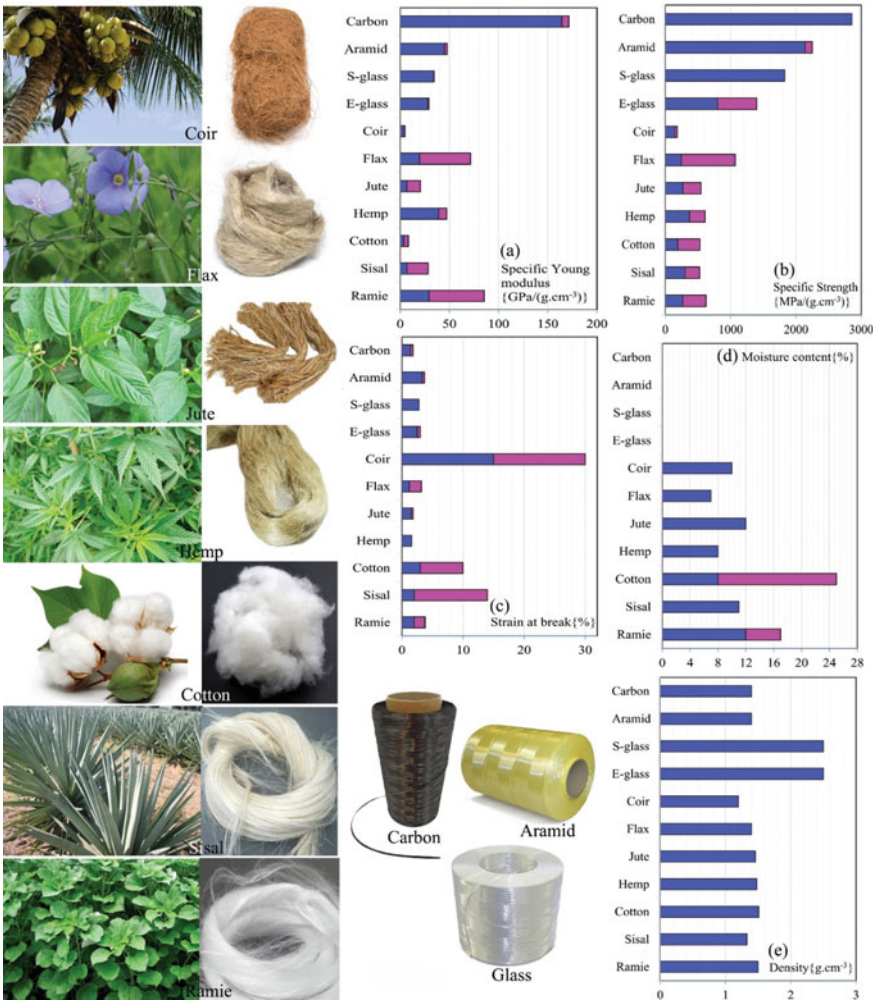

Fig. 4 Physical appearance of plants, the resultant natural fibers as well as synthetic fibers, (**a**)–(**e**) column charts for some of the physical and mechanical properties of plant and synthetic fibers (Ballesteros et al. 2018; Mochane et al. 2019; Siakeng et al. 2019a)

plant fibers are strongly dependent to the crop variety, ecotype, maturity, cultivation place, retting process and fiber processing tools.), less durability (Interfacial adhesion of polymer matrix and fibers must be modified) and price fluctuations. Despite some drawbacks in properties, plant fibers have been generally accepted as the most promising alternative of synthetic fibers in many polymeric composite applications.

All plant fibers are naturally lignocellulosic and comprise of cellulose, hemicellulose, lignin, pectin and waxes, except for cotton fibers. In fact, more than 80% of dried weight of lignocellulosic fibers include cellulose, hemicellulose and lignin.

The small remaining part constitutes of other fiber components such as pectin, waxes and protein (Shafiei et al. 2015; Zhang et al. 2017). The cellulose content of each fiber determines the fiber strength and modulus. Most of the natural fiber properties including the mechanical characteristics depend on the cellulose type, microfiber angle, degree of polymerization and overall cellulose content of the fiber (Siakeng et al. 2019a).

The composition of various fiber components is controlled by the nature of fibers and the soil and environmental conditions, in which the plant is grown. The chemical compositions of some plant fibers are shown in

Table 1 the lignocellulosic fibers are categorized into seven groups based on their origins as:

1. Fibers from bast/stem including jute, flax, hemp, ramie, mesta, kenaf and roselle
2. Fibers from fruit such as coir and oil-palm
3. Fibers from grass/reeds like bamboo, bagasse, corn, sabai, rape, elephant grass, esparto and canary
4. Fibers from leaf including pineapple, sisal, banana, abaca, henequen, agave and raphia
5. Fibers from seed containing cotton, kapok, milkweed and loofah
6. Fibers from stalk like wheat, maize, barely, oat, rice and rye
7. Fibers from wood consisting of hardwood and softwood (Kozlowski and Wladyka-Przybylak 2004; Siakeng et al. 2019a; Sisti et al. 2018).

The bast fibers as reinforcement agents are embedded in the outer layer of bast and encompass the plant stem, thereby stabilizing the plant. With the highest cellulose contents, the bast fibers provide effectual reinforcement effect in the biocomposites. It has been reported that the leaf fibers improve the composite toughness. Moreover, the seed and fruit fibers reportedly eventuate in the elastomeric behavior of the composites (Sisti et al. 2018). Differences in the chemical compositions and physical characteristics results in a wide range of properties for the plant fibers (Kozlowski and Wladyka-Przybylak 2004).

It can be seen in Table 1 that carbohydrates along with lignin are the main components of the lignocellulosic materials. The major components of the plant cell wall are cellulose and hemicellulose carbohydrates (Shafiei et al. 2015). Pectin in lignocellulosic fibers acts like an adhesive and holds the fibers in bundles in the non-fibrous tissues. In lignocellulosic materials, hemicellulose, pectin and lignin play the role of matrix, wherein cellulose fibers are localized as a reinforcement agent (Sisti et al. 2018). In the following part, different components of plant fibers are briefly described.

3.1 Cellulose

As the main component of all plant fibers, cellulose is a linear polymer, which is composed of D-anhydroglucose units. These units are interlinked to each other at carbon-1 and carbon-4 atoms through β-1,4-glucosidic bonds (Saha et al. 2016).

Table 1 Chemical compositions of some common lignocellulosic fibers (Mochane et al. 2019; Siakeng et al. 2019a)

Fiber type		Cellulose (wt%)	Hemi-Cellulose (wt%)	Lignin (wt%)	Pectin (wt%)	Wax (wt%)	Ash (wt%)	Microfibril angle (degree)
Bast	Flax	71	18.6–20.6	2.2	2.3	1.7	–	5–10
	Hemp	68	15	10	1	0.8	0.8	2–6.2
	Jute	61–71	14–20	12–13	–	0.5	0.8	8
	Kenaf	45–57	21.5	8-13	3–5	–	2–5	2–6.2
	Ramie	68.6–76.2	13–16	0.6–0.7	1.9	0.3	–	7.5
Fruit	Coir	32–43	0.15–0.25	40–45	3–4	–	2.7–10.2	30–39
	Oil-palm	65	–	29	–	–	2.4	46
Grass/reeds	Bagasse	55.2	16.8	25.3	–	–	1.5–5	–
	Bamboo	73.83	12.49	10.15	0.37	–	–	–
	Elephant grass	45.6	–	17.7	–	–	5	–
Leaf	Abaca	56–63	20–25	7–9	–	3	3	20–25
	Banana	60–65	6–8	5–10	–	–	9.6	11
	Henequen	77.6	4–8	13.1	–	–	–	–
	Pineapple	70–80	18.8	12.7	1.1–1.2	3.2–4.2	0.9–1.2	8–15
	Sisal	65	12	9.9	10	2	0.6–1	10–22
Seed	Cotton	83–91	3	–	0.6	8–9	–	20–30
Stalk	Rice	41–57	33	8–19	–	8–35	14–20	–
	Wheat	38–45	15–31	12–20	–	–	6.8	–

In cellulose chain, two adjacent glucose molecules named as cellobiose rotates 180 degrees around the chain backbone, relative to the neighboring repeat unit (See Fig. 5a) (Shafiei et al. 2015). Each glucose unit has three hydroxyl groups that can make inter- and intra-molecular hydrogen bonds. Some of these bonds are illustratively shown in Fig. 5b. Therefore, the plant fibers are intrinsically hydrophilic. The inter-molecular O_3–HO_5 hydrogen bonding gives the cellulose a linear and hard structure (Kozlowski and Wladyka-Przybylak 2004). Furthermore, hydrogen bonds cause the cellulose chains to mostly orient in a parallel and ordered structure. The cellulose chains with ordered orientation form the crystalline cellulose owing to lack of side groups. The crystalline cellulose plays the main role in the fiber tensile strength and flexibility (Saha et al. 2016). Cellulose may have crystalline, para-crystalline or amorphous structures depending on the source and cellulose extraction method (Shafiei et al. 2015).

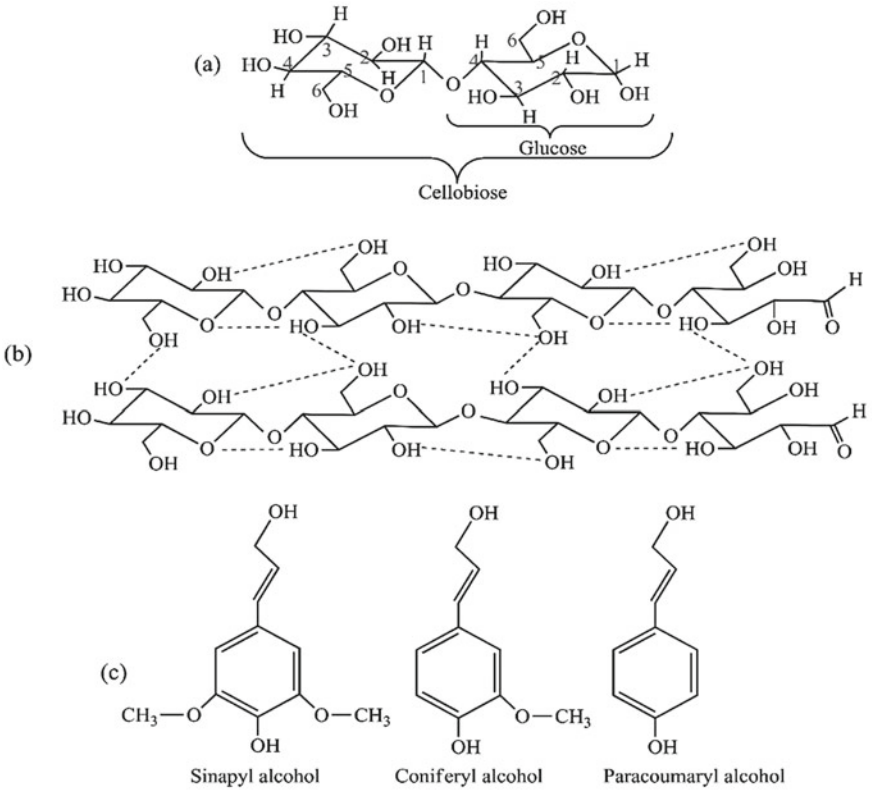

Fig. 5 **a** Cellulose repeating unit, **b** intra- and inter-molecular hydrogen bonds in cellulose respectively shown by blue and red colors and **c** main monomeric units of lignin (Orue et al. 2018; Shafiei et al. 2015)

3.2 Hemicellulose

Hemicelluloses are hetero polymers formed from polysaccharides and polyuronides, which are synthesized and packed in the Golgi vesicles of the plants. Various types of hexosans (mannan, glucosan, galactan and rhamnan) and pentosans (arabinan and xylan) are available in the hemicellulose polysaccharides (Shafiei et al. 2015). Hemicellulose chemically differs from cellulose in several aspects:

1. The hemicellulose macromolecule consists of different sugar units.
2. The degree of polymerization of hemicellulose is 10 to 100 times lower than that of cellulose.
3. Hemicellulose has amorphous structure owing to many chain branches along the polymer backbone.
4. Hemicellulose is more hydrophilic than cellulose and is highly susceptible to acid or alkali hydrolysis. The removal of hemicelluloses from the lignocellulosic fibers increases the tensile strength of fibers (Saha et al. 2016).

3.3 Lignin

Lignin is a complex and crosslinked polymer having an amorphous and 3-dimensional network structure. Different aliphatic and aromatic monomers like p-coumaryl alcohol, P-coniferyl alcohol and sinapyl alcohol compose the lignin networks (Fig. 5). Moreover, the subunits are present in lignin structure with side groups (Saha et al. 2016; Shafiei et al. 2015). The cement like behavior of lignin leads to an improvement in the strength of crystalline cellulose in the layers of plant cell walls, hence resulting in plant growth to reach higher heights. On the other hand, the hydrophobicity of lignin facilitates the water and nutrient transfer (Shafiei et al. 2015). Moreover, lignin protects the plant well, against microbial attacks, moisture and external environmental factors (A. Orue et al. 2018).

3.4 Other Components

As mentioned earlier, more than 80% of dried weight of lignocellulosic materials is composed of cellulose, hemicellulose and lignin. The residual part includes many different materials in small quantities. These materials can be divided into the extractive and non-extractive substances. The first group, which are extracted by polar and non-polar solvents, comprises of fats, fatty acids, isoprene, alcohols, ketones and phenols. The latter group consists of proteins, pectin, alkali-earth carbonates, starch, silica and oxalates (Shafiei et al. 2015).

The quality and properties of lignocellulosic fibers have a great importance in the polymer-based composite performance. The main disadvantage of natural fibers

compared with synthetic fibers is that the natural fibers do not have a constant composition and quality. The reasons behind this go to the climate conditions, crop variety and retting process. For instance, low temperatures and high relative humidity of growing season bring about the formation of more delicate and longer fibers. Besides, the efficiency of retting process, in which pectin is broken down and the fibers are released, considerably affects the fiber quality (Sisti et al. 2018). Nonetheless, the lignocellulosic fibers are applied in different polymer matrices owing to the unique and favorable properties.

The plant fiber-reinforced polymer composites are classified into different groups based on the applications. One of them is the common panel composite, wherein the lignocellulosic material is the main part, such as fiberboards and insulation boards. Polymers are used as binding materials in these applications. Another group of the reinforced composites is attributed to the products in which the lignocellulosic materials as reinforcing fillers are dispersed in a polymer matrix including rubbers, thermoplastics and thermosets. The other group is related to the nonwoven textile composites (Kozlowski and Wladyka-Przybylak 2004). Different polymers are employed in producing lignocellulosic composites including phenolic resins, epoxy resins, polyesters, polyimides, polypropylene (PP), polyurethanes (PU), polyamides (PA), polyethylene (PE), polystyrene (PS), poly(vinyl chloride) (PVC), india-rubber, starch, PLA, cellulose esters, tannin and poly(hydroxy butyric acid) (PHB) (Kozlowski and Helwig 1998; Kozlowski and Wladyka-Przybylak 2004).

Mechanical properties of the composites reinforced by lignocellulosic fibers are considerably affected by various factors such as fiber type, fiber dispersion state in matrix phase, fiber orientation and matrix/filler interfacial adhesion. The fibers having large cellulose content, in which the cellulose micro-fibrils are oriented along the fiber axial direction, show the highest mechanical performance including ramie, hemp and flax (Mochane et al. 2019). However, one may keep in mind that the low interfacial strength of most polymers with lignocellulosic fibers prevents them from competing with the reinforced composites containing synthetic fibers such as glass, carbon and aramid fibers (Kozlowski and Helwig 1998). In fact, the plant fibers have not enough compatibility with most polymers, due to the significant difference in polarity and surface energy. The matrix/filler incompatibility provokes the poor interactions between different components and formation of weak interface (Kozlowski and Wladyka-Przybylak 2004). To overcome the weakness and subsequent consequences, various treatment methods for natural fibers have been developed which are discussed in detail in the following sections.

However, the development of natural fiber-reinforced composites is progressing, and in this sector, a special attention is paid to the biodegradable polymer-based composites reinforced by plant fibers. Biodegradability and sustainability give these green composites a unique opportunity to be introduced as the most promising substitutes for the conventional polymer composites. Among all the biodegradable polymers, PLA is the most frequently used polymer in plant fiber-reinforced composites (Zhang et al. 2017).

4 Lignocellulosic Fiber-Reinforced PLA Composites: Pros and Cons

As mentioned earlier, the plant fibers-reinforced biodegradable polymers are the best candidates for "green composite" production (Mochane et al. 2019). The plant fiber-reinforced PLA biocomposites have received lots of attentions in recent years (Mochane et al. 2019; Siakeng et al. 2019a). Using PLA/plant fibers composites result in less dependence on the exhaustible resources of fossil fuels and less environmental pollution owing to the special characteristics such as eco-friendly, biodegradability, sustainability and renewability (Siakeng et al. 2019a). As it is emphasized in section one, despite some desirable properties, PLA requires to be reinforced by fibers or fillers to improve the performance. The lignocellulosic fiber-reinforced PLA composites have some favorable properties such as high stiffness and specific strength, good processability, recyclability and biodegradability (Siakeng et al. 2019a). However, one may notice that the industrial applications of PLA is limited due to the low availability and high production cost. The incorporation of abundant plant fibers into the biopolymer is in fact an approach to develop sustainable PLA products (Abu Ghalia and Dahman 2017). In order to gain a noticeable market share of plastics, the PLA biocomposites must present properties comparable to the synthetic polymers (Siakeng et al. 2019a). Basically, the performance of the PLA/natural fiber biocomposites depends on different factors including physical and mechanical properties of the components (matrix and reinforcing fibers), matrix/fiber interactions, and orientation of reinforcing fibers (Zhang et al. 2017).

The most important weaknesses of PLA/lignocellulosic fiber composites are the non-uniform properties of the fibers and degree of polymerization, poor matrix/fiber adhesion, high flammability, and moisture sensitivity (Siakeng et al. 2019a). The hydroxyl groups along with other functional groups in the lignocellulosic material makes the plant fibers extremely hydrophilic (Mochane et al. 2019). In other words, the fibers are highly hydrophilic because the plentiful hydroxyl groups in the chemical structure favor the formation of strong intra- and inter-molecular hydrogen bonding (Kozlowski and Wladyka-Przybylak 2004). The strong hydrophilicity of fibers consequently leads to the most important drawback of plant fibers as reinforcement agents, i.e. poor interfacial adhesion between hydrophilic lignocellulosic fibers and hydrophobic polymer matrix (Siakeng et al. 2019a). One may know that matrix/fiber adhesion is determined by the interfacial forces including primary and secondary ones. The primary forces are short range ones that originate from the ionic, metallic and covalent bonds. The secondary or intermolecular forces are provoked by physical attractions such as Van der Waals interactions (Orue et al. 2018). Because of the large differences in polarity and surface energies, weak interfacial forces form between natural fibers and PLA matrix. Consequently, lignocellulosic fibers in PLA matrix have very poor compatibility and wettabililty. The resultant weak interface between the dispersed and matrix phases arises a substantial reduction in the interfacial adhesion and strength. The interfacial strength plays a key role in determining the final properties of the PLA-based biocomposites. The effective transfer of load from

the matrix to the reinforcing fibers has a prerequisite, i.e. adequate matrix/fiber interfacial adhesion. Once the prerequisite is met, the desirable mechanical properties of the biocomposite is attainable (Mochane et al. 2019; Zhang et al. 2017). Generally, the PLA-based biocomposites containing untreated natural fibers show extensive fiber pull-out, regardless of the plant fiber type used in PLA (Huber and Müssig 2008; Mochane et al. 2019). Moreover, weak bonding strength between the reinforcing phase and PLA chains results in matrix breakage and matrix/fiber debonding under stress and mechanical deformations. The scanning electron microscopy (SEM) images of the fractured surfaces of PLA/lignocellulosic fiber biocomposites in Fig. 6 obviously show poor fiber wetting by PLA matrix phase, large-scale debonding and fiber pull-out.

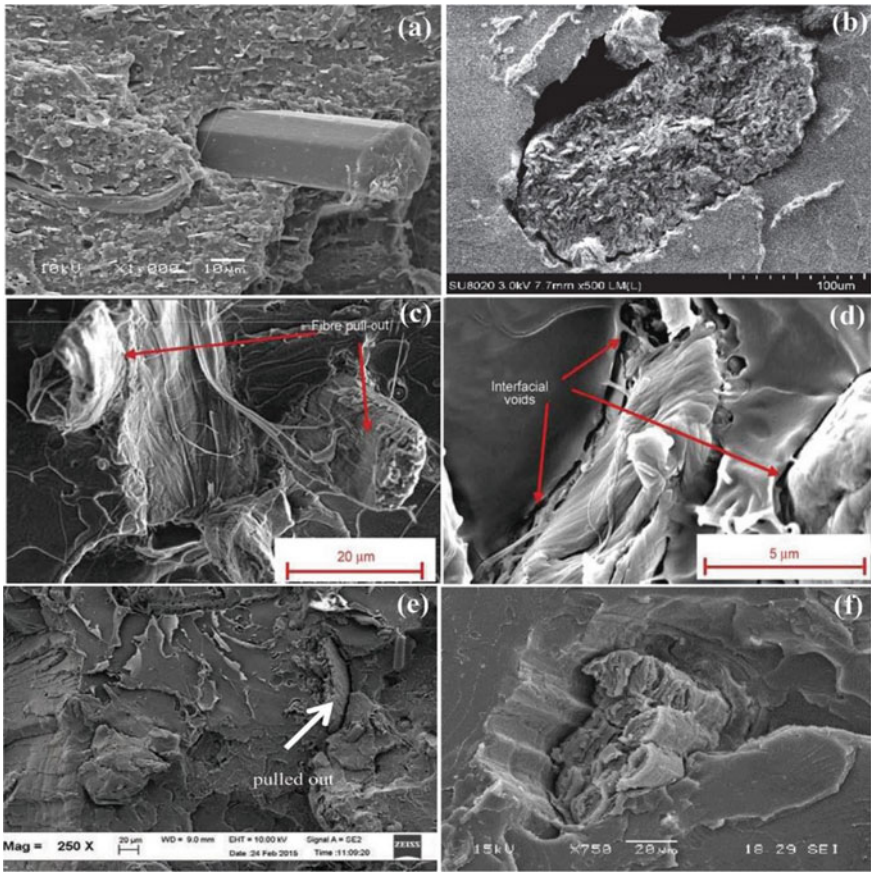

Fig. 6 SEM image of fractured surface of: **a** PLA/flax fiber composite (Liber-Kneć et al. 2015), **b** PLA/coir fiber composite (Sun et al. 2017), **c** and **d** PLA/cellulose fiber composite (Courgneau et al. 2013), **e** PLA/rice straw fiber composite (Yaacob et al. 2016) and **f** PLA/flax fiber composite (Aliotta et al. 2019)

Additionally, the hydrophilic nature of plant fibers eventuates in high water absorption of the biocomposites. The absorbed water content of fibers depends on the relative humidity of the ambient atmosphere, fiber purity and cellulose crystallinity degree. All hydroxyl groups in the amorphous regions of the lignocellulosic fiber structure are accessible sites for water absorption unlike the –OH groups inside the crystalline phase. The biocomposite strength deteriorates by water absorption. Furthermore, the high hydrophilic nature of plant fibers creates another challenge, which encounters in the fiber/matrix mixing process. The challenge attributes to the attainment of a uniform dispersion and distribution state of fibers and prevention of the formation of fiber aggregates in matrix (Kozlowski and Wladyka-Przybylak 2004). Undoubtedly, without uniform dispersion and distribution of reinforcing fibers in matrix, the biocomposite could not show an optimal performance. By improving the fiber/matrix interfacial adhesion, the dispersion state of fibers improves and less voids around the fibers embedded in the matrix are formed.

Clearly, the processing parameters such as temperature, pressure and stress flow fields can be properly adjusted to improve the fiber dispersion state. For instance, intense extensional flow fields in twin-screw extruders can facilitate the formation of more uniform mixture with better dispersion state of the reinforcing fibers. However, this melt-compounding process damage the fibers more considerably, comparing with the process using single-screw extruders. Consequently, the fiber length along with the aspect ratio decrease to higher extents. On the other hand, the mechanical properties of the biocomposite can be improved by adding more fibers to the PLA matrix. Nonetheless, there is an optimum value for the fiber loading. In larger fiber contents, the processability of the composite melt is worsened and more voids and lumens are formed and trapped around the fiber bundles. Consequently, this phenomenon restrains the fiber/matrix melt compaction, hence causing poor mechanical properties such as strength (Mochane et al. 2019).

Reduced thermal stability is another notable drawback of the PLA/lignocellulosic fiber composites comparing with the virgin PLA (Siakeng et al. 2019a). In a study (Yussuf et al. 2010), PLA/rice husk and PLA/kenaf fiber biocomposites, without fiber treatment, showed less thermal stability in comparison with the pure matrix. However, PLA/kenaf fiber composites have higher thermal stability relative to the PLA/rice husk composites owing to different compositions of the filler constituents. Moreover, it has been frequently reported that the tensile strength, strain at break, flexural strength and impact strength of PLA matrix diminish to lower values by adding plant fibers due to the weak interfacial adhesion (Faludi et al. 2013a; Nyambo et al. 2011; Sisti et al. 2018). A brief review on the PLA/untreated plant fiber composites is presented in Table 2. As explained so far, it is obvious that the treatment of lignocellulosic fibers is necessary to improve the performance of the fiber-reinforced PLA biocomposites. Through the literature, researches repeatedly confirm that the surface treatment of plant fibers, as an efficient and effective approach, results in improved matrix/fiber interfacial adhesion, better mechanical performance and lower moisture sensitivity (Siakeng et al. 2019a; Zhang et al. 2017). The fiber treatment methods can be categorized into chemical, physical, physico-chemical and biological modifications (Siakeng et al. 2019a). By applying these methods, the fiber impurities are

Table 2 Some researches on the unmodified lignocellulosic fiber/PLA biocomposites

Fiber type	Fiber content	Processing	Observed results after adding fibers to PLA	Authors (year)
Hemp fibers	1–30 wt%	Compounding by internal mixer/Hot press	• An increment in the elastic modulus up to 5.2 GPa at 20 wt% loading of hemp fibers by increasing the filler content • A decrease in the stress and strain at break by increasing the fiber content	Masirek et al. (2007)
Cotton, flax and hemp	–	Hot press	• The interfacial shear strength of composites was determined by the single fiber fragmentation test. • Poor interfacial adhesion between PLA matrix and fibers results in insufficient stress transfer to break the fibers.	Huber and Müssig (2008)
Wheat straw, corn stover and soy stalks	10–40 wt%	Compounding by twin-screw extruder/Injection molding	• A decrease in the PLA crystallization temperature, T_c • An increase in the flexural and tensile modulus • A decrease in the flexural, tensile and impact strength • More brittle failure mode of PLA • Matrix/fiber debonding, fiber pull-out and fiber fracture are observed on the SEM images of the composite fractured surfaces	Nyambo et al. (2010)
Wheat straw	30 wt%	Compounding by twin-screw extruder/Injection molding	• Increases in the Young modulus, flexural modulus and water absorption • A decrease in the flexural and tensile strength	Nyambo et al. (2010)

(continued)

Table 2 (continued)

Fiber type	Fiber content	Processing	Observed results after adding fibers to PLA	Authors (year)
Corn cob	5–60 vol%	Compounding by internal mixer/Compression molding	• An increase in the Young modulus • A decrease in the tensile strength • Further increase in the fiber content results in more increment in the Young modulus and more decrease in the tensile strength. • Matrix/fiber debonding, fiber pull-out and matrix local yielding are observed on the fractured surface	Faludi et al. (2013a)
Wood	0–60 vol%	Compounding by internal mixer/Compression molding	• An increase in the Young modulus and a decrease in the tensile strength • The addition of more fibers to PLA leads to higher increment in the Young modulus and larger decrease in the tensile strength.	Faludi et al. (2013b)
Wood, micro-crystalline cellulose and corn cob	5–60 vol%	Compounding by internal mixer/Compression molding	• A decrease in the PLA tensile strength for different loadings of fibers • The occurrence of fiber breakage in microscopic observations • Reported the need for using natural fibers with higher strength to prepare the biocomposites having improved properties	Faludi et al. (2014)
Triticale straw	10–40 vol%	Compounding by twin-screw extruder	• A decrease in the PLA thermal stability and PLA HDT • A decrease in the impact strength by increasing the fiber loading • A decrease in the tensile strength with fiber loading of 10 and 20 vol% in contrast to the tensile modulus, flexural modulus and flexural strength	Mihai and Ton-That (2014)

(continued)

Table 2 (continued)

Fiber type	Fiber content	Processing	Observed results after adding fibers to PLA	Authors (year)
Chopped flax fibers	10 wt%	Compounding by twin-screw extruder/Injection molding	• No significant improvement in the average fatigue strength by adding short flax fibers	Liber-Kneć et al. (2015)
Paddy straw powder	5–20 wt%	Compounding by internal mixer/Compression molding	• A decrease in the tensile strength and elongation in break due to poor fiber wetting by PLA matrix • Improved biodegradability of PLA in compost	(Yaacob et al. 2016)
Açaí short fibers	5–10 wt%	Cast molding	• No significant improvement in the flexural modulus by adding fibers to PLA	Santos et al. (2017)
Rice straw	5–15 vol%	Sequential layering and batch-mixed using hot press	• A decrease in the flexural strength by increasing the fiber content in PLA biocomposites	Augustine Saidi et al. (2017)
Wood, bleached kraft pulp and flax fiber	30 wt%	Compounding by twin-screw extruder/Injection molding	• No significant improvement in the tensile strength in contrast to the elastic modulus by adding medium density fiberboard (MDF) fibers • A decrease in the notched impact strength • Microscopic observations of severe fiber pull-out on the fractured surface	Thumm et al. (2018)
Sisal fibers	10–30 wt%	Compounding by internal mixer/Compression molding	• An increase in the tensile modulus • Decreases in the tensile strength and strain at break • Decreases in T_g, T_m and crystallinity degree of PLA at fiber loading of 30 wt%	Lagazzo et al. (2019)

(continued)

Table 2 (continued)

Fiber type	Fiber content	Processing	Observed results after adding fibers to PLA	Authors (year)
Pineapple fibers and coir fibers	30 wt%	Compounding by internal mixer/Hot press	• An increase in the tensile and flexural modulus • Microscopic observations of fiber breakage and pull-out on the fractured surface of the coir fiber-reinforced composites along with weak fiber distribution and some voids on the surface • No voids on the surface of the pineapple fiber-reinforced composites are observed indicating better matrix/fiber interactions	Siakeng et al. (2019b)

eliminated, fiber hydrophilicity is reduced and stronger bonding or adhesion between matrix and reinforcing fibers is formed (Kozlowski and Wladyka-Przybylak 2004). The following section is devoted to different fiber modification methods applied in the PLA/natural fiber biocomposites.

5 Fiber Treatment Methods

5.1 Alkali Treatment

Alkali treatment that is also known as mercerization is one of the most efficient chemical treatment methods, which is widely applied for the surface treatment of plant fibers (Zhang et al. 2017). This simple and effectual method improves the matrix/lignocellulosic fiber adhesion (Orue et al. 2018). One may know that the short-term and long-term compatibility of fibers with polymer matrix mainly depends on the successful removal of the non-cellulosic components of the fiber surface like waxes, pectins, hemicelluloses and lignins. In fact, these impurities hinder matrix/fiber interfacial bonding and makes the biocomposites sensitive to moisture and UV irradiations. The most feasible technique to confront the problem is alkali treatment (Islam et al. 2010).

The main performance of the mercerization method to improve the matrix/fiber adhesion is important from two different aspects:

1. During the mercerization process, the fiber bundles break and fibrillization happens. By the formation of shorter fibers with smaller diameters, the surface area of the reinforcing fibers increases. Therefore, the larger area of matrix/filler interfacial surface is provided for transferring stress from matrix to the reinforcing fibers (Siakeng et al. 2019a; Zhang et al. 2017). The alkali treatment reaction is usually performed by soaking the plant fibers in sodium hydroxide aqueous solution at a predetermined temperature for a particular period of time. Throughout the process, Na^+ ions diffuse into the crystalline cellulose and cause fiber swelling. As a result, the hydroxyl groups on the fiber surface are ionized into alkoxides, which is schematically drawn in Fig. 7. The ionization reaction

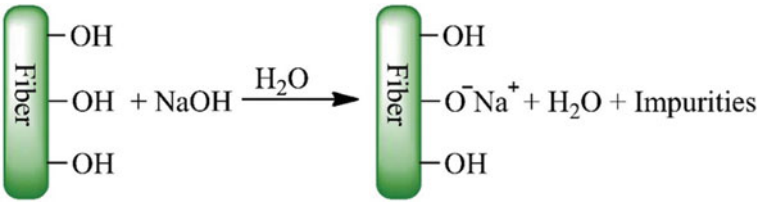

Fig. 7 Proposed alkali treatment reaction of lignocellulosic fibers

in the crystalline regions converts the parent cellulose (cellulose I) to the alkaline cellulose. By washing the treated fibers with water, which subsequently performs after the ionization reaction, the crystalline cellulose regenerates and transforms to the cellulose II having more thermodynamic stability (Aydın et al. 2011; Islam et al. 2010; Kozlowski and Wladyka-Przybylak 2004; Zhang et al. 2017). This transformation is an exothermic and irreversible process (Kozlowski and Wladyka-Przybylak 2004).

2. Through the surface treatment, the non-cellulosic components such as hemicellulose, lignin, waxes and other organic materials are removed from the fiber surface. The removal of natural impurities of fibers occurs alongside the removal of artificial impurities, if any exist (Zhang et al. 2017). Since hydroxyl groups are covered with non-cellulosic substances, the removal of non-cellulosic components thus provides more hydroxyl bonding sites on the fiber surface for more effective adhesion to the matrix (Islam et al. 2010).

Alkaline treatment, based on the mentioned phenomena, results in higher surface roughness. Accordingly, the surface area of plant fibers is enlarged and the mechanical interlocking of fibers with matrix is improved, thereby leading to an enhancement in the interfacial adhesion and compatibility of the fibers and matrix. The mercerization method is applied as a pretreatment method in many modification processes such as silanization, esterification and etherification to increase the cellulose content on the fiber surface and provide more sites for the subsequent treatments (Le Moigne et al. 2014; Way et al. 2012; Zandi et al. 2019). The alkali method also leads to a noticeable augmentation in the amorphous cellulose level (Zhang et al. 2017).

The effects of alkali treatment on various properties of the lignocellulosic fibers are controlled by the treatment process conditions such as the NaOH solution concentration, temperature and duration of the reaction. It is noteworthy that by the removal of non-cellulosic components, some voids can be formed in the fiber structures throughout the process. Moreover, the reactions can depolymerize the native cellulose and collapse the crystalline structures of cellulose (Shafiei et al. 2015). By that, the alkali treatment can lead to a severe damage to the fiber structure and weaken the mechanical properties. Thus, the treatment process must be carried out by using the predetermined optimal conditions of the alkali reaction for each type of the plant fibers. The SEM images of Fig. 8 show the structural changes in the short flax fibers against the NaOH concentration in the aqueous solution over the mercerization process. Taking a look reveals that the fiber bundles break more extensively and fibrillation occurs by increasing the NaOH concentration. Additionally, a decrease in the fiber diameter and an increment in the fiber aspect ratio can be observed after removal of the natural and artificial impurities. Besides, a rougher topography of the fiber surface is obtained after treatment (Aydın et al. 2011).

A literature review on the PLA/lignocellulosic fiber biocomposites show that the alkali treatment method is applied for different types of plant fibers to improve the matrix/filler interfacial bonding (Jandas et al. 2012; Le Moigne et al. 2014; Ander Orue et al. 2016; Saidi et al. 2018; Way et al. 2011, 2012; Zafar et al. 2016). However, different changes in the properties of PLA/lignocellulosic fiber

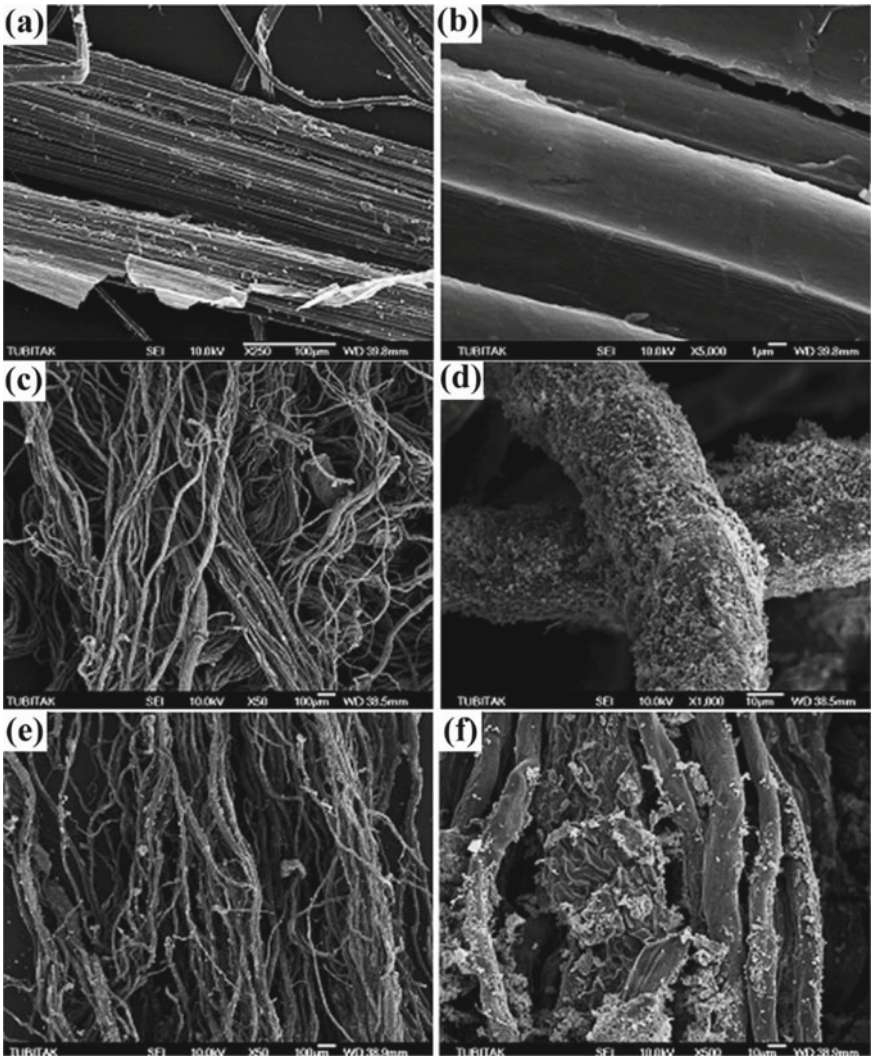

Fig. 8 **a** and **b** Untreated flax fibers, **c** and **d** treated flax fibers with 10% NaOH solution, **e** and **f** treated flax fibers with 30% NaOH solution. Reproduced with permission from (Aydın et al. 2011)

biocomposites have been reported after the mercerization treatment, demonstrating the considerable importance of the treatment process conditions for tailoring the properties of the modified fibers as well as the interfacial phenomena of PLA matrix and lignocellulosic fibers.

In one of these researches (Huda et al. 2008), an effort was made to improve the mechanical and thermal-mechanical properties of laminated PLA/fiber biocomposites by the mercerization treatment of pineapple leaf fibers (PALF). The laminated

biocomposites were prepared by compression molding process through film stacking method. The alkali treatment on PALF was carried out by using 5% NaOH (w/v) solution. The fractured surface of the biocomposites containing untreated PALF was revealed poor distribution and dispersion states of the fibers. Large voids and multi-fiber bundles were also observed on the surface. The fracture was accompanied by severe fiber pull-out and fiber surfaces were completely clean with no stacked residual matrix parts on them indicating poor interactions between PALF and PLA chains. Despite that, the alkali treatment of fibers and the resultant increment in the fiber roughness brought about stronger fiber/matrix interactions and mechanical interlocking. By treating the fibers, the impact strength of PLA matrix increased up to 86% by incorporating modified PALF. Furthermore, the applied alkali treatment led to an increase in the flexural modulus and strength for PALF/PLA biocomposites. The findings of the research have disclose that, at a constant fiber loading, the impact strength and flexural modulus of the biocomposites having alkali treated fibers are higher than even the related data of the biocomposites containing silane-treated fibers (Huda et al. 2008).

In another work (Islam et al. 2010), the PLA/fiber biocomposites having short and long hemp fibers were obtained using compression molding process and film stacking method. In fact, some preforms including short and long fiber mates from both treated and untreated fibers were prepared and applied to shape the biocomposites along with the PLA sheets. The surface treatment of the fibers were done by using NaOH and Na_2SO_3 solutions. In pull-out test, the interfacial shear strength (IFSS) of the treated fibers improved comparing to the untreated fibers. Moreover, the fiber heterogeneous nucleation effect on the PLA crystallization process is intensified by the surface treatment and the corresponding better fiber/PLA interactions. Matrix/fiber debonding, fiber pull-out and holes at the fractured surface of the biocomposite containing treated hemp fibers are observed to a lesser extent. The researchers additionally showed that the alkali treatment leads to higher fracture toughness, tensile modulus, flexural modulus and strength. However, the impact strength of the biocomposites containing the treated fibers is lower than the untreated fiber-reinforced PLA composites. The most probable reason was supposed the occurrence of less fiber pull-out and delamination during crack initiation and propagation in the treated fiber/PLA composite, which leads to a reduction in the dissipated energy (Islam et al. 2010).

The effect of reaction temperature and NaOH solution concentration of alkali modification process on the tensile and flexural properties of wheat straw fiber/PLA biocomposites were studied later by another research group (Pan et al. 2012). The optimum mechanical properties of the mentioned biocomposites were obtained at sodium hydroxide concentration of 2.5% and reaction temperature of 125 °C. At higher reaction temperatures and larger sodium hydroxide concentrations, more hemicellulose and lignin are removed from the fiber surfaces and the fiber microstructure changes more, hence deteriorating the mechanical properties of fibers. However, one may keep in mind that the lower concentrations of NaOH solution in the treatment reaction is more eco-friendly (Pan et al. 2012).

To improve the agricultural waste utilization, skin fibers of durian fruit as a lignocellulosic reinforcement agent were also used for the PLA matrix (Manshor et al.

2014). Durian skin fibers (DSF) are among short lignocellulosic fibers. Poor interface of the untreated fibers with PLA matrix and stress concentration at the end of these fibers result in the formation of microcracks through crack propagation, thereby decreasing the impact resistance of PLA matrix. The fiber surface treatment with NaOH solution has led to an improvement in the impact strength, flexural strength, flexural modulus and thermal stability of the DSF/PLA biocomposites (Manshor et al. 2014).

Besides sodium hydroxide alkali solution, researchers (Siakeng et al. 2018) also applied calcium hydroxide ($Ca(OH)_2$) solution for the chemical treatment of coir fibers (CF) and PALF in the PLA-based biocomposites. It is shown in this research that the fiber diameter of CF and PALF after NaOH treatment change from 220.66 and 79.4 μm to 156.33 and 50.6 μm, respectively. Similarly, the use of $Ca(OH)_2$ treatment induces a reduction in fiber diameter form the mentioned initial ones to 158.66 and 62.78 μm, respectively. Figure 9 shows the SEM images of CF and PALF after NaOH, $Ca(OH)_2$ and silane treatments in this work. As can be observed, the surface of untreated fibers are covered with impurities. By the chemical treatment, the impurities such as waxes are removed from the surfaces, which makes the fiber surfaces cleaner. The CF surfaces after the treatments, especially with NaOH, have many nodes and pinholes, which assists the mechanical bonding of fibers with matrix chains. The effects of $Ca(OH)_2$ treatment on the biocomposite performance were observed to be less pronounced comparing with those of the other employed treatments in this study, i.e. NaOH and silane. Since $Ca(OH)_2$ modification reaction relatively has lower yield in changing the component compositions on the fiber surface, the $Ca(OH)_2$ treated fibers have weaker reinforcing performance and decrease the strength and strain at break of the untreated fiber-reinforced PLA biocomposites. However, the NaOH treatment comparatively causes the strongest interfacial bonding between the fibers and PLA matrix.

Figure 10 represents the interfacial shear strength (IFSS) of PALF and CF after three different chemical treatments used in this work. As it is clear from this figure, the NaOH treatment improves the interfacial adhesion and compatibility of the lignocellulosic fiber/PLA matrix more significantly. The observed improvement stems from the removal of the impurities such as waxes, hemicellulose and lignin, breaking the fiber bundles, enlarging the fiber surface area and increasing the roughness of fiber surface. The positive and negative effects of the fiber chemical treatments on the composite characteristics are also controlled by the fiber nature. In this research, unlike PLA/PALF biocomposites, the mechanical properties of PLA/CF biocomposites do not considerably improve by various chemical treatments of lignocellulosic fibers (Siakeng et al. 2018).

5.2 Organosilane Treatment

Organosilanes are the main group of the coupling agents, which are employed in industrial scales to improve the adhesion between glass fibers and polymeric

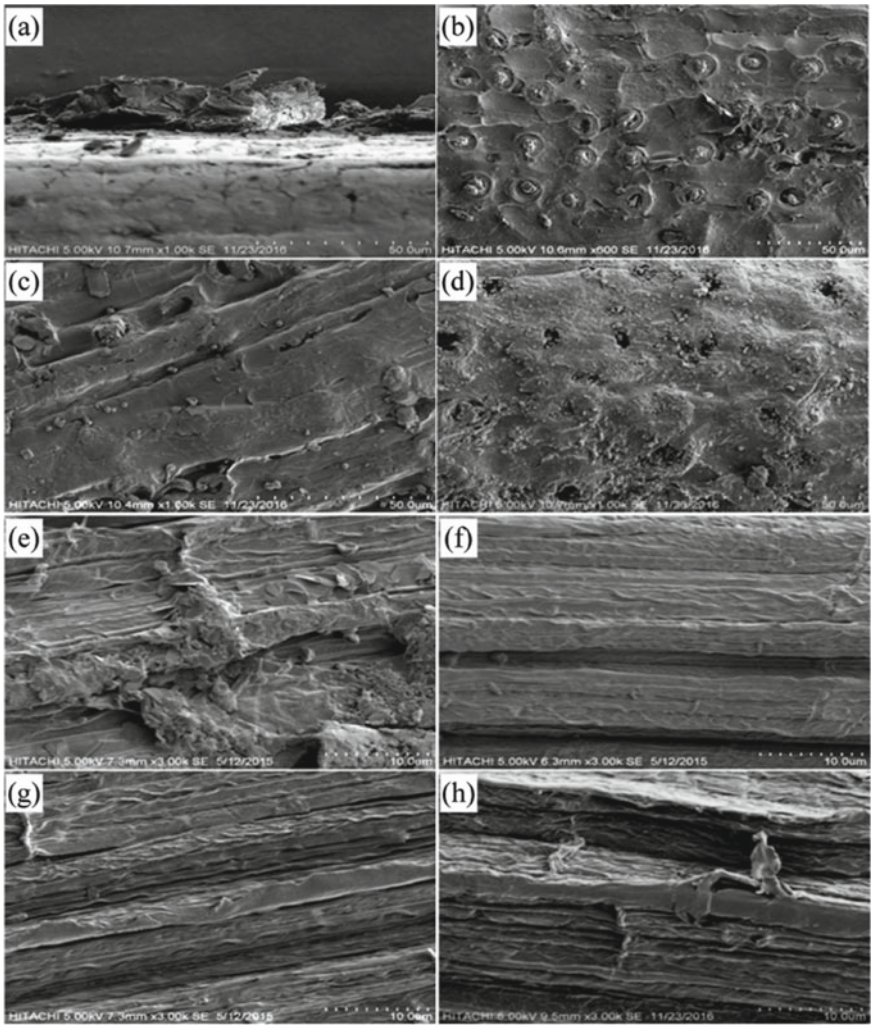

Fig. 9 SEM images of: **a** Untreated CF, **b** CF treated by NaOH, **c** CF treated by silane, **d** CF treated by Ca(OH)2, **e** untreated PALF, **f** PALF treated by NaOH, **g** PALF treated by silane, **h** PALF treated by Ca(OH)2. Reproduced with permission from (Siakeng et al. 2018)

matrices (Zimniewska and Wladyka-Przybylak 2016). The molecules of these effective coupling agents must contain different functional agents in order to develop chemical bonding with both phases, namely polymeric matrix and reinforcing fibers (Zhang et al. 2017). Alkoxysilanes, among organosilanes, have the general structure of $X–R_1–Si(OR_2)_3$. Depending on which atomic groups are substituted for R_1 and R_2, this group of materials is very diverse and widely used to improve the interfacial properties of the lignocellulosic fiber/polymeric matrix biocomposites (González et al. 2012; Huda et al. 2008; Orue et al. 2018; Way et al. 2011, 2012). The OR_2 group

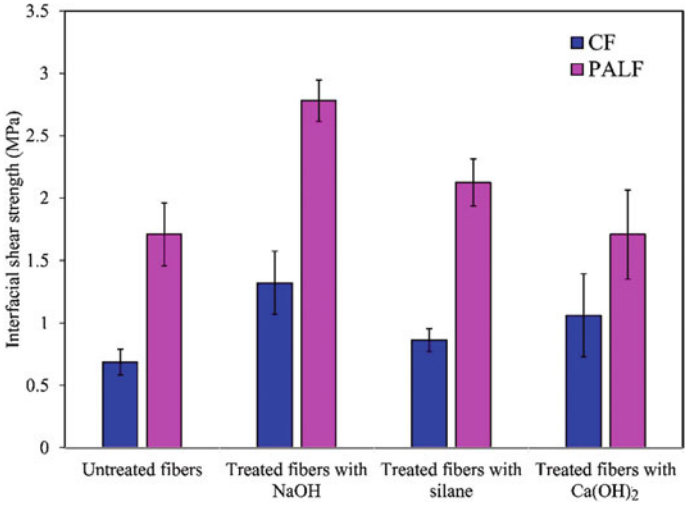

Fig. 10 Interfacial shear strength of treated and untreated coir fibers (CF) and pineapple leaf fibers (PALF). Adapted to (Siakeng et al. 2018)

is a hydrolyzable alkoxy group that can be hydrolyzed in an aqueous environment (Kozlowski and Wladyka-Przybylak 2004). One may know that the siloxane alkoxy groups of the coupling agents can react directly with silanol groups of the glass fiber surfaces in glass fiber-reinforced composites. Unlike that, the lignocellulosic fiber-reinforced composites need some traces of water in the reaction medium in order to form silanol groups in the coupling agent structure. Afterwards, the formed silanol groups participate in the condensation reaction with the hydroxyl groups of the fiber surface (Zhang et al. 2017). Moreover, the X end group in the general structure of the alkoxysilane molecule is an organic functional group that can react with the polymer matrix chain and create covalent bonds between the lignocellulosic fibers and polymer matrix. Figure 11 depicts the proposed reaction scheme between silane coupling agents, lignocellulosic fibers and PLA matrix.

Through the silanization chemical treatment, first the alkoxysilane undergo hydrolysis with water and form silanol groups (step I). Then, the silanol groups in step II participate in condensation reaction with the hydroxyl groups present on the fiber surface. Finally, by choosing a proper functional group X in step III, the chemical reaction between the polymer chain and the grafted silane molecule becomes possible (Zhang et al. 2017). The sinalization treatment minimizes the destructive effects of moisture on the properties of natural fiber-reinforced composites. Moreover, this treatment improves the fiber/matrix interfacial adhesion and correspondingly the composite strength owing to the formed covalent bonding between the matrix chains and reinforcing fibers. The effectiveness of this treatment method on the composite properties depends on the employed organosilane type, treatment solution concentration, reaction temperature and time, moisture content, fiber volume fraction in the biocomposite and reaction medium (water, aqueous solvent or mixture) (Orue

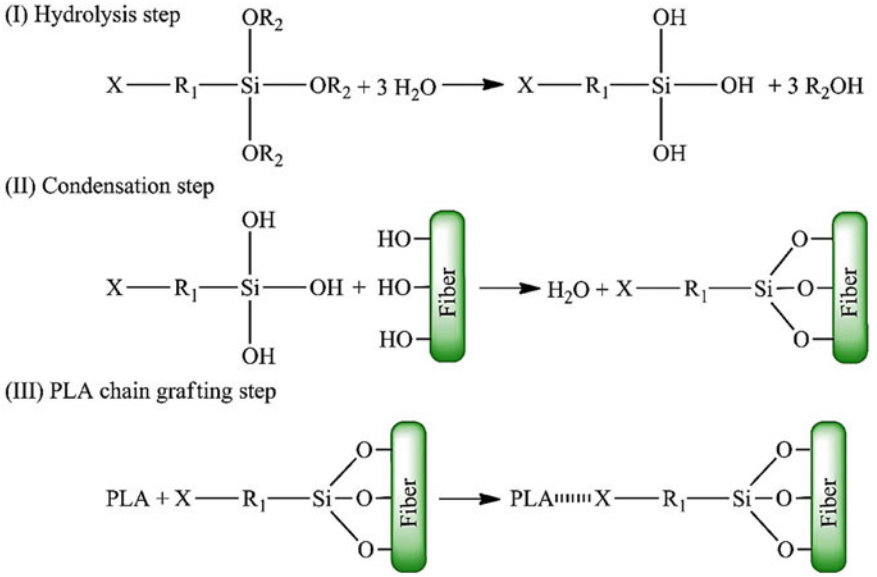

Fig. 11 Proposed schematic reaction pathway for the silanization of lignocellulosic fibers (steps I and II) and grafting onto the PLA chains (step III)

et al. 2018; Zimniewska and Wladyka-Przybylak 2016). The water content in silane treatment is a key factor. The insufficient amount of water leads to the formation of an incomplete monolayer on the fiber surface, while the high water content results in silane polymerization reaction (González et al. 2012). The alkali treatment is commonly applied before the silane modification. In this case, after the creation of silanol groups, more reactive sites on the cleaned fiber surface are accessible to participate in the condensation reactions. The fiber/matrix interfacial bonding is reportedly much more stronger in the bicomposites that undergo silanization surface modification after alkali pretreatment, thereby enhancing the composite tensile strength (Zhang et al. 2017).

A literature review on the use of this treatment in PLA-based biocomposites reveals that the silane treatment conditions have not been controlled well. Therefore, the biocomposite properties have changed in wide ranges, repeatedly resulting in a limited improvement of interfacial strength and other properties (González et al. 2012; Le Moigne et al. 2014; Siakeng et al. 2018). Nevertheless, this treatment has been frequently used to enhance the interfacial adhesion and compatibility of different lignocellulosic fibers in the PLA matrix (Huda et al. 2008; Jandas et al. 2012; Ander Orue et al. 2016; Song et al. 2018; Way et al. 2011, 2012). In one of these studies (González et al. 2012), the PLA biocomposites were prepared with spent kraft and sisal fibers as reinforcement agents through twin-screw extruder melt-compounding and injection molding shaping processes. Different types of silane coupling agents were applied in this work to improve the

thermal and mechanical properties of the PLA-based biocomposites, including 3-aminopropyltriethoxysilane and 3-(trimethoxysilyl)propyl methacrylate. No significant improvement was observed for any of the studied mechanical properties of the obtained biocomposites after silane treatment (González et al. 2012).

Similarly, another research group (Chun et al. 2012) evaluated the effects of coconut shell powder (CSP) on the thermal, mechanical and morphological properties of the PLA biocomposites before and after the fiber silane treatment. A silane coupling agent, 3-aminopropyltriethoxysilane, at concentration of 3% (v/v) in ethanol was applied for treating the filler surface. It is obviously evident in Fig. 12 that the untreated CSP particles are not properly embedded in the PLA matrix and some micro-voids (marked by white arrows) are also discernable at the fractured surface of the bicomposite. At high fiber loading (60 phr), some agglomerates of the untreated CSP particles are also distinguishable. On the other hand, after treating the filler surface with silane coupling agent, the dispersion state of the solid particles becomes more homogenous. As a direct result, the elastic modulus, tensile strength, T_g and crystallinity degree of matrix improve comparing to the untreated CSP-filled biocomposites (Chun et al. 2012).

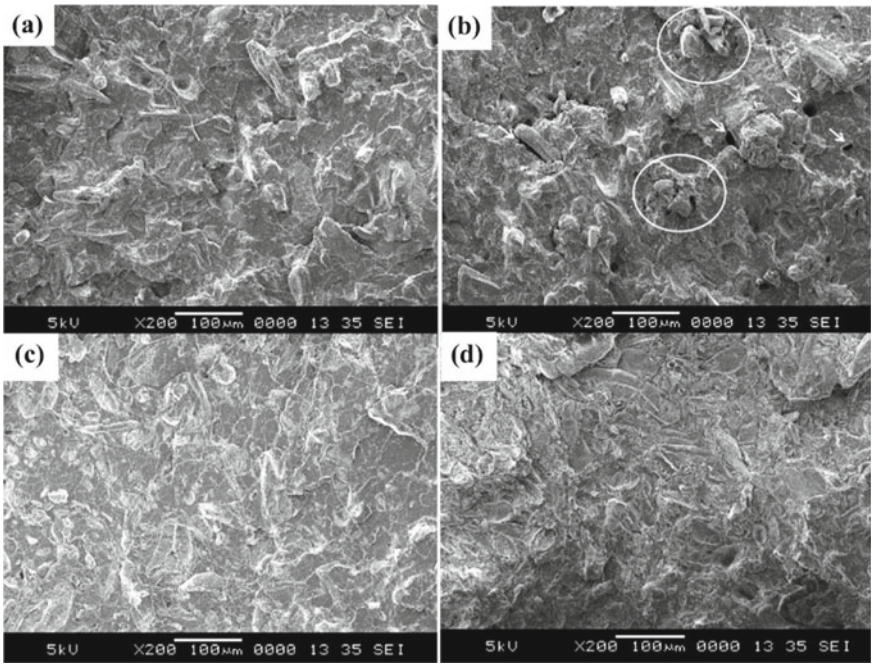

Fig. 12 SEM image of tensile fractured surface of: **a** PLA/untreated coconut shell powder (CSP) biocomposite at a filler loading of 30 phr, **b** PLA/untreated CSP biocomposite at a filler loading of 60 phr, **c** PLA/silane-treated CSP biocomposite at a filler loading of 30 phr and **d** PLA/silane-treated CSP biocomposite at a filler loading of 60 phr. Reproduced with permission from (Chun et al. 2012)

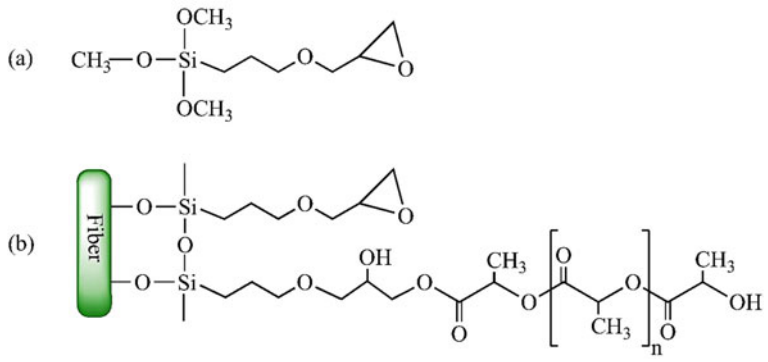

Fig. 13 **a** Chemical structure of the used organosilane coupling agent and **b** proposed silane-grafted fiber/PLA structure. Adapted to (Le Moigne et al. 2014)

More improvements in the mechanical properties of the lignocellulosic filled PLA systems are achievable by optimization of the silane reaction conditions. In this regard, the organosilane treatment method was applied to improve the properties of the PLA/short flax fiber biocomposites (Le Moigne et al. 2014). The effects of different influential parameters of the treatment process including the organosilane solution composition, reaction temperature, fiber soaking time, heating temperature and alkali pretreatment were investigated in this study. To treat the flax fibers, a silane coupling agent, (3-glycidyloxypropyl)trimethoxysilane, with chemical structure shown in Fig. 13 was employed.

By alkali pretreatment, the amount of hydroxyl groups on fiber surfaces as the potential reactive sites for the silane grafting reaction is heightened. Furthermore, the fiber surface roughness also increases that has a positive impact on the fiber/matrix mechanical interlocking. By these mechanisms, the alkali pretreatment provokes improvements in the Young modulus, yield stress and impact strength of biocomposite, particularly comparing with the PLA/silane-treated flax biocomposite (Fig. 14). The silanization treatment of flax fibers, regardless of the alkali pretreatment, leads to a reduction in the fiber hydrophilicity and an increment in the fiber/matrix interfacial adhesion. As can be found in Fig. 14, the organosilane treatment process raises the Young modulus, yield stress, impact stress and equivalent interphase thickness of the PLA-based biocomposite containing untreated fibers. Further studies on the failure mechanisms at the fiber/matrix interface disclose the fact that the adhesive interfacial failure occurs for the untreated fiber-reinforced biocomposite, in which the crack propagation path goes through the matrix as well as fiber/matrix interface. In marked contrast, for the silane-treated fiber/PLA biocomposites, cohesive interfacial failure is observed, which is accompanied by fiber breakage and matrix tearing. Besides, throughout the stress exposure and crack propagation, the silane-treated fibers remained bonded to the PLA matrix. In fact, the observed improvement in the fiber/matrix adhesion over the silanization treatment is induced by the following mechanisms: (I) Chemical coupling, which is formed by

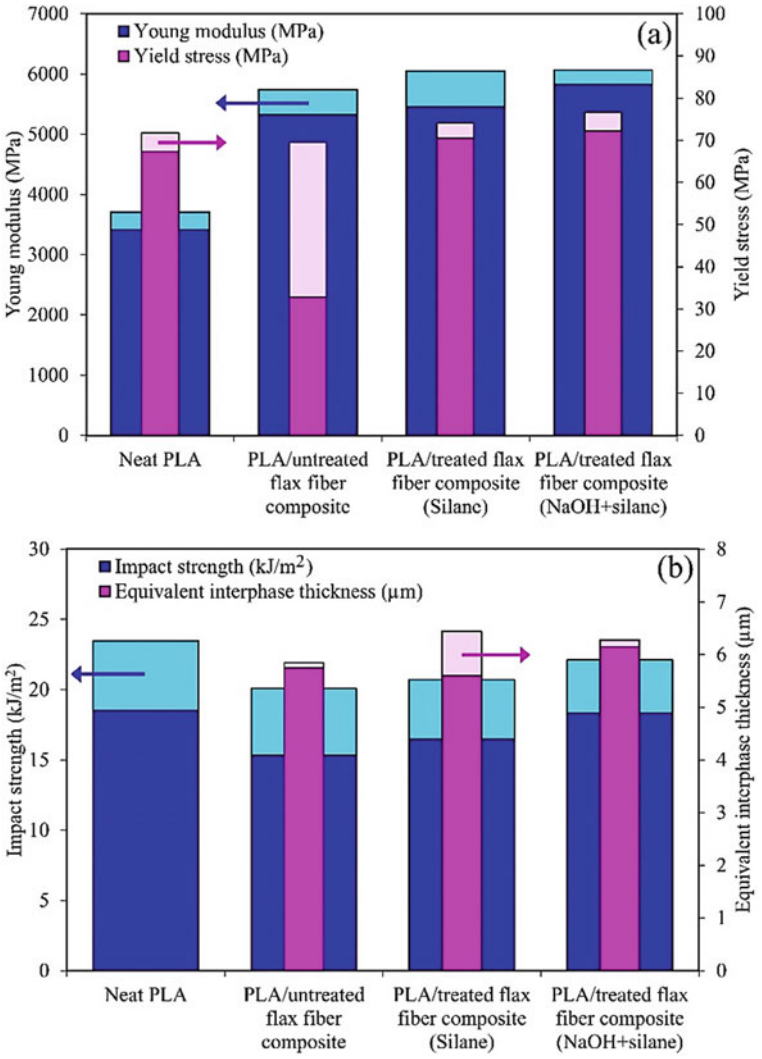

Fig. 14 **a** Young modulus and yield stress, **b** impact strength and equivalent interphase thickness of: neat PLA, PLA/untreated flax fiber biocomposite, PLA/treated flax fiber biocomposite with organosilane modification at a soaking bath temperature of 70 °C (Silane), PLA/treated flax fiber biocomposite with alkali pretreatment and organosilane modification at a soaking bath temperature of 20 °C (NaOH+silane). Adapted to (Le Moigne et al. 2014)

the esterification reaction between the epoxy functional groups of the grafted silane molecules and the end groups of PLA chains. (II) Physical interactions including Van der Waals forces and direct hydrogen bonding between the functional groups of the fibers and PLA chains. The covalent bonds formed between the silane coupling agent, flax fiber surface and PLA matrix chains are depicted in the chemical structure shown in Fig. 13 (Le Moigne et al. 2014).

The beneficial effects of alkali pretreatment on the silane chemical treatment is clearly shown in a study (Zafar et al. 2016). In this research, the PLA/jute fiber biocomposites were prepared using untreated fibers and treated fibers with alkali and silanization treatment. As mentioned, the alkali treatment helps the lignocellulosic fibers to participate in the grafting reaction with the silane coupling agents more extensively. The related mechanism involves in increasing the fiber surface cleanliness and providing more accessible cellulosic hydroxyl groups at the fiber surface. Therefore, one may conclude that the wettability and functionality of the fiber surface are intensified by the pretreatment. The success of the treatment reactions were examined by Fourier-transform infrared (FTIR) spectroscopy and SEM observations. The disappearance of the absorption peak at 1739 cm^{-1} (attributed to the C=O bond of carboxylic and ester groups of hemicellulos), and broadening the absorption peak at 3427 cm^{-1} (related to –OH groups) in the FTIR spectrum of untreated fibers after the chemical treatment provide conclusive evidence on the removal of hemicellulose, pectin, fat and oils through the alkali modification and correspondingly, an increment in the fiber surface functionality. In the FTIR spectrum of the silane-treated fibers, the presence of a peak at 776 cm^{-1} (related to the symmetric stretching vibration of –Si–C- bond), and 1200 cm^{-1} (related to the –Si–O–C- bond) corroborates the occurrence of the condensation reactions between the fiber hydroxyl groups and silanol groups.

It has been reported that the fiber crystallinity degree rises to higher levels after alkali treatment owing to the removal of the non-cellulosic impurities. On the other hand, the fiber crystallinity degree diminishes after silane treatment due to the augmentation in the amorphous cellulose content. The results of tensile test on a single fiber show noticeable increases in the tensile modulus and strength of jute fiber after alkali treatment, whereas the subsequent exposure of alkali-treated fibers to the silane solution in silanization modification worsens the fiber properties. The given explanation is the removal of the soft materials present on the fiber surface after alkali treatment, while the silane treatment in an acidic medium eventuates in the cleavage of β-1,4-glycosidic linkages, hence reducing the fiber strength. In spite of that, the best PLA/jute fiber interfacial strength is reported for the biocomposite containing the jute fibers treated with coupled alkali and silane modifications. The strong fiber/matrix interface for the silane/NaOH treated fibers substantially promotes the interfacial shear strength of the embedded fiber in PLA matrix compared to the untreated fiber (an increment about 112%) (See Fig. 15). In fact, the synergetic effects of the alkali and silanization processes provoke the observed enhancement and considerably shorter pull-out fiber from the PLA matrix (Fig. 15) (Zafar et al. 2016).

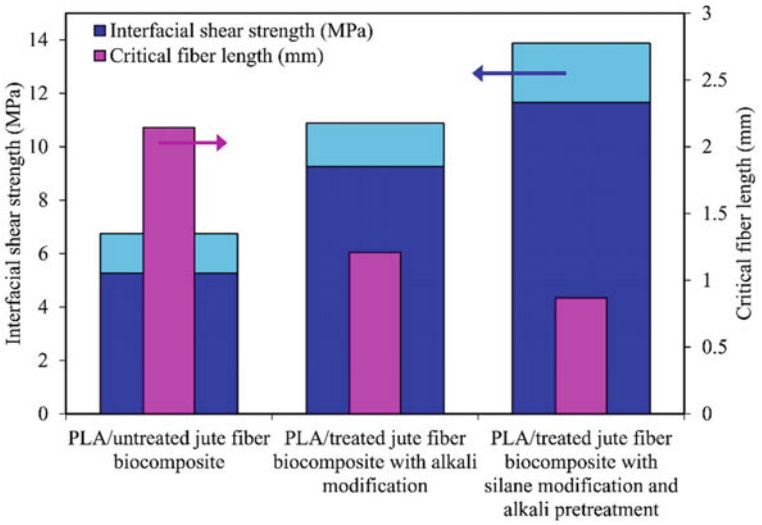

Fig. 15 Interfacial shear strength and critical fiber length for: PLA/untreated jute fiber composite, PLA/treated jute fiber composite using alkali modification and PLA/treated jute fiber composite using alkali pretreatment and silane modification. Adapted to (Zafar et al. 2016)

5.3 Esterification Treatment

Because of the extensive access to the hydroxyl groups available on the surface of lignocellulosic fibers, the esterification treatment has been employed as a suitable treatment method to improve the interfacial interactions in natural fibers/PLA biocomposites. Unlike silane treatment, in which the interfacial coupling is created through the covalent bonding formation between lignocellulosic fibers and matrix, the esterification treatment is done only by functionalizing the fiber surfaces. Over the esterification treatment, the hydrophilic hydroxyl groups are transformed into atomic groups with more hydrophobicity through the ester bonding. Thus, the hydrophobicity of fiber surfaces is intensified and the compatibility between the plant fibers and polymer matrix improves (Zhang et al. 2017).

The esterification reaction normally involves the reactions of organic acids or anhydrides with the fiber hydroxyl groups. The proposed reactions of the hydroxyl groups of the lignocellulosic fibers and anhydride/carboxylic acid groups are depicted in Fig. 16. Different types of esters, depending on the nature of the employed organic acids in anhydride molecules, can be applied in the esterification modification process. The esters with one to four carbon atoms are formate, acetate, propionate and butyrate. Other esters including laurate and stearate contain 12 and 18 carbon atoms, respectively. Furthermore, dicarboxylic esters with double bond in the carbon chain structure like fumarate and maleate are also employed in the esterification treatment (Kozlowski and Wladyka-Przybylak 2004; Zimniewska and Wladyka-Przybylak 2016). It is noteworthy that the longer alkyl group attached to the

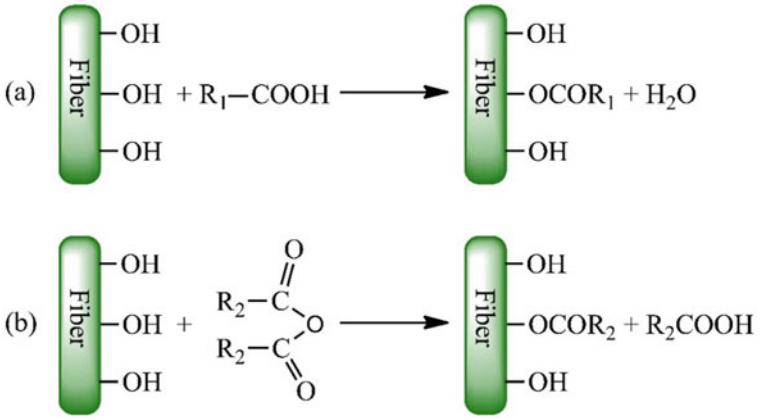

Fig. 16 Proposed reaction scheme of the hydroxyl groups of lignocellulosic fiber with **a** carboxylic acid and **b** anhydrides. Adapted to (Abu Ghalia and Dahman 2017; Way et al. 2011)

ester group gives the lignocellulosic fiber more thermoplasticity. The encountered disadvantage of this treatment method is the requirement of using dried fibers in order to increase the reaction efficiency (Kozlowski and Wladyka-Przybylak 2004). Depending on the applied chemical type to create ester bonding, the acetylation, benzoylation or maleation treatment methods are used to intensify the hydrophobicity of the fiber surface and decrease the fiber moisture uptake (Zhang et al. 2017).

5.3.1 Acetylation Reaction

The acetylation process using acetic anhydride is reported as the most common method to modify wood (Abu Ghalia and Dahman 2017). In recent decades, this method has been also applied on an industrial scale for the treatment of lignocellulosic materials. Various chemical compounds, such as acyl chloride, acetic acid and acetic anhydride, are employed in the acetylation process of lignocellulose (Zhang et al. 2017). One may know that the hydrolysis reaction of acetic anhydride to acetic acid is relatively a highly exothermic rapid reaction and the reaction of fibers with acetic anhydride produces acetic acid as a by-product, which must be removed after the fiber surface treatment (Shafiei et al. 2015). In the acetylation process, using acetic anhydride, the R_2 group (shown in Fig. 16b) is substituted by $–CH_3$ group. Researches have verified that the substitution reaction of acetyl groups with the hydroxyl groups of the amorphous components of lignocellulosic fibers like lignin and hemicellulose is more likely than the reaction with the hydroxyl groups of highly crystalline cellulose. The diffusion constant of the compounds containing acetyl groups is much lower in the closely packed area of the crystals than the amorphous parts. To confront the problem, the plant fibers are commonly treated with alkali solution first (Shafiei et al. 2015). The substitution reaction of fiber contributes to the fiber weight gain owing to

the substitution of the fiber hydroxyl groups with acetyl groups. Since this treatment involves the replacement of the hydrophilic hydroxyl groups by the ester groups with more hydrophobicity, the treated fibers are more hydrophobic and the equilibrium moisture content of fibers diminishes (Kozlowski and Wladyka-Przybylak 2004). One may use catalysts to increase the acetylation reaction rate. The most frequently used catalysts for the acetylation reactions are pyridine, sulfuric acid and potassium and sodium acetate. In case of using a strong acid as catalyst, the proper choice of reaction conditions for the effective fiber treatment is critical, since the reaction can cause the degradation of fiber microstructure and consequently, the deterioration of fiber properties (Orue et al. 2018).

The acetylation treatment of the lignocellulosic fibers is also known as a process for fiber plasticization (Siakeng et al. 2019a). In a research (De Rosa et al. 2011), the effects of acetylation treatment was investigated, using acetic acid, on the mechanical properties of the okra fibers. It was found that the tensile strength and Young modulus of fibers drop to lower values after treatment. The fiber surfaces become cleaner relative to the primary fibers and the fiber hydrophilicity decreases after acetylation treatment, resulting in better wettability between the fibers and hydrophobic resins (Orue et al. 2018). Figure 17 illustrates the SEM images of the cryofractured surfaces of the PLA/rice straw fiber (RSF) biocomposites in the presence of poly (ethylene glycol) (PEG) as a plasticizer. The left- and right-hand columns relate to the biocomposites containing untreated and acetylated fibers, respectively. For preparation the PLA/RSF biocomposites, the acetylation treatment of fibers was performed using acetic acid and acetic anhydride, accompanied by sulfuric acid as a catalyst. The images of the biocomposites containing untreated fibers demonstrate that fiber pull-out and fiber/matrix debonding occur extensively, whereas these phenomena are observed to a lesser extent on the fractured surface the biocomposite containing acetylated RSF. Additionally, the surfaces of treated fibers are covered with a layer of PLA matrix indicating improved interfacial adhesion and fiber hydrophobicity.

The plant fiber-reinforced PLA biocomposites generally show lower moisture gain by replacing the hydroxyl groups with more hydrophobic acetyl groups. In order to diminish the biocomposite sensitivity to moisture, maple fibers (MF) were treated by silanation and acetylation processes after alkali pretreatment (Way et al. 2011). Their findings show that among different treated fibers including untreated MF, treated MF with NaOH, treated MF with silane/NaOH, and treated MF with acetylation/NaOH, the lowest natural moisture content relates to the last one, the fibers treated with acetylation and alkali methods. This property of treated fibers leads to less moisture absorption of the treated fiber-reinforced PLA composites. The melt-compounding in a twin-screw extruder and shaping in an injection molding machine were applied to prepare the PLA/MF biocomposites. Throughout the melt processes, the PLA chains were hydrolyzed and undergone chain scission despite being dried. By the melt processing, the weight-average molecular weight (M_w) of PLA chains in the processed pure PLA and PLA/untreated MF biocomposite diminished by 31% and 41%, respectively (Fig. 18). The residual moisture in the samples assists the hydrolysis reaction of the PLA chains. As a result of less water absorption, the lowest

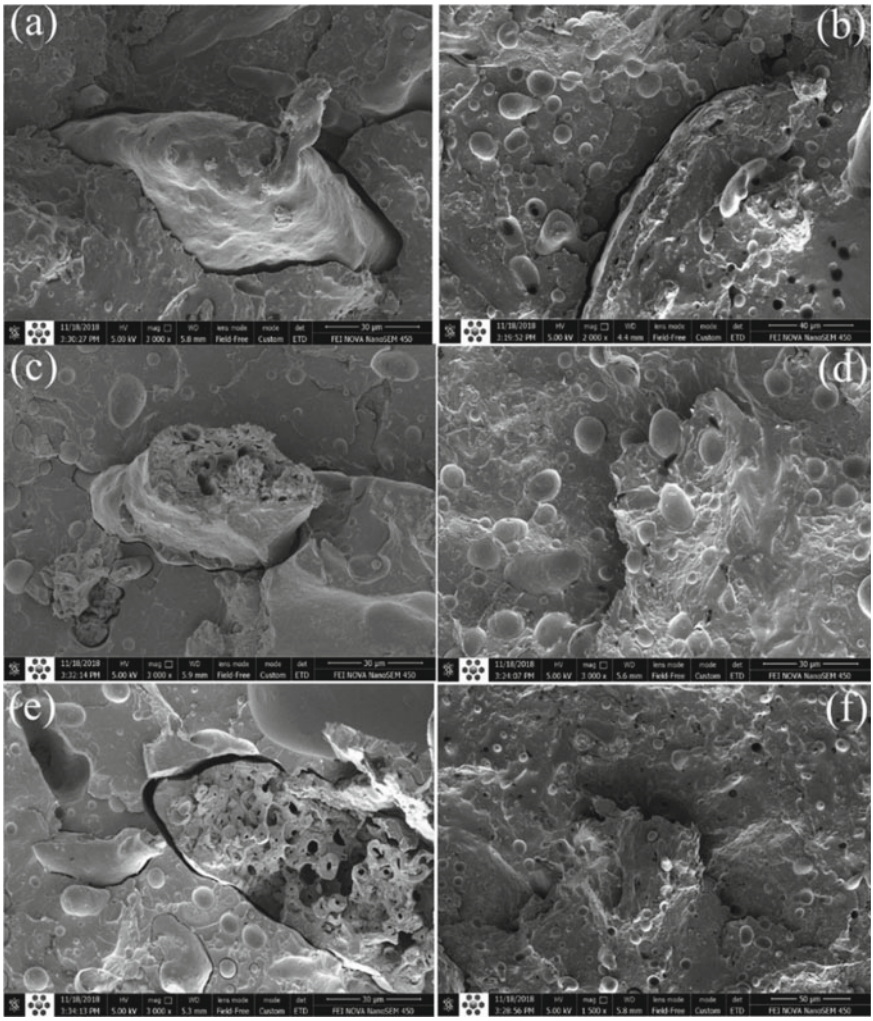

Fig. 17 SEM images of the cryofractured surfaces of PLA/untreated RSF biocomposites (micrographs on the left-hand side) and PLA/acetylated RSF biocomposites (micrographs on the right-hand side) containing 6 phr of PEG at a filler loading of: **a** and **b** 10 phr, **c** and **d** 20 phr, **e** and **f** 30 phr. Author's unpublished data

loss in the PLA molecular weight is determined for the biocomposite containing the acetylated and alkali-treated fibers (Way et al. 2011).

Furthermore, they reported that different properties for tensile and flexural strength were obtained for the PLA biocomposites containing alkali-treated fibers depending on the NaOH solution concentration and treatment reaction time. In this work, it is shown that the tensile and flexural strength of the PLA/MF biocomposite respectively

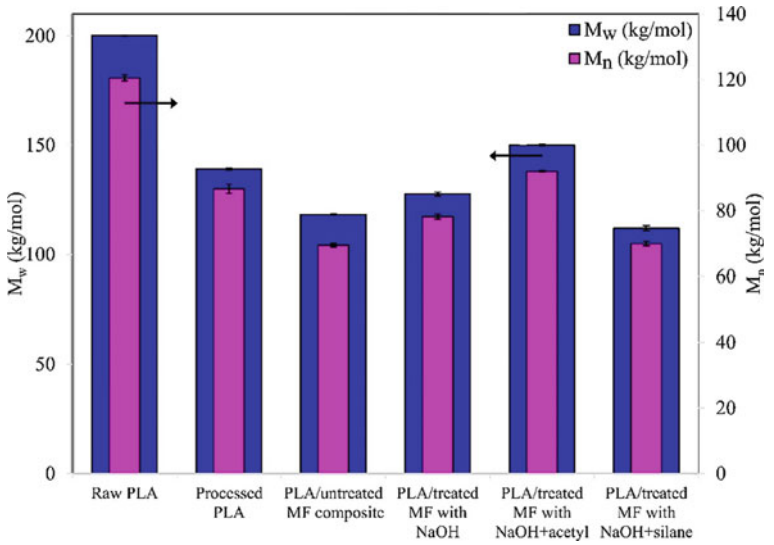

Fig. 18 Weight- and number-average molecular weight (Mw and Mn) of unprocessed raw PLA as well as processed PLA and PLA/MF biocomposites. Adapted to (Way et al. 2011)

decrease by 17 and 16% by using the alkali treatment of fibers. The observed reductions are attributed to the easier initiation of crazes at the fiber/matrix interfaces and fiber tenacity loss over the alkali modification process. Nonetheless, the acetylation process after alkali pretreatment can compensate for the lost strength to some extent, owing to better wettability of the acetylated fibers with PLA matrix and improved fiber/matrix interfacial adhesion. In spite of the improvements, the consecutive treatment processes, i.e. alkali and acetylation reactions, do not result in an improvement in the flexural and tensile strength of the PLA/untreated MF composites (Way et al. 2011).

In a similar study (Jonoobi et al. 2012), the acetylation treatment was employed on the surface of cellulose nanofibers (CNF), which were obtained from the raw kenaf bast fibers. In this research, the fiber pulp was first separated from the kenaf bast fibers by NaOH and bleaching treatments. Afterwards, the acetylation process was performed on the pulp by using acetic anhydride accompanied by the pyridine catalyst. Then, the prepared fibers were dispersed in water and exposed to shear mixing to obtain a suspension of nanofibers. On the FTIR spectra of untreated CNF and acetylated cellulose nanofibers (ACNF), a broad absorption peak at 3330 cm^{-1} and another peak at 1640 cm^{-1} are attributed to the hydroxyl groups and absorbed water of cellulose nanofibers, respectively (Fig. 19). The intensity of these peaks is substantially decreased by the acetylation treatment. In addition, the appearance of two peaks in the FTIR spectrum of ACNF at 1744 cm^{-1} and 1238 cm^{-1}, which are respectively related to the stretching vibration of C=O bond of carbonyl in ester groups and C–O bond of acetyl groups, verifies the successful substitution reaction of the hydroxyl groups with the acetyl ones.

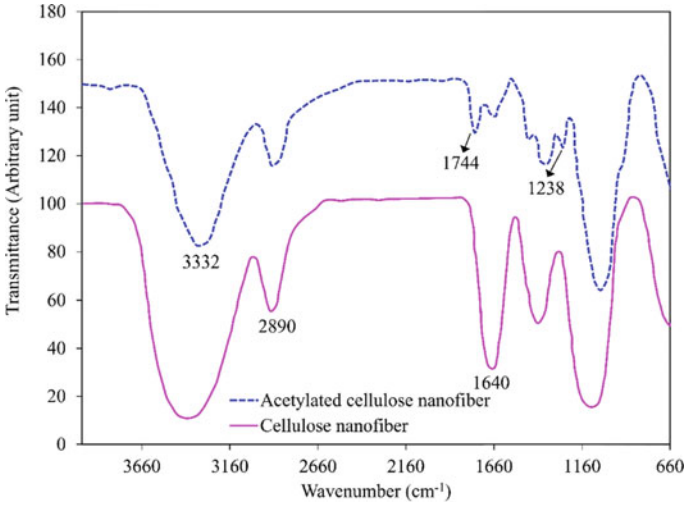

Fig. 19 FTIR spectra of untreated and acetylated cellulose nanofibers (CNF and ACNF). Adapted to (Jonoobi et al. 2012)

It is worthy to note that, after the acetylation process, the water contact angle of fibers increases from 33° to 115°, which reveals the improved hydrophobicity of the treated cellulose fibers. Moreover, the addition of cellulose nanofibers to the PLA matrix increases the storage modulus and decreases tan δ, albeit the variations of storage modulus and damping factor are higher for the acetylated nanofibers. The larger changes show that the acetylated fibers have stronger interactions with the PLA chains and restrict the PLA molecular motions more extensively. Despite that, the crystallinity and thermal stability of the cellulose nanofibers diminish after the acetylation modification. Therefore, the acetylation treatment does not bring about an improvement in the Young modulus and tensile strength of the PLA/untreated CNF biocomposites, though the interfacial adhesion between ACNF and PLA matrix improves (Jonoobi et al. 2012).

5.3.2 Maleation Reaction

Maleate coupling agents are capable of creating effectual chemical bonds between plant fibers and matrix chains. Maleation treatment can be carried out following two procedures. One method is to pretreat lignocellulosic fibers with a maleated polymer. Then, the treated fibers is compounded with polymer matrix. In the second method, plant fiber, polymeric matrix, maleic anhydride (MA) and a peroxide initiator are compounded together via reactive extrusion process, which is a single step one. Afterwards, the prepared compounds are molded into final products by compression or injection molding processes (Zimniewska and Wladyka-Przybylak 2016).

Regardless of the procedure used, to improve the interfacial adhesion of PLA and lignocellulosic fibers, MA grafting reaction must be performed on PLA chains. According to Fig. 20, first the peroxide initiator, which is normally used in maleation treatment methods, creates reactive sites on PLA chains through dissociation and radical transfer reactions. Second, MA molecules are grafted onto PLA chains and form maleic anhydride-grafted PLA (MAPLA) macromolecules. Subsequently, MA functional groups in MAPLA molecules react with the hydroxyl groups of plant fibers by the occurrence of MA ring-opening reaction. The reaction mechanism between MAPLA chains and lignocellulosic fibers involves the thermal activation of graft copolymer and subsequent esterification reaction with lignocellulosic fibers. Thus, the chemical reaction between fibers and PLA chains becomes possible (Orue et al. 2018). Hence, depending on the correct choice of processing conditions, the attainment of higher fiber/matrix compatibility is then within reach (Zhang et al. 2017). The surface energy of lignocellulosic fibers decreases and is put in the range of PLA surface energy by the treatment. As a result, higher wettability of natural fibers is provided by hydrophobic matrix and the interfacial strength improves (Siakeng et al. 2019a; Orue et al. 2018).

Maleation treatment has been used for the chemical modification of the interfaces of PLA-based biocomposites containing different natural fibers such as triticale straw, wheat straw, bamboo and banana fibers (Mihai and Ton-That 2014; Nyambo et al. 2011; Posada et al. 2016; Majhi et al. 2010). Nyambo et al. (2011) in some related studies, MAPLA chains were first obtained via melt mixing process using PLA,

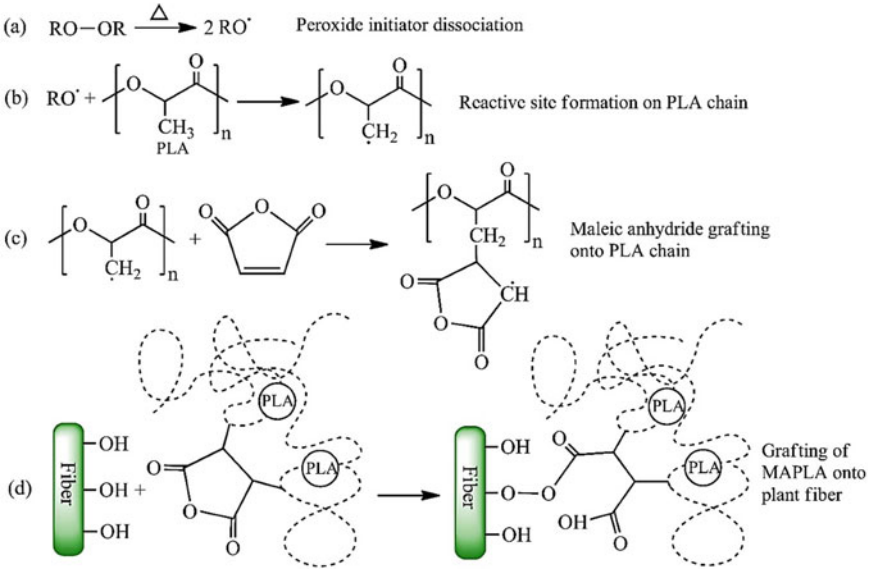

Fig. 20 **a–c** Schematic chemical drawing of maleic anhydride grafting reaction onto PLA chains and **d** grafting reaction of MAPLA on plant fibers. Adapted to (Zhang et al. 2017; Rigolin et al. 2019)

MA, and initiators like 2,5-bis(tert-butylperoxy)-2,5-dimethylhexane (Nyambo et al. 2011; Mihai and Ton-That 2014). Then, in the second mixing process, the resultant compatibilizer was applied in compounding of PLA/natural fiber biocomposites. Their findings reveal that the tensile and flexural modulus and tensile and flexural strength of PLA/untreated fiber biocomposites are improved by adding MAPLA compatibilizer (Mihai and Ton-That 2014; Nyambo et al. 2011).

As mentioned earlier, it is possible to achieve the maleation treatment, both the grafting reaction of MA molecules onto PLA chains assisted by an initiator and ring-opening reaction of MA with fiber hydroxyl groups, through a single step melt-mixing process. It was reported that the tensile modulus and strength of PLA/bamboo fiber (BF) biocomposites were improved by performing this reactive extrusion process (Posada et al. 2016). However, it has been found that the treatment agent of maleic anhydride in the reactive mixing of PLA/natural fiber biocomposites has an optimum value, above it, the composite properties are deteriorated (Majhi et al. 2010). In this study, the interfacial properties of PLA/alkali-treated banana fibers biocomposites were improved using reactive mixing of components in an internal mixer at MA levels of 1, 3 and 5 wt%. It was determined that the highest improvements in the biocomposite properties such as tensile modulus and strength as well as impact strength were achieved at 1 wt% of MA content (Fig. 21) and further increments in MA level led to final properties deterioration. In fact, adding MA improves the properties by creating chemical linkages between PLA chains and fiber surfaces and proper matrix/fiber bonding. By adding more MA to the melt process, the MA content would reach the critical interfacial concentration of the compatibilizer and saturate the matrix/fiber interfaces. Beside the mentioned properties, the maximum

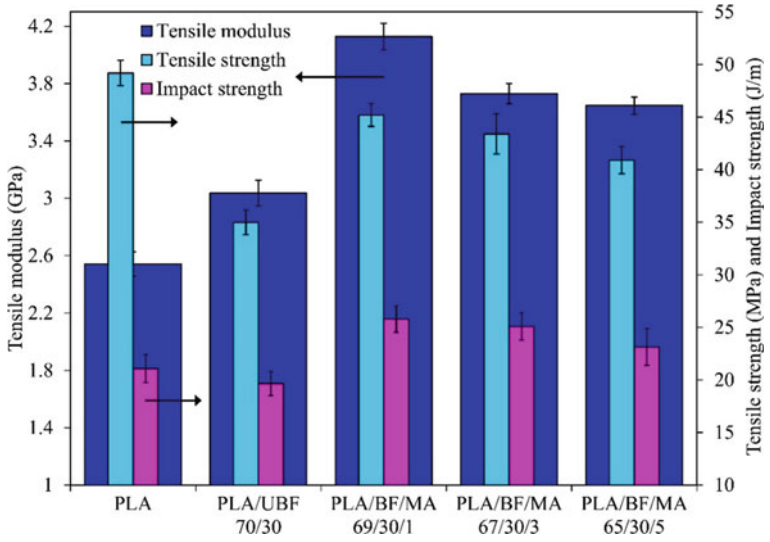

Fig. 21 Maleic anhydride effect on some mechanical properties of PLA/untreated bamboo fibers (UFB) biocomposites. Adapted to (Majhi et al. 2010)

values of T_g, T_c, HDT and storage modulus of treated biocomposites by maleation process were obtained at 1 wt% of MA content.

In similar studies, MAPLA grafted chains were first obtained in twin-screw extruders, using dicumyl peroxide initiator (Kim et al. 2012; González-López et al. 2019). Afterward, 3 wt% of MAPLA were added to PLA/agave fiber, PLA/cassava flour and PLA/pineapple flour biocomposites during extrusion process. The incorporation of MAPLA compatibilizer into melt, during extrusion process, results in the esterification reactions of grafted MA, on the PLA backbone, with hydroxyl groups of lignocellulosic materials (Fig. 20d). In fact, covalent linkages and hydrogen bonding between matrix and the reinforcing filler along with the fiber hydrophobicity reduction over maleation process bring about strong matrix/fiber interfaces. This, in turn, led to relative increment in modulus, strength and hardness of the maleated PLA/agave fiber biocomposites and also relative decrease of impact strength, water absorption and water diffusion coefficient of these biocomposites (Fig. 22) (González-López et al. 2019). In another study, the augmentations in storage modulus, HDT and PLA crystallinity degree through MA esterification reaction in PLA/fiber composite were observed (Kim et al. 2012).

The SEM image of the fractured surface of PLA/agave fiber biocomposites, containing untreated fibers, shows intense fiber pull-out and large quantity of debonded fibers (Fig. 23). At higher magnifications, some interfacial gaps are evident,

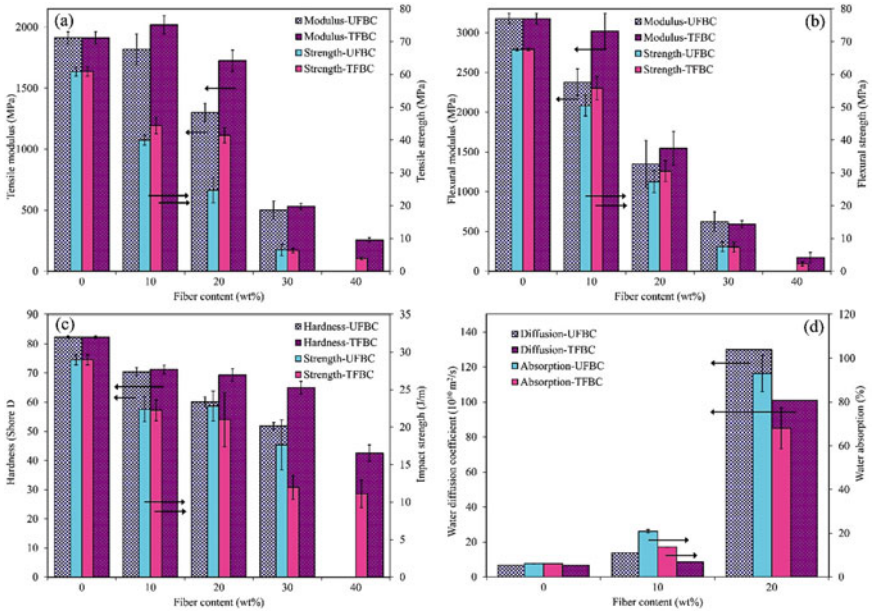

Fig. 22 Mechanical, thermo-mechanical and physical properties of untreated agave fiber/PLA biocomposites (UFBC) and treated agave fiber/PLA biocomposites (TFBC) against fiber loading. Adapted to (González-López et al. 2019)

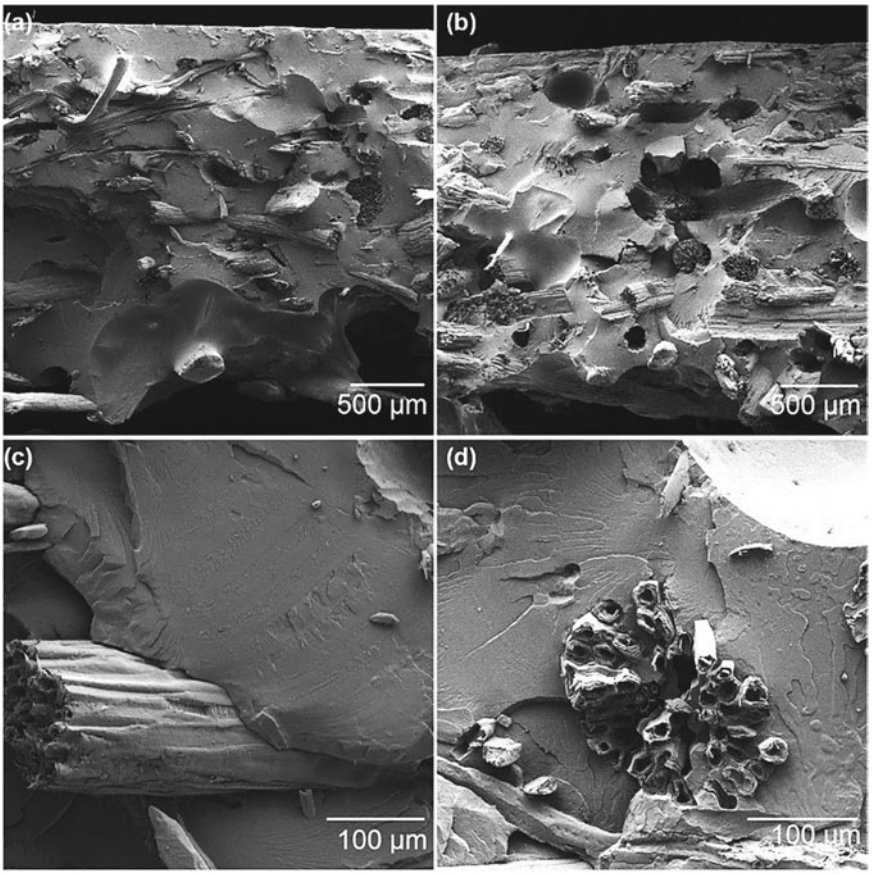

Fig. 23 SEM micrographs of: **a** and **c** untreated agave fiber/PLA biocomposites (UFBC), **b** and **d** treated agave fiber/PLA biocomposites (TFBC) at a fixed fiber loading of 20 wt%. Reproduced with permission from (González-López et al. 2019)

indicating matrix/fiber debonding. On the other hand, the fiber/matrix compatibility of maleated PLA/agave fiber composites was improved and effective stress transfer across matrix/fiber interfaces was obtained. The SEM images of these biocomposites clarify that the failure mostly occurs at the bulk of fibers and matrix, not the interfaces. Therefore, the observed change in the failure mechanism led to a reduction in the impact strength of PLA/treated agave fiber biocomposites compared to PLA/untreated fiber biocomposites, since fiber pull-out requires more dissipated energy during failure (González-López et al. 2019).

Further review of the obtained results in Figs. 21 and 22 and other similar works (Nyambo et al. 2011; Kim et al. 2012), reveals that the esterification treatment with MA has led to some improvements in the properties of PLA/untreated fiber biocomposites, though the properties of MA-treated PLA/fiber biocomposites have worsened

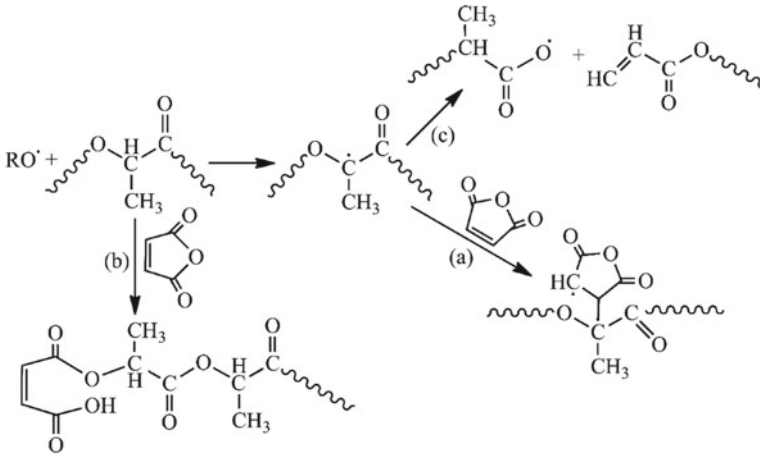

Fig. 24 Main reactions of MA with PLA chains in the presence of organic peroxide that induce an increment in the MAPLA acidity. Adapted to (Rigolin et al. 2019)

comparing with the analogous properties of virgin PLA. It is noteworthy that, despite the improvements in fiber/matrix interfaces by meleation reaction, the acidity of PLA chains increases by MA use. It is in contrast to the MA grafting reaction of polyolefins through reactive extrusion process. The acidity increment of PLA chains over MA grafting reaction was reported up to 342% in one study (Rigolin et al. 2019).

According to Fig. 24, the acidity increase of PLA chains by MA compatibilizer is probable through three reaction pathways: (a) insertion of MA molecules onto PLA chains, (b) condensation reaction of MA anhydride groups with hydroxyl end groups of PLA, and (c) chain scission of PLA macromolecules during reactive extrusion process in the presence of organic peroxide. The occurrence of side reactions along with MA grafting reaction onto PLA backbone leads to the acidity rise of MAPLA. Furthermore, during the melt-mixing process of PLA-based biocomposites containing lignocellulosic fibers, the degradation of PLA chains is likely through hydrolysis reaction, owing to the fiber residual moisture. The hydrolysis reaction of PLA chains is catalyzed by acidic sites. Consequently, PLA molecular weight reduces more considerably in the presence of MAPLA chains. Figure 25 illustrates the reduction of PLA molecular weight in the presence of coir fibers (CF) by adding 5 and 10 wt% of MAPLA. More significant decrease of PLA molecular weight, which stems from the presence of MAPLA compatibilizer, deteriorates the reinforcement effect of maleated fibers, despite stronger PLA/fiber interfaces and interfacial covalent bonding (Rigolin et al. 2019). These findings confirm the necessity of selecting the appropriate processing conditions of MA grafting reaction onto PLA chains to improve the properties of PLA/fiber biocomposites more effectively.

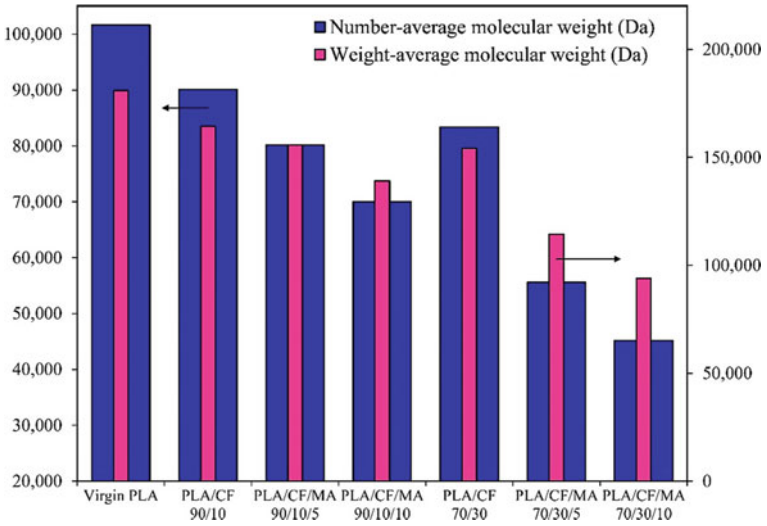

Fig. 25 Changes in average molecular weights of PLA at different coir fiber and MAPLA contents over a melt-mixing process. Adapted to (Rigolin et al. 2019)

5.3.3 Benzoylation Reaction

Benzyl chloride is frequently applied as a chemical agent for reducing the hydrophilicity of lignocellulosic fibers and improving the fiber/matrix compatibility. In benzoylation treatment process, plant fibers are exposed to an aqueous NaOH solution before the fiber reaction with benzoyl chloride to provide more accessible hydroxyl groups of fibers for substitution reaction. After alkali pretreatment, the natural fibers are then modified by benzoyl chloride through esterification reaction (Orue et al. 2018). The reaction scheme of benzoylation treatment is shown in Fig. 26. By mercerization pretreatment and benzoylation reaction, the impurities are removed from the lignocellulosic fiber surfaces and fiber roughness increases. Furthermore, by substitution of benzoyl groups for proton of hydroxyl groups, the fibers become more hydrophobic. In addition, fiber/matrix interfacial adhesion improves and correspondingly, the thermal stability and strength of plant fiber-reinforced composites are enhanced (Siakeng et al. 2019a).

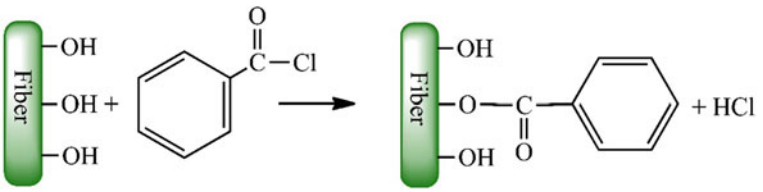

Fig. 26 Esterification reaction of the fiber hydroxyl groups with benzoyl chloride

The aforementioned improvements have been reported for woven jute fabric-reinforced PLLA biocomposites, which were prepared through hot-press molding process, in both weft and warp directions (Khan et al. 2016). In this research, the benzoylation treatment of fabrics resulted in noticeable enhancements in the mechanical characteristics including tensile modulus and strength, flexural modulus and strength, impact strength and elongation at break of virgin PLLA and PLLA/untreated fabrics biocomposites in both warp and weft directions. Figure 27 illustratively shows the mentioned improvements of mechanical properties for PLLA/jute fabrics composites.

For other geometric shapes of the reinforcement agents based on plants, the beneficial effects of benzoylation treatment on properties of PLA/olive husk flour (OHF)

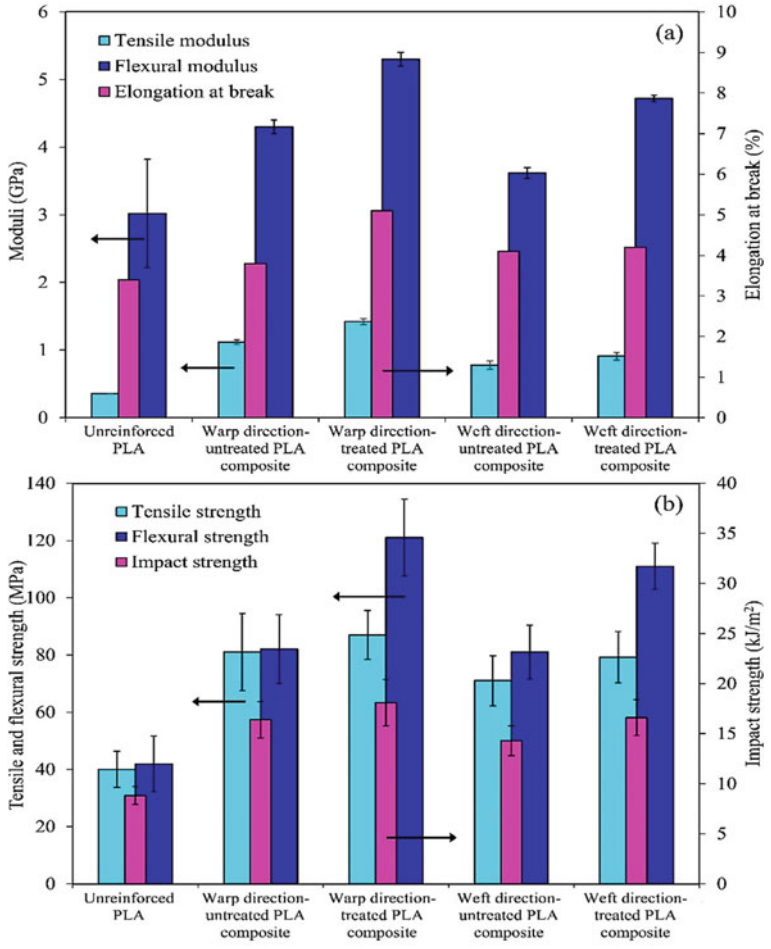

Fig. 27 Mechanical characteristics of virgin PLLA and PLLA/woven jute fabric biocomposites after and before benzoylation treatment. Adapted to (Khan et al. 2016)

biocomposites were investigated and the results were compared with more common chemical modifications including alkali and silane treatments (Isadounene et al. 2017). To treat OHF through benzoylation reaction, the reinforcement agent was first treated by NaOH, then filler particles were exposed to benzoyl chloride solution.

Among different chemical modifications, i.e. alkali, silane and benzoylation reactions, the incorporation of treated OHF particles with benzoyl chloride into PLA matrix did not lead to the best mechanical performance. As can be observed in Fig. 28, the largest Young modulus, tensile strength and elongation at break are comparatively obtained for the PLA biocomposites containing alkali-treated OHF filler. In contrast, for most cases, PLA/OHF biocomposites having benzoylated reinforcement agent show weaker mechanical characteristics comparing with other PLA/treated filler biocomposites at the same OHF loading. The researchers reported that the mercerization treatment had more profound impact on the improvement of matrix/filler interfacial adhesion than silane and benzoylation modifications, through the removal of impurities and increment of filler surface roughness. Moreover, the highest storage modulus and thermal stability were also determined for the biocomposites containing alkali treated OHF particles.

Throughout benzoylation process, the hydroxyl groups of plant fibers are transformed into the benzoate groups. Therefore, the quantities of inter- and intramolecular hydrogen bonds among fiber components diminish to lower values and correspondingly, the natural fibers become more hydrophobic. In a similar manner to acetylation treatment, benzoylation process gives the lignocellulosic fibers thermoplasticity. Reportedly, the reinforcing effect of benzoylated plant fibers in PLA matrix is controlled by the concentration of benzoyl chloride solution after alkali pretreatment (Al-Mobarak et al. 2018, 2019). In the related works, sponge-ground fibers (SGF) obtained from *luffa cylindrica* plant were applied as lignocellulosic reinforcement agent. The influences of three different chemical treatments, i.e. alkali, acetylation and benzoylation processes, on the mechanical, physical, thermal and biodegradation properties as well as antibacterial activity of PLA-based biocomposites were studied.

As can be found in Fig. 29, the highest compression strength was achieved for PLA/benzoylated SGF biocomposite among others, when the treatment aqueous solutions, namely benzoyl chloride, acetic anhydride and NaOH solutions, at a fixed concentration of 5 wt% were applied. Nevertheless, the compression strength of different PLA/treated SGF biocomposites were measured to be close to each other, when the solutions of treatment agents were used at a constant concentration of 10 wt%.

The dependence of the properties of PLA-based green composites on the concentration of treatment agent solutions can be interpreted by studying the morphology and interfacial phenomena of the biocomposites after chemical reactions. The SEM images of fractured surfaces in Figs. 30 and 31 reveal the existence of poor matrix/fiber interface and lots of pores on the interfacial surface of PLA/untreated SGF composite. By fiber modifications using the solutions at a treatment agent concentration of 5 wt%, the matrix/plant fiber interfacial adhesion improves and the fractured surfaces show lower roughness and smaller cracks. As can be observed

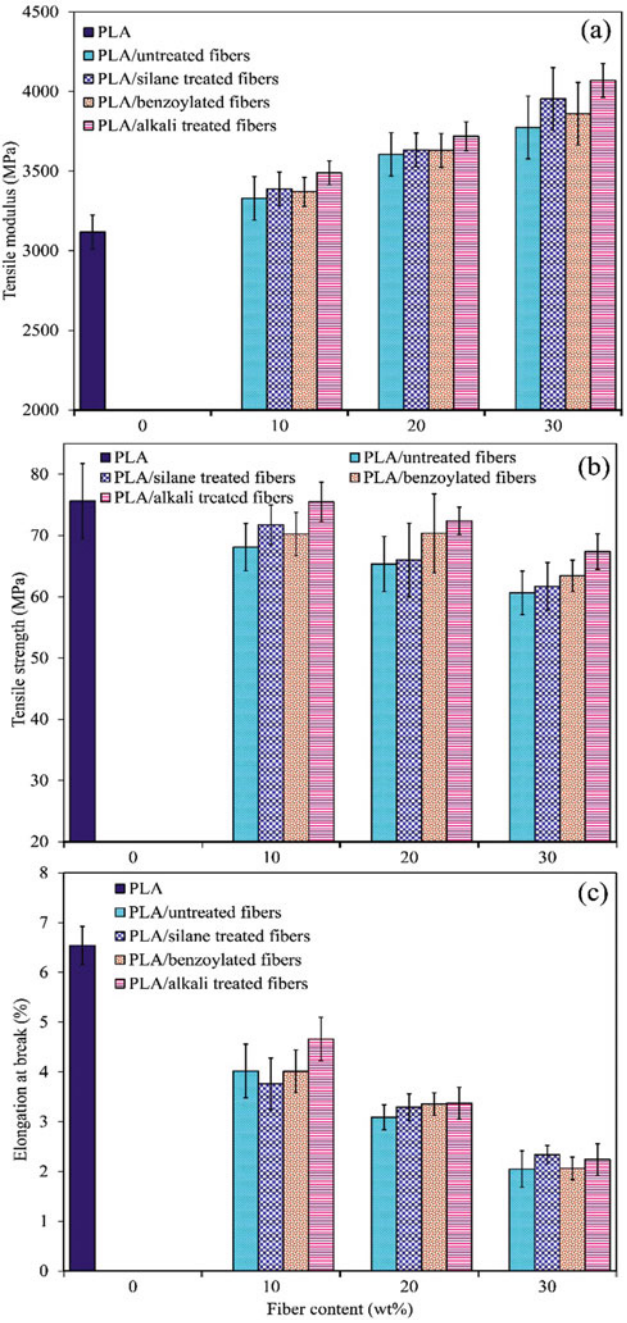

Fig. 28 Mechanical characteristics of virgin PLA and PLA/olive husk flour biocomposites after and before different chemical treatments including alkali, silane and benzoylation modifications. Adapted to (Isadounene et al. 2017)

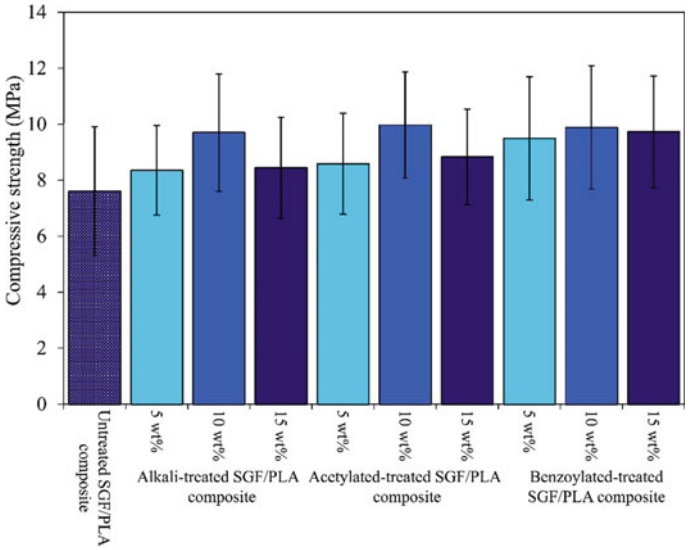

Fig. 29 Effects of the concentration of the treatment agent solutions on the compression strength of PLA/SGF biocomposites at a fixed filler content of 5 wt%. Adapted to (Al-Mobarak et al., 2018; 2019)

in Fig. 30, the lowest surface roughness belongs to the fractured surface of PLA/benzoylated fiber composite. However, an increment in the concentration of treatment agent to 10 wt% leads to the fractured surfaces with more similarity for all biocomposites, which can be seen in Fig. 31. At this concentration, the matrix/fiber interfacial adhesion is enhanced more, hence eliminating the voids.

The concentration of treatment agents resulted in similar trends in the biodegradation rate in soil, T_g and T_m of the prepared green composites. The highest thermal stability and biodegradation rate along with the largest T_g and T_m were attained for PLA/benzoylated SGF composite, in which lignocellulosic fibers were exposed to the benzoyl chloride solution at 10 wt% concentration. Additionally, the antibacterial activity tests using a category of Vero cell line reveal that the benzoylated fiber-reinforced composites do not show any cytotoxicity. At the biocomposite surface, non-cancer cells grow indicating the harmlessness of the prepared biocomposite for human body in biomedical purposes (Al-Mobarak et al., 2018, 2019).

5.4 Bleaching Treatment

Bleaching is a common method for discoloration and whitening of lignocellulosic fibers. Normally, bleaching agents such as hydrogen peroxide (H_2O_2), sodium chlorite ($NaClO_2$) and sodium hypochlorite (NaClO) are used in this method (Zhang et al. 2017). The bleaching agents react with the hydroxyl groups of lignin and

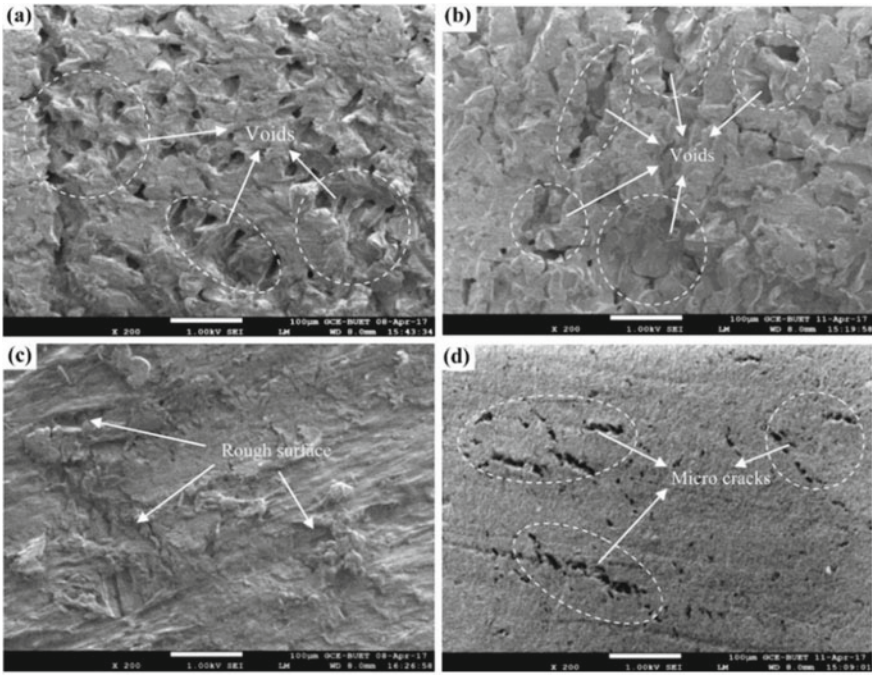

Fig. 30 SEM micrograph of the fractured surface of PLA/SGF composite containing: **a** untreated fibers, **b** alkali-treated fibers, **c** acetylated fibers and **d** benzoylated fibers using the treatment agent solutions at a constant concentration of 5 wt%. (Al-Mobarak et al. 2018) Open Access

degrade the impurity of plant fibers. For instance, $NaClO_2$ releases chlorous acid after acidification reaction. After oxidation, the chemical forms chlorine dioxide (ClO_2). Afterwards, ClO_2 reacts with lignin and removes it from lignocellulosic fibers (Siakeng et al. 2019a). Hydrogen peroxide also, as a bleaching agent, undergoes dissociation reaction in alkaline media and forms perhydroxyl ions (HOO^-) (Fig. 32). The ions attack light absorbing chromophoric groups of lignin and hemicellulose including carbonyl and conjugated carbonyl groups as well as quinones and remove them from fibers after treatment (Marwah et al. 2014). Different studies have employed bleaching method to enhance the properties of PLA/plant fiber biocomposites (Posada et al. 2016; Hou et al. 2006; Razak et al. 2014).

Bleaching process is accompanied with delignification and increases the fiber brightness. On the other hand, the delignification and dewaxying reactions heighten the fiber roughness through bleaching process, which can strengthen the matrix/fiber interfaces by providing mechanical interlocking (Zhang et al. 2017). Bleaching process not only can improve the mechanical performance of natural fiber-reinforced biocomposites, but also it can lead to an improvement in the physical appearance of biocomposites. The incorporation of lignocellulosic fibers into polymer matrices generally eventuates in dark brown products that limits the product applications. As

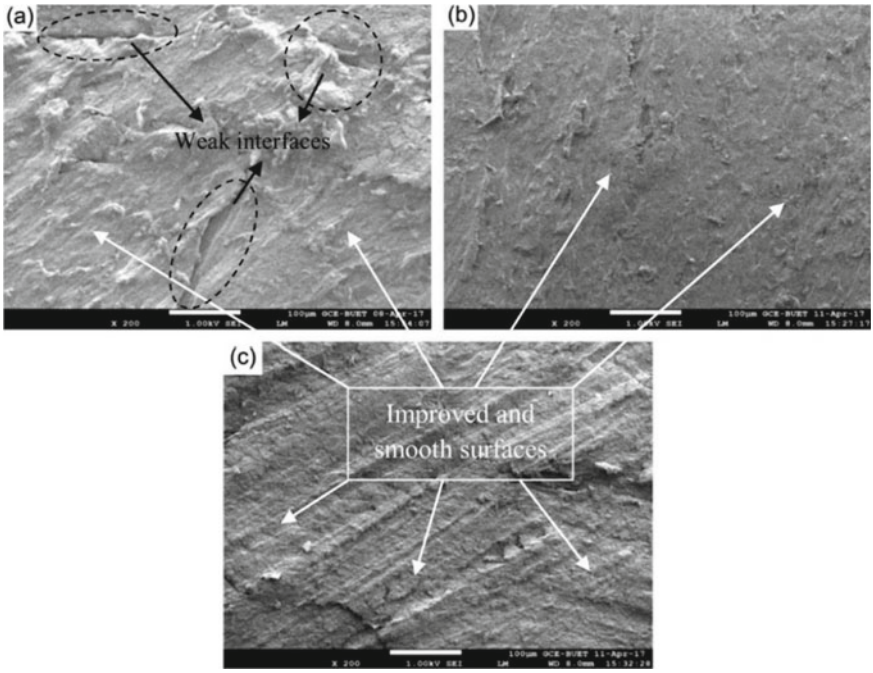

Fig. 31 SEM micrograph of the fractured surface of PLA/SGF composite containing: **a** untreated fibers, **b** alkali-treated fibers, **c** acetylated fibers and **d** benzoylated fibers using the treatment agent solutions at a constant concentration of 10 wt%. (Al-Mobarak et al. 2018) Open Access

$$H_2O_2 + OH^- \longrightarrow H_2O + HOO^-$$

Fig. 32 Reaction scheme of hydrogen peroxide dissociation

can be seen in Fig. 33, bleaching process overcomes the common disadvantage of lignocellulosic fiber-reinforced biocomposites, which is related to fiber brightness. This treatment method can provide a brighter PLA/plant fiber biocomposite that can be also colored by applying different color masterbatches (Marwah et al. 2014; Razak et al. 2014).

As mentioned earlier, it is possible to apply hydrogen peroxide in alkaline media to bleach lignocellulosic fibers. This bleaching agent was used for treating the oil palm empty fruit bunch (OPEFB) and kenaf fibers (Marwah et al. 2014; Razak et al. 2014). In these works, the plant fibers were first treated with warm water. Then, the fibers were dipped in 50 vol% H_2O_2 solution at a pH of 11 and temperature of 70 °C. As it is evident in Fig. 34, the roughness of OPEFB fibers has increased after bleaching treatment and some pores are observable on the fiber surfaces.

As mentioned before, the removal of fiber impurities such as lignin, hemicellulose and waxes can cause an improvement in the fiber/matrix interfacial strength by

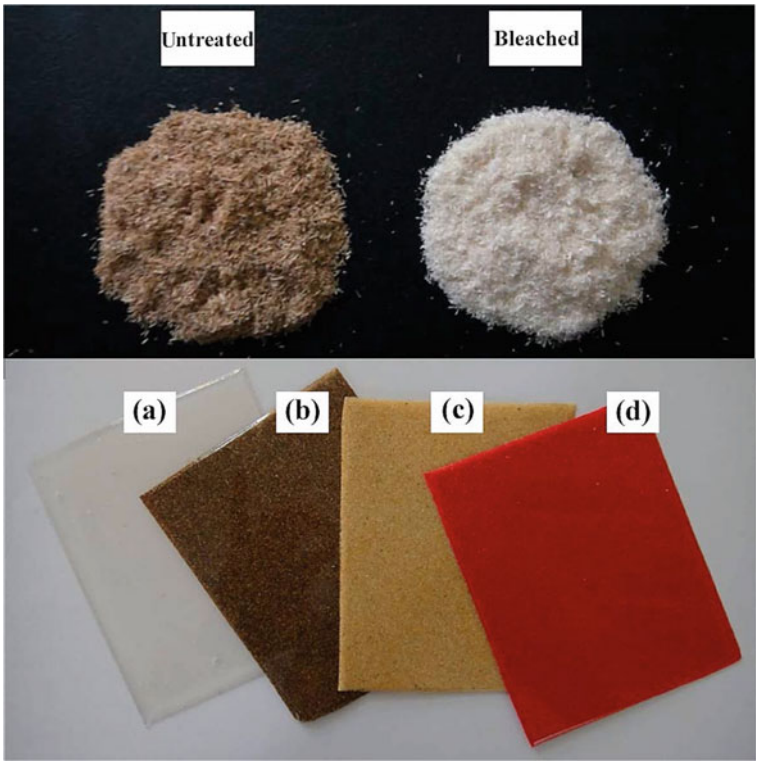

Fig. 33 Upper row: untreated and bleached oil palm empty fruit bunch fibers, lower row: **a** virgin PLA, **b** PLA/untreated fiber biocomposite, **c** PLA/bleached fiber biocomposite, **d** PLA/color masterbatch/bleached fiber biocomposite. (Marwah et al. 2014) Open access

providing mechanical interlocking (Marwah et al. 2014). In this work, X-ray diffraction (XRD) studies reveal that the fiber crystallinity index has changed from 37% to 61% by bleaching modification process. Higher crystallinity degree reinforces the fibers more. Considering that and improved interfacial strength, more efficient stress transfer across fiber/matrix interfaces was attained for PLA/bleached lignocellulosic fiber biocomposites. The fractured surfaces of PLA/OPEFB biocomposites without any treatment in Fig. 35 show significant extents of fiber pull-out and interfacial gaps due to matrix/fiber debonding under load. While smaller gaps and stronger interfacial adhesion can be observable on the fractured surfaces after bleaching treatment. Besides, the tensile modulus and strength, flexural modulus and strength, impact strength and elongation at break were found to be all improved after bleaching treatment. However, one may note that different types of strength and elongation at break of the biocomposites containing bleached fibers were lower than the corresponding values of pure PLA in these researches (Marwah et al. 2014; Razak et al. 2014).

Sodium chlorite was also used for the treatment of pecan nutshell (NS) lignocellulosic material in PLA matrix (Agustin-Salazar et al. 2018). In this research, NS was

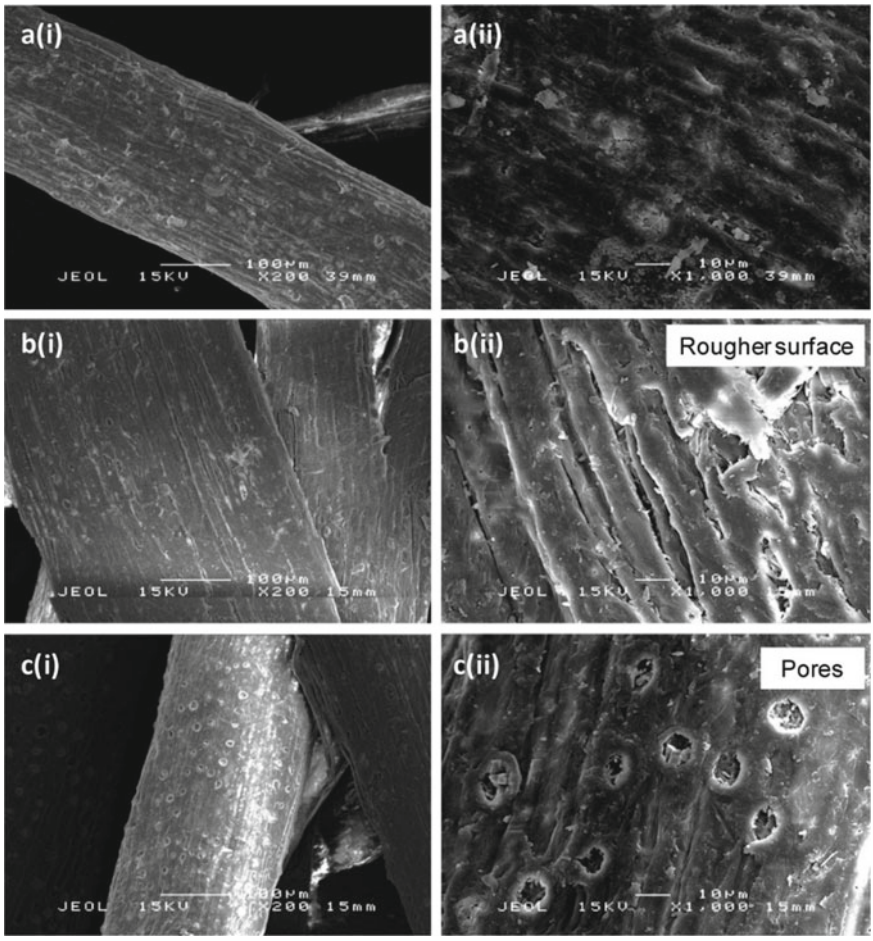

Fig. 34 SEM image of: **a** untreated OPEFB fibers, **b** and **c** bleached OPEFB fibers, the right column is higher magnification images of left ones. (Marwah et al. 2014) Open access

treated in aqueous solutions of acetic acid and sodium chlorite at 90 °C and hollocellulose (HC) part of the lignocellulosic material, i.e. polysaccharide constituents including cellulose and hemicellulose, was extracted (Agustin-Salazar et al. 2018). FTIR and ^{13}CNMR spectroscopic results confirmed the hollocellulose extraction by bleaching treatment. In ^{13}CNMR spectrum of HC sample, there were no peaks of aromatic lignin carbons in chemical shifts of 56, 120 and 170 ppm. Additionally, the presence of NMR peaks in the range of 60–105 ppm attributed to the carbons of cellulose and hemicellulose rings, a peak at 172 ppm related to the carbonyl carbon of acetic ester and a sharp peak at 21 ppm correlated with the methyl carbon of acetyl moiety proved that HC just had cellulose and hemicellulose components.

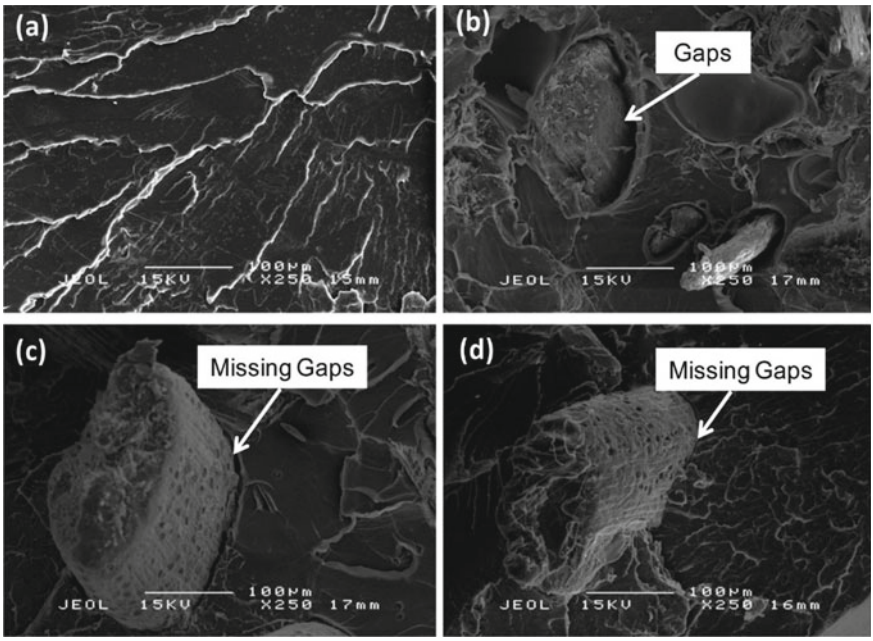

Fig. 35 SEM image of fractured surface of: **a** virgin PLA, **b** PLA/untreated fibers, **c** PLA/bleached fibers and **d** PLA/bleached fibers/color masterbatch samples. The biocomposites contained a fixed fiber loading of 30 wt%. (Marwah et al. 2014) Open access

It is noteworthy that the thermal stability of the biocomposites containing HC decreased, compared to the PLA-based biocomposites containing untreated NS, despite the removal of lignin after bleaching treatment. The viscoelastic properties of the molten biocomposites showed that HC addition to PLA matrix resulted in considerable increments in storage modulus, loss modulus and complex viscosity. The increments are attributed to the restricted molecular motions of PLA chains, hydrodynamical effects of PLA/filler interactions and creation of a 3D particulate network (Agustin-Salazar et al. 2018).

On the fractured surface of PLA/HC biocomposites, some aggregates of separate HC particles in continuous PLA matrix were observed, but the fibers were completely impregnated with matrix and no fiber/matrix detachment was seen. Among all measured mechanical properties, HC filler, obtained from the NS bleaching process, just improved the flexural modulus of PLA to a considerable extent. In this work, the strength and strain at break of PLA/HC biocomposites determined by performing flexural stress-strain tests were equal to the corresponding results of PLA/untreated NS biocomposites. Nevertheless, the impact strength and resilience of the PLA-based biocomposites containing bleached NS were found to be even weaker than the related properties of pure PLA and PLA/untreated NS biocomposites. It was believed that it related to the lack of chemical bonding between bleached lignocellulosic filler and PLA matrix (Agustin-Salazar et al. 2018).

5.5 *Etherification Treatment*

Fiber treatment through the etherification reaction of accessible hydroxyl groups on the surfaces of lignocellulosic fibers leads to an improvement in the mechanical properties and performance of PLA/natural fiber biocomposites. Epoxide, alkyl halides and benzyl chloride are among the chemicals that can be used for etherification fiber treatment. Sodium hydroxide is also applied in etherification treatment reactions. In fact, NaOH plays an important role in the formation of charged intermediate species, which facilitate the nucleophilic addition of fiber surface groups to etherification treatment compounds like benzyl chloride (Avinc and Khoddami 2009). In some of the etherification treatment methods such as benzylation, wherein benzyl chloride is used as the treatment agent, the hydrophilic hydroxyl groups of lignocellulosic materials are substituted by more hydrophobic benzyloxy groups. That can reduce the fiber hydrophilicity. Unlike this method, which is limited to the chemical treatment of fiber surfaces, in epoxide-based etherification methods, the coupling reactions between lignocellulosic fibers and PLA matrix become possible.

5.5.1 Benzylation Reaction

Benzylation reaction, using benzyl chloride, is generally carried out in the presence of sodium hydroxide or after alkali pretreatment. As shown in Fig. 36, the benzylation reaction, also known as "Williamson synthesis", is a nucleophilic reaction between alkoxide and halide ions. By substituting large and non-polar groups of benzyloxy for small and hydrophilic groups of hydroxyl, the intra- and inter-molecular hydrogen bonds among lignocellulosic constituents are reduced and correspondingly, the fiber

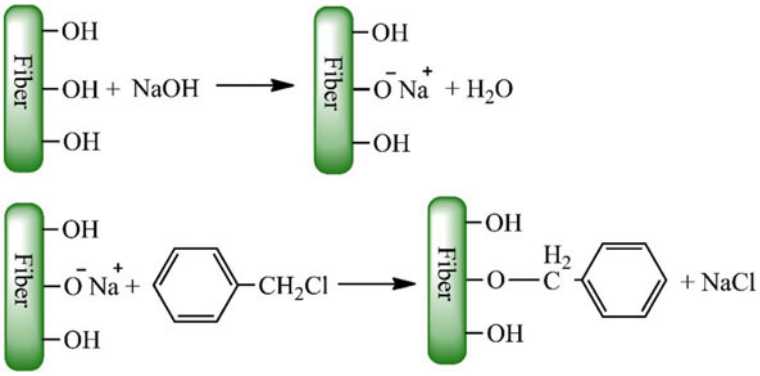

Fig. 36 Proposed reaction scheme of the benzylation treatment of lignocellulosic fibers after alkali pretreatment

thermoplasticity is increased. Reaction time and temperature as well as media alkalinity are effective parameters in benzylation treatment process (Ghorbani Chaboki et al. 2019).

In a research (Ghorbani Chaboki et al. 2019), rice straw fibers were chemically treated in aqueous solution of NaOH and benzyl chloride. In this study, the thermoset-like fibers after etherification process showed T_g in the range of 170 °C, in dynamic-mechanical thermal analysis (DMTA). Adding benzylated rice straw fibers (BRS) to PLA led to an augmentation in T_g of PLA. Table 3 shows the increase in T_g of matrix for different loadings of BRS, i.e. 10, 30 and 50 wt%. The reason behind this increment was believed to relate to improved interactions between thermopalsticized fibers and PLA matrix. The tensile stress-strain results showed that adding BRS fibers having less hydrophilicity and more thermoplasticity can simultaneously improve the Young modulus, yield stress, stress at break and elongation at break of PLA matrix at low fiber loadings (Fig. 37).

Microscopic observations of the fractured surfaces of PLA/BRS biocomposites (Fig. 38) confirm the occurrence of fiber breakage as dominant phenomenon. At 10 wt% loading of BRS, less debonding at fiber/matrix interfaces is observable, which demonstrates the appropriate wettability of BRS fibers with PLA matrix. However, by increasing the reinforcing fiber content, intensified fiber pull-out and interfacial

Table 3 T_g of virgin PLA, BRS and PLA/BRS biocomposites obtained from DMTA analysis, x in PLABRSx codes show the fiber loading (Ghorbani Chaboki et al. 2019)

Sample	T_g (°C) at a frequency of		
	1 Hz	2 Hz	5 Hz
BRS	–	169	172
PLA	54.3	54.6	54.7
PLABRS10	56.10	57.24	58.78
PLABRS30	57.21	58.52	60.19
PLABRS50	60.36	61.16	62.58

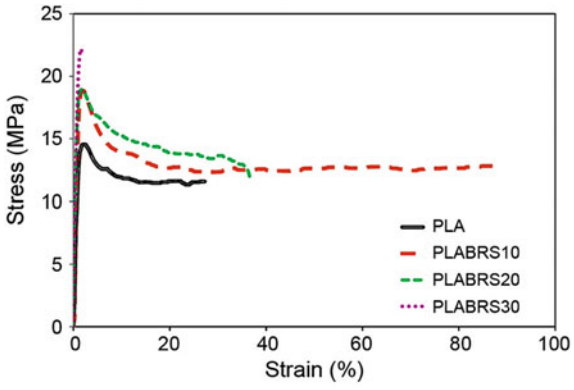

Fig. 37 Stress-strain curves of virgin PLA and PLA/BRS biocomposites, x in PLABRSx codes show the fiber loading (Ghorbani Chaboki et al. 2019)

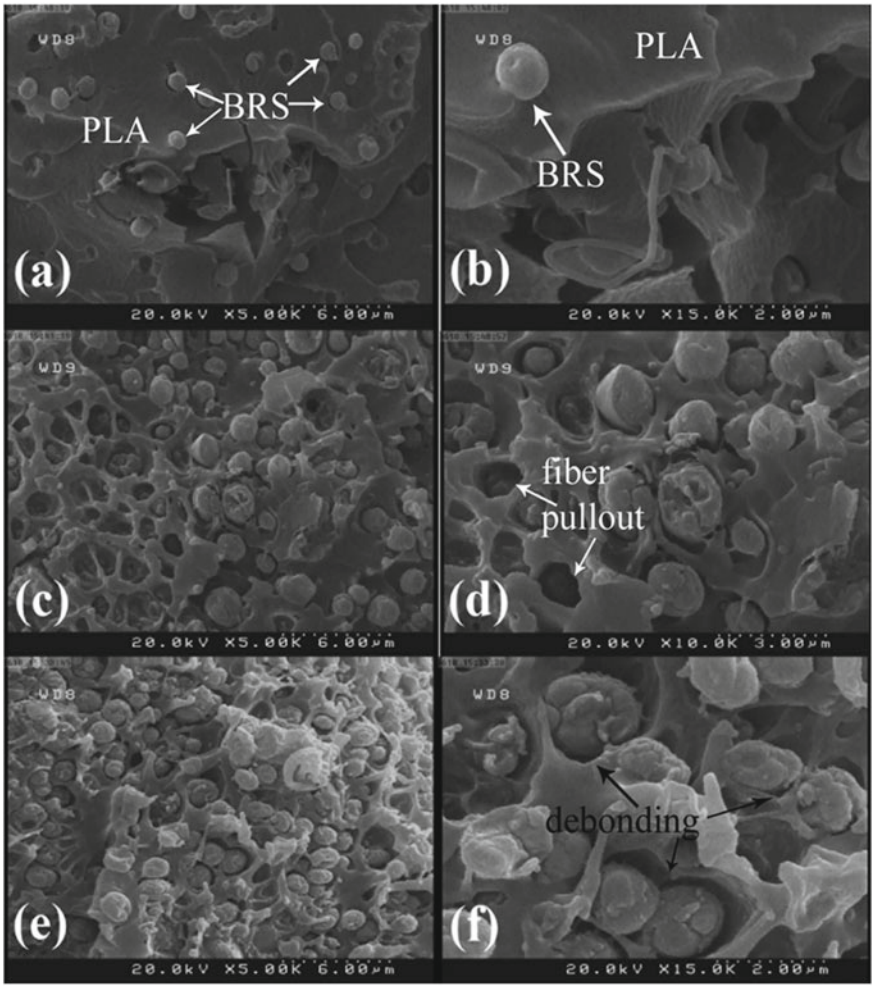

Fig. 38 SEM image of PLA/BRS biocomposites at a fiber loading of: **a–b** 10 wt%, **c–d** 30 wt% and **e–f** 50 wt% (Ghorbani Chaboki et al. 2019)

debonding eventuate in a brittle mechanical failure mode and elimination of yield point in stress-strain curves (Ghorbani Chaboki et al. 2019).

In a similar study (Zandi et al. 2019), rice straw was first undergone alkali treatment with NaOH solution, and after separation of pulp and liquor via alkali pulping process, both products were benzylated. It can be seen in Fig. 39 that benzylated rice straw pulp has higher whiteness owing to the delignification of rice straw through soda pulping and benzylation reactions. The main component of rice straw pulp prepared from alkali treatment has been cellulose, while the main constituents of rice straw pulping liquor have been lignin and hemicellulose.

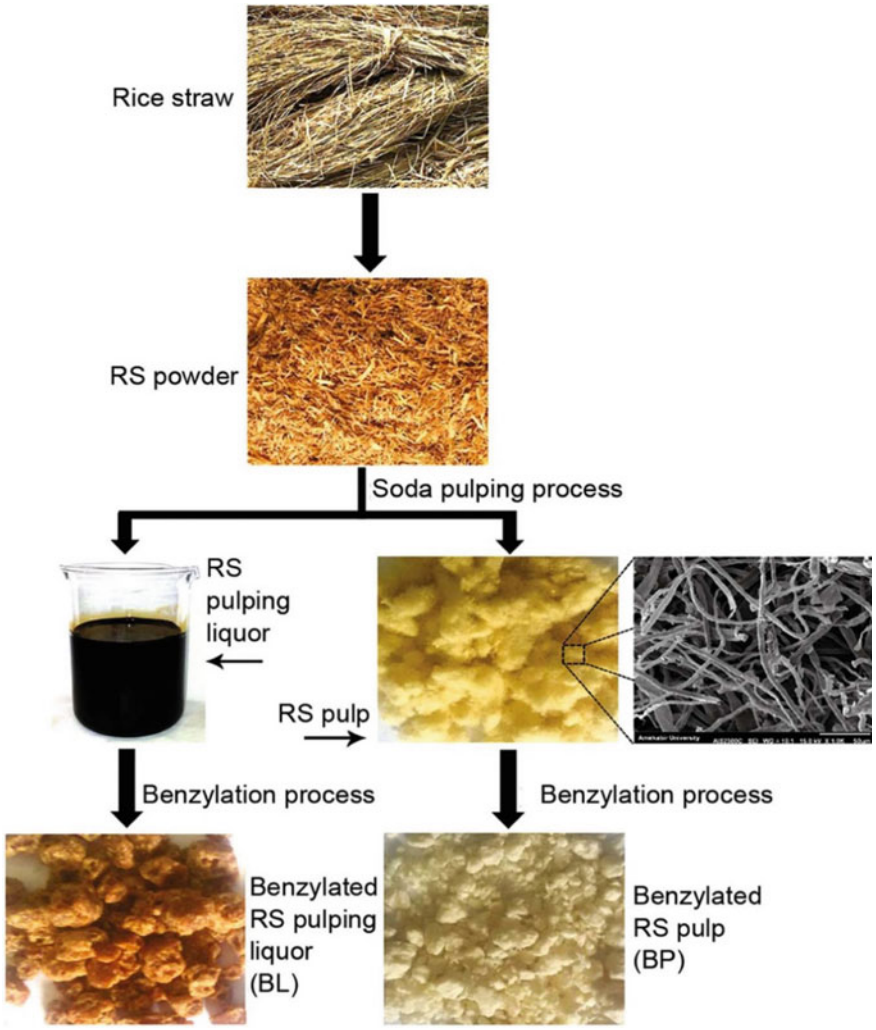

Fig. 39 Scheme of alkali pulping and benzylation processes of rice straw (Zandi et al. 2019)

The SEM images of rice straw products after benzylation process are represented in Fig. 40. As can be seen, there are many pores at surface of benzylated liquor (BL) particles, while benzylated pulp (BP) consists of cellulosic microfibrils. The BL filler, which is more hydrophobic than cellulose, was found to show better interfacial adhesion with PLA matrix. Figure 41 confirms that even on the cryogenically-fractured surface of PLA/BL biocomposites, no sign of fiber pull-out and interfacial debonding is discernable. In Fig. 41c, the coverage of filler surface with a thin layer of matrix is obvious. These phenomena are attributed to the filler hydrophobicity increment after

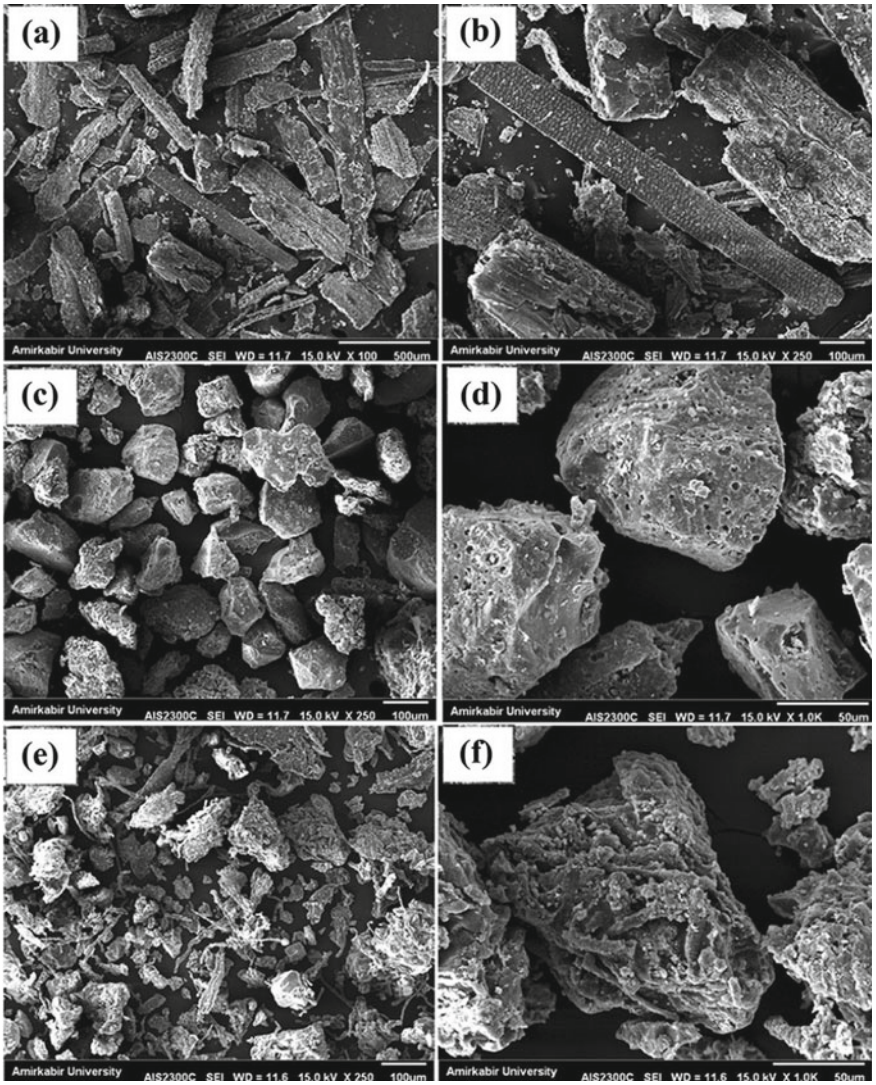

Fig. 40 SEM images of: **a**–**b** untreated rice straw, **c**–**d** BL and **e**–**f** BP (Zandi et al. 2019)

benzylation reaction and better mechanical interlocking with PLA matrix provided by the porosities on BL surfaces.

Thermal analysis results showed that T_m, T_g and vicat softening point of PLA decreased by adding benzylated products of rice straw. As an exception, just the benzylated cellulose fibers at 10 wt% in PLA (PLABP10 composite) had higher softening point than virgin PLA. The resultant decrease of fiber crystallinity degree and increase of fiber thermoplasticity, despite improved interfacial adhesion, are the

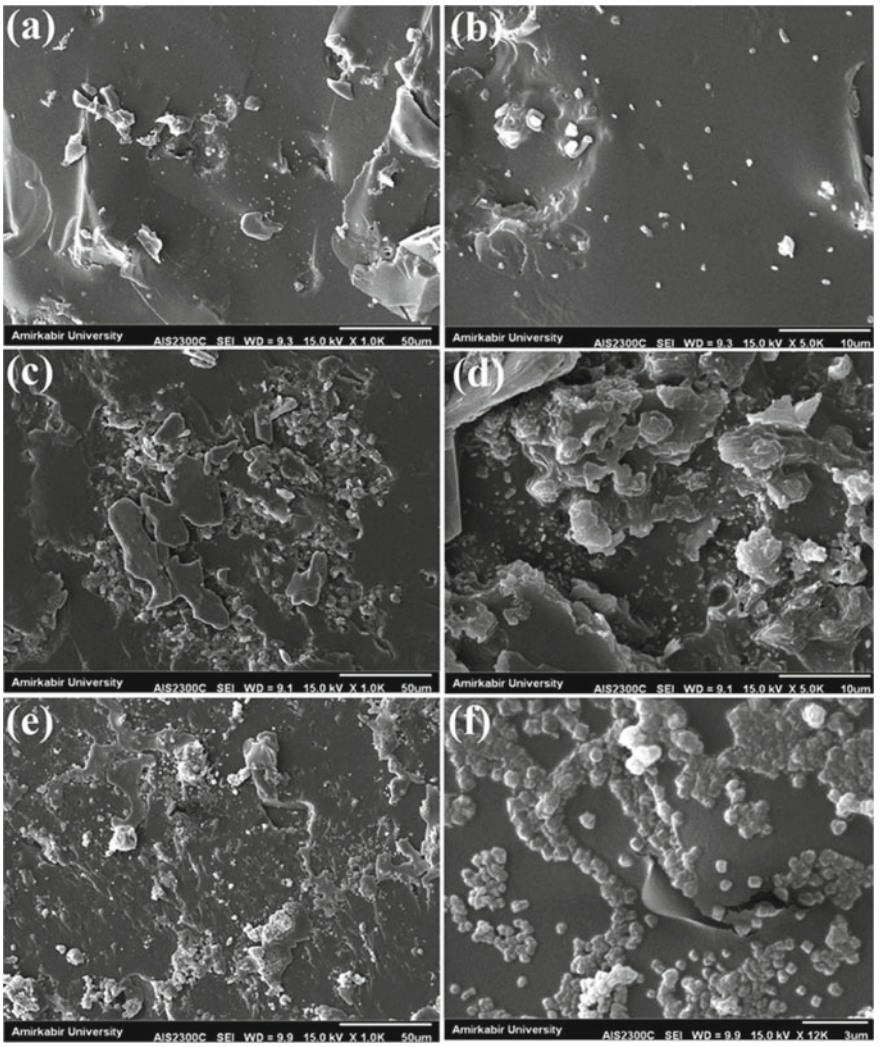

Fig. 41 SEM images of: **a–b** PLABL10, **c–d** PLABL20 and **e–f** PLABL30 biocomposites, x in PLABLx codes shows the filler loading (Zandi et al. 2019)

plausible explanations. Nevertheless, adding the benzylated products of rice straw to PLA matrix brought about a significant rise in matrix crystallinity degree, owing to the effective role of modified fibers as heterogeneous nucleation sites. The increment was observed to be more considerable for benzylated liquor product. Noticeable enhancements in the biodegradation rate of PLA in soil were also found by adding benzylated rice straw fillers. In a similar trend to crystallinity degree, PLA/BL biocomposites have shown higher biodegradation rate than PLA/BP biocomposites, at a constant filler loading (Zandi et al. 2019).

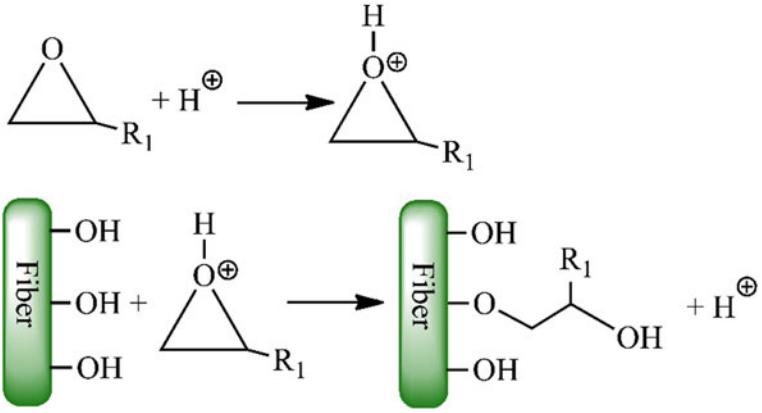

Fig. 42 Opening reaction of epoxide rings by attacking a nucleophile

5.5.2 Epoxide Opening Reaction

Etherification treatment can be also occurred by epoxide opening reaction with a nucleophile attack in the presence of an acid (Fig. 42). One of the epoxides, used for the treatment of lignocellulosic fiber and improvement of natural fibers/PLA compatibility, is glycidyl methacrylate (GMA). GMA has been used for the treatment of rice straw fibers (RSF) in a study (Wu et al. 2013). In order to perform the GMA grafting reaction onto PLA chains, a mixture of GMA and benzoyl peroxide (BPO) was added to molten matrix. The reactions most likely proceed according to Fig. 43a to form GMA grafted PLA (PLA-g-GMA) chains. The fiber surface was treated by tetraethyl orthosilicate as crosslinking agent, H_2O and lactic acid as catalyst in tetrahydrofuran solution. During melt-mixing processes, the opening reaction of epoxide groups and PLA-g-GMA reaction with crosslinking agent grafted onto fiber surfaces became possible (Fig. 41b).

With these reactions, lignocellulosic fibers covalently bond with PLA chains through the formation of several intermediate species. PLA-g-GMA/TRSF biocomposites, in comparison with PLA/RSF biocomposites, showed higher T_g, melting enthalpy, thermal stability, tensile strength and HDT at fixed fiber loadings. However, the treated biocomposites had relatively smaller melt viscosity, water absorption and soil burial biodegradation rate.

The SEM micrographs of fractured surfaces (Fig. 44) reveal the RSF pull-out, which stems from the high surface energy difference of RSF fiber with matrix phase. Better wettability of PLA-g-GMA matrix and higher strength of treated fiber/matrix interfaces led to more homogenous fiber distribution and complete coverage of treated fibers with matrix in such a way that no pull-out can be observable on Fig. 44b. Another notable point is the significant and unique increment in the tensile strength of PLA-g-GMA/TRSF biocomposites. Unlike untreated PLA/RSF biocomposites,

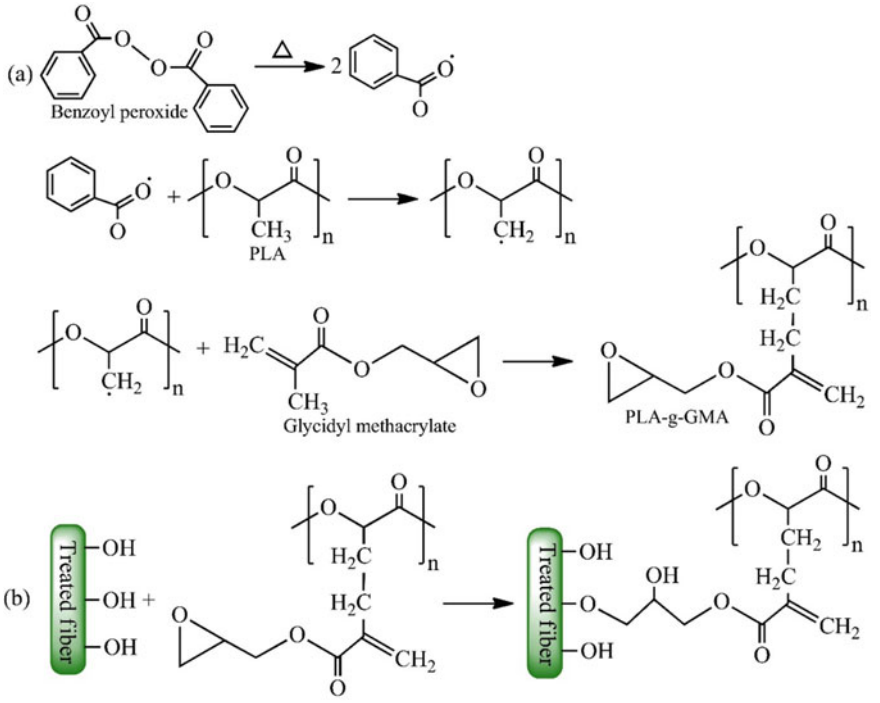

Fig. 43 **a** GMA grafting reaction onto PLA chains and **b** the chemical between PLA-g-GMA and treated rice straw fiber (TRSF). Adapted to (Wu et al. 2013)

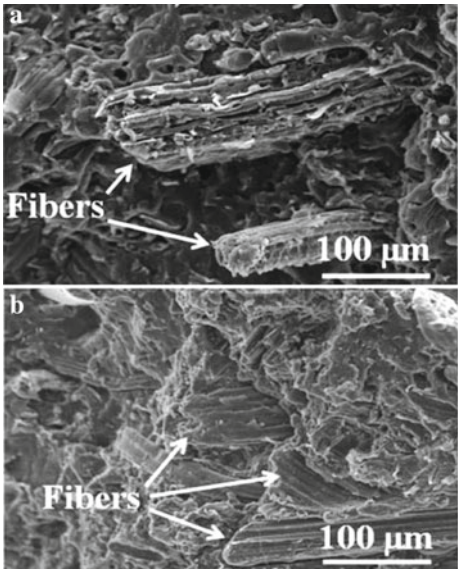

Fig. 44 SEM image of fractured surface of: **a** PLA/RSF and **b** PLA-g-GMA/TRSF biocomposite at a constant fiber loading of 20 wt%. Reproduced with permission from (Wu et al. 2013)

the tensile strength of treated PLA-g-GMA/TRSF biocomposites did not show a decline by increasing the fiber content (Wu et al. 2013).

In a similar study (Liu et al. 2019), the interface of bamboo fibers and PLA matrix was modified using tannic acid (TA, with average 25 hydroxyl groups per molecule) and epoxidized soybean oil oligomers (ESO, with average 4 epoxy groups per molecule). To ensure a proper grafting reaction between the fibers and PLA chains, the fiber surfaces were first sprayed with ESO/TA solution in acetone. Afterward, the dried fibers were melt-compounded with PLA via twin-screw extruder. The utilized epoxide can act as a compatibilizer for fiber/PLA interfaces at high temperatures, through ring opening reaction and covalent bond formation with –OH groups of fibers along with the end groups of PLA chains.

The reason of applying TA has been the localization of epoxy groups at the center of fatty acid (ESO) chains, through which their reactivity is limited owing to steric hindrance. Besides, TA can induce the ring opening reactions of epoxides, due to the presence of many phenolic –OH groups in the chemical structure. Through the fiber treatment, the phenolic –OH groups of TA first react with the epoxy groups of ESO, by which a layer of TA-ESO is formed. Then, in a second step, the epoxy groups of TA-ESO layer can concurrently react with the end groups of PLA and fiber hydroxyl groups. Furthermore, the TA-ESO layer can physically interact with fibers through strong and natural polyphenol-inspired chemistry like hydrogen bonds and $\pi - \pi$ interactions (Fig. 45).

For low concentrations of TA-ESO (0.5 wt%), tensile modulus and strength, elongation at break, tensile toughness, impact strength and storage modulus of untreated PLA/BF biocomposites were improved, because of the formation of chemical bonds

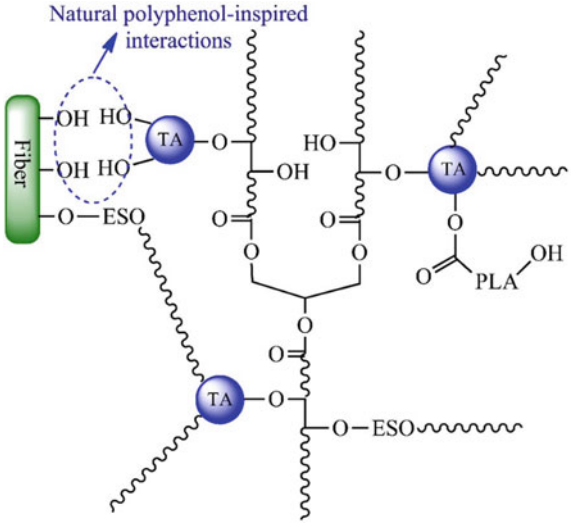

Fig. 45 Physical interactions and chemical linkages of TA-ESO with fiber surfaces and PLA chains. Adapted to (Liu et al. 2019)

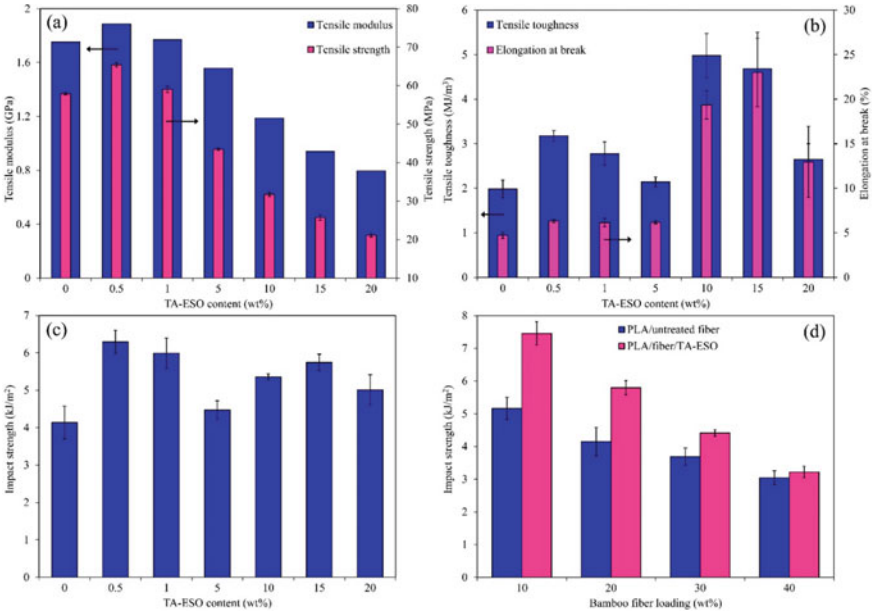

Fig. 46 **a–c** Mechanical characteristics of PLA/BF biocomposites versus TA-ESO concentration, **d** impact strength of untreated and treated PLA/BF biocomposites versus BF loading. Adapted to (Liu et al. 2019)

and TA-ESO flexible layer at the interfaces of PLA/lignocellulosic fiber composites. However, increasing the concentration of TA-ESO gradually changed the role of TA-ESO from a coupling agent to a toughening agent and only the properties of PLA/BF composites such as tensile toughness, impact strength and elongation at break improved at higher TA-ESO contents (Liu et al. 2019).

Figure 46 illustrates the mentioned variations in properties versus TA-ESO concentration. In fact, the phase separation of TA-ESO phase, the formation of dispersed TA-ESO rubbery domains in PLA matrix and correspondingly, toughening of PLA matrix were reported as the explanations. In this chemical treatment, the improvement of the biocomposite properties is just possible by the formation of a thin TA-ESO layer at PLA/fiber interfaces, but in the case of high TA-ESO concentrations and creation of thick and weak interfacial layers of TA-ESO, the biocomposites easily undergo failure under stress. Hence, the concentration of epoxide coupling agent plays a key role in improving the biocomposite performance (Liu et al. 2019).

5.6 Graft Copolymerization

One of the most common topics on reinforced polymers is the treatment of lignocellulosic fibers through graft copolymerization. During this modification process, polymeric chains are synthesized in the presence of fibers and the chains are grafted onto fiber surface through covalent bonds. The polymerization and grafting reactions of polymer chains with fiber surfaces eventuate in the possibility of improving the physical, mechanical and biological properties as well as the surface characteristics and environmental responsiveness of fiber-reinforced composites (Zhang et al. 2017). Grafting proportion and efficiency control the compatibility of lignocellulosic fibers with polymer matrix. Moreover, the type and composition of polymerization initiator, co-monomer type and grafting reaction conditions are determinant parameters in the treatment process as well (Kozlowski and Wladyka-Przybylak 2004; Zimniewska and Wladyka-Przybylak 2016).

Free radical polymerization, ionic and ring-opening polymerizations are different polymerization methods that can be employed in graft copolymerization of lignocellulosic fibers. The ionic polymerization, despite the possibility of further control of polymerization reaction, are not very common for this type of treatment. The explanation is related to the specific conditions required for such reactions and the possibility of side reactions on fiber surfaces during polymerization process (Zhang et al. 2017). On the other hand, free radical polymerization has gained more attention. The chain propagation reaction of radical polymerization can be initiated in different ways by using peroxides, oxidation-reduction agents, UV and γ radiation, cold plasma and etc. For instance, lignocellulosic fibers can be placed in an aqueous solution containing selected ions and exposed to high-energy radiation. As a result of radiation, the lignocellulosic molecules crack down and free radicals are formed. The fibers are then treated by a monomer that is compatible with polymer matrix and the polymerization reaction of monomers is initiated and propagated by the free radicals obtained from fibers. Different types of vinyl monomers, including acrylonitrile, styrene, methyl methacrylate and butyl acrylate, can be employed in this treatment method (Kozlowski and Wladyka-Przybylak 2004; Zimniewska and Wladyka-Przybylak 2016). The free radical polymerization methods such as reversible deactivation radical polymerization (RDRP), atom transfer radical polymerization (ATRP), reversible addition-fragmentation chain transfer polymerization (RAFT) and nitroxide-mediated radical polymerization (NMP) have been widely used in the treatment of lignocellulosic fibers.

In addition, the possibility of ring-opening polymerization and grafting of the resultant polymer chains onto fiber surfaces exists, owing to the hydroxyl groups on lignocellulosic fiber surfaces. The cyclic monomers such as lactides and lactones can be used in ROP reaction and resulted in the synthesis of biodegradable PLLA and poly(ε-caprolactone) (PCL) (Zhang et al. 2017).

In related researches (Qin et al. 2011a, b), the surface of rice straw fibers was treated with butyl acrylate graft copolymerization. The treatment induced an improvement in the tensile strength of PLA up to 6 MPa, at constant weight

percentage of 7.98 wt% for poly(butyl acrylate) (PBA) reacted with RSF. The graft copolymerization of butyl acrylate monomer in the presence of RSF, azobisisobutyronitrile (AIBN) initiator, poly(vinyl alcohol) (PVA) dispersant was performed in distillated water at a temperature of 75 °C. By grafting PBA onto the surfaces of lignocellulosic fibers, the water absorption of PLA/RSF biocomposites was decreased. Since PBA is relatively hydrophobic, the substitution of PBA chains for the hydrophilic hydroxyl groups of fibers and the resultant improvement of fiber/matrix interfacial interactions led to a decrease in the water diffusion of treated biocomposites. As a result of the reduction in the biocomposites hygroscopicity, a smaller drop in the biocomposite properties has been observed due to less water absorption. Moreover, PLA/treated RSF biocomposites show better thermal stability than PLA/untreated RSF biocomposites at a constant fiber loading.

In this research, the SEM images of fractured surfaces of PLA/RSF biocomposites revealed large extent of fiber pull-out, whereas the fiber breakage was dominant phenomenon on the SEM micrographs of fractured surfaces of PLA/TRSF biocomposites. This indicates stronger interfacial bonding and emphasizes on the compatibility role of PBA coverage layer of modified fibers. However, using higher percentages of PBA resulted in weak interfaces and lower PLA/TRSF compatibility. The explanation is the poor distribution of grafted PBA chains, as a flexible polymer, in PLA matrix and the formation of a weak interface. At larger amount of PBA, the fiber surfaces are covered with a layer of stacked PBA, which is discernable on the SEM images of fractured surfaces of PLA/TRSF biocomposites. Therefore, the tensile strength of PLA/TRSF composites decreased by increasing PBA content after showing a maximum value, while strain at break followed an upward trend (Fig. 47). Moreover, it was observed that the heterogeneous nucleation effect of RSF

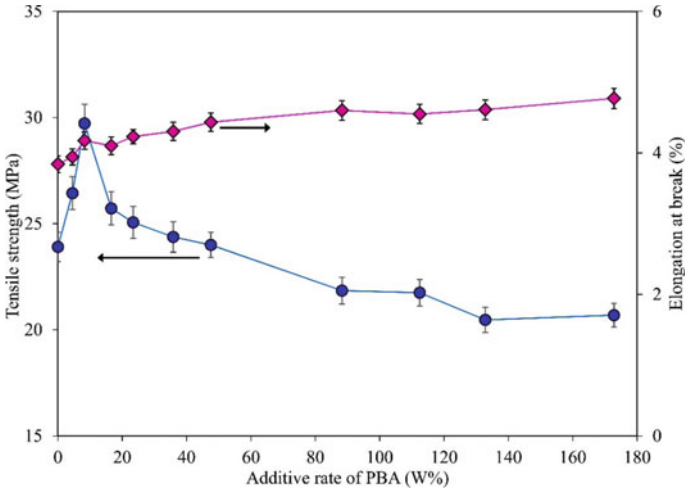

Fig. 47 Relationship between the tensile properties and additive rate of grafted PBA onto the fibers in PLA/RSF biocomposites. Adapted to (Qin et al. 2011b)

surfaces for the PLA chain crystallization has been reduced by PBA grafting. The present PBA chains at fiber surfaces hinder the PLA chains from nucleating on fiber surfaces during the matrix crystallization process. Hence, X_C of PLA in PLA/TRSF biocomposites diminishes and the cold crystallization temperature (T_{CC}) increases to higher values (Qin et al. 2011a, b).

In a similar manner, the graft copolymerization of methyl methacrylate (MMA) monomer was also employed for the treatment of lignocellulosic fibers like RS and agave cellulose fibers in PLA matrix (Zhao et al. 2011; Rosli et al. 2019). It has been reported that poly(methyl methacrylate) (PMMA) has a good miscibility with PLA chains and only one glass transition temperature is observable in the DSC thermograms of PMMA/PLA blends. In one of the related researches (Zhao et al. 2011), MMA admicellar polymerization method was used to create a very thin polymer film on fiber surfaces. The "admicellar" word is derived from "adsorption" and "micelle" and means the monomer polymerization in a surfactant bilayer absorbed on the substrate surface. The surfactant concentration in these conditions must be less than the critical micelle concentration (CMC). Using this innovative method, the researchers first put RSF in cetylpyridinium chloride (CPC) solution to reach the equilibrium absorption of CPC molecules on fiber surfaces. Then, MMA monomer was added to the solution. After reaching the equilibrium adsolubilization of MMA monomer in admiclle, ammonium persulfate initiator was added to the solution and PMMA was polymerized at 70 °C. The fiber treatment with MMA grafting copolymerization was confirmed with FTIR spectroscopy results and microscopic observations.

The microscopic observations demonstrate a large extent of fiber pull-out and interfacial voids for untreated fibers in PLA matrix. On the other hand, with the surface treatment and formation of strong bonds between grafted PMMA and PLA chains, the fiber breakage becomes the dominant phenomenon at fractured surfaces of PLA/RSF biocomposite. Even at higher magnifications, no obvious interface can be perceivable between PMMA-grafted fibers and PLA matrix. As can be seen in Fig. 48, the graft copolymerization treatment of RSF eventuates in an augmentation in the strain at break and tensile strength of PLA/RSF biocomposites. By the chemical treatment, the frictional stress at interfaces increases and correspondingly, the stress transfer efficiency improves. The slight decrease of tensile strength at larger amount of grafted PMMA in Fig. 48 relates to the extra grafted chains at interfaces, which brings about interfacial sliding of PLA and PMMA chains at smaller stresses (Zhao et al. 2011).

The surface treatment of lignocellulosic fibers with graft copolymerization of ε-caprolactone via ROP polymerization was also applied for the improvement of properties of PLA/wheat straw fiber (WSF) biocomposites (Kellersztein et al. 2016). In this copolymerization method, the fibers were first treated with NaOH and then, benzyl alcohol as an initiator, ε-caprolactone monomer and tin octoate ($SnOct_2$) as a catalyst were added to the solution. The ring-opening polymerization was carried out at 95 °C for 22 h. The proposed reaction mechanism of the PCL graft copolymerization on the surface of wheat straw fibers is shown in Fig. 49. The occurrence

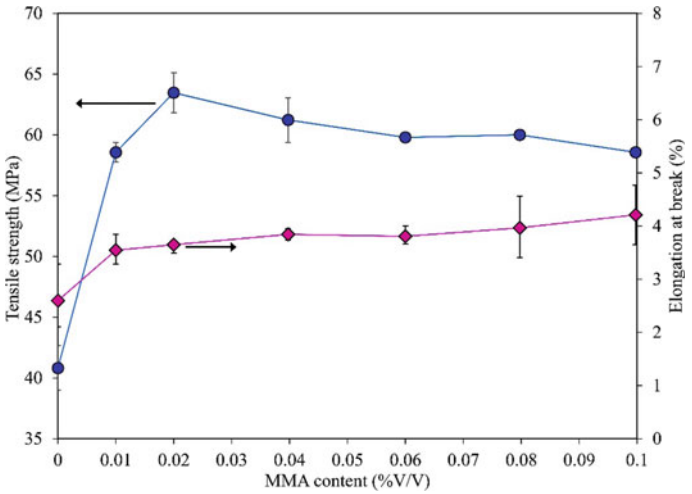

Fig. 48 Relationship between the tensile properties of PLA/RSF biocomposites and MMA content in the graft copolymerization reaction of fibers at a constant filler loading of 30% (v/v). Adapted to (Zhao et al. 2011)

of grafting reaction onto WSF was proven by proton nuclear magnetic resonance (^{1}HNMR) and attenuated total reflectance infrared spectroscopies (ATR).

The addition of PCL-grafted WSF to matrix led to a decrease in the PLA crystallinity degree. It was believed that PCL-grafted chains hindered the crystallization process of PLA owing to the PCL/PLA interactions and entanglements. Additionally, the rheological measurements showed that the complex viscosity of PLA/WSF biocomposites was significantly increased by the graft copolymerization treatment of fibers. In fact, larger frictional forces between PCL-grafted fibers and matrix chains lead to an increase in viscosity. The chemical treatment also resulted in an improvement in tensile and flexural strength as well as strain at break of PLA/WSF biocomposites (Fig. 50). However, it must be noted that the incorporation of PCL-treated fibers into PLA matrix caused a slight decrease in tensile and flexural modulus compared to untreated fibers. It can be attributed to the augmentation of the amorphous part fraction of biocomposites, especially near PCL/PLA interfaces (Kellersztein et al. 2016).

5.7 Acid Hydrolysis Treatment

One of the chemical treatment processes of lignocellulosic fibers is acid hydrolysis modification that is frequently applied after alkaline pretreatment. The acid hydrolysis treatment involves in degradation reactions, through which the average degree of polymerization of lignocellulosic polymers diminishes. Throughout the hydrolysis

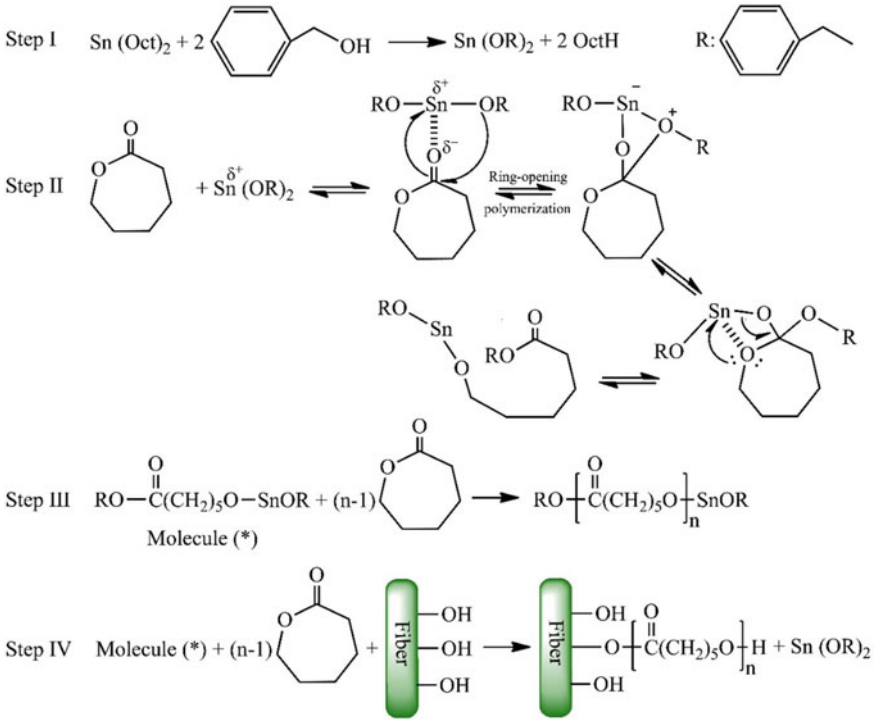

Fig. 49 Proposed reactions of ring-opening polymerization of ε-caprolactone with the surface of wheat straw fiber using benzyl alcohol as an initiator and tin octoate (SnOct2) as a catalyst. Adapted to (Kellersztein et al. 2016)

reaction of plant fibers in an acidic medium, the β-1,4-glucosidic bonds, which are present in the backbones of natural polymers such as cellulose and hemicellulose, or other etheric groups are split up by adding water molecules. By the reaction, shorter fragments from polymeric chains are formed, whereas the polymer basic structures are preserved (Fan et al. 1987). The reaction scheme of the acid hydrolysis reaction of cellulose is shown in Fig. 51. As mentioned, the acidic treatment of lignocellulosic materials can lead to the hydrolysis of lignin, pectin and hemicellulose molecules, thereby removing the amorphous components of plant substance from the cellulosic fibers. The direct result of that is a considerable reduction in the natural fiber diameter and an improvement in the fiber/matrix interfacial adhesion (Araújo et al. 2018).

The acid hydrolysis treatment procedure was employed by Araújo et al. to improve the properties of PLA-based biocomposites containing eucalyptus and mallow fibers (Araújo et al. 2018). The hydrolysis reaction of mallow fibers was carried out after alkali pretreatment while the eucalyptus fibers were exposed to both alkali and bleaching pretreatments before the hydrolysis modification. The hydrolysis reaction was performed using sulfuric acid solutions at various concentrations for different treatment times.

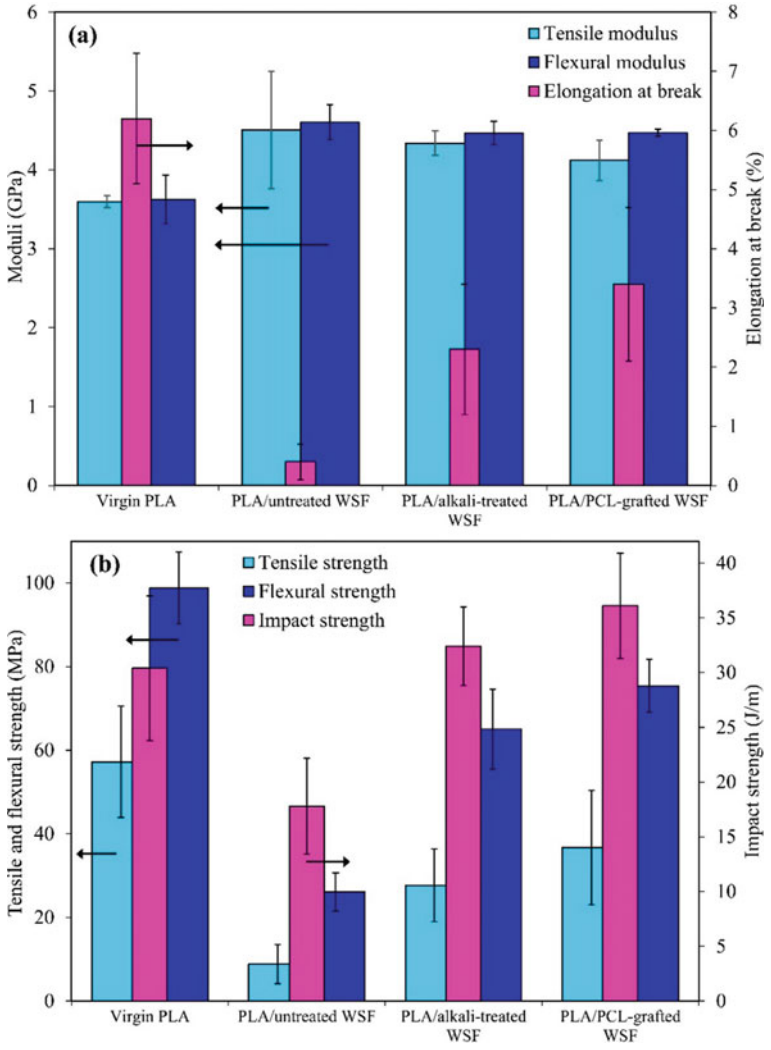

Fig. 50 Mechanical characteristics of virgin PLA and the biocomposites of PLA/untreated WSF, PLA/alkali-treated WSF and PLA/PCL-grafted WSF. Adapted to (Kellersztein et al. 2016)

As can be observed in Fig. 52, the bleached and mercerized eucalyptus fibers have smooth surfaces demonstrating the elimination of lignin and other impurities from the fibers through the pretreatment processes. The treated eucalyptus fibers (FE6 sample), hydrolyzed by using H_2SO_4 solution at a concentration of 10% (v/v) at 80 °C for 240 min, preserved the primary fiber diameter. Despite that, the fiber length was reduced by the hydrolysis treatment. It seems that the hydrolysis reaction weakens the fibers and increases the surface roughness (Fig. 52c–e). The hydrolyzed eucalyptus fibers (FE7 sample) shown in Fig. 52f–h were treated by using sulfuric

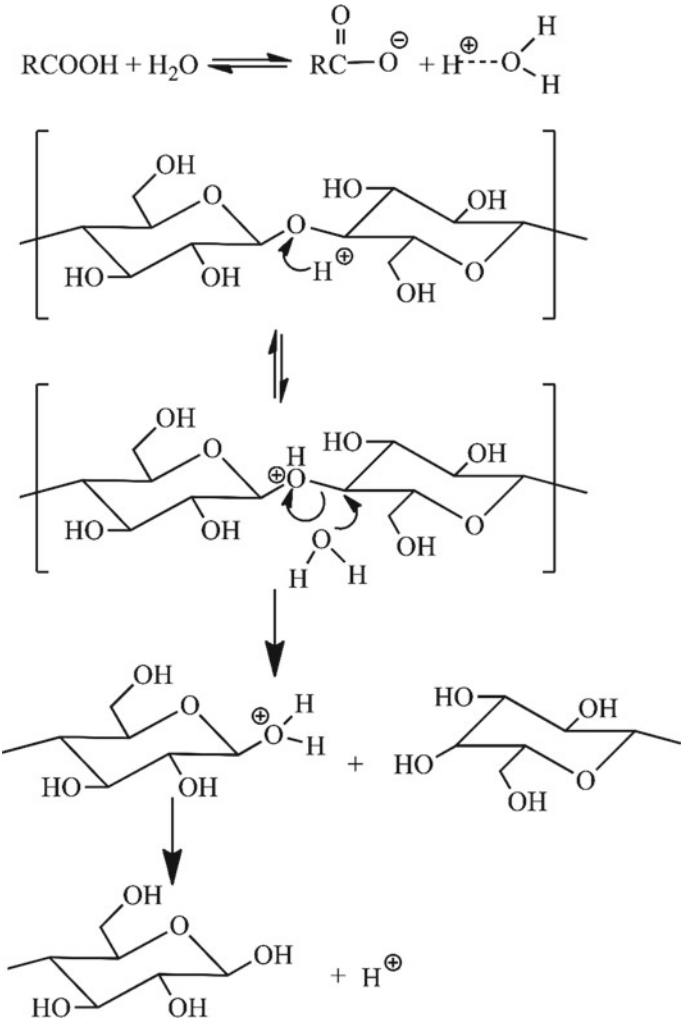

Fig. 51 Mechanism of the acid hydrolysis reaction of cellulose. Adapted to (Lelekakis et al. 2014)

acid solution at a concentration of 50% (v/v) at 60 ∘C for 240 min. As can be seen, the microfibrils were formed at the fiber ends by the chemical treatment. For the modified eucalyptus fibers (FE9 sample) with the SEM images of Fig. 52i–k, the treatment agent of H_2SO_4 solution at a concentration of 30% (v/v) at 60 ∘C for 150 min was applied. These reaction conditions caused a drastic decrease in the primary fiber length and gave the FE9 fibers a rough and brittle appearance. Nonetheless, these hydrolyzed eucalyptus fibers did not show any noticeable changes in the diameter by the treatment (Araújo et al. 2018).

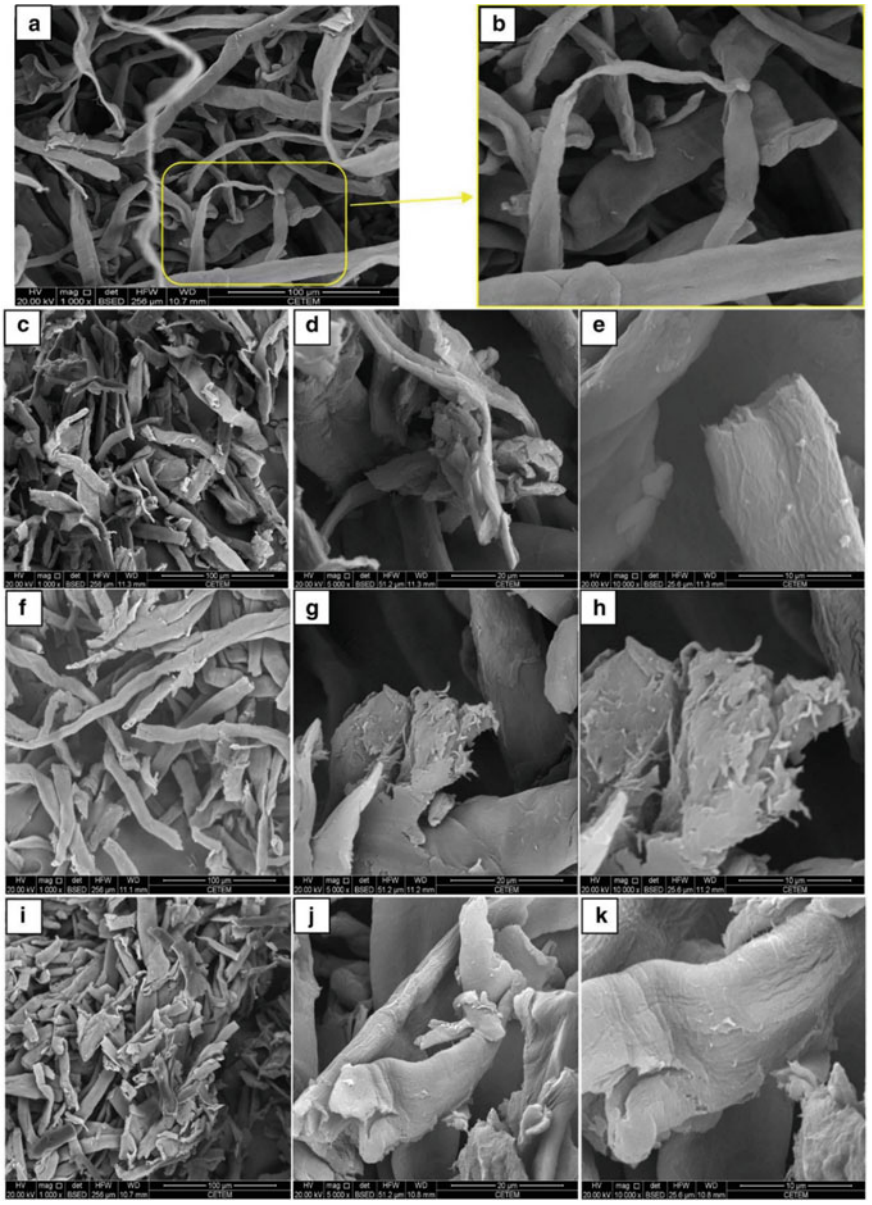

Fig. 52 SEM images of: **a**, **b** untreated eucalyptus fibers, **c**–**e** FE6 fibers, **f**–**h** FE7 fibers and **i**–**k** FE9 fibers. Reproduced with permission from (Araújo et al. 2018)

The XRD analysis confirms that the fiber crystallinity degree diminishes after acidic modification. By acid hydrolysis reaction of eucalyptus fibers, the interface of PLA matrix and reinforcing fibers becomes stronger and the efficiency of the interfacial stress transfer is heightened. The microscopic observations on the fractured surfaces of PLA/eucalyptus fiber biocomposites (Fig. 53) demonstrate that the tendency to fiber pull-out is reduced and less gaps can be discerned at matrix/filler

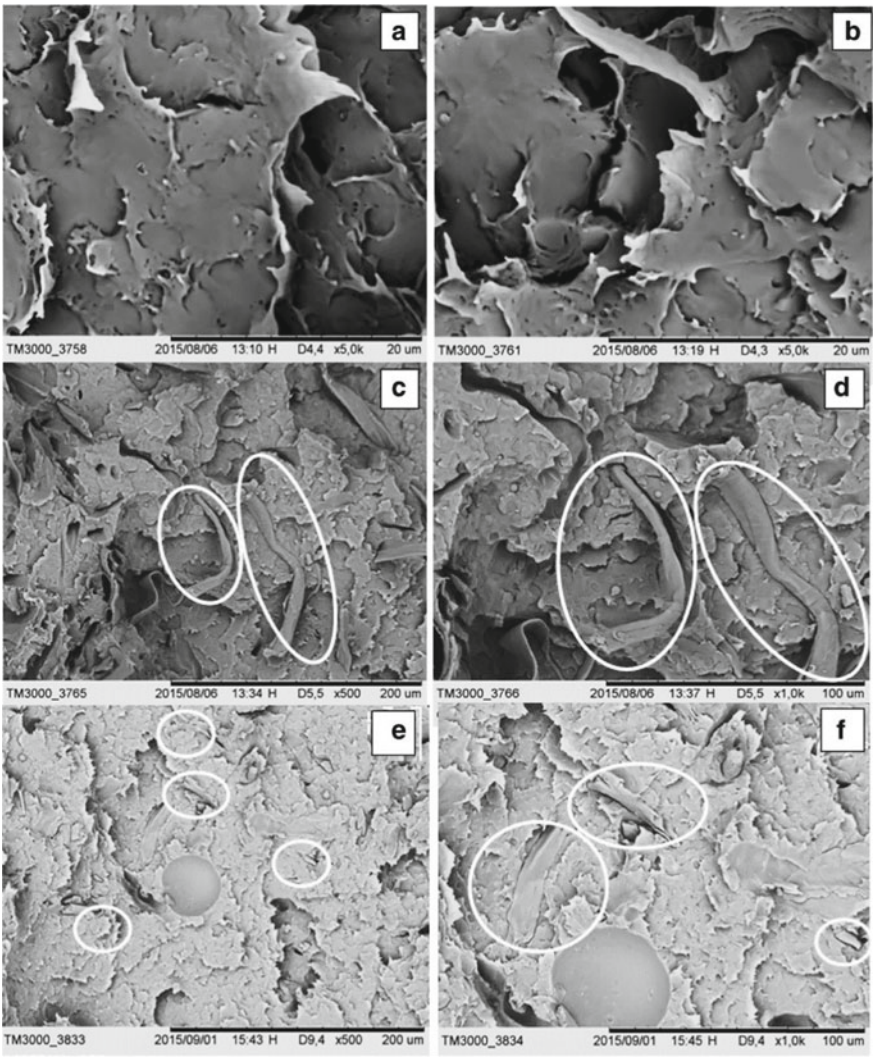

Fig. 53 SEM images of the fractured surface of PLA and PLA/eucalyptus fiber composites: **a**, **b** control sample, virgin PLA, **c**, **d** PLA/untreated fiber composite, **e**, **f** PLA/treated FE9 fiber composite. Reproduced with permission from (Araújo et al. 2018)

interface by the acidic treatment. Furthermore, by improving the interfacial adhesion of PLA/acidic treated eucalyptus fiber phases, the storage modulus at ambient temperature, T_g, PLA crystallinity degree, degradation onset temperature and temperature with maximum thermal degradation rate were raised to higher values comparing with untreated fiber-reinforced PLA composites at the same loading of natural filler (Araújo et al. 2018).

In a similar work, the acid treatment method was used to reinforce the PLA matrix with randomly oriented short *Spartium junceum L.* fibers (Kovačević et al. 2019). For the preparation of fibers, in this work, first the fibers were treated by alkali solution, then were exposed to microwave radiation for 5 min to extract the fibers from plant stems. Different chemical modifications were applied including mercerization, alkali and nanoclay treatments as well as acidic and nanoclay treatment. The PLA-based biocomposites were prepared by the hand lay-up of fibers in mold and then, compression molding. The findings revealed that the alkali treatment decreased the fiber tenacity, whereas the other treatment methods, associated with nanoclay presence, resulted in enhanced fiber strength and tenacity. A comparison between these two methods, which involved in the use of nanoclay, clarifies the coarser surface of the acidic treated fibers (Fig. 54). Citric acid as the treatment agent in acidic modification process had stronger beneficial effects on treating the fiber surface and linking the montrmorillonite nanoparticles with fiber surfaces (Kovačević et al. 2019).

The SEM images of the fractured surfaces of biocomposites shown in Fig. 54 demonstrate the differences in the interfacial strength of PLA matrix and the modified fibers. By alkali treatment, the extent of fiber/matrix debonding and fiber pull-out was reduced comparing with untreated fiber-reinforced PLA composite. In marked contrast, the biocomposite containing the treated fibers with NaOH and nanoclay showed a brittle mechanical behavior and debonding at the interface occurred to large extent. Comparatively, the PLA biocomposite, containing the lignocellulosic fibers modified by citric acid and nanoclay treatment agents, had smoother fractured surface and the fiber pull-out took place to lower extent. By improving the matrix/fiber interfacial strength and void reduction in the PLA-based composite containing treated fibers with citric acid and nanoclay, the highest mechanical properties such as elastic modulus, tensile strength, elongation at break and dissipated energy were attained. The column graph in Fig. 55 confirms the advantages of acidic and nanoclay treatment method in providing the biocomposite with better mechanical performance (Kovačević et al. 2019).

According to the literature, the acid hydrolysis treatment has positive effect on the reinforcing role of plant fibers in PLA matrix. However, the improvements in final properties are controlled by the acid and fiber types, pretreatment reaction conditions, concentration of acidic solution and hydrolysis reaction time.

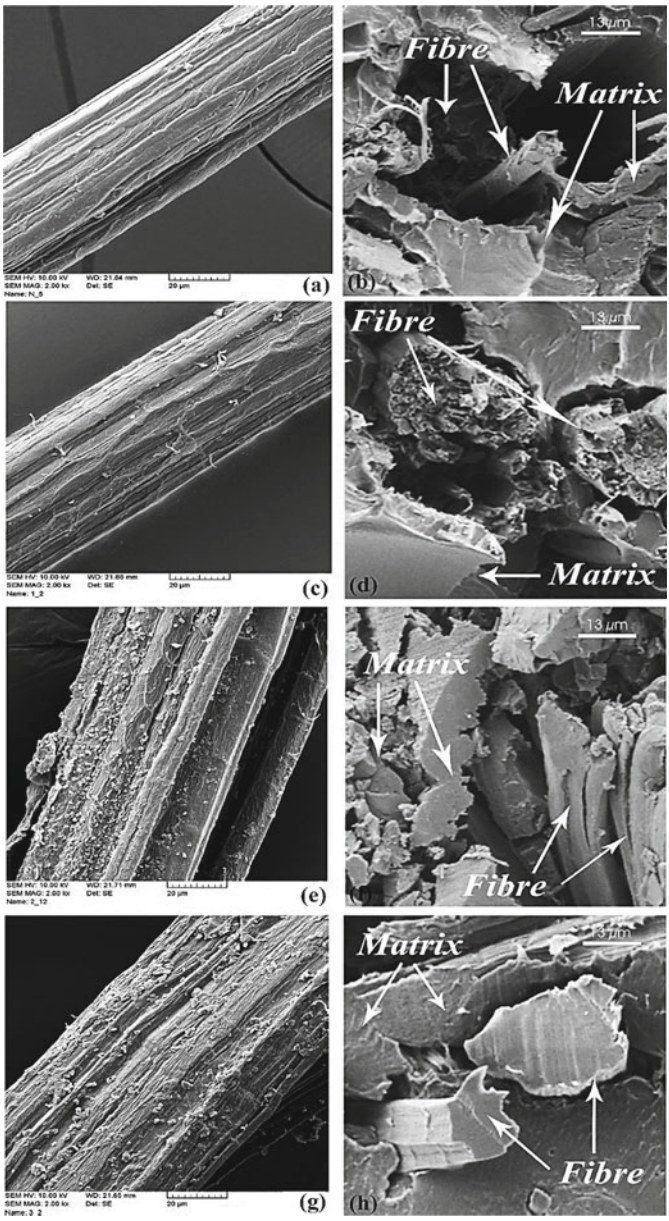

Fig. 54 SEM images of the lignocellulosic fibers (left column) and the fractured surface of PLA/fiber biocomposites (right column): **a** untreated fiber, **b** PLA/untreated fiber, **c** treated fibers with NaOH, **d** PLA/treated fiber with NaOH, **e** treated fibers with NaOH and nanoclay, **f** PLA/treated fiber with NaOH and nanoclay, **g** treated fibers with citric acid and nanoclay, and **h** PLA/treated fiber with citric acid and nanoclay. (Kovačević et al. 2019) Open access

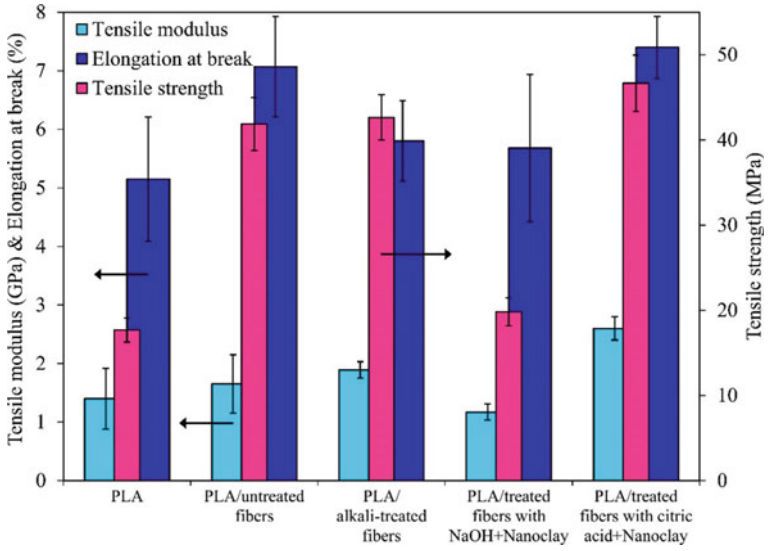

Fig. 55 Mechanical characteristics of PLA and PLA/Spartium junceum L. fiber composites. Adapted to (Kovačević et al. 2019)

5.8 Isocyanate Treatment

The isocyanate treatment of lignocellulosic fibers is carried out by using isocyanates or diisocyanates. Isocyanate treatment agents have –N=C=O functional groups, which are highly reactive against hydroxyl and carboxyl groups. Reportedly, isocyanates can play the common role of coupling agents in plant fiber-reinforced biocomposites (Siakeng et al. 2019a; Orue et al. 2018; Abu Ghalia and Dahman 2017). Isocyanate functional groups can react with the hydroxyl groups of cellulose, hemicellulose and lignin macromolecules and form urethane linkages. In Fig. 56, the reaction mechanism of urethane bond formation is shown. By the reaction, the fiber hydrophobicity and fiber resistance against moisture is enhanced. Besides, the interfacial strength between matrix and natural reinforcement agent is improved (Orue et al. 2018; Kozlowski and Wladyka-Przybylak 2004). The R atomic group in Fig. 56 can consist of different chemical groups like alkyls. The chemical bond formation between the isocyanate treatment agent and PLA chains will become possible, if the R group contains another reactive functional group. Under the circumstances, isocyanate molecules as a coupling agent can form chemical crosslinks between the matrix and lignocellulosic fiber phases (Luo et al. 2014). Despite that, the diisocyanate molecules having two –N=C=O functional groups can simultaneously react with the hydroxyl groups of plant fiber and hydroxyl or carboxyl end groups of PLA chains during the melt-compounding process of PLA/fiber biocomposites, without the need of a reactive functional group in R position. Therefore, the diisocyanate molecules can chemically crosslink the natural reinforcement agent with matrix

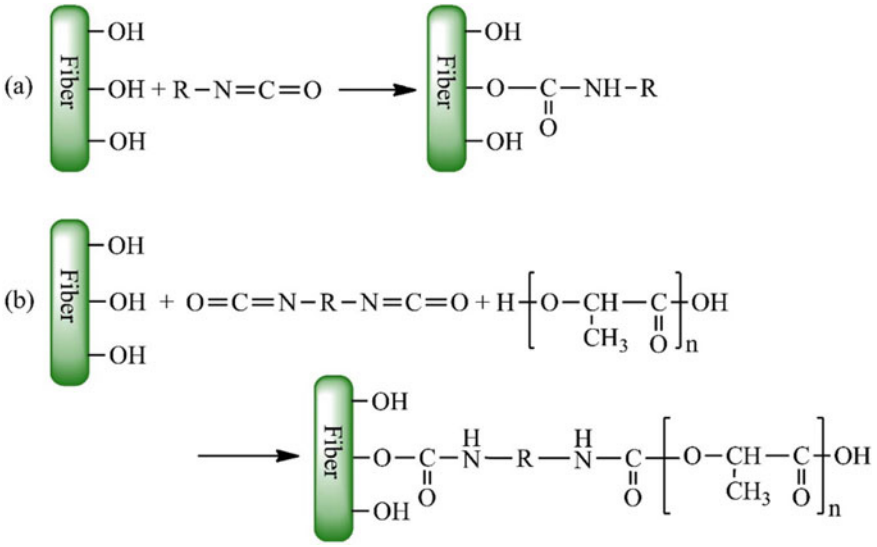

Fig. 56 Reaction scheme of: **a** isocyanate molecule with lignocellulosic fiber, **b** diisocyanate molecule with lignocellulosic fiber and PLA chain

through the formation of urethane linkages (Fig. 56b) (Lee and Wang 2006; Yu et al. 2015).

One of the isocyanate treatment agents, which was applied in a study for the chemical treatment of dry refined soft wood fibers in PLA matrix, has been octadecyl isocyanate (Krouit et al. 2010). By the substitution reaction of isocyanate groups associated with long alkyl groups for the fiber hydroxyl groups, the water contact angle increases from 39° for the pristine fibers to 104° for the isocyanate-treated fibers. Even though the treated lignocellulosic fibers become substantially more hydrophobic, slight changes in the glass transition temperature and mechanical properties of treated PLA/wood fiber composites were observed owing to the lack of chemical bonds between the reinforcing filler and PLA matrix (Krouit et al. 2010).

In a similar work, isocyanate modified epoxy emulsion as a sizing material was employed to improve the properties of the PLA-based biocomposites containing alkali-treated corn fiber (ACF) (Luo et al. 2014). The used sizing material had lots of reactive groups such as epoxy and amino groups. These functional groups can concurrently undergo chemical reactions with the hydroxyl groups of fiber surfaces as well as the hydroxyl and carboxyl groups of PLA chains. Therefore, the sizing material can play the role of a coupling agent and enhance the fiber/matrix interfacial adhesion through the formation of intermolecular linkages between the reinforcing filler and polymeric matrix. In this work, it was found in the SEM micrographs of the fractured surfaces of tensile test samples that large cracks were present at the interfaces of PLA matrix and untreated corn fibers. The alkali treatment of the plant fibers eliminated interfacial voids and cracks, though the interfacial interactions

between PLA matrix and ACF filler were not strong enough to totally suppress the fiber pull-out under stress transfer conditions. By sizing the alkali-treated fibers, not only no interfacial voids and cracks between the fiber and matrix were discernable, but also some stacked PLA residuals were observable on the fiber surfaces, indicating strong interactions between sized-ACF and PLA phases (Luo et al. 2014).

The grafting function of isocyanate treatment agent, used in this work, resulted in considerable enhancements in the properties of PLA/untreated corn fiber (UCF) and PLA/ACF biocomposites (Luo et al. 2014). As can be seen in Fig. 57, the characteristics of corn fiber-reinforced PLA biocomposites including tensile modulus and strength, flexural modulus and strength, HDT, T_g, T_c and crystallinity degree were considerably improved by treating the fibers with the isocyanate sizing material. The used sizing chemical as an effective coupling agent markedly enhanced the corn fiber/PLA interfacial strength and diminished the molecular dynamics of PLA chains. However, the chemical crosslinking of PLA chains with natural fibers led to a reduction in impact strength and elongation at break of the biocomposites.

In comparison to the isocyanate treatment agent with epoxy functional group in R atomic group (Fig. 56), the diisocyanate coupling agent has been reported to be more effectual to modify the PLA/lignocellulosic fiber interfaces and improve the properties of resultant biocomposites (Yu et al. 2015; Lee and Wang 2006). The grafting reaction of diisocyanate chemicals between PLA chains and plant fibers normally take place in melt-mixing processes in the presence of a catalyst.

Some of the used diisocyanate treatment agents in PLA-based biocomposites have been isophorone diisocyanate (IPDI), 4,4′-diphenylmethane diisocyanate (MDI), 1,6-hexane diisocyanate (HDI) and lysine-based diisocyanate (LDI). These chemicals as reactive compatibilizers, having two isocyanate groups, can simultaneously react with both plant fibers and PLA chains and form chemical crosslinks. The findings of related researches have clarified that the use of these reactive compatibilizers substantially improve different properties of PLA/ramie fiber composites including tensile strength and modulus, flexural strength, strain at break, impact strength, T_g, T_c, storage modulus, *Tan* δ peak position, thermal degradation temperature and flow activation energy (Yu et al. 2015; Lee and Wang 2006). Moreover, the effectiveness of diisocyanate coupling agent was reported to be dependent on the diisocyanate chemical structure and content. It can be seen in Fig. 58a and b that IPDI crosslinking agent is the most effective additive to improve the mechanical performance of PLA/ramie biocomposites, among different diisocyanate coupling agents used in this study including MDI, HDI and IPDI (Yu et al. 2015). In addition, the biocomposite properties against the coupling agent content show optimum values, which is evident in Fig. 58c and d. The incorporation of the diisocyanate compatibilizers into PLA/plant fiber composites can bring about considerable improvements in the properties just up to a fixed diisocyanate content and then, the properties level-off. At larger contents of the crosslinking agent, above a critical value, the diisocyanate molecules tend to aggregate and form a thick film on fiber surfaces. The thick film of coupling agent hinders the formation of uniform chemical crosslinks and effective fiber/matrix interactions (Yu et al. 2015; Lee and Wang 2006).

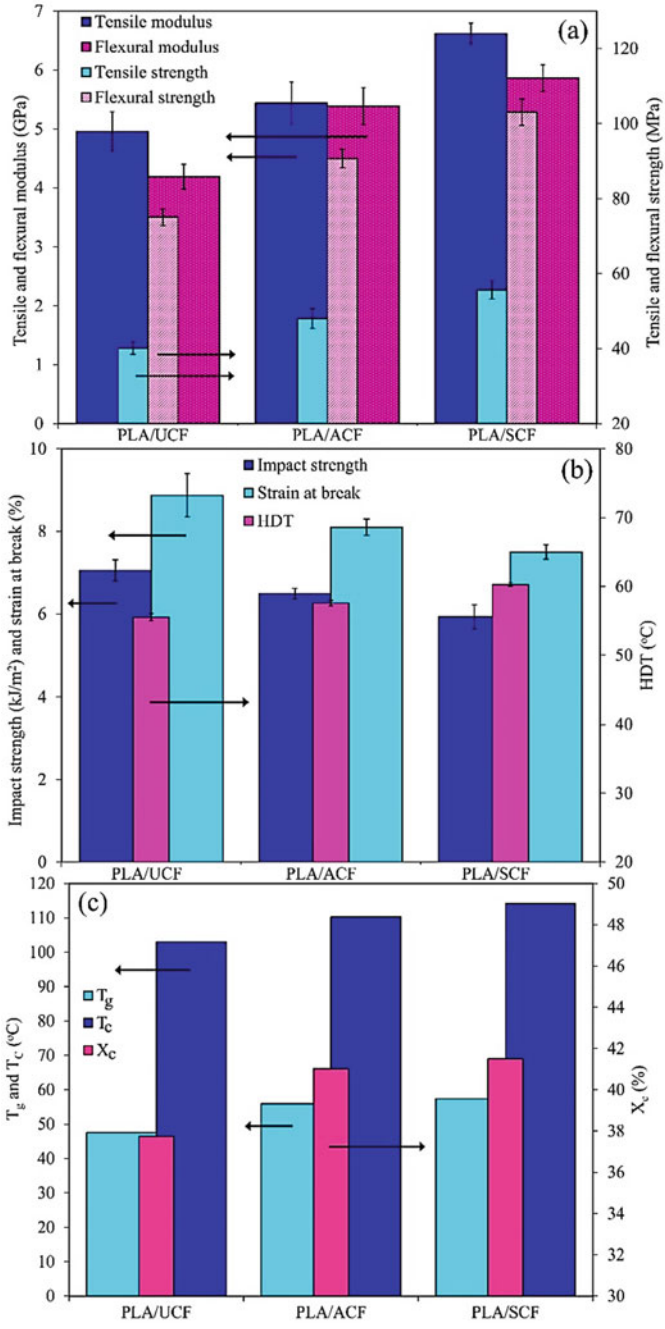

Fig. 57 Different mechanical, thermal and thermo-mechanical characteristics of PLA/untreated corn fiber (UCF), PLA/alkali-treated corn fiber (ACF) and PLA/sizing-treated corn fiber (SCF) composites. Adapted to (Luo et al. 2014)

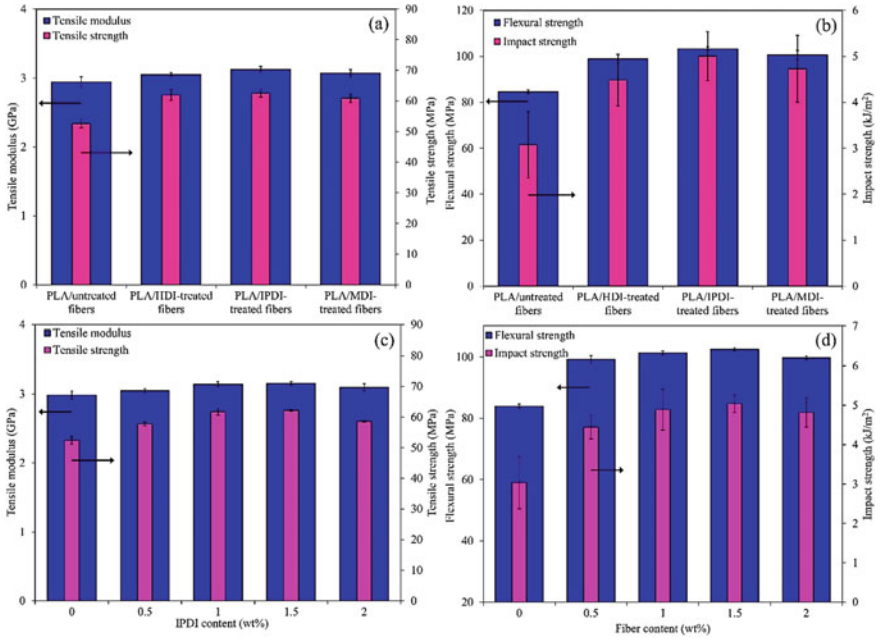

Fig. 58 **a** and **b** Mechanical properties of PLA/ramie fiber biocomposites without/with different diisocyanate treatment agents, **c** and **d** Mechanical properties of PLA/ramie fiber biocomposites without/with IPDI coupling agent at different contents. Adapted to (Yu et al. 2015)

5.9 Peroxide Treatment

Peroxides are chemical compounds with a general structure of R–O–O—R and a characteristic divalent O–O bond. At high temperatures, extremely reactive peroxide molecules decompose and form free radicals (Siakeng et al. 2019a; Kozlowski and Wladyka-Przybylak 2004). The free radical moieties can react with the natural polymers of lignocellulosic fibers like cellulose as well as polymer matrix chains and correspondingly, create some reactive sites on the macromolecules. As a result, the grafting reaction of matrix chains onto fiber surfaces at interfaces becomes possible by the mentioned free radical transfer reactions (Kozlowski and Wladyka-Przybylak 2004; Orue et al. 2018). The proposed scheme of the reactions induced by peroxide treatment agents in PLA/natural fiber biocomposites is shown in Fig. 59. The frequently used organic peroxides in lignocellulosic fiber-reinforced composites are benzoyl peroxide, $(C_6H_5CO)_2O_2$, and dicumyl peroxide, $(C_6H_5C(CH_3)_2O)_2$. The peroxide treatment of plant fibers is normally carried out after alkali pretreatment (A. Orue et al. 2018).

The grafting reactions of PLA chains onto fiber surfaces lead to an increment in the hydrophobicity of lignocellulosic fibers and matrix/fiber interfacial strength (Siakeng et al. 2019a). The peroxide chemical treatment associated with an alkali pretreatment

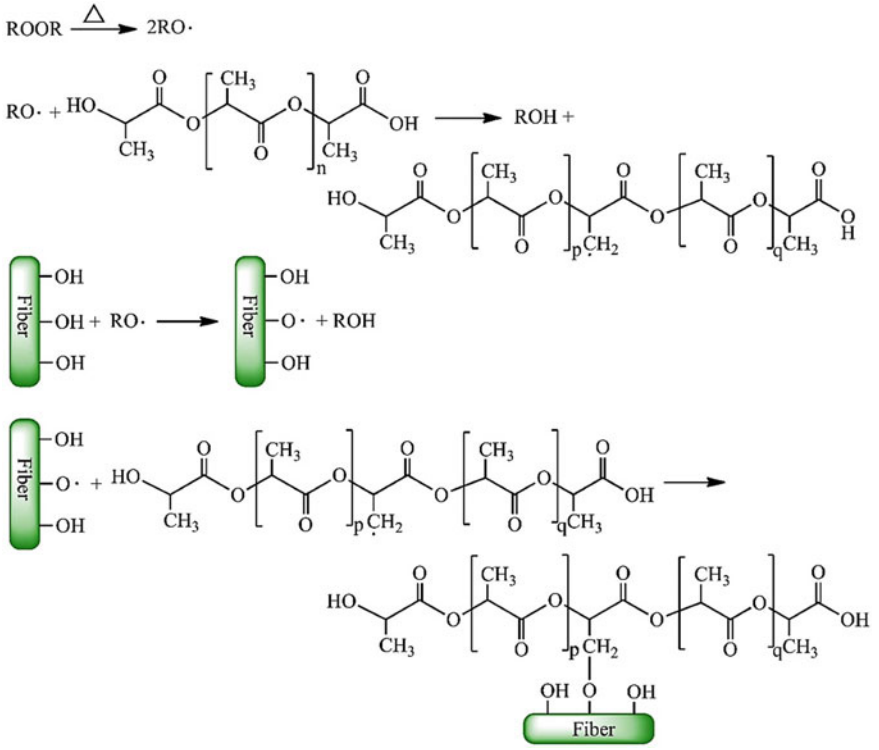

Fig. 59 Proposed reactions induced by the peroxide treatment agent in lignocellulosic fiber-reinforced PLA composites

process was used to improve the interfacial adhesion of the PLA/ramie fiber composites (Choi and Lee 2012). In comparison with unreinforced PLA, PLA/untreated fiber, PLA/alkali-treated fiber and PLA/alkali & silane-treated fiber samples, the PLA-based biocomposites, containing the ramie fibers treated with NaOH and peroxide chemicals, had the lowest thermal expansion in this work. The thermal expansion of biocomposites is closely related to interfacial properties. The presence of cracks, voids and striations at fiber/matrix interfaces brings about a large thermal expansion. The lowest thermal expansion of PLA/peroxide-treated fibers composite is provoked by the grafting reactions of free radical moieties, which result in the PLA chain grafting onto fiber surfaces and conclusively, better interfacial performance. Better matrix/fiber interactions through the formation of covalent linkages caused the largest impact strength for prepared PLA/ramie fiber composites having the plant fibers modified by dicumyl peroxide and NaOH compounds. Despite that, the measurements of the mechanical properties of a single fiber revealed that the peroxide treatment reactions have had a slight impact on the fiber strength and modulus itself (Choi and Lee 2012).

Furthermore, the tensile strength and modulus of the biocomposites containing peroxide-treated fibers were determined to be lower than the ones for PLA/untreated fiber and PLA/alkali-treated fiber composites, at the same filler loadings (Fig. 60). The plausible reasons were believed to be the poor dispersion state of treated fibers and remaining intact fiber bundles in PLA matrix. Although the peroxide chemical

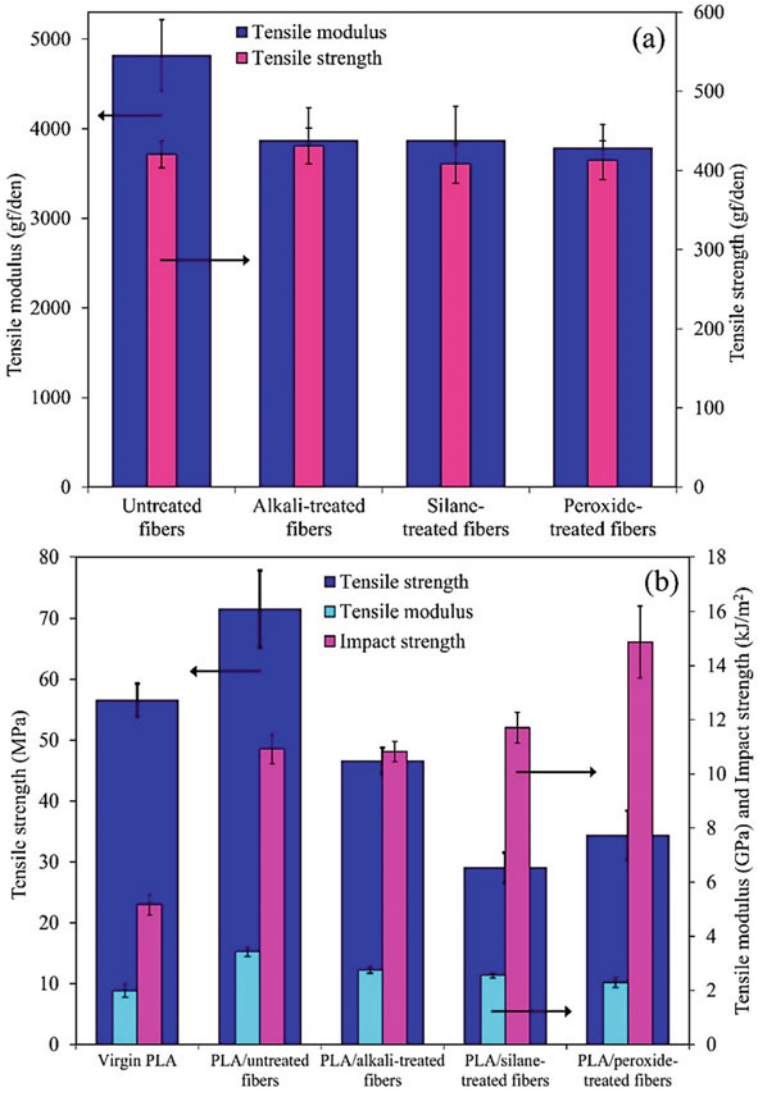

Fig. 60 **a** Tensile strength and modulus of treated and untreated single ramie fiber, **b** tensile properties and notched Izod impact strength of PLA and PLA/ramie fiber composites containing untreated and treated fibers. Adapted to (Choi and Lee 2012)

treatment is noticeably effective in improving the fiber/matrix interfacial adhesion, the final performance of plant fiber-reinforced composites is also controlled by the composite preparation processes. In the reviewed research, the preparation processes consisted of physical mixing of PLA fibers with ramie fibers and then, compression molding (Choi and Lee 2012).

In contrast to this work, in another research, benzoyl peroxide was applied to modify the combined banana/sisal fibers and the PLA-based biocomposites were prepared through twin-screw extruder and injection molding processes (Asaithambi et al. 2014). Over the melt-compounding process, the organic peroxide created highly reactive free radicals, which successfully induced the PLA chain grafting reaction onto the mercerized fiber surfaces. By applying the efficient melt-compounding process and proper function of peroxide treatment agent, the interfacial interactions, wettability and compatibility of PLA chains with the alkali-treated fibers were significantly increased. In these circumstances, the dominant phenomena on the fractured surfaces of PLA/peroxide-treated fibers composites were observed to be fiber fracture and matrix deformation. Nevertheless, fiber aggregates, fiber pull-out and interfacial cavities were greatly evident on the fractured surface of prepared PLA/untreated fibers biocomposites. As can be found in Fig. 61, peroxide chemical treatment prompts considerable improvements in the mechanical characteristics of PLA/sisal and banana fiber composites such as tensile strength and modulus, flexural strength and modulus and impact strength. By inducing strong PLA/fiber interactions through the formation of covalent linkages, the load transfers from matrix to reinforcing fibers with higher efficiencies (Asaithambi et al. 2014).

According to the results, it can be concluded that the properties of the PLA-based biocomposites containing peroxide-treated lignocellulosic fibers are controlled by the reaction conditions of alkali pretreatment and peroxide treatment processes such as peroxide solution concentration and reaction time and temperature along with the melt-mixing and shaping process conditions.

5.10 Permanganate Treatment

Permanganate treatment of natural fibers is generally performed by using potassium permanganate solutions in acetone. Through this chemical treatment, the extremely reactive permanganate ions react with the hydroxyl groups of lignocellulosic fibers (Siakeng et al. 2019a). According to the reaction mechanism shown in Fig. 62, MnO_4^- ions induce grafting copolymerization between PLA chains and plant fibers by forming reactive sites on fiber surfaces. By the permanganate treatment, the hydroxyl groups of fibers are oxidized to carbonyl and carboxyl functional groups and the heteroatom dissociation of carbon-carbon and carbon-oxygen bonds occurs. The created active sites on fibers can provoke the grafting chemical reactions with PLA chains (Zou et al. 2012). Therefore, the resultant chemical interlocking at fiber/matrix interfaces is significantly enhanced the interfacial strength (Orue et al.

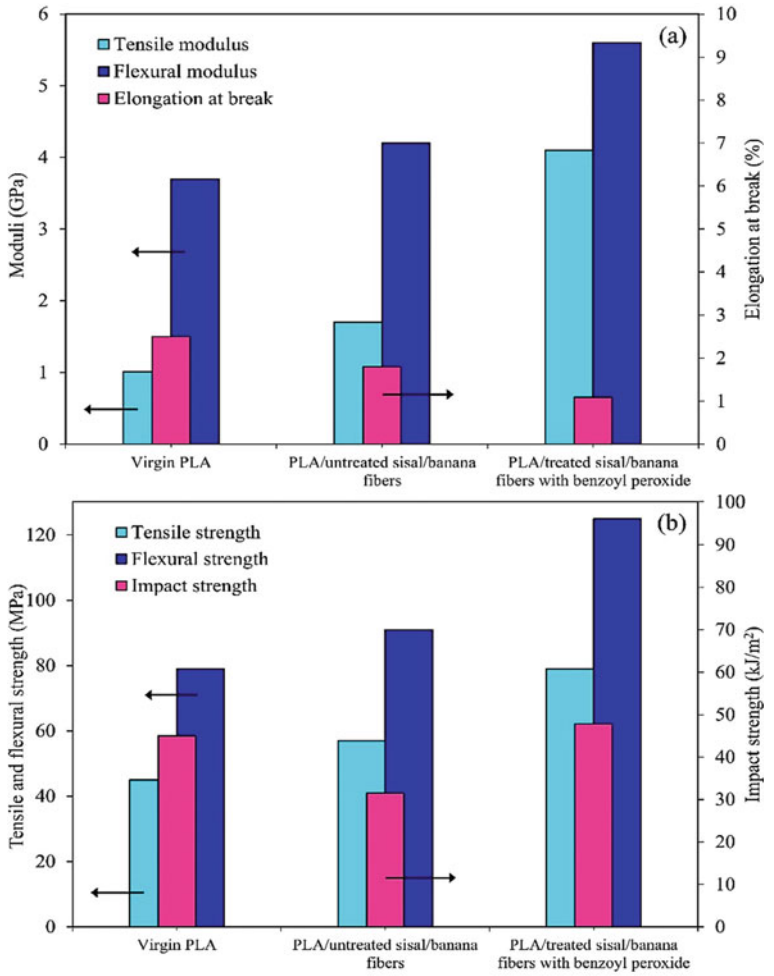

Fig. 61 Mechanical characteristics of virgin PLA, PLA/untreated sisal/banana fibers composites and PLA/peroxide-treated sisal/banana fibers composites. Adapted to (Asaithambi et al. 2014)

2018; Kozlowski and Wladyka-Przybylak 2004). Additionally, the active permanganate ions can also react with the hydroxyl groups of non-cellulosic components of lignocellulosic fibers like lignin and hemicellulose. The occurrence of reactions with non-cellulosic impurities makes the fiber surfaces rougher and fiber/matrix interfaces stronger by providing mechanical interlocking (Zou et al. 2012). In addition to the created mechanical and chemical interlocking, the fiber hydrophilicity is reduced by the graft copolymerization and oxidation reactions induced by permanganate treatment agent (Siakeng et al. 2019a).

The influences of permanganate treatment process on lignocellulosic fibers were investigated on banana fibers (Paul et al. 2010). In this study, banana fibers were

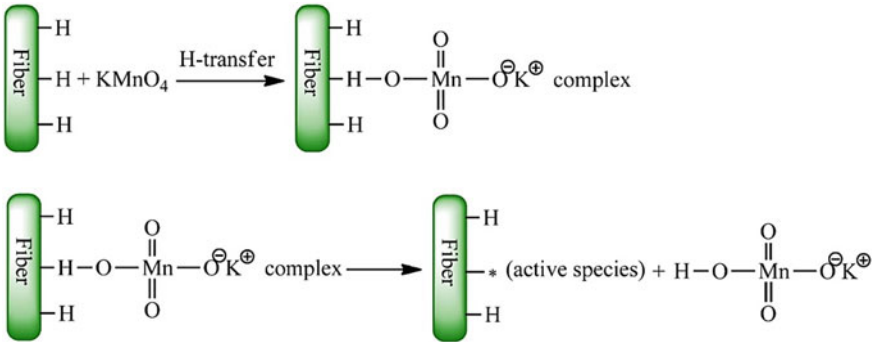

Fig. 62 Probable reactions mechanism involved in the permanganate chemical treatment of lignocellulosic fibers

soaked in 0.5% permanganate solution in acetone for 90 min after alkali pretreatment. The microscopic observations of treated fibers demonstrate an increment in fiber roughness, which can potentially result in stronger matrix/filler interfaces through mechanical interlocking. Moreover, the authors reported that permanganate treatment decreased the acidity and polarity of fibers and adversely, increased the wettability of treated fiber with polymeric matrices (Paul et al. 2010). However, the efficiency of permanganate treatment method to improve the performance of PLA/natural fiber biocomposites is dependent on the treatment solution concentration, fiber soaking time and alkali pretreatment (Orue et al. 2018).

The impacts of permanganate treatment variables on the moisture content as well as structural and mechanical properties of abaca fibers have been also studied (Batara et al. 2019). In this research, it was found that abaca fibers, treated with potassium permanganate solution at concentration of 0.125% for soaking time of 3 min without exposing to mercerization pretreatment, had the highest tensile strength and lowest moisture content. Besides, permanganate modification aroused in rougher and more hydrophobic fibers capable of providing stronger mechanical interlocking. However, an increment in the fiber soaking time, up to 20 min, and the concentration of potassium permanganate solution, up to 0.5%, as well as the fiber exposure to alkali pretreatment were found to damage the fibers and reduce the fiber strength. In severe reaction conditions, the fibrils are separated from each other, fiber bundles are opened and strength of hydrogen bonds inside lignocellulosic fiber diminish. Consequently, the fiber strength worsens. Since the properties of plant fiber-reinforced composites are greatly affected by the performance of reinforcing fibers, a reduction in the fiber strength itself can adversely impact the reinforcement role of fibers in matrix phase (Batara et al. 2019).

The influences of permanganate chemical modification of natural fibers in PLA matrix were evaluated in a study by using short sisal fibers (SSF) and 0.1% $KMnO_4$ solution in acetone (Zou et al. 2012). As can be observed in Fig. 63, permanganate treatment has made the surfaces of sisal fiber (SF) rougher, which can lead to the matrix/dispersed phase mechanical interlocking in PLA/SF biocomposites. In

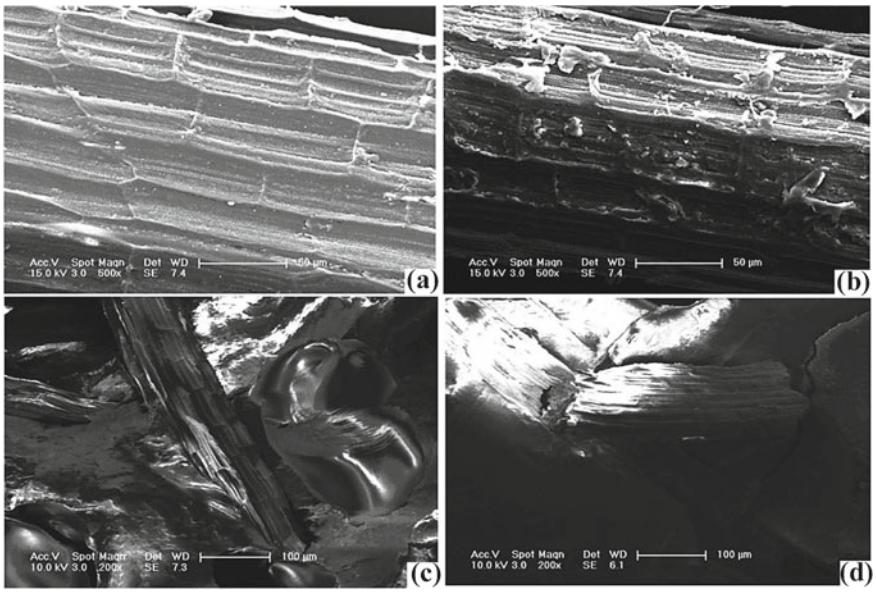

Fig. 63 SEM image of: **a** untreated short sisal fiber, **b** short sisal fiber treated with permanganate solution, **c** fractured surface of PLA/untreated sisal fiber sample and **d** fractured surface of PLA/permanganate-treated sisal fiber sample. Reproduced with permission from (Zou et al. 2012)

fact, the stronger interfacial adhesion of permanganate-treated fibers in PLA matrix induces lower extents of fiber pull-out and interfacial void formation on the fractured surfaces, which is obvious in the SEM images of Fig. 63.

Furthermore, it can be discerned in the SEM image that permanganate-treated fibers are tightly connected to PLA matrix (Zou et al. 2012). By the permanganate treatment of sisal fibers and improvement of interfacial strength, Young modulus and tensile and impact strength of PLA/untreated SSF biocomposites were increased. As can be found in Fig. 64, the reinforcement influences of permanganate-treated SSF are more considerable than the ones for untreated SSF. Nonetheless, among different PLA/treated fiber biocomposites prepared in this work, the biocomposite containing permanganate treated SSF has the lowest tensile and impact strength (Fig. 64). The other chemical treatment methods including acetylation, silane and alkali modifications have been more effective than permanganate treatment in improving the strength of matrix/fiber interface as well as PLA/SSF biocomposite (Zou et al. 2012).

In a similar study, permanganate treatment method was employed to modify unidirectional jute fibers after performing mercerization pretreatment (Goriparthi et al. 2012). The alkali-treated fibers, in this work, were dipped in 0.125% permanganate solution in acetone for 1 min. Additionally, other chemical modifications including silane and peroxide methods were also applied. The results showed that different

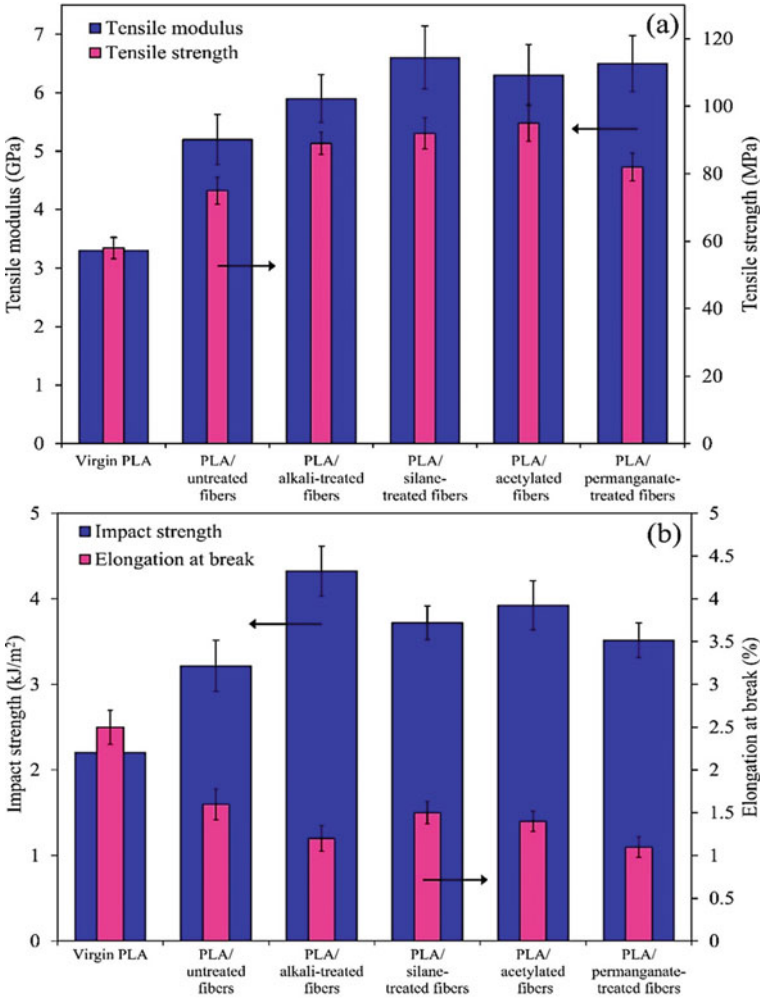

Fig. 64 Mechanical characteristics of virgin PLA, PLA/untreated SSF composite and PLA/treated SSF composites. Different chemical treatment methods were applied to modify the fibers including alkali, acetylation, silane and permanganate procedures. Adapted to (Zou et al. 2012)

properties of PLA/untreated jute fiber and PLA/alkali-treated jute fiber composites were improved by treating the plant fibers with permanganate solution. The mentioned properties include tensile modulus and strength, flexural modulus and strength, storage modulus, glass transition temperature and abrasive wear resistance. In spite of that, the properties of PLA/jute fiber composites containing fibers treated with silane and peroxide methods were better than the ones for PLA-based composite having permanganate–treated fibers (Goriparthi et al. 2012).

5.11 Acrylation Treatment

The acrylation modification is another chemical treatment method that can induce graft copolymerization in natural fiber-reinforced composites. This treatment involves in using acrylics and acrylonitrile monomers. The acrylic monomers can react with lignocellulosic fiber surface through two different reaction paths, (I) free radical reaction and (II) esterification reaction. Dependent on the matrix type used to produce the biocomposite, each one of the reaction paths can be used to modify plant fibers. In the first treatment path, lignocellulosic fibers are exposed to high-energy radiations, hence undergoing chain scission reactions and free radical formation (Orue et al. 2018). Acrylic monomers like acrylic acid are then grafted onto the resultant fiber macroradicals and acrylic monomer polymerization continues through free radical chain polymerization. In contrast, in the second treatment path, acrylic acid monomers react with the fiber hydroxyl groups through esterification reaction. By that reaction, acrylic monomers are grafted onto fiber surfaces and the free radical polymerization of vinyl monomers is performed by adding thermal initiators like organic peroxides. Because of the free radical polymerization of acrylic monomers, it is possible to create chemical linkages between polymeric matrix and lignocellulosic fibers. By the graft copolymerization of acrylic vinyl monomers, treated plant fibers become more hydrophobic and the fiber resistance against moisture improves. Stronger interfacial interactions between lignocellulosic fiber and matrix are provided by acrylation treatment as well (Orue et al. 2018; Siakeng et al. 2019a). The mechanisms of possible chemical reactions involved in the treatment of lignocellulosic fibers with acrylic monomers are shown below (Fig. 65).

In a study, acrylic acid monomer was used to treat sunn hemp fibers (Kalia and Kumar 2013). The fibers were exposed first to NaOH solution, then acrylic acid solution. The appearance of an additional absorption peak in the FTIR spectrum of acrylated fibers at a wavenumber of 1733 cm^{-1} confirmed the presence of carbonyl group of acrylic acid monomer on fiber surfaces. Authors reported that the vinyl polymer was successfully deposited on fiber surfaces, which made the fibers rougher. Contrary

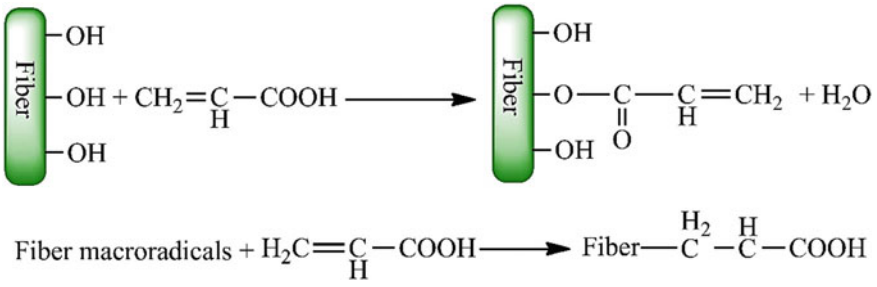

Fig. 65 Probable chemical reactions involved in the treatment of lignocellulosic fibers with acrylic monomers

to the other used chemical modifications, namely peroxide and permanganate treatments, the acrylation method resulted in the fibers with higher thermal stability and crystallinity degree (Kalia and Kumar 2013).

Similar to acrylic monomers, acrylonitrile monomer can be also grafted onto fiber surfaces, polymerized and chemically modified the natural fibers. Acrylonitrile monomer having free radicals can react with lignocellulosic macromolecules through dehydrogenation and oxidation reactions. In addition, the active free radical sites in the system can also react with matrix chains. Therefore, the efficiency of matrix/fiber interlocking is increased by the formation of chemical linkages between matrix chains and plant fibers (Orue et al. 2018). Reportedly, the grafting reaction between cellulose fibers and acrylonitrile monomer can favorably progress without lignin presence (Kozlowski and Wladyka-Przybylak 2004).

The acrylonitrile chemical treatment was applied in a research to modify non-woven jute fiber mat (Khan et al. 2015). To treat the fibers in this work, jute fibers were bleached by using $NaClO_2$ solution. Then, the jute bleached fibers were exposed to acrylonitrile monomer in the presence of $K_2S_2O_8$ initiator and Fe_2SO_4 catalyst. Afterwards, non-woven mats from the treated and untreated fibers were prepared and the PLA-based biocomposites were obtained by using a hot press-molding machine. In this research, the jute fiber mats were also treated by other chemical treatment methods including alkali, bleaching, alkali-acetylation, alkali-permanganate, alkali-benzoylation and bleaching-isocyanate modifications. As can be seen in Fig. 66, just similar to other applied chemical treatments, the jute fiber mats treated by bleaching-acrylonitrile grafting reactions reinforce PLA matrix more effectively comparing to untreated jute mats. By acrylonitrile grafting treatment, the tensile, flexural and impact strength of PLA/bleached jute mat biocomposites improved by 13.5, 7.7 and 10%, respectively. Moreover, the water uptake of PLA/fiber composites containing bleached-acrylonitrile grafted jute mats had been also lower than other corresponding samples. The observed improvements in the properties of these composites are attributed to better compatibility of PLA matrix and jute mats, which stems from the formation of vinyl polymer layer on fiber surfaces and the resultant chemical interlocking (Khan et al. 2015). By the chemical treatments of jute fibers, matrix/fiber interfacial adhesion was improved considerably. The improvement significantly decreased the extent of interfacial debonding and fiber pull-out on the fractured surfaces. Figure 67 shows the SEM images of the fractured surfaces of prepared biocomposites. As can be observed, the acrylonitrile grafting treatment enhances the matrix/fiber interfacial strength and reduces the extent of fiber pull-out remarkably (Khan et al. 2015).

5.12 Modifications Based on Eco-Friendly Chemicals

Among all different modification methods of lignocellulosic fibers, the chemical treatments are the most frequently used methods. This is due to their relative simplicity, low cost and/or high efficiency (Orue et al. 2018; Asha et al. 2017).

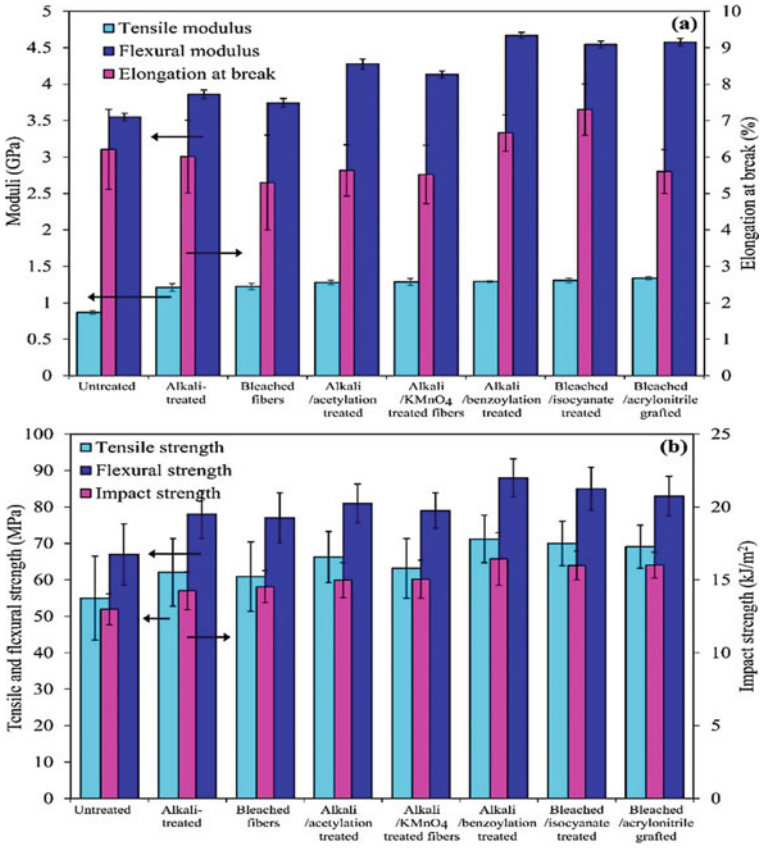

Fig. 66 Mechanical characteristics of PLA/non-woven jute mats composites containing untreated and treated fibers using different chemical modification methods. Adapted to (Khan et al. 2015)

Although many methods of chemical modifications are effective to some extent in improving the properties of natural fiber-reinforced biocomposites, their eco-friendly nature is controversial (Church et al. 2015). In the synthesis of "green" PLA/lignocellulosic fiber composites, the use of eco-friendly and environmentally sustainable methods for the preparation of biocomposites are very important. Many of the mentioned chemical methods involve in the use of toxic chemicals, which are harmful to environment and operator. For example, the used sodium hydroxide in mercerization method is very corrosive, or isocyanates are very toxic and carcinogenic. In addition, some of these methods consist of multi-step reactions that are not energetically efficient (Church et al. 2015; Chaitanya and Singh 2018a). Therefore, these problems affect the environmental acceptability and commercial viability of the treated plant fiber-reinforced biocomposites (Chaitanya and Singh 2018a). As a result, the chemical treatment methods using more eco-friendly and non-toxic

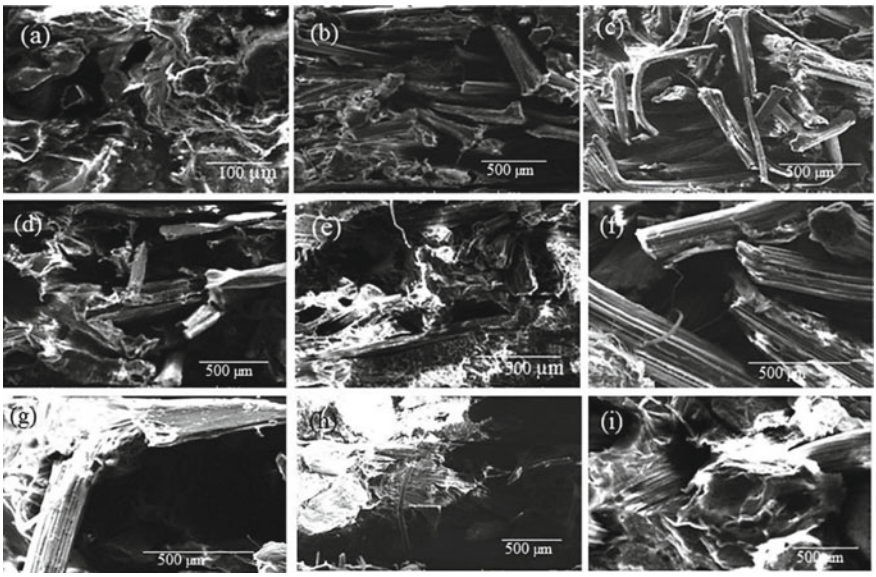

Fig. 67 SEM image of the fractured surface of **a** virgin PLA and PLA/non-woven jute mat composite containing: **b** untreated fibers, **c** bleached fibers, **d** bleached-acrylonitrile grafted fibers, **e** bleached-isocyanate treated fibers, **f** alkali-treated fibers, **g** alkali-acetylated fibers, **h** alkali-$KMnO_4$ treated fibers and **i** alkali-benzoylated fibers. Reproduced with permission from (Khan et al. 2015)

chemical substances, and physical and physiochemical methods along with biological methods are considered as promising alternatives for common chemical methods (Orue et al. 2018).

In order to overcome the problem of interfacial incompatibility in PLA-based biocomposites containing lignocellulosic fibers, the chemical methods using more eco-friendly materials have been developed, instead of complex and harmful chemical processes. In one of the related works, the absorption of amphiphilic block copolymers based on PEG onto fiber surfaces was employed to improve the compatibility of PLA matrix with cellulose fabric, obtained from bamboo fibers (Church et al. 2015). The used copolymers were PEG-block-oleyl ether copolymers (PEG_n–b–C_{18}), which were composed of hydrophilic and hydrophobic amphiphiles and had hybrid function. In the copolymer structures, n refers to the number of PEG units that was 2, 10 and 20 for the copolymers used in this research. These lengths of PEG blocks resulted in the hydrophilic-lipophilic balance (HLB) values of 4, 12 and 15, respectively. For deposition of the copolymers on cellulose fiber surfaces, simple dip-coating method was used for short periods of time. In this treatment method, water or water/acetone solutions of copolymers were applied to obtain micro-crystal suspensions or amphiphilic emulsions. Considering the used treatment agents, this method is superior to common chemical methods in terms of environmental concerns.

By localizing the amphiphilic block copolymers at interface, strong interactions such as inter- and intra-molecular hydrogen bonding emerge across the interfaces of cellulose fibers and PLA matrix. In fact, PEG blocks are extremely flexible and hydrophilic and can form strong hydrogen bonds with cellulose surfaces. Figure 68 demonstrates that the deposition of PEG_n–b–C_{18} copolymers on cellulose fiber surfaces improves the flexural modulus and strength. The highest reinforcing effect belongs to the cellulose fabric treated with PEG_2–b–C_{18} copolymer. PEG_2–b–C_{18} copolymer having smaller HLB, comparing to the copolymers with longer PEG chains, is more hydrophobic. The short PEG blocks result in less fiber slipping and lower degrees of dissociation and restructuring of hydrogen bonding at PEG/cellulose interface in stress transfer conditions. Comparing to the other prepared biocomposites, the fiber treatment with PEG_2–b–C_{18} copolymer caused the largest storage modulus, least damping and maximum shift of T_g to higher temperatures. In other words, the application of this amphiphilic copolymer restrains the molecular motions at interface more considerably and improves the interfacial adhesion of reinforced fabric and matrix more (Church et al. 2015).

More eco-friendly chemical materials, capable of forming chemical linkages, have been also applied to modify PLA/natural fiber biocomposites. In a research, aqueous solution of sodium tetraborate decahydrate (borax) was used to enhance the interfacial bonding between PLA matrix and different lignocellulosic fibers (Birnin-Yauri et al. 2016). The used plant fibers were kenaf core fibers (KCF), oil palm empty fruit bunch fibers (EFBF) and oil palm mesocarp fibers (OPMF). Borax treatment has been suggested as a substitute for mercerization method, since boric acid and borax are less harmful in comparison with NaOH. Borax is relatively eco-friendly

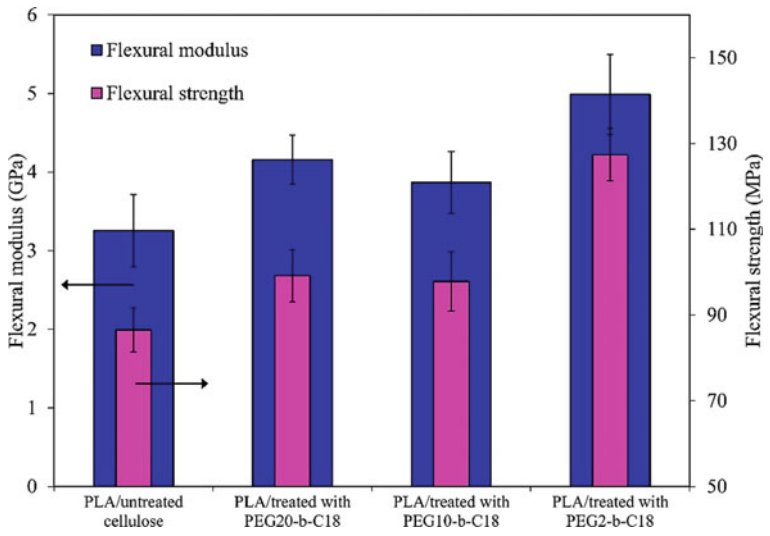

Fig. 68 Flexural modulus and strength of PLA/cellulose fabric biocomposites, effects of the surface treatment of the fabric with PEGn-b-C18 copolymers. Adapted to (Church et al. 2015)

and non-toxic. The borax treatment was found to increase the cellulose content of plant fibers and remove hemicelluloses and waxes from fiber surfaces. Moreover, the lignin concentration was decreased slightly at the surface by the treatment. As it can be seen in FTIR spectra in Fig. 69, the fiber treatment caused the disappearance of the absorption peak at 1718–1725 cm^{-1}, which is attributed to the C=O bond of carbonyl groups in hemicellulose and lignin. Moreover, the intensity of absorption peak related to the stretching vibration of aromatic C=C bonds in lignin at 1610–1619 cm^{-1} decreased indicating the slight removal of lignin after borax treatment. The absorption peak at 1238–1239 cm^{-1}, corresponds to the stretching vibrations of etheric, phenolic and alcoholic C–O bonds, shifted to smaller wavenumbers or totally removed by the treatment. Overall, these results can confirm the elimination

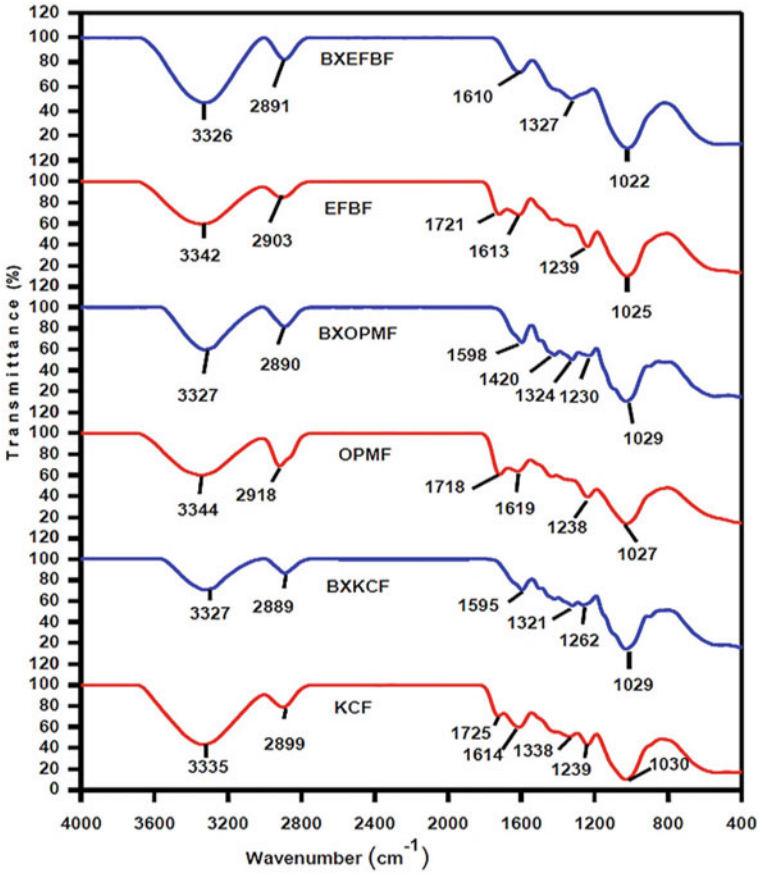

Fig. 69 FTIR spectra of plant fibers with and without borax treatment. The BX letters in front of the fiber names show the use of borax treatment. Reproduced with permission from (Birnin-Yauri et al. 2016)

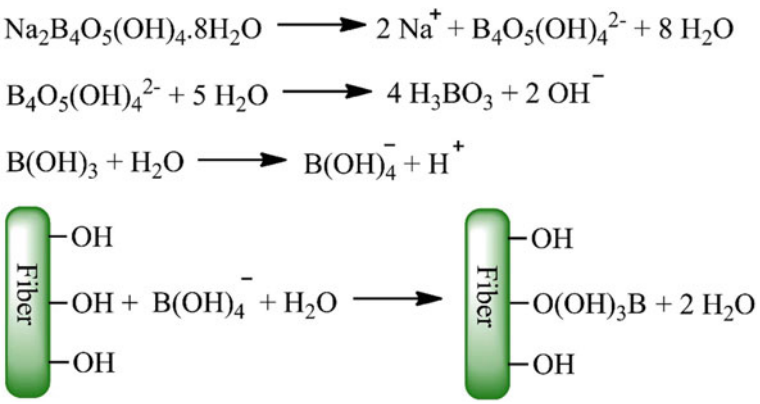

Fig. 70 Proposed chemical reactions involved in the plant fiber treatment with aqueous solution of sodium tetraborate decahydrate, including the reactions of borate ion formation and the reactions of the resultant ions with fiber hydroxyl groups. Adapted to (Birnin-Yauri et al. 2016)

of lignin and waxy constituents from fiber surfaces (Birnin-Yauri et al. 2016). The probable reactions involved in borax treatment are shown in Fig. 70.

The SEM images of the used fibers, in this work, before and after borax treatment have shown that borax-treated EFBF has rough and textured surface. The surface of treated OPMF has relatively more pores, which can assist mechanical interlocking of fiber/matrix phases. For KCF also, clean and rough surface was obtained by the treatment. In fact, borax treatment led to the removal of fiber surface impurities and created stronger fiber/matrix bonding. Therefore, impact, tensile and flexural strength along with flexural modulus and elongation at break of the PLA/plant fiber biocomposites improved via this chemical treatment. Furthermore, the PLA-based biocomposites containing borax-treated KCF, as a secondary fiber at 5 wt% loading, in combination with borax-treated EFBF or OPMF, as a primary fiber at 55 wt% loading, showed a reduction in water uptake and thickness swelling (Fig. 71). The lower hygroscopicity of PLA/borax-treated fiber biocomposites can enhances the composite performance in long term (Birnin-Yauri et al. 2016).

Sodium bicarbonate has been also used as an eco-friendly substitute for ecologically hazardous sodium hydroxide (Chaitanya and Singh 2018a, b). Sodium bicarbonate or baking soda is widely applied in cooking, detergents and biomedical applications such as toothpastes and anti-acid agents. Moreover, this chemical has been used as a biopesticide with no reported negative effect on environment. Baking soda has been employed for the chemical treatment of sisal and Aloe Vera fibers (Chaitanya and Singh 2018a, b). Sodium bicarbonate plays a similar role to sodium hydroxide in the treatment process of fibers (Fig. 72), except that it has milder alkali nature. On that account, longer exposure time of plant fibers in sodium bicarbonate solution is required to achieve the desired results, compared to the treatment in NaOH solutions.

The sodium bicarbonate treatment, similar to alkali treatment with NaOH solutions, removes parenchyma cells and impurities from fiber surfaces. Figure 73 shows

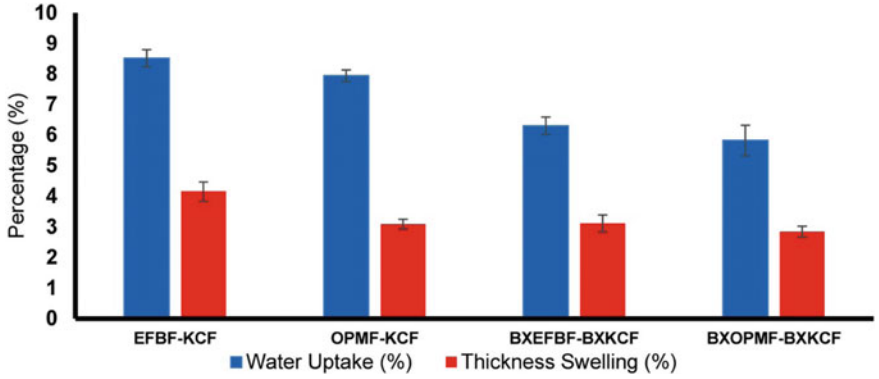

Fig. 71 Dimensional stability of PLA/combined lignocellulosic fibers biocomposites containing untreated and borax-treated fibers. Reproduced with permission from (Birnin-Yauri et al. 2016)

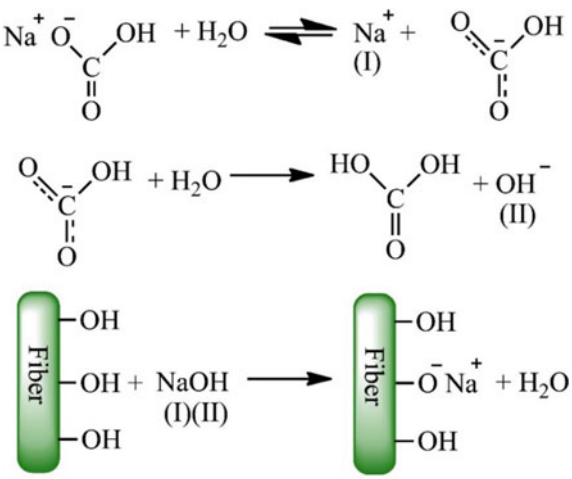

Fig. 72 Proposed chemical reactions involved in the sodium bicarbonate treatment of lignocellulosic fibers

that after 24 h of soaking process, these cells were removed from the fiber surfaces, but no traces of fibrillation can be observable. After 72 h of exposure, fiber fibrillation began and fiber surfaces become rough. Hemicellulose and other impurities were removed from fiber surfaces at this time. At these circumstances, strong hydrogen bonds among inter-fibrillar areas packed the fibers closely. The rearrangement of fibers brought about more fiber homogeneity and stronger load bearing capability. For longer soaking time, more fiber bundles were broken and smaller fibrils with smooth surfaces were obtained (Chaitanya and Singh 2018b).

The changes in the composition of lignocellulosic components of raw Aloe Vera fibers (RAF) after sodium bicarbonate modification at different soaking times (x in TAF-x code) can be found in Fig. 74a. Tensile, flexural and compression strength as well as tensile and flexural modulus of PLA/Aloe Vera fiber biocomposites after

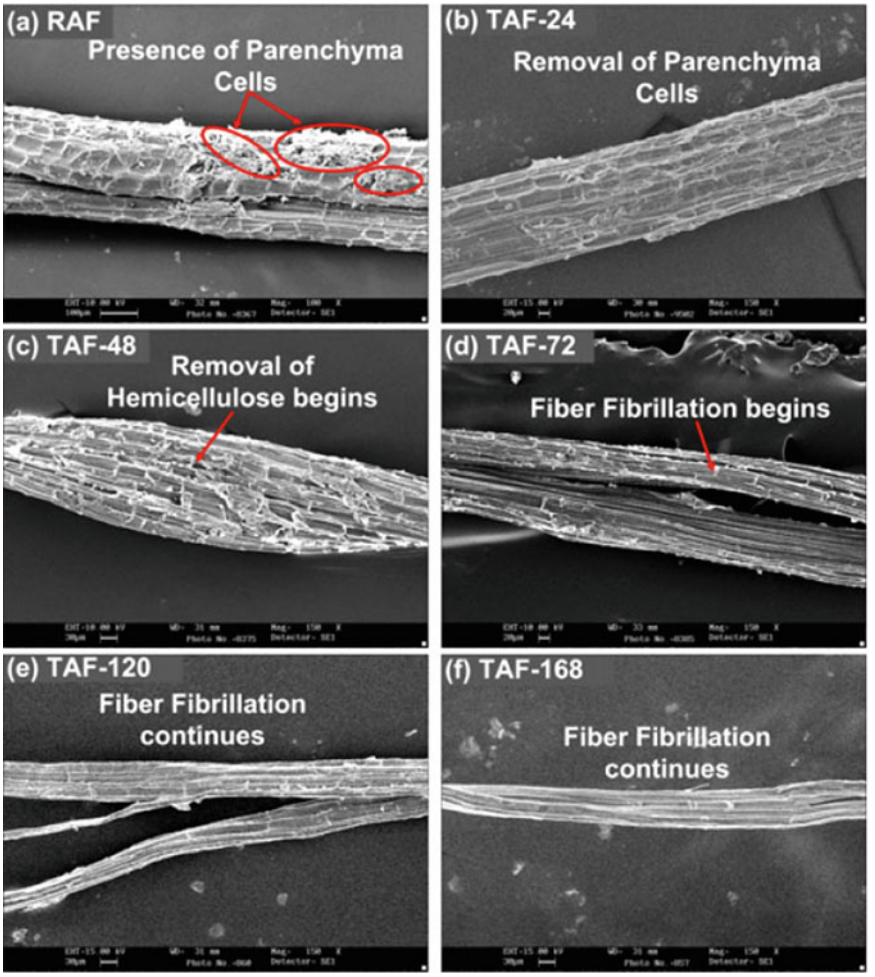

Fig. 73 SEM micrographs of untreated and treated Aloe Vera fibers (TAF), Sodium bicarbonate treatment was used at different soaking times. The soaking time is shown by x in TAF-x codes on the images. Reproduced with permission from (Chaitanya and Singh 2018b)

72 h of soaking time in sodium bicarbonate solution reached the maximum levels, as a result of changing the composition of fiber constituents (Fig. 74b–d). However, increasing the exposure time over 72 h led to weaker fibers with more intensified fibrillation and smoother fiber surfaces. Accordingly, the smoother surfaces result in poor matrix/fiber mechanical interlocking and intensified fibrillation causes more stress concentration at the fiber ends, which increase per unit volume by fibrillation phenomenon. Thus, the mechanical properties of PLA/treated RAF biocomposites were weakened by increasing the treatment times over 72 h, which can be seen in Fig. 74b–d. Unlike the mentioned mechanical properties, the maximum impact

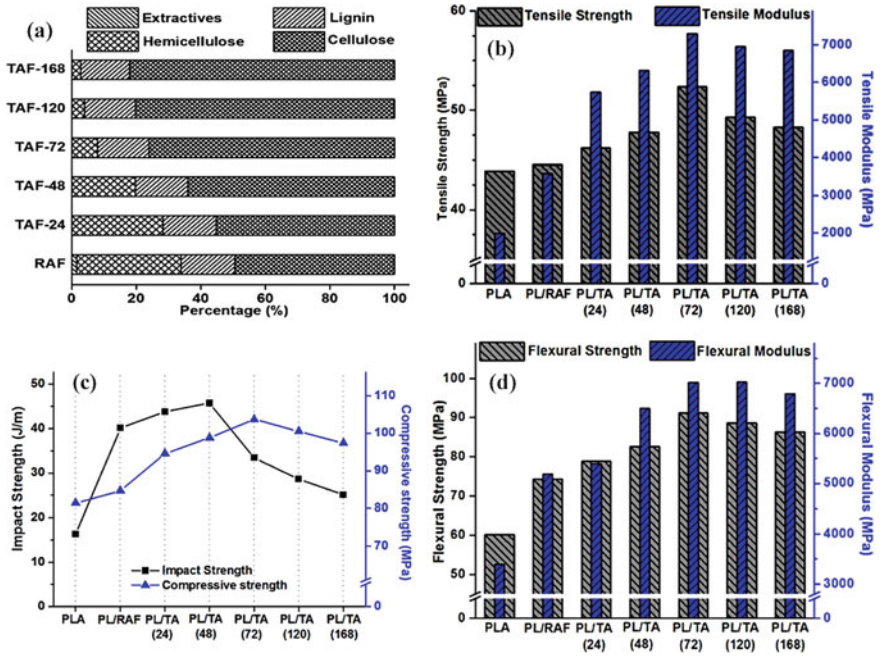

Fig. 74 **a** Composition of lignocellulosic constituents of untreated and treated Aloe Vera fibers (TAF), **b–d** mechanical characteristics of virgin PLA and PLA/Aloe Vera fiber biocomposites containing untreated and treated fibers. Sodium bicarbonate treatment was used at different soaking times (x in TAF-x codes relates to soaking time). Adapted to (Chaitanya and Singh 2018b)

strength was achieved at 48 h of fiber soaking time. This goes to lower extent of fiber pull-out and consequent lower dissipated energy at longer treatment time.

As can be observed in Fig. 75, some microvoids are present on the fractured surface of PLA-based composites containing untreated fibers. Microvoids refer to the points of stress concentration that facilitate the crack propagation. By sodium bicarbonate treatment, fiber/matrix bonding is improved, fiber pull-out is impeded and fiber breakage becomes the dominant phenomenon at the fractured surfaces. However, the improvements were found to be more pronounced up to a certain limit of fiber soaking time (Chaitanya and Singh 2018b). The literature review reveal that it is possible to improve the properties of PLA/natural fiber biocomposites by using non-toxic and eco-friendly chemicals, which can effectively enhance the compatibility of fiber/matrix phases.

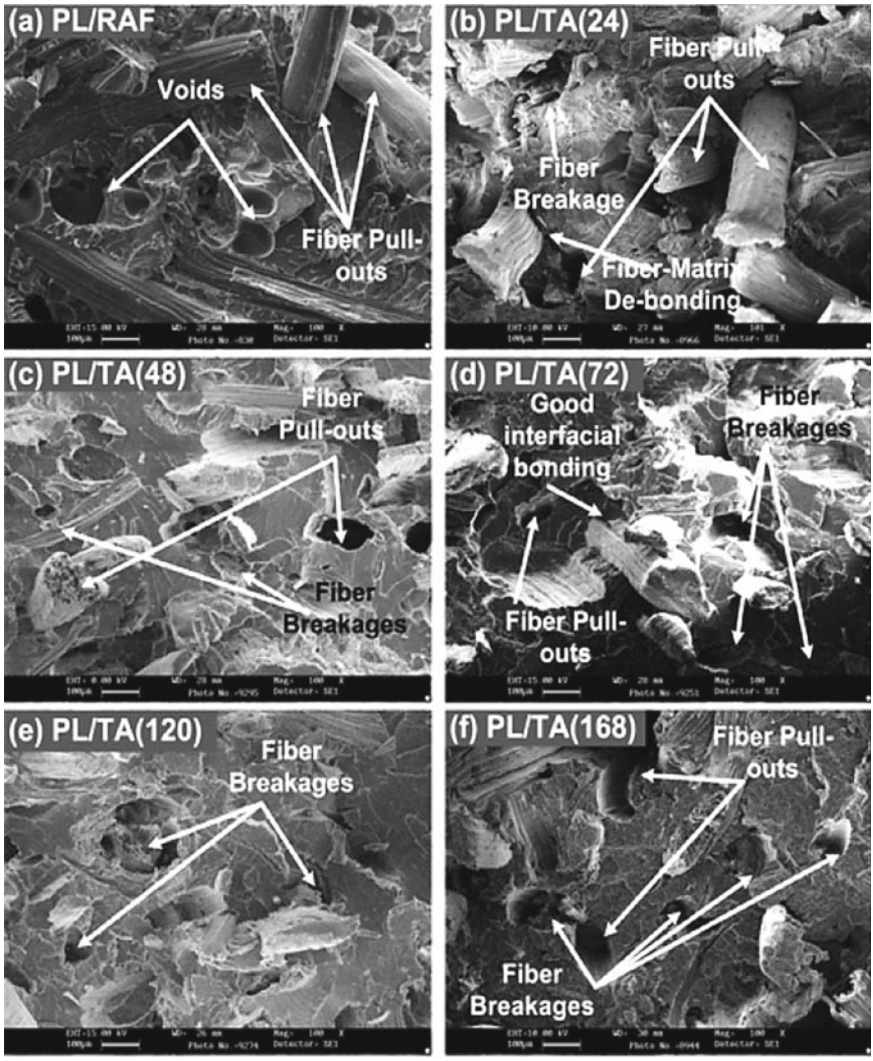

Fig. 75 SEM image of tensile fractured surface of PLA/Aloe Vera fiber biocomposites containing untreated and treated fibers. Sodium bicarbonate treatment was used at different soaking times (x in TAF-x codes relates to soaking time). Reproduced with permission from (Chaitanya and Singh 2018b)

6 Conclusion and Future Perspective

Green composites that consist of lignocellulosic fibers as reinforcing filler and biopolymers as matrices have many beneficial advantages such as availability, renewability, eco-friendly, biodegradability and low density. These biocomposites have been introduced as the most promising alternatives for the products based on synthetic polymers. The plant fiber-reinforced poly (lactic acid) (PLA) biocomposites are the most widely used green composites among others. Although PLA/lignocellulosic fiber biocomposites are sustainable and ecologically friendly, the interface of PLA matrix and plant fibers must be modified to achieve a composite having comparable properties to petroleum-based composites. Different treatment methods including chemical, physical, physio-chemical and biological modifications have been developed to enhance the interfacial strength of matrix/lignocellulosic fibers and correspondingly, the biocomposite final properties. Comparing to other methods, the chemical modifications are the most frequently used procedures. Reviewing the literature, related to the PLA/lignocellulosic fibers systems, reveals the beneficial advantages of chemical treatments such as relative simplicity, lower cost and/or high efficiency.

Different works on PLA/plant fiber biocomposites have shown that the chemical methods can effectively improve the biocomposite properties. The reasons behind that are the increments in fiber roughness and hydrophobicity, improvements in fiber/matrix interfacial adhesion through mechanical interlocking and chemical bonding and removal of impurities from fiber surfaces by performing the chemical treatments. However, the effectiveness of chemical methods depends on the proper choice of reaction conditions. There are some influential variables in chemical treatments that control the extent of improvements. The type of chemical treatment agent, reaction time and temperature, concentration of chemical agent in treatment solutions, pretreatment methods and applied processes for fiber/matrix compounding and shaping are of significance to improve the fiber/matrix interfacial adhesion and biocomposite performance. Reportedly, it has been found that the inappropriate choice of the processing factors involved in chemical treatment methods can lead to even the biocomposite properties deterioration.

As a notable point, the eco-friendly nature of many chemical treatment methods is controversial. Many of chemical methods involve in the use of toxic chemicals, which are harmful to environment and operator. For instance, the used sodium hydroxide in mercerization method is very corrosive, or isocyanates are very toxic and carcinogenic. Therefore, these problems affect the environmental acceptability and commercial viability of the plant fiber-reinforced biocomposites treated by chemical reactions. As a result, some chemical treatment methods using more eco-friendly and non-toxic chemical substances such as sodium bicarbonate have been considered as promising substitutions for common chemical methods. Therefore, the use of eco-friendly and non-toxic chemical compounds will provide treated plant fiber/biopolymer composites with comparable properties to petroleum-based polymers and composites.

References

Al-Mobarak T, Gafur MA, Mina MF (2018) Preparation and characterization of raw and chemically modified sponge-gourd fiber reinforced polylactic acid biocomposites. Mate Sci Appl 09(02). https://doi.org/10.4236/msa.2018.92019

Abu Ghalia M, Dahman Y (2017) Synthesis and utilization of natural fiber-reinforced poly (lactic acid) bionanocomposites. In: lignocellulosic fibre and biomass-based composite materials: processing, properties and applications. Elsevier Ltd, pp 313–345. https://doi.org/10.1016/B978-0-08-100959-8.00015-9

Agustin-Salazar S, Cerruti P, Medina-Juárez LÁ, Scarinzi G, Malinconico M, Soto-Valdez H, Gamez-Meza N (2018) Lignin and holocellulose from pecan nutshell as reinforcing fillers in poly (lactic acid) biocomposites. Int J Biol Macromol 115:727–736. https://doi.org/10.1016/j.ijbiomac.2018.04.120

Ahmed J, Varshney SK (2011) Polylactides-chemistry, properties and green packaging technology: a review. Int J Food Prop 14(1):37–58. https://doi.org/10.1080/10942910903125284

Al-Mobarak T, Mina MF, Gafur MA (2019) Material properties of sponge-gourd fiber–reinforced polylactic acid biocomposites: Effect of fiber weight ratio, chemical treatment, and treatment concentrations. J Thermoplast Compos Mater 32(7). https://doi.org/10.1177/0892705718772880

Aliotta L, Gigante V, Coltelli MB, Cinelli P, Lazzeri A, Seggiani M (2019) Thermo-mechanical properties of PLA/short flax fiber biocomposites. Appl Sci (Switz) 9(18). https://doi.org/10.3390/app9183797

Araújo da SR, de Marques FVM, de Oliveira PF, Rezende CC (2018) Bio-composites based on poly(lactic acid) containing mallow and eucalyptus surface modified natural fibers. J Polym Environ 26(9). https://doi.org/10.1007/s10924-018-1253-0

Asaithambi B, Ganesan G, Ananda Kumar S (2014) Bio-composites: development and mechanical characterization of banana/sisal fibre reinforced poly lactic acid (PLA) hybrid composites. Fibers Polym 15(4). https://doi.org/10.1007/s12221-014-0847-y

Asha AB, Sharif A, Hoque ME (2017) Interface interaction of jute fiber reinforced PLA biocomposites for potential applications. In: Green energy and technology. Springer International Publishing, pp 285–307. https://doi.org/10.1007/978-3-319-49382-4_13

Augustine Saidi M, Gorin A, Kok Heng S, Jayamani E (2017) Effect of layout sequence on the integrity of poly-lactic acid and rice straw fibre composites. In: Materials today: proceedings, vol 4. pp 3150–3157. https://doi.org/10.1016/j.matpr.2017.02.199

Avérous L (2008) Polylactic acid: Synthesis, properties and applications. In: Monomers, polymers and composites from renewable resources, pp 433–450. https://doi.org/10.1016/B978-0-08-045316-3.00021-1

Avinc O, Khoddami A (2009) Overview of Poly(lactic acid) (PLA) Fibre. Fibre Chem 41(6):391–401. https://doi.org/10.1007/s10692-010-9213-z

Aydın M, Tozlu H, Kemaloglu S, Aytac A, Ozkoc G (2011) Effects of Alkali treatment on the properties of short flax fiber-poly(lactic acid) eco-composites. J Polym Environ 19(1):11–17. https://doi.org/10.1007/s10924-010-0233-9

Ballesteros LF, Michelin M, Vicente AA, Teixeira JA, Cerqueira MÂ (2018) Functional properties of lignocellulosic materials. In: Lignocellulosic materials and their use in bio-based packaging. Springer International Publishing, pp 35–47. https://doi.org/10.1007/978-3-319-92940-8_3

Batara AGN, Llanos PSP, De Yro PAN, Sanglay GCD, Magdaluyo ER (2019) Surface modification of abaca fibers by permanganate and alkaline treatment via factorial design. In: AIP conference proceedings. vol 2083. https://doi.org/10.1063/1.5094317

Bigg DM (2005) Polylactide copolymers: effect of copolymer ratio and end capping on their properties. Adv Polym Technol 24(2):69–82. https://doi.org/10.1002/adv.20032

Birnin-Yauri AU, Ibrahim NA, Zainuddin N, Abdan K, Then YY, Chieng BW (2016) Enhancement of the mechanical properties and dimensional stability of oil palm empty fruit bunch-kenaf core and oil palm mesocarp-kenaf core hybrid fiber-reinforced poly(lactic acid) biocomposites

by borax decahydrate modification of fibers. BioResources 11(2):4865–4884. https://doi.org/10.15376/biores.11.2.4865-4884
Chaitanya S, Singh I (2018a) Sisal fiber-reinforced green composites: effect of ecofriendly fiber treatment. Polym Compos 39(12):4310–4321. https://doi.org/10.1002/pc.24511
Chaitanya S, Singh I (2018b) Ecofriendly treatment of aloe vera fibers for PLA based green composites. Int J Precis Eng Manufac Green Technol 5(1):143–150. https://doi.org/10.1007/s40684-018-0015-8
Choi HY, Lee JS (2012) Effects of surface treatment of ramie fibers in a ramie/poly(lactic acid) composite. Fibers Polym 13(2).https://doi.org/10.1007/s12221-012-0217-6
Chun KS, Husseinsyah S, Osman H (2012) Mechanical and thermal properties of coconut shell powder filled polylactic acid biocomposites: effects of the filler content and silane coupling agent. J Polym Res 19(5). https://doi.org/10.1007/s10965-012-9859-8
Church JS, Voda AS, Sutti A, George J, Fox BL, Magniez K (2015) A simple and effective method to ameliorate the interfacial properties of cellulosic fibre based bio-composites using poly (ethylene glycol) based amphiphiles. Eur Polym J 64:70–78. https://doi.org/10.1016/j.eurpolymj.2014.12.024
Courgneau C, Rusu D, Henneuse C, Ducruet V, Lacrampe MF, Krawczak P (2013) Characterisation of low-odour emissive polylactide/cellulose fibre biocomposites for car interior. Express Polym Lett 7(9):787–804. https://doi.org/10.3144/expresspolymlett.2013.76
De Rosa IM, Kenny JM, Maniruzzaman M, Moniruzzaman M, Monti M, Puglia D et al (2011) Effect of chemical treatments on the mechanical and thermal behaviour of okra (Abelmoschus esculentus) fibres. Compos Sci Technol 71(2):246–254. https://doi.org/10.1016/j.compscitech.2010.11.023
Ding WD, Pervaiz M, Sain M (2018) Cellulose-enabled polylactic acid (PLA) nanocomposites: recent developments and emerging trends. In: Functional biopolymers. Springer International Publishing, Berlin, pp 183–216. https://doi.org/10.1007/978-3-319-66417-0_7
Faludi G, Dora G, Renner K, Móczó J, Pukánszky B (2013a) Biocomposite from polylactic acid and lignocellulosic fibers: Structure-property correlations. Carbohydr Polym 92(2):1767–1775. https://doi.org/10.1016/j.carbpol.2012.11.006
Faludi G, Hári J, Renner K, Móczó J, Pukánszky B (2013b) Fiber association and network formation in PLA/lignocellulosic fiber composites. Compos Sci Technol 77:67–73. https://doi.org/10.1016/j.compscitech.2013.01.006
Faludi G, Dora G, Imre B, Renner K, Mõczõ J, Pukánszky B (2014) PLA/lignocellulosic fiber composites: particle characteristics, interfacial adhesion, and failure mechanism. J Appl Polym Sci 131(4):1–10. https://doi.org/10.1002/app.39902
Fan L, Gharpuray MM, Lee Y (1987) Acid hydrolysis of cellulose. In: Cellulose hydrolysis. Biotechnology monographs. Springer, Berlin, Heidelberg. https://doi.org/10.1007/978-3-642-72575-3_4
Ghorbani Chaboki M, Mohammadi-Rovshandeh J, Hemmati F (2019) Poly(lactic acid)/thermoplasticized rice straw biocomposites: effects of benzylated lignocellulosic filler and nanoclay. Iran Polym J (Engl Ed) 28(9):777–788. https://doi.org/10.1007/s13726-019-00743-1
González-López ME, Pérez-Fonseca AA, Cisneros-López EO, Manríquez-González R, Ramírez-Arreola DE, Rodrigue D, Robledo-Ortíz JR (2019) Effect of maleated PLA on the properties of rotomolded PLA-agave fiber biocomposites. J Polym Environ 27(1):61–73. https://doi.org/10.1007/s10924-018-1308-2
González D, Santos V, Parajó JC (2012) Silane-treated lignocellulosic fibers as reinforcement material in polylactic acid biocomposites. J Thermoplast Compos Mater 25(8):1005–1022. https://doi.org/10.1177/0892705711417029
Goriparthi BK, Suman KNS, Mohan Rao N (2012) Effect of fiber surface treatments on mechanical and abrasive wear performance of polylactide/jute composites. In: Composites Part A: applied science and manufacturing, vol 43. https://doi.org/10.1016/j.compositesa.2012.05.007

Hamad K, Kaseem M, Yang HW, Deri F, Ko YG (2015) Properties and medical applications of polylactic acid: a review. Express Polym Lett 9(5):435–455. https://doi.org/10.3144/expresspolymlett.2015.42

Hartmann MH (1998) High molecular weight polylactic acid polymers. In: Biopolymers from renewable resources. Springer, Berlin, pp. 367–411. https://doi.org/10.1007/978-3-662-03680-8_15

Hassan A, Balakrishnan H, Akbari A (2013) Polylactic acid based blends, composites and nanocomposites. In: Advances in natural polymers. Springer, Berlin, pp 361–396. https://doi.org/10.1007/978-3-642-20940-6_11

Hou QX, Chai XS, Yang R, Elder T, Ragauskas AJ (2006) Characterization of lignocellulosic-poly(lactic acid) reinforced composites. J Appl Polym Sci 99(4):1346–1349. https://doi.org/10.1002/app.22236

Huber T, Müssig J (2008) Fibre matrix adhesion of natural fibres cotton, flax and hemp in polymeric matrices analyzed with the single fibre fragmentation test. Compos Interfaces 15(2–3):335–349. https://doi.org/10.1163/156855408783810948

Huda MS, Drzal LT, Mohanty AK, Misra M (2008) Effect of chemical modifications of the pineapple leaf fiber surfaces on the interfacial and mechanical properties of laminated biocomposites. Compos Interfaces 15(2–3):169–191. https://doi.org/10.1163/156855408783810920

Isadounene S, Boukerrou A, Hammiche D, Rodrigue D, Djidjelli H (2017) Effect of fiber surface-treatments on the properties of poly (lactic acid)/olive husk flour biocomposites. J Chem Pharm Res 9(6):332–339

Islam MS, Pickering KL, Foreman NJ (2010) Influence of alkali treatment on the interfacial and physico-mechanical properties of industrial hemp fibre reinforced polylactic acid composites. Compos A Appl Sci Manuf 41(5):596–603. https://doi.org/10.1016/j.compositesa.2010.01.006

Jandas PJ, Mohanty S, Nayak SK (2012) Renewable resource-based biocomposites of various surface treated banana fiber and poly lactic acid: characterization and biodegradability. J Polym Environ 20(2):583–595. https://doi.org/10.1007/s10924-012-0415-8

Jonoobi M, Mathew AP, Abdi MM, Makinejad MD, Oksman K (2012) A comparison of modified and unmodified cellulose nanofiber reinforced polylactic acid (PLA) prepared by twin screw extrusion. J Polym Environ 20(4):991–997. https://doi.org/10.1007/s10924-012-0503-9

Kalia S, Kumar A (2013) Surface modification of sunn hemp fibers using acrylation, peroxide and permanganate treatments: a study of morphology, thermal stability and crystallinity. Polym Plast Technol Eng 52(1). https://doi.org/10.1080/03602559.2012.717335

Kellersztein I, Amir E, Dotan A (2016) Grafting of wheat straw fibers with poly (ε-caprolactone) via ring-opening polymerization for poly(lactic acid) reinforcement. Polym Adv Technol 27(5):657–664. https://doi.org/10.1002/pat.3736

Khan GMA, Shaikh H, Alam MS, Gafur MA, Al-Zahrani SM (2015) Effect of chemical treatments on the physical properties of non-woven Jute/PLA biocomposites. BioResources 10(4). https://doi.org/10.15376/biores.10.4.7386-7404

Khan GMA, Terano M, Gafur MA, Alam MS (2016) Studies on the mechanical properties of woven jute fabric reinforced poly(L-lactic acid) composites. J King Saud Univ Eng Sci 28(1). https://doi.org/10.1016/j.jksues.2013.12.002

Kim KW, Lee BH, Kim HJ, Sriroth K, Dorgan JR (2012) Thermal and mechanical properties of cassava and pineapple flours-filled PLA bio-composites. In: J Therm Anal Calorim. vol 108. https://doi.org/10.1007/s10973-011-1350-y

Kolstad JJ (1996) Crystallization kinetics of poly(L-lactide-co-meso-lactide). J Appl Polym Sci 62(7):1079–1091. https://doi.org/10.1002/(SICI)1097-4628(19961114)62:7%3c1079:AID-APP14%3e3.0.CO;2-1

Kovačević Z, Bischof S, Vujasinović E, Fan M (2019) The influence of pre-treatment of Spartium junceum L. fibres on the structure and mechanical properties of PLA biocomposites. Arab J Chem 12(4). https://doi.org/10.1016/j.arabjc.2016.08.004

Kozlowski R, Helwig M (1998) Lignocellulosic polymer composites. In: Science and technology of polymers and advanced materials. Springer US, Boston, MA, pp 679–698. https://doi.org/10.1007/978-1-4899-0112-5_60

Kozlowski R, Wladyka-Przybylak M (2004) Uses of natural fiber reinforced plastics. In: Natural fibers, plastics and composites. Springer Science+Business Media New York, pp 249–274. https://doi.org/10.1007/978-1-4419-9050-1_14

Krouit M, Naceur Belgacem M, Bras J (2010) Chemical versus solvent extraction treatment: Comparison and influence on polyester based bio-composite mechanical properties. Compos Part A: Appl Sci Manufac 41(6). https://doi.org/10.1016/j.compositesa.2010.01.014

Lagazzo A, Moliner C, Bosio B, Botter, R, Arato E (2019) Evaluation of the mechanical and thermal properties decay of PHBV/sisal and PLA/sisal biocomposites at different recycle steps. Polymers 11(9). https://doi.org/10.3390/polym11091477

Le Moigne N, Longerey M, Taulemesse JM, Bénézet JC, Bergeret A (2014) Study of the interface in natural fibres reinforced poly (lactic acid) biocomposites modified by optimized organosilane treatments. Ind Crops Prod 52:481–494. https://doi.org/10.1016/j.indcrop.2013.11.022

Lee SH, Wang S (2006) Biodegradable polymers/bamboo fiber biocomposite with bio-based coupling agent. Compos Part A: Appl Sci Manufac 37(1). https://doi.org/10.1016/j.compositesa.2005.04.015

Lelekakis N, Wijaya J, Martin D, Susa D (2014) The effect of acid accumulation in power-transformer oil on the aging rate of paper insulation. IEEE Electr Insul Mag 30(3). https://doi.org/10.1109/MEI.2014.6804738

Liber-Kneć A, Kuźniar P, Kuciel S (2015) Accelerated fatigue testing of biodegradable composites with flax fibers. J Polym Environ 23(3):400–406. https://doi.org/10.1007/s10924-015-0719-6

Liu W, Qiu J, Chen T, Fei M, Qiu R, Sakai E (2019) Regulating tannic acid-crosslinked epoxidized soybean oil oligomers for strengthening and toughening bamboo fibers-reinforced poly (lactic acid) biocomposites. Compos Sci Technol 181(April):107709. https://doi.org/10.1016/j.compscitech.2019.107709

LuoH, Xiong G, Ma C, Chang P, Yao F, Zhu Y et al (2014) Mechanical and thermo-mechanical behaviors of sizing-treated corn fiber/polylactide composites. Polym Test 39. https://doi.org/10.1016/j.polymertesting.2014.07.014

Majhi SK, Nayak SK, Mohanty S, Unnikrishnan L (2010) Mechanical and fracture behavior of banana fiber reinforced polylactic acid biocomposites. Int J Plast Technol 14(1 SUPPL.). https://doi.org/10.1007/s12588-010-0010-6

Manshor MR, Anuar H, Nur Aimi MN, Ahmad Fitrie MI, Wan Nazri WB, Sapuan SM et al (2014) Mechanical, thermal and morphological properties of durian skin fibre reinforced PLA biocomposites. Mater Des 59:279–286. https://doi.org/10.1016/j.matdes.2014.02.062

Marwah R, Ibrahim NA, Zainuddin N, Saad WZ, Razak NIA, Chieng BW (2014) The effect of fiber bleaching treatment on the properties of poly(lactic acid)/Oil palm empty fruit bunch fiber composites. Int J Mol Sci 15(8). https://doi.org/10.3390/ijms150814728

Masirek R, Kulinski Z, Chionna D, Piorkowska E, Pracella M (2007) Composites of poly(L-lactide) with hemp fibers: morphology and thermal and mechanical properties. J Appl Polym Sci 105(1):255–268. https://doi.org/10.1002/app.26090

Mihai M, Ton-That M-T (2014) Novel polylactide/triticale straw biocomposites: processing, formulation, and properties. Polym Eng Sci 54(2):446–458. https://doi.org/10.1002/pen.23575

Mochane MJ, Mokhena TC, Sadiku ER, Ray SS, Mofokeng TG (2019) Green polymer composites based on polylactic acid (PLA) and fibers. In: Green biopolymers and their nanocomposites. Springer Singapore, pp 29–54. https://doi.org/10.1007/978-981-13-8063-1_2

Nofar M, Sacligil D, Carreau PJ, Kamal MR, Heuzey MC (2019) Poly (lactic acid) blends: processing, properties and applications. Int J Biol Macromol 125:307–360. https://doi.org/10.1016/j.ijbiomac.2018.12.002

Nyambo C, Mohanty AK, Misra M (2010) Polylactide-based renewable green composites from agricultural residues and their hybrids. Biomacromolecules 11(6):1654–1660. https://doi.org/10.1021/bm1003114

Nyambo C, Mohanty AK, Misra M (2011) Effect of maleated compatibilizer on performance of PLA/wheat straw-based green composites. Macromol Mater Eng 296(8):710–718. https://doi.org/10.1002/mame.201000403

Orue A, Eceiza A, Arbelaiz A (2018) Pretreatments of natural fibers for polymer composite materials. In: Lignocellulosic composite materials. Springer International Publishing AG, pp 137–175. https://doi.org/10.1007/978-3-319-68696-7_3

Orue A, Eceiza A, Peña-Rodriguez C, Arbelaiz A (2016) Water uptake behavior and young modulus prediction of composites based on treated sisal fibers and poly(lactic acid). Materials 9(5). https://doi.org/10.3390/ma9050400

Pan G, Hou X, Dong Z, Zhu J, Huang D, Yang Y (2012) Preparation and properties of long wheat straw fibers used for composite. Adv Mater Res 476–478:843–846. https://doi.org/10.4028/www.scientific.net/AMR.476-478.843

Paul SA, Joseph K, Mathew GDG, Pothen LA, Thomas S (2010) Influence of polarity parameters on the mechanical properties of composites from polypropylene fiber and short banana fiber. Compos A Appl Sci Manuf 41(10):1380–1387. https://doi.org/10.1016/j.compositesa.2010.04.015

Posada JC, Jaramillo LY, Cadena EM, García LA (2016) Bio-based composites from agricultural wastes: polylactic acid and bamboo Guadua angustifolia. J Compos Mater 50(23):3229–3237. https://doi.org/10.1177/0021998315616274

Qin LJ, Qiu JH, Liu MZ, Ding SL, Shao L, Zhang GH, Zhao Y (2011a) Composites of poly(lactic acid) with rice straw fibers modified by poly(butyl acrylate). Mater Sci Forum 675 677:357–360. https://doi.org/10.4028/www.scientific.net/MSF.675-677.357

Qin L, Qiu J, Liu M, Ding S, Shao L, Lü S et al. (2011b) Mechanical and thermal properties of poly(lactic acid) composites with rice straw fiber modified by poly(butyl acrylate). Chem Eng J 166(2):772–778. https://doi.org/10.1016/j.cej.2010.11.039

Razak NIA, Ibrahim NA, Zainuddin N, Rayung M, Saad WZ (2014) The influence of chemical surface modification of kenaf fiber using hydrogen peroxide on the mechanical properties of biodegradable kenaf fiber/poly(Lactic Acid) composites. Molecules 19(3). https://doi.org/10.3390/molecules19032957

Rigolin TR, Takahashi MC, Kondo DL, Bettini SHP (2019) Compatibilizer acidity in coir-reinforced PLA composites: matrix degradation and composite properties. J Polym Environ 27(5). https://doi.org/10.1007/s10924-019-01411-4

Rosli NA, Ahmad I, Anuar FH, Abdullah I (2019) Application of polymethylmethacrylate-grafted cellulose as reinforcement for compatibilised polylactic acid/natural rubber blends. Carbohyd Polym 213:50–58. https://doi.org/10.1016/j.carbpol.2019.02.074

Saeidlou S, Huneault MA, Li H, Park CB (2012) Poly(lactic acid) crystallization. Prog Polym Sci 37(12):1657–1677. https://doi.org/10.1016/j.progpolymsci.2012.07.005

Saha P, Chowdhury S, Roy D, Adhikari B, Kim JK, Thomas S (2016) A brief review on the chemical modifications of lignocellulosic fibers for durable engineering composites. Polym Bull 73(2):587–620. https://doi.org/10.1007/s00289-015-1489-y

Saidi MA, Gorin A, Soon KH, Jayamani E (2018) The optimum sodium hydroxide concentration for high strength pla-rice straw composites. J Mech Eng Sci 12(1):3472–3478. https://doi.org/10.15282/jmes.12.1.2018.14.0308

Santos NS, Silva MR, Alves JL (2017) Reinforcement of a biopolymer matrix by lignocellulosic agro-waste. Procedia Eng 200:422–427. https://doi.org/10.1016/j.proeng.2017.07.059

Savioli Lopes M, Jardini AL, Maciel Filho R (2012) Poly (lactic acid) production for tissue engineering applications. In: Procedia engineering, vol 42. pp 1402–1413. https://doi.org/10.1016/j.proeng.2012.07.534

Shafiei M, Kumar R, Karimi K (2015) Pretreatment of lignocellulosic biomass. In: Lignocellulose-based bioproducts, vol 1. pp 85–154. https://doi.org/10.1007/978-3-319-14033-9_3

Sharif A, Mondal S, Hoque ME (2019) Polylactic acid (PLA)-based nanocomposites: processing and properties. Bio-based Polym Nanocomposites 233–254. https://doi.org/10.1007/978-3-030-05825-8_11

Siakeng R, Jawaid M, Ariffin H, Salit MS (2018) Effects of surface treatments on tensile, thermal and fibre-matrix bond strength of coir and pineapple leaf fibres with poly lactic acid. J Bionic Eng 15(6):1035–1046. https://doi.org/10.1007/s42235-018-0091-z

Siakeng R, Jawaid M, Ariffin H, Sapuan SM (2019a) Mechanical, dynamic, and thermomechanical properties of coir/pineapple leaf fiber reinforced polylactic acid hybrid biocomposites. Polym Compos 40(5):2000–2011. https://doi.org/10.1002/pc.24978

Siakeng R, Jawaid M, Ariffin H, Sapuan, SM, Asim M, Saba N (2019b) Natural fiber reinforced polylactic acid composites: a review. Polym Compos 40(2):446–463. https://doi.org/10.1002/pc.24747

Singhvi MS, Zinjarde SS, Gokhale DV (2019) Polylactic acid: synthesis and biomedical applications. J Appl Microbiol 127(6):1612–1626. https://doi.org/10.1111/jam.14290

Sisti L, Totaro G, Vannini M, Celli A (2018) Retting process as a pretreatment of natural fibers for the development of polymer composites. In: Lignocellulosic composite materials. Springer International Publishing AG, pp 97–135. https://doi.org/10.1007/978-3-319-68696-7_2

Song Y, Zong X, Wang N, Yan N, Shan X, Li J (2018) Preparation of γ -divinyl-3-aminopropyltriethoxysilane modified lignin and its application in flame retardant poly(lactic acid). Materials 11(9):1–13. https://doi.org/10.3390/ma11091505

Sun Z, Zhang L, Liang D, Xiao W, Lin J (2017) Mechanical and thermal properties of PLA biocomposites reinforced by coir fibers. Int J Polym Sci 2017:1–9. https://doi.org/10.1155/2017/2178329

Thumm A, Even D, Gini PY, Sorieul M (2018) Processing and properties of MDF fibre-reinforced biopolyesters with chain extender additives. Int J Polym Sci. https://doi.org/10.1155/2018/9601753

Way C, Dean K, Wu DY, Palombo E (2012) Biodegradation of sequentially surface treated lignocellulose reinforced polylactic acid composites: Carbon dioxide evolution and morphology. Polym Degrad Stab 97(3):430–438. https://doi.org/10.1016/j.polymdegradstab.2011.11.013

Way C, Dean K, Wu DY, Palombo EA (2011) Polylactic acid composites utilising sequential surface treatments of lignocellulose: chemistry, morphology and properties. J Polym Environ 19(4):849–862. https://doi.org/10.1007/s10924-011-0361-x

Witzke DR (1997) Introduction to properties, engineering and prospects of polylactide polymers. Michigan State University

Wu CS, Liao HT, Jhang JJ, Yeh JT, Huang CY, Wang SL (2013) Thermal properties and characterization of surface-treated RSF-reinforced polylactide composites. Polym Bull 70(11):3221–3239. https://doi.org/10.1007/s00289-013-1018-9

Yaacob ND, Ismail H, Ting SS (2016) Soil burial of polylactic acid/paddy straw powder biocomposite. BioResources 11(1):1255–1269. https://doi.org/10.15376/biores.11.1.1255-1269

Yu T, Hu C, Chen X, Li Y (2015) Effect of diisocyanates as compatibilizer on the properties of ramie/poly(lactic acid) (PLA) composites. Compos Part A: Appl Sci Manufac 76. https://doi.org/10.1016/j.compositesa.2015.05.010

Yussuf AA, Massoumi I, Hassan A (2010) Comparison of polylactic Acid/Kenaf and polylactic Acid/Rise husk composites: the influence of the natural fibers on the mechanical, thermal and biodegradability properties. J Polym Environ 18(3):422–429. https://doi.org/10.1007/s10924-010-0185-0

Zafar MT, Maiti SN, Ghosh AK (2016) Effect of surface treatment of jute fibers on the interfacial adhesion in poly(lactic acid)/jute fiber biocomposites. Fiber Polym 17(2):266–274. https://doi.org/10.1007/s12221-016-5781-8

Zandi A, Zanganeh A, Hemmati F, Mohammadi-Roshandeh J (2019) Thermal and biodegradation properties of poly(lactic acid)/rice straw composites: effects of modified pulping products. Iran Polym J (Engl Ed) 28(5). https://doi.org/10.1007/s13726-019-00709-3

Zhang L, Zhong J, Ren X (2017) Natural fiber-based biocomposites. In: Green biocomposites. Springer International Publishing, pp 31–70. https://doi.org/10.1007/978-3-319-46610-1_3

Zhao Y, Qiu J, Feng H, Zhang M, Lei L, Wu X (2011) Improvement of tensile and thermal properties of poly(lactic acid) composites with admicellar-treated rice straw fiber. Chem Eng J 173(2):659–666. https://doi.org/10.1016/j.cej.2011.07.076

Zimniewska M, Wladyka-Przybylak M (2016) Natural fibers for composite applications. In: Fibrous and textile materials for composite applications. Springer Science+Business Media, Singapore, pp 171–204. https://doi.org/10.1007/978-981-10-0234-2_5

Zou H, Wang L, Gan H, Yi C (2012) Effect of fiber surface treatments on the properties of short sisal fiber/poly(lactic acid) biocomposites. Polym Compos 33(10). https://doi.org/10.1002/pc.22295

3D Printing of Continuous Natural Fibre Reinforced Biocomposites for Structural Applications

A. Mugeshwaran, Nalini Ranganathan, R. Joseph Bensingh, and Sanjay K. Nayak

Abstract In last few years, there is a constant demand from several industrial fields for using light-weight components to exhibit high mechanical performance. This demand is met by employing composite materials, especially the fiber reinforced polymer composites. Compare to conventional process shape complexity, infill density, and manufacturing lead times are no longer barriers with additive manufacturing. Therefore, the fabrication of light weight fiber reinforced polymeric composites using additive manufacturing remains the protagonist. In this chapter different types of fiber reinforce composites developed using different additive manufacturing technique are classified based on the length of fiber, aspect ratio, orientation and performance i.e. short, long and continuous fiber reinforced composites. Further the type of continuous natural fiber reinforced composites that are developed using various additive manufacturing technique such as fused deposition modelling (FDM) or Fused Filament Fabrication (FFF), stereolithography (SLA), selective laser sintering (SLS), selective laser melting (SLM), and Direct ink writing (DIW) were reviewed and discussed. In addition, different materials, drawbacks, and strengths associated with different additive manufacturing processes were detailed. Few examples were also presented in the chapter were the 3D Printed structural components has its own real time application in various manufacturing sectors namely automotive, aerospace and aviation.

Keywords Additive manufacturing · Natural fiber · Reinforcement · Polymeric matrix

A. Mugeshwaran · N. Ranganathan (✉) · R. J. Bensingh
SARP: Advanced Research School for Technology and Product Simulation, TVK Industrial Estate, Guindy, Chennai, India
e-mail: nalinranganathan@gmail.com; nalinranganathannr@gmail.com

S. K. Nayak
Central Institute of Plastics Engineering and Technology (CIPET), TVK Industrial Estate, Guindy, Chennai, India

M. T. Hameed Sultan et al. (eds.), *Biocomposite Materials*, Composites Science and Technology, https://doi.org/10.1007/978-981-33-4091-6_6

1 Introduction

Continuous Natural Fiber (CNF) and their biocomposite are being widely used in almost all the structural application due to its massive natural characteristics like lower density, lower cost, and they are renewable and biodegradable with the environment (Pickering et al. 2016). "Green" composites, based on natural fibers derived from plants and biodegradable resins, are in high demand to meet regulatory requirements of recyclability. Several researchers confirmed that the continues natural fiber composites shows significant improvements in stiffness, strength and toughness of composites over fiber reinforced composites, which tends them to utilize in high-tech applications in various engineering sectors such as automotive, aerospace, defense etc. However, properties of the CNF composites depend on various factors matrix intrinsic properties, fiber properties, fiber volume fraction, and interfacial bond strength between the fiber and the matrix, fiber aspect ratio as well as fiber orientation (Ranganathan et al. 2015).

In past decades, the CNF based composite have been developed through various manufacturing processes such as vacuum forming (Delvasto et al. 2010), extrusion (Grande and Torres 2005), injection moulding (Gao and Mäder 2006), and compression (Sreekumar et al. 2007). These conventional fabrication methods for composites require expensive facilities and equipment, such as autoclaves and complex rigid molds, hindering the wide applications. They were also constrained and limited by complexity structure, high mould cost, orientation, and alignment of fibers (Mohanty et al. 2004; Goodship et al. 2015; Faruk et al. 2012). In order to overcome the limitation, the novel method i.e. the 3D Printing/Additive technology for continuous fiber reinforced composites is being developed and studied by many researchers. 3D printing techniques are one of the most promising processes which enhance the light-weight and low-cost processing approaches for reinforced biocomposites when compared to several other composite fabrication methods (Compton and Lewis 2014).The research revolving additive manufacturing to develop structural components using continuous natural fiber composites is in its young stage and burgeoning exponentially throughout the globe. Several additive manufacturing techniques are being involved for the development of structural components which includes fused deposition modeling (FDM) or Fused Filament Fabrication (FFF), stereolithography (SLA), binder jetting (BJ), multi-jet fusion (MJF), selective laser sintering (SLS), selective laser melting (SLM), electron beam melting (EBM), electron beam additive manufacturing(EBAM), big area additive manufacturing (BAAM) (Dugbenoo et al. 2018); Out of which the FDM/FFF, SLA and SLS technologies are being used for developing polymeric composites.

This chapter presents a detailed review of types of natural fibers and 3D printing techniques that are adopted by the researchers for the development of additive manufactured CNF-reinforced biocomposite parts. Additionally, based on the current technological significance and the limitation have been defined.

2 Classification of Short, Long and Continuous Natural Fibers Biocomposites

The natural fibers of cellulose/lignocelluloses fibers are derived from the plant, such as kenaf, hemp, jute, flax, ramie, nettle, pineapple leaf, sisal, date palm, cotton fire, coconut fibers, kapok, bamboo (Al-Oqla and Salit 2017; AL-Oqla and Sapuan 2018; TG YG et al. 2019). On the other hand, wool, silk, hair, and feathers are extracted from the largely consisted proteins of animals and some of the other waste of renewable resources (Saheb and Jog 1999). The natural fibers are classified as short, long and continuous fibers by its aspect ratio (fibers length and diameter) fibers, these fibers are reinforced with polymeric matrix and form biocomposites. Biocomposite materials are defined as composite materials in which at least one of the constituents is derived from natural resources. It is broadly categorized into three types.

i. Reinforcement of synthetic fiber such as carbon fiber, glass fiber, kevlar fiber into bio-matrix such as PLA, PHA, PHB etc.
ii. Reinforcement of natural fibers such as jute, coir, sisal fiber etc. in synthetic/petroleum-derived polymers such as polyethylene (PE), polypropylene (PP) etc.
iii. Reinforcement of bio/natural fibers such as jute, coir, sisal fiber etc. into bio-matrix such as PLA, PHA, PHB etc.

In particular, the natural fiber biocomposites fall under the category of (2) and (3), i.e. the biocomposite materials made from the combination of natural fibers reinforced petroleum-derived polymers or with bio-polymers. Globally, the cellulosic fibers are becoming very interesting for bio-based composite development as they possess advantages with their mechanical properties, low density, environmental benefits, renewability, and economic (Ngo 2018). The bio-based composites are majorly classified as short, Long and continuous fiber composites. In case of short fiber composites, the average size of fiber tends to range below 0.5 inches, whereas in long fiber composites the fibers are normally 0.5, 1.0, or 2.0 inches long (Collett and Campbell 2004) in both the cases namely the short fiber composites and long fiber composites, the fibers are discontinuous. But, in continuous fiber composites the fibers tend to be continuous owing its unique properties. Continuous-fiber composites normally have a preferred orientation, while discontinuous fibers generally have a random orientation. Therefore, the continuous fiber composites are used where higher strength and stiffness are required (but at a higher cost), and discontinuous-fiber composites are used where cost is the main driver and strength and stiffness are less important (Chevali et al. 2010); The benefits and its properties of each category are described in Table 1.

Table 1 The benefits and its properties of each category

Description	Short Fiber Composites	Long Fiber Composites	Continuous Fiber Composites
Processing	Can be processed by many methods	Cannot be processed by many methods	Cannot be processed by many methods
	Compression molding, Extrusion, Hand lay-up, Injection molding, Resin transfer molding, and Sheet molding, Additive Manufacturing	Compression molding, Direct long fiber extrusion technique (D-LFT), Hand lay-up, Resin transfer molding, and Sheet molding	Compression molding, Filament winding, Hand lay-up, Pultrusion, Resin transfer molding and Additive manufacturing
Length of fiber	Lesser than 0.5 Inches	0.5–2.0 Inches	Larger than 2.0 Inches
Aspect ratio	Lower aspect ratio (<100), provide moderate strength, stiffness or creep under loads and with lower endurance compare to LFC or CFC	Higher aspect ratio about 200–3000 (Chevali et al. 2010) provides long fiber composites with increased strength, stiffness or creep under loads and higher fatigue endurance with minimal compression	Longer aspect ratio (Preferable)
Type and orientation	Discontinuous (More randomly dispersed and oriented across the part)	Discontinuous (Not more randomly dispersed and oriented across the part)	Continues (preferred regular orientation arranged across part)
Mechanical performance	They offer lower mechanical performance compare to long and continuous fiber composites, hence could be used forsemi-structural components	They offer lower mechanical performance compare to continuous fiber composite, but higher properties compare to short fiber composites	They provide extreme mechanical performance, thereby indenting to utilize the composite for metal replacements or for structural applications
	Short fiber reinforced polymers were developed to fill the property gap between continuous fiber laminates used as primary structures by the aircraft and aerospace industry and unreinforced polymers used largely in non-load bearing application	The long fiber composite bridges the gap between short and continuous fiber composites, offers better mechanical properties than SFC, but retain their processing conditions (Phelps 2009)	Continuous-fiber composites are normally laminated materials in which the individual layers, plies, or laminae are oriented in directions that will enhance the strength in the primary load direction (Campbell 2010)

3 Continuous Natural Fibers Composites by Additive Manufacturing

Natural fibers are becoming a preferred alternative in reinforced polymer composites, due to the intensive properties such as renewability and biodegradability; in addition, they also possess excellent tensile properties.

Several studies have shown that short (discrete or chopped) fibers extruded as one filament successfully integrated with matrix material are applicable in several AM techniques (Campbell 2010), whereas printing of fibers and matrix materials continuously layer-by-layer have presented successful research. The continuous fiber 3D Printing were started since 2014. The continuous fiber composites in 3D printing may be defined as spool of fibers used to embed very long strands of fiber into parts as they are printed. These fibers in 3D printing provide substantially more strength and stiffness than other short/particulate fiber composites. Tian et al., study has reported that, the use of biocomposite filaments reduces the material cost and environmental impact (Tian et al. 2017). Several studies reported that the continuous fibers are available in different forms such as fiber bundle, yarn, hessian cloth or mat, in case of additive manufacturing technology the continuous fibers are used as fiber bundle with slight twisting. Only limited research studies have been done in 3D printing of the natural fiber-reinforced composite received from fruits and plants. Table 2 reveals about the 3D printed continuous fiber reinforced composites. The development of composite using additive manufacturing involves implementation of fibers after the nozzle directly into the print job using the fibers and matrix. In this process, the fibers are implemented in two ways one is incorporation of fiber 'inside the nozzle' or placing 'after the nozzle'. Generally, the following disadvantages are present in implementing the continuous fiber reinforced composites using 3D printing process.

i. Difficult process controls due to the fiber infiltration parallel to printing and the handling of the fibers.
ii. Possess challenges with resolution, surface finish and in controlling the interfacial (or) thermal bonding between the fiber and matrix.
iii. The inferior mechanical properties and anisotropic behavior.

A study by (Tekinalp et al. 2014). highlighted the challenges associated with 3D printing fibre reinforced composites and evaluated the load bearing potential of composite parts made from carbon fibre and ABS resin feedstock. On the other hand, they have various benefits such as freedom of design, mass customization, waste minimization and the ability to manufacture complex structures, as well as fast prototyping etc.

Table 2 Classification of composite materials used in additive manufacturing technique

SI. No.	Short natural fiber	Polymeric matrix	Additive manufacturing technique	Author/References
1	Sugar cane baggasse	Polyethylene (PE) Polypropylene (PP) Acrylonitrile butadiene styrene (ABS) Polylactic acid (PLA)	Fused deposition modeling (FDM)	Navarrete et al. (2018)
2	Hemp fiber	Polylactic acid (PLA)	Fused deposition modeling (FDM)	Stoof et al. (2017)
3	Recycled cotton fibers	VisiJet-SL (Clear)	Stereolithography (SLA)	Liu et al. (2017)
4	Green tow flax fibers	Geopolymer matrix	Injection molding made to simulate 3D printing using a vibrating table	Korniejenko et al. (2019)
5	Hemp fiber	Recycled polypropylene	Fused deposition modeling (FDM)	Milosevic et al. (2017)
6	Hemp fiber	Polylactic acid (PLA)	Fused deposition modeling (FDM)	Stoof et al. (2017)
SI. No	**Continuous natural fiber**	**Polymeric matrix**	**Additive manufacturing technique**	**Author/References**
1	Flax fiber	Polylactic acid (PLA)	Fused deposition modeling (FDM)/Fused filament fabrication (FFF)	Duigou et al. (2019)
2	Twisted jute fiber	Polylactic acid (PLA)	Fused deposition modeling (FDM)	Matsuzaki et al. (2016)
3	Cotton fibers	Amylopectin	Direct ink writing (DIW)	Jiang et al. (2019)

4 Additive Manufacturing: Continuous Natural Fiber Reinforced Composites

Various 3D printing techniques are being used for the development of continuous reinforcement biocomposites such as fused deposition method (FDM), stereolithography (SLA), selective laser sintering (SLS) and binder jet (3DP). For structural applications, beyond these techniques, FDM, SLS, and 3DP are largely used for the fabrication of CNFRBC (Ngo et al. 2018). The most widely used 3D printing techniques and manufacturing methods and challenges in the 3D printing of the biocomposite are discussed below.

4.1 Fused Deposition Modeling (FDM) in the Natural Fibers-Reinforced Composite

FDM is the nozzle extrusion-based technique where the feedstock material is mounted in the form of spool. Figure 1a, b, shows the schematic representation of Fused Deposition Method (FDM) for developing the continuous natural fiber composite.

Figure 1a, shows that the feedstock material is fed through the printer nozzle and filaments are extruded from a nozzle by the application of controlled heat (Turner et al. 2014) and (Ranganathan et al. 2019). The extrudate will be delivered through the nozzle under controlled melting temperature to build the object by selective depositing; meanwhile, continuous natural fiber is fed from the fiber supply coil and goes through the inner bore of the extrusion head to the nozzle.

Figure 1b, shows that the continuous fiber is immersed in the liquid matrix which is kept below the spool of fiber. In both the cases the, continuous natural fiber is infiltrated and coated by the molten thermoplastic polymer inside the nozzle, and the impregnated composites can be extruded out from the egress of the nozzle. When the extruded material reaches the surface of the part, it solidifies rapidly and adheres to the previous layer so that the fiber can be pulled out continually by the foregoing fiber inside the part. On the other hand, the extrusion head, which is connected to X–Y motion mechanism, can and generate single layer of the part. After one layer is completed, the building platform placed on a lift mechanism moves in the Z-axis direction by an increase equal to the layer thickness. The process is repeated until the part is finished (Murphy and Collins 2018) and (Yang et al. 2017). The schematic representation of FDM process is shown in Fig. 1. FDM is the most widely used method for printing continuous natural fiber reinforced composites.

Various researchers are utilizing the FDM/FFF process for developing continuous natural fibers-reinforced biocomposite for the structural application. The efforts

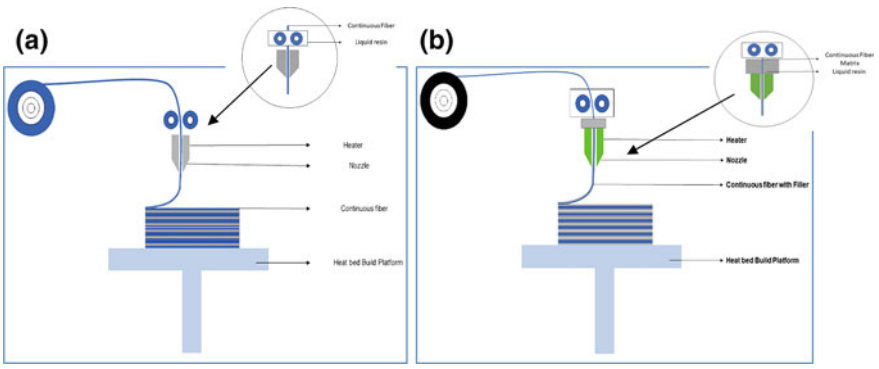

Fig. 1 **a** Fused Deposition method in the continuous natural fiber composite and **b** Fused Deposition method in the continuous natural fiber composite immersed in the liquid matrix

have begun to overcome the geometrical limitation and complexity of the product. Le Duigou et al. developed continuous flax fibers (FF) reinforced PLA composites using FDM process (Duigou et al. 2019). In their study, they have compared and reported the mechanical properties and failure mechanism of FDM printed cFF/PLA part and thermo-compressed continuous synthetic fiber reinforced polymer composites. Similarly, (Duigou et al. 2016) has also investigated the FDM processed continuous wood fiber reinforced thermoplastic composites. The author studied the fiber's anisotropic behavior by printing in different orientations (0 or 90°). Matsuzaki et al. have also utilized the FDM Process to manufacturing continuous natural fibers reinforced PLA composites (Matsuzaki et al. 2016). In their study, they have examined and compared the mechanical properties of the continuously reinforced biocomposite with commercial 3D printing polymer composites.

4.2 Selective Laser Sintering (SLS) in Continuous Natural Fibers-Reinforced Composite

SLS process operated under the principle of laser sintering i.e. high-intensity laser beam such as CO_2/Nd: YAG are used to sinter the powder particles, this process is also known as powder bed fusion, shown in Fig. 2. Reinforcements for SLS-fabricated FRPC are mostly found in the form of discontinuous fibers; synthetic fibers namely carbon fiber, glass fiber or aramid fibers are commonly used. In this process, the raw material or the polymer matrix will be in powder form i.e. polyamide (PA) spherical particles and synthetic fiber will be in uniform diameter around 10 μm. Besides PA, some other bio-polymer composites for instance polycapralactone (PCL)/hydroxyapatite (HA), PEEK/HA and polyethylene (PE)/HA were using SLS (Wang et al. 2017). In this technique the laser-scanning speed, the intensity of the source and layer thickness; needs to be optimized for printing the biocomposite.

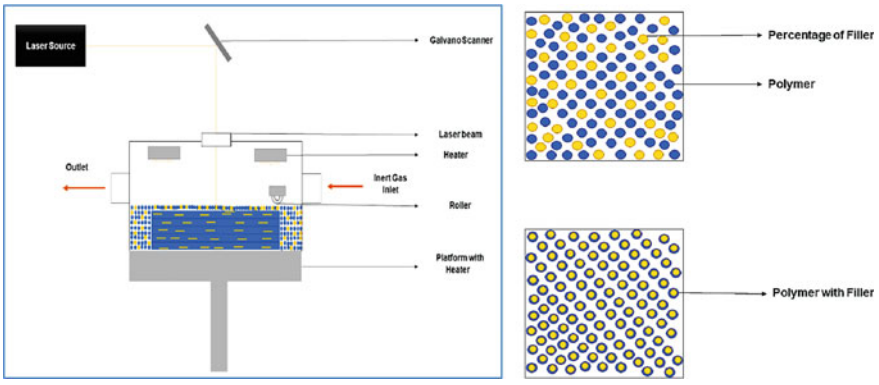

Fig. 2 Selective laser sintering (SLS) for natural fiber reinforced composites

In addition, the build chamber has to be maintained with an inert atmosphere to create the required oxygen-free environment (Goh et al. 2019) and (Goodridge et al. 2011); so that the powdery materials used for printing will be free of moisture, thereby the voids or defects in the printed parts can be avoided.

Saroia et al. employed laser sintering process to manufacture carbon nanofibre reinforced polyamide-12 composite. The mixture of carbon fibers and polyamide was prepared by melt mixing, and the characterization of laser sintered parts was studied (Saroia et al. 2020). Salmoria et al. reported that, the 3D printing of continuous fiber reinforcement composite using SLS is a real challenge (Salmoria et al. 2011). The researchers are working for the development of a proper and standard paradigm for 3D printing of the continuous fiber polymer composite.

Recently, few researchers have utilized the different natural reinforced biocomposite to develop a structural component. They reported that, by optimizing the process parameters the SLS process could be adapted for developing natural fiber reinforced composites. Zhao et al. has optimized the process parameters of SLS, to improve the mechanical properties of the developed biocomposite (Zhao et al. 2017). Zeng et al. developed SLS printed biocomposite components using bamboo flour and co-polyester (BFCP) for various industrial applications (Zeng et al. 2013). Likewise, Simposon et al. developed biocomposites using wood powder as reinforcement in polymeric matrix (Simpson 2018). The powder material processing for the SLS process is quite expensive than other printing techniques. Further, the difficulties persist with material manufacturing and controlling the fiber orientation, interfacial adhesion etc. However, the developed biocomposites found environmentally friendly, non-toxic, and biodegradable materials with low cost.

4.3 Stereolithography (SLA) in Continuous Natural Fibers Composite

Vat photopolymerization selectively cures photopolymer in a vat using ultraviolet (UV) light may be referred as Stereolithography (SLA). In otherwords, the stereolithography (SLA) is a commonly used vat photo-polymerization technique to print FRPC. The Process is also known as direct light processing (DLP). In the SLA process, the low watt laser Nd-Yag laser/UV source is used to cure the liquid photopolymer resin. The build platform is submerged into the liquid photopolymers and is maintained at one-layer height. Then a UV/laser creates the next layer by selectively curing and solidifying the photopolymer resin. This process is called photopolymerization (Feng et al. 2017) and (Guillaume et al. 2017a). Most of the existing SLA systems implement a bottom up approach, scanning each layer, then subsequently moving the base downwards and wiping an additional layer of polymer on top before again photo-polymerizing, represented in Fig. 3. As shown in the figure the platform of the SLA system moves downwards to an incremental amount, by depositing layer by layer. The wipers smooth the top of the deposited resin before the laser

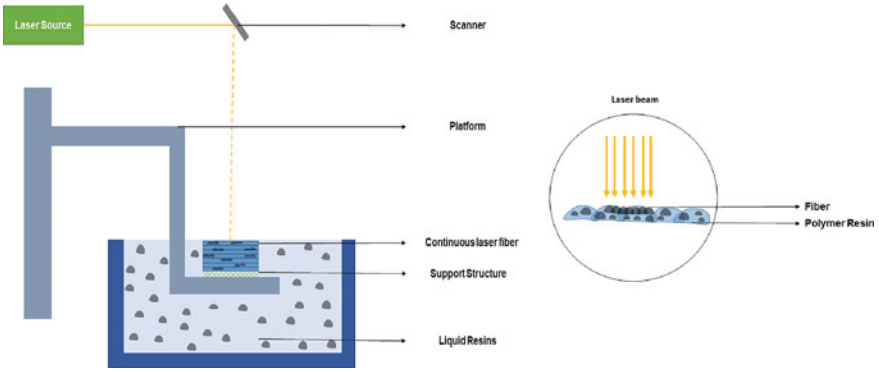

Fig. 3 Stereolithography (SLS) process

cures the corresponding layer patter. The woven mat of fibers are incorporated on bottom layer of solid resin, and then coated with resin. Vat photopolymerization can create composite parts from chopped, woven, or continuous fibers. The creation of composite parts consists of submerging the reinforcing fibers in the UV curable resin, then curing the resin. This technique has the ability to print the higher resolution component. However, the availability of the commercial material is very limited for this process. Research has been carried out on continuous FRPC using glass and carbon fiber bundles and carbon fiber mats as reinforcement (Karalekas and Antoniou 2004). In this continuous FRPC development using SLA, the manual lying or incorporating fiber lying mechanisms (Goodridge et al. 2011).

Recently many researchers are attempting to develop new continuous biocomposites using natural fibers in the SLA process, due to the easy availability of liquid resin. Guillaume et al. a developed poly (trimethylene carbonate) (PTMC) and nano-hydroxyapatite (HA) based cytocompatible 3D porous structure using SLA manufacturing process (Guillaume et al. 2017b). Similarly, Garg et al. developed SLA processed the continuous fiber reinforced composite using Accura60 Resin and carbon fiber (Garg et al. 2001). However, the vat photo-polymerization process has several limitations such as (1) the mechanics of fiber addition, (2) fiber settling, (3) formation of bubbles (voids), (4) increase in resin viscosity (causes poormixing, leading to poor interfacial properties, and (5) laser diffraction and laser energy.

4.4 Direct Ink Writing Technology in Developing Continuous Fiber Reinforced Composite

Direct ink writing (DIW) technology is used to develop continuous natural fiber reinforced thermoplastic composites. In the direct ink writing technology four syringes containing a different composition of magnetic material are used to produce inks with different formulations, thereby the multi-material prints are attained. To produce the

composite inks, SR powder (amylopectin), water, and cotton fibers, without any other chemical or binders were used by (Jiang et al. 2019). In this process the components are added in the proper ratio, mixed well and then subjected to a thermal treatment (causing gelatinization), thus forming the 3D composite pattern. SR composite with 10 wt% cotton fibers from a 400 μm nozzle and (inset) a cellular structure printed via this process were developed and studied by the author. Similarly, the direct ink writing (DIW) system was also used by Sullivan et al. In their study they have used silver nanoparticle ink with a custom-built cell for producing an electrophoretic system to enable deposition of conductive electrodes with controlled thickness with homogeneous mixing of thermite composites (Sullivan et al. 2019).

5 3D Printed Components in Structural Application

The 3D-printing technology emerged to address the rapid prototyping needs of the industry. The technology has outgrown its intended purpose and has its potential for structural applications. Various manufacturing industries have been leveraging the ability of 3D printers to lighten structures by developing lattice structures using fiber reinforced composites. These components are used in various for sectors such as automotive, aerospace and aviation. For example:

i. M/s. AMFG Autonomous Manufacturing Company has produced 3D-printed spacer panels and installed on commercial A320 aircraft.
ii. M/s. Dutch Architecture Company used 3DP to design facades integrated with solar panels, where the angle of the solar panel were optimized automatically based on the location.
iii. M/s. Arevo technology, used continuous carbon fiber/polyetheretherketone (PEEK) for Arevo frame: battery-assisted “ebike”.
iv. M/s. Apis Cor is a San-Francisco-based start-up company has used mobile construction 3D printers that print structural components by adopting additive manufacturing, the construction industry had several advantages like better creativity, design flexibility, less material waste, lower carbon footprint, and more robust structures.

6 Conclusion

In this chapter, the development of CNF and their biocomposite for structural application by using the additive manufacturing process are discussed. The chapter clearly demonstrates the types of natural fibers biocomposites namely short, long and continuous by its aspect ratio (fibers length and diameter) fibers and the different types of fibers (Syntenic fiber, natural fiber and bio added natural fiber) are used as a reinforced with polymeric matrix to form biocomposites. Further the type of continuous

natural fiber reinforced composites that are developed using different additive manufacturing technique was explored. In addition, the chapter also addressed the major advantages and difficulties involved in the printed natural fiber composite by using the various additive manufacturing process the such as fused deposition modelling (FDM) or Fused Filament Fabrication (FFF), stereolithography (SLA), selective laser sintering (SLS), selective laser melting (SLM), and Direct ink writing (DIW). The ability to develop the structural component using natural fiber reinforced composites by using the additive manufacturing process was also discussed detailed.

References

Al-Oqla FM, Salit MS (2017) Materials selection for natural fiber composites. Woodhead Publishing

AL-Oqla FM, Sapuan SM (2018) Investigating the inherent performance characteristic/deterioration interactions of natural fibers in biocomposites for better utilization of resources. J Polym Environ 26(3):1290–1296

Campbell FC (2010) Structural composite materials. ASM international

Compton BG, Lewis JA (2014) 3D-printing of lightweight cellular composites. Adv Mater 26(34):5930–5935

Collett GP, Campbell FC (2004) Curcumin induces c-jun N-terminal kinase-dependent apoptosis in HCT116 human colon cancer cells. Carcinogenesis 25(11):2183–2189

Chevali VS, Dean DR, Janowski GM (2010) Effect of environmental weathering on flexural creep behavior of long fiber-reinforced thermoplastic composites. Polym Degrad Stab 95(12):2628–2640

Delvasto S, Toro EF, Perdomo F, de Gutiérrez RM (2010) An appropriate vacuum technology for manufacture of corrugated fique fiber reinforced cementitious sheets. Constr Build Mater 24(2):187–192

Dugbenoo E, Arif MF, Wardle BL, Kumar S (2018) Enhanced bonding via additive manufacturing-enabled surface tailoring of 3D printed continuous-fiber composites. Adv Eng Mater 20(12):1800691

Faruk O, Bledzki AK, Fink HP, Sain M (2012) Biocomposites reinforced with natural fibers: 2000–2010. Prog Polym Sci 37(11):1552–1596

Feng X, Yang Z, Chmely S, Wang Q, Wang S, Xie Y (2017) Lignin-coated cellulose nanocrystal filled methacrylate composites prepared via 3D stereolithography printing: Mechanical reinforcement and thermal stabilization. Carbohyd Polym 169:272–281

Gao SL, Mäder E (2006) Jute/polypropylene composites I. Effect of matrix modification. Compos Sci Technol 66(7–8):952–963

Garg R, Prud'homme RK, Aksay IA, Janas VF, Tenhuisen KS, Huxel ST (2001) U.S. Patent No. 6283997. Washington, DC: U.S. Patent and Trademark Office. Gu

Goodridge RD, Shofner ML, Hague RJ, McClelland M, Schlea MR, Johnson RB, Tuck CJ (2011) Processing of a Polyamide-12/carbon nanofibre composite by laser sintering. Polym Testing 30(1):94–100

Goodship VD, Middleton B, Cherrington R (2015) Design and manufacture of plastic components for multifunctionality: structural composites, injection molding, and 3D printing. William Andrew

Grande C, Torres FG (2005) Investigation of fiber organization and damage during single screw extrusion of natural fiber reinforced thermoplastics. Adv Polym Technol: J Polym Process Inst 24(2):145–156

Guillaume O, Geven MA, Sprecher CM, Stadelmann VA, Grijpma DW, Tang TT, Yuan H (2017) Surface-enrichment with hydroxyapatite nanoparticles in stereolithography-fabricated composite polymer scaffolds promotes bone repair. Acta Biomater 54:386–398

Guillaume O, Geven MA, Grijpma DW, Tang TT, Qin L, Lai YX, Eglin D (2017) Poly (trimethylene carbonate) and nano-hydroxyapatite porous scaffolds manufactured by stereolithography. Polym Adv Technol 28(10):1219–1225

Goh GD, Yap YL, Agarwala S, Yeong WY (2019) Recent progress in additive manufacturing of fiber reinforced polymer composite. Advan Mater Technol 4(1):1800271

Jiang P, Yan C, Guo Y, Zhang X, Cai M, Jia X, Zhou F (2019) Direct ink writing with high-strength and swelling-resistant biocompatible physically crosslinked hydrogels. Biomater Sci 7(5):1805–1814

Karalekas D, Antoniou K (2004) Composite rapid prototyping: overcoming the drawback of poor mechanical properties. J Mater Process Technol 153:526–530

Korniejenko KINGA, Łach M, Chou SY, Lin WT, Mikuła J, Mierzwiński D, Hebda M (2019, November). A comparative study of mechanical properties of fly ash-based geopolymer made by casted and 3D printing methods. In: IOP conference series: materials science and engineering, vol 660, No 1. IOP Publishing, p 012005

Le Duigou A, Castro M, Bevan R, Martin N (2016) 3D printing of wood fibrebiocomposites: from mechanical to actuation functionality. Mater Des 96:106–114

Le Duigou A, Barbé A, Guillou E, Castro M (2019) 3D printing of continuous flax fibre reinforced biocomposites for structural applications. Mater Des 180:107884

Liu Z, Zhan J, Fard M, Davy JL (2017) Acoustic properties of multilayer sound absorbers with a 3D printed micro-perforated panel. Appl Acoust 121:25–32

Matsuzaki R, Ueda M, Namiki M, Jeong TK, Asahara H, Horiguchi K, Hirano Y (2016) Three-dimensional printing of continuous-fiber composites by in-nozzle impregnation. Sci Rep 6:23058

Milosevic M, Stoof D, Pickering KL (2017) Characterizing the mechanical properties of fused deposition modelling natural fiber recycled polypropylene composites. J Compos Sci 1:7

Mohanty AK, Wibowo A, Misra M, Drzal LT (2004) Effect of process engineering on the performance of natural fiber reinforced cellulose acetate biocomposites. Compos A Appl Sci Manuf 35(3):363–370

Murphy CA, Collins MN (2018) Microcrystalline cellulose reinforced polylactic acid biocomposite filaments for 3D printing. Polym Compos 39(4):1311–1320

Navarrete JIM, Hidalgo-Salazar MA, Nunez EE, Arciniegas AJR (2018) Thermal and mechanical behavior of biocomposites using additive manufacturing. Int J Interact Des Manuf (IJIDeM) 12(2):449–458

Ngo TD (2018) Natural fibers for sustainable biocomposites. Natural and artificial fiber-reinforced composites as renewable sources. p 107

Ngo TD, Kashani A, Imbalzano G, Nguyen KT, Hui D (2018) Additive manufacturing (3D printing): a review of materials, methods, applications and challenges. Compos B Eng 143:172–196

Phelps JH (2009) Processing-microstructure models for short-and long-fiber thermoplastic composites. University of Illinois at Urbana-Champaign

Pickering KL, Efendy MA, Le TM (2016) A review of recent developments in natural fibre composites and their mechanical performance. Compos A Appl Sci Manuf 83:98–112

Ranganathan N, Oksman K, Nayak SK, Sain M (2015) Regenerated cellulose fibers as impact modifier in long jute fiber reinforced polypropylene composites: effect on mechanical properties, morphology, and fiber breakage. J Appl Polym Sci 132(3)

Ranganathan N, Mugeshwaran A, Bensingh RJ, Kader MA, Nayak SK (2019) Biopolymeric scaffolds for tissue engineering application. In: Biomedical engineering and its applications in healthcare. Springer, Singapore pp 249–274

Saheb DN, Jog JP (1999) Natural fiber polymer composites: a review. Advan Polym Technol: J Polym Process Inst 18(4):351–363

Salmoria GV, Paggi RA, Lago A, Beal VE (2011) Microstructural and mechanical characterization of PA12/MWCNTs nanocomposite manufactured by selective laser sintering. Polym Testing 30(6):611–615

Saroia J, Wang Y, Wei Q, Lei M, Li X, Guo Y, Zhang K (2020) A review on 3D printed matrix polymer composites: its potential and future challenges. Int J Advan Manuf Technol 106(5–6):1695–1721

Simpson PG (2018) Additive manufacturing of short-fiber composites via stereolithography Doctoral dissertation, North Dakota State University
Sullivan K, Densmore JM, Duoss E, Gash AE, Kuntz J, Vericella J (2019) U.S. Patent No. 10377090. Washington, DC: U.S. Patent and Trademark Office
Sreekumar PA, Joseph K, Unnikrishnan G, Thomas S (2007) A comparative study on mechanical properties of sisal-leaf fibre-reinforced polyester composites prepared by resin transfer and compression moulding techniques. Compos Sci Technol 67(3–4):453–461
Stoof D, Pickering K, Zhang Y (2017) Fused deposition modelling of natural fibre/polylactic acid composites. J Compos Sci 1(1):8
Tekinalp HL, Kunc V, Velez-Garcia GM, Duty CE, Love LJ, Naskar AK, Ozcan S (2014) Highly oriented carbon fiber–polymer composites via additive manufacturing. Compos Sci Technol 105:144–150
TG YG, MR S, Siengchin S (2019) Natural fibers as sustainable and renewable resource for development of eco-friendly composites: a comprehensive review. Front Mater 6:226
Tian X, Liu T, Wang Q, Dilmurat A, Li D, Ziegmann G (2017) Recycling and remanufacturing of 3D printed continuous carbon fiber reinforced PLA composites. J Cleaner Prod 142:1609–1618
Turner BN, Strong R, Gold SA (2014) A review of melt extrusion additive manufacturing processes: I. Process design and modeling. Rapid Prototyping J
Wang X, Jiang M, Zhou Z, Gou J, Hui D (2017) 3D printing of polymer matrix composites: a review and prospective. Compos B Eng 110:442–458
Yang C, Tian X, Liu T, Cao Y, Li D (2017) 3D printing for continuous fiber reinforced thermoplastic composites: mechanism and performance. Rapid Prototyping J 23(1):209–215
Zeng W, Guo Y, Jiang K, Yu Z, Liu Y, Shen Y, Wang P (2013) Laser intensity effect on mechanical properties of wood–plastic composite parts fabricated by selective laser sintering. J Thermoplast Compos Mater 26(1):125–136
Zhao D, Guo Y, Jiang K, Zhang H (2017) Preparation and selective laser sintering of bamboo flour/copolyester composite and post-processing. J Thermoplast Compos Mater 30(8):1045–1055

Manufacturing Defects in Natural Fibre Composites

Suriani Mat Jusoh

Abstract Generally, defects by word have been determined as abnormality, imperfection, shortcoming, and flaw that impairs quality, function or utility of the materials or system. In manufacturing, the defects or specifically called manufacturing defects are very significant influence for many other properties and performance of the material or system. In literature, manufacturing defects in natural fibre reinforced composites that normally occur during fabrication are classified as misaligned fibres, pockets of undispersed cross-linker, poor wetted resin, resin-rich zone, and voids. The knowledge and determination on manufacturing defect occurrences is important and helps the researcher or manufacturer improve the quality of fabrication process of material and materials performance. This chapter discusses manufacturing defects that have been recognized occurred during the manufacturing process of natural fibre reinforced composite materials by using a non-destructive technique as Optical Microscope (OM) and Scanning Electron Microscopy (SEM). The comeback of manufacturing defects to internal and external fields dictate in many ways of the material properties and performance of final product.

Keywords Composites · Manufacturing defects · Natural fibre composites · Scanning electron microscopy and voids

1 Introduction

In order to overcome all the issues raised due to environment and sustainability, this century has witnessed remarkable achievements in green technology in the field of materials science through the development of biocomposites and the development of high-performance material made from natural resources is increasing. These two facts have been reported by Omar Faruk et al. (2012) as in their review articles entitle *Biocomposites reinforced with natural fibers: 2000–2010*. The properties of natural fibres differ among cited works, because different fibres were used, different

S. M. Jusoh (✉)
Faculty of Ocean Engineering Technology and Informatic, Universiti Malaysia Terengganu, Kuala Nerus, Malaysia
e-mail: surianimatjusoh@umt.edu.my

M. T. Hameed Sultan et al. (eds.), *Biocomposite Materials*, Composites Science and Technology, https://doi.org/10.1007/978-981-33-4091-6_7

moisture conditions were present, and different testing methods were employed. The natural fibre reinforced polymer composites performance depends on several factors, including fibres chemical composition, cell dimensions, microfibrillar angle, defects, structure, physical properties, and mechanical properties, and the interaction of a fibre with the polymer. Talreja (2015) published in their book chapter entitled *Manufacturing defects in composites and their effects on performance* stated that in composite structure, manufacturing defects are imminent, and they can be diminished but not knocked-out. Additionally, the defects are depending on the manufacturing process and their significance varies with the performance requirements applied on the structure. In good engineering approach and practice is, therefore, to allow defects that would not jeopardize safety performance, efficiently production and in return decrease the manufacturing cost. In this chapter, it will discuss manufacturing defects as it has been identified that defects and the comeback of defects to internal and external fields dictate in many ways of many ways of the material properties and performance of final product. Defects are also important for many other properties of materials such as chemical durability, dielectric breakdown, diffusion, and so on. Determination of defects is also important in manufacturing the composite materials because these occurrences of defects will affect the performance and properties of the composite materials. Knowledge on defects occurrence also will help the researcher to improve the manufacturing process during working on composite materials.

2 Manufacturing Defects

Defects can categorize in fibre defects, matrix defects, fibre-matrix defects, and manufacturing defects. During the commercial production of composite materials, defects or specifically may be called manufacturing defects typically occur. It can be claimed that manufacturing defects, flaws or irregularities in products arising from errors in production or manufacturing. In natural fibre reinforced composites, manufacturing defects can be caused by batch-to-batch variations during the prepreg and occasionally by the traditional approach during construction or fabrication technique acknowledged as a hand lay-up method. Manufacturing defects variability could derive from differences in the prepreg tack level during hand lay-up because of variable resin content. In natural fibre composites, it can contain several defects introduced during manufacturing process, which can considerably increase the likelihood of composite failure. Generally, in natural fibre reinforced composite defects may formed during the manufacturing process and include, but are not limited to bonding defects, delamination, fibre misalignment, fibre defects, foreign bodies, incomplete cured matrix, ply cracking, incorrect fibre volume fraction, ply misalignment, porosity or voids in material and wavy fibre. Scheirs (2000) classified manufacturing defects as misalignment of fibres, pockets of undispersed cross-linker,resin-rich zones, regions where resin has poorly wetted the fibre or incomplete curing area and voids.

3 Voids

Campbell (2010) stated the two most prevalent manufacturing defects within solid laminates are porosity and foreign objects. Porosity, in the form of voids, can be introduced in various ways depending on the method of manufacture. Generally, there are many factors causing the porosity or voids in composites. During composite fabrication due to volatile resin components or the air bubbles are not proper controlled during cure and trapped in the matrix are recognized as porosity or voids. During the fabrication or manufacturing process of natural fibre reinforced composites, voids can also develop owing to the occurrence of impurities in the commercial epoxy resins used, which can lead to influence and resulted on the curing behavior of the epoxy resin. These impurities can be oligomers or residues of derives by synthesis reactions. As has been reported by Scheirs (2000), a typical impurity as Chlorohydrins are found in epoxy resin. Roychowdhurty et al. (1992) reported that voids that occurred significantly increased the moisture pick-up and weaken the interfacial adhesion between fibre and matrix had indirectly affected the mechanical properties of the composite materials. In 1980, Bascom et al. had determined the deformation between F-185 resin and glass fibre using Scanning Electron Micrograph (SEM) and as evidence the SEM micrograph showed the occurrence of porous structures in the epoxy resin are clearly observed. The development of porous structures was also determined by Suriani et al. (2012) in her study of Kenaf fibre reinforced epoxy composite by Infrared Thermal Imager. Figure 1 depicted voids or porous structures in epoxy resin as observed in Kenaf fibre reinforced epoxy.

There were two varieties of void classified by Judd and Wright (1978) as into two recognizable types as voids along reinforcement or single fibre and voids between layer or laminae of fibre-matrices. For laminates manufactured using a liquid resin matrix, a cause of void occurrence is air bubbles. These can become trapped in the resin during its manufacturing process or within the laminate as the epoxy resin moves through the fibre, regardless of the process used. De-gassing is a method that can help eliminate voids before resin use. The volatile organic compounds (VOC) is another

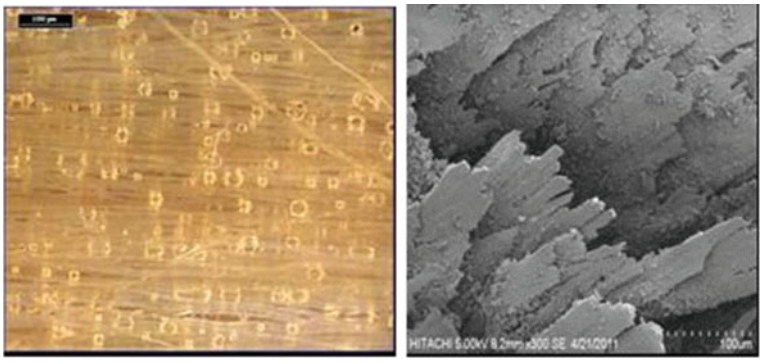

Fig. 1 Voids (Suriani et al. 2012)

factor initiate bubbles within the matrix. These may be essential components of the resin, such as styrene in unsaturated polyester (UPE), or form due to the chemical reaction that takes place during the manufacturing process.

4 Resin-rich Zones

Dewimille and Bunsell (1983) had been discussed about the issue of preferential cracking in the neighborhoods area with resin-rich volume. The swelling of the resin was also claimed due to the occurrence of water that initiated deformation in the resin-rich areas and the weakened interfaces layer in the neighborhood of these areas were subjected to greater stresses that were therefore more likely to fail. In their study, Suriani et al. (2012), stated that resin rich area determined at an area containing more than the maximum allowable resin content which occurs from improper curing or incomplete curing process. Figure 2 depicts areas wetted with resin- rich or known as resin-rich zones, which are not completely cured as has been observed by Optical Microscope (OM) and SEM.

Dong and Tzai (2010) in their study on the composite processing and manufacturing method stated that in liquid composite molding process, resin-rich zones are a prevalent episode determined. Therefore, there is importance to be studied in the design of the composite structure as a preventive action to avoid the failure and indirectly enhanced the final product performance. These resin-rich zones had initiated part to part variation and unwanted residual stress and deformation. The location and size of resin-rich zones have been identified to be affected by both the method of composite manufacturing and the fibre arrangement in the composite.

Fig. 2 Resin rich zones (Suriani et al. 2012)

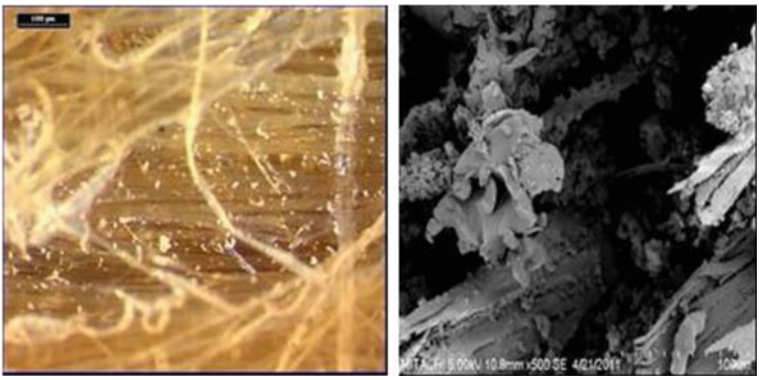

Fig. 3 Pockets of undispersed cross-linker (Suriani et al. 2012)

5 Pockets of Undispersed Cross-Linker

In literature, Scheirs (2000) published that pockets of undispersed cross-linker may be affected by the distribution of curing agents and premature curing or incomplete curing. Figure 3 depicts the pockets of undispersed cross-linker in as determined by Suriani et al. (2012) in their study of kenaf reinforced epoxy composite materials. As claimed by Lapique and Redford (2002), it is significant to understand the mechanical properties and rheological of the adhesive or epoxy resin before testing the properties of composite structures. As consequences, performance in the adhesive or epoxy resin due to premature curing or incomplete curing can influence the results of the interfacial adhesion behavior. Moreover, it may also cause bending in the composite structure during curing process.

6 Misalignment of Fibres

Low dispersion of the fibre-matrix and poor interfacial adhesion or weak bonding of the fibre-matrix are two causes that may affect the misalignment of fibres in fibre reinforced composite materials. As in the literatures stated, the interfacial adhesion between fibre-matrices plays an important role in determining the performance of the fibre reinforced composite materials. Keener and Stuart (2004); Matuana et al. (2001); Saheb and Jog (1999) in their study claimed that heterogeneous systems whose properties are inferior due to poor interfacial adhesion between the fibres and the matrix were lead by the incorporation of fibre (hydrophilic) and polymers (hydrophobics). It may also recognize mainly due to their contradictory hydrophobicity as the polymer matrices are generally hydrophobic and the surface of fibre is hydrophilic thus they are incompatible and forbid efficient bonding between fibre and matrices Khalina et al. (2009) studied the mechanical properties and rheological

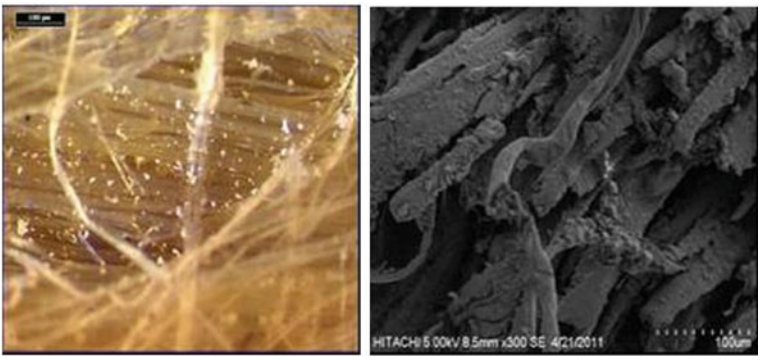

Fig. 4 Misaligned of fibres (Suriani et al. 2012)

of injection moulded short oil palm fibre (OPF) reinforced polymer composites and it was reported that the roughing of the fibre possibly enhanced mechanical properties such as increased interfacial bonding between the fibre and the matrix. Sanadi et al. (2001) has reported that the primary disadvantage of natural fibres reinforced composite is the poor interfacial adhesion due to the hydrophilic profile of cellulose. In fact, all natural fibres are hydrophilic in nature as stated by Mohanty et al. (2000) and Leman (2011) in his study had confirmed that the hydrophilic cellulose is usually incompatible with a hydrophobic matrix material used in the fabrication of fibre-matrix composites or fibre reinforced composite materials. Therefore, this phenomenon initiates to low fibre dispersion and weak fibre-matrix interfacial adhesion and then an effect on misalignment of fibres. Figure 4 depicts the misalignment of fibres that has been discussed by Suriani et al. (2012). These defects occur because of weak interfacial between fibres and epoxy (matrix) and from non-uniform dispersion of fibre/epoxy as has been studied previously by Leman (2011).

Therefore, in the article of the critical factors on manufacturing processes of natural fibre composites Hoa et al. (2012) reported that due to weak interfacial adhesion, pull-out fibres were diluted the matrix content and act as flaws or defects which reduce the effective cross sectional area and, finally influenced poor strength behavior. Moreover, the formation of pull-out fibres agglomeration, due to the inter-fibre hydrogen bonding which prevents thorough poor dispersion of fibres during the manufacturing process and thus decreased the strength behavior and indirectly affects the appearance of the composites (Matuana et al. 2001; Kazayawoko 1999).

7 Incomplete Cure of Fibres-Matrix

The lower performance properties in the final product of natural fibre composite may be initiated by resin failure and numerous resin failures are associated with an incomplete cure or pre-mature cure of fibre-matrix or areas where resin has poorly wetted

the fibres. Gonzaleza et al. (1999) used impregnation method to fabricate the natural fibre composites. It was claimed that natural fibre always experiences poor wetted areas and failed to be wetted completely by following the general manufacturing processes as they are not designed for wetting fibre with tight-packing fibrils. This is due to the viscosity of polymers are normally too high for impregnation process. Alternatively, better fibre pre-impregnation improves a better fibre wetting and thus enhances the mechanical interlocking between fibre- matrices. A coupling agent or compatibilizer used in the surface modifications of fibres for effective stress transfer across the interface were explored. A coupling agent is a chemical substance which is able to react chemically on the both natural fibre and the polymer matrix during processing to promote a stronger bond at the interface as bridges in order to enhance the mechanical properties of resultant composites. Besides, the compatibilizer is a kind of polymeric interfacial agent or polymers with functional groups that graft onto the chain of polymers. Also, as reported by Matuana et al. (2001) the characteristics of the fibre surface to which the coupling agent is adhered is strongly influences the nature of bond formed between a specific coupling agent and fibres. The coupling agents are tetrafunctional organometallic compounds which are commonly known as silane, zirconate, or titanate coupling agents and nowadays, most of the researchers used a coupling agent or compatibilizer to improve the incomplete cure of fibres-matrix.

7.1 Distribution of Curing Agents

As to achieve the optimum curing, good development of mechanical properties and high performance of final product, the curing agents or hardener in a matrix composite needed to be uniformly distributed. The embodiment of the curing agents into a matrix resin commit on the physical mixing of two viscous liquids, problems can sometimes occur due to uneven distribution of the curing agent to fibre-matrices. Apart from incomplete curing, globules of curing agent's rich material can also contribute to failure sites.

7.2 Premature Curing

In a method used for a proper reconstruction of a polymer resin, it is necessary to apply a temperature low than the gel point for curing the polymer; otherwise the cross-linking molecules will not empower sufficient movement to migrate to the reactive sites of the polymer because of the increased viscosity of the resin system. Additionally, if the polymer resin cures prematurely or incompletely at the incorrect curing cycle, insufficient time is available for trapped gases to escape and for flow fronts to sufficiently meld. As a result, cosmetic defects or blisters and weak weld lines can result, which can influence the mechanical properties and may promote failure. Also,

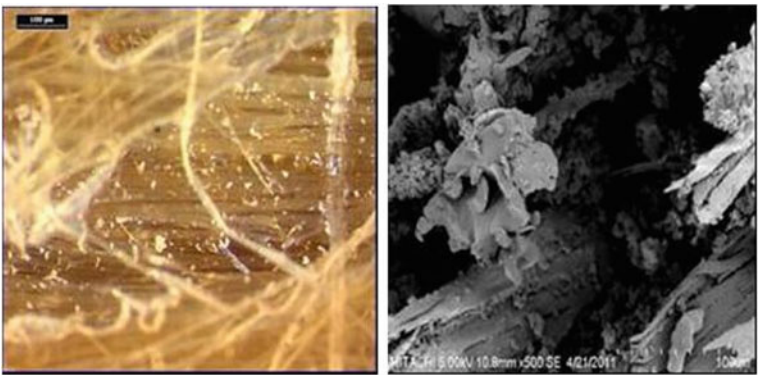

Fig. 5 Poor wetted resin (Suriani et al. 2012)

surface defects in polymer resins can be associated with premature gelation of the resin. As for example, the use of a phenolic resin was generating inadequate parts or defects that were exhibiting hard surface imperfections or fallibility. In this case, the surface imperfections were attributed to the resin reaching gelation before the cavity was filled. Figure 5 depicts the incomplete cure fibre-matrix or poor wetted resin as published by Suriani et al. (2012).

8 Conclusion

Previously most of the research has been performed to study the potential use of natural fibre for various engineering applications and this chapter has specifically discussed the most widely studied on the manufacturing defects in natural fibre reinforced composites materials. The manufacturing of natural fibre reinforced composite materials or biocomposite has been extensively researched and employed in a variety methods and technique in a many applications and determination of manufacturing defects has been significantly influenced and played an important role for a various industries for developing high quality of natural fibres reinforced composite materials or biocomposite materials and simultaneously enhanced mechanical properties behaviour and final product performances.

References

Bascom WD, Bitner JL, Moulton RJ, Siebert AR (1980) Composites 11(1):9–18
Campbell FC (2010) Structural composite materials. ASM International, Materials Park, Ohio
Dewimille B, Bunsell AR (1983) Composites 4(1):35–40

Dong CS, Tsai TC (2010) Formation of resin-rich zones in composites processing. Advan Mater Res 123–125:543–546

Faruk O, Bledzki AK, Fink H-P, Sain M (2012) Biocomposites reinforced with natural fibers: 2000–2010. Prog Polym Sci 37:1552–1596

Gonzaleza AV, Cervantes-Uca JM, Olayob R (1999) Effect of fiber surface treatment on the fiber–matrix bond strength of natural fiber reinforced composites. Compos Part B 30:309–320

Hoa M, Wanga H, Leeb J-H, Hoc C-K, Laua K-T, Lenge J, Hui D (2012) Critical factors on manufacturing processes of natural fibre composites. Compos Part B: Eng 43(8):3549–3562

Judd NCW, Wright WW (Jan/Feb 1978) Voids and their effects on the mechanical properties of composites—an appraisal. SAMPE J 14(1):10–14

Kazayawoko M (1999) Surface modification and adhesion mechanisms in wood fiber-polypropylene composites. J Mater Sci 34:6189–6199

Keener TJ, Stuart RK (2004) Maleated coupling agents for natural fibre composites. Compos A 35:357–362

Khalina A, Jalaludin H, Ansell MP, Khairul Zaman MD, Janius R, Nor Azowa I (2009) Mechanical and rheological properties of injection moulded short oil palm fibre reinforced polymer composites. In: Sapuan MS (ed) Research on natural fibre reinforced polymer composites. Universiti Putra Malaysia Press, Serdang, pp 109–125

Lapique F, Redford K (2002) Intl Adhesion Adhesives 22(4):337–346

Leman Z (2011) Mechanical properties of sugar palm fibre-reinforced epoxy composites. Doctoral Dissertation, Universiti Putra Malaysia, Serdang, Malaysia

Matuana LM, Balatinecz JJ, Sodhi RNS, Park CB (2001) Surface characterization of esterified cellulosic fibers by XPS and FTIR Spectroscopy. Wood Sci Technol 35:191–201

Mohanty AK, Khan MA, Hinrichsen G (2000) Compos Part A 31:143–150

Roychowdhury S, Gillespie JW, Advani SG (1992) Void formation and growth in thermoplastic processing. 3rd conference on computer aided design in composite material technology-CADCOMP 1992. Computational Mechanics Publisher, Southampton, England, pp 89–107

Saheb DN, Jog JP (1999) Natural fiber polymer composites: a review. Adv Polym Technol 18(4):351–363

Sanadi AR, Caufield DF, Kovacsvolgyi G, Destree B (2001) High fiber-low matrix composites: kenaf fibre/polypropylene. Paper presented at the meeting of the 6th international conference on wood fibre-plastic composites, Madison

Scheirs J (2000) Compositional and failure analysis. A practical approach. Wiley, Chichester

Suriani MJ, Ali A, Khalina A, Sapuan SM, Abdullah S (2012) Detection of defects in kenaf/epoxy using infrared thermal imaging technique. Procedia Chem 4:172–178

Talreja R (2015) Manufacturing defects in composites and their effects on performance. In: Irving PE, Soutis C (eds) Polymer composites in the aerospace industry. Woodhead Publishing-Elsevier, Cambridge, United Kingdom, pp 99–113

Carbon-Based Materials Reinforced Ultrahigh Molecular Weight Polyethylene and Biocomposites

Shahira Liza and Nur Hidayah Shahemi

Abstract The chapter represents a comprehensive review of inorganic particles reinforced the ultra-high molecular weight polyethylene (UHMWPE) to promotes better operational properties as compared to pure UHMWPE for orthopaedic applications. A strong interfacial adhesion between UHMWPE matrix-based particle filler is believed to be the major factor influencing the UHMWPE based composite material's properties outcome. Hence, graphene oxide and graphite were reviewed as the potential reinforcement particles due to its special additional properties; biocompatible, high thermal conductivity, hydrophilic behavior and could act as a nucleating agent, which rarely found in other type of materials in current market. UHMWPE based carbon-based reinforced composite with optimum processing parameters and wt% shows improved mechanical properties. UHMWPE reinforced cabon-based particle exhibited remarkable mechanical properties which have the potential to be the alternative materials for joint orthopaedic applications.

Keywords Ultra high molecular weight polyethylene · Composite materials · Graphite · Graphene oxide · Biomedical

1 Introduction

Polymers have become a commended biomaterial for some applications due to its general properties such as chemical inertness, light-weighted, self-lubricated surface, biocompatible and many more. There are several types of polymer available as biomaterials such as PMMA, PEEK, PTFE, PET, UHMWPE (Banoriya et al. 2017). Different types of polymer are best used on particular applications depending on their characteristics and properties. Neat UHMWPE has been widely used as the joint

S. Liza (✉) · N. H. Shahemi
TriPreM I-Kohza, Department of Mechanical Precision Engineering, Malaysia-Japan, International Institute Technology, Universiti Teknologi Malaysia, 54100 Kuala Lumpur, Malaysia
e-mail: shahiraliza@utm.my

N. H. Shahemi
e-mail: nurhidayahshahemi@gmail.com

M. T. Hameed Sultan et al. (eds.), *Biocomposite Materials*, Composites Science and Technology, https://doi.org/10.1007/978-981-33-4091-6_8

bearing implant. It was initially recognized as biomaterial in 1962 when Charnley has clinically verified on its biocompatibility and high wear resistivity (Kurtz 2009).

As a joint implant component, UHMWPE have a notable chemical inertness, low coefficient of friction, high mechanical properties and wear resistance compares to metal and ceramic materials. It has been incorporating as bearing material in artificial joints for the past 50 years. Currently, there are at least two million joint replacements manufactured annually, which majorly involving UHMWPE as part of the joint replacement (Kurtz 2009). However, due to high dynamic loading, heavy articulating activities, oxidation reaction (Laska et al. 2016), and macromolecules interactions in vivo (Sawae et al. 2008), results wear particles shed off from UHWMPE, limits its lifespan and increasing the tendency of adverse reaction with adjacent tissues that causes osteolytic reaction and aseptic loosening (Shahemi et al. 2018). There are numerous studies were done to improve the durability of UHMWPE especially for biomedical application such as by gamma ray irradiation (Liza et al. 2013), vitamin E infusion (Melk and Emami 2018), surface modifications (Chukov et al. 2015) and, composite fabrication (Chukov et al. 2015; Chukov et al. 2014; Wang et al. 2017; Chang et al. 2000). The improvement methods by gamma ray irradiation and vitamin E infusion have been widely used and commercialized. It is by far capable to stretch the UHMWPE lifespan up to 15-20 years. Meanwhile, research studies in UHMWPE based composite is still in infancy stage and yet to be commercialized, yet, interestingly, UHMWPE composites have high potential to improve its durability due to multiple possibilities of unique properties results from the incorporations of other materials with outstanding properties.

Therefore, in order to overcome the limitation and enhancing the properties of neat UHMWPE properties, UHMWPE matrix composite (PMC) is proposed. Other than a standard from ISO 5834-5:2005, which require UHMWPE as the only polymeric materials to be prepared as joint bearing implant component (Maksimkin et al. 2012), there are also several documented studies proven that UHMWPE composite have shown improvement of wear resistance (Xiong et al. 2006; Anderson et al. 2002). Hence, UHMWPE matrix composite is high likely best to be used as the joint implant component.

However, the material properties of UHMWPE composite will only be improved under several aspects. Based on the previous studies of UHMWPE based composites, it stated that the composite material's effectiveness relies on optimum filler composition, particle size and processing parameter (Kurtz 2009). These conditions will likely influence strong interfacial bonding between filler-UHMWPE matrix and well dispersion of particles (Kurtz 2009) which beneficial for stress and load transferability. In addition to that, the surface interaction between macromolecules in lubricants with UHMWPE composite has to be minimize, which believed can be done by altering the surface affinity of UHMWPE composite. An ultimate improvement of UHMWPE composite materials is expected with the complements of these characteristics; relatively good interaction between matrix-filler, and high surface affinity.

2 UHMWPE Biocomposites for Joint Replacement

In the 1970s, the first UHMWPE composite was introduced for the orthopedic implant that commercially known as Poly II. The polymer was reinforced with carbon fiber (CFR-UHMWPE) and has displayed a catastrophic short-term clinical failure (Kurtz 2009) which eventually leads to Poly II abandonment and bad perception of the composite materials as the biomaterial has long remained. The failure of CFR-UHMWPE was unexpected due to the excellent wear properties acquired from the in vitro study. The main cause of the failure was analyzed to be from the poor compatibility between the UHMWPE and CFR. However, with the evolution of composite technology and processing nowadays, UHMWPE composite materials can be found in industrial, military and consumer applications (Puértolas and Kurtz 2014). The current commercial success of UHMWPE composite materials with a wide range of filler has once more incite the curiosity and motivation to a lot of researchers of making this polymer into a composite biomaterials possible.

Particles were mainly reinforced in the UHMWPE to increase wear resistance, some of which have been reported in the literature. Hence, most of the studies found were introducing hard particles as fillers. Dangsheng (2005) found in his study that the reinforcement of carbon fiber (CF) has improved the hardness and wear resistance with increased CF content. However, this study has employed a unidirectional sliding test as the work designed allegedly to screen CF content in the composites. Unfortunately, the data set from the unidirectional sliding test could not be indicative of clinical wear performance as it does not represent the wear mechanism in the hip joint application. Despite the reduction of wear reported for CF/UHMWPE (Dangsheng 2005), the worn surface was dominated with abrasive wear features indicated the plowing effect has involved. Moreover, the drawing out of CF was also remarked on the study, suggested poor compatibility with the polyethylene matrix. In addition, Chukov et al. (2015) stated in their study that the compatibility of CF and UHMWPE can be improved by surface modification using thermal (Stepashkin et al. 2014). The enhanced interfacial interaction has evidently increased the wear properties by reinforcing at least 12 wt% of the CF. However, chipping of the CF/UHMWPE can be easily happened due to the tendency of CF to get agglomerated. The risk of exposing the composite polymer to thermal oxidation might also have an impact on oxidative degradation of the material although not being further discussed in the study.

Other than CF, many previous works have utilized different types of fillers into the UHMWPE matrix. Many authors reported that the mechanical and wear properties can be improved by introducing reinforced ceramics such as zirconia (Plumlee and Schwartz 2009; Salari et al. 2019), zeolite (Chang et al. 2013), TiO_2 (Ozsoy et al. 2015), wollastonite (Zabolotnov et al. 2018). Although wear and mechanical properties have evidently enhanced, the incorporation of ceramic fillers has produced very hard composite materials compared to their respective metal counterface (Brockett et al. 2016; Chang et al. 2013; Plumlee and Schwartz 2009). Hence, increasing the risk of metal wear. The metal wear debris is highly toxic and can cause a direct adverse effect on human health (Delaunay et al. 2010; Neuwirth et al. 2018).

On the other hand, the addition of naturally found biomaterials such as hydroxyapatite (HA) and natural coral (NC) have also been studied (Gupta et al. 2012; Maksimkin et al. 2012; Tripathi and Basu 2012). These fillers were reported to be selected due to their biocompatibility as they were known to have almost the same composition as the human bone (Ge et al. 2009). The friendly behavior towards the human bone system thus suggested that these materials can be gradually absorbed and progressively replaced by newly formed bone (Ge et al. 2009). The reinforcement of HA and NC has proven to improve the mechanical and wear properties with an increasing amount of filler percentage up to 20–40 wt% (Gupta et al. 2012; Maksimkin et al. 2012; Tripathi and Basu 2012). Unfortunately, the plowing and fatigue fracture wear features found on the composite surface suggested that the removal of brittle HA (Gupta et al. 2012; Maksimkin et al. 2012) and NC (Ge et al. 2009) has led these fillers to become the third body abrasive wear. Moreover, the fatigue fracture manifested on wear surface suggested due to the incompatibility between the UHMWPE and HA during the consolidation process (Wang et al. 2009). Therefore, it was noted that these filler reinforcement studies indicated that although the improvement of wear and mechanical properties can be obtained, some material properties have to be compromised.

Due to this reason, several researchers have attempted in maintaining the excellent attributed properties of the polyethylene while increasing its wear resistivity by introducing two type of fillers to complement the compromised properties of the other filler (Chukov et al. 2015; Salari et al. 2019; Wang et al. 2017). Hence, hybrid composite materials were introduced in this field. The fillers were frequently selected from the combination between the hard particles and relatively soft particles. Wang et al. (2017) reported the introduction of reinforcing carbon fiber (CF) and glass fiber (GF) into UHMWPE in their study. CF was selected due to their high tensile strength and elastic modulus; and have evidently displayed improvement of wear and mechanical properties in previous studies (Chukov et al. 2015).

Meanwhile, GF was selected due to its high fracture toughness. The UHMWPE/GF/CF composite sample was reported to possess higher hardness compared to the metal counterface proven by the transferred iron oxide film onto the composite surface. The tightly contained fiber fillers within the UHMWPE matrix has consequently exhibited bulges on the hybrid composite's surface. The resultant combination of the two fillers had shown a significant increment of wear properties due to the contact surface on the hard GF filler with the metal counterface.

Unfortunately, relatively higher toughness and mechanical properties of the UHMWPE/GF/CF sample have produced a large amount of tiny metal debris on the worn surface which plowed through the composite surface and formed high abrasion wear in a long term duration. Meanwhile, the existence of cytotoxic metal debris would also directly affect body system.

On the other hand, Salari et al. (2019) employed two different fillers such as HA and zirconia in their study. HA was used for biocompatibility purpose whereas the brittleness of the HA filler was expected to be supported by zirconia's high mechanical properties and wear resistivity. The hybrid composite material, UHMWPE/HAp-zirconia with amount percentage of 10 wt% and 10 wt%, respectively, has also

proven to reduce the stress exerted by the metal counterface (Salari et al. 2019). As a result, its wear rate has reduced by 61%. The wear properties of UHMWPE/HAp-zirconia have displayed even higher increment compared when using HA as a single filler (Gupta et al. 2012; Wang et al. 2009).

Therefore, it can be indicated that the shortcoming of HA filler can be compensated with the zirconia fillers in the hybridized composite materials. However, from the previous study of UHMWPE/zirconia composite, stated the high mechanical strength of the material has inflicted the wear debris production from the metal counterface. Unfortunately, there was no such discussion involving the metal counterface's wear properties has involved in the study (Salari et al. 2019). Hence, the adverse effect of zirconia incorporation to metal wear debris could not be concluded to be simply resolved by introducing more than one filler into the polyethylene matrix.

Ultimately, it can be concluded that the reinforcement of hard fillers can increase the wear properties of the composite, albeit, higher shear stress would be applied on the metal counterface results metal wear debris formation. The metal wear debris formation would trigger a greater hazardous effect on the body system compared to the UHMWPE wear debris. Therefore, the wear resistivity of the UHMWPE was targeted to improve at a shy value lower than the metal but high enough to resist the materials from getting removed. In order to achieve that, many researchers have diverted their interests into exploring the micro-size and nano-size materials as a filler (Pang et al. 2018; Suñer and Emami 2014). Their potential improved performance may be brought by their larger interface, resulting in more effective load transfer between the matrix and filler interface (Puértolas and Kurtz 2014). Consequently, it increased the subsurface shear strength, thus, improved the wear resistivity of the UHMWPE composites and impeding abrasive properties towards the metal counterface.

3 Graphitic Nanomaterials as Filler

The usage of nanomaterials in the medical field has developed rapidly in bringing novel opportunities for improved biosensors, drug delivery carriers, biomaterials, and biosafety. Carbon nanomaterials possess a unique 0D, 1D, 2D structure with unique mechanical, physical, chemical and thermal properties that are ready to be extensively explored for a wide range especially in medical applications. These excellent properties of the materials are found to be applicable in different areas such as filler material in the implant medical component. Carbon nanomaterials which also known as graphitic materials are categorized in a different type of molecular structure included graphite, graphene, carbon nanotube and other carbon-activated materials as shown in Fig. 1.

The graphitic materials possessed various functional properties such as high aspect ratio, high mechanical strength, low coefficient of friction, high thermal conductivity and hydrophilic (Kim et al. 2010; Liao et al. 2018; Zabolotnov et al. 2018) has lead for a promising filler materials for UHMWPE composite. However, due to its ability

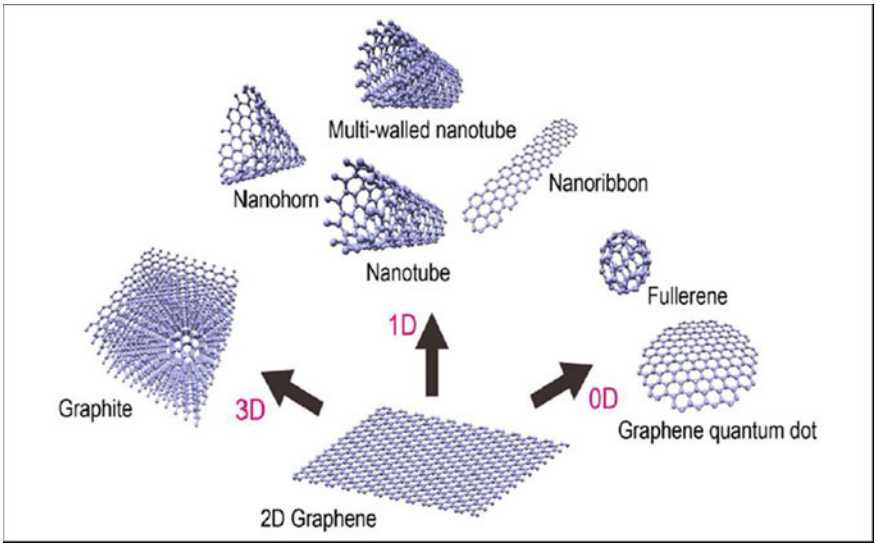

Fig. 1 Graphitic materials in different geometry and functional properties. Reproduced from (Nakano et al. 2018) with permission of Taylor & Francis

to transfer energy level state from sp^1, sp^2, sp^3 at certain conditions (Anwar et al. 2016); the graphitic materials is considered to be an active materials and can be either challenging or advantageous materials to work with (Anwar et al. 2016; Tahir et al. 2018), especially in enhancing the mechanical properties. This is because the final properties of the composite would be unpredictable as the graphitic materials have the propensity to alternate into a different type of bonding after the mixing. As reported by Tahir et al. the different bonding after the mixing can change the hardness and stiffness value which consequently may be related to enhancement or weakening of mechanical properties (Tahir et al. 2018). However, according to Callister in their book (Callister and Rethwisch 2018), due to the symmetrical hexagonal geometry of graphitic materials likes carbon nanotube and graphene; these graphitic materials would likely to exhibit high chemical and structural stability. Thus, it would not be possible for the materials to change their bonding type when incorporated into the polymer matrix in general.

Callister's statement was supported by the previous works that displayed that the reinforcement of the graphitic materials didn't negatively impact the mechanical and wear properties of the composite. For example, Kumar et al. (2015) have reported that the incorporation of only 0.2 wt% multi-walled carbon nanotube (MWCNT) has a significant influence of reducing the wear volume of UHMWPE by 34%. The same pattern of finding was also reported by Sreekanth and Kanagaraj (2015) that the incorporation of 2 wt% multi-walled carbon nanotube (MWCNT) has extensively increased the UHMWPE's mechanical properties by 89%. The severity of wear features on the composite surface was displayed to be reduced as compared

to the neat UHMWPE (Sreekanth and Kanagaraj 2015). Although the wear resistance has increased with the incorporation of a higher amount of MWCNTs, it was reported that the fracture toughness has significantly reduced with the addition of more than 1 wt% (Melk and Emami 2018). That can be indicative of creep deformation reduction. In addition to that, there were also works reported that the incorporation of carbon nanotubes has reduced the ductility and the toughness even lower than the neat UHMWPE (Puértolas and Kurtz 2014). The cause was studied and the drawbacks were determined to be associated with the curviness factor (shape) of the MWCNTs (Puértolas and Kurtz 2014) which segregate the composite structure during solidification, thus weakens the interface between the matrix-MWCNTs granules.

Hence, following the composite fabrication process, there are several routes have been assessed to cater to the problem such as by introducing gamma irradiation (Sreekanth and Kanagaraj 2015) or chemical treatment (Montagna et al. 2017). However, the additional processing steps consuming longer time and relatively larger production costs. Meanwhile, other researchers have started exploring different options to utilize from another type of graphitic materials such as graphite, and graphene-derivatives.

Given that the intrinsic strength and high elastic modulus of graphene are close to 130 GPa and 1 TPa respectively (Anwar et al. 2016), the incorporation of graphene in the UHMWPE was expected to significantly increase the polyethylene's mechanical properties. Since pure graphene could hardly form any sort of bonding with the non-polar polymer matrix, hence, it was treated by various treatment methods. Depending on the methods of treatment that the graphene-derivatives material was produced, it would affect their respective properties. There are at least three types of graphene-derivatives material that have been explored which included reduced graphene oxide (RGO), graphene nanoplatelet (GNP) and graphene nanosheet (GNS). RGO was obtained from chemical exfoliation of graphene and GNP or GNS were obtained from electrostatic spraying technique (Baena et al. 2015).

The introduction of RGO reinforcements into UHMWPE was recorded to reduce the mechanical properties even lower than the neat UHMWPE. The elastic modulus and yield strength were reduced by ranging from 20% to 30% which associated with the reduction of elongation at break (Puértolas and Kurtz 2014). Moreover, although the viscoelasticity and crystallinity measured were no different than the neat UHMWPE (Wieme et al. 2019), the smooth shifting of α-relaxation was detected when the temperature was applied as an indication of slight increment of creep inhibition. On the other hand, Baena et al. (2015) stated in their study that the incorporation of 1.0 wt% GNP displayed an improvement of wear properties by 4.5 times compared to neat UHMWPE. Moreover, the elastic modulus and yield stress were observed to be increased by 125% and 100%, respectively. At the same time, however, the maximum tensile strength and fracture toughness which attained at 0.1 wt% GNP, deteriorated when 1.0 wt% GNP was used. Meanwhile, similar behavior was obtained when GNS was introduced in the UHMWPE. The maximum tensile stress was achieved when 0.25 wt% GNS was reinforced and deteriorated beyond that amount (Montagna et al. 2017).

Based on these findings (Montagna et al. 2017; Suñer and Emami 2014; Zabolotnov et al. 2018) it can be summed up that each graphene-derivatives have potential in improving only some part of mechanical properties such as elastic modulus at an optimum wt% while jeopardizing other mechanical properties like fracture toughness or vice versa. This complication primarily arises due to the high surface area of nanomaterials which have high surface tension, hence tend to repel from interacting with the polymer matrix, and strongly attracted with the common nanoparticles result in agglomeration (Anwar et al. 2016; Ashraf et al. 2018; Yi and Shen 2015).

Consequently, the nanoparticles would be poorly dispersed causes localized stress point, thus, initiate micro-cracks (Ashraf et al. 2018). Although only a small amount of nanoparticles would normally be used as filler loading due to their high surface area to volume ratio, however, the complication of nanoparticle agglomeration would negatively impact the UHMWPE nanocomposite properties (Ashraf et al. 2018). Therefore, in this chapter, the authors suggested pursuing a relatively large size of filler than the nanoparticles; graphite-derivative materials. This approach perhaps could reduce the surface tension between the matrix-filler hence improving the adhesion between them.

Graphite is best known to provide a low coefficient of friction in a humid environment but fails to give low friction and high wear in inert, dry or vacuum environment (Malik et al. 2019). The reason for this behavior is due to the intercalation of water molecules in between the graphite sheets allowing easy shearing of graphite, thus provide lower friction. Additionally, previous tribological studies using graphite flakes have indicated the formation of graphite scrolls at the tribological interface (Yi and Shen 2015). These scrolls are favorable for decreasing the surface energy (Malik et al. 2019; Yi and Shen 2015) and reducing friction in the sliding interfaces. These properties of graphite are high likely favorable for in vivo applications since the graphite will be in a conducive condition where the material will be exposed in a physiological environment, hence, it can be performed efficiently.

Given that graphite and graphite-derivative materials size could be up to 100 μm (Yi and Shen 2015), the surface area to volume ratio was anticipated to be relatively larger compared to graphene nanoparticles. Wang et al. (2018) described that using the untreated graphite can attribute to the resistance by the pressure between the thermoplastic matrix and the graphite filler. The hardness was reported to decrease under the poorly combined graphite and polyethylene. Moreover, due to the anisotropic behavior of graphite, the load transfer capacity of the interface was greatly diminished (Wang et al. 2018).

However, the dispersion of the graphite materials in flakes form (treated) was claimed to be better due to its rough surface aided strong mechanical interlocking to the UHMWPE matrix (Pang et al. 2018). In addition to that, graphite has the high elastic modulus and tensile strength with a stiffness similar to graphene, and so opening the same advantage in regards to functional properties. Although graphite shows promising potentials yet vast to be studied, the findings are rather unpredictable when mixing with another element as composite. The addition of different filler percentages into composites gives different bonding and dimensional stability (Digas

2005). Thus, different bonding gives different hardness and stiffness value. This is due to its weak interlayer bonding which is bonded by Van der Waal forces. On the bright side, as a result of anisotropy, the mono graphene layers in graphite structure can slide with respect to one another quite easily, thus making graphite a good solid lubricant.

As reported by (Sánchez-Sánchez et al. 2018). the incorporation of 1 wt% of graphite has shown an increment of the UHMWPE composite's tensile strength by 8.8%. The exfoliation of the graphite surface has also described assisting in dispersion and enhanced the interfacial adhesion between graphite and UHMWPE matrix (Sánchez-Sánchez et al. 2018). Consequently, the incorporation of graphite into UHMWPE has significantly improved the composite's mechanical properties. The improvement of thermal properties was also recorded to be higher than the neat UHMWPE. However, the increasing amount of graphite in the UHMWPE's amorphous region hindered the mobilization of polyethylene chains during hot pressing. Thus, it reduced the crystallinity degree of the UHMWPE/graphite composite (Sánchez-Sánchez et al. 2018).

Furthermore, other than relying on the coarse surface of graphite to ensure better adhesion and dispersion in UHMWPE matrix (Sánchez-Sánchez et al. 2018), an effective bonding between polyethylene and graphite can be manipulated by altering the surface characteristic and chemical compatibility (Baena et al. 2015). One of the methods is by treating the graphite with a strong oxidizer into graphene oxide (GO). This technique allows the graphite to be functionalized with a hydroxyl group and the epoxide group (Melk and Emami 2018). Previous studies introducing GO as the filler material described that the UHMWPE composite's hardness was increased with increasing GO amount from 0.1 wt% to 1.0 wt% linearly (Puértolas and Kurtz 2014).

The same finding was also reported by Suñer and Emami (2014), when 2 wt% of GO was incorporated into UHMWPE. However, Young's modulus and yield stress have remained constant with the neat UHMWPE. Meanwhile, the toughness of the UHMWPE composite was deteriorated compared to neat UHMWPE (Puértolas and Kurtz 2014). On the contrary, Melk and Emami (2018) described in their study that the addition of GO into UHMWPE has no significant effect on the hardness and so does the mechanical properties altogether. Yet, the incorporation of GO has evidently enhanced the thermal stability of the UHMWPE composite which would have high resistance of plastic deformation due to thermal elevation during sliding activities (Melk and Emami 2018). Unfortunately, the GO reinforcement has led to a reduction of fracture toughness due to the presence of hydroxyl functional groups (OH). In their study (Melk and Emami 2018), it was found that there was a strong correlation between the mechanical behavior of GO and the ratio between epoxide and hydroxyl functional groups contained in the GO. Epoxide-rich GO favors ductility fracture allowing GO to absorb energy and prevent failure through crack initiation (Melk and Emami 2018), whereas, hydroxyl-rich GO favors brittle fracture which was revealed by the coarse fracture morphology and GO pulled out from the polyethylene matrix. Therefore, from the analysis of previous studies, it was noted that the ability of the filler to diffuse with the polyethylene matrix is very important for the improvement of

mechanical and wear properties than neat UHMWPE. Filler's surface characteristics (flakes, exfoliated), size (relatively large than nanoparticles) and functional groups could be utilized to enhance the adhesion bonding between the matrix-filler.

Graphite flakes (GF) were chosen as the filler due to its flaky/exfoliated surface that can be served as the mechanical binding structure with the UHMWPE matrix. Moreover, the relatively large size of GF about 50 μm resulted in lower surface area to volume ratio, minimized the tension between the graphite particles to get agglomerated (Ashraf et al. 2018). On the other hand, GO which recorded to have uneven wrinkles and rough surface also have the same mechanical binding capabilities with the UHMWPE matrix as the GF. The size of GO particles which was about the same as GF (10–30 μm), was presumed to have the same effect of surface tension's mitigation and reduction of agglomeration effect (Pang et al. 2018).

Last but not least, the functional oxygenated groups combined in the GO were relied upon to increase the ductility and mechanical properties as it is easier to be dispersed into UHMWPE matrix and form intercalated composites with polar molecules through the strong interaction (Pang et al. 2018). In conclusion, graphitic materials were chosen as the filler reinforcement in this study. Henceforth, by ensuring the formation of adhesive interfacial matrix-fillers interaction, the effect of reinforcing the graphite-derivatives material into the UHMWPE would be compared and contrast in terms of mechanical, and wear properties.

4 Biomaterial Properties of Graphite Flakes and Graphene Oxide

As described in the previous subchapter, the potential of graphite flakes (GF) and graphene oxide (GO) to enhance the mechanical properties was expected, hence the improvement of wear properties can be anticipated. However, other than being influenced by the mechanical properties of the UHMWPE composite, wear could also be initiated from several other factors such as the interaction of UHMWPE with the synovial fluid's constituents (Murakami et al. 2007) and elevated thermal during sliding activities at the surface contacting load (Burger et al. 2016). Hence, GF and GO were strongly proposed as the reinforcement particles due to its special additional properties; biocompatible, high thermal conductivity, hydrophilic behavior and could act as a nucleating agent, which rarely found in another type of materials in the current market. These have driven us to explore the feasibility of GF and GO reinforced UHMWPE composites for enhanced wear properties as a new type of joint prosthesis bearing material.

4.1 Biocompatibility

Due to the application of the developed UHMWPE composite in this research would be used as the hip implant component. Therefore, the primary concern of the applicability in the human body is the materials' biocompatibility. The risk of wear debris formation during the sliding activities towards the human body was hoping to be minimized. Recently, the usage of carbon-based materials in medical research has been increased such as for photothermal therapy, diagnosis (Rahmati and Mozafari 2018) and drug delivery (Ray and Jana 2017) due to their unique properties. However, the application of the graphene materials in the biological sectors remain infancy as it shows potential toxicity in biological systems ranging from prokaryotes to eukaryotes, depending on its layer number, lateral size, purity, dose, surface chemistry and hydrophilicity (Merola and Affatato 2019; Ray and Jana 2017), which is associated to their respective synthesis procedure. High residual contaminants which normally caused by the usage of toxic surfactants are frequently caused a higher risk of toxicity in biological cells. Thus, the biocompatibility properties of the graphitic materials may be compromised. Biocompatibility refers to the ability of materials to interact with cells, tissues without causing harmful effects. Considering the application of the fabricated composite materials in this study is for an orthopedic implant, hence, biocompatibility is a very important factor to be considered. Unfortunately, the biocompatibility of graphitic materials is uncertain as it often contradictory according to the previous literature (Liao et al. 2018; Gurunathan and Kim 2016). For instance, Liao et al. (2018) stated that GO can interact with the cell membrane of swine spermatozoa, and due to strong forces dragging from the graphene sheets, resulting in membrane damage. In addition to that, (Liao et al. 2018) also indicate that the graphitic materials can also enter cytoplasm due to their small size and sharp edges. Upon penetrating the cells, the material can induce toxicity through the creation of reactive oxygen species (ROS).

On the contrary, according to (Gurunathan and Kim 2016), the cytotoxicity of the graphitic materials is mainly due to the surfactant's remnants during the synthesizing process. Hence, graphitic materials' cytotoxicity can be limited to a low extent by preparing the materials from the green synthesis route. Furthermore, the biocompatibility of the graphitic materials can also be minimized by dispersing them in polymers matrix to form polymer composites (Liao et al. 2018). Since the graphitic materials will be bounded and immobilized in the polymer matrix, there would be no direct interaction with the adjacent cells or tissues, thus minimizing the risk of toxicity.

Moreover, the polymer matrix can act as a seal as it encapsulates the sharp edges of the carbon-based materials, preventing their penetration into the cytoplasm. Therefore, it can be summarized that the biocompatibility of graphitic materials is generally low due to their adverse response with the adjacent cells and tissues resulting in cellular damage. Yet, the cytotoxicity of the carbon-based materials can be lowered depending on their synthesizing process or by dispersing them in

the polymer matrix as the reinforcement filler (Liao et al. 2018; Gurunathan and Kim 2016). This approach opens new opportunities in utilizing graphite derivatives materials, especially for biomedical applications.

4.2 Thermal Conductivity

In joint articulating activities of two bearing surfaces, heat and temperature are commonly involved. These two fundamental concepts were distinguished by thermal energy. Thermal energy is the quantity of microscopic thermal vibrations of particles. Thermal conductivity is a measurement of the heat quantity transferred with respect to its speed and direction. The main heat transfer mode of a solid material corresponds to the transfer of a particle's vibrational energy to adjacent particles without any motion of matter. However, non-conductive materials like polymers need more time for heat conduction which allows the particles' vibrational heat transfer to occur very slowly.

This is due to its semicrystalline structure which consisted of the amorphous and crystalline region. When heat is transferred to the adjacent atom in the crystalline region, the thermal vibration can be diffused relatively faster as it oriented to a single direction due to its orderly mannered particle orientation. Meanwhile, in the amorphous region, the heat diffusion will be disordered and scattered due to the randomly mannered chains which resulted in a long time for the thermal expected to transfer. This means a longer time is required for the heat generated to be dissipated and reach the opposite face of the polymeric material. As a result, the polymer's articulating surface was easily softened and increased the adhesive wear mechanism response. The illustration is shown in Fig. 2 (Burger et al. 2016).

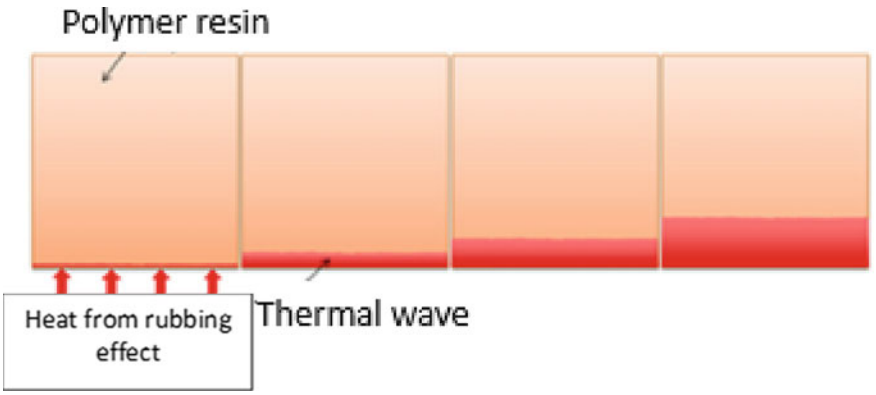

Fig. 2 Heat transfer through the non-conductive polymeric resin material. Reproduced from (Burger et al. 2016) with permission of Elsevier Inc

This has become one of the main drawbacks of maintaining the UHMWPE's durability during the sliding activities for the hip application. Plastic deformation can be spotted in many of the previous retrieval studies (Burger et al. 2007; Choudhury et al. 2018; Laska et al. 2016; Moshkovich et al. 2019) which can be correlated to the early stage of polyethylene's component failure. Naturally, the graphene-based materials that have high thermal conductivity were selected for incorporation in the UHMWPE matrix.

Carbon-based fillers such as graphite (Panin et al. 2014), carbon nanotubes (Gupta et al. 2012), graphene filler (Puértolas and Kurtz 2014), metallic fillers (Ozsoy et al. 2015) were recorded have produced an effective synergistic effect for thermal conductivity improvement. However, compared to carbon-based materials and metallic fillers, carbon nanotube has shown an exceptional increment of intrinsic ability to conduct heat due to their attribution of 3000 $Wm^{-1}K^{-1}$ thermal conductivity property (Anwar et al. 2016; Burger et al. 2016). Hence, it can naturally be deduced that a higher amount (wt%) of high thermal conductivity fillers incorporated in the polymer would result in thermal conductivity increment. Thus, increasing the heat dissipation from the articulating surface.

However, since the thermal can be easily conducted by traveling along the direction of this high thermal conductivity. The thermal conductivity speed would be greatly reduced when it's vibrated through the polymer matrix. The presence of these types of fillers would build good thermal paths. Hence, the size and aspect ratios of the high thermal conductivity fillers played an important role (Burger et al. 2016). Although graphitic and graphitic materials have the thermal conductivity range from 3000 to 5000 $Wm^{-1}K^{-1}$, its nanosize would form more interfaces, leading to high thermal resistance which was proven by the previous study by Park et al. (Burger et al. 2016).

The illustration in Fig. 3 showed the difference of heat diffusion when nanosized fillers and microfillers used as the thermal paths. Therefore, GF and GO with micro size and high thermal conductivity would be used in this study to increase the UHMWPE composite's thermal conductivity. Although, there are many previous studies (Enqvist 2013; Kumar et al. 2015; Suñer and Emami 2014) have reported on the increasing thermal conductivity after the reinforcement of the graphitic filler materials, the relation between thermal conductivity and wear mechanism is rarely discussed.

4.3 Nucleation Promoter

Nucleation is the initial process of crystal formation originated from which a small number of ions, atoms or molecules were arranged in an orderly crystalline manner. In a simpler sentence, it's a site formation in which additional particles are deposited to allow the crystal grow (Lacaze et al. 2017). A highly crystalline region in the material would reflect on its mechanical properties. For example, a metal which is

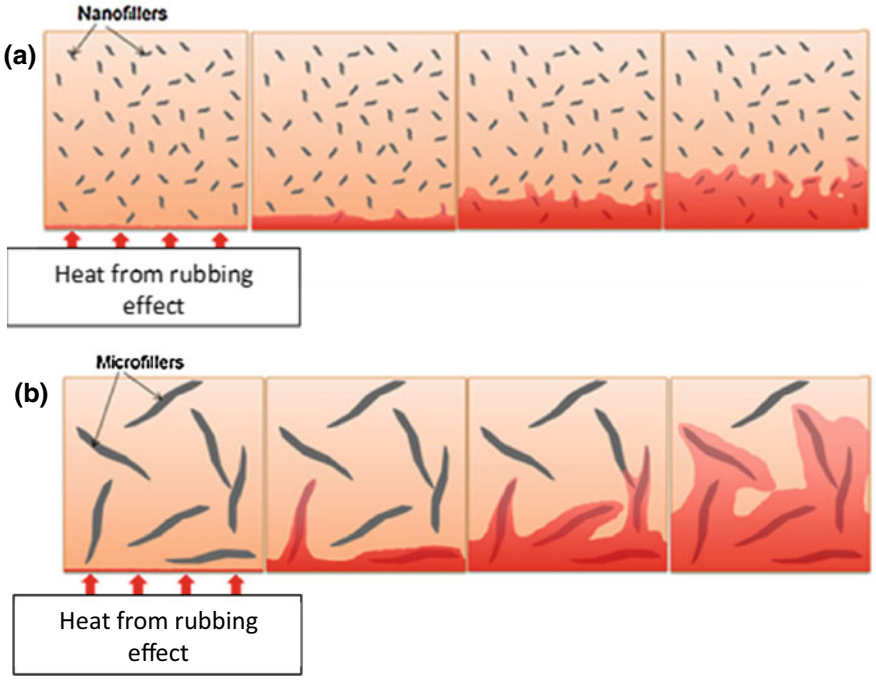

Fig. 3 Heat transfer through the non-conductive polymeric resin material when **a** nanofillers and, **b** microfillers were used. Reproduced from (Burger et al. 2016) with permission of Elsevier Inc

a crystalline material possessed better mechanical properties compared to semicrystalline materials such as a polymer. For the case of semicrystalline UHMWPE, the crystallinity percentage was attempted to be enhanced by using the irradiation of gamma radiation (Laska et al. 2016). However, at some point in the crystallinity percentage, the irradiated UHMWPE was reported to become brittle (Laska et al. 2016).

This is due to the closely packed crystalline region which restricts any molecular movement upon applied load, consequently initiated microcrack formation. The gamma radiation doses on the UHMWPE was studied to achieve the optimum crystallinity degree, thus, improving the UHMWPE mechanical properties (Maksimkin et al. 2012). However, as mentioned in the previous paragraph, the gamma radiation has an adverse effect on the UHMWPE's chemical properties, as the free radicals from the irradiation would accelerate the UHMWPE's oxidation process.

Another method of increasing the polymer's crystallinity degree is by adding a nucleation agent. According to Wieme et al. (2019), the effect of the crystallinity improvement using a nucleating agent was successfully executed without compromising other properties. Nonetheless, the addition of the nucleating agent would incur a higher cost and additional process step for UHMWPE's fabrication, which adding more reason for graphite materials to be used as filler in this study. The nucleation

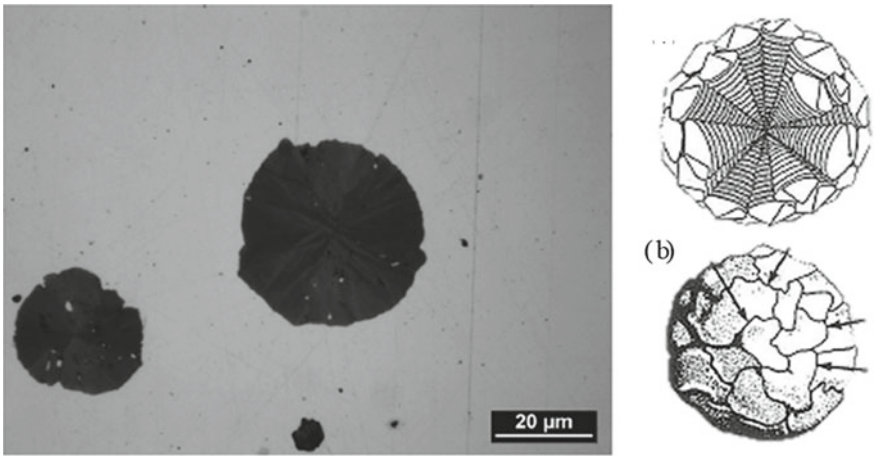

Fig. 4 Optical microscopy micrograph of spheroid showing sector emanating from the center by different type of growth as illustrated in **a** tangential growth (screw-dislocation), **b** nucleation of new layers proceed until two neighbouring interface meet (lateral growth). Reproduced from (Lacaze et al. 2017) with permission of Elsevier Inc

and growth of graphite particles have fascinated researchers since 1995 (Double and Hellawell 1995).

Graphite particle grows by 2D nucleation and forming new graphite layers in a tangential direction, while the overall growth direction is in a radial direction. The graphite growth would increase the nucleation sites and increased the crystallinity percentage (Double and Hellawell 1995; Lacaze et al. 2017). According to Lacaze et al. (2017) there are two types of graphite growth which is tangential growth (screw dislocations) emanating from the graphite spheroid center. The second type of growth is the nucleation of new layers proceeds until two neighboring interfaces meet. The growth of graphite was illustrated in Fig. 4 (Lacaze et al. 2017).

The properties of graphite as a nucleation promoter were also supported by Amini and Abbashian in their finding that both thickening of plates and lateral extension of graphite were observed by the roughening transition at the graphite interface in Ni-C samples. Moreover, Andre de Alburqueque et al. (Vicente et al. 2019) described the growth sequence of graphite associated with the complex silicates formation has successfully served as effective nucleation sites for the crystal formation during solidification in ductile cast iron. On the other hand, when graphite was introduced in the polymer named poly (3-hydroxybutyrate-co-3-hydroxyvalerate) (PHBV), the crystallite size was recorded to be enlarged indicated the crystallization of PHBV chains is promoted due to the presence of graphite (Montagna et al. 2017). Yet, the crystallinity percentage didn't change compared to the near PHBV.

Another study made by Wang and Qiu (2011) by using GO as the filler in the poly(L-Lactic acid) (PLLA) polymer and crystallization behavior was investigated. The experimental results indicate the cold crystallization rate of PLLA is increased

with increasing GO loading as indicative of the nucleating agent effect of GO. However, the crystallization mechanism and crystal structure remain unchanged for both neat PLLA and PLLA/GO composite (Wang and Qiu 2011). Furthermore, there are other previous studies investigating the polymer composite's crystallinity behavior involving graphitic materials as the fillers (Enqvist 2013; Wieme et al. 2019) that successfully displayed their effectiveness of nucleating agent properties. However, as far as the author's knowledge, there is very limited study on utilizing the nucleating promotion properties of the graphitic materials into UHMWPE. Perhaps, the crystallinity behavior of UHMWPE after reinforcing with GF and GO would be one of much valuable knowledge included for future work.

4.4 Hydrophilicity

Polymers can be existed as hydrophilic or hydrophobic depending on the chemical structure of the monomer units. UHMWPE has a long monomer repeating chains of CH and CH_2 as its backbone and CH_3 as its pendant group; known as a non-polar molecule. Hence, UHMWPE is an inherently hydrophobic polymer. On the other hand, polymers with a polar molecule that contains carbonyl or hydroxyl group are recognized as hydrophilic polymers. In the joint application, other than the mechanical sturdiness and elevation of thermal contact, the UHMWPE bearing component which has high hydrophobicity behavior is commonly exposed to wear degeneration due to the protein adsorption effect as well.

Since proteins have a high affinity towards the hydrophobic surface, therefore, it is important to control the UHMWPE hydrophobic properties. An inherent hydrophobic polymer can be modified to have hydrophilic properties and vice versa. The modification that can be done included by changing the surface roughness (Tahir et al. 2018) or applying functional coatings (Shrivastava 2018). However, in this research, the hydrophobicity of UHMWPE is perhaps can be controlled by the reinforcement of hydrophilic filler materials; GF and GO.

According to Andrew et al. (Kozbial et al. 2016), it was found that the graphitic surfaces are intrinsically hydrophilic which is the opposite of the old theory that well accepted with the research community since the 1940s. The freshly produced highly oriented pyrolytic graphite (HOPG) displayed a contact angle of about 64° indicated a relatively high wettability of the graphitic material (Kozbial et al. 2016). Moreover, the surface energy of the HOPG sample was also tested to determine the interface properties that mainly influenced by the polar and dispersive components. The results of total surface energy are relatively highly composed of polar components indicated its hydrophilic behavior.

The theory of pristine graphite's intrinsic hydrophilicity was also supported by Sinha et al. (2014) due to the ability of water molecules' intercalation in between the graphite lamellar. On the other hand, since GO is the treated graphite with a strong oxidizer and functionalized with hydroxyl group and epoxide group (Melk and Emami 2018). Hence, GO would exhibit intrinsic hydrophilic properties. Therefore,

the GO would undoubtedly capable to interact with water molecules. The introduction of GF and GO as filler reinforcement, which has intrinsically hydrophilic properties were presumed could tailor the hydrophilicity of the UHMWPE. According to Suñer and Emami (2014), the reinforcement of GO at 0.1, 0.3, and 0.5 wt% exhibited significantly lower contact angles and significantly enhances wettability compared to neat UHMWPE. The reinforcement of GO at higher wt% (0.7, 1.0, and 2.0 wt%) showed similar contact angle, thus, similar wettability to the lower wt% of reinforced GO particles.

The same finding was also described by Wenchao et al. (Pang et al. 2018) as the contact angle of UHMWPE/GO composite decreases with the increase of GO content, which represents good wettability. Nonetheless, these previous works (Pang et al. 2018; Suñer and Emami 2014) didn't provide the correlation of increasing wettability (hydrophilic properties) with the protein adsorption effect which consequently caused wear degradation. In addition to that, a wettability study that involved graphite as the reinforced filler was also very limited. Therefore, in this research study, the UHMWPE composites would be evaluated for its wettability behavior and would be correlated in reducing the protein adsorption.

5 UHMWPE Composite Fabrication Process

The processing of UHMWPE composite is an important yet very challenging as UHMWPE has a very high viscosity due to its extremely long molecular chains; 2 to 3 million g/mol. Upon heating or under pressure applied, the UHMWPE powder would not turn into a liquid state which limits the polymer from being molded and reinforced by fillers using conventional polymer manufacturing processes; injection molding, conventional screw extrusions (Kurtz 2009; Sánchez-Sánchez et al. 2018). Hence, the dispersion of fillers in the UHMWPE matrix was commonly found to be a segregated structure instead of a random filler distribution (Puértolas and Kurtz 2014).

There was a technique used of enhancing the diffusion between the UHMWPE and filler in a segregated structure, known as a paraffin-assisted melt-mixing process. This technique was believed can reduce the segregated structure which may be considered to introduce structural defects in the microstructure of UHMWPE. Unfortunately, the usage of paraffin could leave unwanted chemical traces especially for the fabrication of biomedical implant components. Furthermore, the usage of large amounts of solvent in the processing introduces serious environmental pollution (Ray and Jana 2017).

Therefore, multiple ongoing works were developed for the UHMWPE composite processing techniques including dry blending the mixture of filler and UHMWPE using blender (Wang et al. 2018), melt blending the mixture of filler and UHMWPE using internal mixer (Puértolas and Kurtz 2014; Suñer and Emami 2014), ball milling technique using the plenary machine (Suñer and Emami 2014) and thermal treatment of the filler by using ultrasonic dispersion technique (Vadivel et al. 2018) prior the

hot pressing for final shape of UHMWPE composites (Pang et al. 2018; Salari et al. 2019; Tai et al. 2012).

Melt-blending or mechanical blending was widely used prior to the compression molding for enhancing fillers' incorporations as it favored by industry owing to its combination of high efficiency and low cost (Kurtz 2009; Merola and Affatato 2019). The fillers can incorporate their own high stiffness and strength to the bulk material and inhibit the propagation of the crack, which can ultimately delay the breakdown of the material (Puértolas and Kurtz 2014; Ray and Jana 2017). In this study, melt-blending was used as it is a more adaptable technique specifically for thermoplastic polymers.

This method does not require any type of solvent, and the graphene or treated graphene can be directly mixed in the molten polymer matrix (Verma and Goh 2019) and generally noted to be simple and common for industrial-based mass production. However, the complex geometries of advanced carbon-based materials and their interactions with high viscosity of polyethylene matrix may easily induce the agglomerations which can also be sabotaging the composite's structural integrity. However, some researchers also utilizing the chemical properties of the fillers itself such as GO owing to its content of oxygen-containing group (Suñer and Emami 2014) which makes dispersion relatively easy in UHMWPE matrix. Other than that, the large interface of GO and GF compared to conventional carbon-based materials have a greater advantage for more effective load-transfer sites between the matrix-filler interface (Abhilash et al. 2016; Anwar et al. 2016; Puértolas and Kurtz 2014). Hence, reducing the poses threats of microstructural failure of the UHMWPE composites.

6 Concluding Remarks and Future Perspective

The chapter summarized on the modification of the UHMWPE joint component. The improvement of UHMWPE wear properties is primarily dependent on the polyethylene's properties itself. The modification of UHMWPE by filler reinforcement was selected. Graphitic materials were introduced as the filler due to their surface characteristics which conveniently allow the formation of adhesive binding to polyethylene matrix. This is important to ensure an improvement of mechanical strengthening supported by the reinforced material. The UHMWPE composite was equipped with extra-functional properties from the graphitic fillers such as high thermal conductivity, high crystallinity, hydrophilic and also biocompatibility. In conclusion, other than being the best filler to improve wear from the mechanical aspects, graphitic fillers is also capable to reduce the wear rate causes by chemical and constituents reactions on the polyethylene component.

References

Abhilash V, Rajender N, Suresh K (2016) X-ray diffraction spectroscopy of polymer nanocomposites. Elsevier Inc., Spectroscopy of Polymer Nanocomposites. https://doi.org/10.1016/B978-0-323-40183-8.00014-8

Anderson BC, Bloom PD, Baikerikar K, Sheares VV, Mallapragada SK (2002) Al–Cu–Fe quasicrystal/ultra-high molecular weight polyethylene composites as biomaterials for acetabular cup prosthetics. Biomaterials 23(8):1761–1768. https://doi.org/10.1016/S0142-9612(01)00301-5

Anwar Z, Kausar A, Muhammad B (2016) Polymer and graphite-derived nanofiller composite: an overview of functional applications. Polym Plast Technol Eng 55(16):1765–1784. https://doi.org/10.1080/03602559.2016.1163598

Ashraf MA, Peng W, Zare Y, Rhee KY (2018) Effects of size and aggregation/agglomeration of nanoparticles on the interfacial/interphase properties and tensile strength of polymer nanocomposites. Nanoscale Res Lett 13:1–7. https://doi.org/10.1186/s11671-018-2624-0

Baena JC, Wu J, Peng Z (2015) Wear Performance of UHMWPE and Reinforced UHMWPE composites in arthroplasty applications: a review. Lubricants 3(2):413–436. https://doi.org/10.3390/lubricants3020413

Banoriya D, Purohit R, Dwivedi RK (2017) Advanced application of polymer based biomaterials. Mater Today 4(2):3534–3541. https://doi.org/10.1016/j.matpr.2017.02.244

Brockett CL, Carbone S, Abdelgaied A, Fisher J, Jennings LM (2016) Influence of contact pressure, cross-shear and counterface material on The wear of PEEK and CFR-PEEK for orthopaedic applications. J Mech Behav Biomed Mater 63:10–16. https://doi.org/10.1016/j.jmbbm.2016.06.005

Burger NDL, de Vaal PL, Meyer JP (2007) Failure ANALYSIS on Retrieved Ultra High Molecular Weight Polyethylene (UHMWPE) acetabular cups. Eng Fail Anal 14(7):1329–1345. https://doi.org/10.1016/j.engfailanal.2006.11.005

Burger N, Laachachi A, Ferriol M, Lutz M, Toniazzo V, Ruch D (2016) Review of thermal conductivity in composites: mechanisms: parameters and theory. Prog Polym Sci 61:1–28. https://doi.org/10.1016/j.progpolymsci.2016.05.001

Callister WD, Rethwisch DG (2018) Materials science and engineering: an introduction, 10th edn, Wiley

Chang N, Bellare A, Cohen RE, Spector M (2000) Wear behavior of bulk oriented and fiber reinforced UHMWPE. Wear 241(1):109–117. https://doi.org/10.1016/S0043-1648(00)00393-8

Chang BP, Akil HM, Nasir RM (2013) Mechanical and tribological properties of zeolite-reinforced UHMWPE composite for Implant application. Procedia Eng 68:88–94. https://doi.org/10.1016/j.proeng.2013.12.152

Choudhury D, Ranuša M, Fleming RA, Vrbka M, Křupka I, Teeter MG, Goss J, Zou M (2018) Mechanical wear and oxidative degradation analysis of retrieved ultra high molecular weight polyethylene acetabular cups. J Mech Behav Biomed Mater 79:314–323. https://doi.org/10.1016/j.jmbbm.2018.01.003

Chukov DI, Stepashkin AA, Gorshenkov MV, Tcherdyntsev VV, Kaloshkin SD (2014) Surface modification of carbon fibers and its effect on the fiber-matrix interaction of UHMWPE based composites. J Alloys Compd 586:459–463. https://doi.org/10.1016/j.jallcom.2012.11.048

Chukov DI, Stepashkin AA, Maksimkin AV, Tcherdyntsev VV, Kaloshkin SD, Kuskov KV, Bugakov VI (2015) Investigation of structure, mechanical and tribological properties of short carbon fiber reinforced UHMWPE-matrix composites. Compos Part B-Eng 76:79–88. https://doi.org/10.1016/j.compositesb.2015.02.019

Dangsheng X (2005) Friction and wear properties of UHMWPE composites reinforced with carbon fiber. Mater Lett 59(2–3):175–179. https://doi.org/10.1016/j.matlet.2004.09.011

Delaunay C, Petit I, Learmonth ID, Oger P, Vendittoli PA (2010) Metal-on-metal bearings total hip arthroplasty: the cobalt and chromium ions release concern. Orthop Traumatol Surg Res 96(8):894–904. https://doi.org/10.1016/j.otsr.2010.05.008

Digas G (2005) New polymer materials in total hip arthroplasty. Acta Orthop 76(315):4–82. https://doi.org/10.1080/17453674078540521

Double DD, Hellawell A (1995) The nucleation and growth of graphite-the modification of cast iron. Acta Metall Mater 43(6):2435–2442. https://doi.org/10.1016/0956-7151(94)00416-1

Enqvist E (2013) Carbon nanofiller reinforced uhmwpe for orthopaedic applications. Luleå University of Technology, Thesis

Ge S, Wang S, Huang X (2009) Increasing the wear resistance of uhmwpe acetabular cups by adding natural biocompatible particles. Wear 267(5–8):770–776. https://doi.org/10.1016/j.wear.2009.01.057

Gupta A, Tripathi G, Basu B, Balani K (2012) Dependence of protein adsorption on wetting behavior of UHMWPE-HA-Al 2O 3-CNT hybrid biocomposites. JOM 64(4):506–513. https://doi.org/10.1007/s11837-012-0295-3

Gurunathan S, Kim J-H (2016) Synthesis, toxicity, biocompatibility, and biomedical applications of graphene and graphene-related materials. Int J Nanomedicine 11:1927–1945. https://doi.org/10.2147/IJN.S105264

Kim H, Abdala AA, MacOsko CW (2010) Graphene/polymer nanocomposites. Macromolecules 43(16):6515–6530. https://doi.org/10.1021/ma100572e

Kozbial A, Zhou F, Li Z, Liu H, Li L (2016) Are graphitic surfaces hydrophobic? Acc Chem Res 49(12):2765–2773. https://doi.org/10.1021/acs.accounts.6b00447

Kumar RM, Sharma SK, Kumar BVM, Lahiri D (2015) Effects of carbon nanotube aspect ratio on strengthening and tribological behavior of ultra high molecular weight polyethylene composite. Compos Part A Appl Sci Manuf 76:62–72. https://doi.org/10.1016/j.compositesa.2015.05.007

Kurtz SM (2009) The origins of UHMWPE in total hip arthroplasty. UHMWPE Biomaterials Handbook: Second Edition: 31–41. https://doi.org/10.1016/B978-0-12-374721-1.00004-3

Lacaze J, Bourdie J, Castro-Román MJ (2017) A 2-D nucleation-growth model of spheroidal graphite. Acta Mater 134:230–235. https://doi.org/10.1016/j.actamat.2017.05.032

Laska A, Archodoulaki VM, Duscher B (2016) Failure analysis of retrieved pe-uhmw acetabular liners. J Mech Behav Biomed Mater 61:70–78. https://doi.org/10.1016/j.jmbbm.2016.01.007

Liao C, Li Y, Tjong SC (2018) Graphene nanomaterials: synthesis, biocompatibility, and cytotoxicity. Int J Mol Sci 19(11):1–36. https://doi.org/10.3390/ijms19113564

Liza S, Haseeb ASMA, Abbas AA (2013) The wear behaviour of cross-linked UHMWPE under dry and bovine calf serum-lubricated conditions. Tribol Trans 56(1):130–140. https://doi.org/10.1080/10402004.2012.732199

Maksimkin AV, Kaloshkin SD, Tcherdyntsev VV, Senatov FS, Danilov VD (2012) Structure and properties of ultra-high molecular weight polyethylene filled with disperse hydroxyapatite. Inorg Mater Appl Res 3(4):288–295. https://doi.org/10.1134/S2075113312040132

Malik R, Tomer VK, Chaudhary V (2019) Hybridized graphene for chemical sensing. Functionalized graphene nanocomposites and their derivatives. Elsevier Inc. https://doi.org/10.1016/b978-0-12-814548-7.00016-7

Melk L, Emami N (2018) Mechanical and thermal performances of UHMWPE blended vitamin E reinforced carbon nanoparticle composites. Compos Part B-Eng 146:20–27. https://doi.org/10.1016/j.compositesb.2018.03.034

Merola M, Affatato S (2019) Materials for hip prostheses: a review of wear and loading considerations. Materials 12(3):1–24. https://doi.org/10.3390/ma12030495

Montagna LS, Montanheiro TLDA, Machado JPB, Passador FR, Lemes AP, Rezende MC (2017) Effect of graphite nanosheets on properties of poly(3-hydroxybutyrate-co-3-hydroxyvalerate). Int. J Polym Sci 2017:1–9. https://doi.org/10.1155/2017/9316761

Moshkovich A, Perfilyev V, Rapoport L (2019) Effect of plastic deformation and damage development during friction of FCC metals in the conditions of boundary lubrication. Lubricants 7(5):1–8. https://doi.org/10.3390/lubricants7050045

Murakami T, Sawae Y, Nakashima K, Yarimitsu S, Sato T (2007) Micro- and nanoscopic biotribological behaviours in natural synovial joints and artificial joints. Proc Inst Mech Eng J 221(3):237–245. https://doi.org/10.1243/13506501JET245

Nakano H, Tetsuka H, Spencer MJS, Morishita T (2018) Chemical modification of group iv graphene analogs. Sci Technol Adv Mat 19(1):76–100. https://doi.org/10.1080/14686996.2017.1422224
Neuwirth AL, Ashley BS, Hardaker WM, Sheth NP (2018) Metal-on-metal hip implants: progress and problems. Biomed Appl Metals pp 73–93. https://doi.org/10.1007/978-3-319-74814-6_3
Ozsoy I, Demirkol A, Mimaroglu A, Unal H, Demir Z (2015) The influence of micro-and nano-filler content on the mechanical properties of epoxy composites. Stroj Vestn-J Mech E 61(10):601–609. https://doi.org/10.5545/sv-jme.2015.2632
Pang W, Ni Z, Wu JL, Zhao Y (2018) Investigation of tribological properties of graphene oxide reinforced ultrahigh molecular weight polyethylene under artificial seawater lubricating condition. Appl Surf Sci 434:273–282. https://doi.org/10.1016/j.apsusc.2017.10.115
Panin SV, Kornienko LA, Suan TN, Ivanova LR, Poltaranin MA, Shil'ko SV (2014) Wear resistance of composites based on ultrahigh molecular weight polyethylene filled with graphite and molybdenum disulfide microparticles. J Frict Wear 35(4):290–296. https://doi.org/10.3103/S1068366614040084
Plumlee K, Schwartz CJ (2009) Improved wear resistance of orthopaedic UHMWPE by reinforcement with zirconium particles. Wear 267(5–8):710–717. https://doi.org/10.1016/j.wear.2008.11.028
Puértolas JA, Kurtz SM (2014) Evaluation of carbon nanotubes and graphene as reinforcements for uhmwpe-based composites in arthroplastic applications: a review. J Mech Behav Biomed Mater 39:129–145. https://doi.org/10.1016/j.jmbbm.2014.06.013
Rahmati M, Mozafari M (2018) Protein adsorption on polymers. Mater Today Commun 17:527–540. https://doi.org/10.1016/j.mtcomm.2018.10.024
Ray SC, Jana NR (2017) Carbon nanomaterials for biological and medical applications, 1st edn. Elsevier Inc
Salari M, Mohseni TS, Bagheri R, Faghihi SMA (2019) Improved wear, mechanical, and biological behavior of UHMWPE-HAp-zirconia hybrid nanocomposites with a prospective application in total hip joint replacement. J Mater Sci 54(5):4259–4276. https://doi.org/10.1007/s10853-018-3146-y
Sánchez-Sánchez X, Elias-Zuñiga A, Hernández-Avila M (2018) Processing of ultra-high molecular weight polyethylene/graphite composites by ultrasonic injection moulding: taguchi optimization. Ultrason Sonochem 44:350–358. https://doi.org/10.1016/j.ultsonch.2018.02.042
Sawae Y, Yamamoto A, Murakami T (2008) Influence of protein and lipid concentration of the test lubricant on the wear of ultra high molecular weight polyethylene. Tribol Int 41(7):648–656. https://doi.org/10.1016/j.triboint.2007.11.010
Shahemi N, Liza S, Abbas AA, Merican AM (2018) Long-term wear failure analysis of UHMWPE acetabular cup in total hip replacement. J Mech Behav Biomed Mater 87:1–9. https://doi.org/10.1016/j.jmbbm.2018.07.017
Shrivastava A (2018) Introduction to plastics engineering. Introduction to plastics engineering, Elsevier Inc. pp 1–16. https://doi.org/10.1016/b978-0-323-39500-7.00001-0
Sinha SD, Chatterjee S, Maity PK, Tarafdar S, Moulik SP (2014) Studies of protein adsorption on implant materials in relation to biofilm formation I. Activity of Pseudomonas aeruginosa on Polypropylene and High density Polyethylene in presence of serum albumin. Retrieved from https://arxiv.org/ftp/arxiv/papers/1411/1411.5108.pdf
Sreekanth PSR, Kanagaraj S (2015) Influence of multi walled carbon nanotubes reinforcement and gamma irradiation on the wear behaviour of UHMWPE. Wear 334–335:82–90. https://doi.org/10.1016/j.wear.2014.12.014
Stepashkin AA, Chukov DI, Gorshenkov MV, Tcherdyntsev VV, Kaloshkin SD (2014) Electron microscopy investigation of interface between carbon fiber and ultra high molecular weight polyethylene. J Alloys Compd 586(1):168–172. https://doi.org/10.1016/j.jallcom.2012.12.045
Suñer S, Emami N (2014) Investigation of graphene oxide as reinforcement for orthopaedic applications. Tribol—Mater Surf Interf 8(1):1–6. https://doi.org/10.1179/1751584X13Y.0000000053

Tahir NAM, Abdollah MFB, Tamaldin N, Amiruddin H, Zin MRBM (2018) A Brief Review on The Wear Mechanisms and Interfaces of Carbon Based Materials. Compos Interfaces 25(5–7):491–513. https://doi.org/10.1080/09276440.2018.1380472

Tai Z, Chen Y, An Y, Yan X, Xue Q (2012) Tribological behavior of UHMWPE reinforced with graphene oxide nanosheets. Tribol Lett 46(1):55–63. https://doi.org/10.1007/s11249-012-9919-6

Tripathi G, Basu B (2012) A porous hydroxyapatite scaffold for bone tissue engineering: physico-mechanical and biological evaluations. Ceram Int 38(1):341–349. https://doi.org/10.1016/j.ceramint.2011.07.012

Vadivel HS, Golchin A, Emami N (2018) Tribological behaviour of carbon filled hybrid UHMWPE composites in water. Tribol Int 124:169–177. https://doi.org/10.1016/j.triboint.2018.04.001

Verma D, Goh KL (2019) Functionalized graphene-based nanocomposites for energy applications. Functionalized Graphene Nanocomposites and their Derivatives. Elsevier Inc. https://doi.org/10.1016/b978-0-12-814548-7.00011-8

Vicente AA, Moreno JRS, Santos TFA, Espinosa DCR, Tenório JAS (2019) Nucleation and growth of graphite particles in ductile cast iron. J Alloys Compd 775:1230–1234. https://doi.org/10.1016/j.jallcom.2018.10.136

Wang H, Qiu Z (2011) Crystallization behaviors of biodegradable poly(L-Lactic Acid)/graphene oxide nanocomposites from the amorphous state. Thermochim Acta 526(1–2):229–236. https://doi.org/10.1016/j.tca.2011.10.006

Wang Q, Liu J, Ge S (2009) Study on biotribological behavior of the combined joint of CoCrMo and UHMWPE/BHA composite in a hip joint simulator. J Bionic Eng 6(4):378–386. https://doi.org/10.1016/S1672-6529(08)60139-0

Wang Y, Yin Z, Li H, Gao G, Zhang X (2017) Friction and wear characteristics of ultrahigh molecular weight polyethylene (UHMWPE) composites containing glass fibers and carbon fibers under dry and water-lubricated conditions. Wear 380–381:42–51. https://doi.org/10.1016/j.wear.2017.03.0069

Wang Z, Guo L, Gao P, Xu S, Liu X, Liu Y, Tong J (2018) Friction and wear properties of polyphenyl ester and graphite filler in the carbon fibre-reinforced ultra-high-molecular-weight polyethylene composites. Mater Sci Tech 49(1):21–29. https://doi.org/10.1002/mawe.201700112

Wieme T, Duan L, Mys N, Cardon L, D'hooge DR (2019) Effect of matrix and graphite filler on thermal conductivity of industrially feasible injection molded thermoplastic composites. Polymers 11(1):4–6. https://doi.org/10.3390/polym11010087

Xiong DS, Lin JM, Fan DL (2006) Wear Properties of nano-Al2O3/UHMWPE composites irradiated by gamma ray against a CoCrMo alloy. Biomed Mater 1(3):175–179. https://doi.org/10.1088/1748-6041/1/3/013

Yi M, Shen Z (2015) A review on mechanical exfoliation for the scalable production of graphene. J Mater Chem A 3(22):11700–11715. https://doi.org/10.1039/c5ta00252d

Zabolotnov AS, Brevnov PN, Akul'shin VV, Novokshonova LA, Doronin FA, Evdokimov AG, Nazarov VG (2018) The wear resistance of composite materials based on ultra-high-molecular-weight polyethylene with fillers of various types. Polym Sci Ser D 11(3):297–302. https://doi.org/10.1134/S1995421218030243

Water Absorption Properties of Natural Fibres Reinforced PLA Bio-Composite

Rozyanty Rahman and Nur Rusyidah Mustapa

Abstract Bio-polymer-based composite has experienced remarkable growth in engineering applications over the last few years. Due to the growing awareness and understanding of environmental concerns, many researchers are interested in finding the best ways to replace existing products that have adverse effects on both the environment and human beings. Since the trends are increasing every year, the uses of natural fibers have become a priority in many industrial sectors and engineering applications because of its biodegradability, low cost materials, low energy usage and renewable resources. Poly (lactic acid) (PLA) is an eco-friendly biodegradable polymer with intrusive qualities such as renewable and compostable. Several studies have been carried out on natural fiber reinforced PLA bio-composite, but there is still no comprehensive review on water absorption behavior of natural fiber reinforced PLA composites. Since water absorption is one of major concern for outdoor applications of bio-composite, this study will be focusing on water absorption properties of natural fiber reinforced PLA composites.

Keywords Natural fiber · PLA · Bio-composite · Water absorption

1 Introduction

Natural fibers are emerging as one of the best fillers in the production of polymer composites owing to their properties that are environmentally favourable. Some of the important properties of natural fibers as compared to their synthetic fibers or reinforcement (i.e. Glass, Acrylic and Polyester) are; readily available with low cost, good mechanical properties, low weight, eco-friendly, biocompatibility and biodegradability (Azwa et al. 2013). Natural fibers used as filler or to some extend as reinforcement are derived from plant-based materials such as banana, hemp, sisal, jute, kenaf blast, flax, date etc. (Saba et al. 2016).

R. Rahman (✉) · N. R. Mustapa
Center of Excellence Geopolymer and Green Technology (CEGeoGTech), School of Materials Engineering, Universiti Malaysia Perlis, 01000 Perlis, Malaysia
e-mail: rozyanty@unimap.edu.my

M. T. Hameed Sultan et al. (eds.), *Biocomposite Materials*, Composites Science and Technology, https://doi.org/10.1007/978-981-33-4091-6_9

Polymer composites are able to absorb moisture in humid atmosphere and/or when immersed in water, especially natural fiber/polymer composites (Yousif and El-Tayeb 2009). This in turn effects the fiber–matrix interface leading to poor stress transfer efficiencies. Furthermore, moisture absorption by natural fibers affects their physical, mechanical and thermal properties (Dhakal et al. 2007). The surface morphology of composites undergone moisture absorption is different to that of dry composites in terms of voids, porosity, swelling, sorption in micro cracking, and disbanding around filler (Athijayamani et al. 2009).

All natural fibers absorb moisture when immersed in water and in humid atmosphere especially in tropical countries. Absorption of moisture by natural fibers causes degradation and decomposition of fiber interface region resulting with poor stress relocation effectiveness and reduction of dimensional and mechanical properties. The major concerns of using natural fibers to reinforce polymer composites is to reduce their tendency to absorb moisture and the result of this moisture absorption on thermal, mechanical, and physical properties of the polymer composite materials (Tserki et al. 2006).

2 Natural Fiber

The utilization of natural fibers as reinforcement in composites has undergone a tremendous growth in industrial applications as well as fundamental work over the last few years. Because of the growing awareness of environmental issues, the government has pushed the industrial sectors towards bio-economy industries and urges researchers to seek for solutions to substitute synthetic materials that could harm the environment. Natural fibers, which can be derived from a natural resource, have been the priorityf in many industrial sectors to make new, environmentally friendly, and biodegradable composite materials. Natural fibers such as jute, kenaf, sisal, and hemp have gained significant interest in recent years because of their biodegradability, renewable, low energy consumption, and low cost (Anuar et al. 2017). Besides, they also have extensive availability and high specific strength, making them an appealing alternative to substitute glass and carbon fiber in a variety of applications, including transport, military applications, building, and construction (Akhtar et al. 2016).

In general, natural fiber can be classified into plant, animal, and mineral types, which can be illustrated in Fig. 1. Examples of animal-based fibers are chitosan, silk, and wool, whereas some examples of plant fibers are flax, sisal, jute, kenaf, and bamboo (Tezara et al. 2016). Numerous studies have proved that natural fibers such as cotton, silk, bamboo, flax, jute, hemp, and kenaf dominate world fiber production and widely used as reinforcing material in bio-composite industries (Gardner et al. 2015). Since the demands for these superior natural fibers are now higher, the researchers not only looked at the use of natural fibers in bio-composite systems but also at different factors influencing the properties of the natural fiber-reinforced composite. Natural fibers are, therefore, undergoing the most intensive work in recent years. Figure 2 displays the topics related to natural fiber-reinforced composite in Science Direct during the past five years.

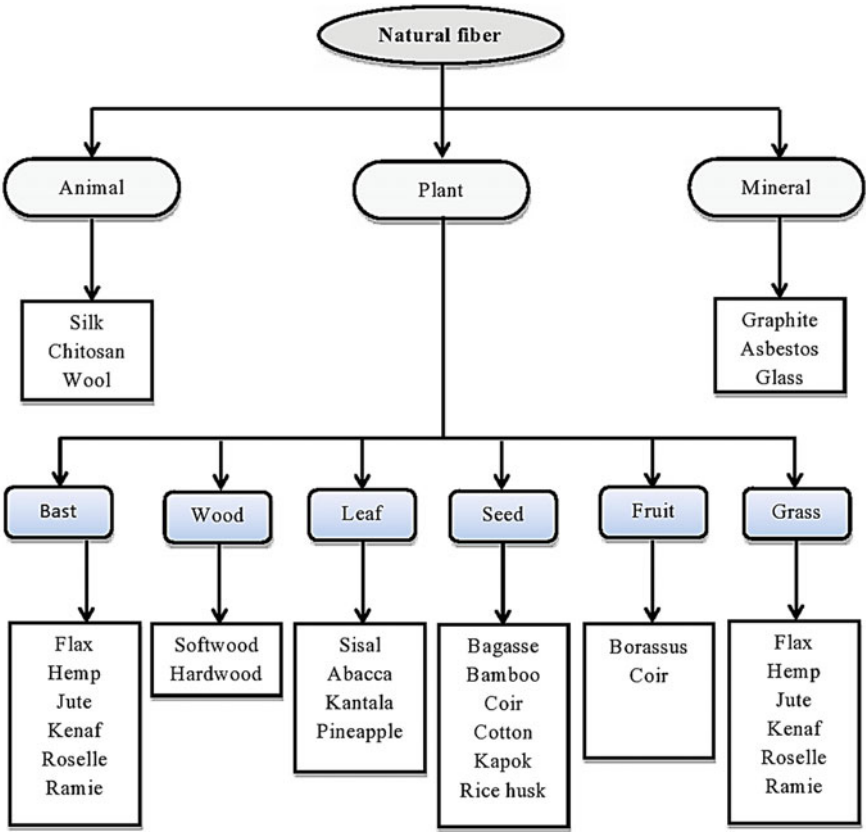

Fig. 1 The classification of natural fiber

2.1 Composition of Natural Fiber

One of the key aspects which contributes to the overall properties of natural fiber is the chemical composition of natural fiber. Natural fiber consisting primarily of cellulose, hemicellulose, pectin lignin, and other water-soluble compounds and wax (Sercer et al. 2009). The percentage of each constituent in natural fiber varies depending on the type of fiber. Cellulose, a fibrous and hydrophilic polysaccharide, acts as a primary component of all plant fiber, making it one of the most abundant compounds in the biosphere. Cellulose consist of a linear chain of glucose monomers joined together by β-1,4 linkages, as shown in Fig. 3a play an integral role in providing strength and stiffness to the fibers (Brigham 2018). Cellulose chains are arranged together in the bundles called micro fibrils. Due to the high presence of hydrogen bonds, the micro fibrils of cellulose are incredibly inflexible and tough (Akil et al. 2011).

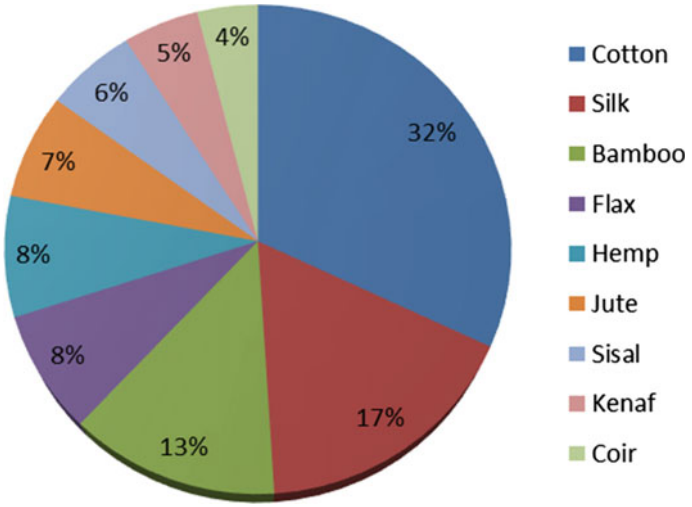

Fig. 2 Natural fiber used in bio-composite related topics in Science Direct from the year 2016 to 2020

Hemicellulose is another branched polymer of less complicated cellulose structure, which is found on the primary cell wall of fiber. Hemicellulose is closely connected with cellulose microfibrils surrounding plant cellulose fibers (Sercer et al. 2009), thereby playing a major role in supporting the cell wall. In addition, hemicellulose also regulates thermal degradation, biodegradation, and the moisture absorption of natural fiber. The chemical structure of hemicellulose is presented in Fig. 3b, whereas the chemical structure of lignin, is illustrated in Fig. 3c. Lignin consists of a broad group of aromatic polymers that arise from the oxidative combinatorial coupling of 4-hydroxyphenylpropanoids. Pectin, as can be observed in Fig. 3d is a linear chain of alpha (1–4) linked D-galacturonic acid which forms the pectin-backbone, a homogalacturonan. Pectin controls the flexibility of plant fiber as well as water solubility (Kumar et al. 2013).

2.2 Properties of Natural Fiber

The properties of natural fiber are extremely variable, and dependent on the environmental conditions. And even after repeating the test, it is difficult to get the same properties. The properties of some commonly used natural fiber are demonstrated in Table 1.

As most of the natural fibers are mainly lignocellulosic fiber, the contents of cellulose in the fiber determine the strength and rigidity of the fiber. Most of the properties of the natural fiber depend on natural fiber composition. For example, the degree of polymerization, microfibril angles, and the percentage of cellulose content

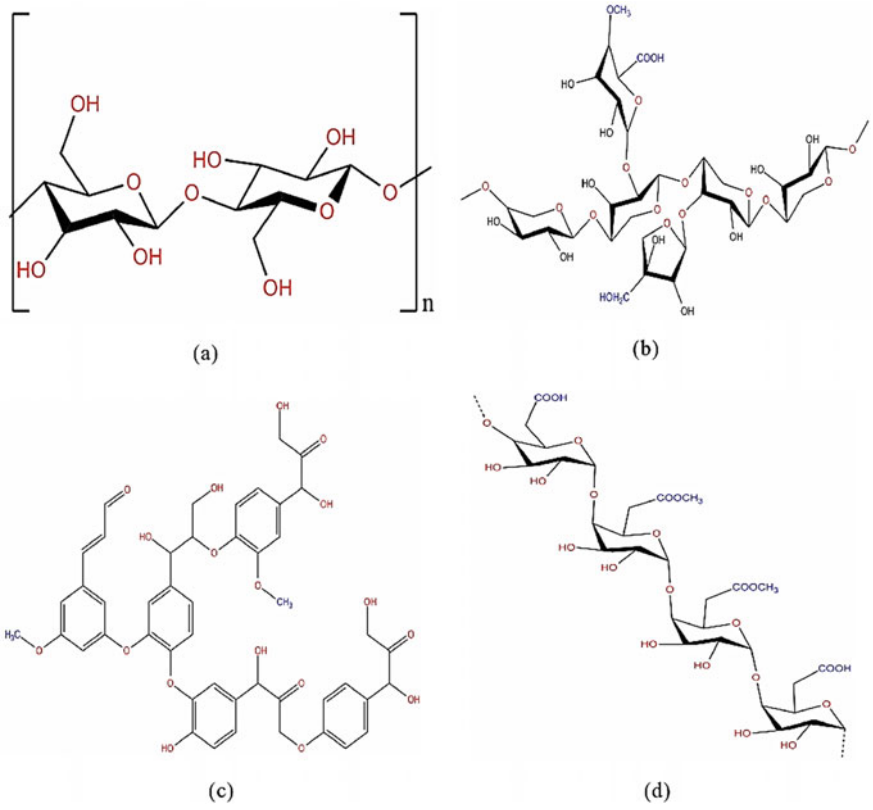

Fig. 3 Chemical structure of **a** cellulose; **b** hemicellulose; **c** lignin; **d** pectin

in the fibers influence the mechanical properties. (Celino et al. 2014). Besides that, at high humidity and temperature, plant fibers can easily be attacked by microorganisms (Chen et al. 2009).

2.3 Hydrophilic of Natural Fiber

In general, plant fibers are hydrophilic due to the existence of functional groups, particularly the hydroxyl group (– OH –) in their chemical structure. Because of this reason, plant fibers can absorb a considerable amount of moisture from the environment mainly depending on their chemical compositions (Parveen et al. 2017). Table 2 shows the moisture absorption of some natural fiber.

Given that natural fibers have been widely used as reinforcement in a composite system, serious consideration needs to be given to the hydrophilic nature of natural fibers, especially for their potential outdoor applications. The ability of natural fiber

Table 1 Properties of some natural fiber

Properties	Density (g/cm^3)	Moisture content (%)	Tensile strength (MPa)	Young's Modulus (GPa)	Elongation at break (%)	Reference
Jute	1.46	5–25	393–773	13–26.5	1.16–1.50	(Gupta et al. 2015)
Hemp	1.4	8	690	30–70	1.6	(Dhakal and Zhang 2015)
Coir	1.2	10	593	6	30	(Naveen et al. 2019)
Kenaf	1.5	–	350–600	40	2.5–3.5	(Ismail et al. 2017)
Sisal	1.33–1.55	10–22	400–700	9.8–38.0	2.5	(Naveen et al. 2019)
Ramie	1.55	–	400–938	61.4–128	1.2–3.8	(Hao et al. 2018)
Cotton	1.5	–	400	12.6	7.0	(Hao et al. 2018)
Flax	1.5	–	345–1100	27.6	2.7–3.2	(Hao et al. 2018)

Table 2 The moisture absorption of some natural fiber

Natural fiber	Moisture absorption (%)
Sisal	110
Coconut	93.8
Bamboo	145
Hemp	85–105
Caesar wood	182
Banana	407
Piassava palm	34–108
Date palm	60–84

to absorb high moisture content will cause the hydrogen bond between fiber and matrix to break and weaken the fiber-matrix interface, hence affecting the mechanical performances of composite (Saikia 2010).

2.4 Fiber-Matrix Interface

The incorporation of hydrophilic natural fiber into the hydrophobic polymer will result in a heterogeneous system whose properties are inferior due to poor fiber-matrix adhesion. One of the major issues in natural fiber reinforced polymer composites is

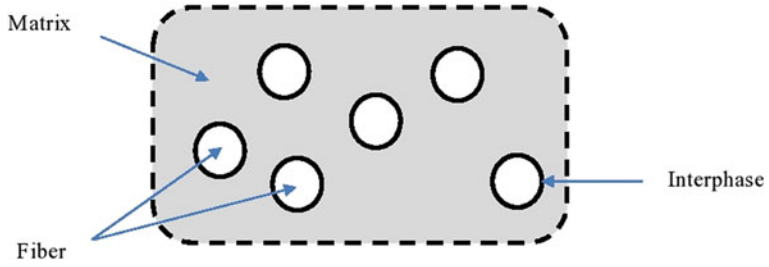

Fig. 4 Schematic illustration of a composite system

the poor interface in the fiber-matrix of the composite system (Ramesh 2016). The incompatible reaction between hydrophilic plant fiber and hydrophobic polymer matrix may contribute to the lack of hydrogen bonding between the matrix and its reinforcement. The agglomeration begins to form when matrix-fibers are not sufficiently bonded. Therefore, chemical and surface treatments are required for the enhancement of the fibers. Figure 4 displays a schematic illustration of a composite system.

2.5 Treatment of Natural Fiber

Despite the beneficial attributes of natural fiber, there are several drawbacks of natural fiber, especially when reinforced with hydrophobic polymer matrices. The disadvantages of natural fiber composite include high water absorption, poor wettability and weak interfacial bonding of fiber-matrix due to the incompatible reaction between hydrophilic fiber and hydrophobic polymer matrix (Al-Maharma and Al-Huniti 2019). Over the last few years, numerous treatments have been developed to improve interfacial bonding, hence achieving better efficiency in the mechanical and water absorption properties. The surfaces of natural fiber are modified to enhance fiber-matrix adhesion. The method of surface modification can be divided into the physical and chemical process method (Siakeng et al. 2018). Both physical and chemical treatment of natural fiber helps to reduce hydrophilicity of fiber and remove impurities from the surface of fiber. Table 3 shows the physical and chemical treatment of natural fiber.

3 Polylactic Acid (PLA)

Global awareness and public concern about material sustainability has urged researchers to partially replace non-biodegradable conventional polymers with biologically based polymers. As the production and consumption of high-volume

Table 3 Physical and chemical treatment of natural fiber

Treatment of fiber	Effect on fibers
Physical treatment	
Corona treatment	Surface oxidation activation by changing the surface energy of fiber. This technique showed significant improvement in mechanical properties
Plasma treatment	The physiochemical structure of fiber is modified without changing the characteristic of composite. This method enhances compatibilization between fiber and matrix in the composite system
Chemical treatment	
Alkaline treatment	Alkaline treatment is used to alter the structure of cellulose and remove impurities from the surface of fiber
Silane treatment	Silane treatment is carried out by immersing the fiber in a weak solution of silane diluted in water/alcohol or water/ketone. This technique is one of the most effective coupling agents which increase adhesion and stability of composite
Maleated coupling treatment	The surface of fiber is modified using well-known coupling agent, MAPP. The addition of MAPP enhances the mechanical properties of composite
Acetylation treatment	Acetylation treatment is the esterification method by using acetyl functional group ($CH_3COO–$) and formed plastization of cellulose fiber. This treatment reduces the hygroscopicity of fiber and increases stability
Benzoylation treatment	This treatment used benzoyl chloride to decrease the hydrophilicity of fiber. It can improve fibre-matrix adhesion, thus increasing the strength of fiber and lower water absorption
Stearic acid treatment	Stearic acid in ethyl alcohol used to enhance interfacial bonding between fiber and matrix
Acrylation and acrylonitrile grafting	In this treatment, good interfacial bonding is obtained when acrylic acid reacts with the hydroxyl group (–OH) of fiber and form more free radical cellulose macro-radicals. This method helps to remove the hydroxyl group from fiber and improve water absorption resistance
Electron beam irradiation (EBI) treatment	Irradiation technique changes the structure, physiochemical, and reactivity of cellulose. This treatment significantly helps to improve thermal stability, interfacial and mechanical properties of composite

polymers worldwide continues to be dominated by fossil-based polymers, the disposal of these non-biodegradable polymers has become a major concern as most plastic waste typically ends up as ocean dumping or solid waste disposal on the land. This problem occurs must be due to its complicated disposal process, which then eventually leads to water pollution and soil contamination (Jamshidian et al. 2010). Subsequently, demands for biodegradable polymers, a group of polymers that can undergo deterioration and completely degrade naturally by the presence of living microorganisms, have slowly increased over the years and are now emerging as a desirable alternative to replace traditional polymers, as they have less detrimental environmental impacts (Ibrahim et al. 2017).

Among various types of biodegradable polymers, Poly (lactic acid) (PLA) has been considered as one of the most advanced and promising bio-based polymers that undergo a broad spectrum of industrial and engineering applications. PLA polymer is bio-based aliphatic polyester that can be derived from renewable resources such as sugar cane, sugar, corn, and potato, and it consists of lactic acid (C3H6O3) as its basic constitutional unit (Avinc and Khoddami 2009). Due to their superior advantageous attributes such as biodegradable, renewable, recyclable, and compostable, interest in using PLA has increased extensively, especially in industrial applications such as structural applications, textiles, packaging, biomedical, and automotive (Ke and Sun 2000). Besides, as a compostable polymer, PLA is used as an alternative to alleviate the issue of municipal solid waste (MSW) disposal (Gupta et al. 2007).

3.1 Structure and Properties of PLA

Poly (lactic acid) (PLA), with a chemical formula of $(C_3H_4O_2)_n$, is a simple chiral polymer composed of a hydroxyl acid with asymmetrical carbon atoms and it exists as two enantiomers, L- and D-lactic acid. Figure 5 illustrates the L- and D-lactic acid isomers. These two isomers have different effects on polarized light, as L-isomer rotates the plane-polarized light in the clockwise direction, while D-isomer rotates the plane in the opposite direction (Casalini et al. 2019). Biologically, PLA can be produced by bacteria fermentation or chemical synthesis. The lactic acid formed by bacteria (homofermentative and heterofermentative) fermentation of carbohydrates exists exclusively as L-lactic acids, which eventually forms a semi-crystalline polymer of Poly (L-lactic acid) with low molecular weights through condensation polymerization of L-lactic acid. Meanwhile, the lactic acid produced through chemical synthesis can be derived by various ratios of L-and D-lactic acid (Farah et al. 2016). The cyclic dimers of lactic acid formed during the chemical reaction as an intermediate step to the production of PLA, typically three different forms, namely L-lactide with two L-lactyl units, D-lactide with two D-lactyl units, and meso-lactide with one L-lactyl unit and D-lactyl unit (Hamad et al. 2015).

PLA is a biodegradable thermoplastic aliphatic polyester with various distinctive features such as high rigidity, strong glossy-like transparency and is readily fabricated (Casalini et al. 2019). PLA has gained a lot of popularity around the world because it is

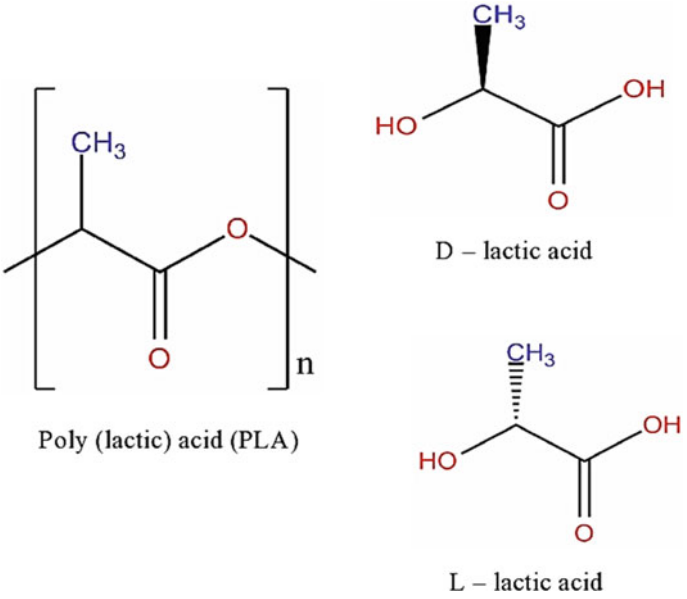

Fig. 5 Chemical structure of PLA and its monomer L-lactic acid and D-lactic acid

derived from the very low toxicity and immunogenicity natural resources. However, due to certain limitations, such as inadequate mechanical and thermal properties, PLA may not have met certain criteria for industrial applications. Although PLA is a relatively stiff polymer with excellent mechanical properties, particularly in tensile strength and flexural strength due to its inherent fragility and low elongation break, the use of PLA in specific industrial applications may have been limited (Gupta et al. 2007). Many recent studies have thus concentrated on various additives such as toughening agents, plasticizers and reinforcing fillers to incorporate with PLA and reduce its limitations, thus being able to compete with other more versatile thermoplastics of commodities such as polypropylene, polyethylene, and polyvinyl chloride (Vroman and Tighzert 2009). Besides, bio-composite approaches by adding natural-based filler or reinforcing agent to PLA will help boost the mechanical properties of PLA without affecting its biodegradability (Casalini et al. 2019).

As polar oxygen linkages occur in its chemical structure, PLA is naturally a hydrophilic biopolymer. However, due to the existence of methyl side groups, the surface of PLA exhibits strongly hydrophobic character (Vroman and Tighzert 2009). Notably, it is believed that the natural hydrophilicity of PLA is responsible for its moderate decomposition based on surrounding temperature and moisture (Ecker et al. 2019). Besides that, PLA, as well as its copolymers, can quickly degrade by the hydrolysis process, and the products from this process are non-toxic to human beings (Tan et al. 2018). During the hydrolysis process, the water breaks the ester bonds that constitute the PLA backbone. The water absorption may lead to moderate changes in the chemical and physical nature of the material.

3.2 *Synthesis of PLA*

The lactic acid serves as the first a building block in the synthesis of PLA. Lactic acid, the most abundant optical active hydroxycarboxylic acid, can be generated either by microbial fermentation or through chemical synthesis (Tan et al. 2018). In chemical synthesis, to produce optically inactive racemic DL-lactic acid, lactic acid is derived from petrochemical resources through the hydrolysis of lactonitrile by strong acid such as sulphuric acid. Meanwhile, the production of lactic acid in microbial fermentation begins with the extraction of starch from plants such as maize, sweet potato, and wheat, or the extraction of sugar from sugar beet. By extracting starch, starch is transformed by enzymatic hydrolysis into fermentable sugars, primarily glucose and dextrose, which is then broken down by microorganisms into smaller parts (lactic acid) (Singhvi and Gokhale 2013). This approach produces optically pure L-(+) or D-(-) lactic acid with an estimated proportion of 95% L-lactic acid and 0.5% D-lactic acid (Vitkevicius 2017). Recently, most of the production of lactic acid around the world comes from microbial fermentation methods. The production of lactic acid can be illustrated in Fig. 6.

There are three major routes to produce PLA from lactic acid; direct polycondensation reaction, ring-opening polymerization, and azeotropic dehydrative condensation as can be demonstrated in Currently, direct polycondensation reaction and ring-opening polymerization are mostly used in industrial applications. The polymerization route to produce PLA from lactic acid is shown in Fig. 7 and Table 4.

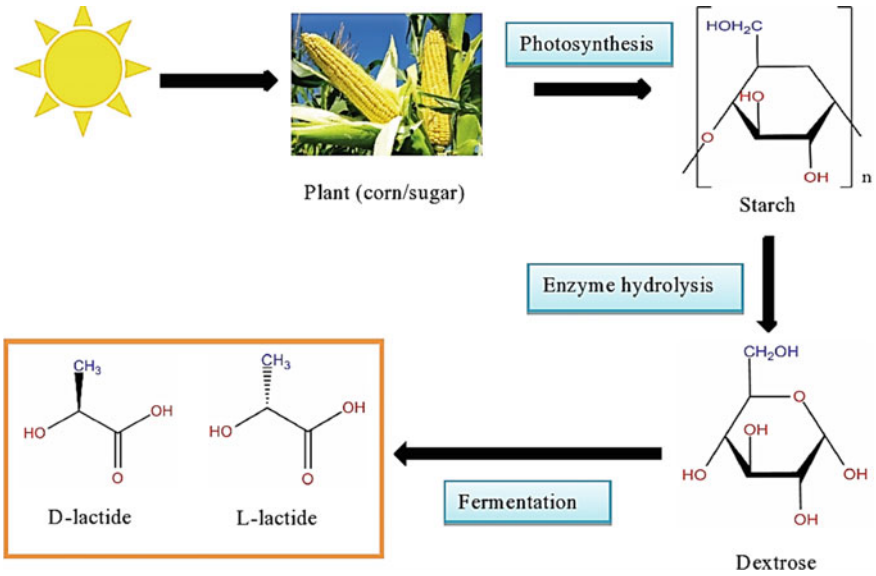

Fig. 6 Production of lactic acid microbial fermentation methods

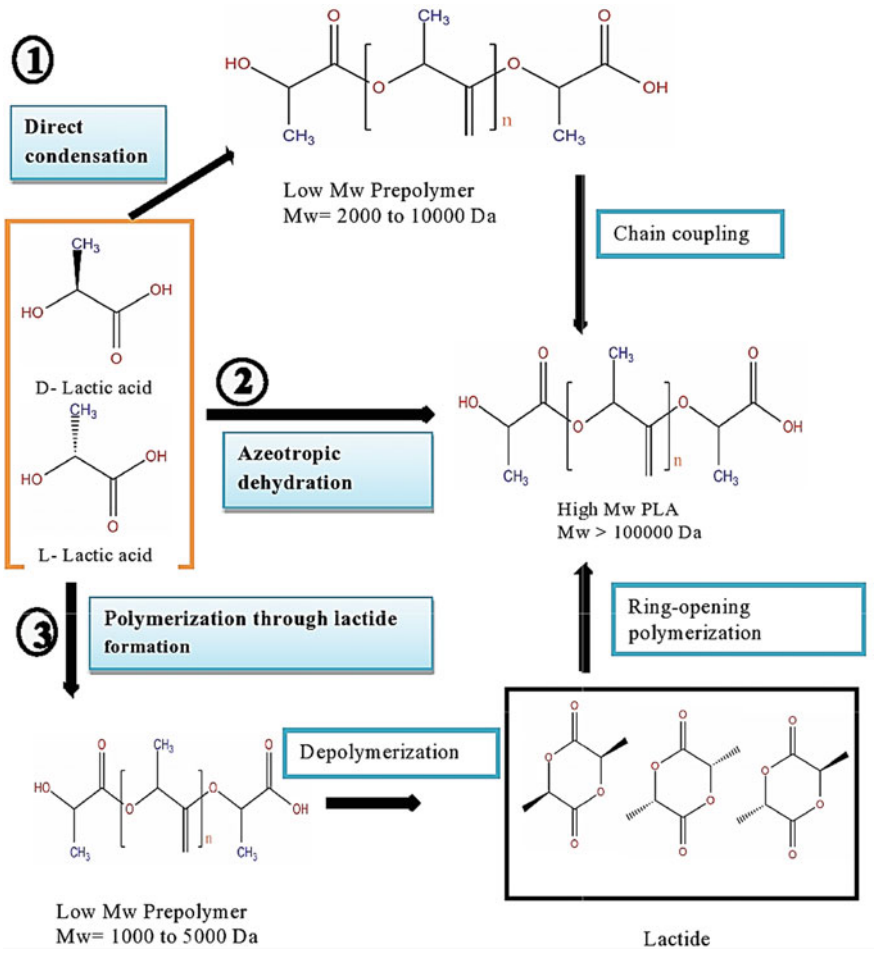

Fig. 7 Polymerization route to produce PLA from lactic acid

4 Natural Fiber Reinforced PLA Bio-Composite

Bio-composite has experienced remarkable development over the past few years, as it becomes a priority in many sectors of industrial engineering. Many researchers around the world have been making attempts to create new materials with improved performance for various industrial and technological applications. A bio-composite, a multi-phase structure consisting of reinforcing and matrix materials derived from natural resources are considered one of today's most promising candidates in advanced materials engineering (Gupta et al. 2016). Biopolymer-based natural fiber has recently become the main interest in material science studies as both matrices and reinforcing agents in this composite system can be extracted from natural resources,

Table 4 Routes to produce PLA from lactic acid (Vitkevicius 2017)

Direct condensation polymerization	Direct condensation polymerization, which can also be known as solid-state polymerization (SSP) or melt condensation, can be carried out without the presence of any organic solvent. Notably, the reaction usually takes place under high temperature (150–200 °C) and vacuum. Although this process is economical, the products obtained from this reaction tend to have a low molecular weight (Mw = 2000–10,000 Da) due to the difficulties to remove water and impurities, which then can be converted into higher molecular weight of PLA by the addition of chain coupling agents
Azeotropic dehydration polymerization	In this process, an organic solvent that is capable of dissolving lactic acid is introduced into the reaction mixture, to ease up the water removal from the refluxed solvent and produce a high molecular weight of PLA. However, these reactions produce many impurities from the solvent and side reactions.
Ring-Opening Polymerization	Ring-opening polymerization, which is considered the most successful and commonly used process to produce a high molecular weight of PLA (Mw > 100,000 Da), is the propagation reaction of cyclic monomers initiated by different ions. This process is carried out under mild conditions, with the presence of a catalyst. Three different stereoisomeric (L–lactide, D–lactide, and meso–lactide) are potentially produced during the formation of lactide from lactic acid. The ratio and sequences of D- and L-lactic acid monomers can eventually produce PLA with desired properties

thus producing more environmentally friendly and environmentally safe materials (Tezara et al. 2016). Among all bio-composites, natural fiber-reinforced PLA bio-composite has been extended to more challenging development to achieve the desirable properties and performances such as high-specific strength, biodegradability and excellent material rigidity (Siakeng et al. 2018). Table 5 summarizes natural fiber studies including their performance on mechanical, physical, and degradation properties.

5 Water Absorption Properties of Natural Fiber Reinforced PLA Bio-Composite

Water absorption behaviour is one of the essential properties that must be considered in a bio-composite environment. Water absorption is a material's ability to absorb water from its surroundings, and it plays a major role in determining the physical, chemical, and structural characteristics of the composite system (Celino et al. 2014).

Table 5 Mechanical, physical and degradation properties of Natural fiber reinforced PLA bio-composite

Properties	Bio-composite	Manufacturing design	Purpose	Result	Reference
Mechanical properties	PLA/coir fiber bio-composite	Bio-composite laminate	Determine the effect of fiber content (5-30 wt%) and fiber treatment on tensile and flexural properties	20 wt% of treated coir fiber achieve optimum tensile and flexural properties	(Bajracharyet al. 2017)
	Hemp Hurd/PLA bio-composite	Extrusion	Determine tensile and flexural properties of composite and effect of the addition of compatibilizer agent, glycidyl methacrylate (GMA)	The mechanical properties of composite greatly improved in GMA grafted PLA/hemp hurd composite	(Dong et al. 2014)
	PLA/cotton gin waste/flax fiber	Compression moulding	Determine flexural properties of composite with different fiber loading	Flexural modulus increased 42% with the addition of 30 wt% cotton gin waste	(Khan et al. 2015)
Physical properties	PLA/jute bio-composite	Compression moulding	Determine the water absorption behaviour of bio-composite and swelling in thickness after immersion in water.	PLA/jute bio-composite present far better water resistance compared to particleboard and hardboard. The swelling thickness of composite decrease as the natural fiber content decrease	(Zandvliet et al. 2014)

(continued)

Table 5 (continued)

Properties	Bio-composite	Manufacturing design	Purpose	Result	Reference
	Starch/PLA/Agave Bagasse fiber bio-composite	Extrusion	Determine water absorption behaviour based on thermoplastic starch (TPS)	TPS hygroscopicity decrease when PLA and fiber content increase	(Gracia et al. 2015)
	PLA/sisal fiber bio-composite	Mixing and compression moulding	Determine the water absorption properties of bio-composite	Water absorption is reduced significantly for combined treated PLA/sisal fiber bio-composites by 136% as compared to untreated composites	(Krishnaiahet al. 2018)
	PLA/sisal fiber bio-composite	Mixing and compression moulding, then composite is compositing into the soil	Determine biodegradation properties of bio-composite	PLA/sisal degrade faster than the pure PLA and the combination of alkali and HIU treated fiber composites show slower degradation as compare to the untreated one	(Krishnaiah et al. 2018)
Degradation properties	PLA/sisal bio-composite	Vertical injection moulding	Determine the thermal degradation of bio-composite	Untreated PLA/sisal has high thermal degradation temperature compared to the treated PLA/sisal, and enzymatic environment increased rate of degradation composite	(Rajesh, et al. 2015)

Hence, the basic understanding of the water interaction with the macromolecule involved in the composite system is important for interpreting and predicting the fiber response when interacting in the matrix in a composite system.

Although natural fiber provides low-cost production and environmentally sustainable material compared to synthetic fiber, the water-absorbing capacity of natural fiber-reinforced composites has become a major concern among researchers. In general, due to the hydrophilicity nature of plant fiber, water absorption of the natural fiber-reinforced composite is higher than synthetic fiber. Hydrophilic natural fiber can cause insufficient adhesion between matrix and fiber when reacting with hydrophobic matrix polymer in a composite system, leading to the poor performance of the composite (Melo et al. 2018). Moreover, it was established that the absorbed moisture would cause detrimental effects on the mechanical properties of the composite (Saikia 2010). Since most natural fiber is a hygroscopic and porous material, the interaction and distribution of water within the composite system plays a vital role in improving the long-term performance of the natural fiber-reinforced composite.

5.1 Sorption Mechanism

Water absorbed by natural fiber reinforced composite exists in the form of free water and bound water. Free water is naturally adsorbed water, and not chemically bound to the fiber. It can pass through the void and crack spaces independently and can easily be removed by controlled heating or evaporation. Meanwhile, bound water disperses molecules of water which penetrate the cell walls and are bound to a polar group of materials (Petinakis et al. 2013).

Once the natural fiber-reinforced composite is exposed to moisture, water molecules migrate through the composite and interact with the active fiber surface site consisting of the hydroxyl groups, thus forming intermolecular hydrogen bonds with fiber and thereby reducing interfacial adhesion between matrix and fiber. The deterioration cycle begins when the fiber starts to swell and develops tension in the interface regions resulting in its fragility and micro-cracking of the matrix around swollen fibers (Melo et al. 2018). The cracks exacerbate water absorption as it stresses the movement of moisture and the capillary by micro-cracks, contributing to fiber deterioration. Excessive absorption of water will increase bound water while diminishing free water. Therefore, the water-soluble material will gradually start to leach from the fiber and eventually cause ultimate debonding between the matrix and the fiber for prolonged exposure to moisture, biological activities such as fungal growth will encourage fiber degradation (Saikia 2010). Due to this process, researchers regarded water absorption as one of the limiting factors that reduce the composite's efficiency. Some different fiber treatment has been implemented to minimize the damaging effects of moisture on the fiber-matrix interface (Girijappa et al. 2019). Figure 8 shows the moisture conditions in a composite's fiber-matrix interface involving bound water and free water and the effects of moisture.

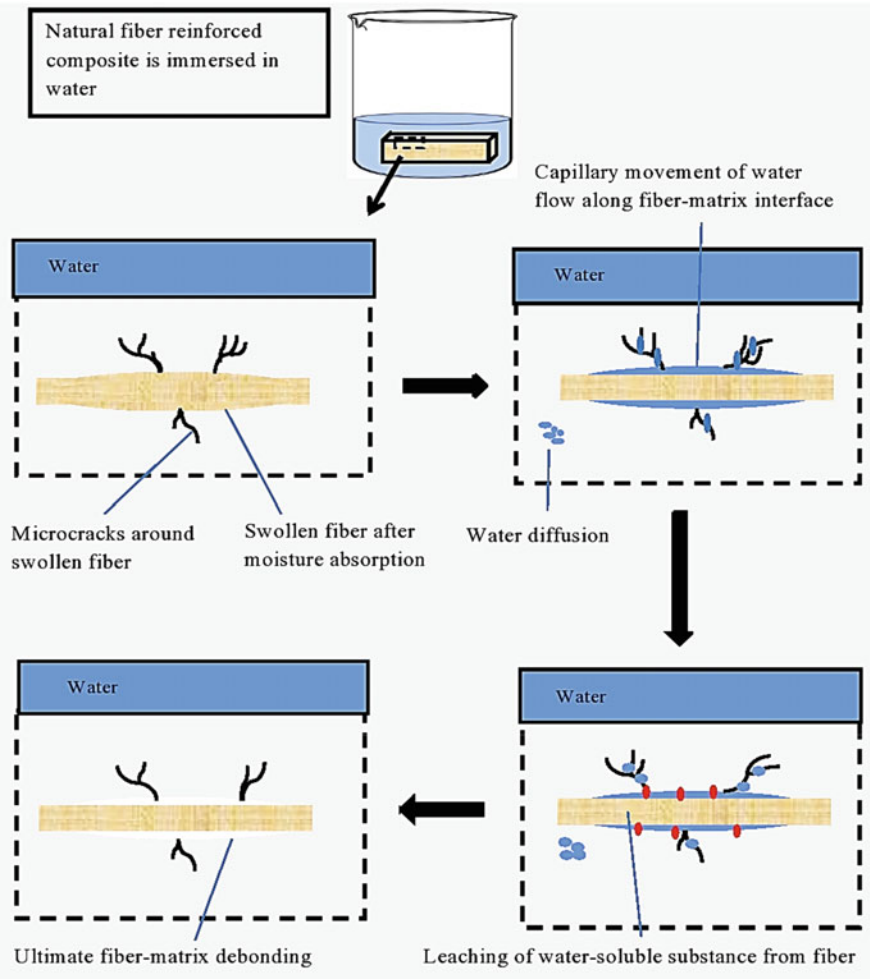

Fig. 8 The effects of moisture in the fiber-matrix interface of the composite

5.2 Water Absorption Behaviour of Natural Fiber Reinforced PLA Bio-Composite

Most of the prior research on water absorption behaviour of natural fiber reinforced PLA bio-composite deals with the hydrophilicity behaviour of plant fibers. Plant fiber is mainly composed of cellulose and hemicellulose that play a major role in moisture absorption. Since most of plant fibers are lignocellulosic fiber, moisture absorption may lead to fiber swollen, thus resulting in the dimensional stability changes (Celino et al. 2014). In some instances, moisture absorption also may affect the mechanical properties of bio-composite.

Anuar et al. 2010 conducted a study on water absorption behaviour of biodegradable PLA-kenaf fiber bio-composite. In their study, PLA-kenaf samples were immersed in three different water which is seawater with a pH of 7.5, tap water with a pH of 7 and river water with a pH of 6. The amount of water absorbed by each sample is weighed every three days until 27 days to determine the rate of water absorption and physical properties of bio-composite. The results obtained from the study showed that the higher the fiber content and immersion time, the higher the amount of water absorbed by the composite. The author also further explained that this phenomenon is due to the basic nature of lignocellulosic fiber that consists of easy accessible hydroxyl group to form intermolecular hydrogen bonds, thus reduce interfacial adhesion between fiber and PLA matrix. Besides that, the authors also stated that the different types of water used in this study were not significantly affected the water absorption rate by PLA-kenaf bio-composite.

Penjumras et al. 2015 have reported a similar trend in their study of water absorption behaviour of Durian Rind cellulose reinforced PLA bio-composite. In their study, water absorption behavior of two different loadings of Durian Rind cellulose (25 and 35 wt%) filled with PLA bio-composite was investigated by immersing the sample in water for 50 days. The results showed that the first 16 days of water immersion, a rapid increase in water absorption rate could be observed. After the next 16 days, the gradual increase of water uptake can be observed, before the composite finally reached an equilibrium point. The equilibrium point is the state where composite no longer absorbs water, and the weight of bio-composite remains unchanged.

In order to overcome the drawback of high water absorption caused by lignocellulosic fiber, a variety of treatments and modifications are introduced to enhance the properties of fiber or composite. Nanthakumar et al. 2018 conducted a comparative study on water absorption properties of bleached and unbleached PLA/sugarcane leaves fiber (SLF) biofilm. The results showed that the water absorption of the unbleached biofilms increased from 5 wt% to 20 wt% of SLF loadings. However, the bleached biofilms showed the opposite result as an unbleached biofilm. It can be observed that the water absorption rate is lower in bleached biofilms. This is because bleaching treatment on SLF surface has improved the surface roughness of fiber, thus enhance filler-matrix adhesion by the interlocking mechanism. Generally, excellent filler-matrix adhesion can lessen the penetration of water molecules into biofilms, resulting in lower water absorption properties of biofilms.

Besides that, Chung et al. 2018 also reported a study on water absorption resistance of an eco-friendly PLA/Kenaf bio-composite using acetylation. In their study, the surface of kenaf was modified using acetylation technique and then was compounded with PLA biopolymer using extrusion and injection molding technique. The hygroscopicity of composites was investigated by immersing the sample in the water at room temperature. The results showed that PLA filled with acetylated kenaf fibers showed lower water absorption compared to untreated PLA/kenaf bio-composite. Lower absorption of water must be due to the replacement of sorption sites consisting of hydroxyl groups with constituting kenaf with acetyl groups.

References

Akhtar MN, Sulong AB, Radzi MKF, Ismail NF, Raza MR, Muhamad N, Khan MA (2016) Influence of alkaline treatment and fiber loading on the physical and mechanical properties of kenaf/polypropylene composites for variety of applications. Prog Nat Sci: Mater Int 26(6):657–664. https://doi.org/10.1016/j.pnsc.2016.12.004

Akil HM, Omar MF, Mazuki AAM, Safiee S, Ishak ZAM, Abu Bakar A (2011) Kenaf fiber reinforced composites: a review. Mater Des 32(8–9):4107–4121. https://doi.org/10.1016/j.matdes.2011.04.008

Al-Maharma AY, Al-Nuhiti N (2019) Critical review of the parameters affecting the effectiveness of moisture absorption treatments used for natural composites. J Compos Sci 3:27. https://doi.org/10.3390/jcs3010027

Anuar H, Zuraida A, Fuad F (2010) Biodegradable PLA-kenaf fibre biocomposite for cleaner environment. paper presented at malaysian science and technology congress (MSTC 2010), Crystal Crown Hotel, Petaling Jaya, Malaysia

Anuar NIS, Zakaria S, Harun J, Wang C (2017) Kenaf/PP and EFB/PP : effect of fibre loading on the mechanical properties of polypropylene composites. *IOP Conf. series: materials science and engineering.* 217(012036). https://doi:10.1088/1757-899X/217/1/012036

Athijayamani A, Thiruchitrambalam M, Natarajan U, Pazhanivel B (2009) Effect of moisture absorption on the mechanical properties of randomly oriented natural fibers/polyester hybrid composite. Mater Sci Eng 517(1–2):344–353. https://doi.org/10.1016/j.msea.2009.04.027

Avinc O, Khoddami A (2009) Overview of poly(Lactic Acid)(PLA) fibre part I: production, properties, performance, environmental impact, and end-use applications of poly(lactic acid) fibres. Fibre Chem 41:391–401

Azwa ZN, Yousif BF, Manalo AC, Karunasena W (2013) A review on degradability of polymeric composite based on natural fibers. Mater Des 47:424–442. https://doi.org/10.1016/j.matdes.2012.11.025

Bajracharya RM, Bajwa DS, Bajwa SG (2017) Mechanical properties of polylactic acid composites reinforced with cotton gin waste and flax fibers. Procedia Eng 200:370–376. https://doi.org/10.1016/j.proeng.2017.07.052

Brigham C (2018) Biopolymers : biodegradable alternatives to traditional plastics. green chemistry. Elsevier Inc. pp 753–770. https://doi.org/10.1016/B978-0-12-809270-5.00027-3

Casalini T, Rossi F, Castrovinci A, Perale G (2019) A perspective on polylactic acid-based polymers use for nanoparticles synthesis and applications. Front Bioeng Biotech 7:1–16. https://doi.org/10.3389/fbioe.2019.00259

Celino A, Freour S, Jacquemin F, Casari P (2014) The hygroscopic behavior of plant fibers: a review. Front Chem 1:43. https://doi.org/10.3389/fchem.2013.00043

Chen H, Miao M, Ding X (2009) Composites: part a influence of moisture absorption on the interfacial strength of bamboo/vinyl ester composites. Compos Part A 40(12):2013–2019. https://doi.org/10.1016/j.compositesa.2009.09.003

Chung T, Park J, Lee H, Kwon H, Kim H, Lee Y, Tze WTY (2018) The improvement of mechanical properties, thermal stability, and water absorption resistance of an eco-friendly pla/kenaf biocomposite using acetylation. Appl Sci 8(3):376. https://doi.org/10.3390/app8030376

Dhakal HN, Zhang Z (2015) The use of hemp fibres as reinforcements in composites. (2015), Elsevier, United Kingdom. pp 86–101. https://doi.org/10.1533/9781782421276.1.86

Dhakal HN, Zhang ZY, Richardson MO W (2007) Effect of water absorption on the mechanical properties of hemp fibre reinforced unsaturated polyester composite. Compos Sci Technol 67(7–8):1674–1683. https://doi.org/10.1016/j.compscitech.2006.06.019

Dong Y, Ghataura A, Takagi H, Haroosh HJ, Nakagaito AN, Lau K (2014) Polylactic acid (PLA) biocomposites reinforced with coir fibres: evaluation of mechanical performance and multifunctional properties. Compos Part A 63:76–84. https://doi.org/10.1016/j.compositesa.2014.04.003

Ecker JV, Haider A, Burzic I, Huber A, Wood K, Eder G, Hild S (2019) Mechanical properties and water absorption behaviour of pla and pla/wood composites prepared by 3D printing and injection moulding. Rapid Prototyping J 4:672–678. https://doi.org/10.1108/RPJ-06-2018-0149

Farah S, Anderson DG, Langer R (2016) Physical and mechanical properties of PLA, and their functions in widespread applications—a comprehensive review. Adv Drug Deliv Rev 107:367–392. https://doi.org/10.1016/j.addr.2016.06.012

Garcia FJ, Nunez RG, Gastinel CFJ, Mendizabal E (2015) Water absorption and thermomechanical characterization of extruded starch/ poly (lactic acid)/ agave bagasse fiber bioplastic composites. Int J Polym Sci 2015:1–7. https://doi.org/10.1155/2015/343294

Gardner DJ, Han Y, Wang L (2015) Wood-plastic composite technology. Curr For Rep 1(3):139–150. https://doi.org/10.1007/s40725-015-0016-6

Girijappa YGT, Rangappa SM, Parameswaranpillai J, Siengchin S (2019) Natural fibers as sustainable and renewable resource for development of eco-friendly composites : a comprehensive review. Front Mater: September 2019. pp 1–14. https://doi.org/10.3389/fmats.2019.00226

Gupta B, Revagade N, Hilborn J (2007) Poly (lactic acid) fiber: an overview. Prog Polym Sci 32:455–482. https://doi.org/10.1016/j.progpolymsci.2007.01.005

Gupta MK, Srivastava RK, Bisaria H (2015) Potential of jute fibre reinforced polymer composites : a review. Int J Fiber Text Res 5(3):30–38. https://www.urpjournals.com

Gupta G, Kumar A, Tyagi R, Kumar S (2016) Application and future of composite materials : a review. Int J Innovative Res Sci Eng Technol 5(5):6907–6911. https://doi.org/10.15680/IJIRSET.2016.0505041

Hamad K, Kaseem M, Yang HW, Deri F, Ko YG (2015) Properties and medical applications of polylactic acid : a review. eXPRESS Polym Lett 9(5):435–455. https://doi.org/10.3144/expresspolymlett.2015.42

Hao LC, Sapuan SM, Hassan MR, Sheltami RM (2018) 2—Natural fiber reinforced vinyl polymer composites. Natural fiber reinforced vinyl ester and vinyl polymer composites. Elsevier Ltd. pp 27–70. https://doi.org/10.1016/B978-0-08-102160-6.00002-0

Ibrahim N, Ab K, Uylan DN (2017) Physical and degradation properties of polylactic acid and thermoplastic starch blends—effect of citric acid treatment on starch structures. BioResources 12(2):3076–3087

Ismail AE, Khalid SNA, Nor NHM (2017) A review on the perforated impact energy absorption of kenaf fibres reinforced composites. IOP Conf Series: J Phys: Conf Series 914(2017):012044. https://doi.org/10.1088/1742-6596/914/1/012044

Jamshidian M, Tehrany EA, Imran M, Jacquot M (2010) Poly-lactic acid: production, applications, nanocomposites, and release studies. Compr Rev Food Sci Food Saf 9:552–571. https://doi.org/10.1111/j.1541-4337.2010.00126.x

Ke T, Sun X (2000) Physical properties of poly (Lactic Acid) and starch composites with various blending ratios. Cereal Chem 77(6):761–768. https://doi.org/10.1094/CCHEM.2000.77.6.761

Khan BA, Wang J, Wang H (2015) Mechanical properties of poly (lactic acid)/ hemp hurd biocomposites using glycidyl methacrylate. Paper presented at The 13th sian Textile Conference, Gelong Australia, 3–6 November 2015, pp 242–245

Krishnaiah P, Thevy C, Manickam S (2018) Morphology water absorption and biodegradable properties of polylactide biocomposites reinforced with sisal fibers. Mater Today: Proc 5(10):22506–22516

Kumar V, Kumari M, Kumar R (2013) Rapid synthesis of graft copolymers from natural cellulose fibers. Carbohydr Polym 98(1):820–828. https://doi.org/10.1016/j.carbpol.2013.06.072

Melo RQC, Santos WRG, Gilson A, Lima B De, Lima WMPB, Silva JV, Farias RP (2018) Water absorption process in polymer composites: theory analysis and applications. Adv Struct Mater 93:219–249. https://doi.org/10.1007/978-3-319-91062-8

Nanthakumar K, Yeng CM, Chun KS (2018) Tensile and water absorption properties of solvent cast biofilms of sugarcane leaves fibre-filled poly (Lactic) acid. J Thermoplast Compos Mater. pp 1–16. https://doi.org/10.1177/0892705718805526

Naveen J, Jawaid M, Amuthakkannan P, Chandrasekar M (2019) 5—Mechanical and physical properties of sisal and hybrid sisal fiber-reinforced polymer composites. Mechanical and physical testing of biocomposites, fibre-reinforced composites and hybrid composites. Elsevier Ltd. pp 428–440. https://doi.org/10.1016/B978-0-08-102292-4.00021-7

Parveen S, Rana S, Fangueiro R (2017) 13—Macro—and nanodimensional plant fiber reinforcements for cementitious composites. Sustainable and nonconventional construction materials using inorganic bonded fiber composites. Elsevier Ltd. pp 343–382 https://doi.org/10.1016/B978-0-08-102001-2.00020-6

Penjumras P, Russly AR, Rosnita AT, Khalina A (2015) Mechanical peoperties and water absorption behavior of durian rind cellulose reinforced poly(lactic acid) biocomposite. Int J Adv Sci Eng Inf Technol 5(5):343. https://doi.org/10.18517/ijaseit.5.5.574

Petinakis E, Yu L, Simon G, Dean K (2013) Natural fibre bio-composites incorporating poly(Lactic Acid). Fiber reinforced polymers—the technology applied for concrete repair. https://dx.doi.org/10.5772/52253

Rajesh G, Prasad AVR, Gupta A (2015) Mechanical and degradation properties of successive alkali treated completely biodegradable sisal fiber reinforced poly lactic acid composites. J Reinf Plast Compos 34(12):951–961. https://doi.org/10.1177/0731684415584784

Ramesh M (2016) Kenaf (*Hibiscus cannabinus L.*) fibre based bio-materials: a review on processing and properties. Prog Mater Sci 78–79:1–92. https://doi.org/10.1016/j.pmatsci.2015.11.001

Saba N, Jawaid M, Alothman OY, Paridah MT (2016) A review on dynamic mechanical properties of natural fibre reinforced polymer composites. Constr Build Mater 106:149–159. https://dpi.org/10.19080/CTFTTE.2017.01.555563

Saikia D (2010) Studies of water absorption behavior of plant fibers. Int J Thermophys 31:1020–1026. https://doi.org/10.1007/s10765-010-0774-0

Sercer M, Raos P, Rujnic-Sokele M (2009) Processing of wood-thermoplastic composites. Int J Mater Form 2(1):721–724. https://doi.org/10.1007/s12289-009-0654-y

Siakeng R, Jawaid M, Ariffin H, Sapuan SM, Asim M, Saba N (2018) Natural fiber reinforced polylactic acid composites: a review. Polym Compos 40(2):446–463. https://doi.org/10.1002/pc.24747

Singhvi M, Gokhale D (2013) Biomass to biodegradable polymer (PLA). The Royal Society of Chemistry 3(33):1–11. 1https://doi.org/10.1039/c3ra41592a

Tan J, Abdel-rahman MA, Sonomoto K (2018) Biorefinery-based lactic acid fermentation : microbial production of pure monomer product. Adv Polym Sci 279:27–66. https://doi.org./10.1007/12_2016_11

Tezara C, Siregar JP, Lim HY, Fauzi FA, Yazdi MH, Moey LK, Lim JW (2016) Factors that affect the mechanical properties of kenaf fiber reinforced polymer: a review. J Mech Eng Sci (JMES) 10(2):2159–2175. https://doi.org/10.15282/jmes.10.2.2016.19.0203

Tserki V, Matzinos P, Panayiotou C (2006) Novel biodegradable composites based on treated lignocellulosic waste flour as filler. Part II. Development of biodegradable composites using treated and compatibilized waste flour. Composites Part A: Applied Science and Manufacturing 37(9):1231–1238. https://doi.org/10.1016/j.compositesa.2005.09.004

Vitkevicius, P. (2017). Synthesis of Polylactic Acid. Master's Thesis in Chemical Engineering. 30 June 2017

Vroman I, Tighzert L (2009) Biodegradable polymers. Materials 2:307–344. https://doi.org/10.3390/ma2020307

Yousif BF, El-Tayeb NSM (2009) Mechanical and wear properties of oil palm and glass fibres reinforced polyester composites. Int J Precision Technol 1(2):213–22

Zandvliet C, Bandyopadhyay NR, Ray D (2014) Water Absorption of jute/ polylactic acid composite intended for an interior application and comparison with wood-based panels. J Inst Eng (India) Series D. 95(1):49–55. https://doi.org/10.1007/s40033-014-0040-x

Characterization of the Time of Phytosanitary Treatment of Frozen or Unfrozen Wood by Microwaves

F. Erchiqui and H. Kaddami

Abstract The traffic and transportation of wood products around the world is one of the causes that have facilitated the migration of pathogens and insects between countries. These biological invasions have resulted in the destruction of plant species, causing significant economic and ecological losses in many parts of the world. To this end, the World Trade Organization, through the International Plant Protection Convention Working Group, has established a standard for phytosanitary measures (ISPM 15), which requires that wood products (pallets, packaging, etc.) be treated according to this standard. It is within this framework that this chapter is included and aims to present a numerical approach to quantify the time required for microwave phytosanitary treatment of wood products. For this purpose, the microwave heat conduction equation is expressed in terms of volumetric enthalpy and numerical resolution is achieved using the finite element method. As an application, we considered three Canadian wooden. For the analysis, we considered a frequency of 2466 MHz, temperatures from −20 to +20 °C and a moisture content of 131%.

Keywords Phytosanitary treatment · Microwave · Orthotropic media · Thermal anisotropy · Enthalpy · Dielectric anisotropy · Finite element analysis

1 Introduction

Circulations of some wood products are identified as one of the dissemination vectors and spread of non-native pathogens and insects in several countries of the world. This biological invasion has caused the destruction of plant species, causing significant economic and ecological disasters in many regions of the world. The Millennium

F. Erchiqui (✉)
School of Engineering, Bioplasturgy Laboratory, University of Quebec in Abitibi-Temiscamingue, Université, Rouyn-Noranda, 445 boul, Québec, Canada
e-mail: fouad.erchiqui@uqat.ca

H. Kaddami
Department of Chemistry, Laboratory of Organomettalic and Macromolecular Chemitry, FST-Marrakech, Cadi Ayyad University, Avenue Abdelkrim Elkhattabi, B.P. 549, Marrakech, Morocco

M. T. Hameed Sultan et al. (eds.), *Biocomposite Materials*, Composites Science and Technology, https://doi.org/10.1007/978-981-33-4091-6_10

Ecosystem Assessment classifies them as one of the main causes of biodiversity loss, along with other factors, such as habitat destruction, climate change and pollution. For example, the North American forest (its extern part) is still endangered by the non-native Asian long-horned beetle (*Anoplophoraglabripennis*) and the emerald ash borer (*Agrilusplanipennis*) (USDA 2003). According to the Food and Agriculture Organization (FAO), this invasion is due mainly the combined effects of the climate change and wide traffic of packaged products. In addition, the devastative risks of these species invasion, which involve many interactions between various spatial and temporal parameters, are difficult to quantify (Yemshanov et al. 2009). Recent estimates of the global economic impacts of these species exceed US$120 billion annually; this includes agricultural, forestry and public health impacts (USDA 2003). In Canada, the economic impact on the agriculture and forestry sectors has been estimated at Can $7.5 billion annually (Yemshanov et al. 2009). To face this new global reality, the International Plant Protection Convention (IPPC) working group promulgated the "International Standards for Phytosanitary Measures 15 (ISPM 15)" regulation in 2009 on the treatment of phytosanitary of all wood and wood-based materials. This standard aims to protect ozone layer and thus forbids polluting and fights against the international dissemination and spread of pathogens, fungi and insects that could endanger agricultures or ecosystems (FAO 2009; Fields et al. 2002). Thereby, ISPM-15 imposed and authorized thermal and chemical treatments of the circulating woods and packaging materials to destructs these pathogens (FAO 2009). Nevertheless, these treatments have economical and ecological side effects and drawbacks. For example Cooper et al. have pointed out the issue of recycling of these materials by raising out the health impact of reusing chemically sanitized wood and wood based materials (Cooper et al. 1996): What is the health hazard to burn borate or Imidacloprid sanitized firewood? What is the generated environmental impact and health hazard if chemically treated materials are recycled for application in outdoor conditions where are subjected to rainfall and sunlight (Nzokou et al. 2008a, b)?

Dielectric heating treatment was ratified in ISPM 15 In 2013. It was proven that this heating technique is very effective in destroying pathogens (Nzokou et al. 2008a, b). Nevertheless, ISPM-15 has indorsed 56 °C as minimum temperature to destroy pathogens in piece of wood thicker than 6 mm when using this technique.

In regard of the heating efficiency of this technique, one of the major advantages is the production of heat inside the material in a short period of time (Norimoto and Gril 1989), (Gašparík and Barcík 2013, 2014), (Oloyede and Groombridge 2000), (Hansson and Antti 2003). Nevertheless, the assessment of the heat distribution generated by dielectric heating in wood and the prediction of the time of its phytosanitary treatment is a very hard task. Indeed, these predictions are tribytary to many parameters such as (i) the non-isotropic dielectric, mechanical and thermal properties of wood, (ii) the product geometry and design, and (iii) its initial temperature and humidity, etc. Moreover, considering the diversity of wood based commercial products how is it possible to make sure of the total destroying of pathogens by dielectric heating treatment? At this stage, several uncertainties concerning the efficiency of such a treatment eliminating pathogens are to be checked. Thus, numerical

simulation and modeling in predicting the processing time become challenging. In these conditions, a multi-physical model is needed for these simulation and modeling and its effectiveness is directly related to how mathematically Maxwell's equations are coupled to conservation equations for wood? (Brodie 2007; Rattanadecho and Suwannapum 2009; Erchiqui et al. 2013; Erchiqui 2013a, b; Rattanadecho 2006; Zhu et al. 2007; Ni and Datta 2002). This raises a big challenge for numerical simulation since this has to consider the combined intricacies of mass and heat transfers, phase change as well as thermomechanical and electromagnetic interactions of a highly hygroscopic, thermally weak conductive and structurally anisotropy material as wood (Torgovnikov 1993; Norimoto and Yamada 1971). Several models are tested in literature to face these major challenges. The empirical model of Beer-Lambert is one of the most used models for Maxwell's equations. This model is valid for semi-infinite medium and can quantify the microwaves energy loss in irradiated material (Erchiqui et al. 2013). Thus, an extensive question evolves: To which extend this model is still applicable for wood considered as finished anisotropic medium. In the case of microwaves as well as for radiofrequency, a criterion of applicability is provided in (Zhu et al. 2007; Erchiqui 2013a, b). This defines a critical thickness of wood sample to respect by considering the penetration depth (cm) of the radiation inside the sample. However, in the case of frozen wood, the ice melting (phase change) during microwave heating should be considered, especially in this case when the medium is considered as anisotropic. This evolves a difficult question from numerical modeling vantage point since one or more moving boundaries are to be considered. To overcome this issue, two ways can be used, in general: resolving independently the equations of energy for the liquid and solid phases, and considering the moving solid–liquid interface (Hu and Argyropoulos 1995a, b; Panrie et al. 1991), or resolving the enthalpy function considered as the equation of energy (Erchiqui et al. 2013). On the other hand, when a phase change is to be considered, several modeling approaches could be found in literature in the area of wood and food sciences (Ohlsson and Bengston 1971; Swami 1982; Rattanadecho 2006; Bhattacharya et al. 2002; Basak and Ayappa 1997; Coleman 1990).

In the present work, which is a synthesis of work we carried out recently, we are treating the phytosanitary treatment of anisotropic frozen wood microwaves heating in order to numerically determine the time of application this kind of dielectric heating. To this end, a finite element 3D approach, involving the enthalpy-volume energy is elaborated. On the other hand, the wood sample is considered of parallelepiped geometry and the incident microwaves are plan and oriented perpendicularly to its faces. For such purpose, three Canadian wood species with different physico-chemical properties have been studied: trembling aspen (Populus tremuloidesMichx), white birch (Betula papyrifera) and sugar maple (Acer saccharum).

2 General Considerations

We assume that in this work the treatment by microwave of the wood species does not induce the degradation of its physical and mechanical properties. This aspect will be considered in this work since the highest temperatures that will be reached are far below the degradation temperature of wood. On the other hand, the focus will be on the numerical modeling aspect, through the consideration of nonlinear thermo-physical and electrical properties. Also, the influence of the mass transfer will not be taken into account in this modeling work. The nonlinear heat conduction problem involving phase changes such as wood freezing is solved using three-dimensional volumetric specific enthalpy based on finite-element analysis. This study focused on a sample cube of wood 22 mm thick. We chose a moisture content of 131% for which the freezing phenomenon is pronounced. The choice of this high moisture content made the modeling process more delicate to handle with since one has to deal with water melting (phase change) during the heating process. The samples considered in this study derive from the external zone of the trunk (see Fig. 1). This choice is justified by geometrical considerations since for this part of the trunk one can easily make the assumption of cylindrical coordinates. On the other hand, this part of the wood (sapwood) is considered to have the tree's storage function. This part of the wood, which is wanted by microorganisms and insects, is frequently subjected to pathogen attack, in contrast to the heartwood, which has a relatively natural resistance to attack by microorganisms owing to the extractives that are stored within its dead cells (disposal site for harmful by-products of cellular metabolism).

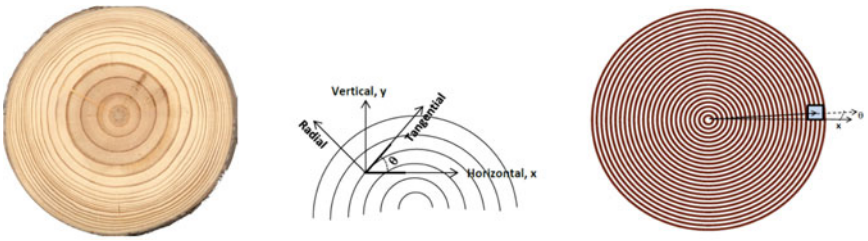

A tree trunk

Geometrical model for a tree trunk

Sample wood used in present modelling

Fig. 1 Wood sample's cross section with illustrations the angle of the ring curves and of the radial and angular position

3 Thermal Properties of Wood

Three principal thermal conductive properties, namely thermal conductivity, specific heat and thermal diffusivity, are to be considered when modeling the heat process of wood. Generally, all three properties vary with the specific gravity SG, based on dry mass and green volume, the wood moisture content MC, expressed as a percentage/fraction of the ovendry mass of the wood and the temperature T. However, the ring orientation on a wood sample has a considerable effect on the rate of heat transfer. An example of a wood sample with curved rings is shown in Fig. 1. The two directions x and y shown in this figure are not exactly radial and tangential directions as defined by the wood anatomical structure; they will be called vertical and horizontal directions in the following. Accordingly, thermal conductivities in both directions on wood samples are usually different from the true radial and tangential direction. However, the thermal conductivities in the x and y directions can be calculated from the following formula:

$$k_x = -k_r \sin\theta + k_t \cos\theta \; and \; k_y = k_r \cos\theta + k_t \sin\theta \tag{1}$$

Obviously, the thermal conductivity values change with the location, the θ angle and the radial position r of the sample. For illustrative purposes, one average angle, defined at the center of mass of the sample relative to the x-axis, is considered. For heat transfer analysis, we consider an angular position close to zero (see Fig. 1). Under these conditions, we have: $k_x \cong k_t$, $k_y \cong k_r$ and $k_z = k_l$. The analytical expressions of the thermal conductivity, in the radial direction of the wood material, according to Kanter, are given in (Steinhagen and Harry 1988). The dependence of the thermal conductivity on temperature is generally low; it increases from 2 to 3% by 10 deg. For several species of wood, the ratio of longitudinal (kL) versus radial (kR) thermal conductivity is around 1.75 and 2.2, while the tangential thermal conductivity (kT) is usually slightly smaller (0.9 to 0.95 times) than the radial conductivity (Kanter 1975; USDA 1977).

The specific heat capacity of wood, Cp, which represents the thermal energy required to produce one-unit change of temperature in one unit of mass, is sensitive to humidity. The presence of water improves the specific heat of the wood because the specific heat of the water is greater than that of the wood.

For specific heat capacity, Cp, which represents the thermal energy required to produce one unit change of temperature in one unit of mass, an increase in moisture improves the specific heat of the wood because the specific heat of the water is greater than that of the wood. The analytical expressions, according to Steinhagen, are given in (Steinhagen and Harry 1988).

Thermal diffusivity, which is a measure of how rapidly a material can absorb heat from its surroundings, is related to thermal conductivity, specific heat capacity and density (Kanter 1975; USDA 1977). Density (kg/m^3), which represents the weight of wood divided by the volume at a given moisture content, is one of the most important physical properties. The analytical expression for density considered in this work is that given in (Simpson and Tenwolde 1999).

Finally, to study wood heating (thawing or not), it is important to quantify the value of the latent heat of wood species. For this purpose, we can use the formula provided by Chudinov (1965):

$$L = L_W \left(\frac{MC - 30\%}{MC + 100\%} \right) \tag{2}$$

L_w is the latent heat of water fusion (334 kJ/kg).

4 Complex Dielectric Properties of Wood

Propagation of electromagnetic waves in materials is determined by their electrical and dielectric parameters. In the case of dielectrics, the parameter of greatest interest is the complex permittivity, ε $(= \dot{\varepsilon} - j\varepsilon'')$, where $j = \sqrt{-1}$. This parameter describes the ability of the material to support an electric field: the real part of ε, known as the dielectric constant, describes the ability of a material to store energy and the imaginary part of the ε, known as the loss factor, describes the ability of a material to dissipate energy, which naturally results in heat generation. Usually, depending on the type of material, the permittivity varies with each phase of the material, since the concentration of molecules and their bonding in the material differ. Several theories have been proposed to describe the permittivity of dielectrics from the constituent elements, concentration and particle size and shape (Zielonka and Gierlik 1999; Phillips et al. 2001). For wood material, complex permittivity varies with the type of wood species, density, frequency, moisture content, temperature and structural orientation. From the electromagnetic point of view, it is desirable to refer to the complex *relative permittivity*, ε_r, as being its permittivity with respect to that of free space, ε_0, such that $\varepsilon = \varepsilon_r \varepsilon_0$.

For wood material, according to (Peyskens et al. 1984), the values of the longitudinal dielectric constant ($\boldsymbol{\varepsilon}_L$) are 1.25–3 times higher than the tangential dielectric constant ones ($\boldsymbol{\varepsilon}_T$), while the ratio of the tangential versus radial dielectric constant ($\boldsymbol{\varepsilon}_R$) is about 0.9 and 1.25.

With regard to the interactions between the material and the electric field, two physical parameters are of primary interest: the absorption and storage of electric potential energy within the dielectric material, and the dissipation or loss of part of this energy when the electric field is removed (James 1975). This dissipation of energy in the material induces effects on heat and mass transfer. To this end, note that the conductive heat process by microwave energy in different directions of wood has two important characteristics: (i) the amplitude of the oscillation of electromagnetic power distribution and (ii) the magnitude of the heat transfer rate. A rigorous mathematical formulation of the heating process requires a good knowledge of the power flux (Poynting vector) associated with electromagnetic microwave propagation, which is a solution of Maxwell's equation in anisotropic dielectric material.

For anisotropic dielectric wood, both the electric charge density (ρ) and the electric currents (***J***) are equal to zero. Furthermore, the following linear interrelations can be established between the electric and magnetic properties (Pozar 2011):

$$\boldsymbol{D} = \overline{\overline{\boldsymbol{\varepsilon}}} \cdot \boldsymbol{E} \text{ and } \boldsymbol{B} = \overline{\overline{\boldsymbol{\mu}}} \cdot \boldsymbol{H} \tag{3}$$

where **E**, **B**, **H**, and **D** are the electric field (V m^{-1}), the magnetic field (Wb m^{-2}), the magnetic induction (A m^{-1}), and the electric displacement (C m^{-2}), respectively. $\overline{\overline{\boldsymbol{\varepsilon}}}$ and $\overline{\overline{\boldsymbol{\mu}}}$ are, respectively, the relative dielectric and permeability tensors. For wood, it is generally believed that the magnetic permeability tensor $\overline{\overline{\boldsymbol{\mu}}}$ is closely approximated by the real tensor $\mu_0 \overline{\overline{\boldsymbol{I}}}$ ($\overline{\overline{\boldsymbol{I}}}$ is the identity tensor) (Erchiqui 2013a, b). μ_0 (H/m) is the permeability of vacuum.

Rotation of the electric field vector E on 180° does not change the dielectric properties of wood materials (Pozar 2011). So, when E is arbitrarily oriented in space and forms an angle θ_1 with the longitudinal direction, angle θ_2 with the transversal direction, and angle θ_3 with the tangential direction, closed-form expressions for calculating the relative dielectric constant, ε', and the dielectric loss tangent, tan δ, is given in (Peyskens et al. 1984).

5 Enthalpy Model for Heating of Orthotropic Media

In anisotropic materials, thermal energy flows at different rates along different directions. This is taken into account by assigning a second-order tensor character to the thermal conductivity. The *x*-component of the heat flux vector q_x becomes (Bergman et al. 2011):

$$q_x = -\left(k_{xx}\frac{\partial T}{\partial x} + k_{xy}\frac{\partial T}{\partial y} + k_{xz}\frac{\partial T}{\partial z}\right) \tag{4}$$

and similarly for the other two directions. For orthotropic materials, heat still travels at different rates along different directions but the heat flux along any direction is driven only by the temperature gradient along that direction, i.e. $k_{ij} = 0$ when i ≠ j. The heat equation then becomes

$$\rho C_p \frac{\partial T}{\partial t} = \frac{\partial}{\partial x}\left(k_{xx}(T)\frac{\partial T}{\partial x}\right) + \frac{\partial}{\partial y}\left(k_{yy}(T)\frac{\partial T}{\partial y}\right) + \frac{\partial}{\partial z}\left(k_{zz}(T)\frac{\partial T}{\partial z}\right) \tag{5}$$

In this paper, we solve the energy equation in terms of the enthalpy function and assume that the interface Γ between the solid (Ω^-) and liquid (Ω^+) phases can be described by a regular function F (x, y, z, t) = 0 (Hu and Argyropoulos 1995a, b). The temperature in the solid and liquid phases is denoted by T_s and T_l respectively. Using a temperature-based formulation, the two energy equations that govern both solid and liquid media are written in the absence of convective motion:

$$\rho^s(T_s)C_p^s(T_s)\frac{\partial T_s}{\partial t} = \frac{\partial}{\partial x}\left(k_{xx}^s\frac{\partial T_s}{\partial x}\right)+\frac{\partial}{\partial y}\left(k_{yy}^s\frac{\partial T_s}{\partial y}\right)+\frac{\partial}{\partial z}\left(k_{zz}^s\frac{\partial T_s}{\partial z}\right),\quad F(x,y,z,t)<0 \tag{6}$$

$$\rho^l(T_l)C_p^l(T_l)\frac{\partial T_l}{\partial t} = \frac{\partial}{\partial x}\left(k_{xx}^l\frac{\partial T_l}{\partial x}\right)+\frac{\partial}{\partial y}\left(k_{yy}^l\frac{\partial T_l}{\partial y}\right)+\frac{\partial}{\partial z}\left(k_{zz}^l\frac{\partial T_l}{\partial z}\right),\quad F(x,y,z,t)>0 \tag{7}$$

where ρ^s [kg/m^3], C_p^s[J/kg/°C] and k^s [W/m/°C] are respectively the density, the specific heat capacity and the thermal conductivity of the material in the solid state. ρ^l [kg/m^3], C_p^l[J/kg/°C] and k^l [W/m/°C] are respectively the density, specific heat capacity and thermal conductivity of the material in the liquid state.

The boundary conditions, also known as the Stefan conditions (Hu and Argyropoulos 1995a, b), allow us to consider the energy jump between the two phases:

$$T_s(x,y,z,t)=T_l(x,y,z,t);F(x,y,z,t)=0 \tag{8}$$

$$\left(k_x^s(T_s)\frac{\partial T_s}{\partial x},k_y^s(T_s)\frac{\partial T_s}{\partial y},k_z^s(T_s)\frac{\partial T_s}{\partial z}\right)\cdot\nabla F-\left(k_x^l(T_l)\frac{\partial T_l}{\partial x},k_y^l(T_l)\frac{\partial T_l}{\partial y},k_z^l(T_l)\frac{\partial T_l}{\partial z}\right)\cdot\nabla F = -\rho.L\frac{\partial F}{\partial t} \tag{9}$$

L is the latent heat [J/kg].

In order to avoid numerical problems in the phase transition region, the variables were changed. The temperature-dependent density ρ(T) and specific heat capacity C_p(T) can be replaced by the volumetric specific enthalpy H(T) defined by (Nedjar 2002):

$$H(T)=\int_{T_{ref}}^{T}\rho(T)c_p(T)dT \tag{10}$$

where T_{ref} [°C] is a reference temperature.

The advantage of using an enthalpy—rather than a temperature-based formulation is that it simultaneously eliminates the doubling of the energy equation and the Stefan conditions. By introducing the volumetric specific enthalpy H(T) at the phase transition, the abrupt jump in the volumetric heat capacity is transformed into a relatively smoother temperature-dependent function. It can be shown that, around phase transition, the curvature of volumetric specific enthalpy H(T) is similar to that of thermal conductivity k(T). H(T) depends strongly on the type of material, although a clear distinction must be made between the following two situations. In the first case, the phase change occurs in an interval $[T_1^s-T_2^f]$. In this case the enthalpy is

defined by:

$$H\left(T \le T_1^s\right) = \int_{T_{ref}}^{T} \rho^s(T) C_p^s(T) dT \tag{11}$$

$$H\left(T_1^s < T \le T_2^f\right) = \int_{T_{ref}}^{T_1^s} \rho^s(T) C_p^s(T) dT + \int_{T_1^s}^{T} \rho(T) \frac{\partial L}{\partial T} dT, \tag{12}$$

$$H\left(T > T_2^f\right) = \int_{T_{ref}}^{T_1^s} \rho^s(T) C_p^s(T) dT + \rho(T) L + \int_{T_2^f}^{T} \rho^f(T).C_p^f(T) dT \tag{13}$$

In the second case, the phase change occurs at a constant temperature so the enthalpy exhibits discontinuity at the fusion temperature, $T_m\left(= \mathrm{T}_1^s = \mathrm{T}_2^f\right)$, and is defined as follows:

$$H(T \le T_m) = \int_{T_{ref}}^{T} \rho^s(T) C_p^s(T) dT \tag{14}$$

$$H(\mathrm{T} > \mathrm{T_m}) = \int_{\mathrm{T_{ref}}}^{\mathrm{T_m}} \rho^{\mathrm{s}}(\mathrm{T}) \mathrm{C_p^s}(\mathrm{T}) \mathrm{dT} + \rho(\mathrm{T}) \mathrm{L} + \int_{\mathrm{T_m}}^{\mathrm{T}} \rho^{\mathrm{f}}(\mathrm{T}).\mathrm{C_p^f}(\mathrm{T}) \mathrm{dT} \tag{15}$$

Zero enthalpy is defined at the saturated solid temperature. For purposes of numerical simulation, the enthalpy method is more reliable. However, the problem remains difficult and highly nonlinear. Following a procedure similar to the enthalpy transform method, the temperature-dependent thermal conductivity can be substituted by the thermal conductivity integral, using Kirchhoff's transformation:

$$\theta_x(T \le T_m) = \int_{T_{ref}}^{T} k_{xx}^s(T) dT;$$

$$\theta_y(T \le T_m) = \int_{T_{ref}}^{T} k_{yy}^s(T) dT;$$

$$\theta_z(T \le T_m) = \int_{T_{ref}}^{T} k_{zz}^s(T) dT; \quad \forall T \tag{16}$$

$$\theta_x(T > T_m) = \int_{T_m}^{T} k_{xx}^l(T)dT;$$

$$\theta_y(T > T_m) = \int_{T_m}^{T} k_{yy}^l(T)dT;$$

$$\theta_z(T > T_m) = \int_{T_m}^{T} k_{zz}^l(T)dT \tag{17}$$

To do so, we consider Leibniz's rule (Flanders 1973) for differentiation under the integral sign in Eqs. (14)–(15) and (16)–(17):

$$\frac{\partial H}{\partial t} = \rho(T)c_p(T)\frac{\partial T}{\partial t} \tag{18}$$

$$\frac{\partial \theta_x}{\partial x} = k_{xx}(T)\frac{\partial T}{\partial x}; \quad \frac{\partial \theta_y}{\partial y} = k_{yy}(T)\frac{\partial T}{\partial y}; \quad \frac{\partial \theta_z}{\partial z} = k_{zz}(T)\frac{\partial T}{\partial z} \tag{19}$$

With these transformations, and taking into account the internal volumetric heat generation of microwave energy P_{wave}, the governing heat equation reduces to a partial differential system, with two mutually related dependent variables H and $\theta = (\theta_x, \theta_y, \theta_z)$:

$$\frac{\partial H(T)}{\partial T} = \left(\frac{\partial^2 \theta_x}{\partial x^2} + \frac{\partial^2 \theta_y}{\partial y^2} + \frac{\partial^2 \theta_z}{\partial z^2}\right) + P_{wave} \tag{20}$$

For microwaves sources, the internal volumetric heat generation of microwave energy P_{wave} is given by the following expression

$$P_{wave}(T) = -Re(\nabla \cdot S) \tag{21}$$

where S is the instantaneous Poynting vector. To solve the problem, we introduce the boundary condition into Eq. (22) as follows:

$$\left(n_x\frac{\partial \theta_x}{\partial x} + n_y\frac{\partial \theta_y}{\partial y} + n_z\frac{\partial \theta_z}{\partial z}\right) + h(T - T_\infty) - \boldsymbol{q} \cdot \boldsymbol{n} = 0 \tag{22}$$

where q [W/m^2] is the radiative heat flux incident, **n** is the outward normal (n_x, n_y, n_z) to the surface h, [W/m^2/°C] is the surface heat transfer coefficient, and T_∞ is the temperature of the surrounding medium (air). The term h ($T–T_\infty$) represents the convection heat transfer from the material to the environment. The incident heat flux depends on the source configuration and the position of the material. The advantage

of using an enthalpy- rather than a temperature-based formulation is that it simultaneously eliminates the doubling of the energy equation and the Stefan conditions (Erchiqui 2013a, b).

5.1 Implicit Time Integration Scheme

Numerical time approximation schemes are used mainly to obtain the transient response. These numerical integration schemes derive recursion relations that relate H(t) at a moment of time t to H(t + Δt) at another moment of time $t+\Delta t$. The solution is then solved step by step starting from the initial conditions at time $t = 0$ until the desired duration of the transient response is calculated. The most common numerical schemes for the solution of Eq. (20) belong to the weighted Euler difference family of time approximations, as follows (Dokainish and Subbraj 1989):

$$H^{n+\theta} = (1-\theta)H^n + \theta H^{n+1}, \text{ with } : \theta = \frac{t - t_n}{\Delta t} \tag{23}$$

The parameter θ varies in the range [0–1]. The θ schemes are unconditionally stable when $\theta \leq 1/2$ and O(Δt) are accurate, with the exception of the $O(\Delta t^2)$–convergent Crank–Nicolson scheme ($\theta = 1/2$). Setting $\theta = 1$ leads to the backward Euler (fully implicit) scheme, which is only first-order accurate but very stable and hence ideally suited for integration. In the present study, we consistently use the semi-implicit Crank–Nicolson scheme (Dokainish and Subbraj 1989). In this case, Eq. (24) becomes:

$$\left(\boldsymbol{K}^*_{n+1} + G^*_{n+1}\right)\boldsymbol{H}_{n+1} = \boldsymbol{K}^*_n.\boldsymbol{H}_n + \boldsymbol{G}^*_n.\boldsymbol{H}^2_n + \boldsymbol{R}^*_{n,n+1} \tag{24}$$

where $\mathbf{K}^*$, $\mathbf{G}^*$ and $\mathbf{R}^*$ are modified global matrices and $\mathbf{H}_{n+1}$ is the vector of global nodal enthalpies at moment t_{n+1}.

6 Electromagnetic-Wave Energy and Poynting's Theorem

The time-dependent power flow density of an electromagnetic wave is given by the instantaneous Poynting vector S (Pozar 2011):

$$S = \frac{1}{2}\boldsymbol{E} \times \boldsymbol{H}^* \tag{25}$$

$\mathbf{E}$ and $\mathbf{H}^*$ are the electric field (V m^{-1}) and the conjugate magnetic field intensity (A m^{-1}), respectively. In general, we are dealing with steady-state harmonic time-varying fields. It is convenient to represent each field vector as a complex phasor by

applying a Fourier transform. Assuming that we have a monochromatic wave, we can write:

$$\boldsymbol{E}(\boldsymbol{r}, t) = e^{-j\omega t}\overline{\boldsymbol{E}}(\boldsymbol{r}) \tag{26}$$

where $\overline{\mathbf{E}}$ is a complex vector and a function of **r** (m), and ω (radian s^{-1}) is the angular frequency of the incident radiation. The other field vectors can be written using the same notation as in Eq. (26).

6.1 Maxwell's Equations and Power Dissipation

A propagating electromagnetic wave is composed of oscillating electric (**E**) and magnetic (**H**) fields. The space and time dependence of these fields are described by the following Maxwell's equations:

$$\nabla \times \boldsymbol{E} = -\frac{\partial \boldsymbol{B}}{\partial t}, \tag{27}$$

$$\nabla \times \boldsymbol{H} = \boldsymbol{J} - \frac{\partial \boldsymbol{D}}{\partial t}, \tag{28}$$

where **E**, **B**, **H**, **J** and **D** are the electric field (V m^{-1}), the magnetic field (Wb m^{-2}), the magnetic induction (A m^{-1}), the current density (A m^{-2}), and the electric displacement (C m^{-2}), respectively.

Considering the definition of the Poynting vector **S**, as in (25), and using both the identity vector and Maxwell's equations with the complex conjugate field **H**, (29) can be derived from (27) and (28) as follows:

$$\begin{aligned}\nabla \cdot \mathbf{S} = \frac{1}{2}\nabla \cdot \left(\mathbf{E} \times \mathbf{H}^*\right) &= -\frac{1}{2}\left[\mathbf{E} \cdot \left(\nabla \times \mathbf{H}^*\right) - \mathbf{H}^* \cdot (\nabla \times \mathbf{E})\right] \\ &= -\frac{1}{2}\left(\mathbf{E} \cdot \frac{\partial \mathbf{D}^*}{\partial \mathrm{t}} + \mathbf{E} \cdot \mathbf{J}^* + \mathbf{H}^* \cdot \frac{\partial \mathbf{B}}{\partial \mathrm{t}}\right)\end{aligned} \tag{29}$$

The vector **S** depends on the explicit electric currents, the temporal variations of the electric displacement, and the magnetic induction.

6.2 The Case of Anisotropic Dielectric Materials

For anisotropic dielectric wood, both the electric charge density (ρ) and the electric currents (***J***) are equal to zero. Furthermore, the following linear interrelations can be established between the electric and magnetic properties:

$$\boldsymbol{D} = \varepsilon_0 \overline{\overline{\boldsymbol{\varepsilon}}} \cdot \boldsymbol{E} \tag{30}$$

$$\boldsymbol{B} = \mu_0 \overline{\overline{\boldsymbol{\mu}}} \cdot \boldsymbol{H} \tag{31}$$

$$\mathbf{J} = 0 \tag{32}$$

where ε_0 is the dielectric permittivity ($= 8.8541 \times 10^{-12}$ F/m) of the free space and μ_0 is the permeability of vacuum ($= 4\pi \times 10^{-7} \cong$ H/m). $\overline{\overline{\boldsymbol{\varepsilon}}}$ and $\overline{\overline{\boldsymbol{\mu}}}$ are, respectively, the relative dielectric and permeability tensors:

$$\overline{\overline{\boldsymbol{\varepsilon}}} = Re(\overline{\overline{\boldsymbol{\varepsilon}}}) - jIm(\overline{\overline{\boldsymbol{\varepsilon}}}) \text{ and } \overline{\overline{\boldsymbol{\mu}}} = Re(\overline{\overline{\boldsymbol{\mu}}}) - jIm(\overline{\overline{\boldsymbol{\mu}}}) \tag{33}$$

with:

$$Re(\overline{\overline{\boldsymbol{\varepsilon}}}) = \begin{bmatrix} \varepsilon'_{\mathrm{LL}} & \varepsilon'_{\mathrm{LR}} & \varepsilon'_{\mathrm{LT}} \\ \varepsilon'_{\mathrm{RL}} & \varepsilon'_{\mathrm{RR}} & \varepsilon'_{\mathrm{RT}} \\ \varepsilon'_{\mathrm{TL}} & \varepsilon'_{\mathrm{TR}} & \varepsilon'_{\mathrm{TT}} \end{bmatrix}, \; Im(\overline{\overline{\boldsymbol{\varepsilon}}}) = \begin{bmatrix} \varepsilon''_{\mathrm{LL}} & \varepsilon''_{\mathrm{LR}} & \varepsilon''_{\mathrm{LT}} \\ \varepsilon''_{\mathrm{RL}} & \varepsilon''_{\mathrm{RR}} & \varepsilon''_{\mathrm{RT}} \\ \varepsilon''_{\mathrm{TL}} & \varepsilon''_{\mathrm{TR}} & \varepsilon''_{\mathrm{TT}} \end{bmatrix} \tag{34}$$

and

$$Re(\overline{\overline{\boldsymbol{\mu}}}) = \begin{bmatrix} \mu'_{\mathrm{LL}} & \mu'_{\mathrm{LR}} & \mu'_{\mathrm{LT}} \\ \mu'_{\mathrm{RL}} & \mu'_{\mathrm{RR}} & \mu'_{\mathrm{RT}} \\ \mu'_{\mathrm{TL}} & \mu'_{\mathrm{TR}} & \mu'_{\mathrm{TT}} \end{bmatrix}, \; Im(\overline{\overline{\boldsymbol{\mu}}}) = \begin{bmatrix} \mu''_{\mathrm{LL}} & \mu''_{\mathrm{LR}} & \mu''_{\mathrm{LT}} \\ \mu''_{\mathrm{RL}} & \mu''_{\mathrm{RR}} & \mu''_{\mathrm{RT}} \\ \mu''_{\mathrm{TL}} & \mu''_{\mathrm{TR}} & \mu''_{\mathrm{TT}} \end{bmatrix} \tag{35}$$

The subscripts L, R, and T are respectively the longitudinal, radial, and tangential directions.

In general, we are dealing here with steady-state harmonic time-varying fields. It is convenient to represent each field vector as a complex phasor by applying a Fourier transform. Assuming that we have a monochromatic wave, we can write:

$$\mathbf{E}(\mathbf{r}, \mathrm{t}) = \mathrm{e}^{-\mathrm{j}\omega \mathrm{t}} \overline{\mathbf{E}}(\mathbf{r}), \tag{36}$$

where $\overline{\mathbf{E}}$ is a complex vector and function of $\mathbf{r}$, and $\boldsymbol{\omega}$ is the angular frequency of the wave. The other field vectors can be written using the same notation of Eq. (36).

Following the application of (30)–(32) and (36), (29) will be reduced to the equation below:

$$\nabla \cdot \boldsymbol{S} = -j\frac{\omega}{2}\left(\left[\varepsilon_0\left(\overline{\mathbf{E}} \cdot \overline{\overline{\boldsymbol{\varepsilon}}} \cdot \overline{\mathbf{E}}^*\right)\right] + \left[\mu_0\left(\overline{\mathbf{H}} \cdot \overline{\overline{\boldsymbol{\mu}}} \cdot \overline{\mathbf{H}}^*\right)\right]\right) \tag{37}$$

Introducing the complex expressions of the dielectric permittivity and the magnetic permeability tensors, we get from (37):

$$\mathrm{Re}(\nabla \cdot \boldsymbol{S}) = -\frac{\omega}{2}\left(\varepsilon_0\left(\overline{\boldsymbol{E}} \cdot \mathrm{Im}(\overline{\overline{\boldsymbol{\varepsilon}}}) \cdot \overline{\boldsymbol{E}}^*\right) + \mu_0\left(\overline{\mathbf{H}} \cdot \mathrm{Im}(\overline{\overline{\boldsymbol{\mu}}}) \cdot \overline{\mathbf{H}}^*\right)\right) \tag{38}$$

$$\mathrm{Im}(\nabla \cdot \boldsymbol{S}) = -2\omega\left(\frac{1}{4}\varepsilon_0\left(\overline{\boldsymbol{E}} \cdot \mathrm{Re}(\overline{\overline{\boldsymbol{\varepsilon}}}) \cdot \overline{\boldsymbol{E}}^{*}\right) + \frac{1}{4}\mu_0\left(\overline{\boldsymbol{H}} \cdot \mathrm{Re}(\overline{\overline{\boldsymbol{\mu}}}) \cdot \overline{\boldsymbol{H}}^{*}\right)\right) \tag{39}$$

Note that (38) shows that the real part of (∇.**S**) is equal to the power dissipated per unit volume in the form of heat. The imaginary part of the complex (∇.**S**), Eq. (39), is equal to 2ω times the net reactive power stored per unit volume and time-average of electric W_e and magnetic W_m. energy densities (Hollis 1983):

$$\langle W_e \rangle = \mathrm{Im}\left(\frac{1}{T}\int_0^T W_e dt\right) = \frac{1}{4}\varepsilon_0\left(\overline{\boldsymbol{E}} \cdot Re(\overline{\overline{\boldsymbol{\varepsilon}}}) \cdot \overline{\boldsymbol{E}}^{*}\right) \tag{40}$$

$$\langle W_m \rangle = \mathrm{Im}\left(\frac{1}{T}\int_0^T W_m dt\right) = \frac{1}{4}\mu_0\left(\overline{\boldsymbol{H}} \cdot \mathrm{Re}(\overline{\overline{\boldsymbol{\mu}}}) \cdot \overline{\boldsymbol{H}}^{*}\right) \tag{41}$$

where W_e and W_m are respectively the instantaneous electric and magnetic energy densities, and T is the period. The quantity ($\langle W_e \rangle + \langle W_m \rangle$) (J/m^3) is the total time average stored energy density of the electromagnetic field in the anisotropic dielectric material.

The real part of the complex (∇.**S**), is equal to 2ω times the net power dissipated per unit volume and time-average of electric $\langle W_e \rangle$ and magnetic $\langle W_m \rangle$ energy densities:

$$P_{wave} = \frac{\omega}{2}\left(\varepsilon_0\left(\overline{\boldsymbol{E}} \cdot \mathrm{Im}(\overline{\overline{\varepsilon}}) \cdot \overline{\boldsymbol{E}}^{*}\right) + \mu_0\left(\overline{\boldsymbol{H}} \cdot \mathrm{Im}(\overline{\overline{\boldsymbol{\mu}}}) \cdot \overline{\boldsymbol{H}}^{*}\right)\right) \tag{42}$$

ε_0 is the dielectric permittivity (= 8.8541 × 10^{-12} F/m) of the free space and $\boldsymbol{\mu}_0$ is the permeability of vacuum (= 4$\boldsymbol{\pi}$ × 10^{-7} ≅ **H**/**m**). $\overline{\overline{\varepsilon}}$ and $\overline{\overline{\boldsymbol{\mu}}}$ are, respectively, the complex relative dielectric and complex permeability tensors. In wood systems, the magnetic permeability tensor $\overline{\overline{\boldsymbol{\mu}}}$ is closely approximated by the real tensor $\boldsymbol{\mu}_0\overline{\overline{\boldsymbol{I}}}$; ($\overline{\overline{\boldsymbol{I}}}$ is the identity tensor), (Kaestner and Bååth 2005). This is what we assumed in this paper. Thus, the power dissipated per unit volume, as in (42), becomes:

$$P_{wave} = \frac{\omega}{2}\varepsilon_0\left(\mathbf{E} \cdot \mathrm{Im}(\overline{\overline{\boldsymbol{\varepsilon}}}) \cdot \boldsymbol{E}\right) \tag{43}$$

Computing the power dissipation involves determining the electric field as a function of the position within the material. If **E** is parallel with one of the three principal directions (longitudinal, radial or tangential) of the wood sample, the power dissipated per unit volume may be simplified as (see Appendix):

$$P_{net} = \frac{\omega}{2}\varepsilon_0\varepsilon_d'' E_d^2 \tag{44}$$

where ε_d'' is the dielectric constant in the principal direction d: longitudinal (L), radial (R) and tangential (T). Assuming the electro-neutrality of wood ($\nabla(\nabla \cdot E) = 0$), we

deduce for each principal direction from Maxwell's equations the expression of Helmholtz's equation of wave propagation (Erchiqui 2013a, b):

$$\nabla^2 \overline{\boldsymbol{E}} - \gamma^2 \overline{\boldsymbol{E}} = 0 \tag{45}$$

where γ is the constant complex propagation $\gamma = \alpha + j\beta$, β is the attenuation constant and α is the phase (a constant). These parameters are related to the dielectric properties of the material and frequency of radiation by:

$$\alpha = \frac{\omega}{c}\sqrt{\frac{\varepsilon'}{2}\left(\sqrt{1+\tan^2\delta}+1\right)} \quad \beta = \frac{\omega}{c}\sqrt{\frac{\varepsilon'}{2}\left(\sqrt{1+\tan^2\delta}-1\right)} \tag{46}$$

$c = 1/\sqrt{\mu_0 \varepsilon_0}$ is the speed of light. The term $\delta\,(= \mathrm{tg}^{-1}(\varepsilon''/\varepsilon'))$ is the dielectric loss angle. The attenuation constant, β, controls the rate at which the incident field intensity decays into a sample. $1/(2\beta)$ is known as the penetration depth (d). The phase constant, α, represents the change of phase of the propagation radiation and is related to the wavelength of radiation by $\lambda = 2\pi/\alpha$.

6.3 *Uniform Plane Wave Propagation and Power Dissipation*

In this paper, we assume that each component of the electric field $\mathbf{E} = \left(\mathbf{E_x}, \mathbf{E_{y,}}, \mathbf{E_z}\right)$ is a uniform plane microwave. Also, each component of a wave is assumed to be incident normally on opposite faces of the sample:

x direction: longitudinal direction L

$$\mathbf{E_x} = \mathrm{E_x(z)}\mathbf{a_x} \tag{47}$$

y direction: radial direction R

$$\mathbf{E_y} = \mathrm{E_y(x)}\mathbf{a_y} \tag{48}$$

z direction: tangentiel direction T

$$\mathbf{E_z} = \mathrm{E_z(y)}\mathbf{a_z} \tag{49}$$

where x is a component of the electric field ($\mathrm{E_x}$), which is a function of the parameter z, y is a component of the electric field ($\mathrm{E_y}$), which is a function of the parameter x, and z is a component of the electric field ($\mathrm{E_z}$), which is a function of the parameter y (see Fig. 2).

For each direction, according to Eq. (45), we have the following expression for Helmholtz's equation of wave propagation:

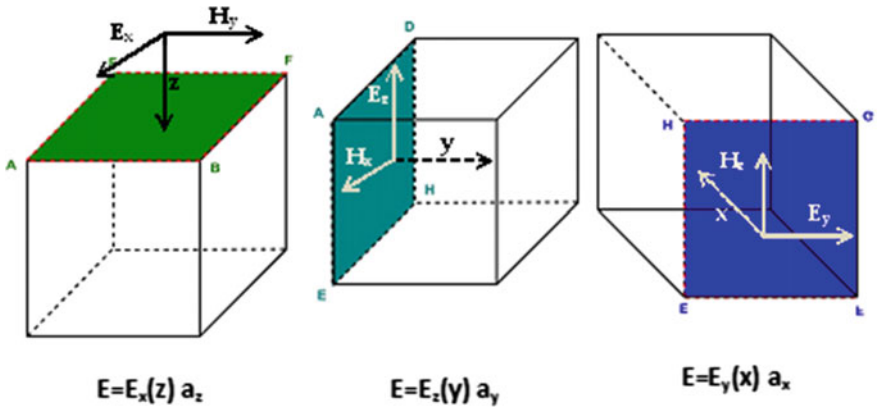

Fig. 2 Schematic of sample wood exposed to plane microwaves from the three principal faces

Longitudinal direction:

$$\frac{d^2E_z}{dy^2}\boldsymbol{a_z} - \gamma_y^2 E_z \boldsymbol{a_z} = 0, \quad 0 \le y \le L_y \tag{50}$$

Radial direction:

$$\frac{d^2E_y}{dx^2}\boldsymbol{a_y} - \gamma_x^2 E_y \boldsymbol{a_y} = 0, \quad 0 \le x \le L_x \tag{51}$$

Tangential direction:

$$\frac{d^2E_x}{dz^2}\boldsymbol{a_x} - \gamma_z^2 E_x \boldsymbol{a_x} = 0, \quad 0 \le z \le L_z \tag{52}$$

L_x, L_y and L_z are, respectively, the length of the sample wood in the x, y and z directions (see Fig. 1). The unit vectors a_z, a_y and a_x are, respectively, the normal to the surface (AEFB), (ADHE) and (HCTE) of the sample wood (see Fig. 2).

The waves travel through the material from right to left with an incident power flux I_0. The regions external to the sample are denoted by index 1 for the left and index 3 for the right. The material is denoted by index 2. The exact solutions for the power absorbed of each principal direction of material are given respectively by the following expressions (Erchiqui 2013a, b):

Longitudinal direction:

$$P^x_{wave} = 2I^x_0\beta^x \left[\frac{e^{-2\beta^x x} + \left(\overline{R}^x_{23}\right)^2 e^{-4\beta^x L_x} e^{2\beta^x x} + 2\overline{R}^x_{23} e^{-2\beta^x L_x} \cos\left(2\alpha^x (x - L_x) - {}^x_{23}\right)}{1 + \left(\overline{R}^x_{12}\right)^2 \left(\overline{R}^x_{23}\right)^2 e^{-4\beta^x L_x} - 2\overline{R}^x_{12}\overline{R}^x_{23} \cos\left({}^x_{12} + {}^x_{23} + 2\alpha^x L_x\right) e^{-2\beta^x L_x}} \right] \tag{53}$$

Radial direction:

$$P_{wave}^{y} = 2I_0^y \beta^y \left[\frac{e^{-2\beta^y y} + \left(\overline{R}_{23}^{y}\right)^2 e^{-4\beta^x L_y} e^{2\beta^y y} + 2\overline{R}_{23}^{y} e^{-2\beta^y L_y} \cos\left(2\alpha^y \left(y - L_y\right) - \frac{y}{23}\right)}{1 + \left(\overline{R}_{12}^{y}\right)^2 \left(\overline{R}_{23}^{y}\right)^2 e^{-4\beta^y L_y} - 2\overline{R}_{12}^{y} \overline{R}_{23}^{y} \cos\left(\frac{y}{12} + \frac{y}{23} + 2\alpha^y L_y\right) e^{-2\beta^y L_y}} \right] \quad (54)$$

Tangential direction:

$$P_{wave}^{z} = 2I_0^z \beta^z \left[\frac{e^{-2\beta^z z} + \left(\overline{R}_{23}^{z}\right)^2 e^{-4\beta^z L_z} e^{2\beta^z z} + 2\overline{R}_{23}^{z} e^{-2\beta^z L_z} \cos\left(2\alpha^z (z - L_z) - \frac{z}{23}\right)}{1 + \left(\overline{R}_{12}^{z}\right)^2 \left(\overline{R}_{23}^{z}\right)^2 e^{-4\beta^z L_z} - 2\overline{R}_{12}^{z} \overline{R}_{23}^{z} \cos\left(\frac{z}{12} + \frac{z}{23} + 2\alpha^z L_z\right) e^{-2\beta^z L_z}} \right] \quad (55)$$

The superscripts x, y z are associated respectively with the longitudinal, radial and tangential directions. θ_{ij} is the phase angle for reflection coefficient at the interface between layers i and j. $\overline{R}_{ij}$ is the absolute value of the complex reflection coefficient.

7 Validation of the Proposed Method

To validate the proposed approach, three situations are considered: (i) heat transfer in one-dimensional raw beef sample exposed to microwave energy (Ayappa et al. 1991), (ii) heat transfer in an orthotropic plate with imposed temperatures (Bruch and Zyroloski 1974) and (iii) heat transfer of frozen wood with phase change: imposed temperatures (Steinhagen and Harry 1988).

7.1 Numerical Heating Validation

To validate the specific volumetric enthalpy-based finite element developed in this work, we consider the results obtained in for a raw beef sample exposed to microwave radiation. In this example, the author solves an isothermal heat conduction equation where the dielectric and thermophysical properties are constants. For our study, we consider a linear mesh with 42 elements and 41 nodes. Figure 3 compares the power distribution and the predicted temperature profile for the raw beef sample exposed to radiation from the left face. The results obtained in (Ayappa et al. 1991) are similar to ours for both formulations.

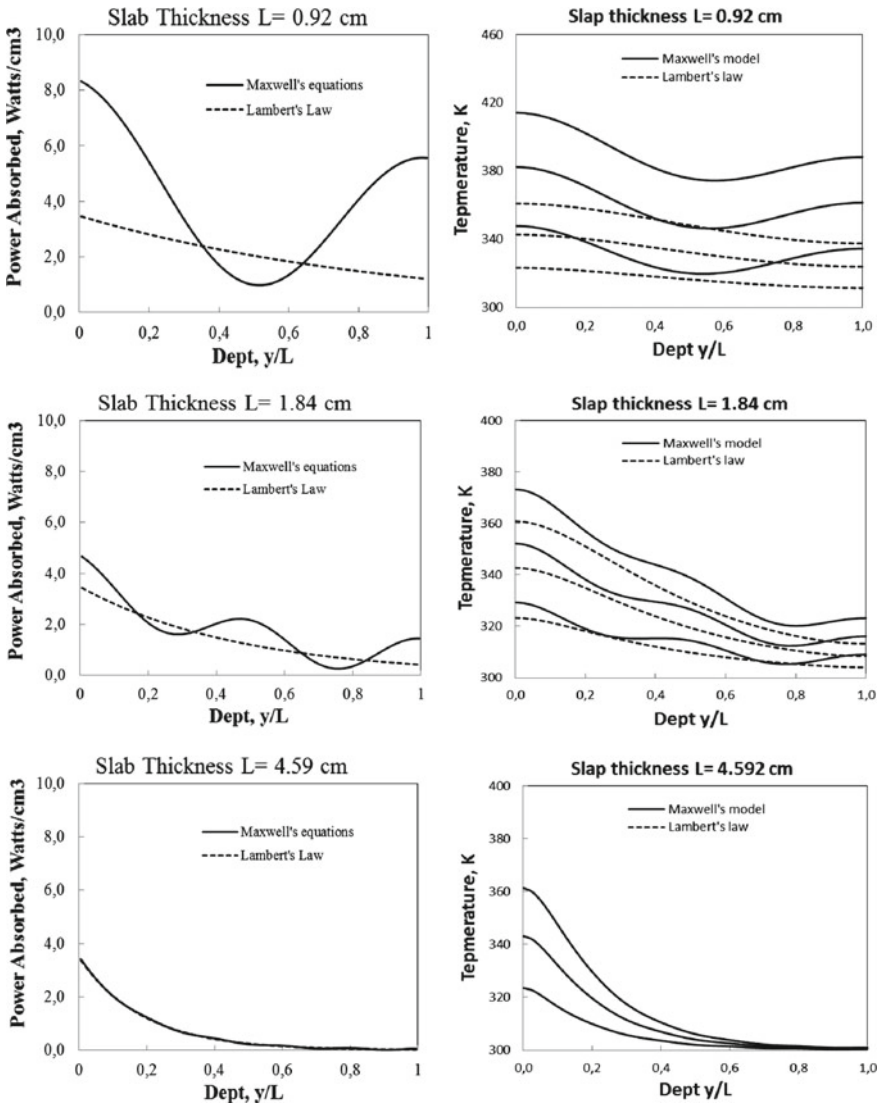

Fig. 3 Influence of slab thickness on power and predicted temperature for raw beef sample exposed to microwave from the left, I0 = 3 W/cm^2, f = 2450 MHz

7.2 Analytical Heat Transfer in an Orthotropic Plate: Imposed Temperatures

For analytical validation, we consider an orthotropic plate subjected to a uniform temperature. The temperature T (x, y, t) across the thickness with time t is computed

Table 1 Geometrical and thermophysical properties of material

Density ρ (kg/m^3)	1.0
Specific heat C_p (J kg^{-1} °C^{-1})	1.0
Thermal conductivity k_x, x direction, (W m^{-1} °C^{-1})	0.2
Thermal conductivity k_y, y direction, (W m^{-1} °C^{-1})	0.4
Length in x direction (m)	1.0
Length in y direction (m)	1.0

using Laplace transforms to solve the 2D energy equation with an imposed temperature (Bruch and Zyroloski 1974). The thickness as well as the physical properties of material used in the numerical validation is given in Table 1. For the finite-element analysis, we consider a quadrilateral mesh with 400 elements and 441 nodes. In the case where the initial temperature of the plate is 30 °C and the imposed temperature is 0 °C, the analytical solution is given by the following equation (Bruch and Zyroloski 1974):

$$T(x,y,t) = \sum_{n=1}^{\infty}\sum_{j=1}^{\infty} A_n \sin\frac{n\pi x}{L_x}\sin\frac{j\pi y}{L_y}\exp\left[-\left(\frac{k_x n^2\pi^2}{L_x^2}+\frac{k_y j^2\pi^2}{L_y^2}\right)\frac{t}{\rho C_p}\right] \quad (56)$$

where:

$$A_n = \left[\frac{120}{\pi^2 jn}\left[(-1)^n - 1\right]\left[(-1)^j - 1\right]\right] \quad (57)$$

where k_x and k_y are respectively the thermal conductivity in the x and y directions. L_x and L_y are respectively the length and width of the plate. Table 2 compares, at t = 0.25 s, the predicted temperature obtained by the theoretical equation with the volumetric enthalpy based on the finite-element method. The results illustrate the excellent agreement between the theoretical and numerical solutions. The agreement is very good with an error of less than 1.0%. For greater precision, a more refined mesh is necessary.

7.3 Experimental Heating Validation: Transient Heating of Frozen Logs

In this section, firstly, we consider the experimental temperature measurements obtained for transient heating of frozen logs (Steinhagen and Harry 1988), then, those obtained in (Peralta and Bangi 2006). For both tests, it involves heating a tree trunk immersed in water at a temperature of 54 °C. In the first case, it is trembling aspen log (radius is 0.3175 m and its initial temperature is −22 °C). In the second

Table 2 Temperature distribution at time = 0.25 s

	X (m)					
Y (m)	0.0	0.2	0.4	0.6	0.8	1.0
0.0	0.000[a]	0.000[a]	0.000[a]	0.000[a]	0.000[a]	0.000[a]
	0.000	0.000	0.000	0.000	0.000	0.000
0.2	0.000[a]	3.832[a]	6.196[a]	6.196[a]	3.832[a]	0.000[a]
	0.000	3.864	6.250	6.250	3.864	0.000
0.4	0.000[a]	6.121[a]	9.898[a]	9.898[a]	6.121[a]	0.000[a]
	0.000	6.163	9.969	9.969	6.163	0.000
0.6	0.000[a]	6.121[a]	9.898[a]	9.898[a]	6.121[a]	0.000[a]
	0.000	6.163	9.969	9.969	6.163	0.000
0.8	0.000[a]	3.832[a]	6.196[a]	6.196[a]	3.832[a]	0.000[a]
	0.000	3.864	6.250	6.250	3.864	0.000
1.0	0.000[a]	0.000[a]	0.000[a]	0.000[a]	0.000[a]	0.000[a]
	0.000	0.000	0.000	0.000	0.000	0.000

[a]Numerical results with *ThermoForm* code

test, it is eastern white pine log (the trunk radius is 0.2285 m and its initial temperature is −23 °C). In (Steinhagen and Harry 1988), it is assumed that logs is subjected to radial heating. In (Peralta and Bangi 2006), it is assumed that logs is subjected to orthotropic heating (radial and longitudinal). For both tests, the heating time is 60 h. The thermo-physical properties of the wood material are given in (Steinhagen and Harry 1988) and (Peralta and Bangi 2006) respectively. For finite element analysis, we consider a quadrilateral mesh (see Fig. 4).

In Fig. 5, we presented the history of the temperature obtained numerically and experimentally in the center of the trembling aspen trunk (Steinhagen and Harry

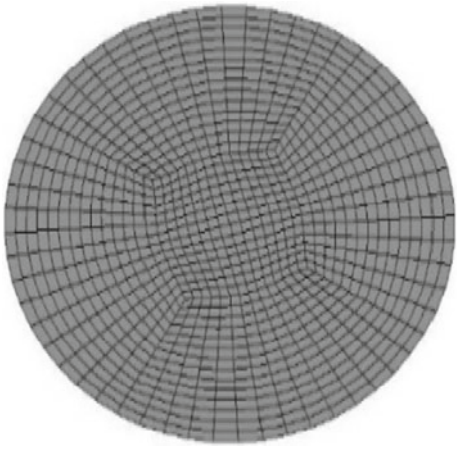

Fig. 4 Circular (2D) geometry mesh

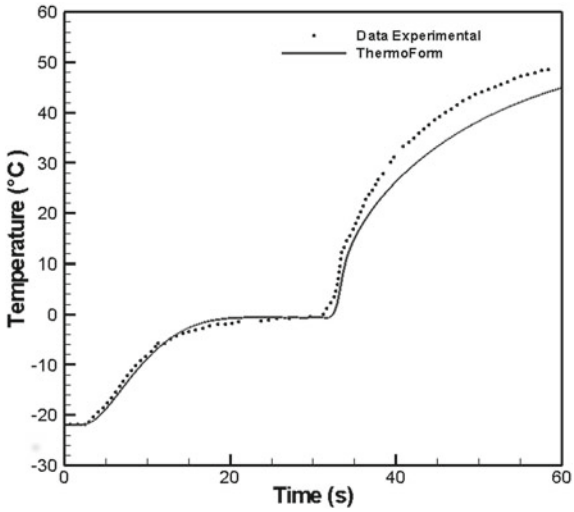

Fig. 5 Experimental end numerical temperature versus heating time at the centre of log

1988). Figure 6 illustrates views of the numerical temperature distribution at different times: 900, 1800, 2700, and 3600 min.

In Fig. 7, we presented the temperature against heating time for three different points located 22.9 cm (location 1), 10.2 cm (location 2), and 2.5 cm (location 3) from the surface of an eastern white pine log (Peralta and Bangi 2006). The numerical results for the heating of frozen wood showed an excellent agreement with the experimental data, in both cases of tests.

8 Numerical Application: Characterization of the Time of Phytosanitary Treatment Wood by Microwaves

This study focused on 22-mm-thick boards. This dimension corresponds to the standard value for boards used in the manufacture of EUR EPAL® pallets. For this, a 3D wood log is considered for three wood species: *trembling aspen, white birch* and *sugar maple*. The log is considered to be orthotropic and its thermal and dielectric properties are functions of temperature, moisture content and structural orientation. The log structure is square ($L_x = L_y = L_z = 2.2$ cm). The principal orientations in sample woods are indicated by x for the longitudinal direction (L), y for the radial direction (R), and z for the tangential direction (T).

To analyze the thermal and dielectric anisotropy effect on thawing frozen wood using microwave energy, we considered the following situation:

$$k_L = 1.8k_R \text{ and } k_T = 0.9k_R \tag{58}$$

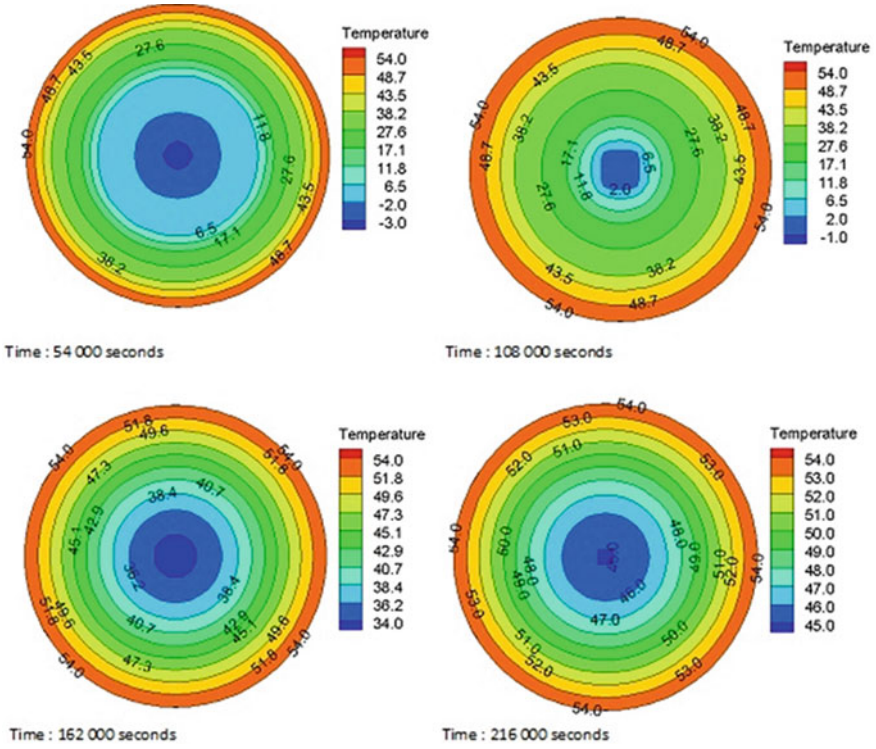

Fig. 6 Temperature versus heating time at the centre of log

$$\boldsymbol{\varepsilon}_{\mathrm{L}} = 1.8\boldsymbol{\varepsilon}_{\mathrm{R}} \text{ and } \boldsymbol{\varepsilon}_{\mathrm{T}} = 0.9\boldsymbol{\varepsilon}_{\mathrm{R}} \tag{59}$$

The wood material is exposed to radiation of equal intensity (1 W/cm^2) and frequency (2466 MHz from six faces): two faces in the x direction, two faces in the y direction, and two faces in the z direction. The initial wood temperature varies from −20 to 20 °C. The no-isothermal complex dielectric properties of the three wood species, for a moisture content (MC) at 131% (MC), are given in (Erchiqui et al. 2020). The specific gravity (SG) is 0.32, 0.48 and 0.55 for aspen, white birch and sugar maple respectively. The no-isothermal longitudinal relative dielectric constant ε' and the relative dielectric loss ε'' are given in reference (Erchiqui et al. 2020). In this application, the density (ρ), specific heat capacity (C_p) and radial conductivity (k_R) are calculated by the formulas provided in (Steinhagen and Harry 1988).

Figure 8 presents, at time 200 s and initial temperature −20 °C, different views of the surface temperature distribution induced by microwave treatment of the aspen trembling, birch white and sugar maple. At this time, Fig. 9 presents, for the trembling aspen log on the half-planes of symmetry (longitudinal, radial and tangential directions), the profiles of temperature distribution predicted from the power dissipation computed from Maxwell's equations.

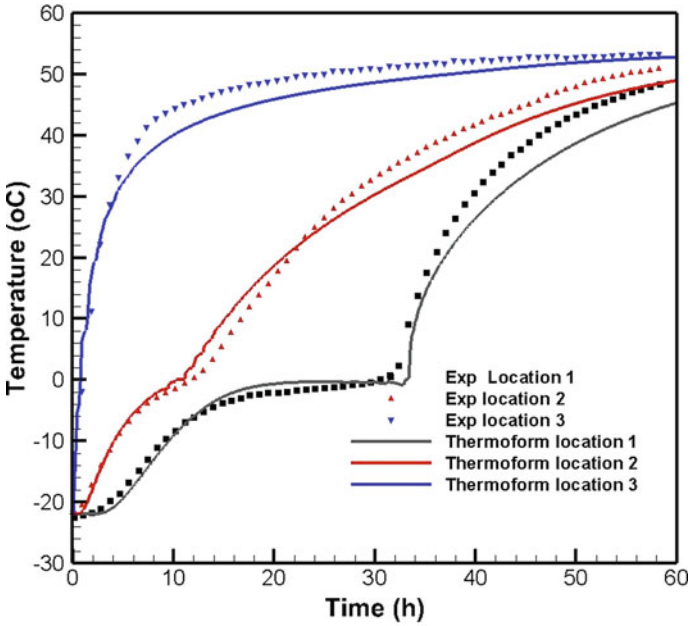

Fig. 7 Experimental and numerical temperature versus heating time for three different points located from the surface of an eastern white pine log

Figure 9(b–d) show different views of the temperature distribution in the longitudinal, radial and tangential directions, respectively. Similarly, Figs. 10 and 11 present the temperature distribution profiles for sugar maple and white birch, respectively. Significant differences can clearly be seen in temperature distribution when comparing the three directions and the three studied woods. In fact, for aspen and sugar maple, the longitudinal direction of the wood is preferred to temperature increase. On the other hand, for white birch, we note that the temperature profile associated with the longitudinal direction dominates at the edges and the center of the sample. Beyond these regions, for white birch, the temperature profile associated with the tangential direction dominates. One can also note that the highest temperatures were reached for the aspen wood sample, followed by white birch.

From the thermo-physical point of view, since the thermal conductivity and specific heat of each of the three hardwoods involve the same formulas, see reference (Steinhagen and Harry 1988), these differences could only be attributed to the differences in the density of these woods. As illustrated in Table 3, aspen is lighter while sugar is the densest wood. Indeed, the heating time increases with the density. This confirmation is due to the dependence of the volume enthalpy on density. In the melting zone (solid ice), the latent melting enthalpy of fusion is proportional to the density (ρ_L). Also, from the electromagnetic point of view, the oscillatory nature of the electromagnetic wave is another parameter which affects the temperature profile. Indeed, the propagation of electromagnetic radiation in a wood medium is a result of

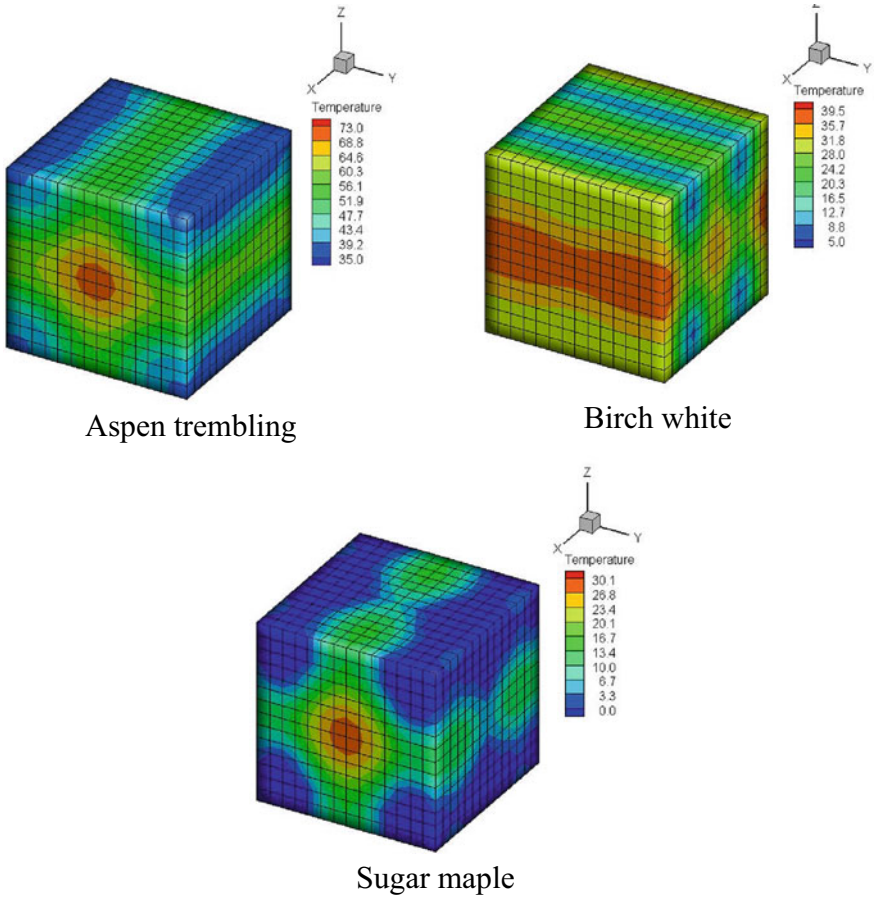

Fig. 8 Surface temperature distribution for aspen trembling, white birch and sugar maple, exposed to microwave at time = 200 s, $I_0 = 1$ W/cm^2, f = 2466 MHz, $T_0 = -20$ °C

a transmitted microwave at the incident face and a reflected microwave from the end surface. This situation, which affects the quality of the signal of the power absorbed by the wood, also affects the temperature profile. Indeed, a slight difference between the dielectric properties in the radial and tangential directions can have significant effects on the temperature profiles and power distributions. Consequently, it is very difficult to predict, from the complex dielectric and thermophysical properties of wood, the evolution of the temperature profile. Under these conditions, the experimental tools for characterization and the numerical modeling (mass transfer, phase change and thermomechanical and electromagnetic interactions) must be considered.

For the following analysis, we denote TA, WB and SM the trembling aspen, white birch and sugar maple. Figures 12, 13 and 14 represent the times required to eliminate 10, 25, 50, 75, and 100% of pathogens by microwave energy from trembling aspen,

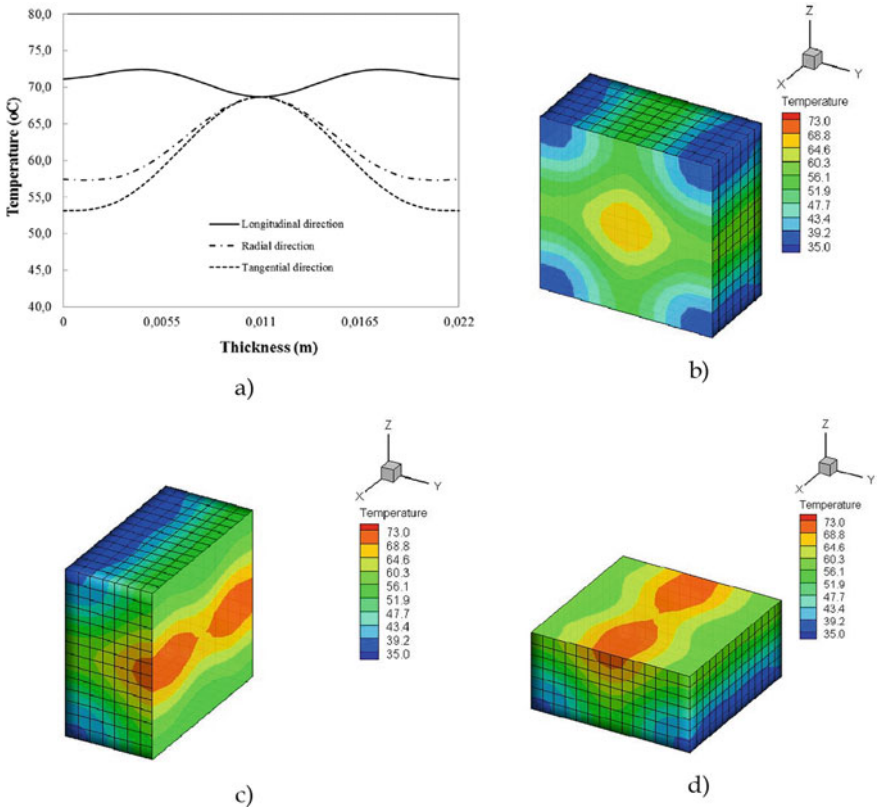

Fig. 9 **a** Temperature profiles distribution and views of the temperature distribution at half-planes of symmetry of **b** longitudinal, **c** radial and **d** tangential direction for aspen trembling sample exposed to microwave at time = 200 s, $I_0 = 1$ W/cm^2, f = 2466 MHz, $T_0 = -20$ °C

white birch, and sugar maple, respectively for initial temperatures of −15, +0 and 15 °C. The percentage of disinfected sapwood is defined as the fraction of wood that reaches the temperature of 56 °C. One can easily note that the required treatment time to reach 100% disinfection increases when the initial temperature decreases. On the other hand, the treatment time of complete disinfection by microwave energy is significantly higher when the initial temperature is below zero. This finding is explained by the accumulation of latent energy in the heating of the solid ice present in the material. Once exceeded, the material temperature increases more easily (thermal conductivity in the liquid region is high). Figure 15 summarizes various minimum times required to achieve 100% disinfection as a function of initial temperature and wood type for lower temperatures and higher temperatures. One can clearly see that the minimum time to achieve 100% disinfection depends strongly on the wood type and on the initial temperature. For example, at the initial temperature of −20 °C, this time is 262, 306 and 380 s for trembling aspen, white birch and sugar maple,

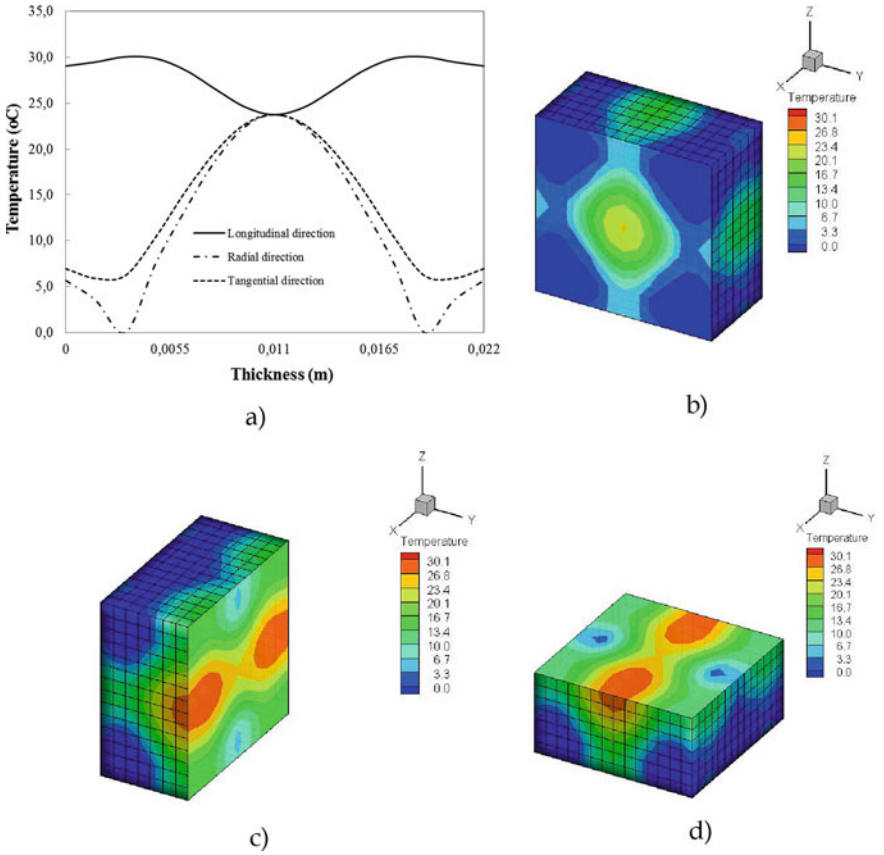

Fig. 10 **a** Temperature profiles distribution and views of the temperature distribution at half-planes of symmetry of **b** longitudinal, **c** radial and **d** tangential direction for sugar maple sample exposed to microwave at time = 200 s, $I_0 = 1$ W/cm^2, f = 2466 MHz, $T_0 = -20$°C

respectively. At + 20 °C, this time is 101 s, 106 s and 132 s for trembling aspen, white birch and sugar maple, respectively.

As a note, the example presented in this chapter concerns the numerical estimation of the phytosanitary treatment time, using microwave energy, for three types of Canadian wood for a simple geometry. However, the approach proposed to model the heat equation in terms of anisotropic enthalpy of volume is, in our opinion, very robust and applicable, a priori, to any type of wood product (frozen or unfrozen). However, in cases where the product to be treated by microwaves is a multi-material with multi-orientation of the thermal conductivity matrices, it is then appropriate to use more appropriate approaches such as the one presented in (Erchiqui and Annasabi 2019). Moreover, this new approach, coupled with Maxwell's equations, is under development.

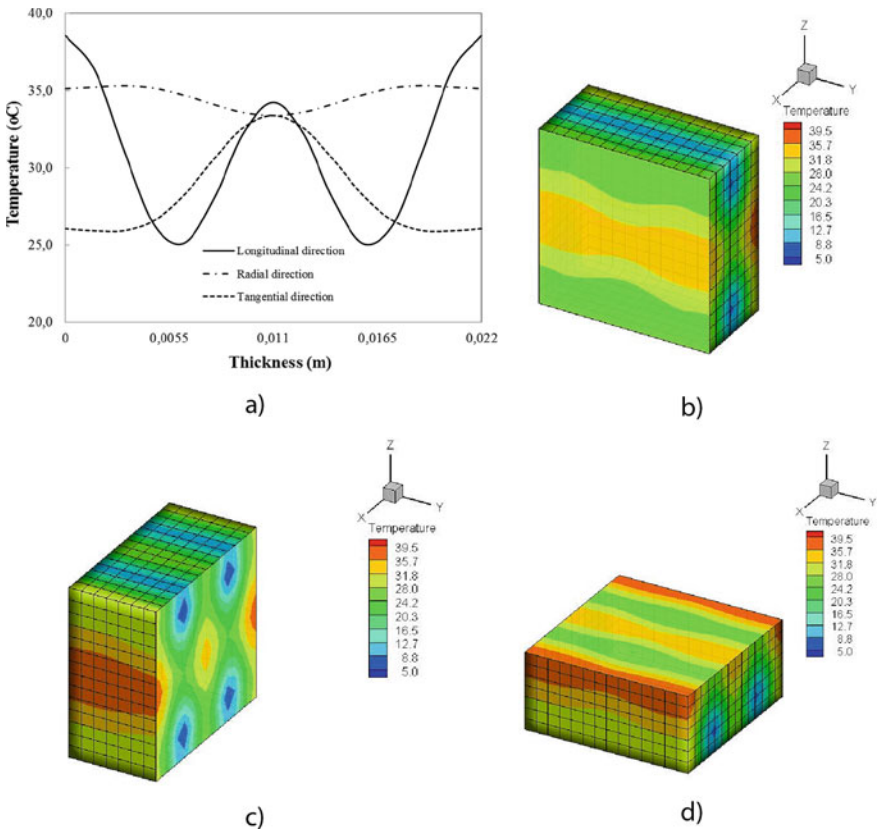

Fig. 11 **a** Temperature profiles distribution and views of the temperature distribution at half-planes of symmetry of **b** longitudinal, **c** radial and **d** tangential direction.for white birch sample exposed to microwave at time = 200 s, $I_0 = 1$ W/cm^2, f = 2466 MHz, $T_0 = -20$ °C

Table 3 Density (MC = 131%, at ambient temperature)

Hardwood	Density (kg/m^3)
Trembling aspen (TA)	808
White birch (WB)	1109
Sugar maple (SM)	1264

9 Conclusion

This chapter describes a numerical approach, based on the 3D finite element method, to estimate the time required to disinfect wood products (frozen or unfrozen). For this, the heat conduction equation in terms of anisotropic volume enthalpy is considered. The study concerns the estimation of the optimal time for the phytosanitary treatment of three species of Canadian wood by microwave in accordance with FAO

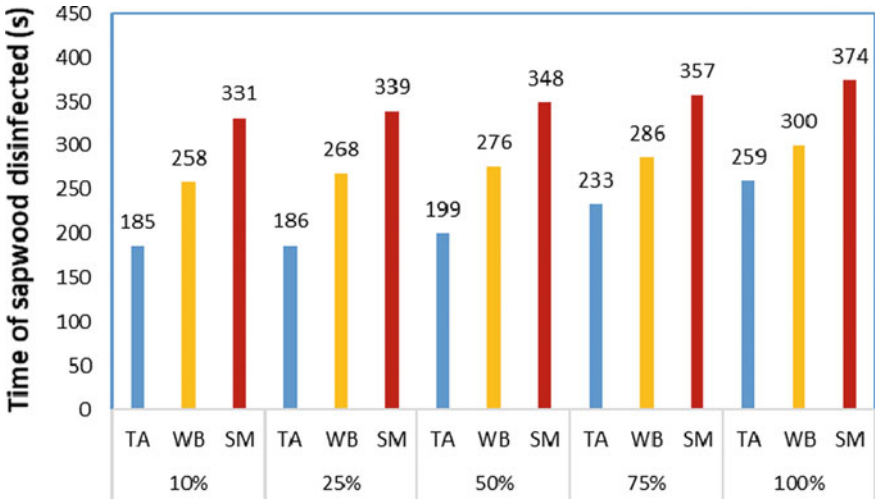

Fig. 12 Heat treatment by microwave energy ($I_0 = 1$ W/cm^2, f = 2466 MHz): Evolution of percentage sapwood disinfected (initial temperature is –15 °C)

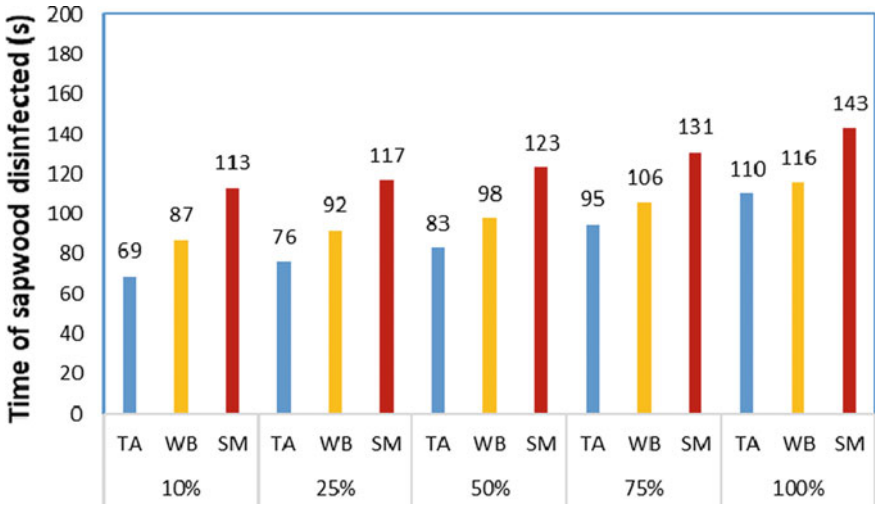

Fig. 13 Heat treatment by microwave energy ($I_0 = 1$ W/cm^2, f = 2466 MHz): Evolution of percentage sapwood disinfected (initial temperature is 0 °C)

International Standard No. 15. The dielectric and thermophysical properties are a function of temperature, moisture content and orientation of the structure. From this modelling study, it was possible to accurately estimate the time required to reach the temperature recommended by the FAO International Standard. This makes it possible to optimize the time and thus the energy of the microwave heat treatment.

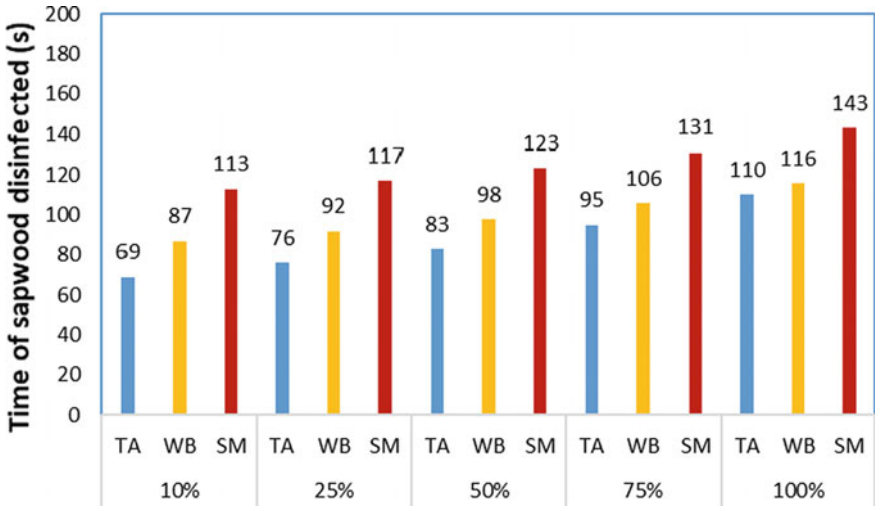

Fig. 14 Heat treatment by microwave energy ($I_0 = 1$ W/cm^2, f = 2466 MHz): Evolution of percentage sapwood disinfected (initial temperature is 15 °C)

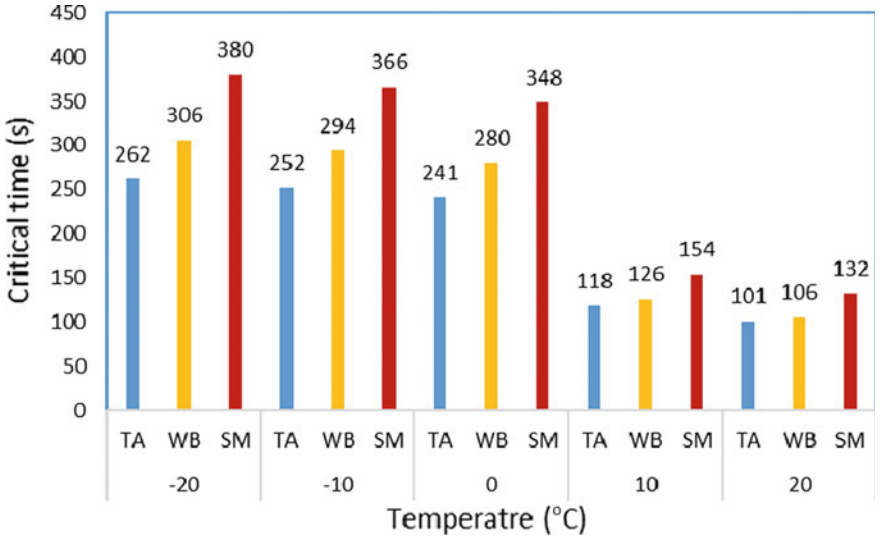

Fig. 15 Effect of initial temperature on critical time* of heat treatment by microwave (MC = 131%, SG = 0.32). *Time required for 100% disinfection. It can also defined as: $t_{crt} = \min\left(t_{crt}^{lon}, t_{crt}^{rad}, t_{crt}^{tan}\right)$

More general cases will be studied in future work to establish the relationship between the treatment time, the initial temperature, the geometry of the sample wood and the physical properties of the wood.

Appendix

Electric Field in Parallel with One of the Three Principal Directions of the Wood

Rotation of the electric field vector **E** on 180° does not change the dielectric properties of wood materials (Vyacheslav Komarov 2012). That is, L, R and T are the principal axes of anisotropy and the tensor $\overline{\overline{\boldsymbol{\varepsilon}}}$ in Eq. (8) may be simplified as

$$\overline{\overline{\boldsymbol{\varepsilon}}} = \begin{bmatrix} \varepsilon_L & 0 & 0 \\ 0 & \varepsilon_R & 0 \\ 0 & 0 & \varepsilon_T \end{bmatrix} = \begin{bmatrix} \varepsilon'_L - j\varepsilon''_L & 0 & 0 \\ 0 & \varepsilon'_R - j\varepsilon''_R & 0 \\ 0 & 0 & \varepsilon'_T - j\varepsilon''_T \end{bmatrix} \tag{60}$$

When **E** is arbitrarily oriented in space and forms an angle θ_1 with L, angle θ_2 with R, and angle θ_3 with T, closed-form expressions for calculation of the relative dielectric constant, ε', and dielectric loss tangent, $\tan\delta$, is derived in (Vyacheslav Komarov 2012)

$$\varepsilon' = \left(\varepsilon'_L \cos^2\theta_1 + \varepsilon'_R \cos^2\theta_2 + \varepsilon'_T \cos^2\theta_3\right) \tag{61}$$

$$\tan\delta = \tan\delta_L \cos^2\theta_1 + \tan\delta_R \cos^2\theta_2 + \tan\delta_T \cos^2\theta_3 \tag{62}$$

with

$$\tan\delta_L = \frac{\varepsilon''_L}{\varepsilon'_L}, \quad \tan\delta_R = \frac{\varepsilon''_R}{\varepsilon'_R}, \quad \tan\delta_T = \frac{\varepsilon''_T}{\varepsilon'_T}, \tag{63}$$

If **E** is parallel to one of the three principal directions of the sample wood ($\theta_i = 0$, *for* $i = 1,\ 2\ or\ 3$), the power dissipated per unit volume, given by Eq. (11), may be simplified as:

$$P_{wave} = -Re(\nabla \cdot \mathbf{S}) = \frac{\omega}{2}\varepsilon_0 \varepsilon''_d E_d^2 \tag{64}$$

ε''_d is the dielectric constant in the principal direction d (L, R or T).

References

Ayappa KG, Davis HT, Crapiste GE, Davis A, Gordan J (1991) Microwave heating: an evaluation of power formulations. Chem Eng Sci 46(4):1005–1016

Basak T, Ayappa KG (1997) Analysis of microwave thawing of slabs with the effective heat capacity method. Am Inst Chem Eng J 43(7):1662–1674

Bergman TL, Lavine A, Incropera FP, DeWitt DP (2011) Fundamentals of heat and mass transfer—7th Edition Incropera. Wiley Edition, ISBN 978-0-470-91323-9

Bhattacharya M, Basak T, Ayappa KG (2002) A fixed-grid finite element based enthalpy formulation for generalized phase change problems: role of superficial mushy region. Int J Heat Mass Transf 45:4881–4898

Brodie G (2007) Simultaneous heat and moisture diffusion during microwave heating of moist wood. Appl Eng Agric 23(2):179–187

Bruch JC, Zyroloski G (1974) Transient two-dimensional heat conduction problems solved by the finite element method. Int J Numeri Method Eng 8(3):481–494

Chudinov BS (1965) Determination of mean effective thermal coefficients of wood. US Forest Service, Washington D.C.

Coleman CJ (1990) The microwave heating of frozen substances. Appl Math Model 14:439–440

Cooper PA, Ung T, Aucoin JP, Timusk C (1996) The potential for reuse of preservative treated utility poles removed from service. Waste Manage Res 14:263–279

Dokainish MA, Subbraj K (1989) A survey of direct time-integration methods in computational structural dynamics. Comput Struct 32(6):1371–1386

Erchiqui F (2013a) 3D numerical simulation of thawing frozen wood using microwave energy: frequency effect on the applicability of the Beer-Lambert Law. Dry Technol 31(11):1219–1233

Erchiqui F (2013b) Analysis of power formulations for numerical thawing frozen wood using microwave energy. Chem Eng Sci 98:317–330

Erchiqui F, Annasabi Z, Koubaa A, Slaoui-Hasnaoui F, Kaddami H (2013) Numerical modelling of microwave heating of frozen wood. Can J Chem Eng 9:1582–1589

Erchiqui F, Annasabi Z (2019) 3D hybrid finite element enthalpy for anisotropic thermal conduction analysis. Int J Heat Mass Trans 136:1250–1264

Erchiqui F, Kaddami H, Slaoui-Hasnaoui F, Koubaa (2020) A. 3D finite element enthalpy method for analysis of phytosanitary treatment of wood by microwave. Eur J Wood Wood Prod 78:577–591

Fields PG, White ND, G (2002) Alternatives to methyl bromide treatments for stored-product and quarantine insects. Ann Revues Entomol 47:331–359

Flanders H (1973) Differentiation under the integral sign. Am Math Monthly 80 (6):615–627

Food and Agriculture Organization, FAO (2009) Regulation of wood packaging material in international trade. International Standards for Phytosanitary Measures no 15 (ISPM 15). In: Food and Agriculture Organization of the United Nations, Secretariat of the International Plant Protection Convention, Rome, Italy

Gašparík M, Barcík Š (2013) Impact of plasticization by microwave heating on the total deformation of beech wood. BioResources 8(4):6297–6308

Gašparík M, Barcík Š (2014) Effect of plasticizing by microwave heating on bending characteristics of beech wood. BioResources 9(3):4808–4820

Gašparík M, Gaff M (2013) Changes in temperature and moisture content in beech wood plasticized by microwave heating. BioResources 8(3):3372–3384

Hansson L, Antti L (2003) The effect of microwave drying on Norway spruce woods: a comparison with conventional drying. J Mater Process Technol 141(1):41–50

Hu H, Argyropoulos SA (1995a) Modelling of Stefan problems in complex configurations involving two different metals using the enthalpy method. Modell Simul Mater Sci Eng 3(1):53–64

Hu H, Argyropoulos SA (1995b) Mathematical modeling and experimental measurements of moving boundary problems associated with exothermic heat of mixing. Int J Heat Mass Transfer 39:1005–1021

Hollis CC (1983) Theory of electromagnetic waves, A coordinate-free approach. McGraw-Hill

James WL (1975) Dielectric properties of wood and hardboard: variation with temperature, frequency moisture content, and grain orientation. USDA Forest Service Research Paper, Forest Products Laboratory

Kaestner PA, Bååth LB (2005) Microwave polarimetry tomography of wood. IEEE Sens J 5(2):209–215

Kanter KR (1975) The thermal properties of wood. Derev Prom 6(7):17–18

Nedjar B (2002) (2002), An enthalpy-based finite element method for nonlinear heat problems involving phase change. Comput Struct 80(1):9–21

Ni H, Datta AK (2002) Moisture as related to heating uniformity in microwave processing of solid foods. J Food Process Eng 22:367–382

Norimoto M, Gril J (1989) Wood bending using microwave heating. J Microw Power Electromagn Energy 24(4):203–212. https://doi.org/10.1080/08327823.1989.11688095

Norimoto M, Yamada T (1971) The dielectric properties of wood V, On the dielectric anisotropy in wood. Wood Res 51:12–32

Nzokou P, Tourtellot S, Kamdem DP (2008a) Sanitization of logs infested by exotic pests: case study of the Emerald Ash Borer (*Agrilus planipennis*Fairmaire) treatments using conventional heat and microwave. USDA, Michigan Dept. of Natural Resources and the Dept. Of Forestry at Michigan State University

Nzokou P, Tourtellot S, Kamdem DP (2008) Kiln and microwave heat treatment of logs infested by the emerald ash borer (*Agrilus planipennis* Fairmaire) (Coleoptera: Buprestidae). Forest Prod J 58(7):68–72

Ohlsson T, Bengston N (1971) Microwave heating profile in foods—a comparison between heating and computer simulation. Microwave Energy Appl Newsl 6:3–8

Oloyede A, Groombridge P (2000) The influence of microwave heating on the mechanical properties of wood. J Mater Process Technol 100(1–3):67–73. https://doi.org/10.1016/S0924-0136(99)00454-9Mori

Panrie BJ, Ayappa KG, Davis HT, Davis EA, Gordon J (1991) Microwave thawing of cylinders. A.I.Ch.E. J 3:1789–1800

Peralta PN, Bangi AP (2006) Finite element model for the heating of frozen wood. Wood Fiber Sci 38(2):359–364

Peyskens E, Pourcq M, Stevens M, Schalck J (1984) Dielectric properties of softwood species at microwave frequencies. Wood Sci Technol 18:267–280

Phillips TW, Halverson SL, Bigelow TS, Mbata GN, Ryas-Duarte P, Payton M, Halverson W, Forester S (2001) Microwave irradiation of flowing grain to control stored-product insects. In: Proceeding of the annual international research conference on methyl bromide alternatives and emissions reductions. San Diego, California, pp 121–122

Pozar MD (2011) Microwave engineering, 4th edn. ISBN-13: 978-0470631553. Wiley

Rattanadecho P (2006) The simulation of microwave heating of wood using a rectangular wave guide: influence of frequency and sample size. Chem Eng Sci 61:4798–4811

Rattanadecho P, Suwannapum N (2009) Interactions between electromagnetic and thermal fields in microwave heating of hardened type I-cement paste using a rectangular waveguide (Influence of frequency and sample size). J Heat Transfer 131(8):1–12

Simpson W, Tenwolde A (1999) Wood handbook-wood as an engineering material. Gen Tech Rep. FPL-GTR=113. Physical properties and moisture relations of wood. Chapter 3. U.S. Department of Agriculture, Forest Service, Forest Products Laboratory, Madison, WI

Steinhagen HP, Harry W (1988) Enthalpy method to compute radial heating and thawing of logs. Wood Fiber Sci 20(4):451–421

Swami S (1982) Microwave heating characteristics of simulated high moisture foods. M.S. Thesis. University of Massachusetts, USA

Torgovnikov GI (1993) Dielectric properties of Wood-based materials. Springer-Verlag, Berlin, Germany

United States Department of Agriculture (USDA) (2003) Importation of solid wood packaging material. Final environmental impact statement. Available at https://www.aphis.usda.gov/plant_health/ea/downloads/swpmfeis.pdf. Accessed Aug 2003

USDA (1977) General technical report, Department of Agriculture Forest Service, thermal conductive properties of wood, green or dry, from −40° to +100 °C: a literature review USDA forest service, FPL-9, U.S.

Vyacheslav Komarov V (2012) Handbook of dielectric and thermal properties of materials at microwave frequency. Artech House, Boston. ASIN: B00AG0382Q

Yemshanov D, Koch FH, McKenney DW, Downing MC, Sapio F (2009) Mapping invasive species risks with stochastic models: a cross-border United States-Canada application for *Sirex noctilio* fabricius. Risk Anal 29(6):868–884

Zhu J, Kuznetsov AV, Sandeep KP (2007) Mathematical modelling of continuous flow microwave heating of liquids (effect of dielectric properties and design parameters). Int J Therm Sci 46:328–341

Zielonka P, Gierlik E (1999) Temperature distribution during conventional and microwave wood heating. Holz Als Roh- Und Werkstoff 57:247–249

Synthesis, Characterization, in Vitro Biocompatibility and Antibacterial Properties Study of Nanocomposite Materials

Che Wan Sharifah Robiah Mohamad

Abstract Nanocomposites are divided into 3 main types namely metals, ceramics and polymers. Apart from that, there are various methods in the production of nanoceramic, namely mechanical, vapor, high temperature and gel solution. Normally, gel solution was use for low cost and easy for handling. Characterization of nanocomposite can be done using various methods either by use the reaction of electrons, ions or radiation. Each characterization will give different features of nanocomposite either in term or surface, element or other characteristic of nanocomposite. Apart from that, nanocomposite is one of the biomaterial materials suitable for use in vivo or even in vitro and also has antibacterial properties. All this factor will enhance the suitability of nanocomposite to be use in engineering field and other related industry.

Keywords Nanocomposite · Synthesis · Characterization · Biocompability and antibacteria

1 Nanocomposites

A nanocomposite is a multiple solid material where one of the phases has one, two or more dimension which is less than 100 nm or the structure was having nano-scale repetitive distance between the different phases that make up the material. Nanocomposites are defined as a promising class of hybrid materials that are mixtures of polymers such as polysaccharides and polylactic-co-glycolic acid (PLGA) with inorganic solids at the nanometric scale. Currently, three broad type of nanocomposites based on their matrix: metal matrix nano composites (MMNC), ceramic matrix nano composites (CMNC) and polymer matrix nano composites (PMNC) (Camargo and Wypych 2009). Nanocomposites are significant to upcoming materials which shows the great changes in all the industrial field. This type of material is also going to be a economical barrier for developing country as a once of medical nanotechnology.

C. W. S. Robiah Mohamad (✉)
Faculty of Electronic Engineering Technology, Universiti Malaysia Perlis (UniMAP), Arau, Perlis, Malaysia
e-mail: robiah@unimap.edu.my

M. T. Hameed Sultan et al. (eds.), *Biocomposite Materials*, Composites Science and Technology, https://doi.org/10.1007/978-981-33-4091-6_11

1.1 Metal Matrix Nano Composites (MMNC)

MMNC consist of a metal matrix filled with nano-particle producing remarkable physical and mechanical properties when compared to those of the matrix. This type of nanocomposite (MMNC) will has high strength in shear/compression process, high electrical and thermal stability, wear and chemical resistance. However, the drawback of MMNC is such as highly corrosive and the example of MMNC are Fe–Cr/Al_2O_3, Fe/MgO, Mg/CNT and etc.

1.2 Ceramic Matrix Nano Composites (CMNC)

The CMNC consist of a ceramic matrix filled with nanofiller as a metal/non-metal/ceramic material mostly resulting in improved optical, electrical and magnetic properties as well as tribological, corrosion-resistance and other protective properties. Other than that, CMNC also will enhanced mechanical properties including fracture toughness, stiffness and strength to certain composite. Just like a MMNC, this type of ceramic nanocomposites is low toughness and brittle. The example of CMNC are Al_2O_3/SiO_2, SiC/C, Al_2O_3/CNT and etc.

1.3 Polymer Matrix Nano Composites (PMNC)

Inorganic or organic nanofiller are incorporated within polymeric matrix to obtain improved properties like impressive and flexural mechanical properties, light weight, electrical conductivity and ductility. This type of PMNC will increases heat and impact resistance, flame retardancy, mechanical strength and decreases gas permeability with respect to certain types of gases such as oxygen, carbon dioxide and water vapour. The disadvantages of PMNC such as low modulus and strength. The example of PMNC are polyester/TiO_2, polymer/CNT, polymer/latered double hydroxides and etc.

2 Synthesis of Nanocomposites

A nanocomposites synthesis is varied from a different solid matric, which a combination of continuous and discontinuous phase with a nano-scale dimension.

2.1 Mechanical Technique

Nanocomposites were synthesized by the solid-state powder processing technique of mechanical alloying in Al–Al_2O_3, TiAl–Ti_5Si_3, and $MoSi_2$–Si_3N_4systems. The mechanically alloyed powders were consolidated to full density by techniques such as vacuum hot pressing, hot isostatic pressing, and combinations of material.

Basically, a synthesis of MMNC were consolidated with Rapid solidification (RSP) (Rohatgi and Schultz 2007), Vapour technique (PVD, CVD), Electrodeposition and chemical method (colloidal and sol–gel processes) and ball milling. However, a different technique will be used for CMNC, which is conventional powder method, polymer precursor route, vapour technique (PVD, CVD), Chemical methods (sol–gel process, colloidal and precipitation approaches, template synthesis) (Camargo and Wypych 2009).

2.2 Enzymatic and Chemical Treatment Technique

Synthesis of nanocomposites using chemical and enzyme treatment techniques involves catalysis reactions and the absorption properties of nanoparticles involved in either metal, ceramic, polymer or biopolymer.

Generally, on irradiation with UV light, these oxides generated holes and released electrons, which reacted with H2 O and O2 molecules, and adhered on the surface. In result, it produces highly reactive oxygen species (ROS) such as peroxides, superoxide, hydroxyl radicals, and singlet oxygen. ROS are capable to degrade organic water pollutants like dyes efficiently (Brillas and Martínez-Huitle 2015). Generation of ROS also has antibacterial effect due to oxydative stress in an aqueous condition, for example, the hydroxyl radical is responsible for inactivation of *Escherichia coli* Han et al. 2016.

Techniques often used for nanocomposite synthesis using Enzymatic and Chemical treatment technique for MMNC is Colloidal and sol–gel processes. The synthesis of CMNC by use template synthesis, precipitation approaches, Colloidal and sol–gel processes, while for PMNC is intercalation of the polymer or prepolymer from solution, In-situ intercalative polymerization, melt intercalation, direct mixture of polymer and polymer and sol–gel process (Camargo and Wypych 2009).

Biocomposites refers to those composites that can be employed in bioengineering field and biofiber (such as wheat, kenaf, hemp, jute, sisal and flax) are one of major component of biocomposites (Usha 2017). Nowadays, the production of biocomposite materials from natural materials (such as plant base, shell, grain) as a new material with improved performance over individual constituent material. Polymers used in the field of health sciences are classified as biopolymers (or biomedical polymers) because of their use in biological systems. These materials are used in biomedical applications such as pharmaceutical, medical device coatings, and resorbable implants that require biocompatibility and nontoxicity (Rudin and Choi 2013).

3 Characterization of Nanocomposites

The nanocomposites were characterized by surface analysis and some other technique to evaluates their properties. The major issue for characterization is to describe the distinctive character of nanocomposite by use external technique to probe into inside structure and properties of material, included nanocomposites element composition, molecular weight and etc.

3.1 Surface Analysis

Nanocomposite surface would not stand alone and this surface were interacted with other material or ambient.

3.1.1 Electron-Beam Techniques (Auger-Electron Spectroscopy)

Auger-Electron Spectroscopy (AES) is a widely used surface analysis technique with several applications across industries including medical device, electronics, hard drive, and other general manufacturing segments. It's basically can be used as a valence—band spectroscopy that is surface sensitive. Observed changes in Auger line shapes have been useful in identifying chemical states of elements at surfaces, particularly carbon, sulfur, nitrogen, and oxygen (Ashok 2016). They are tree basic principle of AES, which is ionization of incident electron transfer of its energy to an inner-shell electron, de-excitation of electron and emission.

A basic application of AES is to determine atomic concentration, elemental, chemical deep profiling, chemical imaging, small feature analysis and etc. The AES have their pros and cons, which means selecting the right testing method is critical for achieving the results we desire such as sample size, sample compatibility, type of material, and other factors. In term of advantages, this technique allow for in-depth surface analysis of conductive and semi-conductive surface because of this technique is able to reveal the composition of a surface. Other than that, the ability of AES analysis to focus the electron beam in small area surface such as a small diameter (1–2 μm) material and to enhanced the accuracy and turnaround of the sample (Auger Electron Spectroscopy). However, AES is not suitable to test a polymer, glass or other insulation material and will cause a result in surface damage for this type of material. To reduce a surface damage, a special technique needs to used and element like hydrogen and helium can't detected because of they have less than 3 electrons. A quantification of is not easy and AES also associated with a relative error rate of 10% in repetitive analysis.

3.1.2 Ion-Beam Technology (IBT)

An ion beam is a type of charged particle beam consisting of ions, generated. Generated and transported under high vacuum conditions in order to avoid beam degradation by collisions with air molecules. In addition, the reaction products used for analysis are also absorbed or scattered by the presence of air, so the vast majority of IBA takes place in a high vacuum chamber (Grime 2017). Ion-beam technology (IBT) have a several type of reflection such as Secondary Ion Mass Spectroscopy (SIMS), Rutherford Backscattering Spectroscopy (RBS), Hydrogen Forward Scattering Spectroscopy (HFSS) in term of their Ion Beam Analysis (IBA) as shown in the Fig. 1. IBA works on the basis that ion-atom interactions are produced by the introduction of ions to the sample being tested. Major interactions result in the emission of products that enable information regarding the number, type, distribution and structural arrangement of atoms to be collected.

IBA can be used for all types of material, provides outstanding uniformity, versatility, and independent ion beam energy. This factor was contributed to huge applications of IBA especially for quantitative analysis of thin film based on their thickness, type of composition, uniformity in depth, solid state reactions and interdiffusion. IBA also use to determines the quantitative measurements of impurities in substrate.

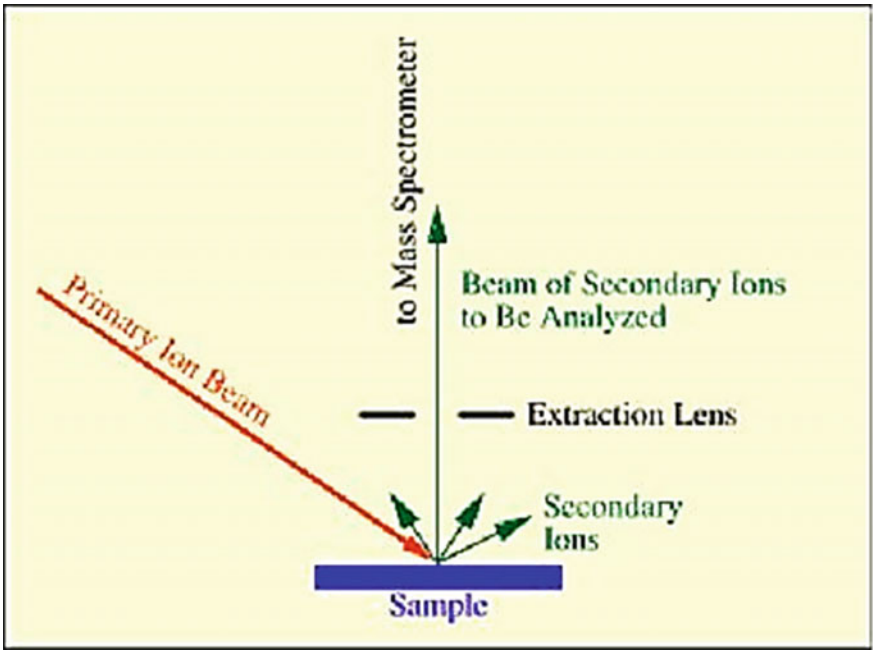

Fig. 1 The type of reflection for Ion-beam technology (IBT) (Muller and Vervoort 2020)

Other than that, this IBA detect a defect distribution in crystal sample and so on. This feature was enhanced the application type of IBA in nanocomposite study especially in surface analysis.

3.1.3 X-ray Technique

X-ray techniques commonly used for the analysis of materials in engineering field and structural components. These techniques included X-ray fluorescence (XRF) spectrometry, X-Ray Photoelectron Spectroscopy, and X-ray diffraction (XRD). These analytical techniques provide qualitative and quantitative information on the composition and structure of materials with precision (Igwebike-Ossi 2017).

The generating of X-rays is important in this technique. Normally the production of X-rays thru electromagnetic radiation (λ, f, E), x-ray radiation and x-ray generation. A basic principle of x-ray technique is ionization/excitation/transfer, de-excitation/relaxation and emission. The x-ray technology, its divide to two type of x-ray scattering, coherent (without a loss in energy) and incoherent scattering (incident x-ray loses some of its energy to the scattering electron) (Fig. 2).

The advantages of using x-rays in analysis are x-rays is the cheapest and most convenient method, x-rays are not absorbed very much by air, so the specimen need not be in an evacuate ed chamber (Igwebike-Ossi 2017). The disadvantage is that they do not interact very strongly with lighter elements, so this could impose a limitation on the elements detectable by X-ray techniques.

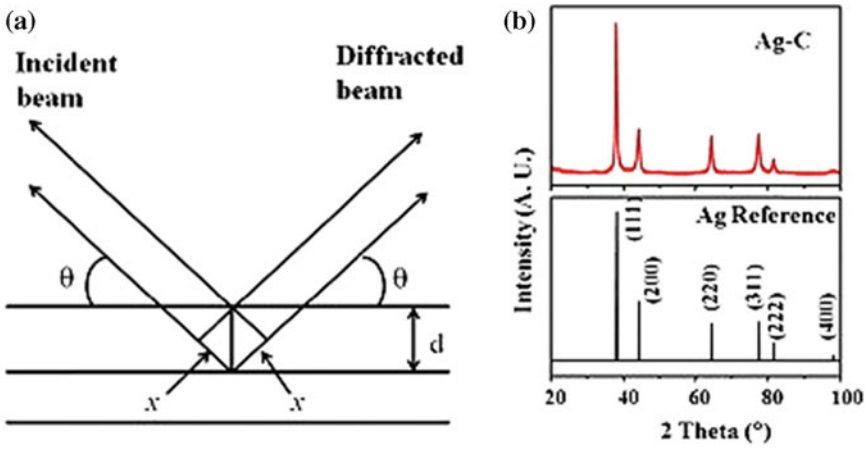

Fig. 2 Example of X-ray diffraction (XRD) result (Bashir and Liu 2015)

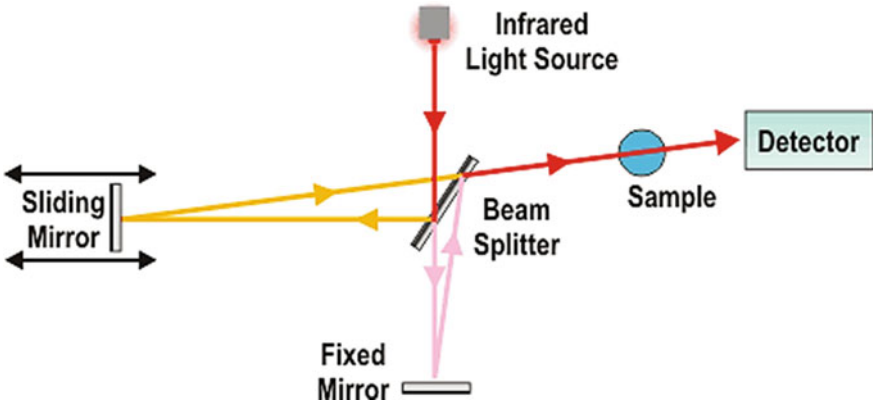

Fig. 3 FTIR principle (John 2018)

3.2 Fourier Transform Infrared Nanomaterials (FTIR)

Fourier transform infrared spectroscopy (FTIR) is a largely used technique to identify the functional groups in the materials (gas, liquid, and solid) by using the beam of infrared radiations. This technique has been considered to be one of the most effective techniques to study and understand the chemical and surface chemistry in various types of membrane (Mudunkotuwa et al. 2014). This type of spectrometer is an optical instrument used to measure properties of light over a specific portion of the electromagnetic spectrum, 5 microns to 20 microns.

The advantages of FTIR in engineering and material analysis is this type of spectroscopy can make an identification of inorganic compounds and organic compounds. The speed of all frequencies is measured simultaneously less than 10 min. Other than that, the sensitivity of FTIR is dramatically improved with their detector and high optical throughput which result in much lower noise level. FTIR also easy to handle and suitable in remote sensing with mechanical simplicity.

Figure 3 shows the basic principle of FTIR as their light beam split into two by the beam splitter which reflected from the moving mirror and fixed mirror, before being recombined by the beam splitter. The movements of the optical path difference based on fixed mirror changes, such that the phase difference changes with time (Clayborne and Morris 2017).

3.3 Photoluminescence (PL) Spectroscopy

Photoluminescence (PL) spectroscopy is a form of light emission spectroscopy in which the light emission comes from a process called photo-excitation. As the light is directed onto a sample, the electrons within the material move into excited

states. (excitation) When the electrons come down from the excited states to their equilibrium states, the energy can be released in the form of light (Zhang 2018).

The PL spectroscopy is a non-contact, nondestructive method of probing materials. It is one of many forms of luminescence (light emission) and is initiated by photoexcitation (i.e. photons that excite electrons to a higher energy level in an atom). Following excitation, various relaxation processes typically occur in which other photons are re-radiated. Time periods between absorption and emission may vary and it depends on type of nanomaterial which are up to milliseconds for Phosphorescence processes in molecular systems; and under special circumstances delay of emission may even span to minutes or hours (Hayes and Deveaud 2002).

3.4 Electron Microscopy

An Electron microscope is a microscope that uses a beam of accelerated electrons as a source for visualization. This type of microscope having a high resolution of image (up to 2 million times), able to magnify objects in nanometers, 3D shape of objects with a greater depth of field (Scanning Electron Microscopy). Types of an electron microscopy is Scanning Electron Microscopy (SEM), Transmission Electron Microscopy (TEM), Field Emission Scanning Electron Microscopy (FESEM).

Advantages of electron microscope is very high magnification (up to 2 million times), incredibly high resolution, material rarely distorted by resolution and diverse application from engineering field, biology and others related industry. However, this electron microscope has a range of disadvantages such as extremely expensive, sample is necessary to coat with very thin layer of metal (such as gold or platinum), sample must be completely dry and energy of the electron beam is very high (Kalsoom et al. 2018).

4 In Vitro Biocompability of Nanocomposites

Biocompatibility is related to the behavior of biomaterials in various contexts. The term refers to the ability of a material to perform with an appropriate host response in a specific situation (Jonathan Black 2006). A measurement of biological reactions and parameters assessing the possibility of using certain materials have been gathered in International Standard ISO 10,993 (PN-EN ISO10993-5:2009 2009) (or other similar standards) to determine if a certain material (or rather biomedical product) is biocompatible. Since the immune response and repair functions in the body are so complicated it is not adequate to describe the biocompatibility of a single material in relation to a single cell type or tissue (Medical Device Technology 2008).

By considering all of the nanocomposite features, during the development of a nanocomposite, all properties of material require to improve from the starting point of synthesis until the end of an experiment. The addition of even a small

concentration or amount of nanoparticles (NPs) to the polymer matrix and then adding the nanocomposite to the body will affect the interaction of material with cells. Interaction with immune cells may result in molecular reactions, which may lead to higher sensitivity to disease and cancer growth and also cause undesired allergic reactions to human body (Kononenko et al. 2015; Hirai et al. 2014; Immunol 2014; Radomski et al. 2005). Understanding how a nanocomposite reacts with cells is a challenge from a toxicological point of view, but is crucial for future solutions in biomedicine. Cell research including human cell lines may provide information on the biocompatibility of nanomaterials (Visani de Luna et al. 2016). The example of metalcomposite is titanium due to its high biocompatibility, low weight, and ease of use (Woods et al. 2009; Hales et al. 2007).

5 Antibacteria Properties of Nanocomposites

Antimicrobial testing can be used for the in vitro investigation of nanocomposites as a potential biomaterial agent. NCCLS (formerly known as the National Committee for Clinical Laboratory Standards) guidelines for nanocomposites of antimicrobial susceptibility testing especially in quality control issues and current methodologies, such as conventional disk diffusion and microbroth dilution tests method (Ginocchio 2002). However, for minimal inhibitory concentration (MIC) and minimum bactericidal concentration (MBC) values for various nanocomposites compound by measuring the effect of decreasing concentration of biochemical in term of inhibition of microbial growth and lowest concentration of an antibacterial agent to kill a specific bacterium, respectively (Holla et al. 2012).

5.1 Diffusion Method

The diffusion methods required to evaluated the antibacterial activity of nanocomposites compounds against Gram positive or Gram negative bacterial.

5.1.1 Agar Well Diffusion (AWD) Method

Nowadays, many microbiology laboratories were use Clinical and Laboratory Standards Institute (CLSI) guidelines as an official antimicrobial routine for bacteria and others microorganism testing. The AWD was used to evaluate the antimicrobial activity of nanocomposite especially from plants or microbial composite. This method was considered as a standard test for certain bacterial pathogen like streptococci, *H. influenzae, H. parainfluenzae, Neisseria* species by using specific culture media such as Mueller–Hinton agar (MHA) medium; various incubation condition

(30–37 °C) and interpretive criteria for inhibition zones was observed and analyses (CLSI 2012).

The basic procedure for ADD methods is involved with inoculation of agar plate with a standardized inoculum of the test microorganism. Then, filter paper discs (about 6–8 mm in diameter), containing the test compound (sample) at a desired concentration, are placed on the agar surface. After that, this Petri dishes are incubated under 37–40 °C for 16–24 h, and the diameters of inhibition growth zones are measured by use calliper or MOTIC software.

5.1.2 Agar Plug Diffusion (APD) Method

Agar plug diffusion methods is often used to determine the antagonism between more than two different type of microorganism (Jiménez-Esquilín and Roane 2005; Elleuch et al. 2010). The APD methods is involved an agar culture of the strain of interest on medium by tight streaks on the plate surface. After certain incubation period, in growing phase, target microbial cells will secrete a metabolite compound which diffuse in the agar medium. Then, after 12–24 h, a target microbial on respective agar is cut aseptically with a sterile cork borer in 2–3 cm, then deposited on the agar surface of another plate previously inoculated by the test microorganism (such as *E. coli*). Tis APD plate will incubate for a few hours then the appearance of the inhibition zone around the agar plug will be visible (Balouiri et al. 2016).

5.2 Dilution Method

The tube dilution test is the standard method for determining levels of resistance to an antibiotic. Serial dilutions of the antibiotic are made in a liquid medium which is inoculated with a standardized number of organisms and incubated for a prescribed time.

5.2.1 Broth Dilution Method

Broth is the most basic methods of antimicrobial susceptibility testing. This method used liquid medium and it is very suitable to test the antimicrobial activity of solid samples like films. McFarland Standards provide a guide to bacterial suspension standardization used for susceptibility screening. The preparation of 0.5 McFarland microbial inoculum for the broth dilution test. Besides, OD_{600} is used to measure and determine the turbidity or concentration of bacteria growth in a solution. OD_{600} is refer to the wavelength in nanometres (nm) and it is used to measure the concentration of a solution (Balouiri et al. 2016).

Broth microdilution method is reproducible to a single doubling dilution of the real end point of a series of dilution Gondal et al. 2016). Broth dilution and microdilution

methods are similar and well established. But microdilution method uses smaller amounts of medium, reagents and tested agents. Because of that, the microdilution method is more economical and less laborious than broth dilution method (Golus et al. 2016). This method is the most suitable ones for the determination of MIC values, as they give the possibility of estimating the concentration of the antimicrobial agent tested (Balouiri et al. 2016). The beginning of process, wells are filled with broth containing various concentrations of antibiotics. Then, inoculated with bacteria and incubated overnight. The minimum inhibitory concentration is determined after 12–24 h incubation.

6 Conclusion

Nanocomposite is one of new material to enhance matrix properties of material. A different type of matrix, such as MMNC is to increase yield stress, tensile strength and creep resistance of material. Meanwhile, a CMNC to increase fracture toughness of material and PMNC to increase modulus, yield stress, tensile strength and also a creep resistance. With the hope that the presence of antibacterial activity for some nanocomposites such as biocomposites will be able to improve and enhanced the application of this material in the biomedical and engineering sectors.

References

Ashok KS (2016) Experimental methodologies for the characterization of nanoparticles, Engineered Nanoparticles

Auger Electron Spectroscopy (2020) Physical Electronic

Balouiri M, Sadiki M, Ibnsouda SK (2016) Methods for in vitro evaluating antimicrobial activity: a review. J Pharm Anal 6(2):71–79

Bashir S, Liu J, (2015) Nanocharacterization, advanced nanomaterial and their applications in renewable energy

Brillas E, Martínez-Huitle CA (2015) Decontamination of wastewaters containing synthetic organic dyes by electrochemical methods. An updated review. Appl Catal B Environ 166–167:603–643

Camargo PHC, Satyanarayana KG, Wypych F (2009) Nanocomposites: synthesis, structure, properties and new application opportunities. Mater Res 12(1):1–39

Clayborne A, Morris V (2017) Fourier transform infrared spectroscopy (FTIR). Physical Chemistry Laboratory

CLSI (2012) Performance standards for antimicrobial disk susceptibility tests, approved standard, 7th ed. CLSI document M02-A11. Clinical and laboratory standards institute, 950 West Valley Road, Suite 2500, Wayne, Pennsylvania 19087, USA

Elleuch L, Shaaban M, Smaoui S et al (2010) Bioactive secondary metabolites from a new terrestrial Streptomyces sp. TN262, Appl Biochem Biotechnol 162:579–593

Ginocchio CC (2002) Role of NCCLS in antimicrobial susceptibility testing and monitoring. Am J Health, Syst Pharm 59(8 Suppl 3):7–11

Golus J, Sawicki R, Widelski J, Ginalska G (2016) The agar microdilution method—a new method for antimicrobial susceptibility testing for essential oils and plant extracts. J Appl Microbiol 121(5):1291–1299

Gondal AJ, Hannan A, Saleem S, Arshad MU (2016) Comparative evaluation of broth and agar dilution techniques for antimicrobial susceptibility testing against multidrug resistant pseudomonas aeruginosa. Pak J Zool 48(5):1517–1522

Grime GW (2017) High-energy ion beam analysis. Encyclopedia of spectroscopy and spectrometry (3rd edn)

Hales NW, Shakir FA, Saunders JE (2007) Titanium middle-ear prostheses in staged ossiculoplasty: does mass really matter? Am J Otolaryngol-head neck med Surg 28:164–167

Han C, Lalley J, Devi N, Cromer K, Mallikarjuna NN (2016) Titanium dioxide-based antibacterial surfaces for water treatment. Curr Opin Chem Eng 11:46–51

Hayes GR, Deveaud B (2002) Is Luminescence from quantum wells due to excitons? Phys Status Solidi A 190(3):637–640

Hirai T, Yoshioka Y, Ichihashi K, Mori T, Nishijima N, Handa T, Takahashi H, Tsunoda S, Higashisaka K, Tsutsumi Y (2014) Silver nanoparticles induce silver nanoparticle-specific allergic responses

Holla G, Yeluri R, Munshi AK (2012) Evaluation of minimum inhibitory and minimum bactericidal concentration of nano-silver base inorganic anti-microbial agent (Novaron(®)) against streptococcus mutans. Contemporary clinical dentistry, vol 3. pp 288–293

Igwebike-Ossi CD (2017) Failure analysis and prevention: X-Ray technique. pp 153–171

Immunol J (2014) 192:118–119; Capasso L, Camatini M, Gualtieri M (2014) Nickel oxide nanoparticles induce inflammation and genotoxic effect in lung epithelial cells. Toxicol Lett 226:28–34

In vitro biocompatibility testing of biomaterials and medical devices, U. Muller, Medical device technology, March 2008

Jonathan Black (2006) Biological performance of materials

John (2018) Fourier transform infrared spectroscopy (FTIR) Principle, instrumentation forum

Jiménez-Esquilín AE, Roane TM (2005) Antifungal activities of actinomycete strains associated with high-altitude Sagebrush Rhizosphere. J Ind Microbiol Biotechnol 32:378–381

Kalsoom A, Shahid AK, Sher BH, Abdullah MA (2018) Scanning electron microscopy: Principle and application in nanomaterials characterization. Handbook of material characterization. pp 113–145

Kononenko V, Narat M, Drobne D (2015) Nanoparticle interaction with the immune system. Arch Ind Hyg Toxicol 66:97–108

Mudunkotuwa IA, Minshid AAI, Grassian VH (2014) ATR-FTIR spectroscopy as a tool to probe surface adsorption on nanoparticles at the liquid–solid interface in environmentally and biologically relevant media. Analyst 139:870

Muller P, Vervoort J (2020) Secondary ion mass spectrometer

PN-EN ISO 10993-5:2009 (2009) Biological evaluation of medical devices Part 5: tests for in vitro cytotoxicity; international organization for standardization: Geneva, Switzerland

Radomski A, Jurasz P, Alonso-Escolano D, Drews M, Morandi M, Malinski T, Radomski MW (2005) Nanoparticle-induced platelet aggregation and vascular thrombosis. Br J Pharmacol 146:882–893

Rohatgi PK, Schultz B (2007) Lightweight metal matrix nanocomposites-stretching the boundaries of metal. Mater Matters, 2.4, 16

Rudin A, Choi P (2013) Chapter 13-Biopolymer, The elements of polymer science and engineering (3rd edn) pp 521–525

Scanning Electron Microscopy (2018) Scientific Data

Usha GK (2017) Synthesis and characterization of biocomposite material, MSc thesis. National Istitute of Technology, Rourkela

Visani de Luna L, Mazarin de Moraes A, Consonni S (2016) Comparative in vitro toxicity of a graphene oxide-silver nanocomposite and the pristine counterparts toward macrophages. J Nanobiotechnol

Woods O, El Fata F, Saliba I (2009) Ossicular reconstruction: Incus versus universal titanium prosthesis. Auris Nasus Larynx 36:387–392

Zhang YH (2018) Light absorption and photoluminescence (PL) spectroscopy, Chemistry Libre-Texts

Enhancement of Local Drug Delivery System Using Different Design of Gentamicin Loaded in Carbonate Apatite Scaffold

N. Mamat, M. Mariatti, Z. A. A. Hamid, and B. H. Yahaya

Abstract A combination of bioactive scaffold with drug delivery of therapeutic agents is a great deal to locally treat bone infections. However, controllable drug release behaviours for different types of drug-incorporated scaffold have been not comprehensively compared. In this study, novel technique was proposed with the addition of bioactive agents in microspheres was incorporated into carbonate apatite (CO_3Ap) scaffold. A simple slurry-dipping method by dispersion of 0.8 wt% suspension of gentamicin (GEN)-loaded polylactic acid (PLA) microsphere (GENMS) using an ultrasonic bath was used to coat the scaffold. GENMS was fabricated by double emulsion. This coated scaffold was compared to the GEN coated scaffold without microsphere and uncoated scaffold with direct loading of GEN. It was confirmed that the microsphere coating did not inhibit the apatite growth of the scaffold when immersed in Hank's Balance Salt Solution for 4 weeks. The drug release profile exhibited the initial burst and sustained drug release could be improved by the presence of GENMS in the coated scaffold. Moreover, the kinetic release study supported the findings of different drug release based on zero-order, first-order, Higuchi and Korsmeyer–Peppas models. The results showed that drug release mechanisms were diffusion and degradation controlled for scaffold, while for coated scaffolds led to diffusion and degradation of chitosan and microsphere. Rougher surface of the scaffold by the adhered GENMS on the scaffold facilitated cell proliferation. In short, this multifunctional coated bioactive scaffold has the potential to enhance cell attachment and provide local of controlled drug delivery for bone tissue engineering improvement.

N. Mamat (✉)
Faculty of Electronic Engineering Technology, Universiti Malaysia Perlis (UniMAP), Arau, Perlis, Malaysia
e-mail: normahira@unimap.edu.my

M. Mariatti · Z. A. A. Hamid
Biomaterials Niche Area Group, School of Materials and Mineral Resources Engineering, Universiti Sains Malaysia, Engineering Campus, 14300 Nibong Tebal, Pulau Pinang, Malaysia

B. H. Yahaya
Regenerative Medicine Cluster, Advanced Medical and Dental Institute (AMDI), Universiti Sains Malaysia, Kepala Batas, Pulau Pinang, Bertam, Malaysia

M. T. Hameed Sultan et al. (eds.), *Biocomposite Materials*, Composites Science and Technology, https://doi.org/10.1007/978-981-33-4091-6_12

Keywords carbonate apatite · Scaffold · Microsphere · Drug delivery · Chitosan · Coating

1 Introduction

One of the key components for successful bone regeneration is the presence of functional bone scaffold with loadings of drug to promote tissue regeneration. The scaffolds have been used as drug delivery such as therapeutic agents (i.e. antibiotic and anti-inflammatory) to enhance the healing process of the bone. Calcium phosphate (CaP)-based bioceramics such as hydroxyapatite [$(Ca_{10}(PO_4)_6(OH)_2)$, HA] is known for its excellent biocompatibility to be used as porous bone scaffold. The apatite found in human bone is consisted by other ions mainly carbonate (CO_3^{2-}) content and traces of Na^+, Mg^{2+}, Fe^{2+}, Cl^- and F^- (Ishikawa 2010). Although the presence of these ions are low, they play an important role in the biochemical reactions of bone metabolism. As a result, CO_3^{2-} containing HA as carbonate apatite (CO_3Ap) has gained much attention due to its chemical composition being closer to bone mineral and favourable for bone growth.

Mimicking bone scaffold to natural bone by chemical composition and improved compressive strength is beneficial in tissue engineering. However, the occurrence of bone infection is a destructive problem which leads to post-operative problems and critically need attention. The current therapy to prevent implant associated infection relies on systemically administrated antibiotics. This conventional treatment poses several major disadvantages. This therapy is difficult to achieve the effective localisation of antibiotics and ineffective once the bacteria anchored and synthesise a biofilm on the surface of implant (Yazdimamaghani et al. (2014)). A very high concentration of a drug in bloodstream and other organs easily produce potential side-effects in the body system. Thus, scaffold loaded with antibiotics can act as a platform for local drug delivery additionally used for bone repair defects while enhance cell proliferation.

Generally, scaffold with drugs directly applied on the surface have very limited loading capacity with the drug diffusion is quite fast. Consequently, this system is not beneficial for certain osteoarticular therapy (Pei et al. 2018). The option of incorporating drugs in the polymer coated scaffolds is attractive as this approach can lead to a more controlled biomolecule release profile during local delivery of therapeutic drugs (Yao et al. 2013; Meng et al. 2013; Araújo et al. 2017). This is supported by an early study by Kim et al. (Kim et al. 2005) that show the homogeneous entrapment of the drug throughout the 3D scaffold structure is possible and the drug release period can be prolonged.

Recent developments concern on the use of microspheres as drug carriers in bone scaffolds. Scaffold fabrication can be formed by incorporating microspheres as a targeted drug delivery system (Francis et al. 2010; Wang et al. 2017). These allow the controlled released of drug and decreased the initial burst of the drug.

Hence, localized delivery of therapeutic substances can reduce the amount of bioactive compounds and release intracellularly in a prolonging time. The incorporated drug-loaded microspheres can offer site-specific delivery of drugs and controlled-release of drugs with distinct release kinetics. Drug-loaded microspheres on the scaffold reduces the side effects and improves the efficiency as it uses a significantly less amount of due to the localized release (Gbureck et al. 2008).

The strategy of incorporating polymer microspheres into 3D scaffolds have been attracted increasingly attention in recent years. However, fabrication and characterization of porous CO_3Ap scaffold loaded with gentamicin (GEN) in chitosan supported with kinetic release properties has not been reported elsewhere. GEN is aminoglycoside antibiotic fulfils some of the criteria for localized application because of its tissue capability, broad- spectrum bactericidal activity and has no deleterious effect on healing process. The objective of this study was to develop GEN loaded CO_3Ap scaffolds. GEN-loaded polylactic acid (PLA) microspheres (GENMS) was formulated and then incorporated to the fabricated CO_3Ap scaffold. Different drug loaded CO_3Ap scaffolds were fabricated and characterized based on their bioactivity, drug release behaviours and cell viability. This study provides a novel method in coating system for controlling drug release of post-operative implantation procedures.

2 Materials and Methods

2.1 Materials

β-TCP ($Ca_3(PO_4)_2$, with grade purum p.a, >96.0%) powder was used as a main component to prepare porous β-TCP scaffold. Polyethylene-imine (PEI, 50 w/v%) was used as a dispersant in β-TCP slurry. Sodium dodecyl sulphate (SDS) powder was used as a pore forming agent while polyvinyl alcohol (PVA) was used as a binder in the ceramic slurry to bind the calcium phosphate particles. Polyethylene glycol (PEG) in liquid form with a specified M_w of 600 g/mol was used as a plasticizer. Denacol EX-622 (aliphatic sorbitol glycidyl ether epoxy) was used as a gelling agent and crosslinker in β-TCP slurry. Distilled water was used as a liquid medium. For transforming β-TCP scaffold to CO_3Ap scaffold, disodium carbonate (Na_2CO_3) solution was used as a carbonate (CO_3^{2-}) source. Medium molecular weight of chitosan (CS, 75–85% deacetylation) was used as a natural polymer solution for coating purpose.

In the fabrication of drug-loaded microsphere, PLA microsphere was fabricated by PLA pellet. Food grade PLA has obtained Food and Drug Administration (FDA) approval. Dichloromethane (DCM) with >99.5% purity was purchased from Merck Millipore and PVA (80% hydrolysis) was purchased from Sigma Aldrich. GEN reagent solution with 10 mg/ml was used as encapsulated drug. For bioactivity test, Hanks' Balanced Salt Solution (HBSS) was used as a supporting solution to investigate the apatite formation.

3 Methods

3.1 Fabrication of GEN Loaded PLA Microsphere

Scaffolds were fabricated using gelate-freeze casting method which is a similar method as described in our previous work (Darus et al. 2018). Fabrication of CO_3Ap scaffold was done using hydrothermal treatment method. Details of the method was described in our previous study (Mamat et al. 2017). The results were based on 5 days hydrothermal treatment in 5 molar Na_2CO_3.

3.2 Fabrication of GEN Loaded PLA Microsphere

GEN-loaded PLA microsphere was fabricated using double emulsion solvent evaporation (ESE). In this study, volume ratio of dispersed phase to continuous phase, 1:3 (PLA: PVA) was used to fabricate PLA microsphere. Firstly, 9 wt.% of PLA pellets was dissolved in 30 ml DCM and followed by dispersion of 1 ml GEN solution (with concentration, 10 mg/ml or 10,000 ppm). This solution is subjected to vigorous homogenization to yield the primary emulsion. Then the primary emulsion was immediately emulsified into 90 ml PVA solution. The mixtures were stirred at ~1250 rpm for 3 min to form secondary emulsion at room temperature. Then, the speed of the stirrer was decreased to ~250 rpm for overnight to allow the evaporation of DCM. The particles of the PLA were formed at the bottom of the flask and was washed, filtered and dried overnight at room temperature before they were collected.

In order to determine the encapsulation efficiency, PLA microspheres loaded with gentamicin at weight 40 mg were fully degraded in 5 ml of 1 M NaOH solution. The samples were left for overnight until it was degraded and ultraviolet (UV) visible spectroscopy was conducted to determine the encapsulation efficiency (EE%). Scanning of absorbance intensity of GEN was detected at 195 nm wavelength. The calculation of EE% and DL% of the GEN were calculated using Equs. 1–3:

$$\text{Encapsulated drug mass(mg)} = \frac{\text{Concentration from data(ppm)} \times 1\text{ml}}{1000} \quad (1)$$

$$\text{Inital drug mass (mg)} = \frac{10\text{mg} \times 1\text{ml}}{\text{ml}} \quad (2)$$

$$\text{Encapsulation Efficiency, EE}(\%) = \frac{\text{Encapsulated drug mass(mg)} \times 100}{\text{Initial drug mass}} \quad (3)$$

3.3 Incorporation GEN into Carbonate Apatite Scaffold

In order to incorporate GEN in the uncoated scaffolds, 2% of GEN solution was prepared by dissolving 0.3 ml (10 mg/ml) of GEN in distilled water at room temperature. The formulation was modified based on the previous work reported by Shah et al. (Shah et al. 2016) by using similar drug. After that, cylindrical shape of CO_3Ap scaffold was immersed in GEN solution for 4 h in vacuum to allow complete infiltration of the drug. The immersed CO_3Ap scaffold was then dried in vacuum oven at 80 °C for 24 h.

3.4 Process on CO_3Ap Scaffold with GEN and GENMS in CS Solution

In order to coat CO_3Ap scaffold with CS containing GEN, GEN was mixed with 0.3 ml of 2% solution (10 mg/ml) in 0.5 wt% CS solution. Firstly, an aqueous suspension of GENMS (0.8 wt%) was mixed in 0.5 wt% CS solution, the formulation was used according to the previous work (Francis et al. 2010). The GENMS suspension in CS was sonicated using an ultrasonic bath (Transsonic TP690) for 15 min to improve the dispersion of the microspheres by separating possible microsphere agglomerations. After both coating solutions were ready, CO_3Ap scaffold with 0.45 g in cylindrical shape with dimension of about 10 mm (diameter) × 2 mm (height) was immersed in the solutions for 4 h in vacuum to allow complete infiltration. The immersed CO_3Ap scaffold was then dried in vacuum oven at 80 °C for 24 h. The scaffolds were weighed before and after the coating process and the amount of GENMS loaded and CS coated on the scaffolds were estimated from the weight change.

4 Characterizations

4.1 Scanning Electron Microscope

Scanning electron microscope (SEM) (Zeiss Supra 55VP, Germany) was used to analyse the morphology of scaffolds and PLA microsphere. Cross-section of porous scaffolds was observed, and pore size were recorded. The morphologies of the sample were captured using secondary mode at an accelerating voltage of 5 kV.

4.2 Bioactivity Test

GEN incorporated CO_3Ap scaffolds in the size of 10 mm (diameter) × 2 mm (height) were soaked in HBSS for 28 days. Each scaffold was soaked in 50 ml of HBSS and kept at 36.5 ± 1 °C for the set period. After immersion in HBSS, the scaffolds were removed, rinsed gently with deionized water, and dried in an oven at 50 °C for 24 h.

4.3 In Vitro Cell Proliferation

Cell study on the samples was carried out with 0.15 g in cylindrical shape. The samples were decontaminated by soaking them 3 times in 70% ethanol for 30 min. After that, the samples were immersed in PBS three times for 15 min each, before being left to dry in sterilized hood for 24 h. Prior to cell seeding, the samples were immersed in Dulbecco's modified Eagle's medium (DMEM) for 30 min. The hFOB 1.19 cells (Homo sapiens, CRL-11372TM, ATCC, Manassas, VA, USA) were cultured in Dulbecco's modified Eagle's medium (DMEM, Gibco Life Technologies)) and supplemented with 10% fetal bovine serum (FBS, Gibco Life Technologies), 1% antibiotic–antimycotic (AA, Gibco Life Technologies). The cells in culture flask (T-25) multiplied in an incubator with humidified atmosphere of 5% CO_2 at 37 °C. Cell proliferation was assessed after 1, 2, 3, 5 and 7 days using PrestoBlue viability reagent (Molecular Probe, Life Technologies). PrestoBlue was added in an amount equal to 10% of the volume in the well. The well was then incubated for 20 min prior to absorbance detection at 570 nm using microplate spectrophotometer (Multiskan Spectrum). The absorbance data were analysed according to formulation provided by manufacturer's instruction (Molecular Probe, Life Technologies).

4.4 Drug Release Test in Vitro

In order to determine the GEN release profile, the uncoated and coated CO_3Ap scaffolds were individually immersed in glass vials containing 10 ml and 0.1 M phosphate buffered saline (PBS) solution. The glass vial placed in shaker with 60 rpm at constant temperature of 37 °C. At pre-determined time intervals, aliquots of 3 ml from each sample were extracted and replenished with fresh PBS solution to maintain the total volume of 10 ml. The drug release study was performed in triplicate for up to 28 days for each group. The level of GEN in the elution was detected by UV–Vis spectrophotometer at a wavelength of 195 nm.

4.5 Degradation Rate

The in vitro biodegradation of the scaffolds was studied by calculating the weight loss the scaffolds over the time. The dry weights after immersion in HBSS were noted as w_t. The percentage weight loss with respect to the initial weight (w_i) was calculated based on Eq. 4 (Olad and Farshi Azhar 2014):

$$\text{Weight loss} = \frac{w_i - w_t}{w_i} \times 100\% \tag{4}$$

4.6 Drug Release Kinetics

The release data of GEN were mathematically fitted to four different kinetic models to fit the results of the in vitro release data; zero-order, first-order, Higuchi and Korsmeyer–Peppas models. These models are often utilized to designate the drug release mechanism from the microsphere (El-Say 2016; Unagolla and Jayasuriya 2018) while Peppas model was the most commonly used model for a mathematical description of drug delivery kinetics and it is often applied to porous ceramic delivery systems (Gbureck et al. 2008). From the linear regression of these plots the correlation coefficient (R^2) values were calculated and compared. Equations 5–8 show the different release kinetic models;

$$\text{Zero-order kinetic} : Q_t = Q_0 + K_0 t \tag{5}$$

$$\text{First-order kinetic} : \ln Q_t = \ln Q_0 + K_1 t \tag{6}$$

$$\text{Higuchi's model} : Q_t = K_{H\sqrt{t}} \tag{7}$$

$$\text{Korsmeyer-Peppas model} : M_t/M_\infty, (Q_t) = kt^n \tag{8}$$

where Q_0 is the initial amount of drug in solution (it is usually zero), Q_t is the amount of drug released in time t, K_0 is the zero-order release constant, K_1 is the first-order release constant, K_H is the Higuchi dissolution constant, M_t/M_∞ is the fraction of drug released at time t, k is the rate constant, and n is the release exponent of the Korsmeyer-Peppas model.

Korsmeyer-Peppas equation was conducted to further confirm that both diffusion and erosion mechanism were involved in releasing the drug by calculating the values of drug release exponent (n). The interpretation of the diffusional constant n for the samples was referred according to Table 1.

Table 1 Categories of release mechanism depending on sample geometry and the release exponent n of the Peppas model (Hess et al. 2017)

Release exponent n		Release mechanism
Cylinder	Sphere	
$n \leq 0.45$	$n \leq 0.43$	Fickian diffusion
$0.45 < n < 0.89$	$0.43 < n < 0.85$	Anomalous (non-Fickian) transport
$n = 0.89$	$n = 0.85$	Case-II transport
$n > 0.89$	$n > 0.85$	Super case-II transport

5 Results and Discussion

5.1 GEN-Loaded PLA Microsphere, Encapsulation Efficiency and Microstructures

Figure 1 shows the bulk shape and microstructure of GENMS fabricated from double ESE. Almost perfect spherical microspheres with a uniform surface morphology are observed from the microstructures.

The percentage of EE and DL of GEN incorporated in GENMS was determined based on standard curve of GEN concentration in the range of 10–400 ppm. From the calculation based on Eq. 1 to Eq. 3, the average of EE of GENMS was 13.97% $\pm$ 0.311. Due to GEN is a very hydrophilic drug, it tends to leach out into water phase when microsphere are fabricated using ESE method which probably made the obtained encapsulation is low (Naraharisetti et al. 2005).

Figure 2 presents SEM morphology of GEN incorporated into CO_3Ap scaffolds. Figure 2a shows the neat CO_3Ap scaffolds with the pure apatite crystal structure without coating layer. Figure 2b shows the morphology of GEN incorporated directly into the CO_3Ap scaffolds (GEN-CO_3Ap scaffolds). This morphology was similar with neat CO_3Ap scaffolds (Fig. 2a) where only apatite crystal structure was

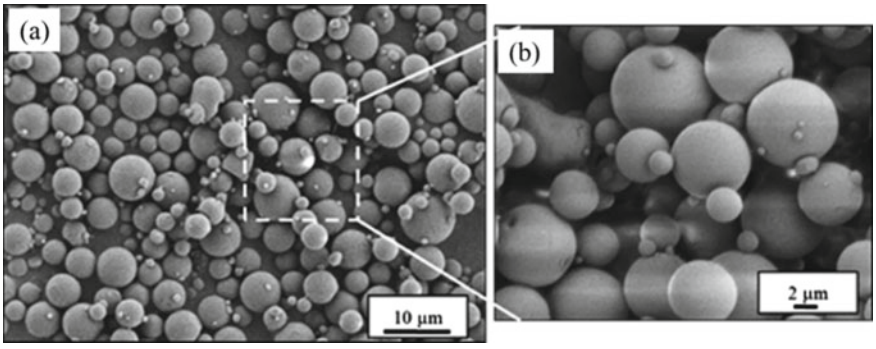

Fig. 1 Microstructure of GENMS fabricated through double ESE technique. (Images were observed at **a** 1500× and **b** 3000 × magnification)

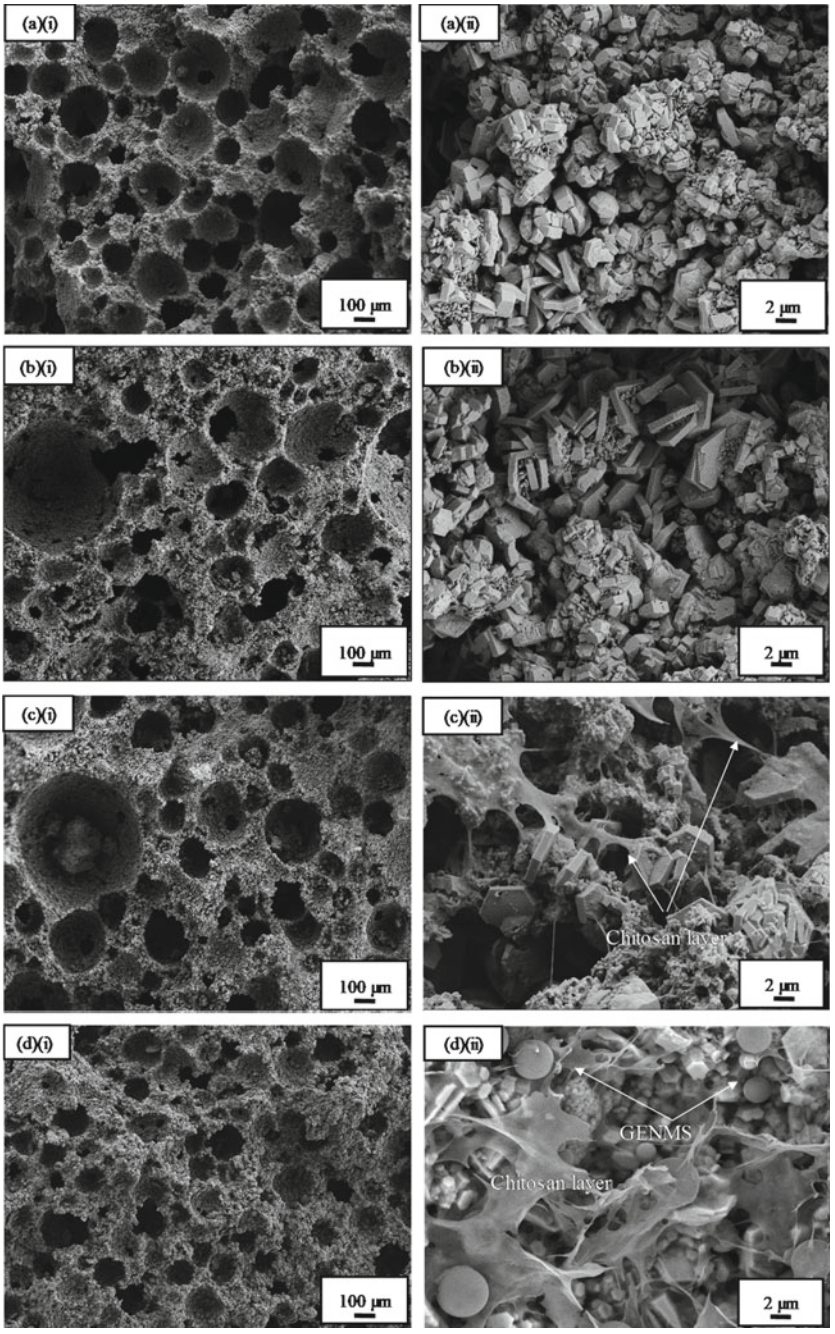

Fig. 2 SEM images of **a** neat CO_3Ap scaffolds **b** GEN-CO_3Ap scaffolds, **c** CS-GEN-CO_3Ap scaffolds and **d** CS-GENMS-CO_3Ap scaffolds

observed. Figure 2c shows the CS-GEN-CO_3Ap scaffolds with a single CS coating layer containing GEN on the apatite structure while Fig. 2d shows the morphology of CS-GENMS-CO_3Ap scaffolds with a mix coating of CS coating layer and GENMS. Both CS-coated CO_3Ap scaffolds (Fig. 2c (i) and (d)(i)) exhibits the retaining pores structure after coating process especially for CS-GENMS-CO_3Ap scaffolds (Fig. 2d) which containing mixed coating layer. It should be noted that pore structures are undistracted as shown in Fig. 2b-d (i) after the coating process. This is to ensure that bone cells could penetrate to the pores of bone scaffold for new bone formation. Therefore, the present study shows that all scaffolds able to maintain their pore size between 100 and 250 μm which is suitable to facilitate cell adhesion and internal mineralized bone formation (Xia et al. 2013).

5.2 Bioactivity Evaluation

5.2.1 Biodegradation

The scaffold acts as a temporary template should be replaced by actual extracellular matrix (ECM). Therefore, the biodegradable behaviour of scaffolds is a great importance because it provides structural support to the newly formed tissue (Swain and Bhattacharyya 2013). Figure 3 shows the biodegradation of scaffolds as a function of immersion time in HBSS at 37 °C for 4 weeks. For day 7 and day 14, degradation rate demonstrated that uncoated scaffold has higher degradation capability (4.6–5.1%) in comparison with coated scaffolds (1–4.4% and 0.8–2.9% for CS-GEN-CO_3Ap and CS-GENMS-CO_3Ap, respectively). This is due to the absence of CS layer delayed the

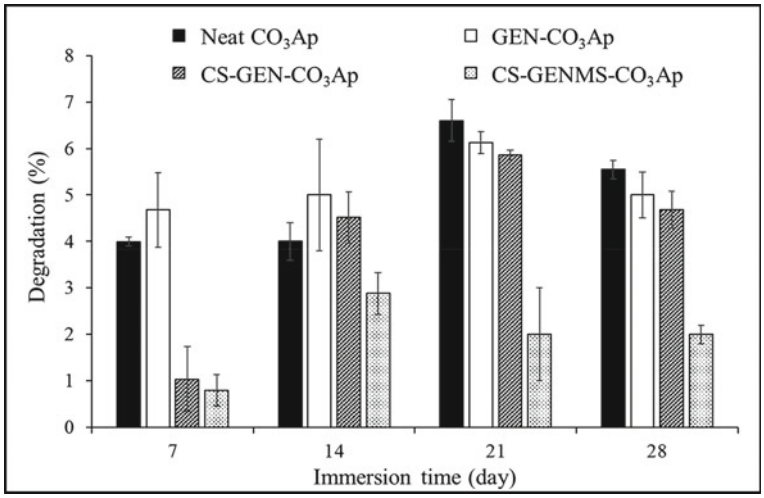

Fig. 3 Biodegradation of uncoated and coated scaffold for 4 weeks immersion in HBSS at 37 °C

scaffold degradation. Moreover, presence of GENMS showed the lowest degradation for the coated scaffolds.

After day 21 and day 28, CS-GEN-CO_3Ap scaffolds shows slightly lower degradation percentage than GEN-CO_3Ap scaffolds. Since CS has hydrophilicity behaviour (Abd-Khorsand et al. 2017), the coated scaffold with GEN shows a quick hydrolysis of its chains during interaction with HBBS solution. However, the quick degradation was controlled by the additional of GENMS for the coated scaffold of CS-GENMS-CO_3Ap scaffolds. This is due to PLA microsphere has $–CH_3$ groups as side chains of a polymer chain and thus PLA surface shows hydrophobicity towards the degradation medium (Dorati et al. 2017; Rakmae et al. 2010). The slow degradation rate of CS-GENMS-CO_3Ap scaffolds may be good, as it can provide a more sufficient time for the newly-formed tissue and the ECM during bone remodeling, while promoting the strength throughout the implantation (Sharma et al. 2016).

5.2.2 Apatite Formation

After 28 days immersion, bonelike apatites were clearly seen on both uncoated and coated scaffolds as shown in Fig. 4. Bonelike apatite grew bigger and fully covered on the surface of GEN-CO_3Ap scaffold (Fig. 4a). The apatite with crystal structure showed flake-like morphology. This precipitation indicated that uncoated scaffold enhanced apatite growth. Figure 4b shows CS-GEN-CO_3Ap scaffold has apatite with the microcracks on the surface. The cracks were formed by shrinkage of the surface layer upon drying after the scaffold being extracted from the HBSS. This is also reported by Francis et al. (Francis et al. 2010) that performed bioactivity of bioglass tablet in SBF solution. Crack development is usually a common morphological feature as a part of the reaction for growing apatite layer, which is typical of bioactive materials (Mancuso et al. 2017). As suggested by previous studies, this behaviour is considered the initial stage of the formation of the apatite layer on scaffold surface (Mancuso et al. 2017; Rahaman et al. 2012).

CS-GENMS-CO_3Ap scaffold shows a dense layer of bonelike apatite with globular and cauliflower shape (Fig. 4c). Even though, the scaffold was coated with GENMS, the scaffold surface was still capable to allow the bonelike apatite growth within 28 days. This is due to direct contact with the surrounding fluid facilitated the ion-exchange process in HBSS and leading to the apatite formation (Kokubo et al. 2009; Yamaguchi et al. 2014). Moreover, during the process of apatite formation, some GENMS could have detached because of the apatite structures growing on the surface of the scaffold. Therefore, this effect would expose scaffold surface to the HBSS, in promoting the apatite formation rate.

It should be noted that, due to uneven surface of the scaffolds, it is very difficult to produce a microsphere coating that fully covers on the entire surface. The CS-GENMS-CO_3Ap has probably some edges that uncovered by the microspheres on the surface. Thus, it provides a potential bioactive surface to facilitate ion exchange and induce apatite formation instead of preventing it.

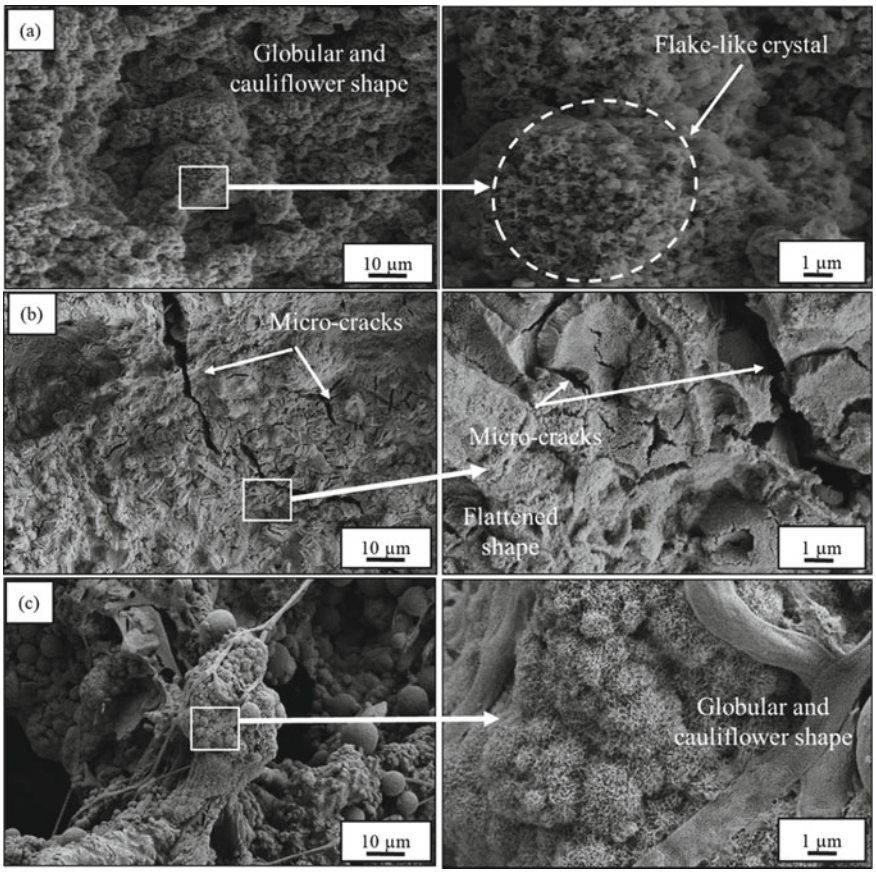

Fig. 4 SEM images of bonelike apatite growth after 28 days immersion on **a** GEN-CO3Ap, **b** CS-GEN-CO3Ap and **c** CS-GENMS-CO3Ap

6 Drug Release Profile and Kinetics Mechanism

Figure 5 reports the cumulative percentage of GEN release profiles from free microspheres of GENMS, uncoated scaffold of GEN-CO_3Ap scaffolds, coated scaffold of CS-GEN-CO_3Ap scaffolds and coated containing GENMS scaffolds of CS-GENMS-CO_3Ap scaffolds. The release profile was measured for 28 days of samples in PBS release medium. GENMS and GEN-CO_3Ap scaffolds were used as references to compare the release kinetics to the coated scaffolds. The drug release profile showed three zones; (a) initial burst release period, (b) induction release period and (c) sustained release period (Macías-Andrés et al. 2017). Burst release and sustained cumulative release mechanisms could be observed by all scaffolds.

From the whole release profile, it obviously showed a lower percentage cumulative of GEN released from the scaffolds compared to the GENMS at each time point.

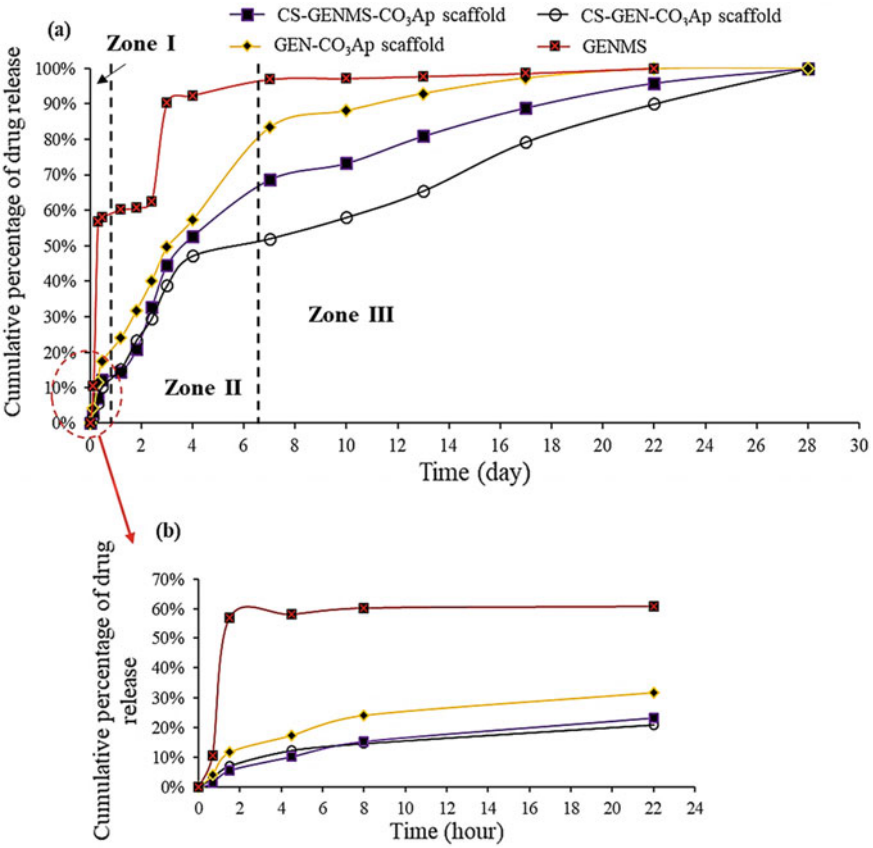

Fig. 5 Cumulative percentage of GEN released in PBS from free GENMS, uncoated and coated scaffolds for **a** 28 days with zone I is initial release, zone II is induction release and zone III is sustained release. **b** the enlargement of cumulative GEN release within 24 h

GENMS exhibited a very high initial burst release with 59% of GEN while 18% from GEN-CO_3Ap scaffolds within 4 h. In the same period, both coated scaffolds released GEN with 11% and 9% for CS-GEN-CO_3Ap scaffolds and CS-GENMS-CO_3Ap scaffolds, respectively. The scaffolds showed similar release profiles but slight differences in the amount of GEN released.

GEN was significantly released from free microsphere at initial stage of zone I. This is shown by sharp slope compared to the release rate shown by those uncoated and coated scaffolds. As can be seen, a secondary burst release occurred by GENMS at approximately day 3. It may be due to the remaining GEN was entrapped deep within the microspheres and comes out only when the microsphere starts to degrade or after water has penetrated sufficiently into the microspheres. Furthermore, much higher drug release rates observed in GENMS was due to much higher surface area to volume shown by GENMS than a scaffold. The possible reason for this burst release

was also assisted by the hydrophilic nature of the drug itself and related to the surface associated GEN.

In the present study, in vitro release experiment carried out in PBS which the dispersed GENMS have their entire surface in contact with the solution. However, for CS-GENMS-CO_3Ap scaffolds only the outermost layer of GENMS on the scaffold were in contact with the PBS solution. In addition, the additional path length of the drug from inner atmosphere to the outer release media required the dissolution and/or degradation of CS layer and/or PLA microsphere to release the GEN.

According to second and third zone profiles with a change in the slope of the release curve, the release of GEN from the uncoated scaffold was higher than those of coated scaffolds. Based on cumulative release for day 7, the cumulative were 83, 68 and 52% for GEN-CO_3Ap scaffolds, CS-GENMS-CO_3Ap scaffolds and CS-GEN-CO_3Ap scaffolds, respectively. It indicated that, the drug release was slower after the GEN was loaded in the coated scaffolds due to the increasing of dissolution path created by CS layer.

In term of coated scaffold, the CS-GEN-CO_3Ap scaffolds and CS-GENMS-CO_3Ap scaffolds were specifically compared to examine the role of GENMS within CS-coated scaffold. As can be seen, the GEN released from CS-GENMS-CO_3Ap scaffold was higher than the CS-GEN-CO_3Ap scaffolds. This is due to the presence of GENMS attached to the scaffold surface reduced the path of drug dissolution from inside of scaffold as compared to CS-GEN-CO_3Ap scaffolds. This also proved that the hydrophobic properties of PLA microsphere were not the barrier factor because the GEN was diffused to the media phase due to its hydrophilic nature. Furthermore, degradation of PLA is very slow (Silva et al. 2018) and thus this mechanism can be neglected within the drug release period in this study. Hence, the present study shows that the diffusion rate of the GEN was higher than the rate of microsphere degradation. It can be concluded that GEN release behaviour depends mainly on drug diffusion and not on polymer degradation (Macías-Andrés et al. 2017). It is also noted that, the components PBS of the release medium used in this work are non-solvents of PLA (Macías-Andrés et al. 2017). Therefore, the shrinkage or swelling of the polymer is negligible which results in a diffusion-controlled drug release behaviour.

In the last zone, GEN was completely released for 22 days from GENMS than those loaded GEN in scaffolds. It is well known that high initial burst showed by GENMS is usually undesirable because the drug released in this period is not available for prolonged release and more importantly it may cause toxic side effects. Therefore, the results demonstrated that scaffold systems can be used to reduce initial burst release while controlling drug release in the prolonging time.

CS coating in the present study seems to be more effective in reducing the initial burst release with a sustained release profile over the time (Yao et al. 2013). This was attributed by the proper dispersion of GEN for both coated scaffolds. As reported elsewhere (Ghorbani et al. 2016; Khodaei et al. 2017), drug, growth factor and genes can be directly mixed into the polymer solution in order to prepare a drug carrier with controlled-release profile. Thus, the result demonstrated that CS-GENMS-CO_3Ap scaffold has the best sustained-release function, which can increase the targeted drug

release using coated CO_3Ap scaffold. Hence, GENMS plays the role to determine an adequate local drug release at defect site.

In order to assess the mechanism of GEN release, the release kinetics for all scaffolds based on in vitro release analysis are presented in Table 2. The release kinetic from GENMS was used as a reference. The release behaviours and related constants of GEN from GENMS and scaffolds were calculated for the zero-order, first-order, Higuchi and Korsmeyer–Peppas model equations. All kinetics models are valid only for the first 60% of drug release (Unagolla and Jayasuriya 2018). Table 2 is used to find the best fit model of the experimental data for each sample type by comparing their correlation coefficient (R^2) values.

The highest values for R^2 indicated that GENMS and CS-GENMS-CO_3Ap followed first-order (log cumulative percentage of drug remaining versus time) release kinetic model while GEN-CO_3Ap scaffolds and CS-GEN-CO_3Ap scaffolds followed Higuchi's release kinetic model (cumulative percentage of drug released versus square root of time). The Higuchi model by GEN-CO_3Ap scaffolds and CS-GEN-CO_3Ap scaffolds indicated that the kinetics of GEN release from both scaffold types was governed by Fickian diffusion. It describes the diffusion-controlled release of water-soluble drugs from porous scaffold systems (matrix) with the assumption of perfect sink conditions and negligible polymer swelling or dissolution (Gbureck et al. 2008). However, this model cannot be well applied to swelling or degradable systems with changes in diffusivity (Gbureck et al. 2008). Thus, a decrease in GEN release over time is expected as the drug is depleted in the matrix and diffusion path length is increased.

In contrast, the first-order release kinetic model reflects reservoir type drug delivery system (Unagolla and Jayasuriya 2018; Xu et al. 2008). The results showed that both GENMS and CS-GENMS-CO_3Ap scaffolds used microsphere as a main source of GEN to be released out. It also related to the release of GEN from the systems where dissolution rate was dependent on the concentration or dissolving of microsphere and coating layer, respectively. Thus, the release of GEN from these samples was slowed down as the dissolving materials increased (Budiasih et al. 2014).

Table 2 Release kinetic parameters calculated from the GEN release data in PBS solution using different mathematical models describing drug release mechanisms (R^2 = correlation coefficient; n = diffusional release exponent representing the type of transport)

Samples	Zero-order kinetic ($Q_t = Q_0 + K_0t$)	First-order kinetic ($\ln Q_t = \ln Q_0 + K_1t$)	Higuchi's model ($Q_t = K_{H\sqrt{}}t$)	Kosmeyer-Peppas model ($Q_t = kt^n$)	
	R^2	R^2	R^2	R^2	n
GENMS	0.6306	0.8059	0.6913	0.6116	0.7011
GEN-CO_3Ap	0.9400	0.9730	0.9851	0.8687	0.7505
CS-GEN-CO_3Ap	0.8048	0.8742	0.9537	0.9402	0.7704
CS-GENMS-CO_3Ap	0.9722	0.9726	0.9391	0.9237	0.7637

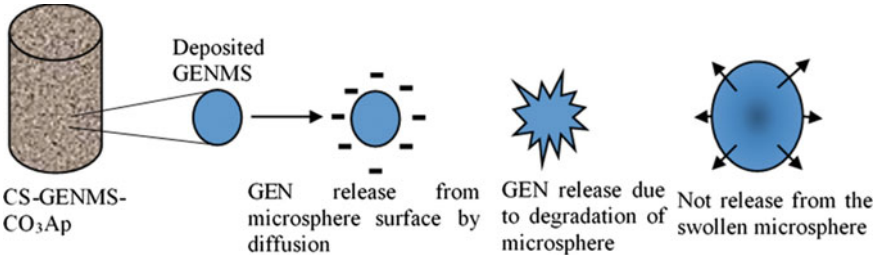

Fig. 6 Mechanism of GEN release from GENMS

The dissolution data of drug release profiles were further fitted into Korsmeyer-Peppas equation (log cumulative percentage of drug released versus log time). The diffusional release exponents (n) were found to be in between 0.7011–0.7704, which attributed to anomalous (non-Fickian) transport for all sample types. According to Gbureck et al. (Gbureck et al. 2008) and Hess et al. (Hess et al. 2017) when $n = 0.43$ (sphere) or $n = 0.45$ (cylindrical) the drug release mechanism is governed by the Fickian diffusion, when $0.43 < n < 0.85$ (sphere) or $0.45 < n < 0.89$ (cylindrical) it is anomalous (non-Fickian) transport and when $n = 0.85$ (sphere) or $n = 0.89$ (cylindrical) it is case II transport.

This analysis was further confirmed that both diffusion and erosion mechanism involved in releasing the drug from the free GENMS, uncoated and coated scaffolds. The incorporation of GEN into microsphere and the scaffold structure was expected to lead to a hindrance in diffusivity and built storage of drug. It may release the trapped GEN while gradually degrade the microsphere (for GENMS), degrade the microsphere and/or CS (for CS-GENMS-CO_3Ap scaffolds), degrade the scaffold (for GEN-CO_3Ap scaffolds) and degrade the CS and/or CO_3Ap scaffolds (for CS-GEN-CO_3Ap scaffolds). Therefore, this mechanism resulted to the observation that the amount of released GEN among these samples were different. In addition, kinetic release mechanism can be in line with the in vitro drug release profile as shown in Fig. 5. Thus, Fig. 6 summarize the release behaviour of GEN in the present study.

7 Cell Proliferation

Effective scaffolds for TE application need higher surface area and void spaces for cell activities. Cell proliferation for the GEN incorporated into CO_3Ap scaffolds was assessed using PrestoBlue assay after culturing for 1, 2, 3, 5 and 7 days (Fig. 7). For day 1 until day 7 of incubation, the scaffolds showed higher cell proliferation compared to the control cell (cell without scaffold) with CS-GENMS-CO_3Ap scaffold has the highest among others. It is believed that, the cell proliferation is dependent on the surface properties of the scaffold whereby the CS-GENMS-CO_3Ap scaffold

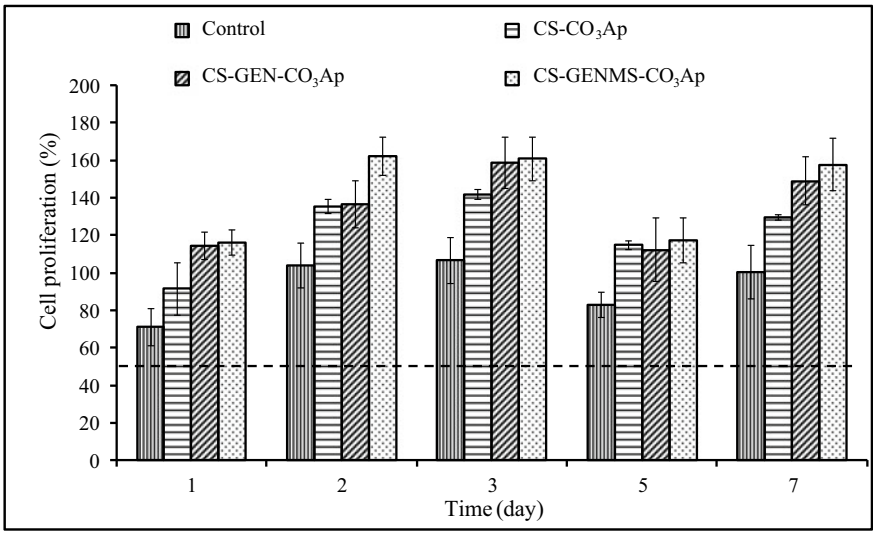

Fig. 7 Rate of proliferation of hFOB cells grown on control, CS-CO_3Ap scaffold, CS-GEN-CO_3Ap and CS-GENMS-CO_3Ap scaffold for 1, 2, 3, 5 and 7 days

provided higher surface roughness due to adherence of GENMS on the CO_3Ap scaffold surfaces. This possible behaviour is illustrated in Fig. 8. These results indicated that more hFOBs proliferated to that scaffolds surface due to more surface roughness

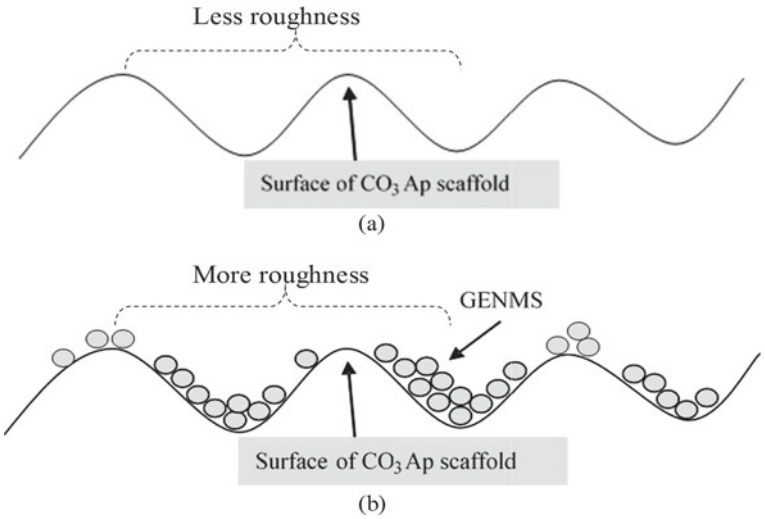

Fig. 8 Possible different surface roughness by **a** CS-GEN-CO_3Ap or GEN-CO_3Ap and **b** how the GENMS attach and fill up uneven surface of CS-GENMS-CO_3Ap

that played an important role in enhancing cell attachment, proliferation and bone matrix formation (Ibrahim et al. 2016).

The results also show that the incorporation of GEN in bone scaffolds improved in osteoblast function rather than scaffold without containing GEN (Farokhi et al. 2016). In addition, cell viability more than 50% demonstrated that drug-delivery scaffolds has no toxicity to hFOBs cells (Ibrahim et al. 2016). As a result, the CS-GENMS-CO_3Ap scaffold has potential application prospects in the infection therapy during bone regeneration.

8 Conclusion

This work has led to the development of novel multifunctional CO_3Ap scaffold for successful bone regeneration. Presence of gentamicin-loaded PLA microsphere (GENMS) in the coated scaffold surfaces has controlled drug release rate while exhibiting more surface roughness to increase cell viability. GEN delivery capability from GENMS-CS-CO_3Ap scaffold was supported with kinetics release results. The drug was released in a slow and sustained manner compared to higher burst release measured from GENMS and from uncoated CO_3Ap scaffold (GEN-CO_3Ap scaffold). Moreover, adherence of GENMS on CO_3Ap scaffold was not distracted to the growth of apatite nucleation for 28 days immersion. GENMS-CS-CO_3Ap scaffold developed in the study exhibit adequate surface roughness, enhanced bioactivity, controlled drug delivery function and biocompatibility, being thus of high interest for bone tissue engineering.

References

Abd-Khorsand S, Saber-Samandari S, Saber-Samandari S (2017) Development of nanocomposite scaffolds based on TiO_2 doped in grafted chitosan/hydroxyapatite by freeze drying method and evaluation of biocompatibility. Int J Biol Macromol 101:51–58. https://doi.org/10.1016/j.ijbiomac.2017.03.067

Araújo M, Viveiros R, Philippart A, Miola M, Doumett S, Baldi G, Perez J, Boccaccini AR (2017) Bioactivity, mechanical properties and drug delivery ability of bioactive glass-ceramic scaffolds coated with a natural-derived polymer. Mater Sci Eng C 77:342–351. https://doi.org/10.1016/j.msec.2017.03.169

Budiasih S, Jiyauddin K, Logavinod N, Kaleemullah M, Jawad A, Samer AD, Fadli A, Eddy Y (2014) Optimization of polymer concentration for designing of oral matrix controlled release dosage form. UK J Pharm Biosci 2:54–61

da Silva D, Kaduri M, Poley M, Adir O, Krinsky N, Shainsky-Roitman J, Schroeder A (2018) Biocompatibility, biodegradation and excretion of polylactic acid (PLA) in medical implants and theranostic systems. Chem Eng J 340:9–14. https://doi.org/10.1016/j.cej.2018.01.010

Darus F, Isa R, Mamat N, Jaafar M (2018) Techniques for fabrication and construction of three-dimensional bioceramic scaffolds: effect on pores size, porosity and compressive strength. Ceram Int 44:18400–18407. https://doi.org/10.1016/j.ceramint.2018.07.056

Dorati R, Detrizio A, Modena T, Conti B (2017) Biodegradable scaffolds for bone regeneration combined with drug-delivery systems in osteomyelitis therapy. Pharmaceuticals 10:3–21. https://doi.org/10.3390/ph10040096

El-Say KM (2016) Maximizing the encapsulation efficiency and the bioavailability of controlled-release cetirizine microspheres using Draper—Lin small composite design. Drug Des Devel Ther 10:825–839

Farokhi M, Mottaghitalab F, Ali M, Ou K, Mao C, Hosseinkhani H (2016) Importance of dual delivery systems for bone tissue engineering. J Control Release 225:152–169. https://doi.org/10.1016/j.jconrel.2016.01.033

Francis L, Meng D, Knowles JC, Roy I, Boccaccini AR (2010) Multi-functional P(3HB) microsphere/45S5 bioglass-based composite scaffolds for bone tissue engineering. Acta Biomater 6:2773–2786. https://doi.org/10.1016/j.actbio.2009.12.054

Gbureck U, Vorndran E, Barralet JE (2008) Modeling vancomycin release kinetics from microporous calcium phosphate ceramics comparing static and dynamic immersion conditions. Acta Biomater. 4:1480–1486. https://doi.org/10.1016/j.actbio.2008.02.027

Ghorbani F, Nojehdehian H, Zamanian A (2016) Physicochemical and mechanical properties of freeze cast hydroxyapatite-gelatin scaffolds with dexamethasone loaded PLGA microspheres for hard tissue engineering applications. Mater Sci Eng C 69:208–220. https://doi.org/10.1016/j.msec.2016.06.079

Hess U, Shahabi S, Treccani L, Streckbein P, Heiss C, Rezwan K (2017) Co-delivery of cisplatin and doxorubicin from calcium phosphate beads/matrix scaffolds for osteosarcoma therapy. Mater Sci Eng C 77:427–435. https://doi.org/10.1016/j.msec.2017.03.164

Ibrahim S, Sabudin S, Sahid S, Marzuke MA, Hussin ZH, Kader Bashah NS, Jamuna-Thevi K (2016) Bioactivity studies and adhesion of human osteoblast (hFOB) on silicon-biphasic calcium phosphate material. Saudi J Biol Sci 23:S56–S63. https://doi.org/10.1016/j.sjbs.2015.10.024

Ishikawa K (2010) Bone substitute fabrication based on dissolution-precipitation reactions. Materials (Basel) 3:1138–1155. https://doi.org/10.3390/ma3021138

Khodaei M, Valanezhad A, Watanabe I (2017) Controlled gentamicin-strontium release as a dual action bone agent: combination of the porous titanium scaffold and biodegradable polymers. J Alloys Compd 720:22–28. https://doi.org/10.1016/j.jallcom.2017.05.236

Kim HW, Knowles JC, Kim HE (2005) Hydroxyapatite porous scaffold engineered with biological polymer hybrid coating for antibiotic Vancomycin release. J Mater Sci Mater Med 16:189–195. https://doi.org/10.1007/s10856-005-6679-y

Kokubo T, Matsushita T, Takadama H, Kizuki T (2009) Development of bioactive materials based on surface chemistry. J Eur Ceram Soc 29:1267–1274. https://doi.org/10.1016/j.jeurceramsoc.2008.08.004

Macías-Andrés VI, Li W, Aguilar-Reyes EA, Ding Y, Roether JA, Harhaus L, León-Patiño CA, Boccaccini AR (2017) Preparation and characterization of 45S5 bioactive glass-based scaffolds loaded with PHBV microspheres with daidzein release function. J Biomed Mater Res—Part A 105:1765–1774. https://doi.org/10.1002/jbm.a.36046

Mamat N, Jaafar M, Abdul Hamid ZA (2017) Fabrication of carbonate apatite based on hydrothermal reaction using freeze-casted β-TCP precursor. Solid State Phenom 264(SSP):3–6. https://doi.org/10.4028/www.scientific.net/SSP.264.50

Mancuso E, Bretcanu O, Marshall M, Dalgarno KW (2017) Sensitivity of novel silicate and borate-based glass structures on in vitro bioactivity and degradation behaviour. Ceram Int 43:12651–12657. https://doi.org/10.1016/j.ceramint.2017.06.146

Meng D, Francis L, Thompson ID, Mierke C, Huebner H, Amtmann A, Roy I, Boccaccini AR (2013) Tetracycline-encapsulated P(3HB) microsphere-coated 45S5 Bioglass®-based scaffolds for bone tissue engineering. J Mater Sci Mater Med 24:2809–2817. https://doi.org/10.1007/s10856-013-5012-4

Naraharisetti PK, Ning Lew MD, Fu YC, Lee DJ, Wang CH (2005) Gentamicin-loaded discs and microspheres and their modifications: Characterization and in vitro release. J Control Release 102:345–359. https://doi.org/10.1016/j.jconrel.2004.10.016

Olad A, Farshi Azhar F (2014) The synergetic effect of bioactive ceramic and nanoclay on the properties of chitosan–gelatin/nanohydroxyapatite–montmorillonite scaffold for bone tissue engineering. Ceram Int 40:10061–10072. https://doi.org/10.1016/j.ceramint.2014.04.010

Pei P, Tian Z, Zhu Y (2018) 3D printed mesoporous bioactive glass/metal-organic framework scaffolds with antitubercular drug delivery. Microporous Mesoporous Mater 272:24–30. https://doi.org/10.1016/j.micromeso.2018.06.012

Rahaman MN, Liu X, Bal BS, Day DE, Bi L, Bonewald LF (2012) Bioactive glass in bone tissue engineering. Biomater Sci Process Prop Appl II Ceram Trans 237:73–82. https://doi.org/10.1016/j.actbio.2011.03.016

Rakmae S, Ruksakulpiwat Y, Sutapun W, Suppakarn N (2010) Physical properties and cytotoxicity of surface-modified bovine bone-based hydroxyapatite/poly (lactic acid) composites. J Compos Mater 45:1259–1269. https://doi.org/10.1177/0021998310377934

Shah MR, Patel RR, Solanki RV, Gupta SH (2016) Estimation of drug absorption in antibiotic soaked bone grafts. Indian J Orthop 50:669–676. https://doi.org/10.4103/0019-5413.193486

Sharma C, Dinda AK, Potdar PD, Chou CF, Mishra NC (2016) Fabrication and characterization of novel nano-biocomposite scaffold of chitosan-gelatin-alginate-hydroxyapatite for bone tissue engineering. Mater Sci Eng C 64:416–427. https://doi.org/10.1016/j.msec.2016.03.060

Swain SK, Bhattacharyya S (2013) Preparation of high strength macroporous hydroxyapatite scaffold. Mater Sci Eng C 33:67–71. https://doi.org/10.1016/j.msec.2012.08.006

Unagolla JM, Jayasuriya AC (2018) Drug transport mechanisms and in vitro release kinetics of vancomycin encapsulated chitosan-alginate polyelectrolyte microparticles as a controlled drug delivery system. Eur J Pharm Sci 114:199–209. https://doi.org/10.1016/j.ejps.2017.12.012

Wang Q, Li J, Xu T, Lu X, Zhi W, Weng J (2017) Porous hydroxyapatite scaffolds containing dual microspheres based on poly(lactide-co-glycolide) and chitosan for bone regeneration. Mater Lett 188:387–391. https://doi.org/10.1016/j.matlet.2016.11.098

Xia Z, Yu X, Jiang X, Brody HD, Rowe DW, Wei M (2013) Acta biomaterialia fabrication and characterization of biomimetic collagen—apatite scaffolds with tunable structures for bone tissue engineering. Acta Biomater 9:7308–7319. https://doi.org/10.1016/j.actbio.2013.03.038

Xu X, Chen X, Ma P, Wang X, Jing X (2008) The release behavior of doxorubicin hydrochloride from medicated fibers prepared by emulsion-electrospinning. Eur J Pharm Biopharm 70:165–170. https://doi.org/10.1016/j.ejpb.2008.03.010

Yamaguchi S, Nath S, Matsushita T, Kokubo T (2014) Controlled release of strontium ions from a bioactive Ti metal with a Ca-enriched surface layer. Acta Biomater 10:2282–2289. https://doi.org/10.1016/j.actbio.2014.01.026

Yao Q, Nooeaid P, Roether JA, Dong Y, Zhang Q, Boccaccini AR (2013) Bioglass®-based scaffolds incorporating polycaprolactone and chitosan coatings for controlled vancomycin delivery. Ceram Int 39:7517–7522. https://doi.org/10.1016/j.ceramint.2013.03.002

Yazdimamaghani M, Vashaee D, Assefa S, Shabrangharehdasht M, Rad AT, Eastman MA, Walker KJ, Madihally SV, Köhler GA, Tayebi L (2014) Green synthesis of a new gelatin-based antimicrobial scaffold for tissue engineering. Mater Sci Eng C 39:235–244. https://doi.org/10.1016/j.msec.2014.03.007